Bernd Lottermoser *Editor*

# Environmental Indicators in Metal Mining

Springer

# Environmental Indicators in Metal Mining

Bernd Lottermoser
Editor

# Environmental Indicators in Metal Mining

Springer

*Editor*
Bernd Lottermoser
Institute of Mineral Resources Engineering
RWTH Aachen University
Aachen
Germany

ISBN 978-3-319-42729-4 ISBN 978-3-319-42731-7 (eBook)
DOI 10.1007/978-3-319-42731-7

Library of Congress Control Number: 2016948102



Printed on acid-free paper

This Springer imprint is published by Springer Nature
The registered company is Springer International Publishing AG Switzerland

# Preface

Today's mineral resource development requires best certainty in decision-making from the beginning of the mine life cycle. Such well-informed decisions need to be based on (a) solid predictions of future market, political, technological and cost trends; (b) a complete understanding of sociopolitical conditions as well as available mining logistics and technologies; (c) a detailed awareness of possible alternatives for mining, processing and environmental measures; and (d) a total deposit knowledge that has been established using best practices.

Total deposit knowledge is the solid understanding of all the pertinent physical and chemical characteristics of a mineral resource. These important characteristics include geological properties, metallurgical performance, geotechnical aspects and likely environmental impacts. These fundamental aspects need to be established early in the life cycle of a mine. Investigations on drill core allow a prediction of the likely geological, metallurgical, geotechnical and environmental characteristics of ore bodies. Among the predictive methods pursued, field and laboratory testing of ores and wastes has gained prominence, and the acquired data are commonly articulated through the use of indicators. Effective indicators are an important component of achieving best certainty for well-informed and fast decisions in mining. Only best certainty in decision-making from the beginning of life of mine will lead to economically viable, technically sound, environmentally responsible and socially acceptable mining projects in the long term.

Indicators are signs or signals that convey messages. They have their value as proxies for measuring conditions that can be difficult or impossible to measure. To be fit for purpose, indicators need to be relevant, easy to understand, reliable and based on accessible data. In agreement with the Organization for Economic Development and Co-operation (OECD), an "environmental indicator" is defined herein as a parameter, or a value derived from parameters, which allows the direct or indirect measurement of environmental quality.

Twenty years ago, Hammond et al. (1995) commented that people sit up and take notice when economic indicators like the Dow Jones dive, house prices drop and unemployment rates rise, yet there were no similar indicators for the

environment. The release of specific pieces of economic data will make millions of individuals reconsider personal financial arrangements. Politicians, industry and business find changes in gross domestic product (GDP), retail sales and industrial production similarly fascinating. Such indicators provide measurements for evaluating the health of our economy, the latest business cycles and how consumers are spending. Economic indicators demonstrate the power of single numbers when their importance is understood by all. Globally recognized indicators are single numbers that clearly communicate changes and risks to significant and complex issues.

As international concerns about the environment and the sustainable development of our natural resources become more pressing, government, business and the public all need informative, definitive and uniform data on the environment. Today, there are key environmental indicators for major environmental issues such as climate change (i.e. $CO_2$ and greenhouse gas emission intensities), ozone layer depletion (i.e. intensities of ozone-depleting substances) and air quality (i.e. $SO_x$ and $NO_x$ emission intensities). The use of environmental indicators is now pursued by international organizations (e.g. OECD, WHO, UN), multinational and national agencies, and the private sector because they allow the prediction, monitoring and assessment of environmental processes. Environmental indicators have become essential tools for assessing environmental processes, supporting decision-making in government and industry, and informing all stakeholders and the public.

Environmental indicators may be used to track current changes to the quality and condition of the air, water, land and ecological systems—and their resident biota—on various geographical and temporal scales. By contrast, the prediction of future environmental conditions and risks allows informed decision-making well before significant impacts on the environment have occurred. Prediction is one of the basic desires of humanity, to discern the future and know what fate holds.

At mine sites, environmental indicators provide information on conditions and processes that exist or may develop during the life-of-mine phases from the exploration to the closure stage. The need for improved understanding of environmental liabilities and risks associated with mining operations has been widely recognized in the mining industry. For example, a number of mining companies have identified that a well-organized and implemented approach to the prediction of acid rock drainage (ARD) can have significant financial benefits, with some suggesting that as little as a 10 % reduction in mine closure liability may be worth tens of millions to individual companies (Dowd 2005).

Therefore, prediction of environmental conditions and risks should be done early in the life of a mine. Mineral resource development is commonly initiated through drilling of geological targets. This book focuses on those activities that should be performed during exploration, prefeasibility and feasibility stages and documents those practices, tests and methodologies that characterize environmental attributes of mineral deposits mainly based on drill core and rock sampling and testing. The acquired data are to yield predictive information on the environmental characteristics of exploitable mineral resources. Such information should be used as inputs into mine planning, mineral processing designs and waste management strategies, which in turn should influence the environmental performance of mining operations

and support more effective resource development, efficient mineral processing, better storage of waste and ultimately improved mine closure outcomes.

Despite the fact that the use of predictive environmental indicators has become part of mineral resource development, a single text explaining the scientific principles of predicting environmental effects of metal mining and the tests and methodologies available to forecast environmental risks is still missing. This book aims to fill the gap and will thereby complement the existing literature. It has been written with students, scientists, regulators and industry practitioners in mind, who already have an understanding of mining, mineral processing, geology, mineralogy and geochemistry. This book will also be of use to those responsible for the preparation and evaluation of environmental impact assessments, mine plans and waste management plans of metal mines.

A mine has a finite lifespan, ranging from the exploration, prefeasibility, feasibility, design, construction, production, decommissioning to the closure phase. Each phase of mine operation requires the use of scientific tools to gain an understanding of environmental processes. Many environmental analyses such as simple water quality measurements are routine environmental measurement tasks at operating mines. Such monitoring tasks only provide insights into the current state of the environment at mine sites, and they have limited use to predict future environmental impacts and risks. Consequently, such monitoring tasks and procedures are not predictive and will not be presented in this work. Also, the book limits the presentation of indicators to those types that are based on the mineralogical and geochemical properties of solid sample media such as rocks, ores, mine wastes, dusts, soils and sediments. Biologically focused indicators based on microbiological, botanical and ecological measurements are more commonly applied to evaluate activities at the operation and closure stages, and hence, they are also not explored in this work. Readers interested in biological indicators are advised to consult the relevant literature.

This book gathers the scientific knowledge on predictive environmental indicators in metal mining. It focuses on indicators that are to be used at the earliest stages of mineral resource development. Thus, this monograph documents early indicators that are relevant to mineral resource development at the exploration to design phases and allow forecasting of waste properties and the possible impacts of mining and mineral processing on land, water and air quality. This book attempts to cover the description of physical and chemical parameters of rocks that could impact on the environment during mineral resource development. This book has been organized into five sections that document the different methodologies and tests of predictive environmental indicators in metal mining:

1. Part I sets the scene as introduction. It states fundamentals and outlines the use of environmental indicators in resource planning and environmental impact assessments.
2. Part II addresses the fundamentals of predicting waste properties. Three reviews on the fundamentals of sulfide oxidation and acid rock drainage (ARD), existing best practices to forecast the likelihood of ARD from wastes and the

technologies available to understand the siting of environmentally significant elements are followed by discussions on novel and improved methods to predict waste behaviour. This chapter also gives details on the various field and laboratory available to predict ARD. Presentations on case studies complete the chapter.

3. Part III describes the methodologies to predict water quality. It provides a review of existing pH testing procedures. A documentation of case studies concludes the chapter.
4. Part IV covers the characteristics of mineral dust and its prediction at mine sites. Mineral dust emission testing is reviewed before improved practices are presented. This chapter also provides case studies.
5. Part V summarizes the techniques to forecast metal transfer processes into plants and impacts on land quality. This chapter explains methodologies applied for the testing of metal bioaccessibility and outlines a new approach for such testing. Documentation of a case study is also given.

Aachen, Germany Bernd Lottermoser

## References

Dowd PJ (2005) The business case for the prevention of acid drainage. In: Proceedings of the 5th Australian Workshop on Acid and Metalliferous Drainage, ACMER, Brisbane, Australia

Hammond A, Adriaanse A, Rodenburg E, Bryant D, Woodward R (1995) Environmental indicators: a systematic approach to measuring and reporting on environmental policy performance in the context of sustainable development. World Resources Institute, Washington

# Acknowledgments

This book arises from a 5-year research project completed under the auspices of the Australian Government's Cooperative Research Centre for Optimising Resource Extraction (CRC ORE). The project focused on reviewing, designing and validating accurate tests that yield predictive information on the characteristics of mineral resources, which may potentially impact on the environmental performance of mining operations. In particular, the team's research activities focused on the prediction of waste, water, air and land quality at metal mine sites.

The editor and authors would like to acknowledge the support of CRC ORE, established and supported by the Australian Government's Cooperative Research Centres Programme. Prof. R. Large, Prof. B. Gemmell and Prof. J. McPhie (Australian Research Council Centre of Excellence in Ore Deposits, CODES, University of Tasmania) gave much appreciated guidance and support for the project to succeed. Thanks are expressed to present and former CRC ORE staff, in particular Dr. S. Walters (research director) for initiating the indicators' research project and to Mr. J. Loraine (chairman of CRC Board), Dr. G. Oldroyd (chairman of Technical Advisory Panel), Mr. A. Bye (CEO), Dr. M. Neville (business manager), Ms. L. Stafford (business manager), and Ms. R. Swanborough (strategy and governance officer) for their support. Dr. K. Goemann, Dr. T. Rodemann, Dr. S. Feig and Dr. A. Townsend (Central Science Laboratory, University of Tasmania) as well as Prof. L. Danyushevsky, Dr. S. Meffre, Dr. P. Olin, Mr. J. Aalders and Ms. S. Gilbert (School of Physical Sciences, University of Tasmania) and Mr. S. McKnight (Federation University Australia) are thanked for helping with the analytical work. Technical, financial and managerial support was provided by Ms. J. Pongratz, Mr. P. Cornish, Ms. K. Mollross and Ms. H. Scott (University of Tasmania). Several individuals and organizations supported work presented in individual chapters (Chapter "Predicting Waste Properties Using the Geochemistry-Mineralogy-Texture-Geometallurgy Approach" Dr. M. Edraki, Centre for Mined Land Rehabilitation, University of Queensland; Prof. D. Bradshaw, Julius

Kruttschnitt Mineral Research Centre, University of Queensland. Chapter "Predictive Waste Classification Using Field-Based and Environmental Geometallurgy Indicators, Mount Lyell, Tasmania" Copper Mines of Tasmania, Mr. L. Brown, Mr. G. Cordery, Mineral Resources Tasmania, Mr. P. Harding, Dr. D. Green).

# Contents

# About the Editor

**Bernd Lottermoser** is a professor in Sustainable Resource Extraction and Director of the Institute of Mineral Resources Engineering at RWTH Aachen University, Germany. In his varied career, he has worked in the mining industry and also in research and academic instruction in Australian, British and German universities. He has authored and coauthored over 200 scientific publications and reports in numerous earth science fields.

# Part I
# Introduction

# Predictive Environmental Indicators in Metal Mining

**Bernd Lottermoser**

**Abstract** Predictive environmental indicators in mining can be defined as '*values derived from parameters that provide quantitative information against which some aspects of environmental risks associated with mineral resource development can be measured*'. At mine sites, such indicators provide information on conditions and processes that may develop during the mine life cycle and after mine closure. They are measures to forecast changes in the quality of the air, water, land and ecological systems. Predicting environmental risks is typically not an attribute that is strongly embedded into the development of mineral resources. However, a more predictive and proactive approach to early environmental characterization and risk assessment should be used early in the life-of-mine stages, because such an approach supports more effective mineral processing, better storage of waste, improved mine closure outcomes and ultimately reduced financial risks and liabilities to operators and regulators.

## What Are Environmental Indicators?

The term 'indicator' originates from the Latin verb 'indicare', translated 'to point out', 'to reveal', 'to show', or 'to give a hint'. Indicators provide details on progress towards goals (Hammond et al. 1995), and environmental indicators in mining communicate advancements towards environmental goals such as the prevention of acid and metalliferous drainage. As generally assumed, an indicator represents information on a matter of greater significance than the actual measurements and data acquired. Thus, an environmental indicator's importance reaches beyond what is analyzed, to larger issues of interest to the mining operator or regulator.

Indicators also provide information in a more readily understood form than complex datasets or models. Indicators may be presented in a tabulated, statistical

B. Lottermoser (✉)
Institute of Mineral Resources Engineering, RWTH Aachen University, Wüllnerstrasse 2, 52062 Aachen, Germany
e-mail: lottermoser@mre.rwth-aachen.de



B. Lottermoser (ed.), *Environmental Indicators in Metal Mining*,
DOI 10.1007/978-3-319-42731-7_1

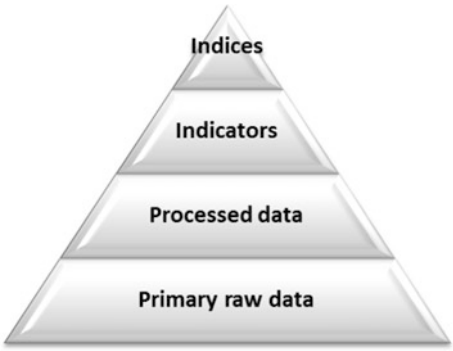


**Fig. 1** The information pyramid, whose base is primary data derived from measurements

or graphical format, yet they are distinct from the raw or processed analytical data. In fact, indicators and their aggregated forms of indices are at the top of the information pyramid and are grounded on analytical data (Fig. 1).

Communication is the main function of indicators: they should enable or promote information exchange regarding the issue they address. Predictive environmental indicators in mining are to improve communication of potential environmental risks and impacts due to mining and mineral processing. Communication demands simplicity and hence, indicators should simplify a complex reality. Such tools need to quantify information so its significance is more apparent, and they have to simplify information about complex phenomena to improve communication.

In a mining context, environmental indicators need to be SMART (i.e. *Sophisticated, Measurable, Accessible, Rapid, Thorough*), having the following characteristics: (1) *Sophisticated*. Indicators must be well grounded in scientific analyses, and the many components need to be aggregated for a targeted purpose. (2) *Measurable*. Indicators must be based on existing or improved best practices and use field and laboratory instruments to yield quantitative data. (3) *Accessible*. Instrumentation needed for data acquisition have to be readily available. (4) *Rapid*. Experience in the mining industry demonstrates that successful indicators need to be rapid and cost-effective in an industrial setting. (5) *Thorough.* Indicators must have been validated for a range of materials and mine settings.

Since the focus of this book is on environmental issues associated with metal mining and particularly the prediction of environmental consequences early in the life-of-mine phases, such indicators need to be defined more precisely. Predictive environmental indicators in mining are defined herein as parameters, or values derived from parameters, that provide quantitative information against which some aspects of environmental risks associated with metal resource development can be measured. In general, a much improved understanding of environmental risks and liabilities is a prerequisite for any sustainable development and management of mine sites.

## Why Predictive Environmental Indicators?

Mining invariably causes a number of environmental effects on air, water, soil and sediment quality, with each mine site having its own unique and specific challenges. In modern mining operations, steps can be taken to minimize impacts on all aspects of the environment before, during and after operation. By carefully pre-planning projects, formulating mine plans, designing waste management procedures, implementing pollution control measures, monitoring the effects of mining, and rehabilitating mined areas, industry can minimize the impact of its activities on the immediate environment.

In fact at operating modern mines, massive volumes of environmental data and statistics are acquired by mining companies on a daily, weekly, monthly, quarterly and yearly basis. Detailed and ongoing analyses of rocks, dust, air, soil, sediment and biota provide temporal resolutions of environmental conditions. Knowing how to interpret and analyse the data is an important skill as environmental data can have far-reaching impacts on the operations of companies. Yet, few professionals wade through all of these massive volumes of data, because the focus should be on broad trends and not on isolated data points as data can change rapidly.

Today, there is a wide variety of approaches, practices and environmental indicators in use for the monitoring and prediction of environmental risks at mine sites. However, it is becoming more and more difficult for students, practitioners and industry professionals to grab the relevance and meaning of these existing environmental indicators, given the amount of data generated and the number and diversity of indicators presently in use.

While operating mines generate vast quantities of environmental data, at exploration and feasibility project sites limited or even no environmental data and statistics are available. Also traditionally, the importance of understanding the environmental risks of mining early in the life-of-mine phases is typically not an attribute that is firmly embedded into the development of mineral resources and pursued with the same rigour. Resource evaluation and testing for beneficiation, mineral processing and recovery attributes of ores take priority. Such a discrepancy is largely due to the outdated and irresponsible perception that mineral processing and metallurgical testing generate immediate project value for the operator and shareholders, whereas environmental testing is only costly or could even stall mineral resource development. In many mineral resource developments, much focus is on the grade and tonnage of ores. Media releases by exploration companies to stock exchanges report in their discoveries of ores on the concentrations of discovered metals over a particular drill core interval. The release of pieces of geological data will still make institutions and individuals gauge the worth of mining companies. Such geological indicators are perceived as measurements for evaluating the value of exploration and mining projects and their companies. In the past, this obsession with grades and tonnages of ore deposits and the one-sighted focus on beneficiation, mineral processing and recovery without considering the

social licence to operate, environmental risks and real closure costs has likely contributed to the extraordinary closure liabilities of some mines today.

Medium-size open pit and underground mines operating in the past 10–15 years cost US$5-15 million to close, while closure of open pit mines operating for over 35 years, with large waste and tailings facilities, can cost upwards of $50 million (World Bank 2002). The occurrence of acid rock drainage (ARD) adds significant costs in terms of waste rehabilitation and water treatment (Fig. 2). Likely costs for ARD mitigation in Australia, Canada, Sweden and the USA, for example, are $US 300 million, $US 1.9–5.3 billion, $US 900 million and $US 32–72 billion, respectively (Tremblay and Hogan 2001). South Africa alone needs to spend as much as $US 1 billion to make ARD water leaking from abandoned mine shafts drinkable (Bloomberg 2014). The estimated costs for total worldwide liability associated the current and future remediation of ARD are approximately US$ 100 billion (Tremblay and Hogan 2001). Hence, planning and acting early on can save tens of millions of dollars in rehabilitation cost upon closure.

Today, government regulators will only permit mining if robust environmental impact statements as well as mine and waste management plans have been developed that consider environmental risks. This is not just a government requirement, with many financiers and stakeholders adopting guidelines to minimising environmental risks as published by the International Finance Corporation

**Fig. 2** ARD waters in the Rio Tinto, Spain. Sulfide oxidation and resultant ARD due to mining have a long history dating back thousands of years (color figure online)

(IFC 2007) or the Equator Principles III (2016). Today, financial institutions, government regulators, and industry best practices demand the use and application of predictive environmental tests and analyses that support environmental risk management and responsible decision-making. Consequently, most jurisdictions require an Environmental Impact Assessment (EIA) or a Social and Environmental Impact Assessment (SEIA) before allowing a mining project to proceed. Such assessments are formal processes that are also used to predict the environmental consequences (positive or negative) of a mining project prior to the decision to move forward with the proposed action. In preparing such assessments, operators identify the actions they intend to implement to limit environmental impacts. Acceptance of the proposed actions is subject to the approval of governmental regulatory agencies. These agencies monitor the activities when the facilities are in operation and upon closure.

A key element of environmental impact assessments includes analyses of ores and wastes for their environmental risks. Over the last few decades, scientists have made some phenomenal advances in their ability to analyse ores and wastes for their properties and observe, quantify and predict environmental impacts at mine sites. For example, the scientific literature is replete with studies on sulfide oxidation, as well as the chemical reactions and processes leading to ARD development.

Despite these scientific advances, mine closure liabilities and particularly the development of ARD waters continue to occur. The reason for this discrepancy appears to be multi-fold (Lottermoser 2012):

1. Environmental management of mineral resources is still a reactive activity, focussing on compliance and monitoring of waste, water, air, soil and sediment quality. This is despite the fact that best practice should pursue predictive test works early in the life cycle of a mine, at the exploration and pre-feasibility stages of mineral resource development.
2. Risk assessments rely on too few predictive tests or none at all, with the inherent variability of rock types hardly considered.
3. Current tests focus on geochemical properties of ores and wastes despite the fact that we mine minerals and not elements!
4. To date, tests for ARD predictionhave been accurate in some cases and misleading in others. The reason for this failure appears to be partly because the existing static tests have inherent limitations (White et al. 1999).
5. Waste classifications rely on simplistic static tests to categorise reject materials as potentially acid forming (PAF), non-acid forming (NAF) and uncertain (UC) wastes. This is despite the fact that such basic tests do not consider other waste types that could produce saline, alkaline or metalliferous neutral mine drainage waters.
6. Notable uncertainty exists in the long-term predictions on water quality. Evaluation of environmental impact statements from 25 mines in the United States showed that 15 of 25 mines (60 %) exceeded surface water quality standards for metals and pH after permitting (Jennings et al. 2008).

7. Tailings and waste rock repositories are not built in accordance with waste repository designs and mine closure plans. Specifically, the capping of waste repositories, the characterization of capping materials and the placement of wastes into repositories need much more attention by contractors and operators (Fig. 3).
8. Rehabilitated mined land and their waste repositories represent poorly understood, young landforms that have not equilibrated with the surrounding landscape, i.e. in terms of weathering and leaching rates.
9. There is little knowledge on how native vegetation interacts with the covers of waste repositories and allows access of oxygen and water to capped wastes at depth.

Regardless, environmental impact assessments and environmental protection are essential parts of a modern mining operation. These aspects become increasingly important as waste production in the mining industry is significant in volume and diverse in composition when compared to other industries (Lottermoser 2010). A key element of these environmental impact assessments includes analyses of ores and wastes for their physical and chemical properties and deduction of likely environmental risks, using environmental indicators.

**Fig. 3** Aerial photograph of a rehabilitated waste rock dump at a gold mine, northern Australia. An exposed, barren sulfide-rich layer is visible on an outer dump batter. A flawed repository design, inadequate waste characterization and poorly supervised waste management practices led to the exposure of potentially acid-forming (PAF) materials, ineffective encapsulation of PAF materials, physical instability of waste rock batters, erosion, vegetation dieback and impacts on ground and surface waters (color figure online)

## The Driving Forces-Pressures-States-Impacts-Responses (DPSIR) Framework and Environmental Indicators

Environmental indicators have been developed for a range of applications, including environmental monitoring, reporting and prediction. In general, environmental indicators are to track changes to the quality and condition of the air, water, land and ecological systems—and their resident biota—on various geographic and temporal scales. At mine sites, such indicators provide information on conditions and processes that exist or may develop during the life-of-mine phases from the exploration to the closure stage.

Predictive environmental indicators should be an integral part of life-of-mine plans, providing information on the physical, chemical and biological environment including waste behaviour, effluent discharges, soil quality, erosion rates and ecosystem success, and increasingly a risk-based estimation of climate change effects on ARD generation and mine site runoff water quality (Nordstrom 2009; Rayne et al. 2009). For example, variable precipitation and seasonal run-off will disrupt water supplies, affect water quality and increase the risk of uncontrolled ARD discharge. Environmental indicators form the basis for long-term site predictions, which in turn allow appropriate life-of-mine costing, the development of closure strategies, scenarios and plans, and the identification of additional research needs and remediation efforts.

Presently, most environmental impact assessments and environmental reports generated for mine developments compile sets of physical, chemical or biological data and relevant indicators. Such reports reflect a systems analysis review of the relations between mining activities and the environment. In order to understand the meaning and importance of environmental indicators, a clear framework is needed that relates the interactions between mine development activities and impacts on the environment.

The DPSIR (Driving Forces, Pressures, States, Impacts, Responses) framework is commonly used to relate human activities to the state of the environment. Within a DPSIR analysis, indicators are assigned to the individual components of the framework to provide clear and specific information on (i) driving forces, (ii) resultant environmental pressures, (iii) the state of the environment, (iv) impacts resulting from changes in environmental quality, and (v) responses to these changes in the environment (Table 1). The DPSIR framework also represents a basis for structuring interconnections during mineral resource development and assessing of how future mining can be sustainably implemented (e.g. Hansen et al. 2013).

Indicators for driving forces describe the activities in societies and reasons for mine developments. Examples of driving forces indicators in mining are economic benefits and independency, resource demand and consumption, employment, or social status. These primary driving forces exert pressure on the environment.

**Table 1** The causal DPSIR (driving forces, pressures, states, impacts, responses) framework for describing the interactions between mineral resource development and the environment

| | Driving forces indicators | Pressure indicators | State indicators | Impact indicators | Response indicators |
|---|---|---|---|---|---|
| Environmental indicators in mining | • Economic benefits<br>• Economic independency<br>• Resource demand and consumption<br>• Employment<br>• Social status | • Tailings or waste rocks produced<br>• Mineral dust released to the atmosphere<br>• Mine water released to the environment<br>• Carbon dioxide emissions<br>• Acid producing potential of wastes | • Concentration of metals in soils, sediments or surface waters<br>• Chemistry of mineral dust settling around the site<br>• Average noise level in the periphery of plant facilities | • Accumulation of metals in plants and animals<br>• Real-time biomonitors (mussels)<br>• Microbial indicators (algae, diatoms, bacteria)<br>• Destruction of wildlife habitat<br>• Biodiversity of aquatic macro-invertebrates<br>• Impacts on human health<br>• Susceptibility of soils to erosion | • Water and waste treatment<br>• Dust suppression<br>• Soil surface condition<br>• Landform stability<br>• Changes in soil nutrients with time<br>• Biomass and microbial mass accumulation<br>• Green cover of mine lease<br>• Vegetation and habitat complexity and dynamics<br>• Percent utilization of total solid wastes<br>• Polluter-pays principle<br>• Emission limitations |
| Life-of-mine stages | • Prospecting, exploration and discovery | • Mine operation<br>• Development and construction | | | • Closure and rehabilitation |
| Life-of-mine activities | • Conceptual planning<br>• Surveys<br>• Target appraisal | • Assessment drilling<br>• Test mining<br>• Mineral processing and metallurgical studies<br>• Mine development | • Ore extraction<br>• Ore processing<br>• Waste production | | • Removal of equipment<br>• Dismantling of facilities<br>• Closure of mine workings<br>• Closure of waste repositories<br>• Revegetation |

Some examples of environmental indicators within the framework and related stages of mineral resource development are given

Pressure indicators describe the release of chemical, physical or biological agents, the use of resources, or the use of land. Pressure indicators, for example, are the amount of tailings or waste rocks produced, or details on the mineral dust released to the atmosphere.

State indicators give a description of the quantity and quality of physical, biological and chemical parameters for a particular area and environmental medium. For example, state indicators describe the concentration of metals in soils, sediments or surface waters, or the chemistry of mineral dust released to the atmosphere.

Due to pressure on the environment, the state of the environment changes. These changes then have impacts on the health and biodiversity of the environment. Impact indicators, for instance, are the number and abundance of aquatic species colonising mining-influenced streams, or the accumulation of metals in colonising plants.

Response indicators refer to responses by the operator or regulator to prevent, remediate, improve or adjust to changes in the state of the environment. Examples of response indicators are water and waste treatment activities, or the amount of revegetated or reclaimed mined land.

For the evaluation of mining activities, the DPSIR framework has a disproportional number of environmental indicators that are response indicators applicable at the end of life-of-mine (Table 1). This relatively large number of response indicators reflects the extensive ecological activities completed at the closure and rehabilitation stage and the significant research efforts conducted on these issues. By contrast, there is a distinctly different and lesser number of established indicators available for the prospecting, exploration, discovery, mine development and construction phases (Table 1). This book attempts to cover the description of physical and chemical parameters of rocks that could impact on the environment during mineral resource development. Consequently, indicators documented in this text represent ‘pressure indicators’ or ‘state indicators’ within the DPSIR framework.

## Conclusions

Prediction of environmental risks is an important aspect of mine development. Predictive environmental indicator tests and methodologies yield prognostic information on the characteristics of metal resources, which may potentially impact on the environmental performance of mining operations. Best practice mine development should be based on the early use of environmental indicators, most appropriately from the exploration stage onwards. In turn, the use of predictive environmental indicators early in the life-of-mine cycle supports more effective mineral processing, better storage of waste, improved mine closure outcomes and ultimately reduced financial risks and liabilities to operators and regulators.

## References

Bloomberg (2014) http://www.bloomberg.com/news/2014-04-10/south-africa-needs-1-billion-to-make-toxic-mine-water-potable.html

Equator Principles III (2016) www.equator-principles.com

Hammond A, Adriaanse A, Rodenburg E, Bryant D, Woodward R (1995) Environmental indicators: a systematic approach to measuring and reporting on environmental policy performance in the context of sustainable development. World Resources Institute, Washington

Hansen SH, Pedersen LC, Vilsgaard KD, Nielsen IE, Hanse SF (2013) Environmental and ethical aspects of sustainable mining in Greenland. J Earth Sci Eng 3:213–224

International Financial Corporation (IFC) (2007) Environmental, health, and safety guidelines for construction materials extraction. International Finance Corporation, Washington 13 pp

Jennings SR, Neuman DR, Blicker PS (2008) Acid mine drainage and effects on fish health and ecology: a review. Reclamation Research Group, Bozeman 29 pp

Lottermoser BG (2010) Mine wastes: characterization, treatment and environmental impacts, 3rd edn. Springer, Berlin 400 pp

Lottermoser BG (2012) Environmental indicators for acid mine drainage: advances in knowledge and challenges ahead. In: Fourie AB, Tibett M (eds) Mine closure 2012. Australian Centre for Geomechanics, Nedlands, pp 3–12

Nordstrom DK (2009) Acid rock drainage and climate change. J Geochem Explor 100:97–104

Rayne S, Forest K, Friesen KJ (2009) Analytical framework for a risk-based estimation of climate change effects on mine site runoff water quality. Mine Water Environ 28:124–135

Tremblay GA, Hogan CM (2001) Mine Environment Neutral Drainage (MEND) manual 5.4.2d: prevention and control. Canada Centre for Mineral and Energy Technology, Natural Resources Canada, Ottawa

White WW, Lapakko KA, Cox RL (1999) Static test methods most commonly used to predict acid mine drainage: practical guidelines for use and interpretation. In: Plumlee GS, Logsdon MJ (eds) The environmental geochemistry of mineral deposits. Part A: processes, techniques, and health issues. Rev Econ Geol 6A:325–338

World Bank (2002) It's not over when it's over: mine closure around the world. World Bank, Washington

# Part II
# Waste Quality

# Principles of Sulfide Oxidation and Acid Rock Drainage

**Anita Parbhakar-Fox and Bernd Lottermoser**

**Abstract** Oxidation of sulfide minerals releases sulfuric acid and dissolved metals, with iron sulfides pyrite ($FeS_2$) and pyrrhotite ($Fe_{(1-x)}S$) recognized as the most common acid-forming minerals. Several factors control the oxidation rate including: the oxidant type, sulfide morphology, microbial action, and trace element contents. Whilst metal sulfides such as galena and sphalerite are less acid-forming, they are typically sources of environmentally significant elements such as Cd, Pb and Zn. Common sulfide oxidation reaction products are metal-sulfate efflorescent salts. Dissolution of these minerals is critical to the storage and transport of acids and metals released upon weathering of mineralized rock or mine wastes. Acid formed by sulfide oxidation can be consumed through reaction with gangue minerals. Neutralization is primarily offered by dissolution of carbonate minerals with calcite and dolomite the most effective. Factors affecting carbonate reactivity include: grain size, texture and the presence of trace elements which can influence a mineral's resistance to weathering. Silicate minerals such as olivine, wollastonite and serpentinite are recognized as effective longer term neutralizers. Lesser neutralizing potential contributions from phyllosilicates, pyroxenes, amphiboles and feldspars have been reported. Micas, clays and organic matter can temporarily adsorb $H^+$ ions through cation exchange reactions, with gibbsite and ferric hydroxide recognized as offering neutralizing capacity under acidic conditions. Ultimately, the balance of acid producing and acid consuming chemical reactions will determine the production of acid rock drainage (ARD).

A. Parbhakar-Fox (✉)
School of Physical Sciences, University of Tasmania, Private Bag 79, Hobart, TAS 7001, Australia
e-mail: Anita.Parbhakar-Fox@utas.edu.au

B. Lottermoser
Institute of Mineral Resources Engineering, RWTH Aachen University, Wüllnerstrasse 2, 52062 Aachen, Germany
e-mail: lottermoser@mre.rwth-aachen.de



B. Lottermoser (ed.), *Environmental Indicators in Metal Mining*,
DOI 10.1007/978-3-319-42731-7_2

## Introduction

Oxidation of sulfidic mine wastes, and the consequent release of acid drainage is one of the main environmental issues facing the mining industry (Hudson-Edwards et al. 2011). The oxidation of sulfides in rock is a natural process which typically occurs slowly as the Earth's surface erodes and underlying rock oxidizes (Lottermoser 2010). However, mining operations can greatly accelerate the oxidation process through various activities (e.g., grinding of sulfidic ore, excavation of sulfidic rock), providing paths for water and oxygen that allow the accelerated release of pollutants into surface and groundwater at rates far greater than the downstream environment can sustain without significant ecological effects (Lottermoser 2010). Sulfide oxidation is controlled by several intrinsic parameters including trace element chemistry, morphology, electrochemical factors and galvanic effects (Parbhakar-Fox and Lottermoser 2015). The complex interplay of these factors coupled with microbiological catalytic effects can result in the production of acid. Each individual parameter has been well studied, but the net effect and complex interplay of these is comparatively less understood. Such acid produced by sulfide oxidation can subsequently be neutralized in the presence of specific minerals including carbonates and select silicates (Lottermoser 2010). The overall process of acid drainage (also referred to as acid mine drainage—AMD, or acid rock drainage—ARD) is the chemical response to acid-producing and acid-consuming weathering reactions (Lottermoser 2010). The individual parameters significantly governing sulfide oxidation are described in this chapter for the most common sulfides in mine waste materials. In addition, the acid neutralizing reactions which can take place in the presence of carbonate and select silicate minerals are also described.

## Pyrite

Pyrite is the most abundant and widespread sulfide mineral in the Earth's crust (Craig et al. 1998; Dold 2005). Upon oxidation, sulfuric acid is produced which can potentially cause liberation of Fe, Mn and Al as well as heavy metals including Cd, Pb and Zn. Discharge to streams, rivers and lakes can adversely impact downstream aquatic ecosystems posing an environmental threat (Evangelou and Zhang 1995). The mechanisms controlling pyrite oxidation are the subject of much research as they involve a complex set of reactions (Egiebor and Oni 2007). Rimstidt and Vaughan (2003) identified that oxidation of pyrite (and marcasite) requires up to seven elementary steps. This is complicated further by the fact that pyrite is a semiconductor, and the reactions are electrochemical in nature. In addition to this, the semiconducting properties of pyrite are critically dependant on the precise composition of the particular pyrite sample, or even the zone or region of a

particular sample undergoing oxidation (Rimstidt and Vaughan 2003). In general, pyrite oxidation may be considered to take place in three major steps (Dold 2005):

- Oxidation of sulfur (Eq. 1);
- Oxidation of ferrous ($Fe^{2+}$) iron (Eqs. 2, 3); and
- Hydrolysis and precipitation of ferric complexes and minerals (Eqs. 4, 5).

$$FeS_{2(s)} + 7/2O_{2(g)} + H_2O_{(l)} \rightarrow Fe^{2+}{}_{(aq)} + 2SO_4{}^{2-}{}_{(aq)} + 2H^{+}{}_{(aq)} \quad (1)$$

$$Fe^{2+}{}_{(aq)} + 1/4O_{2(g)} + H^{+}{}_{(aq)} \rightarrow Fe^{3+}{}_{(aq)} + 1/2H_2O_{(l)} \quad (2)$$

$$FeS_{2(s)} + 14Fe^{3+}{}_{(aq)} + 8H_2O_{(l)} \rightarrow 15Fe^{2+}{}_{(aq)} + 2SO_4{}^{2-}{}_{(aq)} + 16H^{+}{}_{(aq)} \quad (3)$$

$$Fe^{3+}{}_{(aq)} + 3H_2O_{(l)} \leftrightarrow Fe(OH)_{3(s)} + 3H^{+}{}_{(aq)} \quad (4)$$

$$Fe^{3+}{}_{(aq)} + 2H_2O_{(l)} \leftrightarrow FeOOH_{(s)} + 3H^{+}{}_{(aq)} \quad (5)$$

The initial step of pyrite oxidation in the presence of atmospheric oxygen is described in Eq. 1. This is a pH controlled reaction, with oxidation initiated around pH 6 (Evangelou and Zhang 1995). Oxygen directly reacts with pyrite and forms $Fe^{2+}$. This is subsequently oxidised to $Fe^{3+}$ (Eq. 2). Ferric iron has a low solubility around neutral pH but as oxidation proceeds with oxygen, the pH decreases until Eq. 3 is triggered at around pH 4.5. This reaction is catalysed by microbial action (Dold 2005). As the concentration of dissolved $Fe^{3+}$ decreases with increasing pH, $Fe^{3+}$ solubility is limited by the precipitation of ferric hydroxides ($Fe(OH)_3$) and oxyhydroxides (FeOOH). Therefore, if pH increases to >3, the reactions shown in Eqs. 4 and 5 will occur (Lottermoser 2010). These cause the formation of reddish-yellow to yellowish-brown gelatinous flocculants, stains, coatings, slimy sludge, and precipitates in ARD affected streams and seepage areas. The ferric iron resulting from the oxidation of ferrous iron (Eq. 2) is recognized as a more potent oxidant than $O_2$, even at circumneutral pH (Moses and Herman 1991; Moses et al. 1987; Hustwit et al. 1992).

As inferred by these reactions, pyrite oxidation can be either direct (i.e., by oxygen) or indirect (i.e. by oxygen or iron), and can also be biotic (in the presence of microorganisms) or abiotic (Lottermoser 2010). Under abiotic conditions, the rate of pyrite oxidation by ferric iron is controlled by the rate of oxidation of ferrous iron (Dold 2005). Below pH 3, oxidation of pyrite by ferric iron is about ten to a hundred times faster than by oxygen (Dold 2005). Pyrite oxidation will continue indefinitely unless $Fe^{3+}$, $O_2$ or pyrite is removed or if the pH is significantly raised. To simplify this Lottermoser (2010) presented the 'ARD engine' which is summarized in Eq. 6.

$$FeS_{2(s)} + 15/4O_{2(aq)} + 7/2\ H_2O_{(l)} \rightarrow Fe(OH)_{3(s)} + 2H_2SO_{4\ (aq)} + \text{energy} \quad (6)$$

Whilst these reactions are mass and charge balanced, there is no molecular mechanistic or rate reaction meaning (Evangelou and Zhang 1995). Furthermore,

Eqs. 1–6 are gross oversimplifications, with the precise step-wise intermediate reaction mechanisms not detailed (Lottermoser 2010). Thus, these reactions represent approximations only. Several of the main factors influencing pyrite oxidation are discussed in the next sections.

## *Microbial Action*

ARD environments contain diverse microbial communities influenced by temperature, ionic strength and pH. A diverse mixture of organisms have been identified from these communities and are listed in Bond et al. (2000) and Baker and Banfield (2003). Bacteria, Archaea and Eukarya are just a few types which have been identified (Baker and Banfield 2003; Lottermoser 2010). Each specific community is restricted to just a few species due to the limited number of energy deriving reactions available (Baker and Banfield 2003).

Bacteria are the most studied microbes in ARD environments, particularly because of their application in bioleaching as a mineral processing technique (Lara et al. 2010; Chandra and Gerson 2010; Florian et al. 2010). There are four main groups of acid forming bacteria: proteobacteria, nitrospira, firmicutes and acidobacteria. Most research focuses on proteobacteria, with three mesoacidiphilic chemolithotrophic species studied in depth (Evangelou and Zhang 1995; Schippers and Sand 1999):

- *Acidithiobacillus ferrooxidans* (formerly *T. ferrooxidans*), which is able to oxidize $Fe^{2+}$, $S^0$ and metal sulfides as well as other reduced inorganic sulfur compounds;
- *Acidithiobaccillus thiooxidans (*formerly *T. thiooxidans)* can oxidize both elemental sulfur and sulfides to sulfuric acid but not $Fe^{2+}$; and
- *Leptospirillum ferrooxidans,* which oxidizes $Fe^{2+}$ ions only.

Singer and Stumm (1970) stated that microbial mediation accelerates the rate of pyrite oxidation by a factor $>10^6$. However, Morin (2010) regard this as an overestimation, giving evidence from Morth et al. (1972) and Leathen et al. (1953a, b), who reported oxidation to proceed 10–50 times and 2–5 times faster, respectively. Additionally, Olson (1991) calculated that *Acidithiobacillus ferrooxidans* increased pyrite dissolution rates by only $\sim$34 times. More recent examples given in Morin (2010) conclude similar rates over a pH range of 1–8. In reality, the estimate presented in Singer and Stumm (1970) is likely an appropriate general approximation, encompassing the cumulative contribution from all ARD microbes present in a given community.

The mechanisms by which sulfide-microbe interactions occur in the context of ARD formation have been discussed in Nordstrom and Southam (1997), Edwards et al. (1998), Baker and Banfield (2003), and Mielke et al. (2003). More recently, these interactions have been studied in order to improve bioleaching processes (e.g.,

Rohwerder et al. 2003; Lara et al. 2010; Chandra and Gerson 2010; Florian et al. 2010; Tao and Dongwei 2014; Lee et al. 2015; Bryan et al. 2015). It is widely accepted that *Acidithiobacillus ferrooxidans* and *Leptospirillum ferrooxidans* are capable of oxidizing sulfide minerals either directly or indirectly. Edwards et al. (1999) and Mielke et al. (2003) give evidence of direct attachment with cell-sized pits observed on pyrite surfaces. Microorganisms attach to sites of high surface energy, such as scratches, pits, grooves, and steps (Edwards et al. 1998), indicating that these observed pits have preferentially developed on such sites. Here, acidic nano-environments are formed. Indirect reactions involve the production of ferric ions in the solution, which then leach the mineral (Sand et al. 1995; Crundwell 1996). Biofilms are aggregates of microorganisms in which cells adhere to each other and/or to a surface (Tyson et al. 2004; Crundwell 1996, 2003; Sand and Gehrke 2006). The impact of biofilms on sulfide oxidation is an active area of research (Baker-Austin et al. 2010; Ma and Banfield 2011).

## *Pyrite Morphology*

Pyrite oxidation is a surface controlled reaction; therefore morphology is a significant control (Smith and Beckie 2003; Weber et al. 2004; Weisener and Weber 2010). Cubic pyrite is generally less reactive than framboidal forms. Evidence is given in Weber et al. (2004) who compared the behaviour of framboidal and euhedral pyrite taken from an Indonesian Coal Mine (KPC mine, Kalimantan). Samples were subjected to geochemical tests (e.g. acid base accounting, column leaching) and also mineralogical analysis (including X-ray diffractometry, X-ray fluorescence, electron probe microanalysis, and scanning electron microscopy). Results from this study confirmed the most reactive pyrite morphology as framboidal.

Marcasite, the orthorhombic polymorph of (isometric) pyrite is structurally less stable, and is therefore presumed to be the more reactive form of iron disulfide. However, Wiersma and Rimstidt (1984) showed the differences between pyrite and marcasite oxidation rates as less than an order of magnitude, and the differences were in fact within the uncertainty range of the rate measurements. Rimstidt and Vaughan (2003) recognized that there is a very small difference between the chemical potential driving the oxidation of both minerals, thus the differences observed are likely due to variations in the specific surface area of the samples observed.

## *Electrochemical Behaviour and Conductivity*

Whilst the general reactions for pyrite oxidation were previously given, pyrite oxidation is far more complex than these suggest. This is because pyrite is a semi-conducting mineral, and its oxidation is an electrochemical process as

described in Evangelou and Zhang (1995), Rimstidt and Vaughan (2003), Egiebor and Oni (2007), Savage et al. (2008) and Chandra and Gerson (2010). Electrochemical oxidation consists of three steps which occur near-simultaneously in the actual oxidation process (Rimstidt and Vaughan 2003):

- Cathodic reaction,
- Electron transport, and
- Anodic reaction.

The cathodic reaction transfers electrons from the surface of the pyrite to the aqueous oxidant species ($O_2$ or $Fe^{3+}$; Rimstidt and Vaughan 2003). The second step transfers charge from the site of an anodic reaction to replace the electron lost from the cathodic site (Rimstidt and Vaughan 2003). The semiconducting nature of pyrite permits this step to occur. The third step occurs at the anodic site where an oxygen atom of a water molecule interacts with a sulfur atom to create a sulfoxy species (Rimstidt and Vaughan 2003). This releases an electron into the solid, and one or two hydrogen ions to solution. The rate determining step is the cathodic reaction, with electrons transferred to the oxidant from metal sites in the mineral surface and not sulfur sites (Rimstidt and Vaughan 2003).

There are two types of pyrite conductivity: n-type and p-type. These have different Fe:S ratios and can be correlated to trace element content and geological environment of formation (Savage et al. 2008). N-type pyrite can be sulfur deficient (i.e. S:Fe < 2) and may be relatively rich in Co and Ni and formed in high temperature veins. P-type pyrite (S:Fe ratio of >2) is formed in sedimentary and lower temperature hydrothermal deposits with Cu typically absent. Conductivity can vary, but generally p-type pyrites have a lower conductivity than n-type with mean conductivities of 0.5 and 56 $(\Omega\ cm)^{-1}$ respectively (Rimstidt and Vaughan 2003). With regards to which pyrite type has greater potential to form acid, Biegler (1976) concluded that the conduction type of a mineral does not normally influence the oxidation and dissolution reactions. This implies there is no typical rule or relationship, instead the trace element content and its influence on the strength of the pyrite lattice is a more significant control.

## *Trace Element Content*

The trace element content of sulfides has a significant influence on their oxidation. Trace elements can be present in sulfides either as impurities within the crystal structure, or as inclusions. Presence of inclusions causes strain to the crystal structure, diminishing the sulfide's resistance to oxidation (Jambor 1994; Kwong 1995; Plumlee 1999). Trace elements in pyrite typically include Ag, As, Bi, Cd, Co, Hg, Mo, Ni, Pb, Pd, Pt, Ru, Sb, Se, Te, Tl and Zn (Lottermoser 2010). Arsenic has been shown by Plumlee (1999) and Blanchard et al. (2007) to destabilize the pyrite structure and increase the rate of weathering. The influence of other trace elements

is less established. However, Kwong (1993) noted from humidity cell tests that zones in pyrite rich in Cu tend to oxidize faster. Kwong (1993) also noted that Co and Ni increase resistance to oxidation. Kwong (1993) postulated that, when considering the semiconductor nature of pyrite, a positive charge effect arises when an element is substituted with one to its left on the Periodic Table (such as Co for Fe). This results in the suppression of the electron transfer necessary for pyrite oxidation to occur. Generally, there is a limited understanding on trace element effects on pyrite oxidation.

## *Galvanic Effects*

Sulfidic wastes are commonly polysulfidic; if there is direct physical contact between at least two different sulfide minerals, electrons move between the sulfides and a galvanic cell is formed (Kwong et al. 2003; Lottermoser 2010). The sulfide mineral with the highest electrode potential is galvanically protected from oxidation, whilst the mineral with the lowest electrode potential is weathered, leading to selective oxidation (Kwong et al. 2003; Lottermoser 2010). The more electroconductive sulfide mineral oxidises at a slower rate than it would when not in contact with another sulfide. Pyrite, galena and sphalerite are the most common sulfides, and pyrite has the highest electrode potential followed by galena and then sphalerite (Kwong et al. 2003; Lottermoser 2010). If these minerals are in contact, then sphalerite will be preferentially weathered and oxidation of pyrite is reduced. As ARD predictive tests typically require crushed material, galvanic effects on oxidation are not accounted for. Therefore, the rate of pyrite oxidation in a waste rock pile may not be accurately predicted, indicating a need for systematic evaluation of intact waste material to account for these effects.

## *Secondary Minerals*

Secondary precipitates commonly form within pyrite fractures (and possibly as grain rims) upon oxidation. These precipitates may be metal sulfate salts or hydrous ferric oxides (HFOs). On oxidation, these minerals, which have crystallized in fractures, wedge the crystals apart. The exposed surface area therefore increases and further oxidation occurs (Jambor et al. 2000). Variations in exposed surface area can be many orders of magnitude, potentially making this a more important control on oxidation rate than composition or crystal structure as they only cause variations of less than one order of magnitude (Jambor et al. 2000). The formation of secondary minerals is prevalent at mine sites located in seasonally wet-dry climates; consequently in these areas the formation of secondary minerals may influence the rate of sulfide oxidation.

### *Other Factors*

Several other factors influence pyrite oxidation and are explained here in brief. Pyrite oxidation is an exothermic reaction, with temperature controlling the growth of thermophilic bacteria (Lottermoser 2010). The heat produced upon oxidation is poorly dissipated in environments such as waste rock piles (due to the poor heat conductivity of gangue minerals), and the pyritic waste gets warmer (Lottermoser 2010). Overall, oxidation rate doubles with each 10 °C increase in temperature (Smith et al. 1992 *in* Lottermoser 2010).

Also, $O_2$ and $CO_2$ concentrations in the gas and water phases have an effect on oxidation. Generally, oxidation rates increase with higher $O_2$ concentrations. Oxidation of pyrite in oxygenated water is much slower than the oxidation of pyrite in the atmosphere. Changes in $O_2$ concentrations influence the occurrence of aerobic Fe- and S-oxidizing bacteria as they require $O_2$ for their survival (Lottermoser 2010). Above the water table, oxidation rates are catalysed by aerobic bacteria such as *Acidithiobacillus ferrooxidans*. Below the water table, where there are restricted concentrations of dissolved $O_2$, the catalytic effect of aerobic bacteria is not felt. This is applied as a remediation technique with open cuts and mine workings flooded. The absence of aerobic bacteria reduces pyrite oxidation to negligible rates (Lottermoser 2010). Sulfide-oxidizing anaerobic bacteria use $CO_2$ as their sole source of carbon in order to build up organic material for their maintenance and growth (Ledin and Pedersen 1996 *in* Lottermoser 2010). If carbonate material is present in a sulfidic waste rock pile, $CO_2$ will be produced as a result of its dissolution. Elevated concentrations of $CO_2$ in pore spaces have been reported to increase the rate of oxidation of pyrite as the heightened concentrations encourage growth of anaerobic bacteria (Ritchie 1994).

The formation of acidic nano-environments at pyrite surfaces was previously mentioned. The exact pH of these environments is unknown as they require measurements to be made on a sub-microscopic level. However, given the reaction pathways of pyrite oxidation, it is appreciable that, when the pH value falls below 3, the oxidation rate will increase. However, if the pH is above 3, $Fe^{3+}$ will precipitate, removing this oxidizing agent from solution thus slowing oxidation.

The abundance of water is significant as both an essential factor allowing oxidation to progress (Evangelou and Zhang 1995) and also as a reaction medium (Stumm and Morgan 1995). Alternate wetting and drying accelerate the oxidation process and remove oxidation products, leaving a fresh surface exposed for further oxidation (Lottermoser 2010).

## Pyrrhotite

Pyrrhotite ($Fe_{(1-x)}S$) is the name given to a range of nonstoichiometric compounds intermediate to the stoichiometric extremes of troilite (FeS) and pyrite. Pyrrhotite has some unique characteristics relative to the other sulfide minerals as it is a

metallic conductor (the others are semi-conductors) and can undergo both oxidative and non-oxidative dissolution (Becker 2009). The general formula for pyrrhotite is ($Fe_{(1-x)}S$), where X can vary from 0.125 ($Fe_7S_8$) to >0.0. Nicholson and Scharer (1994) give the general equation (Eq. 7) for pyrrhotite oxidation as:

$$Fe_{(1-x)}S_{(s)} + (2 - x/2)O_{2(g)} + xH_20_{(l)} \rightarrow (1 - x)Fe^{2+}{}_{(aq)} + SO_4{}^{2-}{}_{(aq)} + 2xH^{+}{}_{(aq)} \quad (7)$$

From this reaction, one mole of pyrrhotite generates only 0 to <0.25 mol of acid. However, this small amount of acidity is not in accordance with field observations, which indicate that the amount of acid formed is more similar to that of pyrite oxidation (Nicholson and Scharer 1994; Jambor 2003). Jambor (2003) demonstrated 1 mol of pyrrhotite can generate more $H^+$ ions than 1 mol of pyrite when $Fe^{3+}$ is the oxidant (Eq. 8):

$$Fe_7S_{8(s)} + 62Fe^{3+}{}_{(aq)} + 32H_2O\ {}_{(aq)} \rightarrow 69Fe^{2+}{}_{(aq)} + 8SO_4{}^{2-}{}_{(aq)} + 64H^{+}{}_{(aq)} \quad (8)$$

Oxidative dissolution is reported to be 103 times slower than non-oxidative dissolution. Therefore, reaction kinetics will be dominated by non-oxidative dissolution, even if only a small portion of the pyrrhotite surface is dissolving in this manner (Thomas et al. 2003). As regions of pyrrhotite undergo oxidative dissolution, they restructure into a pyrite-like structure, thus textural analysis of samples can indicate the stage of oxidation. Pyrrhotite oxidation can exceed that of pyrite by 20–100 times (Belzile et al. 2004). The more rapid oxidation of pyrrhotite is related principally to the deficiency of Fe in the crystal lattice; with the lattice having a lower stability and thus providing a more conducive environment for oxidation (Nicholson and Scharer 1994; Jambor 2003). Factors which affect pyrrhotite oxidation have been identified; however, the exact nature of their impact is less understood. These factors include crystal structure, pH, temperature, trace metal contents, and bacteria (Belzile et al. 2004; Becker 2009).

## Arsenopyrite

Arsenopyrite (FeAsS) is the most common As-bearing mineral (Corkhill and Vaughan 2009). Under oxidizing conditions, arsenopyrite oxidation releases high concentrations of dissolved As. Corkhill and Vaughan (2009) and Asta et al. (2010) examined in detail the factors and reaction mechanisms controlling arsenopyrite oxidation. As with pyrite, arsenopyrite oxidation is a three-step electrochemical process (Corkhill and Vaughan 2009) involving a mixture of surface and diffusion-controlled processes (Asta et al. 2010). In general, arsenopyrite oxidation can be expressed by the reactions given in Eqs. 9 and 10 (Corkhill and Vaughan 2009):

$$4FeAsS_{(s)} + 11O_{2(g)} + 6H_2O_{(l)} \rightarrow 4Fe^{2+}{}_{(aq)} + 4H_2SO_4{}^{2-}{}_{(aq)} + H_3AsO_3{}_{(aq)} \quad (9)$$

$$FeAsS_{(s)} + 11Fe^{3+}{}_{(aq)} + 7H_2O{}_{(aq)} \rightarrow 12Fe^{2+}{}_{I(aq)} + H_3AsO_3{}_{(aq)} + 11H^{+}{}_{(aq)} + SO_4{}^{2-}{}_{(aq)} \quad (10)$$

Several factors affect oxidation including oxygen and iron availability, microbial action, and pH as detailed in Corkhill and Vaughan (2009) and Asta et al. (2010). Yunmei et al. (2004) identified that oxidation increases exponentially with increasing $Fe^{3+}$ concentration and Asta et al. (2010) confirmed that oxidation is most strongly affected by oxygen concentration, and less by pH and temperature. Under acidic conditions a sulfur-enriched surface layer made up of polysulfides and sulfates and potentially elemental sulfur is developed (Asta et al. 2010). At mildly acidic to basic pH, Fe-phases are precipitated. Fe-coatings on mineral surfaces prevent diffusion of aqueous species through it, and the concentration of As released decreases with time (Asta et al. 2010).

*Acidithiobacillus ferrooxidans*, *Acidithiobacillus thiooxidans* and *Leptospirillum ferrooxidans* all accelerate arsenopyrite oxidation, with mixed cultures most effective, and used in bioleaching (Corkhill and Vaughan 2009). *Acidithiobacillus ferrooxidans* was added to ground arsenopyrite at pH 3.5 in an experiment undertaken by Ehrlich (1964; *in* Corkhill and Vaughan 2009). Twice as much As was brought into solution in its presence, with the pH dropping to 2.5. Other bacteria recognized to have an accelerative impact of arsenopyrite include *Acidithiobacillus caldus*, *Pseudomonas arsenitoxidans* and *Sulpholobus* (Corkhill and Vaughan 2009). Whilst *Leptospirillum ferrooxidans* is now recognized as the most prevalent bacteria in sulfidic mine wastes (Schrenk et al. 1998), few studies have been undertaken on its effects on arsenopyrite oxidation. Mechanisms of direct and indirect bacterial attachment (as discussed for pyrite) are also applicable for arsenopyrite (Corkhill and Vaughan 2009).

## Chalcopyrite

Factors influencing the oxidation of chalcopyrite ($CuFeS_2$) are not as well characterized as for the other Fe sulfides, even though high concentrations of Cu are potentially threatening to the overall health of aquatic organisms (cf. Li et al. 2010; Thurston et al. 2010). Acid production from chalcopyrite oxidation is a combination of $Fe^{2+}$ oxidation and $Fe^{3+}$ hydrolysis, with the general reaction given in Eq. 11. Anaerobic oxidation of chalcopyrite by $Fe^{3+}$ is given in Eq. 12 and also leads to a large drop in pH (Thurston et al. 2010).

$$CuFeS_{2(s)} + 34O_{2(g)} + 2H_2O_{(l)} \rightarrow 4H^{+}{}_{(aq)} + 8Cu^{2+}{}_{(aq)} + 4Fe^{3+}{}_{(aq)} + 16SO_4{}^{2-}{}_{(aq)} + 2Fe_2O_{3(s)} \quad (11)$$

$$CuFeS_{2(s)} + 16Fe^{3+}{}_{(aq)} + 8H_2O_{(l)} \leftrightarrow Cu^{2+}{}_{(aq)} + 2SO_4{}^{2-}{}_{(aq)} + 17Fe^{2+}{}_{(aq)} + 16H^{+}{}_{(aq)} \quad (12)$$

Under aerobic conditions, bacterial impact upon oxidation is observed as reported in Thurston et al. (2010), where a drop in pH was observed almost immediately in the presence of *Acidithiobacillus ferrooxidans* when compared to abiotic controls. Chalcopyrite dissolution is also maximized by high oxidant concentrations, strong oxidants and high temperatures (Kimball et al. 2010). In experiments under such conditions, the mineral is reacted away, forming product layers (elemental sulfur and jarosite). The thickness and density of these can act as barriers that cause the dissolution rate to be controlled by the rate of diffusive transport of reactants to or products away from the chalcopyrite surface (Kimball et al. 2010).

## Sphalerite

Sphalerite (ZnS) is a less acid-forming sulfide than the Fe-sulfides already discussed (Dold 2005; Lottermoser 2010). The composition of sphalerite is highly variable due to substitution of different elements within the ZnS structure. Iron is the most common element substituting into sphalerite and forms a solid solution series with Zn with concentrations reported up to 32 wt% (Stanton et al. 2008). Divalent cations such as Cd and Mn and also In are common, with trace elements Cu and Pb commonly associated with sphalerite, usually by their presence in trace minerals such as chalcopyrite and galena, rather than by substitution into sphalerite (Stanton et al. 2008; Cook et al. 2009). Sphalerite reactivity varies as a function of composition; therefore the amount of acid formed varies. In general, oxidative dissolution of sphalerite does not produce acid but does release $Zn^{2+}$ (Eq. 13), but if Fe is the oxidant, acid is formed as shown in Eq. 14 (Abbassi et al. 2009). The reaction for Fe-rich sphalerite is also given in Eq. 15 (Lottermoser 2010).

$$ZnS_{(s)} + 2O_{2(g)} \rightarrow Zn^{2+}{}_{(aq)} + SO_4{}^{2-}{}_{(aq)} \quad (13)$$

$$ZnS_{(s)} + 8Fe^{3+}{}_{(aq)} + 4H_2O_{(l)} \rightarrow Zn^{2+}{}_{(aq)} + SO_4{}^{2-}{}_{(aq)} + 8Fe^{2+}{}_{(aq)} + 8H^{+}{}_{(aq)} \quad (14)$$

$$(Zn, Fe)S_{(s)} + 3O_{2(g)} + H_2O_{(l)} \rightarrow Fe(OH)_{3(s)} + SO_4{}^{2-}{}_{(aq)} + Zn^{2+}{}_{(aq)} + 2H^{+}{}_{(aq)} \quad (15)$$

Weisener et al. (2003) showed that the higher the concentration of Fe in sphalerite, the more susceptible is the mineral to oxidation. A layer of metal-deficient sulfide is formed on oxidation, which can protect the sphalerite from further oxidation (Weisener et al. 2003). Stanton et al. (2008) reported that the rate of trace element release from sphalerite at pH 2.0–4.0 decreases in the order Zn > Fe > Mn > Pb > Cd > Cu. Balci (2010) showed *Acidithiobacillus*

*ferrooxidans* to control the release of trace metals from sphalerite as well as the metal concentrations in solution by producing Fe-oxyhydroxides.

## Galena

Galena (PbS) dissolution is enhanced at low pH as it dissolves faster in acidic aqueous solutions (Acero et al. 2007). At pH 1, dissolution of galena is pH, not oxygen dependant. At pH 3, this changes and the dissolved $O_2$ content accelerates the rate of dissolution as summarised in Acero et al. (2007). General galena oxidation reactions are given in Eqs. 16 and 17 and show that acid is formed when undergoing non-oxidative dissolution (Abbassi et al. 2009).

$$PbS_{(s)} + 2O_{2(g)} \rightarrow Pb^{2+}{}_{(aq)} + SO_4{}^{2-}{}_{(aq)} \quad (16)$$

$$PbS_{(s)} + 8Fe^{3+}{}_{(aq)} + 4H_2O_{(l)} \rightarrow Pb^{2+}{}_{(aq)} + SO_4{}^{2-}{}_{(aq)} + 8Fe^{2+}{}_{(aq)} + 8H^{+}{}_{(aq)} \quad (17)$$

Reaction products are typically anglesite ($PbSO_4$) and jarosite ($KFe_3(OH)_6(SO4)_2$). Garcia et al. (1995) reported *Acidithiobacillus ferrooxidans* and *Acidithiobacillus thiooxidans* assist galena oxidation, in particular the prior.

## Sulfide Reactivity

The amount of acid formed, reaction rate and resistance to weathering vary between the sulfide minerals (Lottermoser 2010). Reactivity is greatly influenced by the presence and amount of Fe in the sulfide mineral (Plumlee 1999). Therefore, minerals such as galena, Fe-poor sphalerite, covellite (CuS) and millerite (NiS), which are devoid of Fe in their crystal lattice, are far less reactive and do not have the capacity to form significant amounts of acid (Plumlee 1999). Keith and Vaughan (2000) observed sulfide reactivity in tailings impoundments and listed reactivity (from most to least) as pyrrhotite > galena = sphalerite > pyrite = arsenopyrite > chalcopyrite. More recently, Moncur et al. (2009) updated this list to (from least to most resistant to oxidation): pyrrhotite > galena > sphalerite > bornite ($Cu_5FeS_4$) > pentlandite ($(Fe, Ni)_9S_8$) > arsenopyrite > marcasite > pyrite > chalcopyrite > molybdenite ($MoS_2$).

## Efflorescent Salts

Common reaction products of sulfide oxidation are metal-sulfate efflorescent salts. Dissolution of these minerals plays an important role in the storage and transport of acids and metals released upon weathering of mineralized rock, metallic ore deposits

and mine wastes. Composition of the salts reflects the composition of evaporated waters from which the salts form. Typically, these soluble minerals store Fe, $SO_4$, potentially deleterious elements (e.g., As, Cd, Cu and Zn) and acidity. Therefore, these minerals play a significant role in trace-metal cycling (Jambor et al. 2000).

Precipitation of efflorescences is dependent on climate. During dry spells and seasons these minerals are actively precipitating. During rainfall events these minerals readily undergo dissolution releasing their components into the aqueous environment. This sudden flux of dissolved metals is often termed 'first-flush' (Younger and Blachere 2004 *in* Nordstrom 2009a). Efflorescent minerals exist in a variety of forms, as a result of the cation and amount of water molecules present (as reflected in the nomenclature). Generally, they are classed based on their content of divalent, trivalent, di- and trivalent, or monovalent cations. Full descriptions of these are given in Jambor et al. (2000).

A general pyrite oxidation sequence to understand the evolution of efflorescent minerals was established by Jambor et al. (2000). This sequence shows that pyrite oxidation occurs through divalent, to trivalent efflorescences, and finally to jarosite and Fe-oxyhydroxides. Results from laboratory experiments are largely in agreement with field based observations. Identification of these minerals therefore provides an indication of the degree and stage of oxidation. Similar reaction products can be assumed from pyrrhotite.

Arsenopyrite oxidation forms scorodite ($FeAsO_4.2H_2O$), pharmacosiderite ($KFe_4(AsO_4)_3\ (OH)_4{\cdot}6–7H_2O$) and amorphous ferric arsenates (AFA; Harvey et al. 2006; Murceigo et al. 2011). Scorodite is the most studied of these reaction products as it has a low-solubility, thus limiting the concentration of As in ARD waters (Harvey et al. 2006). Copper-rich secondary sulfates such as chalcanthite can form from chalcopyrite oxidation. As stated before, galena oxidation produces anglesite and jarosite (Garcia et al. 1995). Galena is less soluble than anglesite; formation of anglesite rims slows oxidation, but does not completely retard it (Moncur et al. 2009). Sphalerite oxidation typically occurs by particle-size reduction with limited formation of secondary minerals (Moncur et al. 2009). However, a commonly observed alteration product of sphalerite is elemental sulfur (Edwards et al. 2000). An additional source of acidity in a mine waste environment is through precipitation of $Fe^{3+}$ and $Al^{3+}$ hydroxides as shown by Eq. 18 (Lottermoser 2010).

$$2Al^{3+}_{(aq)} + 3H_2O_{(l)} \leftrightarrow Al(OH)_{3(s)} + 3H^{+}_{(aq)} \tag{18}$$

## Acid Neutralizing Minerals

Acid formed from Fe-sulfide oxidation will to some extent react with acid-neutralizing minerals contained within the sample. The pH buffering ranges of the main neutralizing minerals were generally defined by Parker (1999) and are summarized here. Carbonate minerals act as buffers between pH 8.3–6.2, resulting

in the formation of gypsum and carbonic acid. Silicate mineral buffering occurs between pH 6.2 and 5.0, resulting in the liberation of alkali and alkaline earth cations, and the formation of silicic acid (Lottermoser 2010). This progresses at a much slower rate than carbonate dissolution. Exchange buffering takes place between 5.0 and 4.2 (Lottermoser 2010). Sulfuric acid is buffered by $Al^{3+}$ polymer-hydroxo cations, resulting from silicate weathering. These cations are exchanged in interlayers of clay minerals with basic cations. These are released in turn by precipitation and exchange with $H^+$ (Lottermoser 2010). Aluminium and iron buffering occurs between 4.2 and 3.8. Silicate weathering releases Al and Fe oxides, which buffer the available sulfuric acid. Iron is mobilized, resulting in jarosite formation (Lottermoser 2010). Each of these groups is discussed in the following sections.

## *Carbonate Minerals*

The most effective neutralizing minerals (primary neutralizers) are those containing calcium carbonate and magnesium carbonate, including calcite ($CaCO_3$), magnesite ($MgCO_3$), dolomite ($CaMg(CO_3)_2$), and ankerite ($CaFe(CO_3)_2$) (Lapakko 2002; Lottermoser 2010). Dissolution of these carbonates results in the consumption of hydrogen ions, and the release of bicarbonate, calcium and magnesium ions and carbonic acid. Calcite is the most important of all neutralizers when considering its widespread geological occurrence (Lottermoser 2010). Equations 19–21 below represent the dominant acid-neutralizing reactions of calcite above and below pH 6.4. These reactions are reversible if there is a change in temperature, loss of water or loss of carbon dioxide and will cause the re-precipitation of carbonates (Lottermoser 2010).

$$\text{at pH} > 6.4\text{: } CaCO_{3(s)} + H^{+}_{(aq)} \leftrightarrow HCO^{-}_{3\ (aq)} + Ca^{2+}_{(aq)} \tag{19}$$

$$\text{at pH} < 6.4\text{: } CaCO_{3(s)} + 2H^{+}_{(aq)} \leftrightarrow H_2CO_{3\ (aq)} + Ca^{2+}_{(aq)} \tag{20}$$

$$CaCO_{3(s)} + H_2SO_{4(aq)} \leftrightarrow CaSO_{4(s)} + CO_{2(g)} + H_2O_{(l)} \tag{21}$$

Calcite dissolves most rapidly relative to dolomite and magnesite, whose dissolution rates are one and four orders of magnitude slower (Lapakko 2002). Fe and Mn carbonates do not provide net acid neutralization under oxidizing conditions, due to hydrolysis and precipitation of these metals, resulting in acid production (Paktunc 1999; Lapakko 2002). However, despite this there are numerous examples where siderite has been considered as contributing to the neutralizing potential (Gilbert et al. 2003). Factors affecting calcite reactivity are similar to those of the sulfides, with grain size, texture and the presence of trace elements either increasing or decreasing the mineral's resistance to weathering (Lottermoser 2010).

## *Silicate Minerals*

Silicate minerals offer less neutralization than carbonate minerals and are less soluble at moderate pH (see tables given in Mills et al. 2015 and Bowell et al. 2000). Nevertheless, non-carbonate mineral dissolution can maintain neutral conditions, if the rate of acid production is slow. Furthermore, they are relatively abundant, making them potentially significant neutralizers (Bowell et al. 2000). Neutralizing effectiveness increases with increasing mineral surface area. This in turn increases with increasing mineral content and decreasing grain size (Lapakko 2002; Jambor et al. 2002).

Nesbitt and Jambor (1998) discussed the role of mafic minerals in neutralizing ARD in tailings from the Waite-Amulet tailings impoundment, Canada. They concluded that phyllosilicates, pyroxenes, amphiboles and feldspars were effectively solid bases with a noticeable neutralizing potential (NP). High levels of Mg were recorded in the most neutralized waters suggesting that the dissolution of Mg-bearing phyllosilicates (i.e., chlorite) contributed to the neutralizing potential. Jambor et al. (2002) explored this further by undertaking a series of static tests to define the neutralizing potential of selected silicate and aluminosilicate minerals. From their sample suite (comprising of olivines, pyroxenes, amphiboles, feldspars, micas, chlorites, clays, garnets, apatites and serpentines), only olivine, wollastonite and serpentinite were recognized as having a significant NP (i.e. >20 NP value). The authors also investigated compositional differences and reported that in general, compositional variation and polymorphism within a group do not have a profound effect on neutralizing potential. In the case of the feldspar group, sodic and potassic feldspar were recorded as yielding little NP, and even Ca-bearing members were recorded as giving little NP until well into the field of anorthite.

## *Exchangeable Cations*

Exchangeable cations ($Ca^{2+}$, $Mg^{2+}$, $Na^{+}$, $K^{+}$) are present at the exchange sites of micas, clays and organic matter (Strömberg and Banwart 1999). They can be replaced by cations dissolved in weathering solutions. Dissolved $H^{+}$ and $Fe^{2+}$ ions, produced on sulfide oxidation, compete for cation exchange sites and are temporarily adsorbed. General reactions are given in Eqs. 22 and 23 (Lottermoser 2010).

$$\text{Clay}-(\text{Na}^{+})_{(s)} + Fe^{2+}{}_{(\text{aq})} \leftrightarrow \text{clay}-\left(\text{Fe}^{2+}\right)_{(s)} + \text{Na}^{+}{}_{(aq)} \tag{22}$$

$$\text{Clay}-\left(\text{Ca}^{2+}\right)_{0.5(s)} + H^{+}{}_{(aq)} \leftrightarrow \text{clay}-(\text{H}^{+})_{(s)} + 0.5\text{Ca}^{2+}{}_{(aq)} \tag{23}$$

## Hydroxide Minerals

Dissolution of aluminosilicate minerals such as kaolinite releases dissolved $Al^{3+}$. If this precipitates as gibbsite ($Al(OH)_3$), then an acid-producing reaction will occur (Eq. 18). However, if gibbsite already exists, then it can provide additional neutralizing ability because it can consume dissolved hydrogen ions as shown in Eq. 24 (Lottermoser 2010). Ferric hydroxide solids can also be redissolved in acidic waters, also consuming hydrogen ions as shown in Eq. 25 (Lottermoser 2010).

$$Al(OH)_{3(s)} + 3H^{+}_{(aq)} \leftrightarrow Al^{3+}_{(aq)} + 3H_2O_{(l)} \quad (24)$$

$$Fe(OH)_{3(s)} + 3H^{+}_{(aq)} \leftrightarrow Fe^{3+}_{(aq)} + 3H_2O_{(l)} \quad (25)$$

## Conclusions

Oxidation of sulfide minerals (i.e., pyrite) occurs via inorganic and biologically-mediated pathways and releases sulfuric acid and dissolved metals. Processes of pyrite oxidation are generally controlled by several factors including pH, oxidant type ($O_2$ or $Fe^{3+}$), oxidant concentration, mineral morphology, microbial and trace element contents. Oxidation is further complicated by the electrochemical nature of pyrite.

Other sulfides have differing acid-forming potential and rates of reaction. This is dependent on the amount of Fe present, with Fe-sulfides generating the most acidity. Sulfides which do not contain Fe in their crystal lattice (e.g., galena, Fe-poor sphalerite) do not have the capacity to generate large amounts of acid, but can be sources of potentially deleterious metals such as Cd, Pb and Zn. Sulfide reactivity is generally in the order of pyrrhotite > galena—sphalerite > pyrite—arsenopyrite > chalcopyrite. Product layers can develop on oxidation which can control the rate of diffusion and thus the overall rate of oxidation. Additionally, secondary efflorescent minerals may form particularly in semi-arid and arid regions; these represent temporary stores of sulfate and metals, which on dissolution will be released along with acidity. An additional source of acidity in mine waste is the precipitation of $Fe^{3+}$ and $Al^{3+}$ hydroxides.

Acid formed by sulfide oxidation can be consumed through reaction with gangue minerals. Neutralization is primarily offered by dissolution of carbonate minerals of which calcite is the most effective. Some neutralization is offered from silicate mineral dissolution, particularly olivine, wollastonite and serpentine. However, the rate of dissolution is much slower than that of carbonates. Additionally, clay minerals and Al and Fe hydroxides have a neutralization capacity, but the likely net-neutralizing contribution is small compared to that of calcite. The balance of all

chemical reactions occurring within a particular mine waste will determine if the material will turn acid, and produce ARD (Lottermoser 2010). Consequently, significant environmental problems are posed because ARD chemistry can be harmful to receptors (e.g., flora and fauna) in proximity to mine sites (Ma and Banfield 2011).

## References


Abbassi R, Khan F, Hawbolt K (2009) Prediction of minerals producing acid mine drainage using a computer-assisted thermodynamic chemical equilibrium model. Mine Water Environ 28:74–78

Acero P, Cama J, Ayora C (2007) Rate law for galena dissolution in acidic environment. Chem Geol 245:219–229

Asta MP, Cama J, Ayora C, Acero P, de Giudici G (2010) Arsenopyrite dissolution rates in $O_2$-bearing solutions. Chem Geol 273:272–285

Baker BJ, Banfield JF (2003) Microbial communities in acid mine drainage. FEMS Microbiol Ecol 44:139–152

Baker-Austin C, Potrykus J, Wexler M, Bond PL, Dopson M (2010) Biofilm development in the extremely acidophilic archaeon *'Ferroplasma acidarmanus'* Fer1. Extremophiles 14:485–491

Balci NC (2010) Effect of bacterial activity on trace metals release from oxidation of sphalerite at low pH (< 3) and implications for AMD environment. Environ Earth Sci 60:485–493

Becker M (2009) The mineralogy and crystallography of pyrrhotite from selected nickel and PGE ore deposits and its effect on flotation performance. Unpublished DPhil thesis, University of Pretoria, Pretoria

Belzile N, Chen YW, Cai MF, Li Y (2004) A review on pyrrhotite oxidation. J Geochem Explor 84:65–76

Biegler T (1976) Oxygen reduction on sulfide minerals: part II. Relation between activity and semiconducting properties of pyrite electrodes. J Electroanal Chem 70:265–275

Blanchard M, Alfredsson M, Brodholt J, Wright K, Catlow CRA (2007) Arsenic incorporation into $FeS_2$ pyrite and its influence on dissolution: a DFT study. Geochim Cosmochim Acta 71:624–630

Bond PL, Druschel GK, Banfield JF (2000) Comparison of acid mine drainage microbial communities in physically and geochemically distinct ecosystems. Appl Environ Microbiol 66:4962–4971

Bowell RJ, Rees SB, Parshley JV (2000) Geochemical predictions of metal leaching and acid generation: geologic controls and baseline assessment. In: Cluer JK, Price JG, Struhsacker EM, Hardyman RF, Morris CL (eds) Geology and ore deposits 2000: the great basin and beyond: Geological Society of Nevada symposium proceedings, Reno/Sparks, pp 799–823

Bryan CG, Watkin EL, McCredden TJ, Wong ZR, Harrison STL, Kaksonen AH (2015) The use of pyrite as a source of lixiviant in the bioleaching of electronic waste. Hydrometall 152:33–43

Chandra AP, Gerson AR (2010) The mechanisms of pyrite oxidation and leaching: a fundamental perspective. Surf Sci Rep 65:293–315

Cook NJ, Ciobanu CL, Pring A, Skinner W, Danyushevsky L, Shimizu M, Saini-Eidukat B, Melcher F (2009) Trace and minor elements in sphalerite: a LA-ICP-MS study. Geochim Cosmochim Acta 73:4761–4791

Corkhill CL, Vaughan DJ (2009) Arsenopyrite oxidation—a review. Appl Geochem 24:2342–2361

Craig JR, Vokes FM, Solberg TN (1998) Pyrite: physical and chemical textures. Miner Deposita 34:82–101

Crundwell FK (1996) The formation of biofilms of iron-oxidising bacteria on pyrite. Min Eng 9:1081–1089

Crundwell FK (2003) How do bacteria interact with minerals? Hydrometall 71:75–81

Dold B (2005) Basic concepts of environmental geochemistry of sulfide mine-waste. XXIV Curso Latinoamericano de Metalogenia UNESCO—SEG, Lima, Peru

Edwards KJ, Schrenk MO, Hamers RJ, Banfield JF (1998) Microbial oxidation of pyrite: experiments using microorganisms for an extreme acid environment. Am Mineral 83:1444–1453

Edwards KJ, Goebel B, Rogers TM, Schrenk MO, Gihring TM, Cardona MM, Hu B, McGuire MM, Hamers RJ, Pace NR, Banfield JF (1999) Geomicrobiology of pyrite ($FeS_2$) dissolution: case study at Iron Mountain, California. Geomicrobiol J 16:155–179

Edwards KJ, Bond PL, Druschel GK, McGuire MM, Hamers RJ, Banfield JF (2000) Geochemical and biological aspects of sulphide mineral dissolution: lessons from Iron Mountain, California. Chem Geol 169:383–397

Egiebor NO, Oni B (2007) Acid rock drainage formation and treatment: a review. Asia Pac J Chem Eng 2:47–62

Evangelou VP, Zhang YL (1995) A review: pyrite oxidation mechanisms and acid mine drainage prevention. Crit Rev Env Sci Technol 25:141–199

Florian B, Noel N, Sand W (2010) Visualization of initial attachment of bioleaching bacteria using combined atomic force and epifluorescence microscopy. Min Eng 23:532–535

Garcia O, Bigham JM, Tuovinen OH (1995) Sphalerite oxidation by *Thiobacillus fertooxidans* and *Thiobacillus thiooxidans*. Can J Microbiol 41:578–584

Gilbert SE, Cooke DR, Hollings P (2003) The effects of hardpan layers on the water chemistry from the leaching of pyrrhotite-rich tailings material. Environ Geol 44:687–697

Harvey MC, Schreiber ME, Rimstidt JD, Griffith MM (2006) Scorodite dissolution kinetics: implications for arsenic release. Environ Sci Technol 40:6709–6714

Hudson-Edwards KA, Lottermoser BG, Jamieson HE (2011) Mine wastes: past, present, future. Elements 7:375–380

Hustwit CC, Ackman TE, Erikson PE (1992) The role of oxygen transfer in acid mine drainage (AMD) treatment. Water Environ Res 64:817–823

Jambor JL (1994) Mineralogy of sulfide rich tailings and their oxidation products. In: Blowes DW, Jambor JL (eds) The environmental geochemistry of sulfide mine wastes. Mineralogical Association of Canada, Short Course Series 22, pp 59–102

Jambor JL (2003) Mine-waste mineralogy and mineralogical perspectives of acid-base accounting. In: Jambor JL, Blowes DW, Ritchie AIM (eds) Environmental aspects of mine wastes. Mineralogical Association of Canada, Short Course Series 31, pp 117–145

Jambor JL, Nordstrom DK, Alpers CN (2000) Metal-sulfate salts from sulfide mineral oxidation. Rev Mineral Geochem 40:303–350

Jambor JL, Dutrizac JE, Groat L, Raudsepp M (2002) Static tests of neutralization potentials of silicate and aluminosilicate minerals. Environ Geol 43:1–17

Keith CN, Vaughan DJ (2000) Mechanisms and rates of sulfide oxidation in relation to the problems of acid rock (mine) drainage. In: Environmental mineralogy: microbial interactions, anthropogenic influences, contaminated land and waste management, mineralogical society series 9, pp 117–139

Kimball BK, Rimstidt JD, Brantley SL (2010) Chalcopyrite dissolution rate laws. Appl Geochem 25:972–983

Kwong YTJ (1993) Prediction and prevention of acid rock drainage from a geological and mineralogical perspective. MEND report 1.32.1, NHRI contribution CS-92054, Ottawa, Ontario

Kwong YTJ (1995) Thoughts on ways to improve acid drainage and metal leaching prediction for metal mines. US geological survey water resources investigations report, pp 95–4227

Kwong YTJ, Swerhone GW, Lawrence JR (2003) Galvanic sulfide oxidation as a metal-leaching mechanism and its environmental implications. Geochem Explor Env Anal 3:337–343

Lapakko KA (2002) Metal mine rock and waste characterization tools: an overview. Metal Mining and Sustainable development website#67. http://pubs.iied.org/pdfs/G00559.pdf

Lara RH, Valdez-Pérez D, Rodríguez AG, Navarro-Contreras HR, García-Meza JV (2010) Interfacial insights of pyrite colonized by *Acidithiobacillus thiooxidans* cells under acidic conditions. Hydrometall 103:35–44

Leathen WW, Braley SA, McIntyre ID. (1953a) The role of bacteria in the formation of acid from certain sulphuric constituents associated with bituminous coal, Thiobacillus thioxidans. Appl Microbiol 1:61–64

Leathen WW, Braley SA, McIntyre ID (1953b) The role of bacteria in the formation of acid from certain sulphuric constituents associated with bituminous coal, II Ferrous-iron oxidising bacteria. Appl Microbiol 1:65–68

Lee E, Han Y, Park J, Hong J, Silva RA, Kim S, Kim H (2015) Bioleaching of arsenic from highly contaminated mine tailings using *Acidithiobacillus thiooxidans*. J Environ Manag 147:124–131

Li J, Kawashima N, Kaplun K, Absolon VJ, Gerson AR (2010) Chalcopyrite leaching: the rate controlling factors. Geochim Cosmochim Acta 74:2881–2893

Lottermoser BG (2010) Mine wastes: characterization, treatment and environmental impacts, 3rd edn. Springer, Berlin 400 pp

Ma S, Banfield JF (2011) Micron-scale $Fe^{2+}/Fe^{3+}$, intermediate sulfur species and $O_2$ gradients across the biofilm–solution–sediment interface control biofilm organization. Geochim Cosmochim Acta 75:3568–3580

Mielke RE, Pace DL, Porter T, Southam G (2003) A critical stage in the formation of acid mine drainage: colonization of pyrite by *Acidithiobacillus ferrooxidans* under pH-neutral conditions. Geobiology 1:81–90

Mills C, Robertson A, Shaw S (2015) Acid rock drainage, EnviroMine. http://technology.infomine.com/enviromine/ard/home.htm

Moncur MC, Jambor JL, Ptacek CJ, Blowes DW (2009) Mine drainage from the weathering of sulfide minerals and magnetite. Appl Geochem 24:2362–2373

Morin KA (2010) The science and non-science of minesite-drainage chemistry. MDAG Internet Case Study#37. www.mdag.com/case_studies/cs37.html

Morth AH, Smith EE, Shumate KS (1972) Pyrite systems: A mathematical model contract report for the US protection agency. EPA-R2 72 002

Moses CO, Herman JS (1991) Pyrite oxidation at circumneutral pH. Appl Geochem 55:471–482

Moses CO, Nordstrom DK, Herman JS, Mills AL (1987) Aqueous pyrite oxidation by dissolved oxygen and by ferric iron. Geochim Cosmochim Acta 51:1561–1571

Murceigo A, Álvarez-Ayuso E, Pellitero E, Rodríguez MA, García-Sánchez A, Tamayo A, Rubio J, Rubio F, Rubin J (2011) Study of arsenopyrite weathering products in mine wastes from abandoned tungsten and tin exploitations. J Hazard Mater 186:590–601

Nesbitt HW, Jambor JL (1998) Role of mafic minerals in neutralizing ARD, demonstrated using a chemical weathering methodology. In: Cabri LJ, Vaughan DJ (eds) Short course handbook on ore and environmental mineralogy. Mineralogical Association of Canada 27, pp 403–421

Nicholson RV, Scharer JM (1994) Laboratory studies of pyrrhotite oxidation kinetics. In: Alpers CA, Blowes DW (eds) Environmental chemistry of sulfide oxidation, ACS symposium series 550. American Chemical Society, Washington, DC

Nordstrom DK (2009) Acid rock drainage and climate change. J Geochem Explor 100:97–104

Nordstrom DK, Southam G (1997) Geomicrobiology of sulfide mineral oxidation. Rev Mineral Geochem 35:361–390

Olson GJ (1991) Rate of pyrite bioleaching by *Thiobacillus ferrooxidans*: results of an interlaboratory comparison. Appl Environ Microbiol 57:642–644

Paktunc AD (1999) Mineralogical constraints on the determination of neutralising potential and prediction of acid mine drainage. Environ Geol 39:103–112

Parbhakar-Fox A, Lottermoser BG (2015) A critical review of acid rock drainage prediction processes and practices. Min Eng 82:107–124

Parker G (1999) A critical review of acid generation resulting from sulfide oxidation: processes, treatment and control. Aust Miner Energy Environ Found Melbourne 11:1–182

Plumlee GS (1999) The environmental geology of mineral deposits. In: Plumlee GS, Logsdon MJ (eds) The environmental geochemistry of mineral deposits part A: processes, techniques and health issues. Rev Econ Geol 6A:71–116

Rimstidt JD, Vaughan DJ (2003) Pyrite oxidation: a state-of-the-art assessment of the reaction mechanism. Geochim Cosmochim Acta 67:873–880

Ritchie AIM (1994) Sulfide oxidation mechanisms: controls and rate of oxygen transport. In: Jambor JL, Blowes DW (eds) The environmental geochemistry of sulfide mine wastes. Short course series, Mineralogical Association of Canada 22, pp 201–246

Rohwerder T, Gehrke T, Kinzler K, Sand W (2003) Bioleaching review part A: progress in bioleaching: fundamentals and mechanisms of bacterial metal sulfide oxidation. Appl Microbiol Biotechnol 63:239–248

Sand W, Gehrke T (2006) Extracellular polymeric substances mediate bioleaching/biocorrosion via interfacial processes involving iron (III) ions and acidophilic bacteria. Res Microbiol 157:49–56

Sand W, Gerke T, Hallman R, Schippers A (1995) Sulfur chemistry, biofim, and the (in)direct attack mechanism—a crictical evaluation of bacterial leaching. Appl Microbiol Biotech 43:961–966

Savage KS, Stefan D, Lehner S (2008) Impurities and heterogeneity in pyrite: influences on electrical properties and oxidation products. Appl Geochem 23:103–120

Schippers A, Sand W (1999) Bacterial leaching of metal sulfides proceeds by two indirect mechanisms via thiosulfate or via polysulfides and sulphur. Appl Environ Microbiol 65:319–321

Schrenk MO, Edwards KJ, Goodman RM, Hamers RJ, Banfield JF (1998) Distribution of *Thiobacillus ferrooxidans and Leptospirillum ferrooxidans* for generation of acid mine drainage. Science 279:1519–1522

Singer PC, Stumm W (1970) Acidic mine drainage: the rate-determining step. Science 167:1121–1123

Smith L, Beckie R (2003) Hydrologic and geochemical transport processes in mine. In: Jambor JL, Blowes DW, Ritchie AIM (eds) Environmental aspects of mine wastes. Mineralogical Association of Canada, Short Course Series 31, pp 51–72

Stanton MR, Gemery-Hill PA, Shanks WC, Taylor CD (2008) Removal of zinc and trace metal release from dissolving sphalerite at pH 2.0 to 4.0. Appl Geochem 23:136–147

Strömberg B, Banwart SA (1999) Experimental study of acidity-consuming processes in mining waste rock: some influences of mineralogy and particle size. Appl Geochem 14:1–16

Stumm W, Morgan JJ (1995) Aquatic chemistry, 3rd edn. Wiley, New York 1040 pp

Tao H, Dongwei L (2014) Presentation on mechanisms and applications of chalcopyrite and pyrite bioleaching in biohydrometallurgy—a presentation. Biotechnol Rep 4:107–119

Thomas JE, Skinner WM, Smart RC (2003) A comparison of the dissolution behaviour of troilite with other iron(II) sulfides; implications of structure. Geochim Cosmochim Acta 67:831–843

Thurston RS, Mandernack KW, Shanks WC (2010) Laboratory chalcopyrite oxidation by *Acidithiobacillus ferrooxidans*: Oxygen and sulfur isotope fractionation. Chem Geol 269:252–261

Tyson GW, Chapman J, Hughenholtz P, Allen EE, Ram RJ, Richardson PM, Solovyev VV, Rubin EM, Rokhsar DS, Banfield JF (2004) Community structure and metabolism through reconstruction of microbial genomes from the environment. Nature 428:37–43

Weber PA, Thomas JE, Skinner WM, Smart RC (2004) Improved acid neutralisation capacity assessment of iron carbonates by titration and theoretical calculation. Appl Geochem 19:687–694

Weisener CG, Weber PA (2010) Preferential oxidation of pyrite as a function of morphology and relict texture. NZ J Geol Geophys 53:22–33

Weisener CG, Smart RC, Gerson AR (2003) Kinetics and mechanisms of the leaching of low Fe-sphalerite. Geochim Cosmochim Acta 67:823–830

Wiersma CL, Rimstidt JD (1984) Rates of reaction of pyrite and marcasite with ferric iron at pH 2. Geochim Cosmochim Acta 48:85–92

Yunmei Y, Yongxuana Z, Williams-Jones AE, Zhenmina G, Dexian L (2004) A kinetic study of the oxidation of arsenopyrite in acidic solutions: implications for the environment. Appl Geochem 19:435–444

# Prediction of Sulfidic Waste Characteristics

**Anita Parbhakar-Fox and Bernd Lottermoser**

**Abstract** Inadequate prediction of acid rock drainage (ARD) can result in the reputational damage of mine operators, the spending of significant costs for post-closure management and lasting impacts to ecosystems. Instead, accurate prediction of ARD will allow a reduction of environmental risks and associated financial liabilities. At present, the mining industry use a range of static and kinetic chemical tests to measure the balance between the acid generating and acid neutralizing potentials of mine waste materials. The resulting data are used to prepare risk assessments and design waste classification schemes. However, associated with these established tests and practices are several shortcomings including: inadequate sampling; performance of a limited number of tests; late initiation of kinetic trials; classification using restricted waste classification categories; and no consideration given to biological and physical parameters that can influence ARD formation. Therefore, current practices only provide a broad indication of ARD potential over time. Fundamentally, ARD is a multifaceted process controlled by several variables, and therefore new tests and protocols developed in this area must reflect this.

## Introduction

Environmental indices are not effectively embedded into the mine plan of potential ore deposits during early life-of-mine stages. Instead, testwork for resource evaluation, beneficiation, mineral processing and metal recovery is prioritized. The resulting models from such testwork provide guidance with regards to how exactly

A. Parbhakar-Fox (✉)
School of Physical Sciences, University of Tasmania, Private Bag 79, Hobart, TAS 7001, Australia
e-mail: Anita.Parbhakar@utas.edu.au

B. Lottermoser
Institute of Mineral Resources Engineering, RWTH Aachen University, Wüllnerstrasse 2, 52062 Aachen, Germany
e-mail: lottermoser@mre.rwth-aachen.de



B. Lottermoser (ed.), *Environmental Indicators in Metal Mining*,
DOI 10.1007/978-3-319-42731-7_3

to extract and process ore, with little consideration given to the resulting waste products (e.g., waste rock or tailings). However, when considering that ore typically represents a much smaller volume of material than waste, the characterization of waste units should be of significant importance, as this will continue to be exposed at the Earth's surface, increasing the risk for acid rock drainage (ARD) formation. In financial terms the absence of in-depth environmental characterization can be considered a shortcoming as there are many examples of significant post-mining costs due to subsequent ARD management (e.g., Wheal Jane, UK, Johnson and Hallburg 2005; Iron Mountain, California, US, Jamieson et al. 2005).

Guidelines for ARD testwork are given in several handbooks including the Global Acid Rock Drainage (GARD) Guide, a web-based Wikipedia-style handbook first published in 2009 by the International Network for Acid Prevention (INAP). This provides up-to-date information on how to undertake ARD prediction, documents potential rehabilitation options and gives advice on management strategies.

Whilst the GARD Guide provides information on how to undertake ARD prediction; it focuses on using a testing regime similar to the wheel approach for drainage chemistry prediction (Morin and Hutt 1999; Fig. 1). The wheel comprises eight categories, which are either field or laboratory based tests. The wheel


**Fig. 1** The 'wheel' approach for predicting drainage chemistry (Morin and Hutt 1999). (Reprinted from Morin KA, Hutt NM (1999) Kinetic test and risk assessment for ARD. In: Proceedings of the 5th annual BC metal leaching and ARD workshop, Vancouver, pp 1–10, with permission from K Morin) (color figure online)

approach focuses its attention on geochemical testing, several of which are suitable to use during early life-of-mine stages (e.g., static and net acid generation testing), and others for later stages (e.g., geochemical monitoring). Although mineralogy is included in the wheel, detailed guidelines on when or how to use mineralogical techniques or data are not given.

Consequently, Smart et al. (2002) published a more structured protocol for ARD prediction (included in the GARD Guide) specifically to be followed during pre-feasibility/feasibility stages of mining. It differs from the wheel approach in that advanced geochemical tests are recommended for use to resolve the characteristics of ambiguous (i.e., classified as uncertain) samples. However, this updated approach suffers from the same major limitation in that mineralogical data is sparsely collected with its application restricted to when geochemical classifications are reported as uncertain. The mining industry standard approach to ARD prediction is to use geochemical testing. However, due to their relatively high cost per sample (e.g., US$80 to US$200 for acid-base accounting packages), performance on an appropriate number of samples (Table 1) is not always possible, resulting in an ARD waste block model populated with too few data points. Ultimately, funding is the factor responsible for inadequate ARD prediction and characterization testwork, of which the inevitable result is insufficient deposit-wide characterization and ineffective waste management strategies. Thus, the biggest environmental challenge facing the mining industry is undertaking accurate, but cost-effective ARD (and metal leaching) prediction testwork. In this chapter, the tests and protocols used for predicting ARD from sulfidic mine wastes (e.g., tailings, waste rock) are summarized, with the benefits and limitations associated with each briefly discussed.

**Table 1** Suggested initial number of samples and test work (adapted from Australian Government Department of Industry, Tourism and Resources, 2007 *in* Price 2009)

| Phase | Description |
|---|---|
| Exploration: prospect testing | At least 3–5 representative samples should be tested for each key lithology/alteration type |
| Exploration: resource definition | At least 5–10 representative samples should be tested for each key lithology/alteration type |
| Pre-feasibility | Several hundred representative samples of high and low grade ore, waste rockand tailings should be collected for geochemical work.<br>Sufficient samples to populate a block model with reliable distribution of static test data on ore, waste and wall rock<br>Kinetic tests should be established for at least 1–2 representative samples for each key lithology/alteration type |
| Feasibility | Continue to refine block model if necessary and conduct sufficient mineralogical test work to cross check data for key lithologies<br>If there are insufficient data to assess drainage chemistry and provide a convincing management plan for approval, additional sampling, test work and refinement of block models will be required |

## ARD Prediction: Testwork and Protocols

In order to achieve best practice prediction of ARD in terms of risk, quantity and longevity, several testsmust be performed on a particular sample. A single test alone cannot be used due to the uncertainties and limitations associated with each existing test methodology. As shown by Table 1, at each stage in the life-of-mine cycle there is a necessity for performing ARD testwork, though the type of assessment and number of samples for evaluation varies. At the exploration stages where environmental characterization funds are typically limited, desk study assessments such as consultation of geoenvironmental ore deposit models are given preference. Once an operation moves into pre-feasibility/feasibility stages, then access to drill core is allowed, and geochemical static testwork permitted. At this stage, kinetic test cells should also be established. Once mining is in the fully operational extraction stage, static tests are recommended for quality control testing to allow for the checking of classifications. This is of importance as during this stage, waste blocks are transported to the piles and placed according to the waste management strategy developed at the previous stage (i.e., pre-feasibility/feasibility). In the following section, the commonly used tests are outlined.

### *Geoenvironmental Ore Deposit Modelling*

Planning of future mines and remedying of existing threats to human health, ecosystems and water resources, requires a thorough understanding of the underlying physical and chemical processes and their interactions. Therefore, as ore deposits are unique and complex environments, a detailed understanding of the site conditions is required. Diverse physical, social and political factors require characterization to fully understand the environmental signature; these include geography, baseline geochemistry, geology, hydrology, hydrogeology and climatic regime. Increasing understanding of necessary processes and links between them can be addressed by focused studies involving investigations into a source-pathway-receptor approach. This information is used to build a conceptual site model. This is used in turn to assess the potential environmental risks of mining and to develop a strategy to manage these.

On a broader scale, distinct geoenvironmental signatures for the majority of deposits types have been recognized (Ficklin et al. 1992; Kwong 1993), leading to the publication of geoenvironmental ore deposit models (Du Bray 1995; Seal et al. 2002). They are intended as analogues for similar ore-deposits, providing surrogate environmental data. In general, massive sulfide deposits are recognized as the most likely to produce acid metalliferous drainage. Whilst some information is provided as to the environmental signatures of each ore deposit, there are several limitations including the lack of quantification and the bias of models to North American sites (i.e. no climatic or hydrological diversity). Furthermore, models were recognized as too site specific, or too general. Despite their limitations, they are periodically

updated, e.g. carbonatite deposits (Verplank et al. 2014). Plumlee (1999) looked beyond classifying by ore deposit type and identified instead the environmental signatures based on the most common host rock lithologies and alteration styles. Carbonates were recognized as the most neutralizing lithology, and acid sulfate argillic and phyllic alteration as the most acid forming alteration styles.

Future developments in site characterization must focus on developing more detailed conceptual site models, which incorporate the use of tools such as biotic ligand models. Sharing data in a manner similar to the international static test database (Hutt and Morin 2000) could lead to the development of regional-scale deposit models, which would have a greater application than geoenvironmental ore deposit models as they would incorporate relevant climatic and hydrological data, which are key factors controlling the formation of ARD and the release of metals.

## *Selection, Storage and Preparation of Samples*

The most critical part of a predictive ARD investigation is sample selection. An adequate number of samples must be obtained to characterize all lithological types as well as all types of alteration and weathering. As site conditions greatly vary (as explained in the previous section), there is no set number of samples that should be taken, and no set rule as to from which intervals they should be obtained. Instead, there are recommended minimum guidelines, and also a general outline of sampling throughout the development of a mining operation (Table 1). Once samples have been obtained, they should be correctly stored to prevent further oxidation. Sample preparation ahead of analysis is dictated by the analytical procedures selected for use. The majority of geochemical and bulk-mineralogical tests require crushing and grinding samples to <74 μm (200 mesh) or <120 μm (120 mesh), and <9.5 mm (3/8 in.) or 6.4 mm (1/4 in.) for laboratory kinetic tests. Ensuring QA/QC procedures are being undertaken is essential to prevent cross contamination of samples during preparation.

## *Geochemical Characterization*

Geochemical characterization typically includes the measurement of sulfur, carbon, metals and metalloids in a sample. Total sulfur and carbon are commonly measured using combustion in a high-temperature furnace and subsequent analysis of the gases using infrared spectrometry methods. Methods for measuring sulfide concentration include the chromium reducible sulfur method. Sulfur and carbon values are used in calculations of the acid producing and acid neutralizing potentials (Downing and Giroux 1993; Borden 2003; Weber et al. 2005; Hakkou et al. 2009). Measurement of total metals and metalloids is commonly achieved through X-ray fluorescence (XRF) or inductively coupled plasma (ICP) spectrometry methods. Field portable XRF (pXRF) devices allow for rapid measurement of these,

however, the quality of data is poorer. Chemical leach methods to determine metal contents and mobility include the toxicity characteristic leach procedure (TCLP) and synthetic precipitation leach procedure (SPLP), and the BCR extraction procedure. However, undertaking these tests on a geostatistically reliable number of samples would prove difficult (i.e. cost and labour intensive); therefore they have limited application in predictive ARD testwork. Whilst lithogeochemical models using whole-rock XRF data for predicting ARD have been developed (Downing and Madeisky 1997; Lawrence and Scheske 1997; Paktunc 2001), they also have limited application. Redevelopment of these approaches is required as this information is routinely collected; thus by using it, there is potential to cost-effectively develop predictive ARD block models.

## *Static Tests*

Static tests are rapid (measured in hours and days) screening tests. The most common static test procedure—acid-base accounting (ABA)—requires the calculation of the maximum potential acidity (MPA) and measurement of the acid neutralizing capacity (ANC). The difference between these values gives an indication of the acid forming potential. Measurement of the paste pH is also required. Net acid generation (NAG) tests are another type of static testing that measure acid release at different pH levels. Other static tests include the net carbonate value (NCV) and acid buffering characterization curve (ABCC) tests.

### Acid-Base Accounting (ABA)

Acid-base accounting involves the calculation of net acid producing potential (NAPP). NAPP is a two component procedure in which the difference between MPA and ANC is deduced and used to assess the net acid producing or acid consuming capacity of a sample. Values can be expressed in either kg$H_2SO_4$/t as in Australia and Asia Pacific region, or kg $CaCO_3$/t as in North America. Alternatively, ANC can be subtracted from MPA to give the Net-Neutralizing Potential (NNP), however this is a less commonly used calculation. A third is the neutralizing potential ratio (NPR). All three calculations are shown in Eqs. 1, 2 and 3.

$$\text{Net Acid Producing Potential or NAPP} = \text{MPA} - \text{ANC} \quad (1)$$

$$\text{Net Neutralizing Potential or NNP} = \text{ANC} - \text{MPA} \quad (2)$$

$$\text{Neutralizing Potential Ratio or NPR} = \text{ANC}/\text{MPA} \quad (3)$$

MPA or acid potential (AP) is calculated directly from $S_{Total}$ or $S_{Sulfide}$ values. The $S_{Total}$ or $S_{Sulfide}$ value is multiplied by the stoichiometric factor of 30.6 to give the

MPA value in kg $H_2SO_4$/t. (a factor of 31.25 is used to give MPA in kg $CaCO_3$/t). This factor is determined from the stoichiometry of pyrite oxidation (Weber et al. 2005). However, the inaccuracy of using this factor for samples containing sulfides other than pyrite has long since been recognized. Paktunc (1999) stated that if the sample being tested contains pyrrhotite in addition to pyrite, then overestimation of MPA/AP values may occur up to 1.5 times.

The ANC (or neutralizing potential NP) is a quantitative measurement of a solid phase sample's capacity to neutralize aqueous acidity (Morin and Hutt 2009). It is calculated by a titration method, of which several exist with the most common summarized in Table 2. The most widely used is the Sobek method (White et al. 1999; Bezaazoua et al. 2004; Jambor et al. 2006). This method has subsequently been modified, and several additional methods exist. There is no standard method; rather one is used in accordance with environmental legislation in that particular country. For example, the US. EPA-600-compliant Sobek et al. NP method is the standard method in the United States (Morin and Hutt 2009). In Australia, the Commonwealth, state and local Governments have legislation guidelines in place

**Table 2** Procedure conditions for the determination of acid neutralizing capacity (ANC) (Mills et al. 2015)

| Test | Acid | Amount of acid added | End pH of acid addition | Test duration | Test temperature | Minerals dissolved |
|---|---|---|---|---|---|---|
| Sobek | HCl | Determined by fizz test | 0.8–2.5 | Until gas evolution ceases (test includes titration up to 3 h) | Elevated (c.90 °C) | Calcite, dolomite, Ca-feldspar, anorthoclase, orthoclase, albite, olivine, pyroxene, hornblende, augite, biotite |
| Modified Sobek | HCl | Determined by fizz test | 2.0–2.5 | 24 h | Ambient | Ca + Mg carbonates and some Fe carbonate, biotite, chlorite, amphibole and olivine |
| BCRI Initial | $H_2SO_4$ | To reach pH 3.5 | 3.5 | 16–24 h | Ambient | Ca + Mg carbonates and possibly chlorite and limonite |
| Lapakko | $H_2SO_4$ | To reach pH 6.0 | 6.0 | Up to 1 week | Ambient | Ca + Mg carbonates |
| Sobek-siderite correction | Procedure as for Sobek, but with peroxide correction for siderite | | | | | Ca + Mg carbonates |
| Net carbonate value | Method uses combustion infrared analysis, not acid digestion | | | | | Calcite, dolomite, ankerite, siderite |
| Inorganic carbon carbonate | Method uses LECO furnace or equivalent, not acid digestion | | | | | Calcite, dolomite |

that are relevant to mine site ARD management. However, the Sobek and modified Sobek methods are the most widely used (Comarmond 1997). Alternative methods to titrations were presented in Hutt and Morin (2000) by calculating ANC based on carbonate contents (e.g., net carbonate value (NCV) and inorganic carbonate carbon; Table 2). Lengke et al. (2010) demonstrated the application of the NCV, which is the favoured method by mining companies such as Newmont Ltd.

There are no commonly used methods to determine silicate ANC (as for carbonate ANC). Instead their neutralizing capacity has been determined through analysis of tailings hydrogeochemistry (Nesbitt and Jambor 1998), or targeted acid-digest experiments (Jambor et al. 2002, 2007). Miller et al. (2010) presented a method to calculate the contribution of silicate to ANC (termed $ANC_{nc}$). It uses solution assay data for cations resulting from acid neutralization reactions of silicate minerals—principally Na, K, Ca, Mg and Al phases. Limitations of ABA procedures were outlined in White et al. (1999), Dobos (2000), Jambor (2003) and Weber et al. (2004) and are summarized below.

- $S_{Total}$ values may not account for different acid yields from species such as non-ferrous sulfides, chalcopyrite and arsenopyrite; in the absence of mineralogical data, the general assumption is that all S represents pyrite. Such an approach is considered conservative, as pyrite produces more acid per mole than these listed sulfides.
- ANC titration tests utilize fixed reaction stoichiometries to calculate acidity yield. However, for minerals such as pyrrhotite, a number of reaction pathways are available, not all producing the same acid yields.
- ANC values are affected by differences in titration protocols chiefly the sample particle size, amount of acid added, back titration endpoint and digestion duration.
- Errors may arise from deducing carbonate concentrations from total carbon values. The presence of organic carbon and/or graphite in the sample leads to overestimation of mineral carbonate and hence acid neutralizing capacity. Additionally, siderite is added to the ANC budget. This is a real problem in many coal and gold deposits, where siderite is the dominate carbonate material.
- ABA assumes that all ferrous ions are oxidized to ferric (that is, precipitated as ferrihydrite), that iron sulfosalts and other iron salts are not produced, and that all sulfides are oxidized to sulfates.
- In real samples that are partly or completely oxidized, sulfate sulfur is treated as sulfide sulfur, even though acid yields may be zero (from mineral species such as gypsum), or different from pyrite (such as from jarosite). This leads to conservative errors.
- ABA predicts the final result of completed reactions with the assumption that no significant chemical species are lost during the ‘reactions’. On a mine-site, intermediate products may be removed by leachates from the reacting solids.
- ABA assumes that, in the presence of excess acid, all available carbonate reacts. This may not be realistic, since coarse-grained calcite in waste-rock piles may be coated or ‘armoured’ by precipitated gypsum during early neutralization

reactions. Subsequently, acid will not directly contact the armoured calcite, leading to acidic leachates where none were predicted. This may be a major long-term issue.

- ABA is largely concerned with the balance between acid-producing and acid-consuming minerals. However, it does not yield any information on metal releases and concentrations in drainage waters.

### Net Acid Generation (NAG) Tests

Net Acid Generation (NAG) tests evaluate the ARD forming potential of a sample without separate estimation of MPA and ANC. This is achieved by using $H_2O_2$ to rapidly oxidize sulfide minerals, allowing the product to react with the acid neutralizing minerals present (Miller et al. 1997; Smart et al. 2002). A summary of the main types of NAG tests are given below.

- Single addition NAGtesting is the most widely used, and involves the addition of 250 ml of 15 % $H_2O_2$ to 2.5 g of pulverized sample in a 500 ml wide mouth conical flask, or equivalent. This is placed in a fume-hood and the sample is left to react until effervescing ceases, pending which the sample is heated for c. 2 h. The pH of the cooled liquor is taken (termed NAG pH), and then is titrated first to pH 4.5 as this is the starting pH of the solution, and then pH 7.0 using NaOH (if NAG pH > 2 then must be titrated with 0.1 M and if $\leq 2$ then 0.5 M). The NAG pH value is the more traditionally used value from this analysis and is used with NAPP values for waste classification. Limitations of this test include the effect of organic matter present in samples releasing organic acids and causing anomalously low pH values; and the temperature rise in this test causing catalytic decomposition of $H_2O_2$ before all reactive sulfides have oxidized. Considering these, Stewart (2004) proposed the development of 'advanced' NAG tests, the most common of which are summarized below.
- The sequential NAG (sNAG) test essentially involves repetition of the single addition NAG test. At the end of each NAG test stage (pre-titration with NaOH), the sample is filtered and the NAG pH and titrated acidity of the solution are measured. The NAG test is then repeated on the solid residue cyclically until the NAG pH > 4.5. The individual NAG acidities are then summed to give a total sequential NAG acidity in kg $H_2SO_4$/t (Stewart et al. 2006). This test is time consuming and labour-intensive, therefore only a small number of samples should be tested and cross-compared with single-additional NAG results. Furthermore, the quantity of $H_2O_2$ to be used in the tests is unpredictable, thus the cost of this test per sample cannot be precisely estimated.
- The multiple addition (mNAG) test is simpler than the sNAG test as it involves stepped addition of $H_2O_2$ to 2.5 g of sample in three intervals: 100, 100 and 50 ml. Between each addition the NAG solution is left to react and then heated to assist interaction of any acidity generated with the gangue before the next peroxide addition (Stewart 2004). The test is performed as if a single-addition

test after each measure of $H_2O_2$ (i.e. left to react, heated and cooled), and the NAG pH and titration steps are performed after the reaction of the final 50 ml measure of $H_2O_2$.

- The kinetic NAG test (kNAG) involves recording of temperature, pH and sometimes EC during a single addition NAG test to provide an indication of reaction kinetics (Smart et al. 2002; Stewart 2004). These data can provide an insight into the behaviour of the material under field conditions. The pH trend gives an estimate of the relative reactivity and may be related to prediction of lag times and oxidation rates similar to those measured in leach columns (Smart et al. 2002).

### Additional Static Test Methods

The carbonate bomb test is used to estimate the calcite contents of a sample as developed by Müller and Gastner (1971). Essentially the carbonate bomb is a 25 cm × 6 cm device to which a manometer calibrated in % $CaCO_3$ is attached. 1 g of dried and ground sample is placed into the main cylinder into which a smaller plastic container containing 5 ml HCl is carefully inserted. The gasket, cap and manometer are correctly attached and sealed and the bomb is then tipped to allow the sample and acid to react with a light shaking employed to ensure that all the rock powder comes into contact with the acid. Calcite and aragonite react immediately by effervescing strongly with the reaction completed after 10 s and a reading is taken. Dolomite reaction is much slower, if calcite and dolomite are both present, then a reading after 10–15 s yields calcite proportion and after 15 min dolomite. Hughes et al. (2007) used the carbonate bomb test as part of an assessment of the most effective and efficient field-investigation techniques for characterizing coal mine wastes. Results showed a high degree of correlation between Sobek ANC and Carbonate Bomb results ($R^2 = 0.97$), proving its use as a field-indicator of ANC which was found to be effectively used with paste pH data as a rapid field-based proxy for MPA.

The acid buffering characteristic curve (ABCC) method was initially developed by Miller and Jeffery (1995) to identify how effectively ANC has been calculated through routine methods (e.g. Sobek). Essentially, the test involves slow titration of a sample with acid, while continuously monitoring pH. ABCC results provide an indication of what portion of the ANC measured in a sample is readily available. The technique is useful in assessing whether a sulfidic sample with NAPP < 0 and NAG pH = 4.5 has enough readily available carbonate to render it non-acid producing (Smart et al. 2002). Stewart et al. (2006) refined this method by optimizing test configurations for ranges of the ANC values as the volume and concentration of HCl at each addition is varied according to set ANC ranges, but the time between additions (approximately 15 min) is kept constant. In addition, these authors also generated a set of standard carbonate curves for each ANC range. The carbonates tested were calcite, dolomite, ferroan dolomite, magnesite and siderite. In general,

high HCl volumes and concentrations are used for high ANC samples and low HCl volumes and concentrations are used for low ANC samples. Cumulative kg $H_2SO_4$/t added is plotted against pH measured to obtain the buffering curve. Examples of ABCC application are presented in Stewart et al. (2006).

## *Kinetic Tests*

Kinetic tests are dissolution tests conducted to aid prediction of drainage quality from mine wastes. They are either laboratory- or field-based with the main methods summarized in Table 3. They are performed after static tests, and are primarily used on samples classified as acid forming to measure the lag time to and longevity of acid formation. Samples classified as uncertain can also be tested to define their behaviour allowing for a definite classification to be assigned.

Humidity cell and column leach tests are the dominate laboratory based procedures. The ASTM 5744-96 and the MN DNR are the most widely used humidity cell procedures. A standard humidity cell is operated on a weekly cycle that comprised of 3 days of dry air, 3 days of moist air and a rinse with distilled water on the seventh day. These tests are designed to accelerate weathering and model rates of oxidation in the field as well as the chemical release (Lapakko 2002). A limitation of humidity cell tests is that they are conducted using a single, weekly flushing of a constant nature. However, precipitation at an actual mine site may vary significantly during wet and dry season. Additionally, humidity cell tests use a sufficiently large volume of water with reaction products expected to be removed. Removal of all reaction products may not occur in the field due to much lower water to rock ratios, incomplete flushing, and the occurrence of chemical reactions along the flow-path. Furthermore, equilibrium conditions expected in waste rock piles may not be realized in the test due to short contact times between the test solid and solution.

Column leach tests are less standardized than humidity cell tests and are recommended for use in conjunction with these by the USEPA (2003). They monitor leachate quality over time by cyclic (weekly or monthly) sampling. Data is gathered on the sulfide reactivity, oxidation kinetics, metal solubility and the leaching behaviour of the test materials. As an alternative, Smart et al. (2002) developed the free draining column leach test. Lesser used kinetic tests include the Soxhlet, BCRC and shake flask and batch reactor tests. The latter two tests include steps to examine the impact of mine waste bacteria on acid formation.

Field tests are identified as the most accurate method of testing a mine waste sample, however they are costly, and are required to evolve over long time periods (e.g. decades). The benefit is that mine wastes are exposed to the correct climatic and hydrological conditions; however, a significant limitation is that they are not established early enough to aid with waste planning at the pre-feasibility or feasibility stages of mine operation. Field based tests can either be small scale (e.g. 2 m $\times$ 2 m) or large scale trials piles such as those constructed at the Freeport,

**Table 3** Main kinetic tests commonly used in determining ARD potential (values shown in US dollars; United States Environmental Protection Agency 2003)

| Humidity cells | Soxhlet extraction | Column tests | BC research confirmation | Batch reactor | Field tests |
|---|---|---|---|---|---|
| *Summary of test method* | | | | | |
| 2.38 mm particle size<br>200 g of rock exposed to 3 days dry air, 3 days humidified air, and rinsed with 200 mL on day seven<br>Cost: $425–850 | Particle size not presented<br>T = 70 °C<br>T = 25 °C<br>Water passed through sample is distilled and recycled through sample<br>Cost: $200–500 | Variable particle size<br>Columns containing mine waste are leached with discrete volumes or recirculating solutions<br>Cost: dependant on scale | −400 mesh particle size<br>15–30 g added to bacterially active solution at pH 2.2 to 2.5, T = 35 °C.<br>If pH increases, sample is non-acid producer. If pH decreases, ½ original sample mass is added in each of the two increments<br>Cost: $170–340 | −200 mesh particle size<br>Sample/water slurry is agitated<br>200 g/500 mL<br>Cost: $425–850 | Field scale particles<br>800–1300 metric ton test piles constructed on liners flow and water quality data collected. Some tests which began in 1977 are still ongoing<br>Costs are initially high, subsequent costs are comparable |
| *Advantages* | | | | | |
| Models AP and NP well and models wet/dry<br>Approximates field conditions and rate of acidity per unit of sample<br>Moderate ease of interpreting results<br>Large data sets are generated | Results in short time, and assessment of interaction between AP and NP | Models AP and NP<br>Models effect of different rock types<br>Models wet/dry and models different grain sizes | Simple to use<br>Low cost<br>Assesses potential for biological leaching | Able to examine many samples simultaneously and relatively simple equipment | Uses actual mine waste under environmental conditions can be used to determine drainage volume mitigation methods can be tested<br>Evolved over long time periods (decades) |
| *Disadvantages* | | | | | |
| Moderate-hard to set-up<br>Results take long time, and some special equipment is needed | Moderate-hard to use and need special equipment<br>Moderate-hard interpretation in developmental stage and relationship to natural processes not clear | Difficult interpretation<br>Not practical for large number of samples<br>Large volume of sample<br>Loss of data generated, long time and potential problems; uneven leachate application | Duration of test longer than most tests, with some special equipment required<br>Difficult interpretation if pH change is small<br>Does not model initial AP step, and long time for pH to stabilize | Subject to large sampling errors and lack of precision | Expensive initial construction |

Indonesia (Andrina et al. 2006) and the Diavik diamond mine, Canada (Smith et al. 2009). Large scale piles require installation of instrumentation including thermistors and lysimeters to monitor the in-pile geochemical conditions. Leachates collected from these piles are compared against laboratory based geochemical tests to check their accuracy. These piles can also be used to test potential remediation methods. For example, Andrina et al. (2006) examined various methods of limestone addition and different covers and their impact on acid formation.

A potential error in predicting ARD likelihood and risk from kinetic tests is the precipitation of minerals like gypsum during kinetic testing. Precipitation of this removes calcium and sulfate from solution. Calcium in leachate reflects the rate of neutralizing potential dissolution, and aqueous sulfate indicates the rate of acid formation. Calculations indicate that the precipitation of as little as 15–30 % of gypsum can lead to incorrect predictions of high ARD likelihoods (Morin and Hutt 1998). Data from the International Kinetic Database suggests that this error is rare, however appropriate kinetic-test closedown procedures are required to verify whether secondary minerals have accumulated (Morin and Hutt 1998). Misinterpretation of kinetic test data is perhaps the biggest error, with lower ARD likelihoods predicted (Morin and Hutt 1998). Additionally, there is a general lack of standardization with these tests, which whilst allowing for flexibility in experimental design, comparisons of results from different kinetic trials becomes complicated. However, despite this kinetic tests are the best geochemical tests to use to predict ARD formation and metal leaching from a sample.

## *Mineralogical Characterization*

The mineralogy of a sample has the strongest influence on oxidation processes. Therefore, a clear understanding of the mineralogy is required to accurately predict the potential for ARD formation. In many instances where ARD systems are studied in order to assess or predict water quality, mineralogy is largely ignored. The reasoning for this is that detailed environmental mineralogy is regarded as time consuming and expensive, and additionally it requires the employment of a dedicated environmental mineralogist. In recent years, it has been acknowledged that mineralogical characterization is necessary as shown in the wheel approach (Morin and Hutt 1999). Most recently, the GARD Guide (2016) recognized the importance of characterizing mineralogy whilst logging drill core (i.e., evaluating the sulfide and carbonate content), and as part of kinetic testing (Parbhakar-Fox et al. 2013).

Mineralogy can be assessed using a range of tools ranging from the simple (e.g. optical microscopy) to the advanced (e.g. laser ablation ICPMS). Selection of the most appropriate tools for use is dependent on what aspect of the mineralogy is sought to be understood. For example, is the bulk mineralogical composition required for calculating the calcite:sulfide ratio (Paktunc 1999), or is the elemental composition of a selected mineral required to understand its potential for weathering (e.g. iron in sphalerite)? Further considerations and examples of their

application in ARD prediction studies are given in Blowes and Jambor (1990), Paktunc (2001), Lapakko (2002), Jambor (2003), Raudsepp and Pani (2003), Weber et al. (2005), McLemore et al. (2009), Al et al. (2007), Diehl et al. (2007), Ohlander et al. (2007), Savage et al. (2008), Cook et al. (2009), Weisener and Weber (2010) and Parbhakar-Fox et al. (2011).

## *Waste Classification*

Samples are classified in terms of their acid forming potential following extensive geochemical, static, kinetic and mineralogical characterization. There are many classification methods employed, therefore only those used routinely used are presented. Sulfide and calcite contents can be used to classify samples based on mineralogy as shown in Paktunc (1999). However, more commonly classifications are based on static geochemical results. As stated earlier, NAPP, NAG and NPR analyses are three methods used to calculate the acid-forming or acid-neutralizing potential of a sample following the measurement of MPA and ANC. NAPP values >20 kg $H_2SO_4$/t indicate that the rock unit has acid forming potential. In Australia, the convention is to use NAPP versus NAGpH data to classify samples after static testing. Samples are classified as:

PAF = potentially acid forming: when NAPP > 0 kg $H_2SO_4$/t and pH < 4.5
NAF = non-acid forming: when NAPP < 0 kg $H_2SO_4$/t and pH > 4.5
UC = uncertain: when NAPP < 0 kg $H_2SO_4$/t but pH < 4.5; or NAPP > 0 kg $H_2SO_4$/t and pH > 4.5

$S_{Total}$ values are also consulted when evaluating these classifications. Miller (1996) and Smart et al. (2002) recommended additional classifications (e.g., PAF high-capacity, PAF-low capacity), however, in subsequent publications these terms are infrequently used, with the use of only PAF, NAF and UC favoured. As stated, samples classified as UC are subjected to detailed mineralogical classification and advanced geochemical testing. Alternative classification methods are presented in Weber et al. (2006) and Hughes et al. (2007). Weber et al. (2006) consider NAGpH against paste pHto provide an indication to the lag time to acid formation, thus classifying the risk. In reality, several classification methods should be used to cross-check the static test data and should be performed alongside interpretation of geochemical and mineralogical data. Kinetic test data are not classified in the same manner as samples have already been classified prior to testing. Most waste rock schemes are based on classifications from static test data. However, these schemes are limited to just three or four categories of waste rock. Whether or not they accurately reflect the geological variability is not yet known. Formal establishment of additional waste categories following static testing would be one way in which waste classification could be improved, ultimately resulting in better mine planning.

## Conclusions

The prediction of ARD from sulfidic rocks and mineral processing products is possible using geological modeling, mineralogical descriptions, geochemical characterization, static and kinetic tests. Since the 1970s, static tests have been and still are standard industry practice.

The most widely used static method quantitatively balances the acid generated from the oxidation of sulfides against the acid consumption of carbonates and other minerals (i.e. acid-base accounting). Numerous static tests have been developed but all of them are screening methods to evaluate particular samples (e.g. acid-base accounting, pH methods, net acid generation tests, carbonate bomb test acid buffering characteristic curve method). As waste and drainage predictors, static tests have been accurate in some cases and misleading in others. These tests may under- or overestimate the acid production of a particular sample. As a result, numerous authors have proposed improvements and alternatives to existing static tests. These proposed methods seek to provide better estimates of sulfur speciation and acid producing minerals in the waste.

These data are evaluated using a range of waste classification methods, with samples classified as potentially acid forming (PAF), non-acid forming (NAF) or uncertain (UC). Additional classes have been used in individual studies (PAF high-capacity, PAF-low capacity), however their use has yet to be formally established. These values are used to calculate the Net Acid Producing Potential (NAPP) Net Neutralizing Potential (NNP) or Neutralizing Potential Ratio (NPR), depending on the requirements imposed by the mine regulator.

Results from static testwork are used to help select samples for long-term kinetic weathering tests, which are studied as drainage quality predictors. A wide-range of kinetic tests exist (e.g. humidity cells, column leach tests, soxhlet extraction), with test selection dependent on guidelines set by the mine regulator. The details of kinetic tests differ, but all methods attempt to mimic cyclic wetting/drying and flushing of wastes. They can run for a minimum of weeks, but the most useful results are obtained if these are run for several years.

The reason for the failure of static teststo accurately predict sulfide oxidation and ARD appears to be multi-fold—partly because some of the existing static tests have inherent limitations. The greatest criticism of static laboratory methods is the vast differences between testing conditions and the field. However, despite their limitations, they provide mine operators with some guidance and an insight into potential ARD formation.

One of the greatest challenges of ARD prediction is the successful upscaling of laboratory results to field scale. Currently, there is no consensus on which static method/test most accurately reflects field conditions. Questions have arisen regarding the length of laboratory test times and extrapolation to field weathering time. Research therefore continues on improving predictive static tests and methods. In particular, cost-effective static tests which consider all factors including biologicaland geometallurgical properties must be developed with a new prediction

methodology globally established (Parbhakar-Fox and Lottermoser 2015). Such a protocol must consider or speed up weathering time, address the known limitations of existing static testing procedures, and ultimately represent more accurately the actual waste behaviour in the long term and real field conditions.

## References

Al TA, Blowes DW, Martin CJ, Cabri LJ, Jambor JL (2007) Aqueous geochemistry and analysis of pyrite surfaces in sulphide-rich mine tailings. Geochim Cosmochim Acta 61:2353–2366

Andrina J, Wilson GW, Miller S, Neale A (2006) Performance of the acid rock drainage mitigation waste rock trial dump at Grasberg mine. In: Proceedings from the 7th international conference on acid rock drainage, pp 30–44

Bezaazoua B, Bussieré B, Dagenais AM, Archambault M (2004) Kinetic tests comparison and interpretation for prediction of the Joutel tailings acid generation potential. Environ Geol 46:1086–1101

Blowes DW, Jambor JL (1990) The pore-water geochemistry and the mineralogy of the vadose zone of sulphide tailings, Waite Amulet, Quebec, Canada. Appl Geochem 5:327–346

Borden RK (2003) Environmental geochemistry of the Bingham Canyon porphyry copper deposit, Utah. Environ Geol 43:752–758

Comarmond J (1997) Chemical methods for predicting the acid mine drainage/acid rock drainage potential of mine wastes in Australia. Environmental division, ANSTO. http://www.environment.gov.au/ssd/publications/ssr/pubs/ssr125-appendices.pdf

Cook NJ, Ciobanu CL, Pring A, Skinner W, Danyushevsky L, Shimizu M, Saini-Eidukat B, Melcher F (2009) Trace and minor elements in sphalerite: a LA-ICP-MS study. Geochim Cosmochim Acta 73:4761–4791

Diehl SF, Koenig AE, Hageman PL, Smith KS, Fey DL, Lowers HA (2007) From the micro to the macroscale: a textural and chemical perspective of characterising waste-rock material. In: Proceedings from the 2007 society for mining, metallurgy and exploration (SME) annual meeting and exhibit, and the 109th national western mining conference, Denver, Colorado. Society for Mining, Metallurgy and Exploration, Littleton, pp 7–21

Dobos SK (2000) Potential problems with geologically uncontrolled sampling and the interpretation of chemical tests for waste characterisation and ARD prediction. In: Proceedings from the 4th Australian ARD workshop on acid and metalliferous mine drainage. Australian Centre for Minerals Extension and Research, Brisbane, pp 25–29

Downing BW, Giroux G (1993) Estimation of a waste rock ARD block model for the Windy Craggy massive sulphide deposit, northwestern British Columbia. Explor Min Geol 2:203–215

Downing BW, Madeisky HE (1997) Lithogeochemical methods for acid rock drainage studies and prediction. Explor Min Geol 6:367–379

Du Bray EA (1995) Preliminary compilation of descriptive geoenvironmental mineral deposit models. United States Geological Survey, Open-file Report, pp 95–831

Ficklin WH, Plumlee GS, Smith KS, McHugh JB (1992) Geochemical classification of mine drainages and natural drainages in mineralized areas. In: Proceedings from the 7th international water-rock interaction conference. Park City, Utah, pp 381–384

GARD (Global Acid Rock Drainage) Guide (2016) The international network for acid prevention (INAP). http://www.gardguide.com/

Hakkou R, Bezaazoua M, Bussiere B (2009) Laboratory evaluation of the use of alkaline phosphate wastes for the control of acidic mine drainage. Mine Water Environ 28:206–218

Hughes J, Craw D, Peake B, Lindsay P, Weber P (2007) Environmental characterisation of coal mine waste rock in the field: an example from New Zealand. Environ Geol 52:1501–1509

Hutt NM, Morin KA (2000) Observations and lessons from the International Static Database (ISD) on neutralizing capacity. In: Proceedings from the 5th international conference on acid rock drainage, vol 1. Society for Mining, Metallurgy and Exploration, Littleton, pp 603–611

Jambor JL (2003) Mine-waste mineralogy and mineralogical perspectives of acid-base accounting. In: Jambor JL, Blowes DW, Ritchie AIM (eds) Environmental aspects of mine wastes. Mineralogical Association of Canada, Short Course Series 31, pp 117–145

Jambor JL, Dutrizac JE, Groat L, Raudsepp M (2002) Static tests of neutralization potentials of silicate and aluminosilicate minerals. Environ Geol 43:1–17

Jambor JL, Dutrizac JE, Raudsepp M (2006) Comparison of measured and mineralogically predicted values of the Sobek Neutralization Potential for intrusive rocks. In: Proceedings from the 7th international conference on acid rock drainage, pp 820–832

Jambor JL, Dutrizac JE, Raudsepp M (2007) Measured and computed neutralization potentials from static tests of diverse rock types. Environ Geol 52:1019–1031

Jamieson HE, Robinson C, Alpers CN, Nordstrom DK, Poustovetov A, Lowers HA (2005) The composition of coexisting jarosite-group minerals and water from the Richmond mine, Iron Mountain, California. USGS Published Research 475. http://digitalcommons.unl.edu/usgsstaffpub/475

Johnson DB, Hallburg KB (2005) Acid mine drainage, remediation options. Sci Total Environ 338:3–14

Kwong YTJ (1993) Prediction and prevention of acid rock drainage from a geological and mineralogical perspective. MEND report 1.32.1, Ottawa, Ontario

Lapakko KA (2002) Metal mine rock and waste characterization tools: an overview. Posted on the acid drainage initiative—Metal Mining Sector. www.mackay.unr.edu/adti

Lawrence RW, Scheske M (1997) A method to calculate the neutralization potential of mining wastes. Environ Geol 32:100–106

Lengke MF, Davis A, Bucknam C (2010) Improving management of potentially acid generating waste rock. Mine Water Environ 29:29–44

McLemore V, Heizler L, Donahue K, Dunbar N (2009) Characterization of weathering of mine rock piles: example from the Questa Mine, New Mexico, USA. In: Proceedings from the 8th international conference on acid rock drainage, Skelleftea, pp 1–10

Miller S, Jeffery J (1995) Advances in the prediction of acid generating mine waste materials. In: Proceedings from the 2nd Australian ARD workshop on acid and metalliferous mine drainage. Australian Centre for Minerals Extension and Research, Brisbane, pp 33–43

Miller SD (1996) Advances in acid mine drainage prediction and implications for risk management. In: Proceedings of the 3rd international and 21st annual minerals council of Australia, vol 1, Environmental Workshop, pp 14–18

Miller SD, Robertson A, Donahue T (1997) Advances in acid drainage prediction using the Net Acid Generation (NAG) test. In: Proceedings from the 4th international conference on acid rock drainage, Vancouver, pp 533–549

Miller SD, Stewart W, Rusdinar Y, Schumann R, Ciccarelli JM, Li J, Smart R (2010) Methods for estimation of long-term non-carbonate neutralization of acid rock drainage. Sci Total Environ 408:2129–2135

Mills C, Robertson A, Shaw S (2015) Acid rock drainage at Enviromine. http://technology.infomine.com/enviromine/ard/home.htm

Morin KA, Hutt NM (1998) Kinetic test and risk assessment for ARD. In: Proceedings of the 5th annual BC metal leaching and ARD workshop, Vancouver, pp 1–10

Morin KA, Hutt NM (1999) Internet case study #15: prediction of minesite-drainage chemistry using the "wheel" approach. http://www.mdag.com/case_studies/cs11-99.html

Morin KA, Hutt NM (2009) Internet case study #32: on the nonsense of arguing the superiority of an analytical method for neutralization potential. www.mdag.com/case_studies/cs32.html

Müller G, Gastner M (1971) The Karbonate-Bombe, a simple device for determination of the calcium carbonate content in sediments, soils and other minerals. N Jb Miner Mh 10:466–469

Nesbitt HW, Jambor JL (1998) Role of mafic minerals in neutralizing ARD, demonstrated using a chemical weathering methology. In: Cabri LJ, Vaughan DJ (eds) Short course handbook on ore and environmental mineralogy. Mineralogical Association of Canada 27, pp 403–421

Ohlander B, Müller B, Axelsson M, Alakangas L (2007) An attempt to use LA-ICP-SMS to quantify enrichment of trace elements on pyrite surfaces in oxidizing mine tailings. J Geochem Explor 92:1–12

Paktunc AD (1999) Mineralogical constraints on the determination of neutralising potential and prediction of acid mine drainage. Environ Geol 39:103–112

Paktunc AD (2001) MODAN a computer program for estimating mineral quantities based on bulk composition, Windows version. Comput Geosci 28:883–886

Parbhakar-Fox A, Lottermoser BG (2015) A critical review of acid rock drainage processes and practices. Min Eng 82:107–124

Parbhakar-Fox A, Edraki M, Walters S, Bradshaw D (2011) Development of a textural index for the prediction of acid rock drainage. Min Eng 24:1277–1287

Parbhakar-Fox A, Lottermoser BG, Bradshaw D (2013) Evaluating waste rock mineralogy and microtexture during kinetic testing for improved acid rock drainage prediction. Min Eng 52:111–124

Plumlee GS (1999) The environmental geology of mineral deposits. In: Plumlee GS, Logsdon MJ (eds) The environmental geochemistry of mineral deposits part A: processes, techniques and health issues. Rev Econ Geol 6A:71–116

Price WA (2009) Prediction manual for drainage chemistry from sulphidic geologic materials. CANMET Mining and Mineral Sciences Laboratories, Canada

Raudsepp M, Pani E (2003) Application of Rietveld analysis to environmental mineralogy. Mineralogical Association of Canada, Short Course 3, pp 165–180

Savage KS, Stefan D, Lehner S (2008) Impurities and heterogeneity in pyrite: influences on electrical properties and oxidation products. Appl Geochem 23:103–120

Seal II RR, Foley NK, Wanty RB (2002) Introduction to geoenvironmental models of mineral deposits. In: Seal II RR, Foley NK (eds) Progress on geoenvironmental models for selected mineral deposit types, US Geological Survey Open-File Report 02-195

Smart R, Skinner WM, Levay G, Gerson AR, Thomas JE, Sobieraj H, Schumann R, Weisener CG, Weber PA, Miller SD, Stewart WA (2002) ARD test handbook: project P387A, prediction and kinetic control of acid mine drainage. AMIRA International Ltd., Melbourne

Smith LJ, Neuner M, Gupton M, Moore M, Bailey BL, Blowes DW, Smith L, Sego DC (2009) Diavik waste rock project: from the laboratory to the Canadian arctic. In: Securing the future and 8th ICARD: proceedings of the conference, Skellefteå, Sweden, pp 40–50

Stewart W (2004) Development of acid rock drainage prediction methodologies for coal mine wastes. PhD. thesis, University of South Australia, Adelaide

Stewart WA, Miller SD, Smart R (2006) Advances in acid rock drainage (ARD) characterisation of mine wastes. In: Proceedings from the 7th international conference on acid rock drainage, Missouri, pp 2098–2119

United States Environmental Protection Agency (2003) Nationwide identification of hardrock mining sites. Report 2004-P-00005

Verplank PL, Van Gosen BS, Seal RR, McCafferty AE (2014) A deposit model for carbonatite and peralkaline intrusion-related rare earth element deposits. U.S. Geological Survey Scientific Investigations Report 2010-5070-J

Weber PA, Hughes JB, Conner, LB, Lindsay P, Smart R.St.C (2006) Short-term acid rock drainage characteristics determined by paste pH and kinetic NAG testing. In: 7th International Conference on Acid Rock Drainage (ICARD), St. Louis, North America, Cypress prospect, New Zealand, pp 2289–2310

Weber PA, Thomas JE, Skinner WM, Smart St RC (2004) Improved acid neutralisation capacity assessment of iron carbonates by titration and theoretical calculation. Appl Geochem 19: 687–694

Weber PA, Thomas JE, Skinner WM, Smart St RC (2005) A method to determine the acid-neutralisation capacity of rock samples. Can Mineral 43:1183–1192

Weisener CG, Weber PA (2010) Preferential oxidation of pyrite as a function of morphology and relict texture. NZ J Geol Geophys 53:22–33

White WW, Lapakko KA, Cox RL (1999) Static test methods most commonly used to predict acid mine drainage: practical guidelines for use and interpretation. In: Plumlee GS, Logsdon MJ (eds) The environmental geochemistry of mineral deposits part A: processes, techniques, and health issues. Rev Econ Geol 6A:325–338

# Micro-analytical Technologies for Mineral Mapping and Trace Element Deportment

**Ron F. Berry, Leonid V. Danyushevsky, Karsten Goemann, Anita Parbhakar-Fox and Thomas Rodemann**

**Abstract** Quantifying the texture, mineralogy and mineral chemistry of rocks in the mine environment is required to predict the value of a deposit and maximize extraction efficiency. Scanning electron microscopy supported by recognition of minerals by characteristic X-ray emissions is the preferred mineral mapping method in the mining industry at present. This system is fully mature and supported by highly optimized software. Laser Raman mapping may compete for some of this space in the future. Very coarse scale mineral maps are possible from drill core images but these cannot be used to measure the key parameters required for most mine planning. Trace elements can be highly concentrated in rare minerals so that they are easy to detect but very difficult to accurately measure due to sampling problems, or they may be very dispersed and difficult to detect at all. There are a range of tools available to support trace element deportment and most studies will need to use more than one methodology. The key new development of the last decade is the emergence of laser ablation inductively coupled plasma mass spectrometry for the measurement of most elements at sub-ppm level. There are still many trace and minor elements for which accurate models of deportment are extremely difficult.

R.F. Berry (✉) · L.V. Danyushevsky · A. Parbhakar-Fox
School of Physical Sciences, University of Tasmania, Private Bag 79,
Hobart, TAS 7001, Australia
e-mail: Ron.Berry@utas.edu.au

L.V. Danyushevsky
e-mail: l.dan@utas.edu.au

A. Parbhakar-Fox
e-mail: Anita.Parbhakar@utas.edu.au

K. Goemann · T. Rodemann
Central Science Laboratory, University of Tasmania, Private Bag 74,
Hobart, TAS 7001, Australia
e-mail: Karsten.Goemann@utas.edu.au

T. Rodemann
e-mail: Thomas.Rodemann@utas.edu.au



B. Lottermoser (ed.), *Environmental Indicators in Metal Mining*,
DOI 10.1007/978-3-319-42731-7_4

## Introduction

Quantifying the texture, mineralogy and mineral chemistry of rocks in the mine environment contributes to the prediction of three components of mine planning: processing performance, value of mine products and the environmental cost of the project. The element deportment explains the grade and recovery of mine concentrates. The value of the concentrate is also affected by the presence of penalty elements. For example in iron ore, Al and P are significant penalty elements. In base metal concentrates typical penalty elements are Sb, As, F and Hg. The number of penalty elements in smelting is increasing and the grade at which they apply is decreasing as environmental monitoring at the smelting site becomes more stringent.

For environmental assessment of mining we need to focus on the characterization of mine waste and prediction of mineral and element behaviour in the environment. This is a complex area (Smith and Huyck 1999; Plumlee 1999). There are environmental challenges associated with all the mine waste streams: process water, mine water, mine waste, dust and tailings. The environmental impact of these streams is strongly affected by the mineralogy and trace element composition of both the ore and waste components of the mine.

This chapter concentrates on how mineral mapping and trace element methods can contribute to a discussion of the methods and impacts of mining. It is restricted to methods that are employed by industry and researchers now, or which are on the fringe of economic application. The methodologies include conventional mineral mapping techniques (optical microscopy, SEM/EDS, infrared) and emerging technologies (Laser Raman, X-ray CT). In trace element mapping the conventional scanning electron microscope (SEM) based energy dispersive spectroscopy (EDS) and wavelength dispersive spectroscopy (WDS) element mapping is compared with micro-X-ray fluorescence, micro-proton-induced X-ray emission (PIXE), and laser ablation inductively coupled plasma mass spectrometer (LA-ICPMS). More sophisticated analytical tools such as X-ray absorption near-edge spectroscopy (XANES), synchrotron-based microanalysis and surface techniques (e.g. X ray photoelectron spectroscopy) are not included. The aim is to promote a better understanding of how mineralogical information is collected and used for problem solving in the mining industry.

## Mineral Mapping

Mineral mapping is carried out at a range of scales. There is a constant tension between the need to get high precision results on a sample and the extent to which the samples measured are representative of the material that will be processed. In the past, studies have failed to properly represent the spatial variability of the orebody. A relatively small number of samples have been well characterized. Sampling statistics were carefully monitored to make sure the sample sent for measurement

was properly represented but very little attention was paid to whether this sample was representative of the ore and waste that may be produced across the life of the mine.

More recently, this problem has been realized and attempts have been made to use less precise but cheaper tests to define the variability before large scale sampling is carried out for robust testing. This problem has not yet been solved. Mineralogy tests are available for major minerals but textural attribute and trace mineral abundance measurements are very expensive to carry out in the numbers required to define the ore body variability.

Petrology and many geology studies are based on intact textures. They provide a first look at the material but cannot provide the statistical support needed for rigorous predictions of mine performance. Representivity requires that tests are carried out on particles. Most authors (e.g. Geelhoed 2011) suggest that for particulate material a reasonable sampling error is achieved where 1000s of particles are measured, and more are required where a trace element, such as Au, is concentrated in a trace mineral.

When measuring grain size and shape parameters, it is important not to modify the grain size in the sample preparation. The usual recommendation is to have a particle size at least five times the largest grain size to be measured. For example, in liberation prediction it is important to recognise grains coarser than the mill grind size. Putting these two requirements together means that the particle size studied must be greater than 0.5 mm (cf. $\sim$1 mm of Sutherland 2007). In a sample sieved to +0.6−1.2 mm, a typical grain mount has 200–500 particles. Berry and Hunt (2011) suggest that the error on the P50 grain size estimate for chalcopyrite was about 10 % relative in a low grade Cu deposit using a single grain mount.

Mineral mapping is expensive and should be used with care. The experimental design should include a clear statement of what data is required that can only be generated from mineral maps. Grain size distribution can be the rate controlling factor for reactions in the environment but often modal mineralogy is more important. Bulk methods for mineralogy have significant advantages over mineral maps in estimating modal mineralogy. For accurate mineral mapping the scanning electron microscope remains the method of choice but for the spatial variation of the deposit a cheaper protocol is required and in some circumstance optical microscopy or even classification of drill core images may be useful.

## *Automated Optical Microscopy*

Generation of mineral maps by optical methods has a long history, but early attempts were limited by the lack of digital images and computing capacity. Modern optical analysis of mineral textures was summarized by Higgins (2006). Automated recognition has largely been applied to opaque minerals (e.g. Pirard 2004; Pirard et al. 2007; Lane et al. 2008). However, transparent mineral can be analysed using object-oriented multi-spectral methods (Berry et al. 2008).

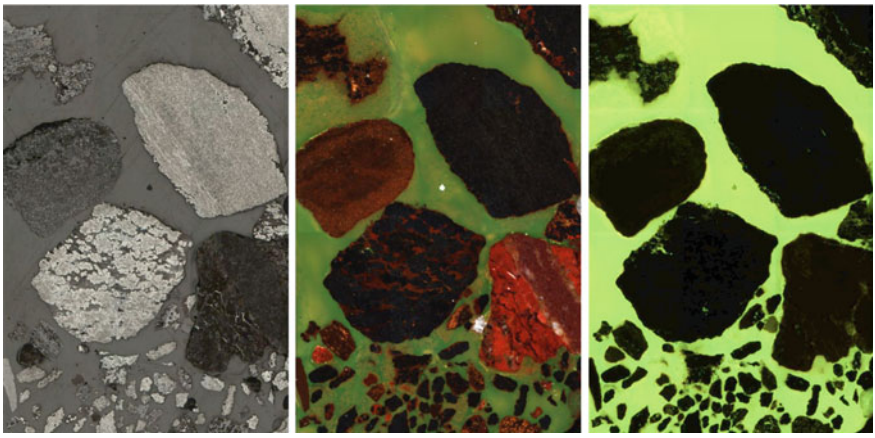

**Fig. 1** Grain mount of iron ore as polished block. *Left* reflected light, *Middle* reflected light cross polarized, *Right* fluorescent image (field of view 1.5 mm wide) (color figure online)

Automated optical mineral identification requires a microscope with a high precision stage (position reproducibility better than 1 micron) that allows direct tiling of frames and good registration of multiple images. For large scale imaging a 5× objective lens gives 10 μm resolution. This provides the best balance between resolution, depth of focus and field of view. For best results great care is required with colour balance and shading correction. Multiple transmitted and reflected light images are required for accurate classification. For particle mounts a fluorescence dye can be added to the resin to aid recognition of particle boundaries (Fig. 1). Classification accuracy varies from 85 to 95 % in simple systems with less than eight significant minerals. Trace mineral recognition is not recommended unless the mineral has outstanding optical properties.

The optical mineral mapping protocol occupies a discrete niche in the environmental geometallurgy toolset. In a few cases such as separating hematite from magnetite and marcasite from pyrite, optical microscopy is better than SEM-EDS mapping, which could prove particularly useful in acid rock drainage (ARD) prediction studies. Where only the opaque minerals need to be identified then optical microscopy can be effective. If the aim is the recognition of both transparent and opaque minerals, and especially if there are less than ten minerals involved, then object-oriented multi-spectral software provides an efficient environment for the development of the complex rules base required.

## *SEM-EDS Mapping*

Scanning electron microscopes (SEM) with fast energy dispersive X-ray detectors (EDS) are currently the method or choice for mineral mapping in the minerals

industry (e.g. Goodall and Scales 2007). The SEM has a high resolution with an excellent depth of field, so it is easy to map quickly at a large range of magnifications while the sample stays in focus. The usual sample is a grain mount (particles) with a polished surface coated with carbon. The main limit to mapping resolution is the interaction volume between the electron beam and the sample. For a typical 15–25 keV electron beam this is up to 5 µm diameter and 5 µm deep. For higher resolution a lower accelerating voltage is required but can make recognition of the minerals using characteristic X-rays more difficult as the K· X-ray lines of many elements are not activated at this electron energy. At 7 keV the interaction volume is 0.3–0.5 µm across, depending on mineral density and mean atomic number.

The standard image on a SEM is the secondary electron (SE) image. The SE image is based on low energy electrons that are the result of inelastic scattering. SE images predominantly show topography which is of little use in mineral mapping. However, it can be useful in recognising if bacterial catalysis of ARD has taken place, with pits seen on pyrite mineral surfaces, or to observe morphological changes during ARD evolution (e.g., Weber et al. 2004). An alternative image available on most SEMs is the back scattered electron (BSE) image which is strongly controlled by the sample mean atomic number (Howell et al. 1998). This image has lower sensitivity to surface imperfections and topography, but a high quality final polish of the sample surface (e.g. 0.25 micron diamond) are still required to prevent topographical information masking compositional variations. It provides a robust basis for mineral mapping (Fig. 2). The BSE image is based on high energy primary electrons re-emerging from the sample surface with some of their energy left. Its application in environmental characterization studies is well documented (e.g., Weisener and Weber 2010; Smart et al. 2010).

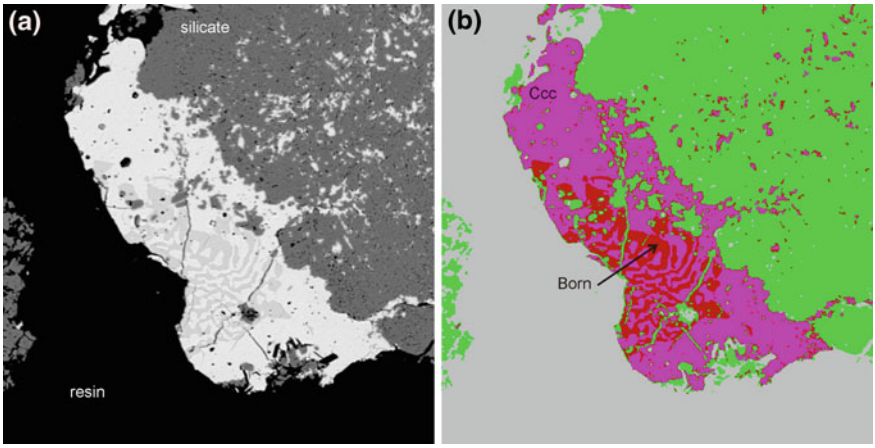


**Fig. 2** **a** BSE map of vermicular bornite in chalcocite. **b** Classification of sulfides (Ccc-chalcocite, Born-bornite) based on BSE intensity (color figure online)

Major advances in beam current and detectors have led to substantial improvements in SEM-EDS mapping over the last 20 years. There are two commonly used software solutions for mineral mapping:

(a) Collect an X-ray spectra at every pixel (Gottlieb et al. 2000), or
(b) Use a BSE map to recognize objects and then collect the X-ray spectra from each object (Gu 2003; Fandrich et al. 2007).

The former method is more robust but the second is quicker. All SEM-EDS methods require a mineral spectra library to undertake the classification step, i.e. matching a spectrum obtained from an X-ray analysis of the unknown to one stored in the mineral spectra library. The library is key resource that has to be established for each project. While library spectra can be collected with moderate count times, during the analysis the count time for each spectrum is a key decision which defines the speed and accuracy of the analysis.

## *Laser Raman Spectroscopy*

Raman scattering is the inelastic scattering of photons. When photons are scattered from an atom or molecule, most photons are elastically scattered (Rayleigh scattering). About 1 in 10 million photons are scattered by an excitation, with the scattered photons having an energy different from the incident photons by the energy level of one of the electrons involved in chemical bonding in the material. These differences are the same as the absorption energies in infrared spectroscopy but are measured as a difference from the incident laser light energy rather than at a fixed wavelength. Thus electron energy differences that would normally be far into the infrared can be moved to the visible light range and the spatial resolution of laser Raman analysis defined by the spot size of the laser beam rather than the optical resolution of infrared light. The Raman effect differs from the process of fluorescence. In fluorescence, the incident light is completely absorbed and the fluorescence photon is emitted after a resonance lifetime. Fluorescent light is a feature of the material and does not change with the laser frequency.

Laser Raman spectroscopy is a rapidly developing field in mineralogy. Raman spectroscopy is used to identify a wide variety of minerals and, in some instances, to provide chemical and structural information (Das and Henry 2011). It is useful for mineral identification across the whole range of minerals: silicates, oxides and sulfides. It has spatial resolution down to 1 μm. However, historically, this technology was too slow for routine mapping functions. Recently, a new generation of fast-mapping laser Raman spectrometers have been released with mapping rates of 50 ms/pixel. This rate is similar to the SEM-EDS mapping systems 15 years ago, when the first SEM-EDS software was evolving. A modern Raman instrument is a desktop machine based around a conventional optical microscope. Raman

spectroscopy is a low-cost, rapid, high-resolution technique which requires minimal sample preparation and is well suited to mine waste recognition (Levitan et al. 2009; Stefaniak et al. 2009; Das and Henry 2011).

Polymorphs such as pyrite and marcasite have the same chemical formula and identical composition. They cannot be differentiated by normal SEM-EDS mapping. However, marcasite is more reactive than pyrite and the proportion of marcasite is significant in mineral processing and environmental impact of mining. The Raman spectrum of marcasite is different from pyrite (Hope et al. 2001).

The presence of carbonaceous material is important in predicting leach extraction behaviour (Helm et al. 2009) and $fO_2$ buffering potential of mine waste. Carbonaceous material is easily recognized by Raman spectroscopy (Wopenka and Pasteris 1993) but not by SEM-EDS mapping. Mapping of carbonaceous material is feasible (Fig. 3), but care must be taken in selection of laser frequency to avoid fluorescence.

Raman spectroscopy is increasingly being used in the analysis of oxidized waste materials. It can be used to identify a wide range of environmentally sensitive minerals such as arsenates (Filippi et al. 2007, 2009). It also has potential application to the recognition of dust mineralogy (e.g. Huang et al. 2013) but few examples are publicly available.

## *X-Ray CT*

X-ray computed tomography (X-ray CT) was initially implemented in the medical field, and is an emerging technology in mineral mapping (Kyle and Ketcham 2015). The technology is developing dramatically from a purely research interest 10 years ago to active application in porosity mapping (Knackstedt et al. 2009) and diamond search (Firsching et al. 2012) today. Gold deportment is likely to be the next widespread commercial implementation in the minerals industry (Dominy et al. 2011).

X-ray CT depends on the attenuation (absorption) of X-rays by materials. At low to medium energies (up to 100 keV) X-rays are largely attenuated by photoelectric absorption. This process is controlled by electron density which is a monotonic function of atomic number. Each element has additional capacity to absorb above specific energies associated with the characteristic absorption edges for that element. For common elements in the Earth these absorption edges are less than 10 keV, but high atomic number elements have higher energy absorption edges (e.g. K absorption edge for Au is 81 keV, and for U is 115 keV). At higher energies, the predominant effect is Compton scattering, which is less dependent on atomic number (Fig. 4). As a result, compositional differences have a greater impact on X-ray CT contrast at lower energies, whereas contrast at higher energies is linearly dependent on differences in density. To image materials that differ in composition (elemental) but not mass density, X-rays <100 keV are used. Diamond search uses this difference (Basis Material Decomposition: BMD) to identify the high density but low atomic number diamonds (Firsching et al. 2012). No

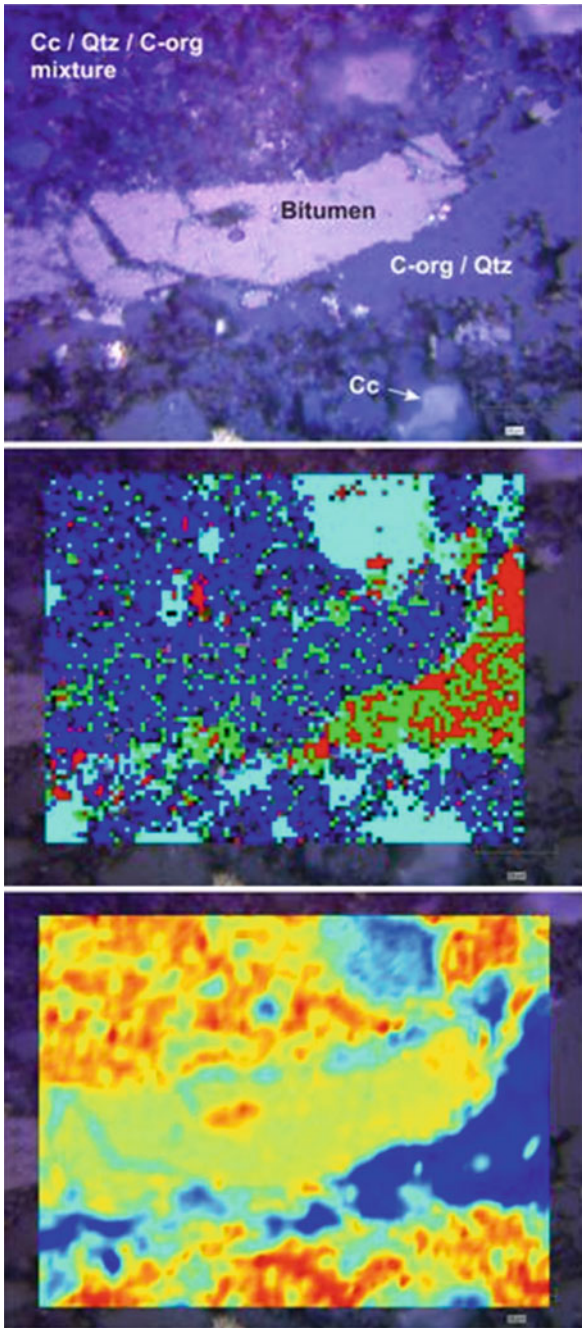


**Fig. 3** *Top* reflected light image; *Middle* hierarchical cluster analysis for all components recognized. Colours for clusters: *blue* Carbon, *green* quartz, *red* sulfide (possibly marcasite), *cyan* calcite. *Bottom* heat (warm colours) map shows the probability the pixel is mostly graphite. Note, the central bitumen region shows lower intensity than true graphite which reflects the different spectra of organic C. *Cc* calcite, *qtz* quartz, *C-org* carbonaceous material (color figure online)

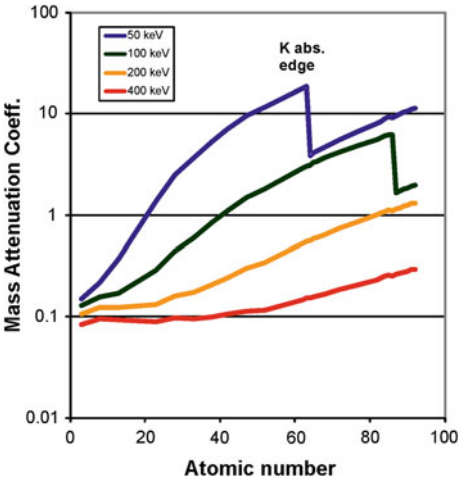


**Fig. 4** X-ray mass attenuation coefficient ($cm^2/g$) across atomic number range for four X-ray energies (based on data in Hubbell and Seltzer 1996) (color figure online)

application of this technique for the development of environmental indicators has been found to date.

## *Core Imaging*

### Visible Light

High quality core photographs are technically feasible. A pixel size of 100 μm (250 dpi) gives excellent quality and allows for recognition of grains larger than 0.5 mm. This resolution is not sufficient to determine grain size distribution in most ores. Theoretical optical resolution limits should allow a higher resolution to be achieved but experiments suggest little extra information is obtained because of the surface roughness.

Lighting is of prime importance to producing a high quality photographic record of the core. All the evidence suggests that the core must be kept wet to give good results. With wet core, specular reflection from the water surface is common and the lights must be placed to avoid this problem.

For a photographic record that enhances direct comparison of core intervals it is important that lighting is stable over the life of the project. The protocol must include a colour balance check every day. A light intensity standard should be recorded on a daily basis so any drift in conditions can be corrected. A shading correction is essential if mineral maps are to be produced. In saturated pixels all colour information is lost. If mineral maps are to be produced, the brightness should be adjusted to avoid saturated pixels.

Low quality mineral maps can be produced from core images (Fig. 5). A few minerals can be conclusively identified but most of the core is classified into

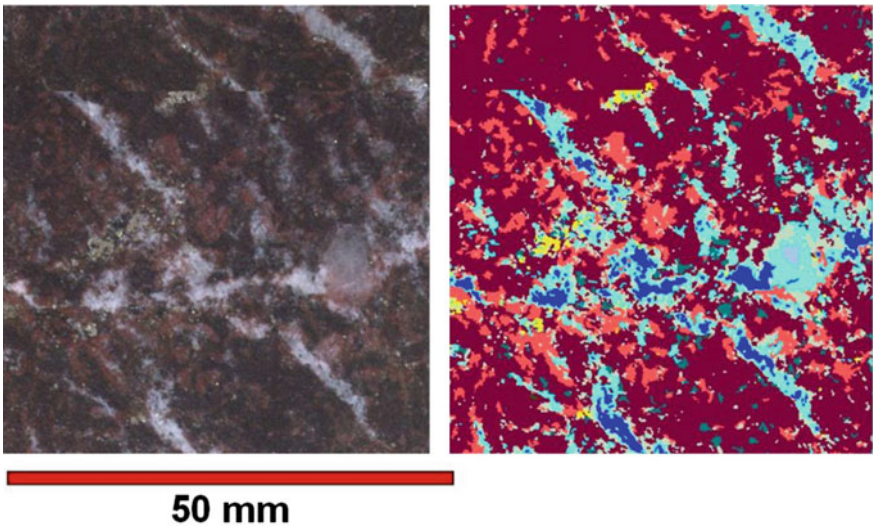


**Fig. 5** High quality core image from cut core (*left*) and the derived mineral map (*right*) including coarse grained chalcopyrite (*yellow*) (color figure online)

mineral associations. This is most effective where the ore is coarse grained and minerals have a high visual contrast. These maps provide a textural basis for classification. They are not competitive with other methods where the main aim is determining the mineralogy of core intervals.

## Infrared Mapping

A recent advance has been the development of "high" resolution infrared mapping devices suitable for core. Core scanning devices can measure maps in near infrared (NIR) and short wave infra-red (SWIR) bands at 0.5 mm pixels. These devices are excellent for mapping the distribution of IR active minerals such as hydrous silicates and carbonates. The spatial resolution means they cannot be used to recognize mineral grains or even grain aggregates except in the coarsest grained rocks. Thermal infrared (TIR) maps which include a wider range of minerals are now possible but have poor spatial resolution.

The infrared core scanning devices typically have optional high resolution visible light photography but the IR imperative is that core is completely dry so the visible light images lack the clarity that might otherwise be expected.

Core scale mineral mapping using IR hyperspectral mapping is limited by its spatial resolution. This emerging technology is yet to find its correct niche in environmental geometallurgy.

## Trace Element Deportment

All the problems of sampling support and representivity discussed for mineral mapping also affect trace element deportment. The most extreme sampling problems are for trace elements that are concentrated at high level in trace minerals. For this case, sampling errors dominate over all other sources of error. This topic has received extensive study for precious metals (e.g. Smee and Stanley 2005) but not for other trace elements.

The first indication for trace element deportment can be found in element correlation tables based on whole rock geochemistry. This information can save a lot of effort by targeting the initial search at specific minerals. Based on that data the methods can be selected from those below. It is very difficult to determine the distribution of 100 % of a trace element. Commonly only 75 % of the trace element assay is accounted for in deportment studies.

### *Electron Probe Micro Analysis (EPMA)*

The classical method for measuring trace and minor elements in minerals is electron probe micro analysis (EPMA). This is a SEM-based method with an electron beam hitting the target and producing characteristic X-rays which are measured with wavelength dispersive spectrometers (WDS) or with solid state crystals that can determine the energy of the individual X-rays (EDS). For EPMA, a specialized SEM is used that has an optical microscope to set the specimen position and is designed for high regulated beam currents. Major developments have been in the new electron sources, $LaB_6$ crystal and field emission (FE), which provide a much smaller spot size where the electron beam hits the sample.

The WDS are much more expensive, include many high precision moving parts, have very high spectral resolution ($\sim$5 eV) and measure characteristic wavelengths sequentially. A full feature EPMA system has five WDS so that five elements can be measured at once. Modern developments are low noise gas flow detectors, large area analysing crystals and high speed counting electronics. In typical spot mode WDS methods have a detection limit of 50–300 ppm (e.g. F: 200 ppm, Si, Fe: 60 ppm, Co, Ni: 100 ppm, Cu, Zn: 130 ppm, As: 170 ppm, Se, Ag: 200 ppm, Au, Hg, Pb, Bi: 300 ppm). Under optimum circumstance in research condition some elements can be detected below 10 ppm (Wark and Watson 2006). In mapping mode the detection limit is much higher.

EDS are cheaper with no moving parts, have lower spectral resolution (120–140 eV at Mn K$\alpha$ peak) and measure all wavelengths at once. The low spectral resolution means that the continuous X-rays provide a higher background against which to measure the characteristic X-rays and as a result the detection limit for most elements is much higher. This is especially true when measuring L X-ray lines (elements with atomic number >30). In addition overlap between characteristic X-ray

lines is much more common for L and M X-ray lines. The EDS detectors have improved in the last 15 years with liquid $N_2$ free detectors, better spectral resolution, larger area detectors and especially higher effective count rates. The computing power has greatly improved the background estimation and full peak series deconvolution of these devices is now standard (Ritchie et al. 2012). In normal circumstances, in spot mode, a detection limit of 0.1 % is an achievable and in optimal circumstances detection limits of 200 ppm have been reported (Donovan 2011).

The normal mode of operation for EPMA is spot analysis. Up to 20 elements are analysed using a 1–10 μm spot (5–14 μm diameter analysed area) in 2 to 5 min. Major elements take 20–40 s, five elements at a time. Errors are 3–5 % relative for elements >500 ppm. Spots can be pre-programmed individually, in scan lines or over a grid. A few hundred analyses can run unattended overnight. Acquisition conditions for X-ray element mapping depend on the elements being measured (X-ray energies to be excited) and the stability of mineral(s) being mapped. For silicates and carbonates, 15 keV accelerating voltage and 100 nA beam current are typically used. For sulfides, 20 keV and 100–300 nA are commonly used. Maps range from 512 * 384 pixels to 4096 * 4096 pixels (Fig. 6). Pixel sizes are usually 1–20 μm. Five WDS X-ray lines are measured in each scan. Major elements can be measured using EDS at the same time. Maps are usually accumulated at 10–100 ms/pixel. At 100 ms/pixel (detection limit around 1000 ppm), it takes 450 h to complete a single pass of 4096 * 4096 pixels, so trace element mapping is usually done over small areas or at low resolution. A more realistic scan time is 11 h with a 2048 * 2048 pixel area and 10 ms/pixel ($\sim$3000 ppm detection limit). For lower detection limits other techniques such as LAM-ICP-MS are preferred.

The electron microprobe analyser has an important role in measuring trace element abundances in the range 200–5000 ppm using spot mode. Trace element maps can be generated in WDS mode for elements where the important

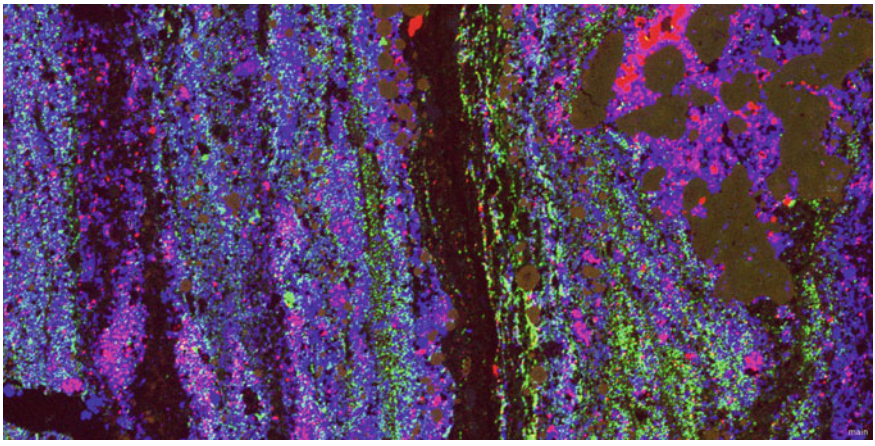

**Fig. 6** EPMA map of fine grain massive sulfide ore. 1536 * 768 pixels at 1 μm/pixel. Cu in *red*, Pb in *green* and Zn in *blue* (color figure online)

compositional range is above 1000 ppm. Most elements above atomic number 4 can be measured but for routine application the element range is F to U (atomic number 9–92). It is suitable for most elements of interest in environmental impact assessments such as As, Bi, Cd, Ni and F. EDS detectors on modern SEMs, especially with FE electron sources, will measure the same elements with a detection level 3× to 5× higher.

## *Micro XRF*

In the last 10 years it has been possible to routinely focus X-rays onto a spot as small as 10 μm. The X-rays are generated by a standard X-ray tube and focused through a mono- or poly-capillary optic. When high energy X-rays hit a target they generate characteristic X-rays from the target (at energies much less than the source beam). The advantage of using an X-ray source to generate X-ray fluorescence (XRF) is that there is a much lower background of continuous X-rays so detection limits are lower, the sample does not need to be coated, and the measurement can be carried out in air if only high atomic number elements are to be measured. The disadvantages are that X-rays are hard to focus so intensities are low, XRF is not effective for light elements (below Na), and the primary X-ray beam has very high penetration so the analysis is an integration of the composition down to 100s of microns depth for more energetic characteristic X-rays. At small spot sizes, up to 100 μm, the X-ray intensity of the primary beam is low so that analysis is slow.

Our experiments with micro XRF suggest it has limited application in environmental indicators. It may be suitable for mapping of delicate materials (unsuitable for a vacuum), where the very long count times needed for realistic detection limits have to be accepted because no other technique can be applied. A new generation of micro XRF is now appearing which may overcome some of the problems experienced.

## *Laser ICP-MS*

The laser ablation inductively coupled plasma mass spectrometer (LA-ICP-MS) combines three specific elements. The sample is usually mounted in a resin block (25 mm diameter) and placed in a sample chamber below the laser. The sample chamber is flushed with Ar gas. Helium gas is bled in through an internal small sample enclosure. The laser beam is turned on and ablates the surface. Fine particles are carried by the He and then Ar gases through a set of plastic mixing tubes to the plasma. At the plasma the particles are vaporized and ionized before introduction into a fast switching quadruple mass spectrometer which measures various atomic weight ions.

LA-ICP-MS is an in situ technique with moderate spatial resolution. Sample preparation is relatively simple requiring a moderately polished surface and no

coating. The major advantage of this technique is the very low detection limit for most elements. There are substantial consumable costs, mainly for inert gases He and Ar, which limit application in mapping to specific high value areas. There are a range of interferences from charged oxides and argides, which make some elements difficult to measure in a typical rock matrix. In addition, the results are sensitive to machine drift which can affect absolute abundance measurements. Laser ablation rates are matrix sensitive so that the mineral must be known before the raw counts can be converted to element abundance.

The major application for LA-ICP-MS is to provide rapid trace element analytical capabilities with a typical detection limit of 0.1–20 ppm. It is possible to detect some heavy elements at ppb level. In analytical mode the typical analysis time is about 90 s.

In mapping mode the sample is rastered under the laser beam in a series of closely-spaced lines. The ablated material takes several seconds to reach the mass spectrometer so a correction must be made for this delay. To minimize the delay a small volume ablation cell is required. Good quality maps (Fig. 7) require long term laser stability. Typically a first run is made to pre-ablate the sample to remove surface contamination of trace elements. Map quantification has low precision and spot measurements are made after the map has been compiled to get absolute abundances of the elements in the zones that are distinguished.

LA-ICP-MS mapping has lower spatial resolution than SEM-based mapping, and is 10 to 100 times slower. It is also destructive with 5 µm of material ablated from the surface during mapping. LA-ICP-MS mapping has detection limits from 100 to 1000 times lower than SEM-WDS maps. The main application of this technique is in mapping trace elements such as Au, As and Bi to determine the possible path of these elements in the mineral processing system.

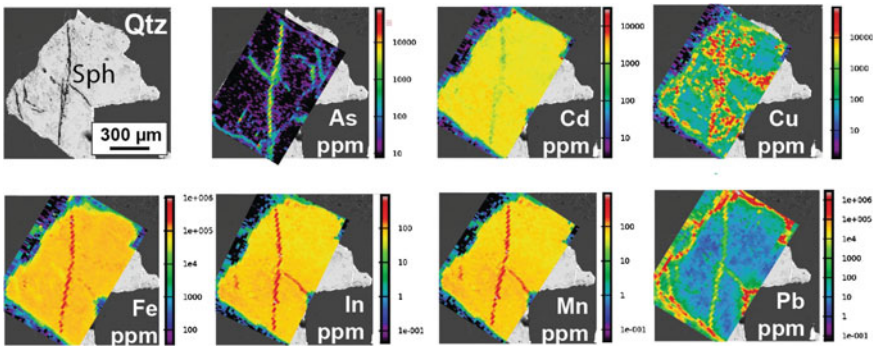


**Fig. 7** Maps showing the distribution of seven trace elements in a grain of sphalerite (BSE map at *top left*). Sample after 10 weeks of leaching in a kinetic test. As concentrated in fractures. Pb concentrated in fractures and around the grain. Fe, In and Mn still homogeneously distributed and showing no evidence of leaching (color figure online)

### *Other Techniques*

Just as an electron beam can generate characteristic X-rays in EPMA, a high energy proton beam will generate characteristic X-rays when it hits a solid target (Ryan 2000). This is the basic concept of PIXE (proton-induced X-ray emission analysis). The proton beam is accelerated to very high energy (>1000 keV), which gives a high ratio of characteristic X-ray emission to the continuous X-ray spectrum (bremsstrahlung). The lower background leads to lower detection limits. The typical PIXE machine uses an EDS detector so the detection limit is still more than 1 ppm. The spot size can be as small as 1 micron but resolution is affected by spreading and depth penetration of the beam just as with the SEM. The high energy proton beam has much higher depth penetration (several tens of microns) than typical electron beams and this means the depth resolution is less than the lateral variation on the maps. For imaging, the proton beam is rastered across the surface just as with small area EPMA maps. However, at this time the PIXE appears to be limited to research only applications by cost and availability.

Where sub-micron resolution trace and minor element mapping is required, ion beams (charged atoms) can be used to splutter material from the surface of a specimen that is then transferred into a mass spectrometer for measurement. This is known as secondary ion mass spectrometry (SIMS). The most common secondary ion used is mass filtered oxygen ($16O^-$) with $Cs^+$ used where a positive ion is required. Typical applications map at 10 μm pixel resolution and measure isotopes and trace elements (down to sub ppm concentration levels). SIMS analysis for sub-microscopic gold in sulfides is commercially available. It has a much smaller spot size than LA-ICP-MS and a higher detection limit (250 ppb). Because of speed (cost) considerations it is losing market share to LA-ICP-MS in trace element mapping. The cost and time preclude the widespread use of SIMS in the minerals industry, with applications limited to specific highly targeted solutions.

## Conclusions

There are many ways to map mineral distributions. The optimum method depends on the aim.

(a) Where 3D connectivity is a key theme, as in porosity mapping, the X-ray CT systems are rapidly improving and already look competitive for specific problems.
(b) For high resolution mineral maps in complex systems (multi-mineral, fine grain size) the SEM-EDS mapping systems are the best today. The laser Raman mapping systems may be competitive in this field within a few years.
(c) For a simple system (e.g. iron ore) or where only a few minerals need to be mapped the automated optical microscope may be a cost competitive system. The optical method cannot compete in sparse phase search with the SEM-EDS

mapping. It does have advantages of the SEM-EDS system in a few specific problems such as mapping assemblages that contain polymorphic minerals (e.g. marcasite and pyrite).

(d) Mapping the surface of rough samples is available via laser Raman spectroscopy and while slow at the moment may be routine within 2 years. The confocal capacity of these systems also allows maps below the surface where minerals are transparent to the laser light.

(e) PIXE has significant advantages for mapping the chemistry of objects below the surface.

The SEM-EDS mapping systems dominate mineral mapping at present. They are highly optimized with efficient commercial software support. Competing systems will find it difficult to change this within the next 5 years. In that period, the alternative methods are likely to encroach as niche methods in specific problems that lend them an advantage.

Trace element deportment is a complex problem. Before starting the search for trace element sources in a specific project it is essential to consider the options. When attempting to find trace elements to define the deportment there are several possible scenarios:

- Trace element is concentrated as a major (stoichiometric) element in a trace mineral: Sparse phase SEM-EDS mapping to recognize all relevant trace minerals. Examples are: Au in gold and electrum; F in fluorite; As in arsenopyrite, cobaltite, realgar, orpiment and enargite; Bi in Bi metal, bismuthinite and some sulfosalts; Cd in greenockite; Pb in galena and some sulfosalts; Sb in stibnite and some sulfosalts; Ni in Ni sulfides; U in uraninite, coffinite and carnotite.
- Trace element is concentrated as a minor element in a minor mineral: SEM-EDS point counting to recognize all relevant minor minerals. EPMA or EDS to measure minor element abundance in mapped minerals. Examples are: F in apatite, mica, amphibole, tourmaline; As in pyrite and low-As sulfosalts; Cd in sphalerite; Pb in low Pb sulfosalts; Ni in pyrite, olivine, mafic minerals, clays; U in apatite, zircon, allanite, monazite, REE phosphates.
- Trace element is dispersed at trace level in a common mineral: SEM-EDS point counting or QXRD to measure abundance of common mineral. LA-ICP-MS to measure trace element content of the host minerals. Examples are: Au in pyrite and arsenopyrite; Bi in pyrite; Cd in pyrite; Pb in feldspar; Sb in pyrite; U in feldspar.

In many cases, the element of interest may be found in more than one of these scenarios. In all cases, some combination of techniques will probably be required to find the location of most of a trace element in a sample. The big change in trace element deportment studies over the last few years has been the emergence of the LA-ICP-MS as an efficient high throughput device with sub-ppm detection limits for most elements.

## References

Berry RF, Hunt J (2011) Grain size in geometallurgy: review of progress. Geometallurgical mapping and mine modelling (AMIRA P843A). Technical Report 8, pp 61–75, Nov 2011

Berry RF, Walters SG, McMahon C (2008) Automated mineral identification by optical microscopy. In: Ninth International Congress for Applied Mineralogy, Brisbane, pp 91–94

Das S, Henry MJ (2011) Application of Raman spectroscopy to identify iron minerals commonly found in mine wastes. Chem Geol 290:101–108

Dominy SC, Platten IM, Howard LE, Elangovan P, Armstrong R, Minnitt RCA, Abel RL (2011) Characterisation of gold ores by X-ray computed tomography—part 2: applications to the determination of gold particle size and distribution. In: Dominy SC (ed) First AusIMM international geometallurgy conference (GeoMet) 2011, pp 293–309

Donovan JJ (2011) High sensitivity EPMA: past, present and future. Microsc Microanal 17:560–561

Fandrich R, Gu Y, Burrows D, Moeller K (2007) Modern SEM-based mineral liberation analysis. Int J Mineral Process 84:310–320

Filippi M, Doušová B, Machovič V (2007) Arsenic in contaminated soils and anthropogenic deposits at the Mokrsko, Roudný, and Kašperské Hory gold deposits, Bohemian Massif CZ. Geoderma 139:154–170

Filippi M, Machovič V, Drahota P, Böhmová V (2009) Raman micro-spectroscopy as a valuable additional method to XRD and EMPA in study of iron arsenates in environmental samples. Appl Spectroscop 63:621–626

Firsching M, Nachtrab F, Mühlbauer J, Uhlmann N (2012) Detection of enclosed diamonds using dual energy X-ray imaging. In: 18th World conference on nondestructive testing, 16–20 April 2012, Durban, South Africa, pp 1–7

Geelhoed B (2011) Is Gy's formula for the fundamental sampling error accurate? Experimental evidence. Min Eng 24:169–173

Goodall WR, Scales PJ (2007) An overview of the advantages and disadvantages of the determination of gold mineralogy by automated mineralogy. Min Eng 20:506–517

Gottlieb P, Wilkie G, Sutherland D, Ho-Tun E, Suthers S, Perera K, Jenkins B, Spencer S, Butcher A, Rayner J (2000) Using quantitative electron microscopy for process mineralogy applications. JOM 52:24–25

Gu Y (2003) Automated scanning electron microscope based mineral liberation analysis. J Min Mat Charact Eng 2:33–41

Helm M, Vaughan J, Staunton WP, Avraamides J (2009) An investigation of the carbonaceous component of preg-robbing gold ores. World gold conference 2009, The Southern African Institute of Mining and Metallurgy, 2009

Higgins MD (2006) Quantitative textural measurements in igneous and metamorphic petrology. Cambridge University Press, Cambridge

Hope GA, Woods R, Munce CG (2001) Raman microprobe mineral identification. Min Eng 14:1565–1577

Howell PGY, Davy KMW, Boyde A (1998) Mean atomic number and backscattered electron coefficient: calculations for some materials with low mean atomic number. Scanning 20:35–40

Huang Q, McConnell LL, Razote E, Schmidt WF, Vinyard BT, Torrents A, Hapeman CJ, Maghirang R, Trabue SL, Prueger J, Ro KS (2013) Utilizing single particle Raman microscopy as a non-destructive method to identify sources of PM10 from cattle feedlot operations. Atmos Environ 66:17–24

Hubbell JH, Seltzer SM (1996) Tables of X-ray mass attenuation coefficients and mass energy-absorption coefficients from 1 keV to 20 MeV for elements Z = 1 to 92 and 48 additional substances of dosimetric interest. NIST. http://www.nist.gov/pml/data/xraycoef/index.cfm/

Knackstedt MA, Latham S, Madadi M, Sheppard A, Varslot T, Arns C (2009) Digital rock physics: 3D imaging of core material and correlations to acoustic and flow properties. Lead Edge 28:28–33

Kyle JR, Ketcham RA (2015) Application of high resolution X-ray computed tomography to mineral deposit origin, evaluation, and processing. Ore Geol Rev 65:821–839

Lane GR, Martin C, Pirard E (2008) Techniques and applications for predictive metallurgy and ore characterization using optical image analysis. Min Eng 21:568–577

Levitan D, Hammarstrom JM, Gunter ME, Seal RR, Choul IM, Piatek N (2009) Mineralogy of mine waste at the Vermont asbestos group mine, Belvidere Mountain, Vermont. Am Miner 94:1063–1066

Pirard E (2004) Multispectral imaging of ore minerals in optical microscopy. Min Mag 68:323–333

Pirard E, Lebichot S, Kreir W (2007) Particle texture analysis using polarized light imaging and grey level intercepts. Int J Miner Process 84:299–309

Plumlee GS (1999) The environmental geology of mineral deposits. In: Plumlee GS, Logsdon MJ (eds) The environmental geochemistry of mineral deposits part A: processes, techniques and health issues. Rev Econ Geol 6A:71–116

Ritchie NWM, Newbery DE, Davis JM (2012) EDS measurements of X-ray intensity at WDS precision and accuracy using a silicon drift detector. Micros Microanal 18:892–904

Ryan CG (2000) Quantitative trace element imaging using PIXE and the nuclear microprobe. Int J Imag Sys Technol 11:219–230

Smart RStC, Miller SD, Stewart WS, Rusdinar Y, Schumann RE, Kawashima N, Li J (2010) In situ calcite formation in limestone-saturated water leaching of acid rock waste. Sci Total Environ 408: 3392–3402

Smee BW, Stanley CR (2005) Sample preparation of 'nuggety' samples: dispelling some myths about sample size and sampling errors. Explore 126:21–26

Smith KS, Huyck HLO (1999) An overview of the abundance, relative mobility, bioavailability, and human toxicity of metals. In: Plumlee GS, Logsdon MJ (eds) The environmental geochemistry of mineral deposits part A: processes, techniques and health issues. Rev Econ Geol 6A:29–70

Stefaniak E, Alsecz A, Frost R, Mathe Z, Sajo IE, Torok S, Worobiec A, Griekent R (2009) Combined SEM/EDX and micro-Raman spectroscopy analysis of uranium minerals from a former uranium mine. J Hazard Mat 168:416–423

Sutherland D (2007) Estimation of mineral grain size using automated mineralogy. Min Eng 20:452–460

Wark DA, Watson BE (2006) TitaniQ: a titanium in quartz geothermometer. Contrib Mineral Petrol 152:743–754

Weber PA, Stewart WA, Skinner WM, Weisener CG, Thomas JE, Smart RStC (2004) Geochemical effects of oxidation products and framboidal pyrite oxidation in acid mine drainage prediction techniques. Appl Geochem 19: 1953–1974

Weisener CG, Weber PA (2010) Preferential oxidation of pyrite as a function of morphology and relict texture. NZ J Geol Geophys 53:22–33

Wopenka B, Pasteris JD (1993) Structural characterisation of kerogens to granulite-facies graphite: applicability of Raman microprobe spectroscopy. Am Miner 78:533–557

# Predicting Waste Properties Using the Geochemistry-Mineralogy-Texture-Geometallurgy Approach

**Anita Parbhakar-Fox**

**Abstract** Established protocols for predicting acid rock drainage (ARD) principally utilise geochemical testwork for classifying waste materials. However, ARD formation is dictated by the mineralogy of the sampled material, and indeed textural relationships of both acid forming and neutralizing mineral phases present. In order for such characteristics to be understood, a logical and structured approach to ARD prediction must be adopted. Motivated by this, the three-stage geochemistry-mineralogy-texture-geometallurgy (GMTG) approach was developed. This integrates a range of techniques, with the resulting sample classification based on diverse analyses. This intends to eradicate the possibility of identifying samples as 'uncertain' as is the case with established protocols. At stage one, termed 'pre-screening' simple tools including paste pH, portable XRF, measurement of sulfur, environmental logging and geometallurgical techniques are used. Samples identified as inert (non-acid forming, non-metalliferous) are not prioritized for further testing. At stage-two termed 'screening', established screening tools are used including net acid producing potential (NAPP) and net acid generation (NAG) tests with samples classified by establish criteria. At stage three, termed 'defining', only samples identified as acid forming are subjected to in-depth characterization to identify controls on oxidation, as well as advanced geochemical tests to confirm classifications assigned at the conclusion of stage-two. The GMTG approach has potential applications at operations that are at the early life-of-mine (e.g. prefeasibility) and also post-closure phase (e.g. abandoned sites).

A. Parbhakar-Fox (✉)
School of Physical Sciences, University of Tasmania, Private Bag 79,
Hobart, TAS 7001, Australia
e-mail: Anita.Parbhakar@utas.edu.au



B. Lottermoser (ed.), *Environmental Indicators in Metal Mining*,
DOI 10.1007/978-3-319-42731-7_5

## Introduction

Whilst understanding of sulfide oxidation processes and acid rock drainage (ARD) formation has improved over the past decades (Price 2009; Lottermoser 2010; Jamieson 2011), ARD predictive protocols have not developed as such. The wheel approach (Morin and Hutt 1998) and the AMIRA P387A approach (Smart et al. 2002) are the most widely used protocols by which waste rock is classified in terms of ARD formation (e.g., Weber et al. 2005a; Marescotti et al. 2008). However, both protocols suffer from limitations, such as the absence of textural measurements and no integration of geometallurgical data. Therefore, a new, up-to-date approach is required by the mining industry to efficiently identify sources of ARD in order to improve waste rock management. Such an approach should not focus on improving the current geochemical screening tests, but should offer better guidance with regards to test selection and application, as well as providing guidelines for evaluating mineralogy and texture over a range of scales.

Ultimately, the key to improving ARD prediction and waste rock classification is to increase the number of samples analysed so as to account for the geological variability of the ore deposit. Such an approach has been successfully adopted in other predictive disciplines such as geometallurgy, whereby samples are obtained at least every 2 m for analyses (Alruiz et al. 2009). Downing and Giroux (1993) provide an example whereby such an approach was adopted for ARD prediction. Their investigation was part of the pre-feasibility study undertaken at the Windy Craggy VMS (Besshi-type) deposit in northwestern British Columbia, Canada. Over 1200 split core samples were subjected to acid-base accounting (ABA) tests with Fe and S assay data for over 1700 samples also used to create a waste rock model consisting of over 100,000 units. However, deposit-wide application of screening geochemical tests in this manner may be considered uneconomical at other mine sites. Therefore, an efficient pre-screening stage (ideally performed in the field) by which an ore deposit or waste rock pile can be classified is required. The GARD Guide (2015) provides a description of what should be included in such a stage. However, it largely revolves around a desk study, and whilst core logging is recommended, no structured guidance is provided on how to assess acid forming potential. Instead, a pre-screening stage must offer detailed guidance for systematically undertaking mineralogical and textural evaluations in order to address the limitations posed by current techniques. Such an approach must have application at both historic and operational mine sites to ensure consistency when data evaluation is undertaken by both mine operators and regulators.

Here, a geochemistry-mineralogy-texture-geometallurgy (GMTG) approach is presented as a means of improving waste classification (Fig. 1). This comprises of three stages of tests, within which two require parallel geochemical, mineralogical and textural analyses in order to fully characterize ARD potential and predict metal/metalloid leaching potential. Each stage is performed sequentially. A range of tests were evaluated (Parbhakar-Fox 2012), with the most effective selected for inclusion in the GMTG approach. This approach also proposes the Acid Rock Drainage Index (ARDI) a novel

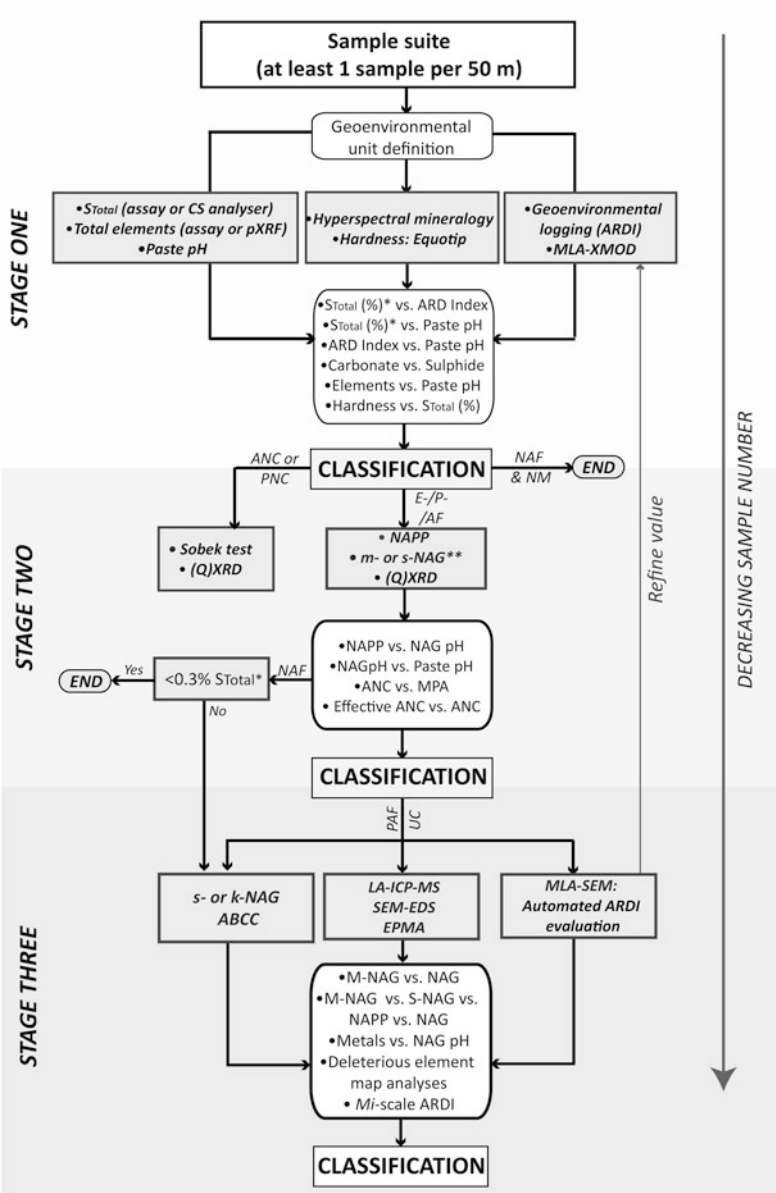


**Fig. 1** Proposed geochemistry-mineralogy-texture-geometallurgy (GMTG) approach for ARD prediction (Parbhakar-Fox and Lottermoser 2015). *MLA-XMOD* mineral liberation analysis-modal mineralogy analysis, *NAPP* net acid producing potential, *ANC* acid neutralizing capacity, *NAG* net acid generation, *MPA* maximum potential acidity, *m-, s- and k- NAG* multi-, sequential- and kinetic-NAG, *LA-ICP-MS* laser ablation inductively coupled plasma mass spectrometry, *SEM-EDS* scanning electron microscopy—energy dispersive spectrometry, *EPMA* electron probe micro analysis, *EAF* extremely acid forming, *AF* acid forming, *PAF* potentially acid forming, *ANC* acid neutralizing capacity, *PNC* potential neutralizing capacity (* indicates $S_{Sulfide}$ can be used instead; ** if $S_{Total} > 0.3$ wt%, mNAG test should be performed) (reprinted from Parbhakar-Fox and Lottermoser 2015, with permission from Elsevier)

textural evaluation scheme performed on hand-specimen and petrological thin section samples as part of stage-one (Parbhakar-Fox et al. 2011; Parbhakar-Fox 2012). After full GMTG analyses, waste is adequately classified, with groups classified as acid forming (AF), or extremely acid forming (EAF) recommended for kinetic testing, and a management/rehabilitation plan formulated.

In this chapter, mine sites in pre-feasibility/feasibility or operational stages are generically referred to as 'operational' and historical or abandoned mines are collectively referred to as 'historical'. As the GMTG approach aims to have application at both operational and historical mine sites, some protocol variation is required (e.g., with regards to sample selection) as explained throughout this chapter. With each stage analytical sophistication increases and the number of samples analysed decreases. Stage-one is for pre-screening samples and identifying those required for analysis by routine screening tests which are undertaken at stage-two. Samples with significant acid forming potential are advanced to stage-three, whereby controls on sulfide oxidation are identified through detailed characterization. Thus, as each stage increases, selection of samples for further analyses is determined by mineralogical characteristics. The following sections detail each stage of the GMTG approach and provide rationale for the chosen methods/tests.

The specific objectives of this chapter are: (a) to introduce a protocol for predictive ARD testing of ores and waste rocks which has the potential for incorporation into resource block modeling or for assisting in characterizing abandoned mine operations; (b) to describe a protocol by which samples are better identified for detailed microtextural sulfide characterization and kinetic testing (following the methodology presented in Parbhakar-Fox et al. 2013a, b) to define the application of geometallurgical tools in ARD predictive studies.

## Sample Selection

Sample selection is the most critical aspect of an investigation aimed at determining the acid-forming potential of mine wastes (Downing 1999; Price, 2009). Poor sampling techniques and inadequate sample selection can contribute to excessive variance, difficulties in interpretation, and incorrect assessment (Downing 1999; Morin 2010; Kentwell et al. 2012; Pearce and Gutierrez 2015). Sampling guidelines are provided in the literature, particularly for operational mines (e.g., Price 2009; GARD Guide 2015). This section builds upon these recommendations, and proposes sample selection guidelines for GMTG analyses.

### *Operational Sites*

Samples selected for the GMTG approach at a mine in the early stages of operation (e.g., pre-feasibility, feasibility), must be representative of geological, lithological

and alteration units in accordance with the GARD Guide (2015). Additionally, samples must be representative of the relative amounts and particle size of each type of material (Downing 1999). When sampling drill core, Price (2009) recommended that samples should be collected at least 50 m laterally and vertically in order to create a statistically significant waste rock model. Composite samples as used in Hammarstrom et al. (2003), Borden (2003) and Lengke et al. (2010) should be avoided as potentially they could mask geological variability. Downing (1999) reasoned that whilst rigorous sampling can be costly, remediation and reclamation plans developed as a consequence of poor sampling and analysis can become even more expensive, hence the importance of a detailed initial assessment. He argued that costs should not pre-determine the number of samples taken and analysed, but should be dependent on the amount necessary to increase confidence in the data. Therefore, the GMTG approach recommends that at least a 5 m linear sampling programme should be employed to obtain samples for stage-one testing. This interval is not fixed and can be changed to a more appropriate value between 2 and 50 m as determined by site geological personnel. Sampling should be undertaken on all drill holes; however, a tighter sampling campaign can be developed for low-grade ore/waste rock/overburden zones. Such a strategy is aligned with the expected number of samples as published in guidelines given by the Australian Government Department of Industry, Tourism and Resources (2007).

## *Historical Sites*

Theoretically, the most effective sampling campaigns are those based on rock volume per lithology. However, often a limitation is that for historical piles, these values (i.e., rock volume and number of lithologies) are unknown. This limitation manifests in published examples of waste rock characterization at historical mine sites as relatively low numbers or composited samples are used (e.g., Munroe et al. 1999; Hammarstrom et al. 2003; Harris et al. 2003; Ashley et al. 2004; Akabzaa et al. 2007; Marescotti et al. 2008; Changul et al. 2010). However, some guidelines do exist. First, the USEPA (1994) outlined two strategies, one of which (proposed by an unnamed consultancy) stated that 8–12 samples should be collected from each significant rock type (whereby a significant rock type is presumed to be 1–2 % of the total mine rock volume). The second strategy recommended that one sample (1.5 kg) should be collected per 20,000 t of waste rock, or approximately 50 samples per 1 Mt (USDA Forest Service 1992). The British Columbia (BC) AMD taskforce (1989) recommend 25 samples as a minimum should be collected from 1 Mt geological units, or 1 sample for every 40,000 t. A limitation of this strategy is that as waste volume increases, the number of samples decreases (i.e., for a unit of 10 Mt the minimum sample number is 250 or one sample for every 125,000 t).

Downing (1999) recommended consultation of waste rock curves to deduce the minimum number of samples required with an example developed by the British Columbia Acid Mine Drainage Task Force (1989).

## Geoenvironmental Unit Definition

Examples of ARD prediction and waste rock characterization indicate that no formal methods of differentiating between waste rock lithologies are employed (Hammarstrom et al. 2003; Harris et al. 2003; Ashley et al. 2004; Changul et al. 2010; Song and Yanful 2011). Consequently, materials identified as sulfidic are not categorized by sulfide type or texture, thus questioning the effectiveness of waste management strategies and rehabilitation plans which consider sulfidic material as one entity (Harris et al. 2003; Ashley et al. 2006). Therefore, a mesotextural classification method is proposed whereby all samples are initially grouped as per lithology, mineralogy, texture and element content.

A geological description of each sample is first logged with particular attention given to estimating modal mineralogy, texture and alteration type. Alteration can either increase (e.g., advanced argillic, argillic and phyllic) or decrease (propylitic, carbonate, fine-grained potassic) the acid forming capacity as documented in Plumlee (1999), whereby neutralizing potential (NP) values for minerals commonly observed in waste rock material were given. Fine-grained pale minerals are common constituents of these alteration assemblages (e.g., kaolinite, dickite, sericite). Such minerals require differentiation as they differ in their NP and susceptibility to weathering (Sverdrup 1990; Bowell et al. 2000; Dold and Fontboté 2001).

The application of short-wave infrared (SWIR) spectroscopy in determining pale, fine-grained alteration minerals has been demonstrated in ore-deposit characterization studies (e.g., Thompson et al. 1999; Herrmann et al. 2001; White et al. 2010). Mineral identification is based on absorption spectra collected from clean, dry, flat, rock surfaces (Gifkins et al. 2005). SWIR therefore has potential to improve mineral identification of altered waste rock samples, thus aiding mesotextural grouping.

Field-portable X-ray fluorescence (pXRF) analysis has in recent years been used in mine site characterization studies for determining element concentrations (e.g., Melquiades and Appoloni 2004; Haffert and Craw 2010; Higueras et al. 2012). For the purpose of mesotextural classification, pXRF analysis is recommended to chemically differentiate between lithologies. At this stage, several areas of a clean, flat, dry sample can be analysed with the results averaged.

Following these analyses, grouping of samples displaying similarities in mineralogy, texture and elemental content is possible. By defining and populating groups, the schedule of analysis is improved with all samples subjected to stage-one tests geochemical tests, and at least 10 % of samples from each group subjected to mineralogical and textural characterization. By grouping samples based on their mineralogical and chemical characteristics, a more organized approach to ARD testing is introduced that guides sample selection in later GMTG stages.

## GMTG Approach: Stage-One

### *Geochemical and Mineralogical Characterization*

A portion of each sample should next be milled to <75 µm and from this splits homogenized and used in sulfur, pulverized paste pH and portable XRF analysis. At least 5 % of samples per geoenvironmental unit should be submitted for X-ray diffractometry (XRD) and validation XRF analysis. If mineral liberation analysis (MLA) data (as calculated based on a point-count method) exist, this information can also be used to determine the bulk mineralogy (in place of XRD).

### *Textural Evaluations*

Texture is evaluated using the acid rock drainage index (ARDI) method. As the ARDI features in the pre-screening stage, a ranking system to efficiently evaluate samples is adopted. Previous examples of ranking in petrological evaluations are presented in Blowes and Jambor (1990), Oyen et al. (1998) and Moncur et al. (2009, 2015), with several criticized due to their subjective nature (Mills et al. 2011). As the ARDI is intended to be performed manually (i.e., by site-geologists), the subjective nature of ranking can only be minimized by clearly defining each score. Therefore, reference examples must be provided (including photographs, diagrams and/or criteria tables) prior to its undertaking.

The ARDI evaluates acid forming sulfide minerals individually by five parameters (A to E) as shown in Fig. 2. Parameters A to C focus on characterizing sulfide minerals and are ranked from either 0 or 1(low: not acid forming) to 10 (high: acid forming). Only Fe-sulfides (e.g., pyrite, pyrrhotite, arsenopyrite and chalcopyrite) are assessed by the ARDI as these are the most acid forming sulfides (Hammarstrom et al. 2003; Lottermoser 2010; Jamieson 2011). Non-Fe bearing sulfides such as galena (PbS) and sphalerite (ZnS) are not directly evaluated, but their presence is considered by Parameters D and E. Assessment by all parameters must be undertaken if acid forming sulfides are identified, or else the ARDI value is void. If sulfide minerals are not identified in a sample, it is classified as non-acid forming. Where sulfides are identified, a maximum of twenty Fe-sulfide phases are assessed (by Parameters B to E) if present. Otherwise, the maximum number identified is assessed, and the ARDI values must be appropriately scaled. A high value indicates acid formation, a low value indicates low or inert acid forming potential, and a negative value indicates an acid neutralizing capacity (Table 1). Values between 10 and 0 indicate that a sample is either non-acid forming or has a potential neutralizing capacity and must be resolved when cross-checking these values with other data collected in this stage. A brief description of each parameter is given in the following sections, with diagrammatic examples given in Parbhakar-Fox et al. (2011).

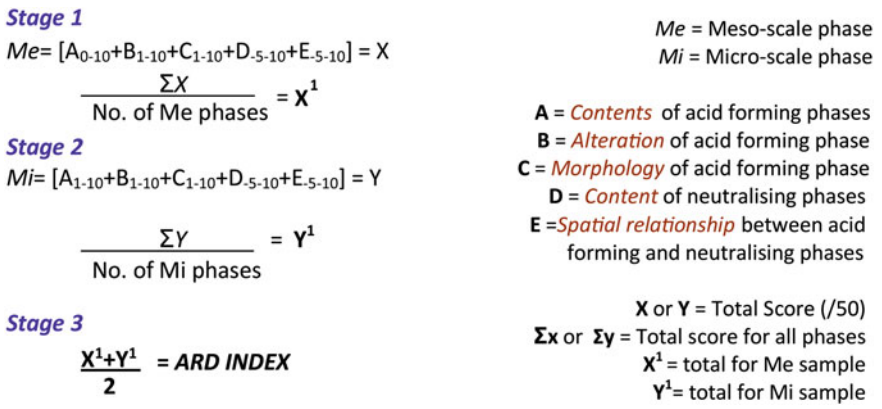


**Fig. 2** Acid Rock Drainage Index (ARDI) calculation

**Table 1** ARDI classification

| ARDI score | Classification |
|---|---|
| 50 to 41 | Extremely acid forming |
| 40 to 31 | Acid forming |
| 30 to 21 | Potentially acid forming |
| 20 to 11 | Non-acid forming/inert |
| 10 to 0 | Non-acid forming/ANC |
| −1 to −10 | Acid neutralizing capacity |

*ANC* acid neutralizing capacity)

Parameter A is a proxy for maximum potential acidity (MPA) and requires an estimation of the modal contents of iron-sulfides. For a meso-scale evaluation, a 3 cm × 3 cm area is selected, and on the micro-scale the entire petrographic thin section is evaluated. The higher the contents, the greater the acid reservoir as MPA is calculated based on $S_{Sulfide}$ or $S_{Total}$ quantity. If a score of 0 is given (i.e. no sulfides present), then no further assessment is required and the sample considered NAF.

Parameter B is adapted from sulfide alteration index (SAI) of Blowes and Jambor (1990). However, iron-sulfides are inversely scored. Fresh, unaltered sulfides score 10, partially obliterated/weathered sulfides score 5, and those largely replaced by secondary minerals are given a low score. A maximum of twenty iron-sulfide phases are assessed if present. Otherwise, the maximum number is assessed, and the number of phases evaluated is considered when assigning the final ARDI value.

Parameter C evaluates morphology, thus it considers the available surface area for sulfide oxidation, but this is based on observation only (i.e. no detailed measurements). Generally on the meso-scale, a disseminated sulfide texture scores high, and a massive sulfide texture low. On the micro-scale, framboidal pyrite will score

high because of the large surface area available for oxidation (Smith and Beckie 2003). Euhedral pyrite would score much lower as its regular shape offers a much smaller surface area for oxidation.

Parameter D evaluates the neutralizer contents i.e., the presence of neutralizing minerals directly surrounding the acid forming sulfide phases evaluated by parameters B and C. On the meso-scale, the modal mineralogy of an area twice the maximum diameter of the iron-sulfide is assessed. At the micro-scale, the evaluated area is the field of view selected to observe the sulfide phase. If acid forming phases are abundant, a high scored is given (e.g. 80 % sulfides scores 8). If neither acid forming nor neutralizing phases are identified, then 0 is given (e.g. pyrite 100 % surrounded by quartz). If the area is 100 % dominated by primary neutralizing minerals then −5 is given. A range is given for primary neutralizers as without staining, carbonates are harder to discern between in hand specimen and thin section (Hitzman 1999). If both acid forming and neutralizing minerals surround the phase, values are subtracted to give a final score (e.g. 80 % sulfide and 20 % calcite = 7). Secondary neutralizing minerals identified in Bowell et al. (2000) and Jambor et al. (2002) are scored half that of primary neutralizers (i.e. if 100 % dominated by a secondary neutralizer, then −2.5 is given).

The mineral association of the acid forming sulfide phases is examined by Parameter E (i.e., evaluation of acid former/neutralizer spatial relationship). If the iron-sulfide phase is in direct contact with another sulfide (acid or not acid forming), a positive score is assigned; e.g. if 100 % in contact with other sulfides, then the maximum score 10 is given. The lower the percentage contact, the lower the score. If the acid forming phase is 100 % directly in contact with primary neutralizing minerals, then the minimum score of −5 is given. If the acid forming phase is fully bounded by an inert mineral (i.e. quartz), then a value of 0 is given.

## *Geometallurgical Testing*

### Hyperspectral Logging

The use of hyperspectral instruments for mineral identification down drill hole is recommended. The advantage of hyperspectral instruments (e.g., HyLogging™ systems) is that they are automated platforms to rapidly and systematically collect infrared spectroscopic reflectance data at dense sample spacing from drill core, chips or powders (Huntington et al. 2006). Such a technique is best suited to an operational site whereby drill core trays can be loaded into core trays and analysed in a push-broom manner. For a historical site, if hand specimen samples are available they can be individually placed in core trays and analysed. This technique is responsive to the chemical composition and crystal structure of a mineral. Thus, mineral

identification is made possible based on the resulting 'spectral fingerprint' or 'signature' observed in the spectral response curve (Huntington et al. 2006). Hyperspectral logging has several advantages over other mineral identification techniques (e.g., XRD and automated SEM instruments including MLA and QEMSCAN) through its rapidity (a HyLogger can analyse up to 1000 m of core per day), its low cost per sample, and its non-contact, non-destructive approach (Huntington et al. 2006). Based on this, hyperspectral loggers have an application in the GMTG approach, but at stage-one only, as the data is qualitative. If used in conjunction with $S_{Total}$ and paste pH values, it can assist with domaining, whereby relative carbonate intensities can assist in identifying zones with neutralizing capacity.

### Mineral Hardness: Equotip

Measuring the susceptibility of a lithology to weathering is required to understand how rapidly acid forming minerals will become exposed in a waste rock pile. For example, if Fe-sulfides are encapsulated in minerals such as quartz (Mohs hardness 7), they are less likely to be acid forming than those encapsulated in clays (Mohs hardness 1 to 2). Therefore, the application of EQUOtip, which represents a non-destructive, core-based measurement technique, was explored (Keeney 2008). The Leeb (Ls) hardness value (0 to 1000) is automatically calculated, using the quotient of the rebound velocity over the impelled velocity multiplied by 1000 (Keeney 2008). The impact body rebounds faster from harder test samples than it does from softer ones, resulting in a greater value. The GMTG approach recommends the use of an EQUOtip 3 (Proceq) instrument. Average values for each 1 m interval must be calculated based on measurements taken at 2.5 cm intervals. Care must be taken to ensure that half-core PQ drill core materials are used. Samples with smaller thickness will return incorrect hardness results. Hardness criteria must be defined prior to data collection based on initial testwork. Such criteria should be site-specific, with validation/calibration testwork performed using established hardness measurement techniques e.g., Vickers hardness test. Equotip values are used alongside total-sulfur values for comparison to indicate ARD risk. This has the potential to allow for a low-cost, first-pass understanding of lag-time to ARD on a deposit-scale.

## *Stage-One Classification*

Classification of stage-one data follows the principle of cross-checking as recommended in Morin and Hutt (1998). Only through such data comparisons can a well-reasoned classification be assigned, as previous protocols do not consider acid forming potential on a range of scales in the manner that the GMTG approach does

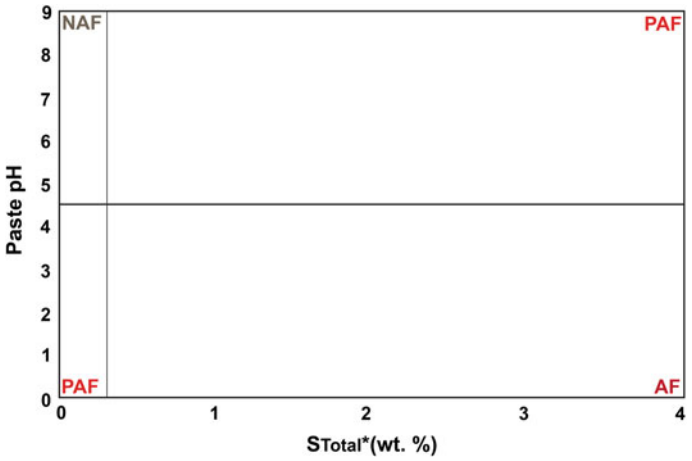


**Fig. 3** GMTG pre-screening plot of paste pH versus $S_{Total}$ (wt%) with proposed classification fields shown. *NAF* non-acid forming, *PAF* potentially acid forming, *AF* acid forming (* indicates that sulfide-sulfur values can be used in place)

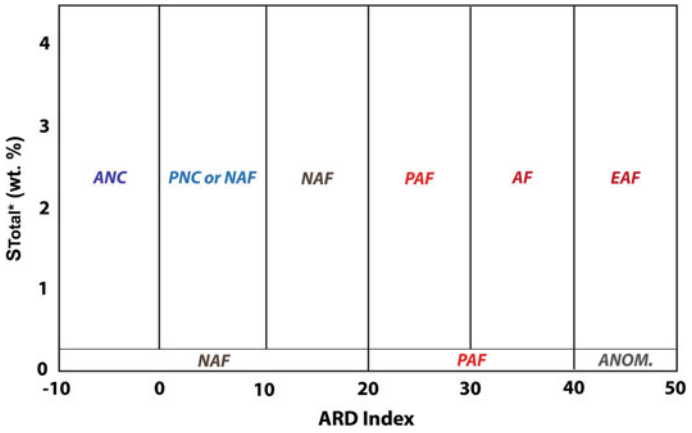


**Fig. 4** GMTG pre-screening plot of acid rock drainage index (ARDI) values versus $S_{Total}$ (wt%). *ANC* acid neutralizing capacity, *PNC* potential neutralizing capacity, *NAF* non-acid forming, *PAF* potentially acid forming, *AF* acid forming, *EAF* extremely acid forming, *Anom.* anomalous (*indicates that sulfide-sulfur values can be used in place)

(e.g., pulverized sample (<75 μm) used in paste pH and $S_{Total}$ analyses, intact samples for ARDI and hyperspectral evaluations). Whilst some of the classification schemes selected for inclusion have already established (e.g., paste pH vs. $S_{Total}$), the classification fields have been refined. Classification plots for stage-one data are shown in Figs. 3, 4, 5, 6, 7, 8 and Tables 2 and 3.

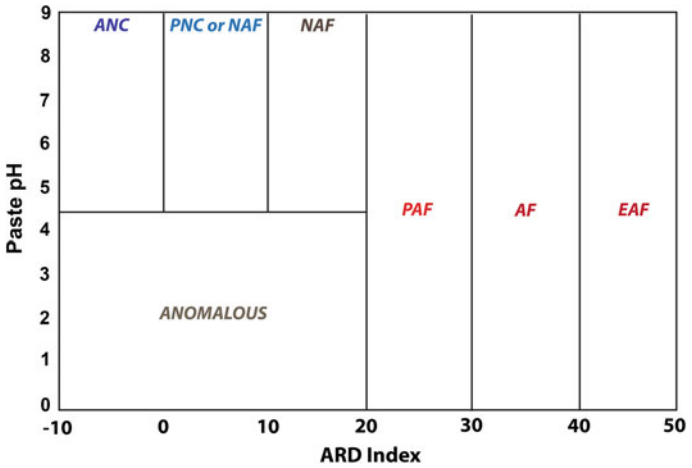


**Fig. 5** GMTG pre-screening plot of acid rock drainage index (ARDI) values versus paste pH. *ANC* acid neutralizing capacity, *PNC* potential neutralizing capacity, *NAF* non-acid forming, *PAF* potentially acid forming, *AF* acid forming, *EAF* extremely acid forming

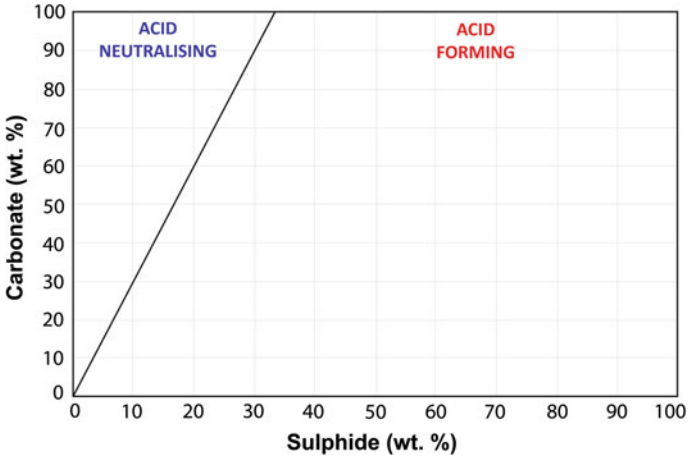


**Fig. 6** GMTG pre-screening plot of carbonate (wt%) versus sulfide (wt%). Modified from Paktunc (1999) and Craw (2000)

Samples classified as NAF, low-risk and non metalliferous at the end of stage-one require no further analyses by the GMTG approach. This ensures that no further efforts (i.e., time and budget) are spent on unnecessary characterization work (e.g., NAPP/NAG), with only acid forming or neutralizing samples focussed upon in stage-two and stage- three.

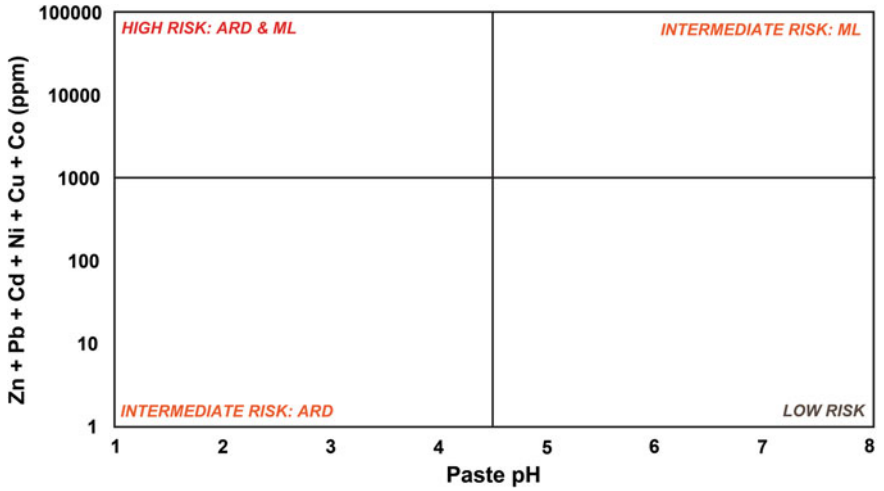


**Fig. 7** GMTG pre-screening modified Ficklin plot of metal contents versus paste pH. *ARD* acid rock drainage, *ML* metal leaching

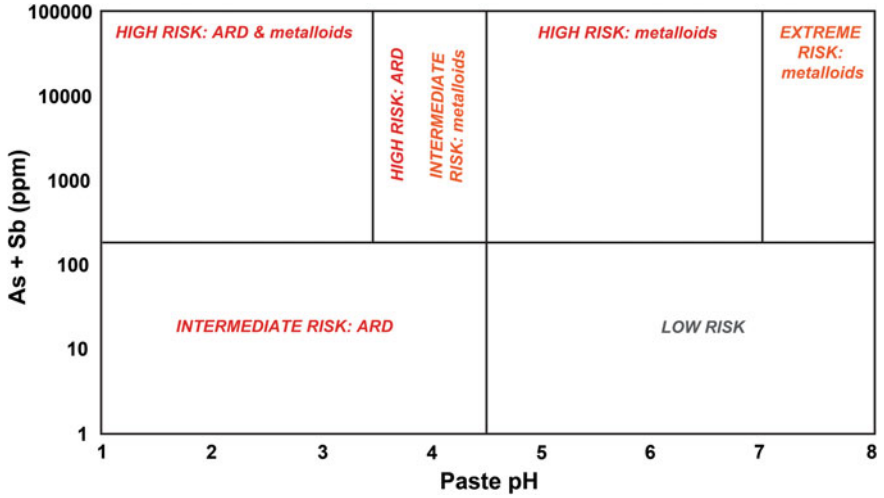


**Fig. 8** GMTG pre-screening plot of metalloid contents versus paste pH

**Table 2** Hyperspectral data classification for assessing acid neutralizing capacity (ANC) and identifying potentially acid forming (PAF) samples

| Hylogger (relative carbonate intensity value) | $S_{Total}$ (wt%) | Paste pH | Classification |
|---|---|---|---|
| High | <0.3 | >6 | ANC (high capacity) |
| High | >0.3 | >6 | ANC (low capacity) |
| High | >0.3 | <6 | PAF/ANC poor |
| High | <0.3 | <6 | ANC poor |
| Low | <0.3 | <6 | ANC poor/PAF (low capacity) |
| Low | >0.3 | >6 | PAF/ANC poor |
| Low | >0.3 | <6 | PAF |
| Low | >0.3 | >6 | PAF |

**Table 3** ARD risk classification based on mineral hardness (Equotip), $S_{Total}$ and paste pH

| Equotip hardness | $S_{Total}$ | Paste pH | Classification |
|---|---|---|---|
| Hard | <0.3 | >6 | Low risk |
| Soft | <0.3 | >6 | Low risk |
| Hard | <0.3 | <6 | Low risk |
| Soft | <0.3 | <6 | Low risk |
| Hard | >0.3 | >6 | Low-medium risk |
| Soft | >0.3 | >6 | Medium risk |
| Hard | >0.3 | <6 | Medium risk |
| Soft | >0.3 | <6 | High risk |

## GMTG Approach: Stage-Two

Routine geochemical tests are exclusively used in stage-two of the GMTG approach. Both NAPP and NAG tests are recommended for samples identified as PAF, AF or EAF by stage-one. Additionally, element assay analyses (focused on As, Cd, Cu, Co, Ni, Pb, Sb, Zn) are recommended for such samples, unless field portable XRF (pXRF) and validation XRF values are in very strong agreement, in which case, a lesser number per geoenvironmental unit would be required. Additional mineralogical analyses can be performed as part of this stage if required (i.e., XRD on samples containing several sulfides to determine the exact proportion of acid forming sulfides present). Such analyses can allow for improved validation and calibration of hyperspectral data. A brief explanation of NAPP and NAG test selection rationale is given in this section, followed by an outline of stage-two data classification.

## *NAPP and NAG Tests*

Maximum potential acidity (MPA) calculation requires determination of $S_{Total}$, with values obtained from the carbon-sulfur analysis (or alternative method) performed at stage-one. The convention of expressing values in kg $H_2SO_4$/t is adopted in this approach (cf. Smart et al. 2002). If quantitative mineralogy has been undertaken, the opportunity exists to refine calculation of MPA using sulfide-sulfur values to improve accuracy or Fe-sulfide-sulfur values, with these values multiplied by 30.6 (Stewart 2005).

Despite arguments presented in Morin and Hutt (2009), it is of importance to select an appropriate method for determining ANC from one of the many existing methods outlined in White et al. (1999), Smart et al. (2002), Price (2009) and the GARD Guide (2015). Therefore, the Sobek method is included in the GMTG approach. This method is more widely accepted as an industry standard method, with results collected in a shorter turn-around time, making them of greater use in an industry context. The GMTG approach recommends the use of certified reference materials KZK-1 (sericitic schist) and NBM-1 (altered feldspar porphyry) from CANMET (Natural Resources, Ottawa) for testing when these experiments are conducted. Both have been used in other ARD studies (e.g., Paktunc 2001; Goodall 2008).

The single-addition NAG test is recommended as part of stage-two as it is the simplest and most established of the six NAG methods (Chap. "Principles of Sulfide Oxidation and Acid Rock Drainage"). Examples of its application are presented in Hammarstrom et al. (2003), Tran et al. (2003), Stewart et al. (2006), Sapsford et al. (2008) and Broadhurst et al. (2009). The main application of NAG test results here is for screening against paste pH values (as calculated in stage-one) and to provide a value to cross check NAPP data.

## *Stage-Two Classification*

Traditional NAPP versus NAG pH plots are used to classify samples as PAF, NAF or UC. However, some discrepancy lies in the cut-off criterion to use for NAG pH. For example, Weber et al. (2006) used pH 4, whereas Stewart et al. (2006), Moon et al. (2008) and Broadhurst (2007) favoured the use of pH 4.5. The latter is used here as the cut-off criterion (Fig. 9). The use of NAG pH versus paste pH values was proposed by Weber et al. (2006), however, its application has not been widely demonstrated, despite the fact that it offers an assessment of lag-time to ARD and thus classifies risk. Weber et al. (2006) used it to classify coal mine samples. Therefore, as both NAG and paste pH data are collected through stage-one and stage-two testing, this classification has been modified slightly (to define fields as EAF and AF) and is included as part of stage-two data interrogation (Fig. 10). It is noteworthy that as more fields are defined, the cut-off criterion used between high

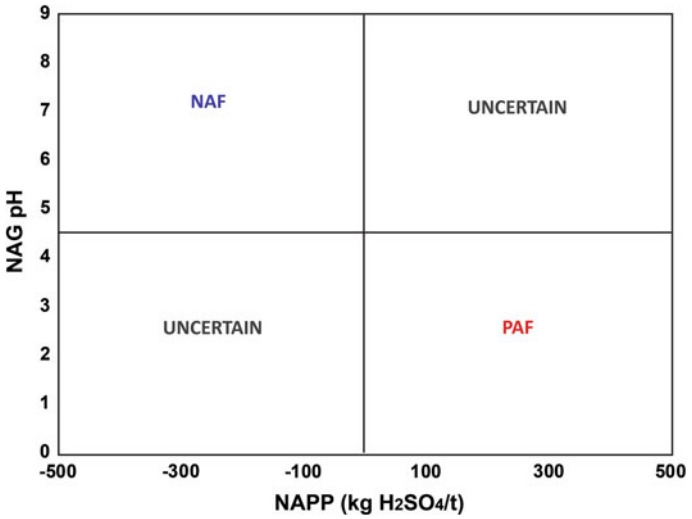


**Fig. 9** GMTG stage-two screening plot of NAPP versus NAG pH. Abbreviations: *NAF* non-acid forming; *PAF* potentially acid forming. Modified after Smart et al. (2002)

risk and medium risk samples is set slightly lower to pH 4, following the value suggested by Sobek et al. (1978).

In a similar manner to carbonate versus sulfide ratio plots (shown at stage-one), ANC and MPA ratio plots are recommended as shown in Fig. 11. However, they are most effectively used if the MPA has been recalculated in terms of sulfide-sulfur. Otherwise, application of the ANC versus $S_{Total}$ plot presented in Smart et al. (2002) can be used in their place. To refine estimates of geochemical risk, NAG pH data can be used in place of paste pH when compared against element concentrations (Figs. 7 and 8). These refined geochemical data plots should be compared alongside those produced for paste pH as they provided an indication of the current situation, and NAG pH plots represent an extreme condition whereby all acid forming sulfide has reacted.

Sample selection for further testing requires careful consideration as stage-three tests are not mandatory. Instead, a select combination of tests is recommended to clarify or further investigate specific questions. In general, samples identified as highly acid forming by stage-one (i.e., consistently AF or EAF), PAF by NAPP versus NAGpH, and EAF or AF by NAG pH versus paste pH will require further testing. Samples identified with high metal/metalloid concentrations and sulfides are recommended for detailed microanalysis to determine the sulfide mineral chemistry and identify controls on oxidation as outlined in Egiebor and Oni (2007). To observe sulfide microtextures, MLA and SEM analyses should be performed. Advanced NAG testing is only recommended for ambiguous samples (i.e.,

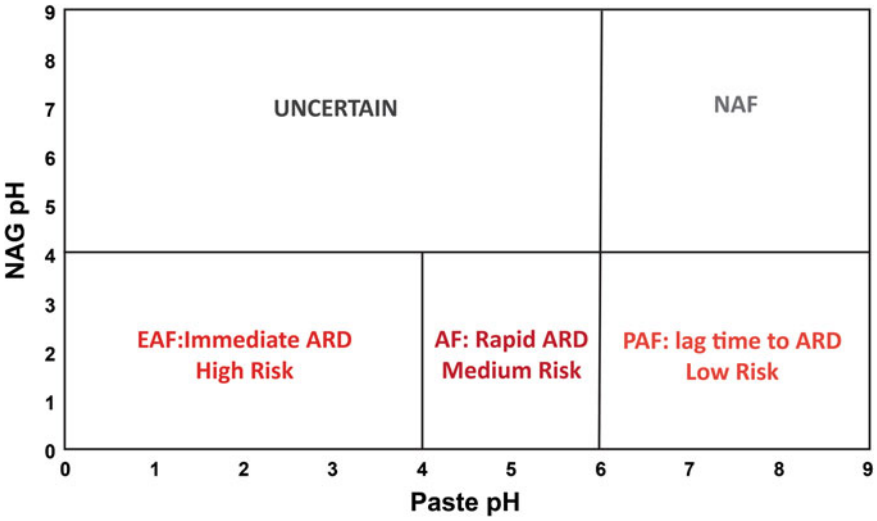


**Fig. 10** GMTG stage-two screening plot of NAG pH versus paste pH. *NAF* non-acid forming, *PAF* potentially acid forming, *AF* acid forming, *EAF* extremely acid forming. Modified from Weber et al. (2006)

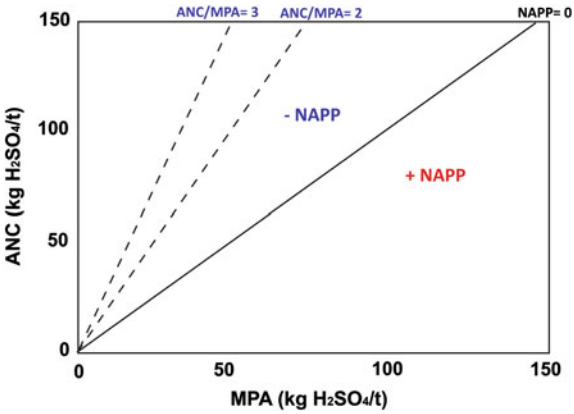


**Fig. 11** GMTG stage-two screening plot ANC versus MPA. *ANC* acid neutralizing capacity, *MPA* maximum potential acidity, *NAPP* net acid producing potential. Modified from Smart et al. (2002)

conflicting classifications), with XRD subsequently recommended (if it has not already been performed on these individual samples and if classifications remain inconclusive). Samples with high ANC values are recommended for additional acid buffering characteristic curve (ABCC) testing in order to determine the effective neutralizing capacity.

## GMTG Approach: Stage-Three

Similar to stage-one of the GMTG approach, a combination of geochemical, mineralogical and textural techniques is applied to characterize in detail appropriately selected samples. Unlike stage-one, sophisticated technologies are used, therefore a much smaller number of samples is analysed. This section provides an explanation of each selected test or technique and outlines how these can be used for ARD prediction/waste classification.

### *Advanced Testwork*

Stage-three involved refining the geochemical ARD estimate through the performance of advanced NAG tests, with multi-addition NAG (m-NAG) and sequential NAG (s-NAG) tests performed on all EAF/AF/PAF samples and laboratory based k-NAG testing for at least one sample per EAF/AF/PAF classified mesotextural group. Detailed textural studies and trace element characterization should also be undertaken on these samples, using MLA-SEM, EPMA and LA-ICP-MS. Primary sulfide and secondary weathering minerals identified through XRD and ARDI evaluations should be targeted, with the aim of quantitatively and spatially measuring potentially deleterious element contents to allow for modelling of future metal liberation. Based on these analyses NAPP, NAG, s-NAG and m-NAG values should be compared alongside sample mineralogy, texture and $S_{Total}$ values. From this, a final acid forming potential classification can be assigned. The programme is then concluded, with highly acid forming samples prioritized for detailed kinetic test work (e.g. laboratory based column leach tests).

### *Stage-Three Classification*

Classification of stage-three results first requires comparison of advanced NAG test results with stage-two geochemical test results (i.e., NAPP and NAG). This allows for variation between results to be calculated. It is unlikely that the overall sample classification will change from the previous stages. However, if significant differences are observed between advanced NAG test results and either the single-addition NAG or NAPP tests, additional samples from that particular mesotextural group are recommended for advanced NAG analysis. This is to identify if the error is an anomaly, or representative of a systematic error. Each geochemical test should be plotted against the other, with deviations from the model line (1:1) examined. Additionally, all results should be plotted on a summary graph or comparison table to allow for a direct comparison of data. Classification of microanalytical data is less defined than when using geochemical and quantitative

mineralogical results. A numerical ranking scheme based on observations (similar to that proposed by the ARDI) has not been proposed for BSE images collected during SEM analysis. Instead, the observations made from microanalyses are intended to provide in-depth characterization of each (potentially) acid forming mesotextural group. However, quantitative element data can be used with NAG pH data (stage-two) to produce highly specific Ficklin style plots (following those shown in Figs. 7 and 8). Additionally, element distribution can be directly correlated with mineralogy through overlying mineral and element maps. Individual elements should be screened against each other to determine relationships using correlation matrices (e.g., Harris et al. 2003; Ashley et al. 2006) thus enhancing the understanding of the potentially deleterious elements sources at a given site. Additionally, these values should be screened against locally determined baseline and guideline values (e.g., ANZECC 2000; WHO 2006). This will provide a clear indication of the mesotextural groups posing significant environmental risk at a given site.

## Final Classification

Classification results from each stage of the GMTG approach should be collated in a summary table. At the end of each stage, a final classification is assigned per mesotextural group based on the frequency of classifications within that particularly stage. For example, if the majority of classifications are PAF, the group is 'PAF'. Mesotextural groups classified at the end of stage-three as 'EAF: high risk' are recommended for kinetic testing. These groups should be considered by site managers/operators as separate entities when formulating waste rock management/rehabilitation plans, as they have unique sulfide mineralogy and texture, and therefore specific acid forming characteristics and potential deleterious element issues.

## Conclusions

Current methodologies used at the prefeasibility stage of mine operations to characterize waste rock extensively utilize laboratory based geochemical tests. Whilst mineralogical analyses are recognized as an integral part of predicting acid formation, they are not effectively used. Furthermore, routine textural analysis is largely absent from sample classification protocols despite its direct control on acid formation. Therefore, an integrated geochemistry-mineralogy-texture-geometallurgy (GMTG) approach is introduced in this chapter. It is designed for waste rock classification with potential applications at both historical and operational mines sites. This approach aims to use well established routine tests and classification methods, but also explores the application of additional techniques (e.g., LA-ICP-MS,

MLA-SEM) which have not been widely used in ARD prediction or waste rock classification studies. The GMTG approach is arranged in three-stages, with analytical sophistication increasing per stage, and the number of samples analysed decreasing. Samples selected for GMTG analyses are arranged into mesotextural groups as defined following routine geological hand-specimen evaluations, pXRF analysis and if required mineral identification using SWIR instrumentation (e.g., PIMA, TerraSpec).

Stage-one is a pre-screening stage, and comprises of simple, inexpensive tests, some of which can be performed in an onsite laboratory (e.g., paste pH). A simple evaluation scheme termed the ARD Index (ARDI) is proposed to evaluate texture. The ARDI assesses acid forming sulfide minerals individually by five categories A-E, specifically chosen based on the direct influence on acid formation. High scores indicate acid formation, low scores indicate low or no acid forming potential, and negative scores indicate an acid neutralizing capacity. Samples classified as NAF require no further GMTG testing. All others are subjected to stage-two analyses with the exception of those classified as having either a PNC or an ANC which require stage-two ANC testing only.

Stage-two uses routine geochemical tests to cross-check stage-one results and determine the actual acid forming or neutralizing capacity of samples. Mesotextural groups identified as PAF by stage-two and AF/EAF by stage-one require stage-three testing. At stage-three a carefully selected sub-set of samples is recommended for advanced NAG tests, and microtextural analyses to characterize microscale controls on acid formation as ultimately these dictate the acid forming nature of a sample. Representative samples from mesotextural groups with high ANC values (by stage-two) and several carbonate minerals should be scheduled for ABCC testing to determine the effective ANC. All of these data should be tabulated and from this, samples from EAF/AF mesotextural groups can be selected for kinetic testing if required. Based on GMTG testing, improved waste rock management plans can be developed as EAF/AF mesotextural groups are identified as separate entities that have a unique sulfide mineralogy and textures and therefore, acid forming characteristics.

## References

Akabzaa TM, Benoeng-Yakubo BK, Seyire JS (2007) Impact of mining activities on water resources in the vicinity of the Obuasi mine. W Afr J App Ecol 11:101–109

Alruiz OM, Morrell S, Suazo CJ, Naranjo A (2009) A novel approach to the geometallurgical modelling of the Collahuasi grinding circuit. Miner Eng 22:1060–1067

ANZECC (2000) Australian guidelines for water quality monitoring and reporting. National Water Quality Management Strategy Paper No. 7, Australian and New Zealand Environment and Conservation Council & Agriculture and Resource Management Council of Australia and New Zealand, Canberra

Ashley PM, Lottermoser BG, Collins AJ, Grant CD (2004) Environmental geochemistry of the derelict Webbs Consols mine, New South Wales, Australia. Environ Geol 46:591–604

Ashley PM, Craw D, Tighe MK, Wilson NJ (2006) Magnitudes, spatial scales and processes of environmental antimony mobility from orogenic gold-antimony mineral deposits, Australasia. Environ Geol 51:499–508

Australian Government Department of Industry, Tourism and Resources (2007) Managing acid and metalliferous drainage. Leading Practice Sustainable Development Program for the Mining Industry, Canberra

Blowes DW, Jambor JL (1990) The pore-water geochemistry and the mineralogy of the vadose zone of sulphide tailings, Waite Amulet, Quebec, Canada. Appl Geochem 5:327–346

Borden RK (2003) Environmental geochemistry of the Bingham Canyon porphyry copper deposit, Utah. Environ Geol 43:752–758

Bowell RJ, Rees SB, Parshley JV (2000) Geochemical predictions of metal leaching and acid generation: geologic controls and baseline assessment. Geol Ore Depos Great Basin Beyond Proc 2:799–823

British Columbia Acid Mine Drainage Task Force (BCAMDTF) (1989) Draft acid rock drainage technical guide—volume 1. Prepared by Steffen Robertson and Kirsten (SRK), Vancouver, British Columbia

Broadhurst JL (2007) Generalised strategy for predicting environmental characteristics of solid mineral wastes—a focus on copper. PhD thesis. University of Cape Town, South Africa

Broadhurst JL, Hesketh A, Harrison STL (2009) An integrated approach to the management of sulphide tailings and mitigation of acid mine drainage. In: Proceedings from the 8th international conference on acid rock drainage, Skelleftea, pp 1–10

Changul C, Sutthirat C, Padmanahban G, Tongcumpou C (2010) Assessing the acidic potential of waste rock in the Akara gold mining, Thailand. Environ Earth Sci 60:1065–1071

Craw D (2000) Water-rock interaction and acid neutralisation in a large schist debris dam, Otago, New Zealand. Chem Geol 171:17–32

Dold B, Fontboté L (2001) Element cycling and secondary mineralogy in porphyry copper tailings as a function of climate, primary mineralogy and mineral processing. J Geochem Explor 74:3–55

Downing BW (1999) ARD sampling and sample preparation. http://technology.infomine.com/enviromine/ard/sampling/intro.html

Downing BW, Giroux G (1993) Estimation of a waste rock ARD block model for the Windy Craggy massive sulphide deposit, northwestern British Columbia. Explor Min Geol 2:203–215

Egiebor NO, Oni B (2007) Acid rock drainage formation and treatment: a review. Asia Pac J Chem Eng 2:47–62

GARD (Global Acid Rock Drainage) guide (2015) The international network for acid prevention (INAP). http://www.gardguide.com/

Gifkins C, Herrmann W, Large R (2005) Altered volcanic rocks: a guide to description and interpretation. University of Tasmania, CODES Special Publication, Hobart

Goodall W (2008) Automated mineralogy in the prediction of acid rock drainage: accessible mineralogy using QEMSCAN®. In: Proceedings from the 2008 society for mining, metallurgy and exploration (SME) annual meeting and exhibit, society for mining, metallurgy and exploration, Littleton, Colorado, pp 1–9

Haffert L, Craw D (2010) Geochemical processes influencing arsenic mobility at Bullendale historic gold mine, Otago, New Zealand. NZ J Geol Geophys 53:129–142

Hammarstrom JM, Piatek NM, Seal RR, Briggs PH, Meier AL, Muzik TL (2003) Geochemical characteristics of TP3 mine wastes at the Elizabeth copper mine superfund site, Orange County, Vermont. Open-file report 03-431: 83. United States Geological Survey, United States

Harris DL, Lottermoser BG, Duchesne J (2003) Ephemeral acid mine drainage at the Montalbion silver mine, north Queensland. Aust J Earth Sci 50:797–809

Herrmann W, Blake MD, Doyle MG, Huston DL, Kamprad J, Merry N, Pontual S (2001) Short wavelength infrared (SWIR) spectral analysis of hydrothermal alteration zones associated with base metal sulphide deposits at Rosebery and western Tharsis, Tasmania, and Highway-Reward, Queensland. Econ Geol 96:939–955

Higueras P, Oyarzun R, Iraizoz JM, Lorenzo S, Esbri JM, Martinez-Coronado A (2012) Low-cost geochemical surveys for environmental studies in developing countries: Testing a field portable XRF instrument under quasi-realistic conditions. J Geochem Explor 113:3–12

Hitzman MW (1999) Routine staining of drill core to determine carbonate mineralogy and distinguish carbonate alteration textures. Miner Deposita 34:794–798

Huntington JF, Quigley M, Yang K, Roache T, Young C, Roberts I, Whitbourn LB, Mason P (2006) A geological overview of HyLogging 18,000 m of core from the eastern goldfields of Western Australia. In: Proceedings from the 6th International mining geology conference, AusIMM Publication Series No. 6, Darwin, Australia, pp 45–50

Jambor JL, Dutrizac JE, Groat L, Raudsepp M (2002) Static tests of neutralization potentials of silicate and aluminosilicate minerals. Environ Geol 43:1–17

Jamieson HE (2011) Geochemistry and mineralogy of solid mine waste: essential knowledge for predicting environmental impact. Elements 7:381–386

Keeney L (2008) EQUOtip hardness testing: Aqqaluk (including a guide on how to use EQUOtip). Technical report 2, P843 GeM, Australian mineral industries research association (AMIRA), Melbourne

Kentwell D, Garvie A, Chapman J (2012) Adequacy of sampling and volume estimation for pre-mining evaluation of potentially acid forming waste: statistical and geostatistical methods. In: Proceedings from the life-of-mine conference, Brisbane, pp 1–16

Lengke MF, Davis A, Bucknam C (2010) Improving management of potentially acid generating waste rock. Mine Water Environ 29:29–44

Lottermoser BG (2010) Mine wastes: characterization, treatment and environmental impacts, 3rd edn. Springer, Berlin 400 pp

Marescotti P, Azzali E, Servida D, Carbone C, Grieco G, De Capitani L, Luccheti G (2008) Mineralogical and geochemical spatial analysis of a waste rock dump at the Libola Fe-Cu sulphide mine (Eastern Liguria, Italy). Environ Earth Sci 61:187–199

Melquiades FL, Appoloni CR (2004) Application of XRF and field portable XRF for environmental analysis. J Radioanal Nucl Chem 262:533–541

Mills C, Robertson A, Shaw S (2011) Acid rock drainage at Enviromine. http://technology.infomine.com/enviromine/ard/home.htm

Moncur MC, Jambor JL, Ptacek CJ, Blowes DW (2009) Mine drainage from the weathering of sulfide minerals and magnetite. Appl Geochem 24:2362–2373

Moncur MC, Jambor JL, Ptacek CJ, Blowes DW (2015) Long-term mineralogical and geochemical evolution of sulfide mine tailings under a shallow water cover. Appl Geochem 57:178–193

Moon Y, Song Y, Moon HS (2008) The potential acid producing capacity and factors controlling oxidation tailings in the Guryong mine, Korea. Environ Geol 53:1787–1797

Morin KA (2010) The science and non-science of minesite-drainage chemistry, MDAG Internet Case Study #37. www.mdag.com/case_studies/cs37.html

Morin KA, Hutt NM (1998) Kinetic test and risk assessment for ARD. In: Proceedings of the 5th annual BC metal leaching and ARD workshop, Vancouver, Canada

Morin KA, Hutt NM (2009) On the nonsense of arguing the superiority of an analytical method for neutralising potential. www.mdag.com/case_studies/cs32.html

Munroe EA, McLemore VT, Kyle P (1999) Waste rock pile characterisation heterogeneity and geochemical anomalies in the Hillsboro Mining District, Sierra County, New Mexico. J Geochem Explor 67:391–405

Oyen CW, Fountain KB, McClellen GH, Eades JL (1998) Thin-section petrography of concrete aggregates: alternative approach for petrographic number evaluation of carbonate aggregate soundness. Soils Geol Found 1619:18–25

Paktunc AD (1999) Mineralogical constraints on the determination of neutralising potential and prediction of acid mine drainage. Environ Geol 39:103–112

Paktunc AD (2001) MODAN a computer program for estimating mineral quantities based on bulk composition: windows version. Comput Geosci 21:883–886

Parbhakar-Fox A (2012) Establishing the value of an integrated geochemistry-mineralogy-texture approach for acid rock drainage prediction. PhD thesis. University of Tasmania, Australia
Parbhakar-Fox A, Lottermoser BG (2015) A critical review of acid rock drainage prediction methods and practices. Min Eng 82:107–124
Parbhakar-Fox A, Edraki M, Walters S, Bradshaw D (2011) Development of a textural index for the prediction of acid rock drainage. Min Eng 24:1277–1287
Parbhakar-Fox A, Lottermoser BG, Bradshaw D (2013a) Evaluating waste rock mineralogy and microtexture during kinetic testing for improved acid rock drainage prediction. Min Eng 52:111–124
Parbhakar-Fox A, Lottermoser BG, Bradshaw D (2013b) Cost-effective means for identifying acid rock drainage risks: integration of the geochemistry-mineralogy-texture approach and geometallurgical techniques. In: Proceedings from the 2nd AusIMM international geometallurgy conference (GeoMet), Brisbane, Australia, pp 143–154
Pearce JI, Gutierrez J (2015) Opportunistic AMD sampling from multi-discipline drilling programs for large mining companies. In: Proceedings from the 10th international conference on acid rock drainage and international mine water association, Santiago, pp 1–11
Plumlee GS (1999) The environmental geology of mineral deposits. In: Plumlee GS, Logsdon MJ (eds) The environmental geochemistry of mineral deposits part A: processes, techniques and health issues. Rev Econ Geol 6A:71–116
Price WA (2009) Prediction manual for drainage chemistry from sulphidic geologic materials. CANMET Mining and Mineral Sciences Laboratories, Canada
Sapsford DJ, Bowell RJ, Dey M, Williams KP (2008) Humidity cell tests for the prediction of acid rock drainage. Min Eng 22:25–36
Smart R, Skinner WM, Levay G, Gerson AR, Thomas JE, Sobieraj H, Schumann R, Weisener CG, Weber PA, Miller SD, Stewart WA (2002) ARD test handbook: project P387A, prediction and kinetic control of acid mine drainage. AMIRA International Ltd, Melbourne
Smith L, Beckie R (2003) Hydrologic and geochemical transport processes in mine waste rocks. In: Jambor JL, Blowes DW, Ritchie AIM (eds) Environmental aspects of mine wastes. Short Course Ser 31:51–72
Sobek AA, Schuller WA, Freeman JR, Smith RM (1978) Field and laboratory methods applicable to overburden and minesoils. EPA 600/2-78-054, p 203
Song Q, Yanful EK (2011) Oxygen influx and geochemistry of percolate water from reactive mine waste rock underlying a sloping channeled soil cover. Appl Geochem 26:655–665
Stewart WA (2005) Development of acid rock drainage prediction methodologies for coal mine wastes. PhD dissertation, University of South Australia
Stewart WA, Miller SD, Smart R (2006) Advances in acid rock drainage (ARD) characterisation of mine wastes. In: Proceedings from the 7th international conference on acid rock drainage, Missouri, pp 2098–2119
Sverdrup HU (1990) The kinetics of base cation release due to chemical weathering. Lund University Press, Lund
Thompson AJB, Hauff PL, Robitaille AJ (1999) Alteration mapping in exploration: application of short-wave infrared (SWIR) spectroscopy. Soc Econ Geol Newsl 39:16–27
Tran AB, Miller S, Williams DJ, Fines P, Wilson GW (2003) Geochemical and mineralogical characterisation of two contrasting waste rock dumps—the INAP waste rock dump characterisation project. In: Proceedings from the 6th international conference on acid rock drainage, Cairns, pp 939–948
US Environmental Protection Agency (1994) Acid mine drainage prediction (EPA 530-R-94-036 NTIS PB94-201829). http://water.epa.gov/polwaste/nps/upload/amd.pdf
USDA Forest Service (1992) A conceptual waste rock sampling program for mines operating in metallic sulfide ores with a potential for acid rock drainage. Department of Agriculture, Forest Service, Ogden, Utah

Weber PA, Hughes JB, Conner LB, Lindsay P, Smart RC (2006) Short-term acid rock drainage characteristics determined by paste pH and kinetic NAG testing: cypress prospect, New Zealand. In: Proceedings from the 7th international conference on acid rock drainage, Missouri, pp 2289–2310

White WW, Lapakko KA, Cox RL (1999) Static test methods most commonly used to predict acid mine drainage: practical guidelines for use and interpretation. In: Plumlee GS, Logsdon MJ (eds) The environmental geochemistry of mineral deposits part A: processes, techniques, and health issues. Rev Econ Geol 6A:325–338

White A, Robb VM, Robb LJ, Waters DJ (2010) Portable infrared spectroscopy as a tool for the exploration of gold deposits in tropical terrains: a case study at the Damang deposit, Ghana. Society of Economic Geologists Special Publication 15, Littleton, Colorado, pp 57–84

WHO (2006) Working Together for Health. The World Health Report. http://www.who.int/whr/2006/whr06_en.pdf

# Chemical Staining Techniques for Drill Core Characterization

**Anita Parbhakar-Fox, Nathan Fox, Jake Moltzen and Bernd Lottermoser**

**Abstract** Accurate mineralogical identification is critical across the mining value chain from host rock characterization and alteration mapping, to mineral processing and environmental management. Advanced techniques for rapid mineralogical identification in drill core including hyperspectral scanners (e.g., HyLogger™, Corescan™) are becoming increasingly available to the mining industry. However, their high associated costs and logistical problems with deploying to field sites means that these techniques are not yet ubiquitously available. Mineral specific chemical staining techniques for carbonate and feldspar minerals offer a rapid and cheap alternative to hyperspectral scanning and more traditional mineral identification techniques (e.g., X-ray diffractometry, electron microprobe analysis). This contribution provides an updated review of chemical staining procedures for carbonate and feldspar minerals and how they can be used to map the distribution and texture of these minerals in drill core. Used under controlled health and safety conditions, chemical staining of drill core can assist with identification and mapping of these minerals during exploration activities (i.e., resolving alteration assemblages), feasibility studies (i.e., indicating ore grindability and flotation cell pH) and environmental assessments (i.e., domaining short and long term acid neutralization capacity).

A. Parbhakar-Fox (✉) · N. Fox · J. Moltzen
School of Physical Sciences, University of Tasmania, Private Bag 79, Hobart, TAS 7001, Australia
e-mail: Anita.Parbhakar@utas.edu.au

N. Fox
e-mail: Nathan.Fox@utas.edu.au

J. Moltzen
e-mail: Jake.Moltzen@stategrowth.tas.gov.au

B. Lottermoser
Institute of Mineral Resources Engineering, RWTH Aachen University, Wüllnerstrasse 2, 52062 Aachen, Germany
e-mail: lottermoser@mre.rwth-aachen.de



B. Lottermoser (ed.), *Environmental Indicators in Metal Mining*,
DOI 10.1007/978-3-319-42731-7_6

## Introduction

Mineralogy directly influences the way we explore for and recover mineral deposits. Each deposit is unique and requires extensive mineralogical characterization to optimize extraction (e.g., blasting) and processing (e.g., comminution, flotation) and to predict environmental impacts (e.g., acid rock drainage, ARD). Detailed mineralogical characterization at the deposit scale enhances our understanding of geological processes (e.g., hydrothermal ore formation) and can provide valuable mineralogical vectors for further exploration (e.g., brownfields exploration). But from an extractive perspective, mineral characterization allows detailed understanding of the geometallurgical properties of a deposit and offers the opportunity to predict environmental characteristics defined by mineralogy such as acid forming potential and acid neutralizing capacity. Laboratory-based, high-technology techniques for mineral identification include automated mineral analysers (e.g., mineral liberation analyzers, MLA) and X-ray diffractometry (XRD). A new generation of hyperspectral drill core scanners that utilize shortwave-infrared (SWIR) and long-wave or thermal-infrared (LWIR/TIR) technology, have emerged based largely on CSIRO's push-broom HyLogging systems (Huntington et al. 2006). Such scanners are capable of rapid and routine mineralogical analysis directly in drill core. Together, these techniques continue to transform the way that ore deposits are characterized by accurate mineralogical identification.

However, these technologies are expensive and although they are becoming more widely available, they are not always accessible. Such advanced technologies may be inaccessible either due to their high-associated purchase or running costs, or impracticalities for field or field-laboratory locations. As a cost effective alternative, we have revisited well-established staining methods that offer a simple, rapid and cost effective alternatives for the identification of carbonate and feldspar minerals in both drill core and hand specimens. These mineral groups directly influence geometallurgical processing by impacting on ore hardness (grindability) and pH conditions during mineral processing, e.g. during flotation (Baum 2014). Both carbonates and feldspars also offer short- and long-term acid neutralizing capacity in waste rock or tailings environments (Jambor et al. 2000; Weber et al. 2005), making accurate mineralogical domaining critical for improved characterization of waste rock materials (e.g., Parbhakar-Fox et al. 2011).

This chapter provides a summary of the chemical staining techniques available for the identification and distinction of carbonate and feldspar minerals and validation testing using X-ray diffractometry (XRD) and electron probe microanalysis (EMPA). Although microanalytical mineral identification is considered more accurate and robust, chemical stains represent rapid and cost-effective phase identification techniques that effectively provide mineralogical information on a small scale (e.g., μm) in field- or site-based laboratories.

## Chemical Staining Practices

Staining techniques utilize chemical or organic reagents to identify a range of common alteration and gangue minerals including carbonates, feldspars and sulfates (e.g., Gabriel and Cox 1929; Friedman 1959; Reid 1969; Green 1993; Hitzman 1999; Walker and Cohen 2006). When applied to thin sections, sawn rock slabs or drill core, the mineralogy and textural relationships of primary and alteration minerals can be observed. Stains can also be applied to crushed rock sampled from conveyors, for example in the aggregates and industrial minerals and mining sectors. Samples are etched with acid before application of chemical stains or reagents. Due to the hazardous nature of some chemicals, occupational health and safety factors must be considered for certain working environments. Table 1 summarizes the acids and reagents used for staining carbonate and feldspar minerals.

### *Carbonate Staining*

Carbonate minerals (e.g., calcite, dolomite and ankerite) are common primary ore minerals or products of hypogene and supergene alteration in a range of Cu, Au, Pb,

**Table 1** Reagents used for chemical staining of carbonate and feldspar minerals

| | Etching acid | Concentration (%) | Staining reagent | References |
|---|---|---|---|---|
| *Carbonates* | | | | |
| Calcite, ferroan calcite, witherite, cerussite | HCl | 2[a] | Alizarin-red S or sodium alizarinosulfate ($C_{14}H_7NaO_7S$) | Freidman (1959) |
| Ferroan dolomite, ferroan calcite | HCl | 2 | Potassium ferricyanide ($K_3Fe(CN)_6$) | Freidman (1959) |
| Dolomite, magnesite | HCl | 2 | Titan/thiazole yellow ($C_{28}H_{19}N_5Na_2O_6S_4$) | Freidman (1959) |
| *Feldspars* | | | | |
| Potassium feldspar | $HF_{(aq)}$ | 52[b] | Sodium cobaltinitrate ($Na_3CO(NO_2)_6$) | Gabriel and Cox (1929), Bailey and Stevens (1960) |
| Plagioclase feldspar | $HF_{(aq)}$ | 52[b] | (1) Barium chloride ($BaCl_2$)<br>(2) Potassium rhodizonate ($C_6O_6K_2$) | Bailey and Stevens (1960) |

[a]2 % HCl solution is prepared by diluting 2 ml of concentrated HCl in 100 ml of deionized water
[b]Hydrofluoric acid (HF) is highly toxic, causing burns and long term calcium degradation of bones if in contact with skin. HF should only be used in approved and tested fume hoods and appropriate personal protective equipment should be used

**Table 2** Staining colours generated by reagents on carbonate minerals

| Mineral | Alizarin red-S (ARS) | Potassium ferricyanide (PF) | Titan yellow (TY) |
|---|---|---|---|
| Calcite ($CaCO_3$) | Red to pink | Unstained | Unstained |
| Aragonite ($CaCO_3$) | Red to pink | Unstained | Unstained |
| Ferroan calcite (Ca, Fe)$CO_3$ | Pink to pale pink | Pale to deep blue | Unstained |
| Witherite ($BaCo_3$) | Red | Unstained | Unstained |
| Cerussite ($PbCO_3$) | Mauve | Unstained | Unstained |
| Dolomite ($CaMg(CO_3)_2$) | Unstained | Unstained | Red to orange |
| Ferroan dolomite (Ca(Mg,Fe) $CO_3)_2$ | Unstained | Pale to deep turquoise | Unstained |
| Rhodocrosite ($MnCO_3$) | Unstained | Pale brown | Unstained |
| Magnesite ($MgCO_3$) | Unstained | Unstained | Red to orange |
| Siderite ($FeCO_3$) | Unstained | Unstained | Unstained |
| Ankerite ($CaMg(CO_3)_2$) | Unstained | Unstained | Unstained |

Zn and Fe deposits. Similarities in the diagnostic properties (e.g., hardness, colour, HCl reactivity) of the carbonate-group minerals makes accurate differentiation of individual carbonate minerals in hand specimen challenging. Chemical staining imparts coloured precipitates onto acid etched mineral surfaces to allow visual differentiation between calcite, ferroan calcite, dolomite, ferroan dolomite, witherite and cerussite (Table 1). Hitzman (1999) highlighted the importance of routine rock and drill core staining to identify carbonate textures and mineralogical zonation in the Irish Zn-Pb district, McArthur River Zn-Pb-Ag district and Ruby Creek Cu-Co deposits. Rock samples, drill core or crushed aggregates are initially etched for 2–3 min with 2 % hydrochloric acid (HCl). The HCl etch and the staining chemicals can be applied with paintbrushes to intact rock, or crushed aggregates immersed in these stains. Etching with a concentration of HCl > 2 % will promote vigorous reaction, with the carbonate minerals generating $CO_2$ bubbles that prevents reaction and adhesion of the stains. Table 2 summarizes the diagnostic colours imparted by each carbonate stain on reaction with the listed carbonate minerals. Alizarin red-S (ARS) stains calcite red and ferroan calcite pink, whereas dolomite and ferroan dolomite are unstained by this reagent. Potassium ferricyanide (PF) stains ferroan calcite pale to deep blue and ferroan dolomite turquoise, but it does not stain calcite. Dolomite is stained red to orange by titan yellow, which does not affect any other mineral except magnesite (Table 2). Evamy (1963) proposed ARS + PF as a method to differentiate four different carbonates (calcite, red; Fe-calcite, turquoise; Fe-dolomite, pale blue; ankerite, dark blue).

## *Feldspar Staining*

The feldspars comprise a group of aluminosilicate minerals with similar chemical and physical properties. Compositionally, the alkali feldspars (K-feldspars) form a

**Table 3** Staining colours generated by reagents on feldspar-group minerals

| Mineral and formula | Chemical reagents | |
|---|---|---|
| | Sodium cobaltinitrate | Barium chloride *plus* potassium rhodizonate |
| *Alkali feldspars* | | |
| Orthoclase, $KAlSi_3O_8$ | Yellow | Unstained |
| Microcline, $KAlSi_3O_8$ | Yellow | Unstained |
| Adularia, $KAlSi_3O_8$ | Yellow | Unstained |
| Sanidine $(K,Na)(Si,Al)_4O_8$ | Yellow | Unstained |
| Anorthoclase $(Na,K)AlSi_3O_8$ | Weak yellow | Red to pink |
| *Plagioclase feldspars* | | |
| Albite $NaAlSi_3O_8$ | Unstained | Unstained |
| Oligioclase $(An_{90\text{-}70})$, $(Na,Ca)(Si,Al)_4O_8$ | Unstained | Red-pink |
| Andesine $(An_{70\text{-}50})$ $(Na,Ca)(Si,Al)_4O_8$ | Unstained | Red |
| Labradorite $(An_{50\text{-}30})$ $(Na,Ca)(Si,Al)_4O_8$ | Unstained | Red |
| Bytownite $(An_{30\text{-}10})$ $(Ca,Na)(Si,Al)_4O_8$ | Unstained | Red |
| Anorthite $(An_0)$, $CaAl_2Si_2O_8$ | Unstained | Red |

solid solution from potassium (orthoclase) to sodium (albite) end-members, whereas the plagioclase feldspars form a solid solution from sodium- (albite) to calcium-rich (anorthosite) end-members (Table 3; Deer et al. 2001). The K-feldspar group contains several polymorphs including orthoclase, microcline and adularia, which show varying degrees of structural disorder (Deer et al. 2001). As a major constituent of plutonic and volcanic rocks the composition and abundance of feldspar minerals is fundamental to rock classification. K-feldspar is diagnostic of zones of potassic alteration, typically located in the core of most porphyry Cu-Au deposits and some iron-oxide-copper-gold deposits (e.g., Seedorf et al. 2005; Sillitoe 2010). Although hydrothermal K-feldspar may appear pink in colour due to microscopic hematite inclusions, it can also be white making it indistinguishable from other feldspar minerals, particularly when fine-grained in hand specimens. Adularia, a low temperature polymorph of orthoclase, is common in low-sulfidation epithermal veins and associated alteration envelopes (Simmons et al. 2005). Zones of texturally destructive secondary plagioclase (albite to oligioclase) related to sodic-calcic alteration (plagioclase-actinolite) occur in the deepest parts of some porphyry deposits, including Yerington (Dilles et al. 2000) and Cadia East (Fox et al. 2015), and in the regionally extensive alteration surrounding iron-oxide-copper-gold deposits (e.g., Mount Isa; Williams et al. 2005). The feldspar group minerals may have similar physical properties (e.g., colour, hardness), when observed in the field or core-shed, leading to misidentification and errors with visual classification of igneous rock types and alteration during sampling and drill core logging. Identification of feldspar alteration (e.g., K-feldspar vs. plagioclase feldspar) and their associated textures (e.g., vein infill, vein envelope, replacement) can assist with exploration, particularly on the fringes of mineralized centres in the field

or in exploration diamond drill core. From a mineral processing perspective, zones of intense feldspar alteration can affect the comminution process, and in some cases, may lead to early modifications of ball and SAG mill design, e.g. Cadia Valley, New South Wales (Keeney 2010; Bonnici 2012). Thus, early identification of feldspathic ore and waste rock can improve the long-term efficiency of blasting, crushing and processing circuits.

Staining methods for the identification of alkali feldspar (e.g., Gabriel and Cox 1929; Keith 1939; Chayes 1952) and plagioclase feldspar (Bailey and Stevens 1960) are well established. Staining has been widely used to assist visual discrimination of minerals for point counting in transmitted light microscopy (Keith 1939) and more generally for fast discrimination between feldspar groups in hand specimens (Chayes 1952; Bailey and Stevens 1960). Despite careful safety considerations associated with using strong acids, feldspar staining techniques can be routinely applied to large rock samples and voluminous sample numbers. Staining has an advantage over other techniques (such as optical petrography or SEM analyses which are either too costly or inadequate for processing large sample numbers). Furthermore, feldspar and carbonate staining techniques enhance mineralogical and textural features such as phenocrysts, vein or breccia infill and alteration envelopes making it an effective mineral mapping technique.

## *Chemical Safety Considerations*

For carbonate staining, samples are first etched using dilute hydrochloric acid. Considering the low concentrations (1–2 %), there is no immediate health and safety risks from regular application to rocks. The materials safety data sheets for commonly used Alizarin-red S and titan yellow stains indicate that if ingested, these stains may be toxic and may be an irritant in case of direct skin contact. To mitigate against any potential risks, appropriate personal protective equipment including safety glasses, lab coat, enclosed shoes and gloves is recommended.

Feldspars are highly insoluble in most acids (e.g., HCl, $HNO_3$), except under sustained experimental conditions. Hydrofluoric acid (HF) is the only strong acid capable of etching feldspars in the short term. Ammonium bifluoride ($NH_4HF_2$) has been proposed as a safer alternative to conventional hydrofluoric acid and may be used for total digestion of refractory minerals (e.g., zircon), prior to solution ICPMS geochemistry (Zhang et al. 2012). However, the material safety data sheet (MSDS) for ammonium bifluoride carries similar associated health risks as HF, including corrosion and burns on exposure to skin and eyes and lung damage if exposed to vapours (hydrogen fluoride). The potential health and safety implications associated with using HF will likely preclude feldspar staining in field environments and at field laboratories or offices. Acid etching using HF should only be carried out in laboratories fully equipped with a fume hood, running water and safety showers, and appropriate eye, skin and face protection should be always be worn.

## Materials and Methods

### *Carbonate Staining*

In order to test various carbonate staining methodologies, a range of carbonate-rich samples were selected. Twenty samples from the Palaeoproterozoic Koongie Park Formation (Western Australia, WA) were chosen as this unit, having been subjected to carbonate-associated base metal mineralization, contains both calcite and dolomite. Additionally, five calcite-rich drill core slabs from a porphyry-Cu deposit in New South Wales (NSW) were obtained, as well as pure dolomite and calcite samples. To test whether stains can also be used on grain mount samples and to assist in automated mineralogical classification using reflected light microscopy (i.e., to distinguish carbonates), two waste rock and run-of-mine (ROM) samples from two Australian mine sites (RDW-1, CE-2) were investigated. These samples were dry sieved to a range of size fractions (125–250, 250–500, 500–1000, 1000–2000, 2000–4000 μm), with grains subsequently mounted in resin (after being rinsed with ethanol to remove fines).

Prior to staining, samples were etched using dilute hydrochloric acid (HCl) for 2–3 min and subsequently washed under running water. Next, samples were stained using a dual stain ARS-PF dissolved in HCl. Titan yellow was selected as the most appropriate dolomite stain for use in this study following the recommendations given in Friedman (1959), who reviewed the application of dolomite specific stains. The experimental procedure adopted is summarized in Fig. 1. Staining tests on drill core samples were undertaken in the order: (1) ARS-PF mixed solution and (2) titan yellow. The use of applying both stains was also explored to stain both calcite and dolomite in one procedure, rather than removing the stain and re-coating with another.

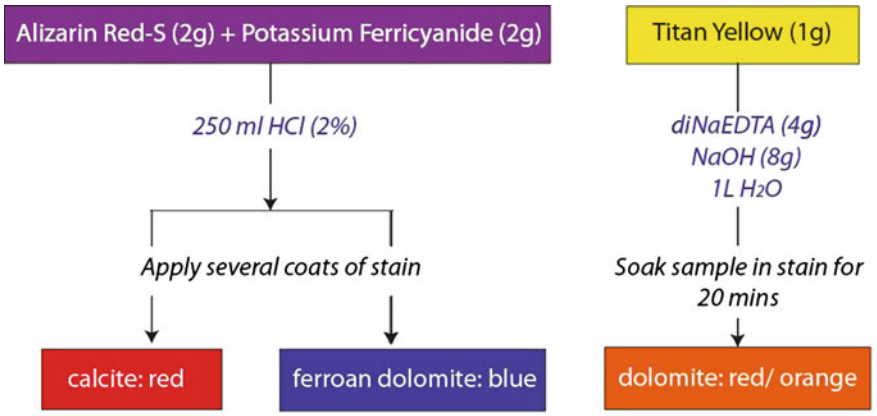


**Fig. 1** Stain preparation, application and carbonate response colours used in this study (color figure online)

Samples were imaged before and after each test and subsequently washed in both dilute HCl and water, with the sample surface cleaned with wet/dry paper to ensure the full removal of each stain. Prior to undertaking the next staining test, samples were re-etched with dilute HCl and stained. After these preliminary drill core tests, grain mount samples (n = 7), which contained significant calcite and/or dolomite (as indicated by XRD analyses), were subjected to the most effective procedure, with results presented in the following sections.

Validation testwork was performed on grain mount samples using a FEI Quanta 600 Mineral Liberation Analyzer-Scanning Electron Microscope (Central Science Laboratory, University of Tasmania). Grain mounts samples were first cleaned with ethanol before being carbon coated. Next, samples were subjected to X-ray modal (XMOD) analyses in order to rapidly identify each mineral phase present (cf. Gu 2003; Fandrich et al. 2007), with back scattered electron (BSE) images also collected. Post processing first involved classifying the XMOD spectra against the general CSL mineral library. Next, colours were only assigned to carbonate (blue and red) and sulfide (orange and yellow) minerals. All other minerals were coloured white. For each sample, classified XMOD and BSE frames were stitched together to produce images of whole samples. Finally, both images were overlain using GIMP image processing software.

## *Feldspar Staining*

Four samples of porphyritic to coarse equigranular igneous rocks, containing both plagioclase and alkali feldspars, were chosen for examination of feldspar staining techniques. A sample of white coarse granite from eastern Tasmania (14G1A), pink equigranular granite from eastern Tasmania (Sample 14G2A), a white equigranular granite from western Tasmania (Sample 14G4A) and a quartz latite porphyry from Bingham Canyon (14BC1A) were used in this study.

Each sample was cut, ground and washed prior to analysis. The strict occupational health and safety requirements (including use of all personal protective equipment outlined previously), must be followed before using hydrofluoric acid. The following method has been modified from techniques developed by Gabriel and Cox (1929) and Bailey and Stevens (1960). Samples were etched in 52 % hydrofluoric acid (HF) which was applied directly to the rock surface using a paintbrush inside a fully operational fume hood. The etching acid was removed after 60 s in running water. Concentrated sodium cobaltinitrate solution, the stain for alkali feldspar, was applied to the etched area, also using a paintbrush, allowed to react for 60 s before removal in running water. The sample was dried either in an oven (60 °C) or using a hot air dryer. The two-stage stain for plagioclase feldspar can be applied on top of the alkali feldspar stain with no need to re-etch using HF. A solution of 5 % barium chloride is first applied to the etched area and allowed to react for 60 s before washing in running water. Each sample was again dried before application of potassium rhodizonate solution on the etched area and again allowed

to react for 60 s before washing in running water and then dried. Each sample was digitally imaged before and after staining to facilitate identification of stained phases. Representative areas of each sample were analyzed using a Cameca SX100 wavelength dispersive electron microprobe at the University of Tasmania to validate the results of the staining experiments. Analyses were normalized according to the procedure outlined by Deer et al. (2001).

## Results

### *Carbonate Drill Core Staining*

Results from select carbonate-rich drill core samples (n = 4) subjected to the four staining tests are presented here. The sample shown in Fig. 2a is a chlorite-carbonate-sphalerite schist, with the carbonate mineralogy dominated by dolomite. When stained with ARS + PF, a bright blue was observed in the finer-grained upper right hand portion (Fig. 2b), indicating the pervasive distribution of fine grained ferroan dolomite. Some blue coloration was seen in the lower portion of the sample, indicating the presence of coarser ferroan dolomite, along with coarse red clots of calcite. Fine grained calcite was also pervasive in the matrix of the lower, coarser portion of the sample. Etching after staining (i.e., to highlight

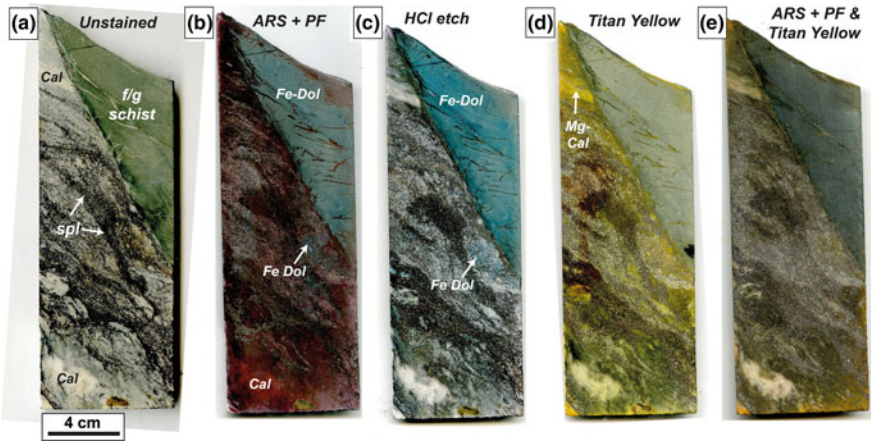


**Fig. 2** Drill core staining on a chlorite-carbonate-sphalerite schist sample (Koongie Park Formation, WA): **a** unstained sample; **b** stained with a combination of Alizarin red-S (ARS) and potassium ferricyanide (PF) with ferroan dolomite *stained blue*, and calcite *stained red*; **c** post ARS-PF staining etch with HCl, with the Fe-Dol rich areas exhibiting a stronger stain colour; **d** stained with titan yellow (c. 3 h) with Mg calcite identified only; **e** ARS-PF staining following titan yellow with only ferrous dolomite identified (*dark blue*). *Cal* calcite, *Fe-Dol* ferroan dolomite, *f/g* fine-grained, *Mg-cal* magnesium rich calcite, *spl* sphalerite (color figure online)

ferroan dolomite rich-zones) confirmed observations of ferroan dolomite distribution, with a stronger blue colour demonstrated (Fig. 2c). Staining with titan yellow (c. 3 h) indicated that pure dolomite is unlikely present in this sample (Fig. 2d). Calcite in the upper left portion stained yellow indicating that it is Mg-rich (Fig. 2d), thus there are two chemical forms of calcite present. The fine-grained ferroan dolomite exhibited a faint dark-blue colour (Fig. 2e) when stained using the ARS +PF followed by the titan yellow method, however, no calcite was easily identifiable when compared to Fig. 2b.

Results from a carbonate-talc schist sample are presented in Fig. 3, which contains large, boudins of dolomite and quartz surrounded by foliated calcite and

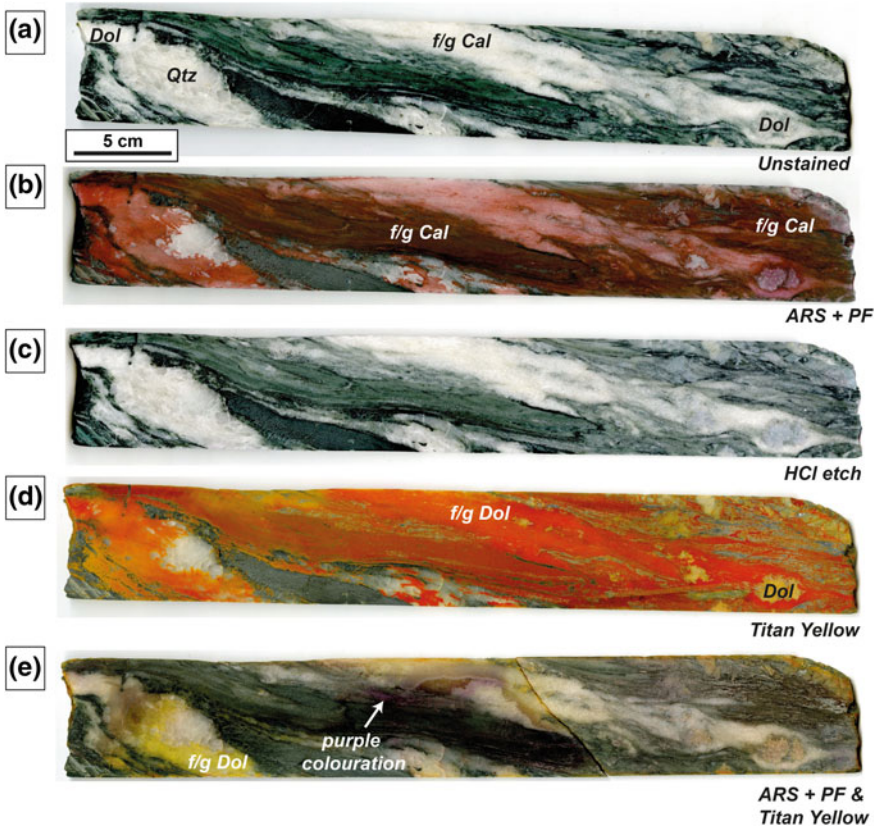


**Fig. 3** Drill core staining on a carbonate-talc schist sample (Koongie Park Formation, WA): **a** unstained sample, **b** stained with a combination of Alizarin red-S (ARS) and potassium ferricyanide (PF) with calcite *stained red*; **c** post ARS-PF staining etch with HCl, confirming the absence of ferroan dolomite; **d** stained with titan yellow (c.16 h) with abundant fine grained dolomite identified (*stained red*) and coarser dolomite clasts *stained yellow*; **e** ARS-PF staining following titan yellow with only some dolomite identified (*yellow*). *Cal* calcite, *Dol* dolomite, *f/g* fine-grained (color figure online)

talc (Fig. 3a). Staining with ARS + PF identified fine-grained calcite within the fabric, and white vein material. However, it was not evenly distributed, with a portion towards the bottom left of the sample unstained as was the coarse clotted quartz (Fig. 3b). No ferroan dolomite was observed, as confirmed by the post-stain HCl etch (Fig. 3c), with the original pre-staining appearance of the sample restored (cf. Figure 3a). Staining with titan yellow (c. 16 h) showed a strong response in the white vein material, suggesting the presence of fine-grained dolomite intergrown with minor calcite (Fig. 3d). The dolomite boudins show a weak yellow stain. Staining using ARS-PF followed by titan yellow resulted in weak purple colouration at the margins of the white vein material, and a strong yellow dolomite-rich zone in the bottom left hand corner (Fig. 3e). Calcite did not demonstrate a stain response.

A dolomite breccia sample (also containing calcite) is shown in Fig. 4a. When stained using the ARS-PF solution, all carbonate material (i.e., white in Fig. 4a) assumed a pink-pale red colour, with a faint blue colour seen in the bottom left portion of the sample (Fig. 4b), indicating that dolomite is closely associated with pervasively distributed calcite (possibly overprinted during a later stage alteration event). The post staining HCl etch showed small distinct patches of ferroan dolomite (Fig. 4c). Staining with titan yellow (c. 3 h) showed only the weak fixation of stain to the dolomite clasts, with a pale pink to orange-red colour demonstrated (Fig. 4d). Finally, a combination of staining using now titan yellow first, followed by ARS-PF, highlighted the presence of ferroan dolomite (dark blue clots) and a general pale pink colouration was generally imparted, and now a large clast of ferroan dolomite was clearly observed in the bottom left hand corner.

Finally, a dolomitic sample with radiating pyrite following ‘pipe’ like structures in dolomite was tested (Fig. 5a). Staining with ARS-PF showed strong colouration across the majority of the sample, however, in proximity to pyrite veins, a blue colour was observed, but rather than depicting the presence of ferroan dolomite, it was caused by the reaction of pyrite to the acidic staining solution (Fig. 5b). The absence of ferroan dolomite was confirmed in the post-stain HCl etch, with no strong blue colours seen (Fig. 5c). Staining with titan yellow (c. 3 h) showed a weak response, with some pale pink-orange patches observed (Fig. 5d). Finally, the combined use of titan yellow followed by the ARS-PF stain showed the strong presence of calcite in the upper left portion, an a weak pink colour elsewhere, however, pyrite appeared to stain blue (Fig. 5e).

## Validation Using Automated EDS-SEM

A grain mount comprising a coarse-sized fraction (RDW-1, 1000–2000 μm) was analyzed by EDS-SEM using an XMOD mode to automatically identify carbonate minerals. The results are overlain on the corresponding BSE image in Fig. 6a, with examples of calcite identified in the enlarged inset image. XMOD analysis readily identified carbonate and sulfide minerals due to the relatively coarse grain size of the sample. Dolomite (not shown) was observed locally intergrown with silicate

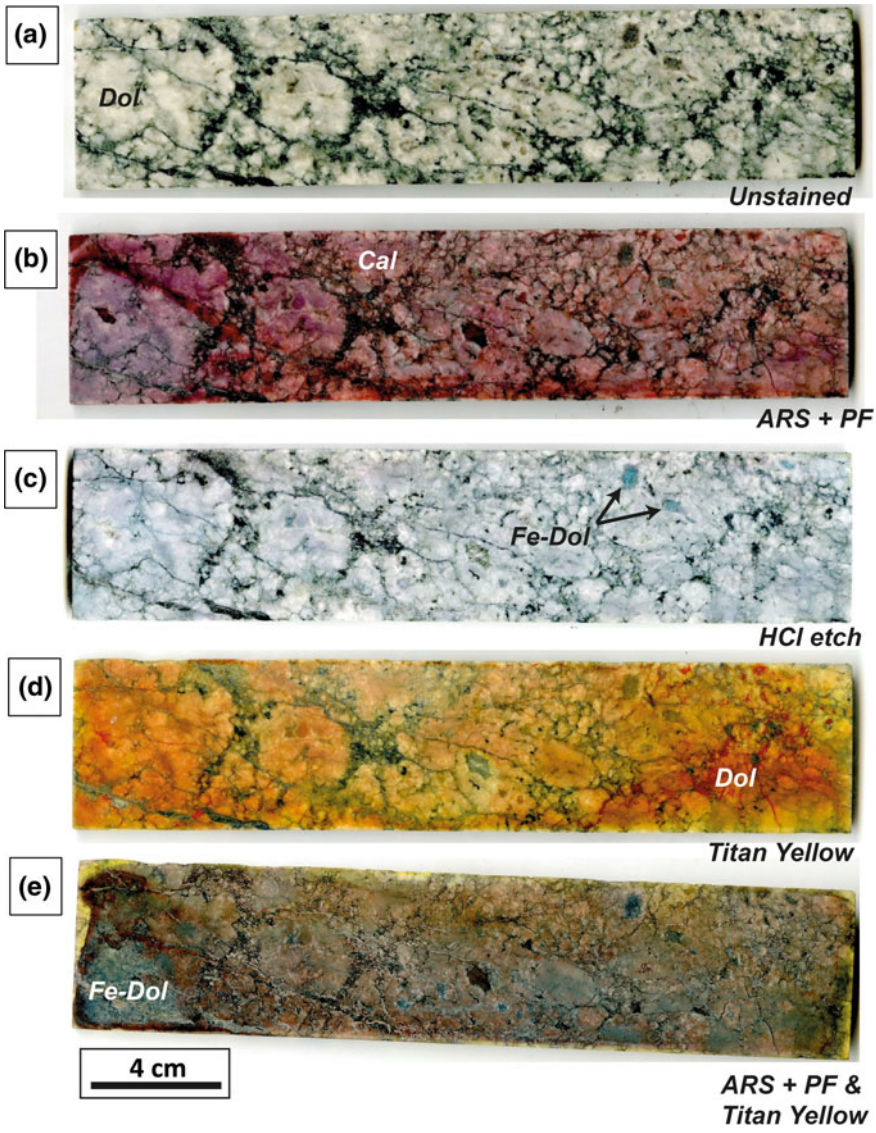


**Fig. 4** Drill core staining of a carbonate breccia sample (Koongie Park Formation, WA): **a** unstained sample; **b** stained with a combination of Alizarin red-S (ARS) and potassium ferricyanide (PF) with pervasive calcite *stained red*; **c** post ARS-PF staining etch with HCl, confirming the presence of ferroan dolomite clots; **d** stained with titan yellow (c. 3 h) with dolomite clasts assuming a weak *pink-orange-red* colour; **e** *titan yellow* followed by ARS-PF staining with only dolomite and ferroan dolomite clearly identified (*blue*). *Cal* calcite, *Dol* dolomite, *Fe-Dol* ferroan dolomite, *f/g* fine-grained (color figure online)

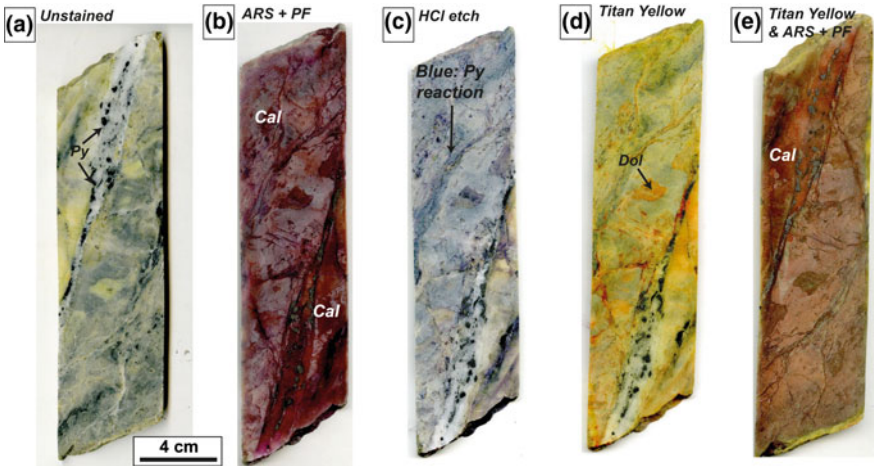


**Fig. 5** Drill core staining of a dolomite-rich sample containing pyrite (Koongie Park Formation, WA): **a** unstained sample; **b** stained with a combination of Alizarin red-S (ARS) and potassium ferricyanide (PF) with the *bottom right portion* stained intensely *red* indicating the presence of calcite; **c** post ARS-PF staining etch with HCl, confirming the absence of ferroan dolomite, but a blue colouration observed around pyrite veins; **d** stained with titan yellow (c. 3 h) with some dolomite identified (*stained pink-red*); **e** *titan yellow* followed by ARS-PF staining with only some dolomite identified (*yellow*). *Cal* calcite, *Dol* dolomite, *Py* pyrite (color figure online)

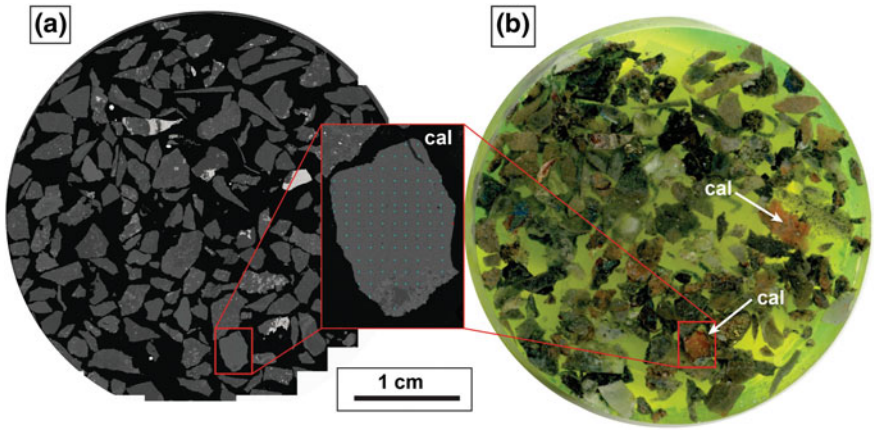


**Fig. 6** Waste rock sample (RDW-1 1000–2000 μm) as grain mount: **a** Back scattered electron (BSE) image with overlaid XMOD of the grain mount (*inset*) calcite grain (as depicted by *blue dots*) with minor silicate mineral intergrowths observed at the bottom of the grain. **b** The same mount stained using ARS-PF highlighting calcite (cal) grains in *pink* (color figure online)

phases, with both ferroan and non-ferroan dolomite distinguished. The resolution of XMOD analyses can be improved by modifying the point count to a shorter pixel

distance. Whilst this increases the analysis time, the accuracy is improved. For this application, XMOD is preferred over the more time consuming extended back-scattered electron liberation analysis (XBSE) mapping, which for this particular size fraction took more than 2 h (including analysis and post-processing) making XBSE a more costly technique.

To validate the XMOD results using the staining techniques and vice versa, the grain mount was stained using ARS-PF procedure after removal of the carbon coating. The calcite grains readily identified in the sample by XMOD (Fig. 6a) were also recognized by carbonate staining (Fig. 6b) demonstrating a distinct pink-staining response.

## *Feldspar Staining*

The alkali feldspars analyzed range in composition from end-member orthoclase ($Or_{99}Ab_1An_0$) in pink granite sample 14G2A to sanidine ($Or_{70.5}Ab_{28}An_{0.5}$) in sample 14BC1A. Chemical staining (Fig. 7), with sodium cobaltinitrate creates a bright yellow precipitate on the surface of the alkali feldspar (Fig. 7g, h). Hieratite, $K_2SiF_6$, is a highly reactive fluorosilicate, is precipitated on the surface of alkali feldspar after HF etching (Sclar and Fahey 1972). Concentrated sodium cobaltinitrate solution applied to the etched sample reacts with hieratite to form a diagnostic insoluble yellow precipitate of potassium sodium cobaltinitrate ($K_2Na[Co(NO_2)_6]$; Fiegl 1958). The brightness and intensity of the precipitate is proportional to the amount of potassium in the feldspar such that orthoclase produces a more intense yellow colouration than sanidine (Fig. 8). Although no anorthoclase was analysed in this study, sodium cobaltinitrate has been reported to be relatively insensitive to anorthoclase, likely due to the lower $K_2O$ content (Chayes and Zies 1961; Deer et al. 2001). Significantly, the calcium content of anorthoclase suggests that it may also be susceptible to staining by the plagioclase feldspar method of Bailey and Stevens (1960). Plagioclase analyzed in this study ranges from end-member albite ($Or_0Ab_{99.5}An_{0.5}$) in pink granite sample 14G2A to andesine ($Or_3Ab_{65}An_{32}$) in white granite sample 14G1A (Figs. 7 and 8). Plagioclase feldspar in HF-etched rocks stains red after application of barium chloride and potassium rhodizonate. The intensity of the diagnostic red precipitate depends on the calcium (anorthite) content of the feldspar. With moderate contents of anorthite ($An_{>10}Ab_{<90}$), oligioclase and andesine stain a distinctive brick red colour (Fig. 7), whereas albite ($An_{<10}Ab_{>90}$) adopts only a weak pink colouration (Fig. 7). Pure albite ($An_{0.8}Ab_{98.4}Or_{0.8}$) in pink granite sample 14G2A appears to adopt no stain, although the albite itself has a pink colouration in the unstained sample (Fig. 7g, h).

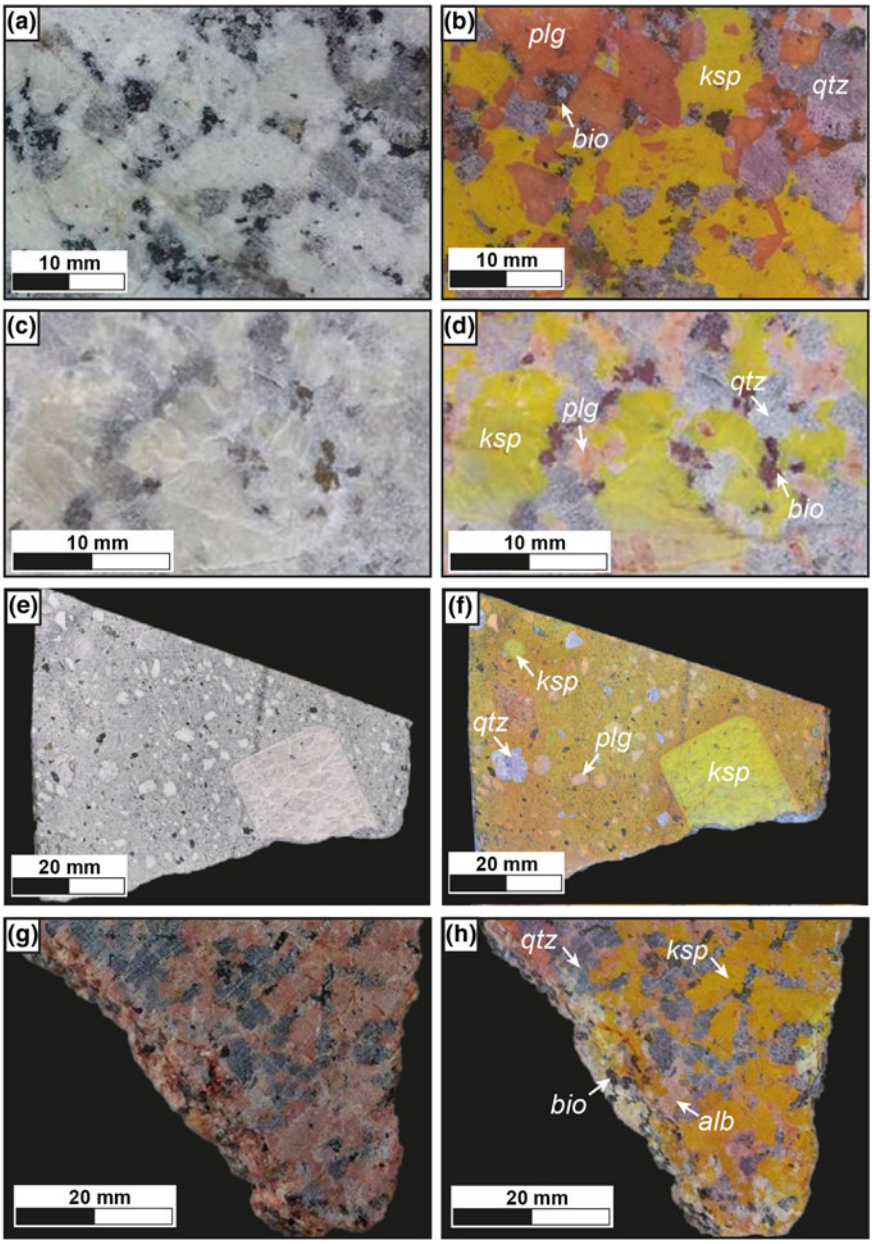


**Fig. 7** Results of feldspar staining of igneous rocks (*left hand side*—unstained, *right hand side*, stained): **a**, **b** granite 14G1A; **c**, **d** granite 14G4A; **e**, **f** quartz latite porphyry, 14BC1A; **g**, **h** granite 14G2A. *alb* albite, *bio* biotite, *ksp* alkali feldspar, *plg* plagioclase, *qtz* quartz (color figure online)

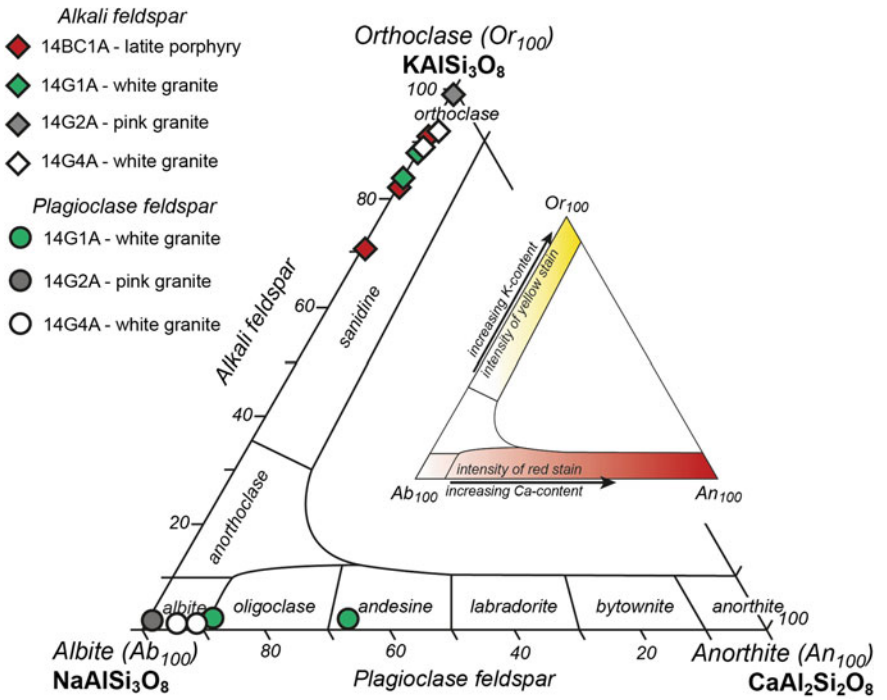


**Fig. 8** Ternary diagram showing the end-member compositions of feldspars and the results of electron microprobe analyses completed on granite samples in this study. The *inset* ternary diagram summarizes the compositional control on colour variations after chemical staining (color figure online)

## Conclusions

Rapid and cost-effective techniques for drill core characterization are required for deposit-wide geological characterization from the earliest life-of-mine stages (e.g., exploration). Early identification of environmental and geometallurgical liabilities, which could be economically detrimental later in the mine life, will influence the overall economic performance of mining projects.

Chemical staining techniques are diagnostic for specific carbonate-group and feldspar-group minerals and can be applied during exploration activities (i.e., resolving alteration assemblages), feasibility studies (i.e., indicating ore grindability and flotation cell pH) and environmental assessments (i.e., domaining short and long term acid neutralization capacity). Staining techniques can readily be used in the field or in the core shed to enhance accurate drill core logging and mineralogical domaining. Consequently, a series of chemical stains was performed by this study for carbonate and feldspar groups to explore the strengths and weakness of existing staining techniques. Outcomes of these activities were as follows:

- Chemical staining of drill core samples using either ARS-PF or titan yellow is effective for identifying calcite and ferroan dolomite, however, as this stain is acidic, reaction with sulfides was observed, with false stains (blue) seen adjacent to sulfide minerals.
- The titan yellow stain was inconsistent in its reaction with dolomite, with a much longer reaction time required for a strong staining response (c. 16 h) than prescribed by Freidman (1959).
- A combined use of both ARS-PF and titan yellow (in either order) was not effective in simultaneously staining both calcite and dolomite.
- Chemical staining of grain mounts stained calcite a diagnostic pink colour.
- Feldspar staining techniques are specific to end-member compositions—colour variations depend on the chemical composition of the feldspars.

The necessity remains to develop a one-step carbonate staining procedure, as this will assist with environmental drill-core logging, for which industry protocols need to be formally established. Such staining will improve the deposit-wide definition of neutralizing potential without the requirement for more expensive analyses (e.g., hyperspectral logging) which may not necessarily be undertaken on waste-rock drill holes. A more detailed understanding of the effects of carbonate texture (e.g., micritic, sparry) on neutralizing potential must also be explored. Additionally, low-cost methods for quantifying trace elements (e.g., Pb, Zn) in carbonates must be established, because under acid conditions they are potentially liberated, impacting on leachate quality. Regardless of these deficiencies and challenges, chemical staining techniques offer rapid, texturally informative alternatives to high-end X-ray imaging or mapping techniques.

## References

Bailey EH, Stevens RE (1960) Selective staining of K-feldspar and plagioclase on rock slabs and thin sections. Am Mineral 45:1020–1025

Baum W (2014) Ore characterization, process mineralogy and lab automation a roadmap for future mining. Min Eng 60:69–73

Bonnici N (2012) The mineralogical and textural characteristics of Cu-Au deposits related to mineral processing attributes. PhD thesis. University of Tasmania, Australia

Chayes F (1952) Notes on the staining of potash feldspar with sodium cobaltinitrite in thin section. Am Mineral 37:337–340

Chayes F, Zies EG (1961) Staining of alkali feldspars from volcanic rocks. Carnegie Institute, Washington Year Book 60, pp 172–173

Deer WA, Howie RA, Zussman J (2001) Rock forming minerals vol 4A: framework silicates: feldspars, 2nd edn. The Geological Society, London

Dilles JH, Barton MD, Johnson DA, Proffett JM, Einaudi MT (2000) Part I. Contrasting styles of intrusion-associated hydrothermal systems. Society of Economic Geologists Guidebook Series 32, Society of Economic Geologists, Littleton, Colorado

Evamy BD (1963) The application of a chemical staining technique to a study of dolomitisation. Sediment 2:164–170

Fandrich R, Gu Y, Burrows D, Moeller K (2007) Modern SEM-based mineral liberation analysis. Int J Miner Process 84:310–320

Fiegl F (1958) Spot tests in inorganic analysis, 5th edn. Elsevier, Amsterdam

Fox N, Cooke DR, Harris ACH, Collett D, Eastwood G (2015) Porphyry Au-Cu mineralization controlled by reactivation of an arc-transverse volcanosedimentary subbasin. Geology 43:811–814

Freidman GM (1959) Identification of carbonate minerals by staining methods. J Sed Petrol 29:87–97

Gabriel A, Cox EP (1929) A staining method for the quantitiatve determination of certain rock minerals. Am Mineral 14:290–292

Green OR (1993) The use and applications of stains and dyes in geological techniques. Sci Technol 28:226

Gu Y (2003) Automated scanning electron microscope based mineral liberation analysis—an introduction to JKMRC/FEI mineral liberation analyser. J Miner Mater Character Eng 2:33–41

Hitzman MW (1999) Routine staining of drill core to determine carbonate mineralogy and distinguish carbonate alteration textures. Miner Deposita 34:794–798

Huntington JF, Quigley M, Yang K, Roache T, Young C, Roberts I, Whitbourn LB, Mason P (2006) A geological overview of HyLogging 18,000 m of core from the eastern goldfields of Western Australia. In: Proceedings from the 6th international mining geology conference, Aus IMM Publication Series No. 6, Darwin, Australia, pp 45–50

Jambor JL, Dutrizac JE, Chen TT (2000) Contribution of specific minerals to neutralisation potential in static tests. In: Proceedings from the 5th international conference on acid rock drainage, Denver, pp 551–565

Keeney LM (2010) The development of a novel method for integrating geometallurgical mapping and orebody modelling. PhD thesis, University of Queensland, Australia

Keith ML (1939) Petrology of the alkaline intrusives at blue mountain ontario. Geol Soc Am Bull 50:1795–1826

Parbhakar-Fox A, Edraki M, Walters S, Bradshaw D (2011) Development of a textural index for the prediction of acid rock drainage. Min Eng 24:1277–1287

Reid WP (1969) Mineral staining tests, Colorado School of Mines. Mineral Ind Bull 12:1–20

Sclar CB, Fahey JJ (1972) The staining mechanism of potassium feldspar and the origin of hieratite. Am Mineral 57:287–291

Seedorff E, Dilles JH, Proffett JM, Einaudi MT, Zurcher L, Stavast WJA, Barton MD, Johnson DA (2005) Porphyry-related deposits: characteristics and origin of hypogene features. Economic Geology 100th Anniversary Volume. Economic Geology Publishing Company, Littleton, Colorado, pp 251–298

Sillitoe RH (2010) Porphyry copper systems. Econ Geol 105:3–41

Simmons SF, White NC, John DA (2005) Geological characteristics of epithermal precious and base metal deposits. Economic geology 100th anniversary volume. Economic Geology Publishing Company, Littleton, Colorado, pp 485–522

Walker JD, Cohen HA (2006) The geoscience handbook. American Geological Institute, Alexandria, Virginia

Weber PA, Thomas JE, Skinner WM, Smart RC (2005) A methodology to determine the acid neutralization capacity of rock samples. Can Mineral 43:1183–1192

Williams PJ, Barton MD, Johnson DA, Fontbote L, De Haller A, Mark G, Oliver NHS, Marschik R (2005) Iron oxide copper gold deposits: geology, space-time distribution, and possible modes of origin. Economic geology 100th anniversary volume. Economic Geology Publishing Company, Littleton, Colorado, pp 371–405

Zhang W, Hu Z, Lui Y, Chen H, Gao S, Gashnig RM (2012) Total rock dissolution using ammonium bifluoride ($NH_4HF_4$) in screw top Teflon vials: a new development in open-vessel digestion. Anal Chem 84:10686–10693

# Prediction of Acid Rock Drainage Using Field-Based Testing Tools

**Anita Parbhakar-Fox, John Aalders, Laura Jackson and Bernd Lottermoser**

**Abstract** Tests currently used by the industry for acid rock drainage (ARD) prediction heavily utilize static geochemical tests. Instead, effective tools which allow for early domaining should be utilized as they can be performed on a greater number of samples, allowing for deposit-wide environmental characterization. These must be simple enough to perform in the core shed or field-laboratory to keep cost and turn-around time to a minimum. Simple field-based pH tests and chemical staining should be performed. In addition, mineralogical characterization methods for drill core materials i.e., an ARD focused logging code and the use of portable instruments (i.e., pXRF, Equotip) should be pursued. This chapter presents several field tools appropriate for ARD prediction. These tools were developed, tested and validated using drill core and waste rock materials obtained from several Australian mines with differing geology, mineralogy and mineralization style. This chapter demonstrates that by utilizing these field based tests, industry has the opportunity to achieve: (i) effective ARD prediction testwork; (ii) detailed deposit-wide characterization, (iii) development of best practice waste management plans; and (iv) identification of the most suitable rehabilitation options.

A. Parbhakar-Fox (✉) · J. Aalders · L. Jackson
School of Physical Sciences, University of Tasmania, Private Bag 79, Hobart, TAS 7001, Australia
e-mail: Anita.Parbhakar@utas.edu.au

J. Aalders
e-mail: John.Aalders@utas.edu.au

L. Jackson
e-mail: lauraj0@utas.edu.au

B. Lottermoser
Institute of Mineral Resources Engineering, RWTH Aachen University, Wüllnerstrasse 2, 52062 Aachen, Germany
e-mail: lottermoser@mre.rwth-aachen.de



B. Lottermoser (ed.), *Environmental Indicators in Metal Mining*,
DOI 10.1007/978-3-319-42731-7_7

## Introduction

Oxidative dissolution of sulfidic minerals present in mine waste materials (e.g., waste rock, tailings) can produce acid rock drainage (ARD) and release sulfate and potentially deleterious elements (e.g., As, Ag, Cd, Cr, Cu, Hg, Ni, Pb, Sb, U and Zn; Dold 2014; Jamieson et al. 2015). In order for mining operations to adequately control and manage ARD during the entire life-of-mine, a comprehensive approach to ARD prediction must be adopted, the benefits of which include minimization of environmental impacts, and the reduction of financial liabilities associated with closure. Such an approach requires: (i) analysis of an adequate number of samples; and (ii) a short turn-around time frame in which to collect pertinent ARD data to allow for basic waste classification.

The current industry approach to ARD prediction relies upon using static and kinetic geochemical tests. However, limitations of static testing have long-since been established, neither of which are suited to performing on sample numbers as recommended by the regulator (Price 2009). For example, a basic net acid producing potential (NAPP) and net acid generating (NAG) package costs US$77 (Australian Laboratory Services 2016) and can take at least 5 days (on sample receipt) for data to be reported. Performing such screening tests on best practice number of samples (e.g., 500 samples) would cost at least US$38,500, excluding sample preparation and handling costs. Additional mineralogical testwork would likely be required (average cost per sample: US$50-150), and any further geochemical testing (i.e., sulfide-sulfur determination, pH testing, advanced NAG tests) would result in significant financial expenditures. Achieving total deposit knowledge becomes a costly pursuit. Thus, an alternative approach, which uses simple tools to domain ARD risks, should be adopted and implemented as early as exploration stages. Furthermore, such tools have potential to be used at abandoned mines sites whereby limited budgets for site characterization and rehabilitation exist.

Fundamentally, the mining industry requires a field-appropriate ARD prediction ‘toolbox’ that permits such data to be collected more time-efficiently and cost-effectively. If such tests can be readily performed at mine sites, then better selection of samples for detailed ARD testwork is likely (i.e., stages 1 and 2 of the GMTG approach). Considering this, several tools for rapid field-based ARD prediction are presented and discussed in this chapter. Several of these tools also feature during geoenvironmental unit definition and stage-one of the GMTG approach. However, their practical applications are presented here. The tools discussed here include: (i) carbonate staining; (ii) field-based pH testing, (iii) field portable instruments; and (iv) ARD focused logging, with validation testwork performed to establish the benefits of each tool. Practical examples are shown from materials collected at four Australian mine sites representing different deposit styles.

## Materials and Methods

Drill core and waste rock samples were collected between 2007 and 2013. A range of field-appropriate tests were performed on these materials. A brief description of each site is given below, followed by a summary of sample preparation techniques, and a brief outline of the analytical methods performed.

### *Site and Sample Descriptions*

#### Polymetallic Massive Sulfide Pb-Zn-Cu-Au-Ag Deposit

Site 1 is an operational polymetallic (Pb-Zn-Cu-Au-Ag) massive sulfide deposit located on the west coast of Tasmania, Australia. The deposit is hosted within the Cambrian Mt. Read volcanic belt. Multiple stratabound massive sulfide lenses host the mineralization within a fault bound sequence. Drill core samples (n = 51) from five drill holes were selected to provide a range of materials from non-mineralized or marginal lithologies (i.e., those likely to be designated waste). These included massive carbonates, black slates, chlorite-silica altered rhyolitic breccias and sericite or chlorite-silica altered sandstones.

#### Volcanogenic-Magmatic Cu-Au-Ag Deposit

Site 2 is a hybrid volcanogenic-magmatic system also located in west Tasmania, Australia. The mineralization is largely Cu-Au-Ag, but also contains significant intersections of Pb-Zn-Ag. The deposit is hosted in an intense microcrystalline silica alteration package. A 70 m interval of drill core was selected for testing field methods and included both carbonate-rich breccia (sandstones, limestones and conglomerates, in a variety of textural forms including fragmental, clastic and veined; upper 40 m), and sulfide-rich schist material (chalcopyrite and pyrite rich; lower 30 m).

#### Iron-Oxide Copper Gold Deposit

Site 3 is located in the Cloncurry district in north Queensland, Australia and is an iron-oxide copper gold (IOCG) in the eastern part of the Mount Isa Inlier. The deposit is hosted by plagioclase-phyric meta-andesitic volcanic rocks. These are locally intercalated with siliciclastic calc-silicate-rich (scapolite-bearing) and graphitic metasedimentary rocks and metadiorites. Host rocks have been affected by Na-Ca alteration, characterized by hematite-bearing albite, disseminated

biotite-magnetite and garnet-potassium feldspar-biotite alteration. Drill core offcuts (n = 30) from two drill holes were used.

**Lode Au-Deposit**

Site 4 is an abandoned Au operation located in north Queensland, Australia. This site comprises of three open pits, four waste rock piles, heap leach pads and relict mining infrastructure. The dominant lithologies identified in the remaining waste rock piles are hydrothermally altered rhyolite flows and tuffs that host sulfide bearing quartz lodes. Sulfide mineralogy consisting of pyrite ± arsenopyrite ± galena ± sphalerite. Fifty-one waste rock samples were collected to provide a range of lithologies from four different locations across the former operations.

## *Sample Preparation*

Full drill core (site 1), drill core off-cut (site 3) and waste rock (site 4) samples were sawn in two to allow for photography and logging of fresh surfaces. One portion was subjected to crushing and milling to <63 μm (UTAS) for geochemical and mineralogical testwork. The other portion was kept intact for mineralogical assessments, carbonate chemical staining, and analyses using field tools. Drill core from site 2 was received cut (i.e., half core), thus chemical staining for geometallurgical testwork was performed first, followed by the selection of representative samples every 1 m for validation of geochemical and mineralogical analyses, with these samples also crushed and milled to <63 μm (UTAS).

## *Staining*

All drill core samples from sites 1 and 2 were subjected to staining. Prior to staining, drill core materials were etched with dilute hydrochloric acid (HCl) for 2–3 min, and subsequently washed with water. Samples were then left to dry for approximately 30 min. Site 1 samples were placed directly in a plastic container containing the stain and left to soak for approximately 15 min in a dual stain comprising the organic dye Alizarin red-S (ARS) and potassium ferricyanide (PF) dissolved in HCl. For site 3, samples were stained directly with the same stain using a paintbrush. The ARS produces a pink to red stain on any carbonate that will react with dilute acid. The more reactive carbonates such as calcite and aragonite stain red, but the less reactive such as dolomite and siderite, remain unstained (Freidman 1959; Hitzman 1999). Pure dolomite does not stain with ARS-PF unless iron is substituted into its lattice (Hitzman 1999). The PF stain is more effective at identifying ferrous carbonates, as it reacts with ferrous iron causing a precipitate of

Turnbull's blue to form (Dickinson 1966). Siderite does not react with this stain. Therefore, where zones of high acid neutralizing capacity (ANC) are reported, but no staining colour is observed, the effective ANC can be considered low as siderite is not an effective carbonate neutralizer. After staining, samples were imaged to allow for comparison against unstained images.

## *Environmental Logging*

Textural analyses are not routinely performed in ARD prediction assessments despite the direct control of texture on acid formation. Considering this, Parbhakar-Fox et al. (2011) developed the 'ARD Index' (or ARDI) specifically for the textural evaluation of drill core and waste rock materials. ARDI values are used alongside sulfur assay or paste pH data to allow the ARD domaining as part of stage-one of the GMTG approach. At site 1, the ARDI was performed on all drill core samples (n = 51), over an 8.5 cm × 5.5 cm size area, with the area most dominated by sulfides chosen for assessment, as the most conservative ARDI value was sought.

## *Field Measurements*

### Field pH Testing

Paste pH testing represents the most efficient manner by which to assess a sample's immediate acid forming characteristics (Chap. "pH Testing Methods for Sulfidic Mine Wastes"). The ASTM D4972-01 (2007) method was used on fresh drill core materials from sites 1 and 2 following recommendations given in Noble et al. (2012). For older drill core material (site 3) and weathered materials from site 4, the AMIRA P387A method (Smart et al. 2002) was used. The pH value of each tested sample was measured in triplicate, with the standard deviation calculated as <0.5.

An accelerated paste pH methodology using a hot electrolyte solution to encourage faster reaction kinetics was trialed. Select pulverized (<63 μm) materials from sites 1 and 3 (n = 20) were tested using three different electrolyte solutions: (i) tap-water; (ii) deionized water (DI); and (iii) 0.01 M $CaCl_2$. Certified reference materials (CRM) KZK-1 and NBM-1 (CANMET; Natural Resources, Ottawa) were also tested. These solutions were heated to 100 °C and poured onto 10 g of sample weighed out in 50 ml glass beakers, with a 1:2 solid: solution ratio used. Once poured, beakers were stirred for 30 s and allowed to cool to room temperature. Triplicate measurements for both pH (S.D. = <0.01) and EC (S.D. = <0.05 μs/cm) were taken after 1 h.

Whilst the paste pH test provides an indication of a sample's current acid forming characteristics, it does indicate a samples future ARD generating potential.

Instead, field NAG tests have the potential to be used on site as a predictive pH test. Whilst Stewart (2005) listed several variables which could be modified to establish such a test, no formal methodology exists. Considering this, the NAG test was here revised by undertaking the following: (i) exclusion of the heating step; (ii) variation of hydrogen peroxide strength (to 7.5 %); (iii) variation of digestion time (30 min); and (iv) variation of the quantities of $H_2O_2$ added (5 aliquots of 50 ml). These methods were tested using samples from site 1 and the CRM NBM-1. Measurements of pH were again taken in triplicate, with standard deviation calculated as <0.01.

### Short-Wave Infrared Spectroscopy (SWIR)

The application of short-wave infrared (SWIR) spectroscopy in determining pale, fine-grained alteration minerals has been demonstrated in ore deposit characterization studies (e.g., Thompson et al. 1999; White et al. 2010). Mineral identification is based on absorption spectra collected from clean, dry, flat rock surfaces (Gifkins et al. 2005). SWIR therefore has potential to improve mineral identification of altered drill core samples for ARD characterization. Two instruments were selected for testing in this research on samples from site 2: (1) a portable infrared mineral analyzer (PIMA; manufactured by Integrated Spectronics, Australia); and (2) a TerraSpec spectroradiometer (manufactured by analytical spectral device (ASD) Inc.) with RS3 software (version 4.0.23). The PIMA measures reflected light in the 1.3–2.5 μm region in approximately 600 spectral channels (Kruse 1994). It is a contact instrument in which the head of the spectrometer is placed in direct contact with the rock (Kruse 1994). An internal light source is used to illuminate the sample, with the data automatically reduced to reflectance relative to an internal standard (Kruse 1994). TerraSpec is a compact and field portable precision instrument with a full spectral range (350–2500 nm), a 5 nm spectral resolution, and rapid data collection (1/10th of a second per spectrum). Materials from site 3 were tested using the TerraSpec only, however in this study, both intact pieces and homogenized powders from each 1 m interval were analyzed to assess which is a more appropriate sample type.

### Portable X-Ray Fluorescence (pXRF)

Accurately measuring chemistry and comparing these data to ARD parameters (e.g., paste pH, $S_{Total}$) allows for a first-pass indication of potential leachate quality issues which may arise towards the life-of-mine end (i.e., mine closure). This in turn allows the development of appropriate waste management plans. Field-portable XRF (pXRF) instruments have in recent years been used in mine site characterization studies for determining element concentrations (e.g., Haffert and Craw 2010; Higueras et al. 2012). Most recently, Parbhakar-Fox et al. (2014) discussed its application in mesotextural classification at abandoned mine sites. In this study, a

hand-held Olympus-InnovX instrument was used on intact drill core (three areas selected) and homogenized powders at site 1, and powders taken at 1 m intervals at site 3, with reference standards NIST 2781, GXR3-538 and GXR4-2843 used throughout the analyses. A benchtop Innov-X X50 XRF instrument was used to analyze waste materials collected from site 2. Both homogenized powders and intact portions (three areas analyzed) were tested in this particular study. The instrument was routinely calibrated by the material supplied by the manufacturer during the analyses (i.e., after ever 10th measurement).

### Equotip Analyses

Mineral hardness a proxy for weathering can be easily measured using an Equotip instrument and is included in stage-one of the GMTG approach (see Chap. "Predicting Waste Properties Using the Geochemistry-Mineralogy-Texture-Geometallurgy Approach"). It is practically tested here in the environmental toolbox context, with the data providing an opportunity to perform ARD domaining. At site 3, EQUOtip data was collected on-site for two drill holes (section lengths 290 and 320 m). For each 2 m interval, measurements were taken every 2.5 cm (total: ca. 24,000 data points collected). Data were validated against uniaxial compressive strength (UCS) values, commonly used by industry to determine rock hardness (Keeney 2008). The down-hole profiles of Equotip results had a 5 % smoothing applied to the curve to minimize the variability in the profiles (Keeney 2008). Equotip values were used alongside total-sulfur values for comparison with NAG pH versus paste pH data. This has the potential to allow for a low-cost first-pass understanding of lag-time to ARD on a deposit-scale.

## *Geochemical and Mineralogical Validation Testing*

Rapid and accurate measurement of $S_{Total}$ (wt%) was performed on samples from sites 1 and 2 using an Eltra C-S 2000 instrument. For sites 2 and 3, samples were analyzed for $S_{Total}$ using a Thermo Finnigan 1112 Series Flash Elemental Analyzer instrument. Appropriate standard materials were analyzed on both instruments during all analyses. In addition, the total element chemistry of samples from site 2 was measured for comparison against pXRF data using a Philips PW1480 X-ray Spectrometer.

Acid neutralizing capacity (ANC) was measured by the Sobek method at ALS Brisbane for samples from all sites. Multi-addition net acid generation (mNAG) testing was performed on materials from all sites following the AMIRA P387A method (Smart et al. 2002).

Mineralogical determination of material from sites 1 and 3 was performed using a benchtop Bruker D2 Phaser. Samples were analyzed for 1 h (Fe-filtered CoKα radiation, fixed divergence slit: 1 mm; range: 4° to 90° 2 theta; 0.020 step size),

with the resulting spectra processed in Eva 2.1 software, whereby minerals were identified using the ICDD PDF 2012 database. Quantitative XRD results were obtained using Topas version 2.0 and refinement of the most suitable mineral structures available in the current software package databank. Mineralogical analyses for samples from sites 2 and 3 were performed at Federation University Australia, using a traditional Siemens D501 diffractometer (Fe-filtered CoKα radiation, 35 kV, 30 mA, step scan 0.03θ/2θ at 1.0°/2θ/min, fixed 1° divergence and receiving slits and a 0.15° scatter slit). Mineral phases present were identified by computer-aided (X'pert and Eva) searches of the 2008 ICDD PDF4/Minerals subfile. Quantitative XRD results were obtained using SiroQuant© version 3.0 and refinement of the most suitable mineral structures available in the current software package databank.

## Results and Discussion

### *Domaining Neutralizing Potential: Use of Staining*

Validation of chemical staining must first be undertaken, because it is possible to generate a false positive, if for example, a stronger strength of acid is used during the sample preparation. An example of validation against XRD is presented in Fig. 1. This sample, from site 2, was stained with at least four coats painted on. Carbonate in drill core is observed as clasts (in limestone conglomerates) and veins. The Alizarin red S-potassium ferricyanide (ARS-PF) stain appropriately reacted with calcitic material in both textural forms; with the pink stain appropriately uptaken as shown in Fig. 1 with corresponding XRD data confirming this as calcite.

Using drill core from site 1, an investigation to determine if stains painted directly on are as effective as soaked drill core directly in the stain was undertaken. A slight pink coloration was noted on application of two coats of stain (Fig. 2a), however, a much stronger staining response was observed when the drill core sample was soaked in the stain bath (Fig. 2b). These results indicate that, whilst soaking core returns the best staining response, staining is a time efficient domaining tool for active operations. Painting at least four coats directly onto drill core (in trays) will return accurate results, providing the stains have been correctly prepared. The drill core should be imaged (e.g., high resolution photography) pre- and post-staining with the images available to the geological staff when logging to assist with their estimates of the modal mineralogy. It is recommended that a systematic validation campaign is undertaken to ensure the accuracy of the stain responses. For example, one representative sample of each geoenvironmental unit encountered every 50 m could be selected for XRD analysis. At abandoned operations, soaking waste materials may be a feasible option if a constrained sample set representing each geoevironmental unit is collected for characterization.

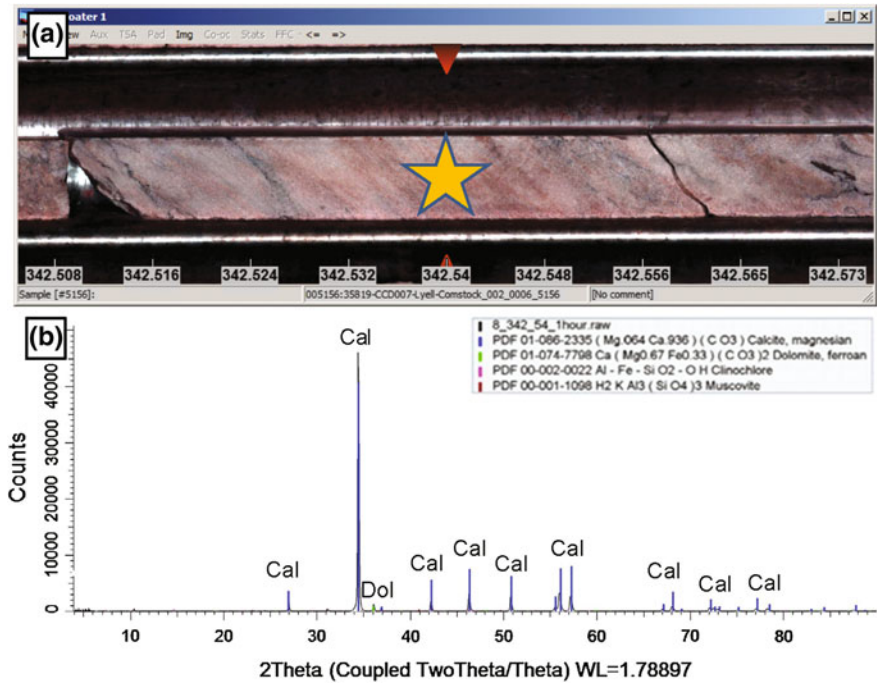


**Fig. 1** Drill core sample from site 2 (hybrid volcanogenic-magmatic Cu-Au-Ag deposit, Tasmania: **a** Carbonate-stained drill core, with the *pink colour* indicating the presence of calcite; **b** X-ray diffraction pattern of area starred in A confirming the dominance of calcite, thus verifying the application of drill core chemical staining for calcite identification and domaining of acid neutralizing capacity. *Cal* calcite, *Dol* dolomite (color figure online)

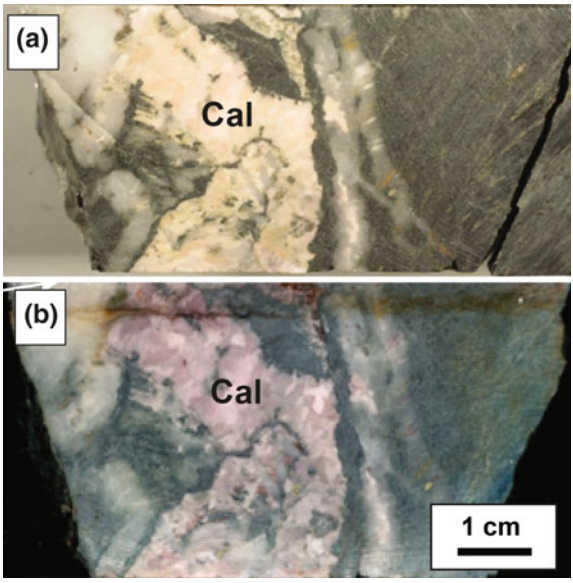


**Fig. 2** Photograph images of drill core from site 1 (polymetallic massive sulfide deposit, Tasmania); **a** after several coatings of stain; **b** after soaking in stain bath for 30 min. The *pink colour* seen in both examples indicates the presence of calcite, thus identifying effective acid neutralizing capacity (color figure online)

## *Domaining Neutralizing Potential: Use of SWIR*

Whilst major rock forming minerals can easily be recognized in hand-specimen based on their different rock properties (i.e., hardness, lustre, habit), hydrothermally altered minerals are much harder to identify. Typically, they can appear pale and fine-grained and with such a grain size that the potential for participating in neutralizing reactions is much greater (cf. Plumlee 1999). Homogenized powder samples from site 4 (abandoned Au-mining operations) were used in this study to compare two commonly used SWIR instruments, namely the portable infrared mineral analyzer (PIMA) and TerraSpec. Muscovite was confirmed by XRD as the dominant alteration mineral in hydrothermally altered rhyolite samples. Two examples of typical PIMA and TerraSpec results are shown in Fig. 3. Results from PIMA analyses showed greater deviation from the reference spectra for sample 1 (Fig. 3a), and were aspectral from sample 2 (Fig. 3c). Spectra collected by TerraSpec instrumentation (Fig. 3b, d) were better defined (i.e., less noise), and show better agreement with the reference spectra. Based on these results, the

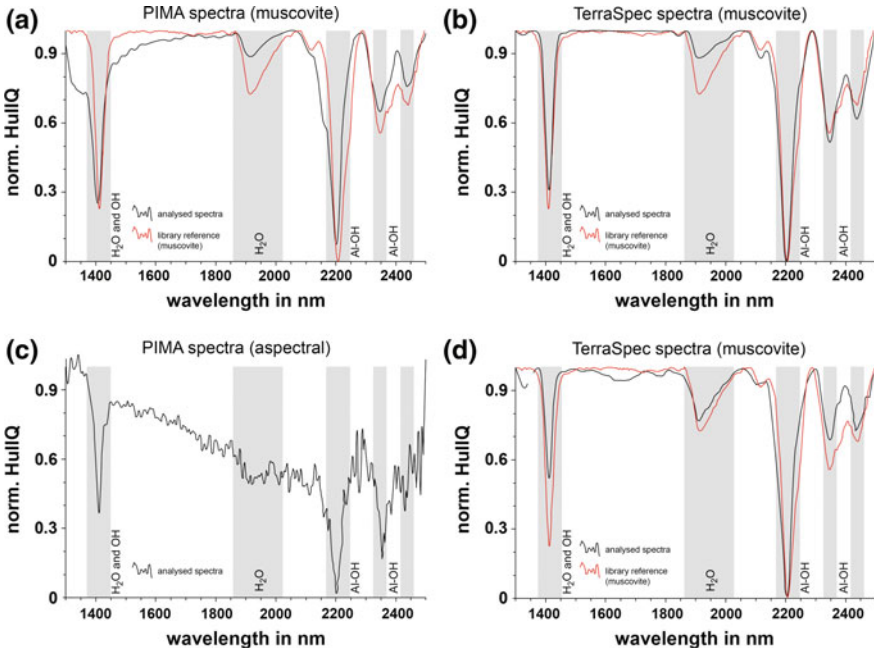


**Fig. 3** Example of alteration mineral identification in Site 4 (abandoned lode-Au mine, Queensland) waste rock materials: **a** sample A analysed on a PIMA instrument with muscovite identified; **b** sample A analysed on a TerraSpec instrument with muscovite confidently identified; **c** sample B analysed on a PIMA instrument with an aspectral result; and **d** sample B analysed on a TerraSpec instrument with muscovite confidently identified (reprinted from Parbhakar-Fox et al. 2015, with permission from Gecamin) (color figure online)

TerraSpec is given preference for use. Furthermore, the TerraSpec is not restricted to analysis of pale-coloured minerals like PIMA and can detect a greater range of minerals including iron-oxyhydroxides.

In order to identify the best sample type for TerraSpec analysis, both powdered and intact drill core materials from site 1 were tested. For powdered samples, noisy spectra were collected, which were classified as aspectral, therefore, preference is given to using intact drill core. Validation testwork can itself add both time and cost, particularly if mineralogical analyses like XRD (using a conventional instrument) or EPMA are required. Therefore, we tested the use of TerraSpec for such validation, and found it was less accurate than XRD.

Whilst the TerraSpec was able to confidently identify the presence of calcite, muscovite and chlorite in 52 % of the samples, it occasionally misidentified minerals such as tourmaline and epidote, which were neither logged, nor detected by XRD. Furthermore, whilst the TerraSpec instrument correctly detected the presence of carbonate minerals in 52 % (i.e., identified as calcite) of these samples, the exact carbonate mineral type was only correctly identified in 10 % of samples when compared to XRD. This is likely explained by having performed these analyses on intact drill core (i.e., non-homogenized, randomly selected areas for analysis); therefore there is a high likelihood of conflicts when compared to XRD data. Based on these results, it is evident that applications of TerraSpec for ARD (specifically ANC) domaining are limited.

## *Assessing Acid Forming Characteristics*

### Standard Paste pH Testing

Paste pH measurements are shown in Fig. 4 with data compared against NAG pH and total sulfur measurements as recommended by the GMTG approach (Chap. "Predicting Waste Properties Using the Geochemistry-Mineralogy-Texture-Geometallurgy Approach"). Classification by the paste pH versus NAG pH (Fig. 4a) allows for the different geochemical characteristics of these materials to be observed. Drill core from sites 1 (massive sulfide) and 3 (IOCG) were the lowest risk—with two modal populations observed (i.e., NAF and PAF). Waste materials from site 4 showed a spread through all categories, indicating that both extremely acid forming materials and inert waste materials are present at this site. Drill core from sites 2 was the most consistent in terms of the majority of samples classified as having some degree of acid forming potential. If instead a geochemical plot of paste pH versus total sulfur is constructed (Fig. 4b), similar classifications, particularly for those materials with end-member type (i.e., NAF, EAF) behaviour are returned. For example, a significant portion of site 4 samples remain classified as NAF, and all site 2 samples are classified as AF and PAF. Sites 1 and 3 samples tend to cluster around the PAF/NAF cutoff, however, a higher percentage of samples classify in the PAF field than in the previous geochemical plot (Fig. 4a). This is due to the

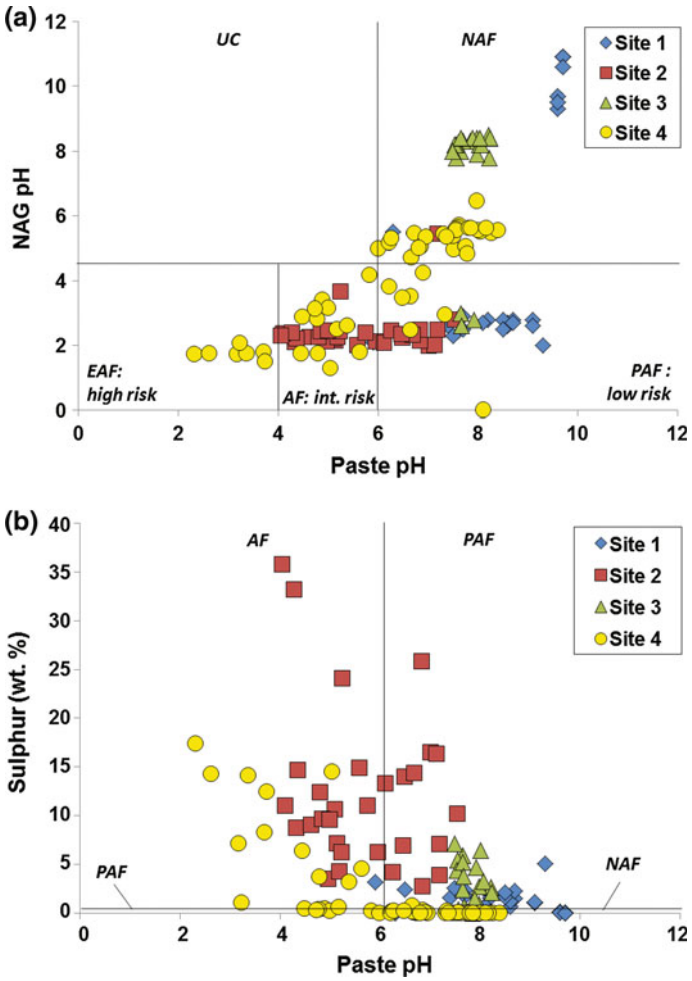


**Fig. 4** Paste pH measurements performed on drill core and waste materials from sites 1, 2, 3 and 4: **a** NAG pH compared against paste pH (after Weber et al. 2006); **b** total sulfur compared against paste pH (after Parbhakar-Fox et al. 2011). *AF* acid forming, *EAF* extremely acid forming, *PAF* potentially acid forming, *NAF* non-acid forming, *UC* uncertain, *int.* intermediate ($n = 254$) (color figure online)

presence of less-reactive sulfides (i.e., chalcopyrite, sphalerite) in the paste pH test (relative to pyrite). Whilst not as accurate as the NAG pH versus paste pH classification, these data confirm that the paste pH versus total sulfur classification is sufficient for use in domaining ARD potential for a range of materials. This classification is particularly suited to identifying 'end-member' characteristics, which has the benefit of allowing early screening of samples for more detailed testwork (i.e., through the GMTG approach) and those geoenvironmental units which are potentially inert.

### Accelerated Paste pH Testing

Accelerated paste pH experiments using DI water, tap water and ASTM D4921-01 as the (heated) electrolyte were compared against the standard (non-heated) ASTM D4921-01 method for sites 1 and 2 drill core materials (Fig. 5). In general, for site 1 the accelerated ASTM D4921-01 method returned the lowest pH values by up to 2.3 units. Results from both accelerated water electrolyte experiments were in close approximation ($R^2 = 0.995$). However, when values were compared against standard ASTM D4921-01 method data, they were neither consistently higher, nor lower (pH unit difference range of +1.2 to −2.2). A similar trend was seen for site 2, with the accelerated ASTM D4921-01 test returning the lowest pH values for the accelerated tests. When these were compared against the standard ASTM D4921-01 method, an inconsistent trend was once against observed with a pH unit different range of +1 to −2.25. These results confirmed that accelerated testing is encouraging reaction kinetics to proceed quicker, as all differed to the standard ASTM method. However, the degree of difference is dependent on the individual mineralogy of each sample.

The purpose of these experiments is to evaluate whether accurate paste pH data can be collected if there is no access to $CaCl_2$ solution or DI water. For the majority of samples and indeed the two standards, there are very few classification conflicts (i.e., NAF vs. PAF), with a cut-off of either pH 6 (regarded as highly conservative)

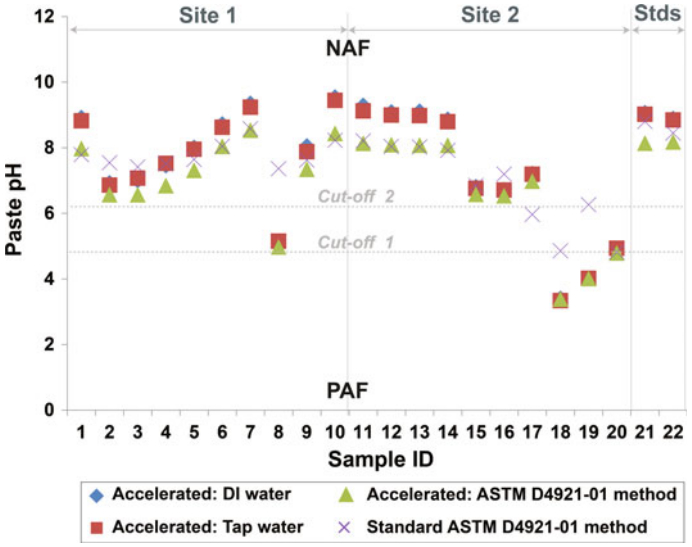


**Fig. 5** Paste pH test results for samples from site 1 (1–10; polymetallic massive sulfide deposit) and site 2 (sample ID 11–20; hybrid volcanogenic-magmatic Cu-Au-Ag deposit), KZK-1 (sample 21) and NBM-1 (sample ID 22) standards. Data from four experiments (3 accelerated, and one standard) are shown, with two NAF/PAF cut-offs shown (at pH 6 and pH 4.5). *NAF* non-acid forming, *PAF* potentially acid forming (color figure online)

or pH 4.5. Bulk mineralogical assessments of samples 8, 17, 18 and 19 indicated these as pyritic samples. Therefore, the lower pH readings generated by the accelerated methods better approximate the NAG pH data for these samples (pH values of 2.9, 2.1, 2.4 and 2.4 respectively), resulting in a more appropriate paste pH value (and classification). These experiments show that for simple ARD domaining, heating a solution (tap water, DI water or $CaCl_2$) will provide a sufficient paste pH value. However, caution must be exercised when using these data. Validation of a select (and mineralogically diverse) number of samples (i.e., 10 %) using a standard procedure should be performed to establish whether and where classification discrepancies lie.

## Field NAG Testing

To evaluate the potential for a field NAG test, 10 different samples from site 1 (massive sulfide) were chosen in addition to the NBM-1 standard, with results presented in Fig. 6. In general, the exclusion of the heating step appeared to generate the most erroneous results compared to the standard single addition test, particularly for samples 7, 8 and 9, whereby pH results of 10.1–10.6 were measured. The mineralogy of these samples revealed a composition of quartz, chlorite and muscovite, with minor calcite. Potentially, calcium hydroxide may have formed during this reaction (i.e., dissolution of calcite), causing this elevated pH. Sample 10 reported a pH value lower with no heating step, so the error is in fact

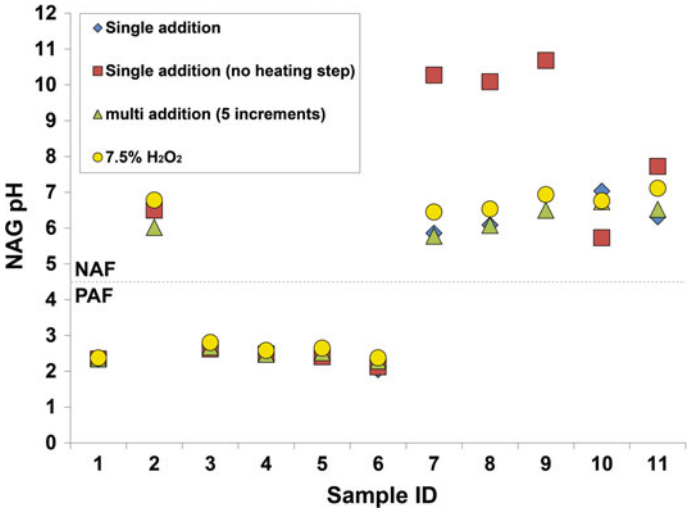


**Fig. 6** Field NAG test results for site 1 (polymetallic massive sulfide deposit, Tasmania) samples (sample ID 1–10) and an NBM-1 standard (sample ID 11). Data from four experiments are shown, with the NAF/PAF cut-off shown (set at pH 4.5, after Smart et al. 2002). *NAF* non-acid forming, *PAF* potentially acid forming. NB. The 15 % $H_2O_2$ pH = 5 (color figure online)

non-systematic. Considering this, exclusion of the heating step is not recommended. A comparison of single addition against multi addition (in 5 × 50 ml additions) showed no significant differences, with only slightly lower pH values recorded from the stepped addition. This slight variation did not alter the final classification of the samples (as NAF or PAF). Using a lower strength $H_2O_2$ (7.5 %) resulted in values within a range of −0.2 to 0.8 pH units different to single addition values. Again, these values did not alter the classification of the samples. These experiments show that excluding the heating step to reduce the turnaround time is not an option due to the inaccurate results returned. Instead, using a lower strength $H_2O_2$ in stepped increments is the best approach to cost-effective accurate testing.

### Sulfur Determination

Measurements of sulfur are essential for the calculation of MPA, and can also be used as a simple proxy for domaining ARD likelihood. However, if measurement of sulfur is performed via laboratory analyses, turn-around time may be significant (i.e., >48 h) with analyses performed off-site. Alternatively, sulfur can be measured efficiently using a portable XRF or a benchtop element analyzer. To test the accuracy of the various sulfur measurement techniques, waste rock materials from site 4 (abandoned Au-mine) were selected to compare measurements from an: (i) benchtop analyzer; (ii) traditional XRF instrument; and (iii) pXRF. Results are shown in Fig. 7. Data from the benchtop analyzer and XRF were in close approximation ($R^2$ = 0.9979), however, data from the pXRF was in less agreement when compared with both methods ($R^2$ = 0.886 against EA; $R^2$ = 0.8917 against XRF).

Considering current technology, pXRF should be used for the measurement of potentially deleterious elements including As, Cu, Cd, Pb, Zn (cf. Parbhakar-Fox et al. 2014), but the technique appears to have limited applications for S. Instead, sulfur should be determined using a benchtop element analyzer (e.g., Eltra CS 2000 instrument), which has been shown to generate accurate sulfur data as required for the calculation of MPA. Instead, S data from a pXRF instrument could be used to aid the identification of samples requiring such testwork, i.e., those with relatively high sulfur (i.e., above the specified total-sulfur cut-off).

### Determination of Bulk Chemistry

Often, the focus of early environmental assessments is on characterizing the pH of the future leachate. However, having an understanding of the chemistry of the mine waste is just as critical to define the environmental characteristics of each geoenvironmental unit. Often, this is overlooked, with the reasoning related to cost, i.e., bulk elemental analyses are priced upwards of US$30/sample (ALS 2016). In addition, to appropriately schedule such analyses the sample mineralogy must be known prior to ensure that the correct digestion procedures are used (e.g., aqua

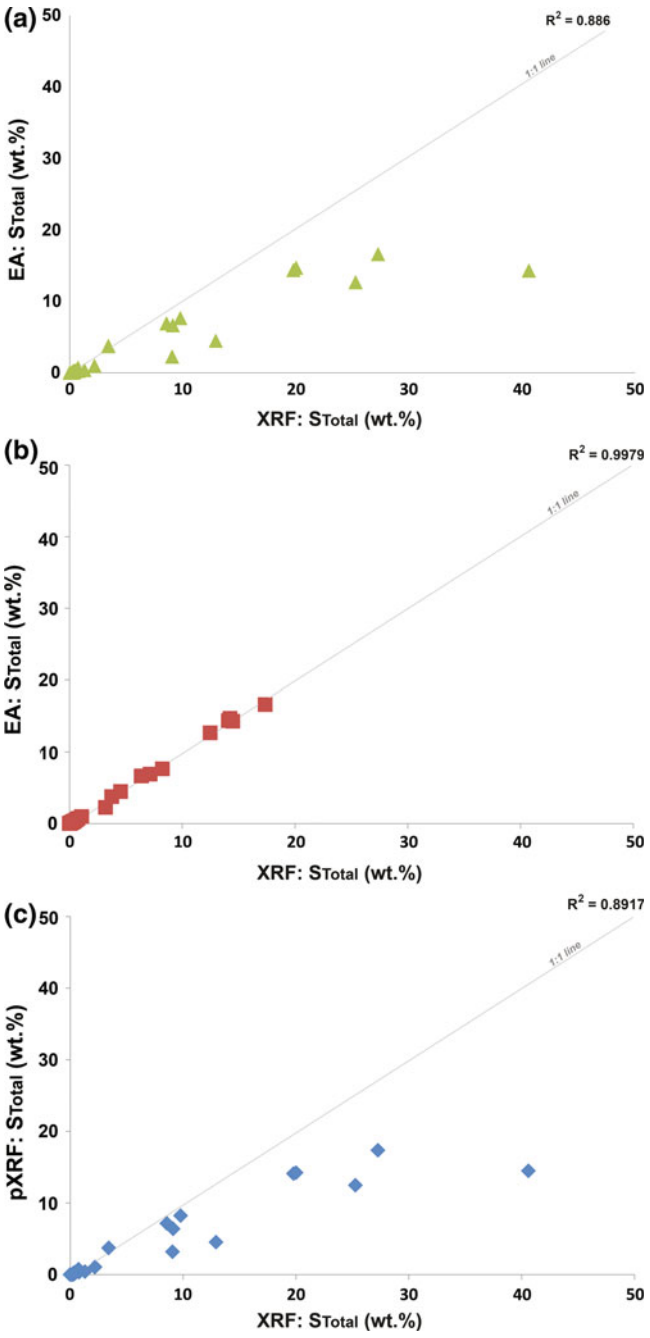


**Fig. 7** Total sulfur measurements on samples from site 4 (abandoned lode Au-operations, Queensland; *n = 51*) made by three different analytical instruments: **a** portable XRF instrument versus an element analyzer; **b** element analyzer versus XRF instrument; and **c** portable XRF versus XRF instrument (color figure online)

regia, four-acid digest) in order to return accurate data for elements of interest. Undertaking such analyses is inappropriate for field-domaining. Despite its generation of inaccurate sulfur data, the use of pXRF should be explored and again, used in the context of providing an indication of which samples contain high/low metal(loid) contents. To test this, bulk chemistry was measured by XRF and pXRF for the same samples from site 4 (abandoned Au mine). Results for six elements commonly of environmental concern measured above their detection limit are shown in Fig. 8. Both techniques returned results in very close agreement (range of

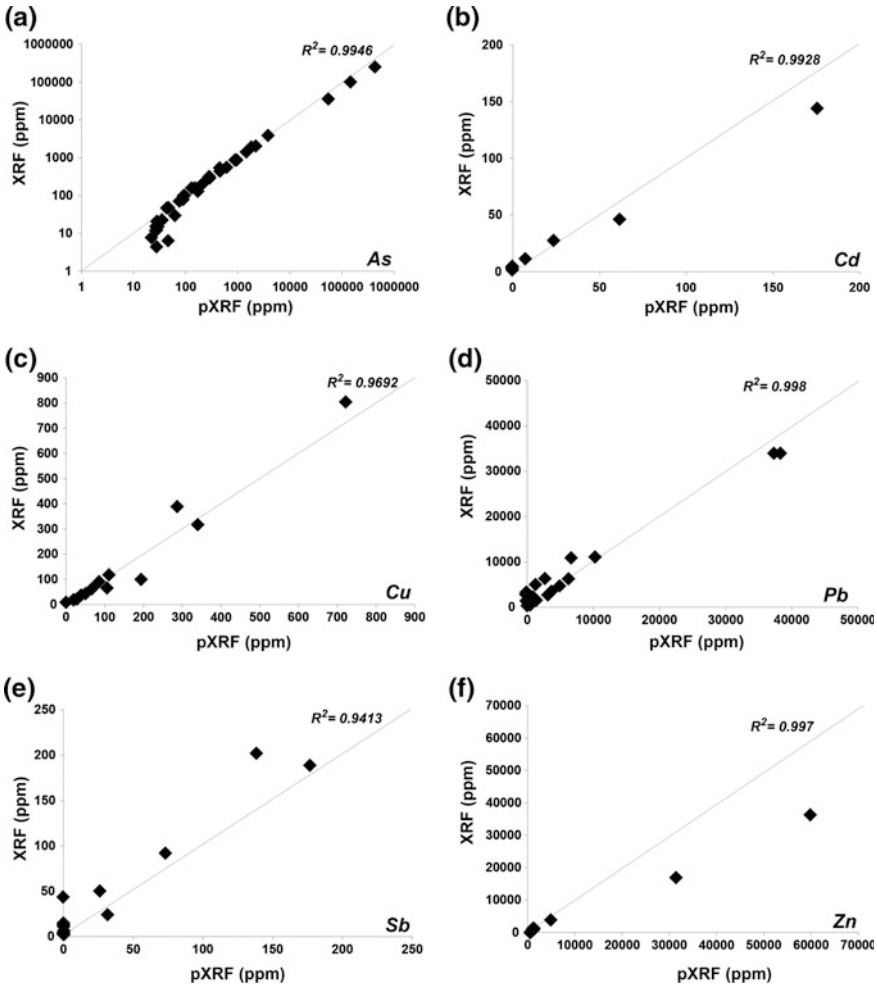


**Fig. 8** Concentrations (ppm) of selected elements: As (**a**); Cd (**b**); Cu (**c**); Pb (**d**); Sb (**e**); and Zn (**f**) measured in waste rock materials from site 4 (abandoned lode-Au operation, Queensland) by portable XRF (pXRF) and XRF techniques ($n = 51$) (reprinted Parbhakar-Fox et al. 2015, with permission from Gecamin)

$R^2$ = 0.9413 for Sb, to $R^2$ = 0.998 for Pb). This indicates that element data collected from pXRF is relatively accurate and can be used in classification schemes such as Ficklin plots (Plumlee 1999). A similar conclusion as to the accuracy of pXRF instruments for waste classification purposes at the MacArthur River Mine, Australia was made by Landers et al. (2014). In this study, the authors undertook a field and laboratory geochemical investigation to assess the potential for metal release, saline drainage and ARD from overburden materials. Their results were used to derive a waste rock classification guide for mine geologists to classify their materials onsite to aid correct placement of materials. Six waste types were identified based on pXRF measurement of Cu, Pb and in addition to pH values and sulfur. These categories were validated with standard NAPP and NAG test results. Such an approach should be adopted at all operation sites with access to a pXRF instrument.

The type of sample to use in pXRF tests should also be considered, as at both operational and abandoned sites, the most time and cost-effective sample type for testing is an intact piece of rock/drill core. However, more accurate results (i.e., comparable to XRF) are generated from homogenized powders. Both homogenous powders and intact drill core from site 1 (polymetallic massive sulfide deposit) were examined with results for the sum of metals (as considered in Ficklin plots) shown in Fig. 9. In general, there is positive correlation between both datasets ($R^2$ = 0.81), with powdered samples generally returning higher values. From an efficiency and domaining perspective, collection of data on intact drill core is preferred; however, subjective (bias) sampling is introduced through identifying a particular interval for analysis. Furthermore, over a given interval (i.e., 1 or 5 m), if one final value is to

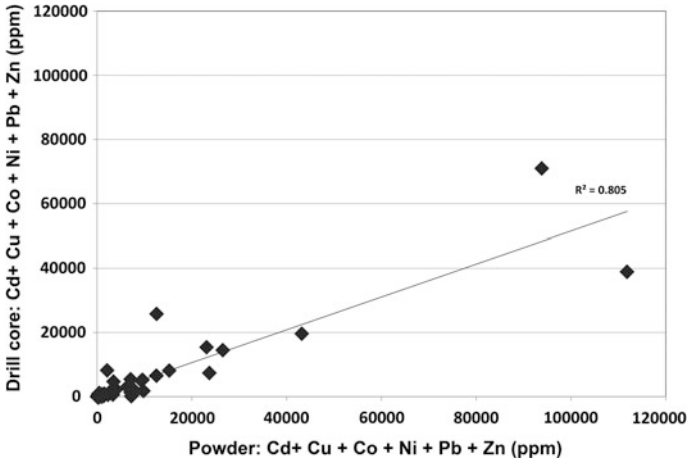


**Fig. 9** Total metal concentrations (Cd, Cu, Co, Ni, Pb, Zn in ppm) measured by portable XRF (pXRF) in drill core and homogenized powdered sample material collected from site 1 (polymetallic massive sulfide deposit, Tasmania, n = 51) (reprinted from Parbhakar-Fox et al. 2015, with permission from Gecamin)

be utilized, how many analysis should be performed, and should an average value calculated and used? If analysis on drill core is to be pursued, a standard operating procedure must be enforced. To reduce such sampling issues, pXRF should be performed on powdered materials (again, it would be advantageous to use the same powdered materials as in $S_{Total}$ and paste pH testing). In doing so, appropriate certified reference materials (as used here) and described in Hall et al. (2014) and Piercey and Devine (2014) should also be analyzed. Additionally, samples should be systematically selected for validation (using routine whole-rock analysis techniques) and if necessary, specific correction factors developed.

## Using Hardness for Waste Classification

Equotip hardness data are here considered as an indicator for weathering behaviour. For example, samples classified by Equotip as very soft are considered to weather at a fast rate, whereas samples which are classified as very hard are predicted to weather slowly. Interpretation of data in this manner is purely qualitative and therefore, its application is restricted to domaining. Additionally, no consideration is given to grain size and the presence of fractures, with the latter influencing weathering rate by acting as conduits for oxygen and water (Plumlee 1999). Despite these limitations, Equotip values were considered against lithology and sulfur assay values in order to assess the potential for, and lag time to acid formation (Fig. 10a, b). If a mineral hardness value was <648 Ls, it was classified as soft in accordance with Keeney (2008), with a sulfur cut-off of 0.3 wt% used. These values were compared against GMT stage-two NAG pH versus paste pH classifications. In this study, thirteen lithological groups were identified (termed EH 1 to EH 13) based on their lithology and alteration mineralogy.

The predicted lag time to ARD for EH 633 based on Equotip and assay data varied between NAF (i.e., hard zone with relatively low $S_{Total}$) and AF (rapid rate of ARD formation, medium risk) as shown in Fig. 10a. More variation was observed for EH 635, particularly from 860 to 1020 m with NAF, PAF and AF zones identified (Fig. 10b). In general, these classifications were more conservative than those assigned by NAGpH versus paste pH, with the most common conflict the classification of a zone as PAF rather than NAF (i.e., EH 633, ~970 m; Fig. 10a). However, in EH 635 a NAF zone was identified from ~1030 to ~1075 m by this classification, but by the NAGpH versus paste pH classification, ~1030 to ~1060 m was identified as PAF (Fig. 10b). Thus, this hardness/assay classification is unlikely to be used as an accurate indication of lag-time to acid formation. Instead it can be used to provide a general indication of weathering rate prior to NAGpH or kinetic NAG geochemical data being reported. This study indicates the potential assistance of Equotip data when performing field-based ARD studies. If paste pH data also exists, this can be used to refine the domaining exercise.

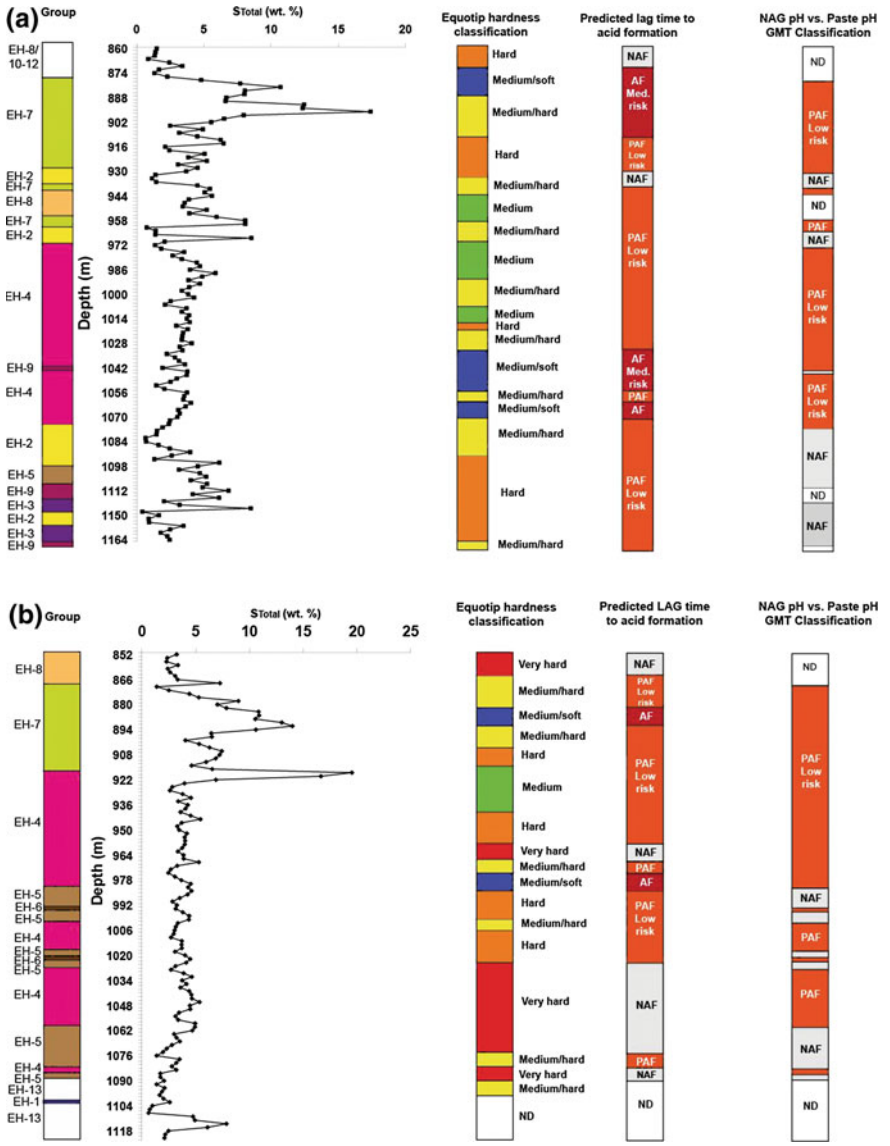


**Fig. 10** Domaining of lag time to acid formation based on $S_{Total}$ values (obtained from assay analyses) and Equotip hardness (measured by Keeney 2008) in drill core materials from site 3 (operational IOCG); **a** drill hole EH633, and **b** drill hole 635. NAGpH versus paste pH classifications are also shown for comparison. *AF* acid forming, *PAF* potentially acid forming, *Med* medium, *NAF* non-acid forming, *ND* no data (reprinted from Parbhakar-Fox et al. 2013, with permission from AusIMM) (color figure online)

## Geoenvironmental Logging

A validation study of the acid rock drainage index (ARDI) was performed on drill core materials from site 1 (polymetallic massive sulfide deposit), whereby ARDI values collected in mesotextural scale drill core material only were compared against geochemical data (Fig. 11). The ARDI was able to correctly identify samples with acid forming capacity (PAF, AF and EAF) when compared against total sulfur (Fig. 11a), NAPP (Fig. 11b) and NAG pH values (Fig. 11c). The ARDI was more conservative in its classification of samples with neutralizing capacity, with several identified as NAF by the ARDI (Fig. 11d).

In this instance, the ARDI was considered more accurate, as it evaluated the content of sulfides in proximity to, and the mineral associations of carbonate minerals. This study demonstrates the application of the ARDI, consequently, more mine sites may adopt such an ARD focused logging code in order to populate their mine database with this environmental attribute. Additionally, this method can be performed at mining operations in various stages of the life-of mine; for example: during exploration on hand specimen samples, during mine operations to check the correct placement of waste materials, and upon post-closure at historic or abandoned sites.

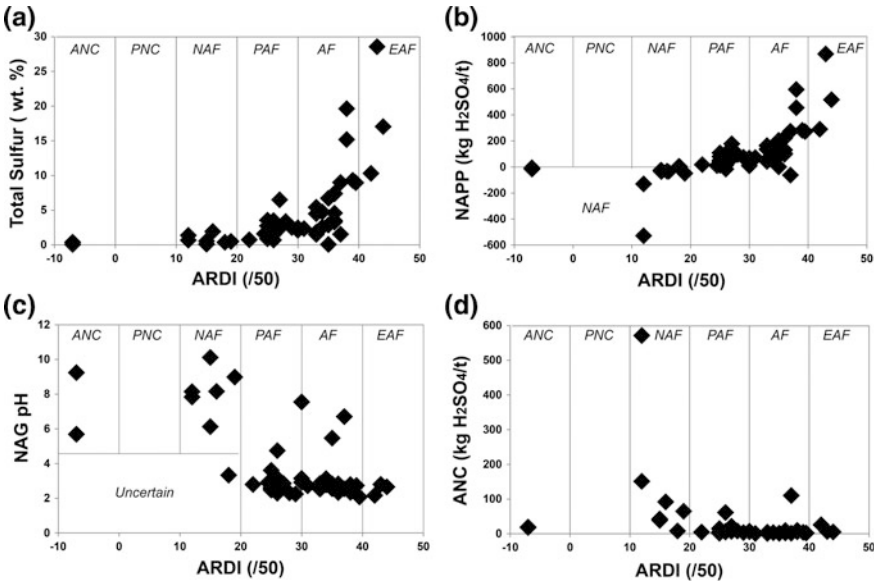


**Fig. 11** Comparison of acid rock drainage index (ARDI) scores given to site 1 (polymetallic massive sulfide deposit) drill core materials ($n = 51$) against: **a** total sulfur (wt%); **b** net acid producing potential (NAPP; kg $H_2SO_4$/t); **c** net acid generation (NAG) pH; and **d** acid neutralizing capacity (ANC; kg $H_2SO_4$/t) (reprinted Parbhakar-Fox et al. 2015, with permission from Gecamin)

## Conclusions

To effectively select the most appropriate samples for detailed geochemical and mineralogical ARD test work, a pre-screening testing stage is required. Such a stage must allow for an appropriate number of samples to be evaluated to build an environmental database of information allowing for the construction of a deposit-wide ARD model. Such a pre-screening stage must utilize efficient and cost-effective field-based tools. This will permit site-based staff to characterize their own materials, thus reducing turn-around time for obtaining ARD relevant data, and improving the quality of decision making with regards to waste management (e.g., scheduling, handling and placement). A range of both existing and newly developed tools were examined in this study using materials collected from four Australian mine sites.

Our studies indicate that chemical staining is an appropriate technique by which to identify the presence of carbonates, if traditional mineral identification methods fail (e.g., if it is very fine-grained and present in the rock matrix). Whilst the best stain responses are returned from soaking drill core directly in chemical stains, it may not be practical to perform in a field laboratory. Painting stains directly onto core provides sufficient results. Carbonate staining responses should be used to assist with environmental logging using a site-specific ARDI. In addition, short-wave infrared data collected can be used to confirm the presence of carbonate minerals. However, such analysis should only be performed on intact drill core materials and not on homogenized powders. In order to classify the geochemical behaviour of the materials, paste pH tests should be performed and plotted against portable XRF data (collected from homogenized powders) on Ficklin plots. Whilst preference is given to the use of a standardized paste pH methodology (e.g., ASTM D4921-01), in order to be an effective and predictive field tool, it requires modification. First, it should be simplified (i.e., if access to $CaCl_2$ or DI water is not possible). The use of hot $H_2O$ as an electrolyte was tested (e.g., accelerated paste pH test), with these results returning similar classifications to those collected from standard testing and NAG pH tests. Development of a field NAG test was investigated, with variables in a single addition test modified. From these experiments, it was found that reducing the $H_2O_2$ strength to 7.5 % was the most effective method. Caution must be exercised, as both accelerated paste pH and field NAG results should be used for domaining purposes only. Sulfur data, a crude proxy for the presence of sulfides, should be collected using benchtop instruments (if no assay data exists in the geological database), and used with mineral hardness values (as collected by Equotip) and paste pH to domain lag-time to ARD.

The benefit of utilizing these simple techniques suitable for performance in a core shed or field-lab is that it enables a database of ARD data to be collected and held on site, thus allowing for in-house expertise to be established. Ultimately, this will lead to an improved quality of waste management strategies, and better forecasting of appropriate of rehabilitation options. Additionally, as demonstrated by using materials from site 4 (abandoned lode-Au operations, Queensland, Australia),

these simple field-techniques can be used at mines in the final life-of-mine stage, i.e. post-closure, enabling regulators the opportunity to undertake detailed site characterization and to develop an appropriate rehabilitation strategy based on real environmental properties.

## References

American Society for Testing and Materials ASTM D4972–01 (2007) Standard test method for pH of soils, ASTM D4972-01(2007). ASTM International, West Conshohocken, Pennsylvania

Australian Laboratory Services (2016) Schedule of services and fees

Dickinson JAD (1966) Carbonate identification and genesis as revealed by staining. J Sediment Petrol 36:491–505

Dold B (2014) Mineralogical and geochemical controls in biomining and bioremediation. In: Parmar N, Singh A (eds). Geomicrobiol Biogeochem 39:119–135

Freidman GM (1959) Identification of carbonate minerals by staining methods. J Sediment Petrol 29:87–97

Gifkins C, Herrmann W, Large R (2005) Altered Volcanic Rocks: a guide to description and interpretation. University of Tasmania, CODES Special Publication, Hobart

Haffert L, Craw D (2010) Geochemical processes influencing arsenic mobility at Bullendale historic gold mine, Otago, New Zealand. NZ J Geol Geophys 53:129–142

Hall GEM, Bonham-Carter GF, Buchar A (2014) Evaluation of portable X-ray fluorescence (pXRF) in exploration and mining: phase 1, control reference materials. Geochem Explor Environ Anal 14:99–123

Higueras P, Oyarzun R, Iraizoz JM, Lorenzo S, Esbri JM, Martinez-Coronado A (2012) Low-cost geochemical surveys for environmental studies in developing countries: testing a field portable XRF instrument under quasi-realistic conditions. J GeochemExplor 113:3–12

Hitzman MW (1999) Routine staining of drill core to determine carbonate mineralogy and distinguish carbonate alteration textures. Miner Deposita 34:794–798

Jamieson HE, Walker SR, Parsons MB (2015) Mineralogical characterisation of mine waste. Appl Geochem 57:85–105

Keeney L (2008) EQUOtip hardness testing: Aqqaluk (including a guide on how to use EQUOtip). Technical report 2, P843 GeM, Australian Mineral Industries Research Association (AMIRA), Melbourne

Kruse FA (1994) Identification and mapping of minerals in drill core using hyperspectral image analysis of infrared reflectance spectra. http://www.spectralcameras.com/files/Applications/Kruse_Core94.pdf

Landers M, Usher B, Faulkner D, Marianelli P, Masterman K (2014) Field and desktop waste rock classification guide for a metalliferous mine in the northern territory, Australia. In: Proceedings from the 8th Australian workshop on acid and metalliferous drainage. ACMER, Brisbane, pp 159–172

Noble TL, Lottermoser BG, Parbhakar-Fox A (2012) Evaluating pH tests for mine water prediction. In: Proceedings from the 3rd International Congress on Water Management in the Mining Industry. GECAMIN, Chile, pp 504–512

Parbhakar-Fox A, Edraki M, Walters S, Bradshaw D (2011) Development of a textural index for the prediction of acid rock drainage. Min Eng 24:1277–1287

Parbhakar-Fox AK, Lottermoser BG, Bradshaw D (2013) Cost-effective means for identifying acid rock drainage risks—integration of the geochemistry-mineralogy-texture approach and geometallurgical techniques. In: 2nd AusIMM international geometallurgy conference, Brisbane, pp 143–154

Parbhakar-Fox A, Edraki M, Hardie K, Kadletz O, Hall T (2014) Identification of acid rock drainage sources through mesotextural classification at abandoned mines of Croydon, Australia: implications for the rehabilitation of waste rock repositories. J Geochem Explor 137:11–28

Parbhakar-Fox AK, Aalders J, Lottermoser BG (2015) Effective field-based testing tools for rapid ARD prediction. In: 10th international conference on acid rock drainage and IMWA annual conference, Santiago, Chile, pp 890–905

Piercey SJ, Devine MC (2014) Analysis of powdered reference materials and known samples with a benchtop, field portable X-Ray fluorescence (pXRF) spectrometer: evalution of performance and potential applications for exploration lithogeochemistry. Geochem Explor Environ Anal 14:139–148

Plumlee GS (1999) The environmental geology of mineral deposits. In: Plumlee GS, Logsdon MJ (eds) The environmental geochemistry of mineral deposits part A: processes, techniques and health issues. Rev Econ Geol 6A:71–116

Price WA (2009) Prediction manual for drainage chemistry from sulphidic geologic materials. CANMET Mining and Mineral Sciences Laboratories, Canada

Smart R, Skinner WM, Levay G, Gerson AR, Thomas JE, Sobieraj H, Schumann R, Weisener CG, Weber PA, Miller SD, Stewart WA (2002) ARD test handbook: project P387A, prediction and kinetic control of acid mine drainage. AMIRA International Ltd., Melbourne 42 pp

Stewart WA (2005) Development of acid rock drainage prediction methodologies for coal mine wastes. PhD thesis. University of South Australia, Australia

Thompson AJB, Hauff PL, Robitaille AJ (1999) Alteration mapping in exploration: application of short-wave infrared (SWIR) spectroscopy. Soc Econ Geol Newsl 39:16–27

Weber PA, Hughes JB, Conner LB, Lindsay P, Smart RC (2006) Short-term acid rock drainage characteristics determined by paste pH and kinetic NAG testing: cypress prospect, New Zealand. In: Proceedings from the 7th international conference on acid rock drainage, Missouri, pp 2289–2310

White A, Robb VM, Robb LJ, Waters DJ (2010) Portable infrared spectroscopy as a tool for the exploration of gold deposits in tropical terrains: a case study at the Damang deposit, Ghana. Society of Economic Geologists Special Publication 15, Littleton, Colorado, pp 57–84

# Prediction of Acid Rock Drainage from Automated Mineralogy

**Anita Parbhakar-Fox, Bernd Lottermoser, Richard Hartner, Ron F. Berry and Taryn L. Noble**

**Abstract** Automated mineralogy tools are now commonly used during mineral processing for particle characterization to help mine operators evaluate the efficiency of the selected mineral processing techniques. However, such tools have not been efficiently used to assist in acid rock drainage (ARD) prediction. To address this, the computed acid rock drainage (CARD) risk grade protocol was developed. The CARD risk grade tool involves: (1) appropriate selection of samples (i.e., following a geometallurgical sampling campaign); (2) careful preparation of a particle mount sample; (3) analysis on a mineral liberation analyser (MLA) using the X-ray modal analysis (XMOD) function; (4) processing of the XMOD data to produce a whole particle mount backscattered electron (BSE) image and a corresponding image of classified XMOD points; (5) fusion of both images to obtain particle area data; (6) calculation of the CARD risk ratio based on carbonate and sulfide particle areas, relative reactivities ($pH_{CaCl_2} - pH_{mineral + CaCl_2}$) and acid forming/neutralizing values (calculated based on mineral chemistry and stoichiometric factors, kg $H_2SO_4$/t); and (7) classification of CARD risk ratios ranging from extreme risk to very-low risk. Testing of the CARD risk grade tool was performed on materials selected from several mine sites representative of both run-of-mine ore

A. Parbhakar-Fox (✉) · R.F. Berry · T.L. Noble
School of Physical Sciences, University of Tasmania, Private Bag 79, Hobart, TAS 7001, Australia
e-mail: Anita.Parbhakar@utas.edu.au

R.F. Berry
e-mail: Ron.Berry@utas.edu.au

T.L. Noble
e-mail: Taryn.Noble@utas.edu.au

B. Lottermoser
Institute of Mineral Resources Engineering, RWTH Aachen University, Wüllner-Strasse 2, 52062 Aachen, Germany
e-mail: lottermoser@mre.rwth-aachen.de

R. Hartner
E. 7076, Ehome 2 Apartment Duong D3 Phuoc Long B Ward, Ho Chi Minh City, Vietnam
e-mail: r.hartner@mail.com



B. Lottermoser (ed.), *Environmental Indicators in Metal Mining*,
DOI 10.1007/978-3-319-42731-7_8

and waste. This testing proved that CARD can be effectively used to map ARD risks on a deposit scale and forecast geoenvironmental risk domains at the earliest life-of-mine phases.

## Introduction

Various attempts to directly predict acid formation using mineralogical techniques have been made over the past two decades. Examples of acid rock drainage (ARD) focused optical mineralogy studies are given in Blowes and Jambor (1990), Gunsinger et al. (2006) and Moncur et al. (2009, 2015) in which the sulfide alteration index (SAI), primarily developed for tailings classification, is used. However, the SAI is limited by the lack of consideration given to the dissolution of adjacent metal sulfides (and release of metals) under acid conditions (i.e., sulfide mineral-associations are not considered). Other techniques used to predict acid formation include calculation of neutralizing potential (NP) directly from estimates based on whole-rock geochemical analysis and modal mineralogy (Lawrence and Scheske 1997; Downing and Madeisky 1997; Paktunc 1999). Limitations associated with each of these methods have been widely documented, most recently in Plante et al. (2012).

In principle, a simple mineralogical screening method based on intact mineralogy is required. This method should be used to screen and classify ARD risk, allowing for deposit-wide ARD domaining. Thus, the overarching aim of this research was to develop a new computed ARD (CARD) risk grade protocol, whereby samples can be (a) rapidly assessed using a mineral liberation analyser (MLA) instrument, and (b) appropriately classified based on a statistically-sound assessment of the intact mineralogy and mineral particle area.

## Background

Techniques used to predict acid formation based on mineralogy include calculation of neutralizing potential (NP) values from whole rock geochemical data e.g., Lawrence and Scheske (1997), Paktunc (1999), Plante et al. (2012). In reality, such mineralogical approaches are under-utilized due to the requirement of quantitative data as part of their calculation (e.g., bulk geochemistry, bulk mineralogy). In recent years, automated mineralogical testwork has been performed using established instruments including the FEI Mineral Liberation Analyser (MLA) and Quantitative Evaluation of Minerals by SCANning electron microscopy (QEMSCAN), with newer instruments and software also now available (e.g., TIMA, Zeiss Mineralogic). They allow for the combination of backscattered electron (BSE) image analysis, X-ray mineral identification and advanced imaging and pattern recognition analysis as detailed in Gu (2003), Fandrich et al. (2007) and Gottleib (2008). Their

applications in non-environmental mining-related disciplines (i.e., applied mineralogy, metallurgical processing) are well established, with examples presented in Bruckard et al. (2010), Chapman et al. (2011), Hunt et al. (2011) and Rizmanoski (2011). MLA represents a unique automated method of combining back scattered electron (BSE) image analysis, X-ray mineral identification and advanced imaging and pattern recognition analysis (Gu 2003; Fandrich et al. 2007).

Parbhakar-Fox et al. (2011) included MLA analyses in the GMT three-stage approach to ARD prediction as an advanced mineralogical technique. Polished mounts were recommended for preparation from samples classified by stage-one and stage-two of the GMT approach as acid forming (AF) or extremely acid forming (EAF). Such samples are subjected to sparse phase liberation-Lite (SPL-Lite), extended back scattered electron (XBSE), or grain-based X-ray mapping (GXMAP) analyses depending on mineralogy. Few practical examples of MLA application in mine waste characterization studies exist. For example, Aranda et al. (2009) used XBSE technique to characterize four mine waste types identified at the Antamina Cu-Zn-Mo mine, Peru. Similarly, Buckwalter-Davis et al. (2012) used pixel spaced X-ray (GXMAP), sparse phase liberation (SPL-Lite) and XBSE techniques to characterize six tailings samples from the former New Caloumet Pb-Zn mine, Canada. Most recently, Parbhakar-Fox et al. (2014) also used the XBSE technique for acid rock drainage index evaluations on ten waste rock types at the abandoned Croydon lode-Au mine, Australia. These studies indicate that MLA techniques are best utilized in detailed studies whereby only a few samples are characterized in depth, thus proving its assignment at stage-three of the GMT approach (Parbhakar-Fox et al. 2011).

Despite the ever growing applications of automated mineralogy tools in ore deposit, mineral processing and metallurgical investigations, there are no published examples of their use in predictive ARD studies. This is likely because data collection on a sufficient number of samples for early life-of-mine characterization (Price 2009) is inefficient in terms of both cost and time. Therefore, using MLA in such a manner does not assist in obtaining pertinent environmental information to allow for deposit-wide ARD domaining. This chapter documents the development of a simpler and cost-effective MLA method, which potential to assist with ARD block modeling, and therefore has potential application at the early stages of mining operations.

## Sampling and Sample Preparation

Sample selection for CARD risk grading should ideally take place during early stages of mine operation (e.g., exploration, pre-feasibility), and must be representative of geological, lithological and alteration units in accordance with the GARD Guide (2015). Additionally, samples must be representative of the relative amounts and particle size of each type of material (Downing 1999). Further, Downing (1999) reasoned that whilst rigorous sampling can be costly, remediation and reclamation

plans developed as a consequence of poor sampling and analysis can become even more expensive, hence the importance of a detailed initial assessment. He argued that costs should not pre-determine the number of samples taken and analysed, but should be dependent on the amount necessary to increase confidence in the data.

Considering this, the CARD protocol requires a systematic campaign to be employed; preferably one that mirrors assay or geometallurgical sampling (e.g., 1 in every 2 or 5 m). Once samples have been selected, sample preparation protocols with regards to crushing and grinding for assay should follow those used routinely in mineral processing. In most cases, half core is progressively crushed until 100 % passes approximately 3.3 mm. At this particle size distribution, sub-sampling (i.e., using cone and quarter or riffle methods) can be undertaken with statistical confidence. A sub-sample of this crushed material can be used to prepare 63–125 μm CARD particle mounts (i.e., bulk material milled to this size fraction). By undertaking a campaign that mirrors assay/geometallurgy sampling, data complementary to CARD risk grading will be collected, allowing for cross-checks using environmental geometallurgy indicators to be performed (Parbhakar-Fox and Lottermoser 2014). Such a sampling interval is not fixed, and should be site-specific. For example, it can be changed to a more appropriate value between 2 and 50 m (Price 2009) as determined by site geological personnel. Such sampling should be undertaken on all drill holes (i.e., also low-grade sulfidic ore and waste holes). Adopting such a campaign provides the data to construct an appropriate first-pass ARD block model. Additionally, the expected number of samples as published in guidelines given by the Australian Government Department of Industry and shown in Price (2009) will be approximated.

The mass of individual samples collected is generally dictated by the types of tests to be undertaken, and the associated QA/QC protocols. Typically, 500 g is sufficient to conduct a comprehensive list of geochemical static tests, though 1 kg is preferred (Price 2009). As the CARD risk grade protocol requires mineralogical assessment (with potential for additional geochemical testing for validation purposes or further diagnostic ARD work), 500 g of sample must be obtained as a minimum, with an intact rock slice kept for reference. At a mining operations in pre-feasibility/feasibility, drill core is typically required for other testing (e.g., resource evaluation, geometallurgy, geotechnics), therefore obtaining the required amount may be compromised. In this instance, at least 250 g should be obtained for environmental testing.

## Data Acquisition and Processing

Whilst detailed information regarding particle size, shape and mineral association can be obtained using the previously mentioned MLA-techniques, collecting such data is both costly and time inefficient, with analyses potentially taking >6 h per circular (approx. 2.5 cm diameter) polished block if the mineralogy is complex. Therefore, using the MLA in such a manner does not assist in obtaining relevant

information which would allow for deposit-wide ARD domaining. Instead, the simpler and more rapid X-ray modal analysis (XMOD) technique was applied. It is based on a point counting method, whereby mineral identification is determined by one X-ray analysis at each counting point.

XMOD analyses in this research were performed using a FEI Quanta 600 SEM-MLA instrument (equipped with 2 EDAX ultra-thin window Si (Li) energy dispersive X-ray detectors) at the Central Science Laboratory, University of Tasmania. The input parameters recommended are: 300 frames; 20,000 particles; 60 min time; with the BSE standard set to nickel. On average, data acquisition takes approximately 40 min or less per particle mount. As each XMOD frame is analyzed (X and Y spacing = 47 pixels), a corresponding BSE image is also collected. X-ray spectra were saved for off-line classification. Data processing first included classification of X-ray spectra against a site-specific mineral library (using MLA software). Once classified, only sulfide and carbonate minerals were assigned colours (e.g., pyrite = yellow, calcite = blue), with all other minerals coloured white (e.g., silicates, oxides). Individual XMOD and BSE frames were stitched together to create two congruent whole particle mount images (Fig. 1). Finally, both image files were saved in the *.bmp* format to allow for further processing.

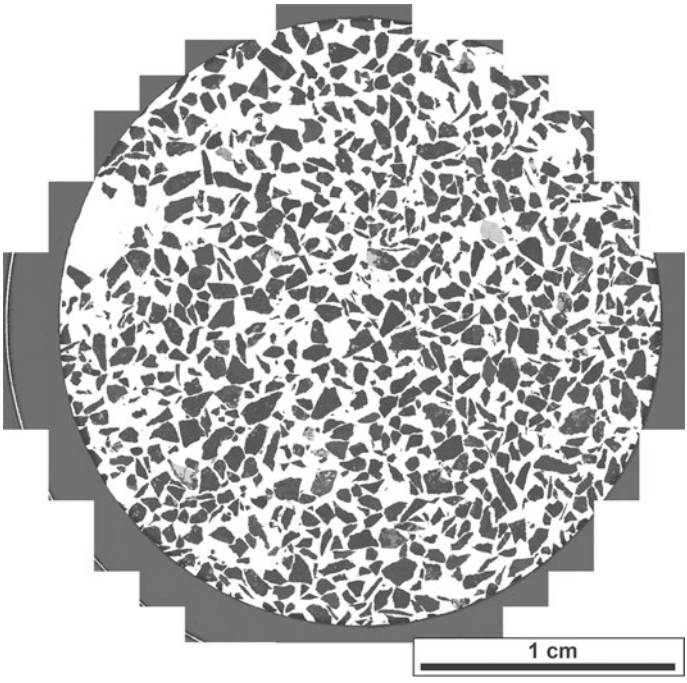


**Fig. 1** Example of stitched BSE image of whole grain mount (*circle diameter* = 2.5 cm)

## Image Fusion

To process the acquired MLA data and extract the desired mineralogical information, Definiens eCognition Developer 8.0 software was used. Previous examples of its application in mineral processing are given in Hartner et al. (2011) and Hartner (2012), where integration of digital optical microscopy (DOM) and automated SEM-based mineralogy (e.g., MLA) datasets was explored. This software follows an object-oriented approach towards automated image analysis by providing a range of innovative features and algorithms. It differs from other software by classifying image objects identified in an image segmentation step, rather than classifying based on single-pixels (Hartner 2012). For the purpose of CARD risk grading, a specific rule code was written. This code first fuses the congruent BSE and XMOD images; and next 'grows out' sulfide and carbonate phases only (Fig. 2). Acid-consuming silicates (e.g., serpentine, chlorite, potassium feldspar) are not counted as they are slower weathering and contribute a comparatively low neutralizing potential (Jambor et al. 2007). The exported pixel area data is saved as a *csv* file. Finally, the particle area per mineral is calculated by multiplying the pixel total for each by 3.52 µm (i.e., the pixel size). Image processing time per sample was approximately 5 min. An example of classified particle mount image with carbonates and sulfides extracted is shown in Fig. 3.

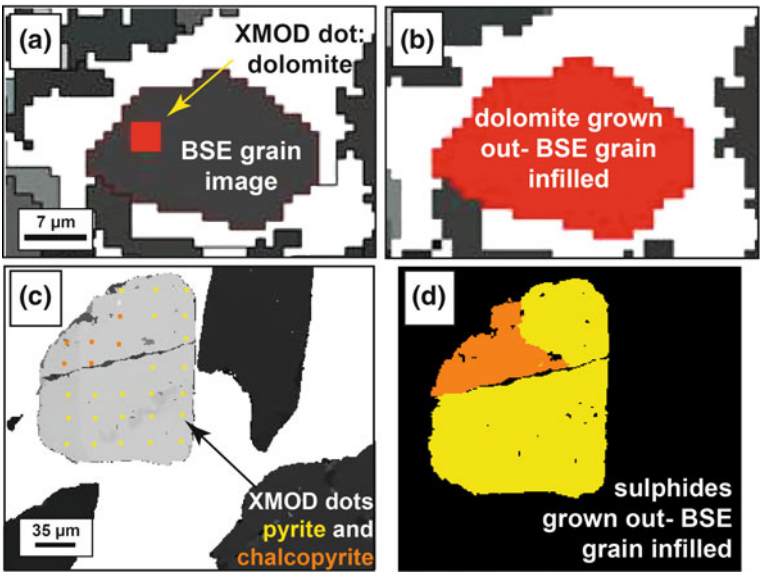


**Fig. 2** Examples of eCognition Developer output images; **a** *Red* classified XMOD dot indicating dolomite over BSE image; **b** fused image with dolomite grown out; **c** sulfide phase with pyrite and chalcopyrite intergrown over BSE image; **d** fused image with sulfides grown out (color figure online)

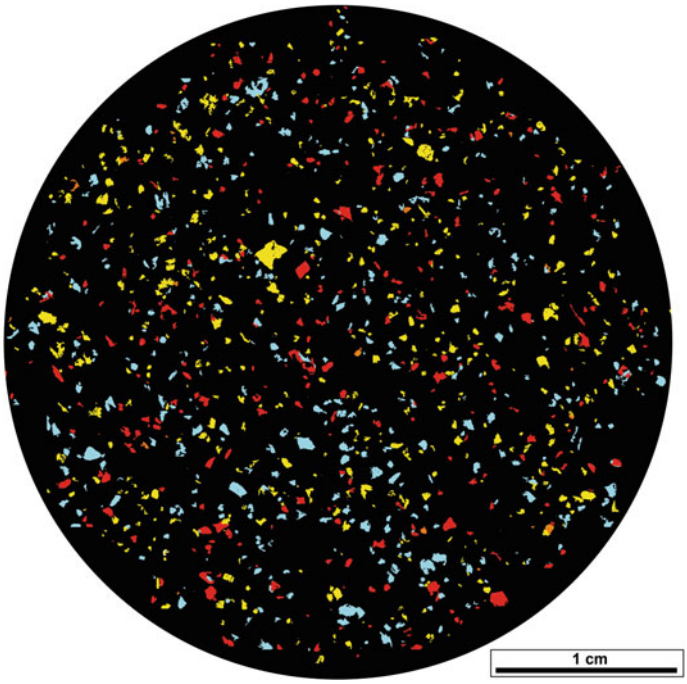


**Fig. 3** Example of a fused and classified image with carbonate and sulfide phases shown (*yellow* = pyrite; *red* = dolomite; *blue* = calcite) (color figure online)

## Relative Reactivity Rates

The occurrence and magnitude of ARD is controlled by the kinetics of acid-producing and -consuming reactions. Therefore, the reactivity of samples needs to consider the balance of these two type reactions. Thus, reactivity values were developed using real geochemical data representative of field-conditions (i.e., pH values). Abrasion pH values (defined as the value obtained by grinding a mineral in water; Stevens and Carron 1948) were previously used as indicators of rock weathering (Grant 1969). For unweathered materials, these values can be adopted and used as measures of immediate reactivity, providing they are immersed in an appropriate electrolyte solution (Noble et al. 2015). Values for the most common sulfide and carbonate minerals following the American Society for Testing and Materials (ASTM) D4972.13 (2013) method were used here (Table 1). To avoid ambiguity, siderite is not included in the CARD protocol as it is can be described as both acid forming and neutralizing (Plumlee 1999). Several less common sulfide and carbonate minerals (e.g., stibnite, rhodochrosite) were not tested by Noble et al. (2015). Instead, abrasion pH values from Stevens and Carron (1948) were used. To standardize abrasion pH values, the absolute difference from the $CaCl_2$ electrolyte control solution pH (6.4; n = 10; Noble et al. 2015) was

**Table 1** Abrasion pH values of common sulfide and carbonate minerals relevant to CARD risk grade classification and their assigned CARD reactivity value

| Mineral | Formula | Abrasion pH | CARD reactivity value | References |
|---|---|---|---|---|
| *Sulfides* | | | | |
| Arsenopyrite | FeAsS | 5.34[a] | 1.06 | Noble et al. (2015) |
| Chalcopyrite | $CuFeS_2$ | 4.22[a] | 2.18 | Noble et al. (2015) |
| Galena | PbS | 6.70[a] | 0.3 | Noble et al. (2015) |
| Pyrite | $FeS_2$ | 3.86[a] | 2.54 | Noble et al. (2015) |
| Pyrrhotite | $Fe_{(1-X)}S$ | 7.38[a] | 0.98 | Noble et al. (2015) |
| Sphalerite | ZnS | 8.04[a] | 1.64 | Noble et al. (2015) |
| Stibnite | $Sb_2S_3$ | 7.5[b] | 1.1 | Stevens and Carron (1948) |
| *Carbonates* | | | | |
| Calcite | $CaCO_3$ | 8.33[a] | 1.93 | Noble et al. (2015) |
| Dolomite | $CaMg(CO_3)_2$ | 8.87[a] | 2.47 | Noble et al. (2015) |
| Magnesite | $MgCO_3$ | 9.32[a] | 2.92 | Noble et al. (2015) |
| Rhodochrosite | $MnCO_3$ | 6.5[b] | 0.1 | Stevens and Carron (1948) |
| Azurite | $CuCO_3$ | 7[b] | 0.6 | Stevens and Carron (1948) |
| Smithsonite | $ZnCO_3$ | 7[b] | 0.6 | Stevens and Carron (1948) |
| Cerussite | $PbCO_3$ | 6[b] | 0.4 | Stevens and Carron (1948) |

[a]Median; n = 9
[b]General value given as determined based on litmus paper testing

calculated for each. For sulfides, this value was calculated by Eq. 1 and for carbonates by Eq. 2. This was designated as the so-called "CARD reactivity value". If no abrasion pH data existed, then a value of 0 was given, and the mineral is not considered further in the final CARD calculations (Eqs. 3–5).

$$(\mathrm{pH}(\mathrm{CaCl_2}) - \mathrm{pH}\ (\mathrm{mineral} + \mathrm{CaCl_2})) = \mathrm{CARD\ relative\ reactivity\ (sulfide)} \quad (1)$$

$$(\mathrm{pH}(\mathrm{mineral} + \mathrm{CaCl_2}) - \mathrm{pH}\ (\mathrm{CaCl_2})) = \mathrm{CARD\ relative\ reactivity\ (carbonate)} \quad (2)$$

## Acid Producing/Neutralizing Values

In order to allow for the calculation of the CARD risk grade value, acid producing (AP)/neutralizing potential (NP) values are required. Acid producing potential (AP) was determined by multiplying the weight of sulfur in the mineral by the stoichiometric factor of 31.25 (to cast in comparable terms with NP values; Lawrence and Wang 1996). These values were divided by 1000 to give a scaled value appropriate for use in the CARD risk grade equation (termed the 'CARD AP value'), with final values shown in Table 2. This table gives values for when oxygen or iron is used as the sulfide oxidant (Plumlee 1999), as opposed to only considering acid formation from when just oxygen is used. For example, sulfide minerals such as sphalerite and galena are regarded as non-acid forming when oxygen is the oxidant (Dold 2010). However, if iron is the oxidant (i.e., under conditions pH <3.5) then both sphalerite and galena will produce acid, and potentially will release significant quantities of metals such as Zn, Cd and Pb into the resulting leachate (Egiebor and Oni 2007). Therefore, because CARD risk grading aims to be conservative in its estimate of acid forming potential, it regards

**Table 2** Acid production (AP) values for common sulfide minerals and their scaled CARD value

| Mineral | Formula | AP (kg $H_2SO_4$/t) | CARD AP value |
|---|---|---|---|
| *Common sulfides known (inferred) to generate acid with oxygen as the oxidant* | | | |
| Arsenopyrite | FeAsS | 616 | 0.61 |
| Bornite | $Cu_5FeS_4$ | 799 | 0.80 |
| Enargite | $Cu_3AsS_4$ | 1018 | 1.02 |
| Orpiment | $As_2S_3$ | 1222 | 1.22 |
| Pyrite | $FeS_2$ | 1670 | 1.67 |
| Pyrrhotite | $Fe_{(1-X)}S$ | 1177 | 1.18 |
| Realgar | AsS | 937 | 0.94 |
| Stibnite | $Sb_2S_3$ | 885 | 0.85 |
| Tennantite/tetrahedrite | $(Cu,Fe,Zn)_{12}As_4S_{13}$/$(Cu,Fe,Zn)_{12}Sb_4S_{13}$ | 889/793 | 0.89/0.79 |
| *Common sulfides that may generate acid with ferric iron as the oxidant* | | | |
| Chalcopyrite | $CuFeS_2$ | 1092 | 1.09 |
| Cinnabar | HgS | 431 | 0.43 |
| Covellite | CuS | 1048 | 1.05 |
| Galena | PbS | 419 | 0.42 |
| Greenockite | CdS | 693 | 0.69 |
| Millerite | NiS | 1104 | 1.10 |
| Pentlandite | $(Fe,Ni)_9S_8$ | 1038 | 1.04 |
| Sphalerite | ZnS | 1033 | 1.03 |

AP values calculated using individual mineral chemistries (www.webmineral.com), following the equation of Lawrence and Wang (1996) with a conversion factor of 31.25 used

most sulfides as acid forming regardless of their oxidant type. Neutralizing potential values for common carbonate minerals have been compiled in a similar manner (Table 3), with data from the published literature (measured experimentally) used, as well as values calculated based on stoichiometry. These values have also been normalized (i.e., divided by 1000) to give a scaled 'CARD NP value' (Eqs. 3–5) appropriate for use in the next steps.

$$\mathrm{AP}/1000 = \mathrm{CARD\ AP\ value\ (sulfide)} \tag{3}$$

$$\mathrm{NP}/1000 = \mathrm{CARD\ NP\ value\ (carbonate)} \tag{4}$$

## CARD Calculation

Calculation of the CARD risk grade value is based on similar principles to acid base accounting, whereby the net acid producing potential (NAPP) is calculated by subtracting the maximum potential acidity (MPA or AP) from the acid neutralizing capacity (ANC or NP). Therefore, CARD calculation can be regarded as 'textural acid base accounting'. Calculation of the final CARD risk grade value is shown in Eqs. 5–8. Equations 5 and 6 show the first step of the CARD calculation. For each individual sulfide and carbonate phase identified, a CARD value must be calculated by multiplying the particle area data (determined from eCognition processing) by the CARD relative reactivity as calculated from abrasion pH values (Table 1), and finally the scaled CARD acid producing or neutralizing potential value (Table 2).

**Table 3** Neutralizing potential (NP) values for common carbonate mineral and their scaled CARD value

| Mineral | Formula | NP (kg $CaCO_3$/t) | Scaled CARD value | References |
|---|---|---|---|---|
| Calcite | $CaCO_3$ | 1000 | 1 | Jambor et al. (2007) |
| Cerussite | $PbCO_3$ | 374 | 0.37 | Calculated[a] |
| Dolomite | $CaMg(CO_3)_2$ | 1086 | 1.09 | Jambor et al. (2007) |
| Ankerite | $Ca(Fe,Mg,Mn)(CO_3)_2$ | 970 | 0.97 | Calculated[a] |
| Magnesite | $MgCO_3$ | 1187 | 1.19 | Calculated[a] |
| Rhodochrosite | $MnCO_3$ | 870 | 0.87 | Calculated[a] |
| Azurite | $CuCO_3$ | 580 | 0.58 | Calculated[a] |
| Smithsonite | $ZnCO_3$ | 798 | 0.80 | Calculated[a] |

[a]Calculated using individual mineral chemistries (www.webmineral.com) and normalizing them to that of calcite (i.e., % $CaCO_3$ in carbonate × 16.67 = NP)

For each sulfide/carbonate phase:

$$\text{Sulfide} = \text{particle area} \times \text{CARD relative reactivity} \times \text{CARD AP} \quad (5)$$

$$\text{Carbonate} = \text{particle area} \times \text{CARD relative reactivity} \times \text{CARD NP} \quad (6)$$

The next step is to calculate the CARD risk grade value (Eq. 7) whereby the final value for all sulfides (calculated individually in Eq. 5) and carbonates (calculated individually in Eq. 6) summed, and the two values subtracted. As with NAPP values, a positive CARD value indicates acid forming potential, and a negative CARD value indicates net-neutralizing potential.

$$\Sigma[\text{Sulfides}] - \Sigma[\text{Carbonates}] = \text{CARD risk grade value} \quad (7)$$

Because calculations include particle area data (in μm), these values are numerically large and potentially cumbersome to interpret. Therefore, calculating the CARD grade ratio is recommended (Eq. 8). However, division by '0' (i.e., absence of carbonates or sulfide) returns an erroneous value. In the absence of sulfides, but with carbonates present, the sample is to be automatically assigned as very low risk (with an arbitrary maximum value for the particular dataset given). In the absence of carbonates, but with sulfide present, the sample is to be assigned extreme risk (with an arbitrary minimum value for the dataset given). This final value provides an indication of the ARD risk, with resulting classifications presented in Table 4.

$$\frac{\Sigma[\text{Sulfides}]}{\Sigma[\text{Carbonates}]} = \text{CARD risk ratio} \quad (8)$$

**Table 4** ARD risk classification scheme, showing CARD risk ratio, risk grade and description of ARD risk classes

| CARD risk ratio | CARD risk grade | Description of ARD risk classes |
|---|---|---|
| $\leq 0.1$ | Extreme risk | Dominance of acid forming minerals, absence of neutralizing minerals |
| 0.11–0.59 | High risk | Dominance of acid forming minerals, low proportion of neutralizing minerals |
| 0.6–0.99 | Moderate risk | Dominance of acid forming minerals, some neutralizing minerals present |
| 1–3.9 | Potential risk | Whilst acid forming and neutralizing minerals are both present, insufficient content of neutralizing minerals present to buffer acid long-term |
| 4–9.9 | Low risk | Net-neutralizing capacity likely |
| $\geq 10$ | Very low risk | Longer term net-neutralizing capacity likely<br>The higher the ratio, the more neutralizing the sample material |

## Examples of CARD Risk Grading

Mineralogical and geochemical analyses as well as CARD testing was performed on bulk samples (both waste rock and run-of-mine, approximately 2 kg prepared to 63–125 μm) collected from eight different mine sites in Australia (n = 10; Tables 5 and 6). A geochemical and mineralogical summary of each is given in the following section, with critical assessment relative to CARD risk grading.

**Table 5** Bulk mineralogy [as measured by XRD, values in %] for 10 samples collected from several Australian mine sites representative of different deposit types (*<1 %)

| Sample | 1 | 2 | 3 | 4 | 5 | 6 | 7 | 8 | 9 | 10 |
|---|---|---|---|---|---|---|---|---|---|---|
| *Silicates* | | | | | | | | | | |
| Chlorite | – | 3 | 3 | 4 | 2 | – | 13 | – | – | – |
| Hornblende | 14 | – | 8 | – | – | – | – | – | – | |
| Muscovite | 9 | – | – | 48 | 28 | | 11 | 10 | 6 | 16 |
| Orthoclase | 13 | 34 | 18 | – | – | – | – | – | – | 3 |
| Plagioclase | 39 | 37 | 35 | – | – | – | – | – | – | 3 |
| Quartz | 15 | 19 | 25 | 37 | 43 | 15 | 49 | 8 | 9 | 44 |
| Topaz | – | – | – | – | – | – | – | – | – | 29 |
| Tourmaline | – | – | – | – | – | – | – | – | – | * |
| *Sulfides* | | | | | | | | | | |
| Galena | – | – | – | – | 4 | 4 | 3 | – | – | – |
| Pyrite | 3 | 2 | * | 10 | 1 | 1 | 6 | 4 | 7 | 3 |
| Pyrrhotite | – | – | – | – | – | – | 2 | 16 | 15 | – |
| Sphalerite | – | – | – | – | 7 | 8 | 12 | – | – | – |
| *Carbonates* | | | | | | | | | | |
| Calcite | 7 | 5 | 10 | * | – | – | – | – | – | – |
| Dolomite | – | – | – | – | 3 | 3 | 3 | – | 23 | – |
| Siderite | – | – | – | – | 11 | 66 | – | 39 | 21 | – |
| Magnesite | – | – | – | – | – | – | – | 12 | 13 | – |
| *Oxides/fluorides* | | | | | | | | | | |
| Cassiterite | – | – | – | – | – | – | – | – | – | * |
| Fluorite | – | – | – | – | – | – | – | 3 | 3 | – |
| Magnetite | – | – | – | – | – | – | * | – | – | – |
| Sellaite | – | – | – | – | – | – | – | 8 | 3 | – |
| Sphene | – | – | – | – | – | – | * | – | – | – |
| *Sulfates/arsenates* | | | | | | | | | | |
| Jarosite | – | – | – | * | * | 2 | – | – | – | * |
| Scorodite | – | – | – | – | – | – | – | – | – | * |

**Table 6** Geochemical and CARD risk grade values for 10 samples collected from several Australian mine sites representative of different deposit types

| Sample number | Sulfur (wt%) | ANC (kg $H_2SO_4$/t) | MPA (kg $H_2SO_4$/t) | NAPP (kg $H_2SO_4$/t) | NAG pH | Geochemical classification | CARD ratio | CARD risk classification |
|---|---|---|---|---|---|---|---|---|
| 1 | 1.21 | 92 | 37 | −55 | 9.6 | NAF | 0.72 | Moderate |
| 2 | 1.06 | 72 | 32 | −40 | 8.4 | NAF | 1.8 | Potential |
| 3 | 1.11 | 111 | 34 | −77 | 7.6 | NAF | 3.1 | Low |
| 4 | 15.18 | 4 | 465 | 461 | 2.1 | PAF | 0.01 | Extreme |
| 5 | 3.83 | 56 | 117 | 61 | 6.5 | UC | 0.3 | High |
| 6 | 4.35 | 274 | 133 | −141 | 6.6 | NAF | 0.13 | High |
| 7 | 13.84 | 40 | 424 | 384 | 3.1 | PAF | 0.01 | Extreme |
| 8 | 13.86 | 393 | 424 | 31 | 2.9 | PAF | 0.19 | High |
| 9 | 14.71 | 365 | 450 | 85 | 2.9 | PAF | 1.04 | Potential |
| 10 | 3.79 | 0 | 116 | 116 | 2.2 | PAF | 0 | Extreme |

## *Porphyry-Cu-Au Deposit, NSW*

Samples 1, 2 and 3 are run-of-mine (ROM) samples collected from porphyry-Cu-Au operations in New South Wales (NSW). The mineralogy of sample 1 is silicate dominated, but also contains calcite and lesser pyrite (Table 5). Geochemically, this sample is classified as non-acid forming (NAF; Table 6). However, whilst the sample's NAPP is −55 kg $H_2SO_4$/t, the 3:1 ratio of ANC to MPA to allow for effective neutralization has not been achieved. Therefore, its classification as NAF is misleading, as calcite will be rapidly consumed (Brough et al. 2013). Instead, the sample was classified as moderate risk by the CARD risk grade. This is a more appropriate classification when considering the rate of carbonate consumption, and the consequent PAF characteristics the sample will exhibit.

Sample 2 has similar mineralogy to sample 1 (Table 5). Geochemically, this sample is classified as NAF (Table 6), but again, does not have a 3:1 ratio of ANC to MPA. By the CARD classification, this sample is identified as potential risk indicating that in ARD terms, this material is not inert. This CARD classification aligns with the mineralogy.

Sample 3 is also silicate dominated, but has significant carbonate content and only trace sulfide (Table 5). Geochemically, this sample is classified NAF (Table 6) with sufficient ANC to buffer any acid produced. The CARD risk classification is in agreement, and identifies this as a low risk sample, with significant ANC.

## *Massive Sulfide Deposit (Cu-Ag-Au-Pb-Zn), Tasmania*

Samples 4 to 7 are bulk waste rock materials collected from four massive sulfide deposits located on the western coast of Tasmania. The mineralogy of sample 4 (from a Cu operation) is silicate dominated with major pyrite, and only trace calcite (Table 5). Geochemically, this sample is classified as PAF (Table 6) with a NAPP value of 461 kg $H_2SO_4$/t. However, based on the high pyrite content, CARD risk grade refined this classification identifying it as extreme risk, due to the absence of acid neutralizing carbonates.

The mineralogy of sample 5 (from a former Ag-Pb operation) is silicate dominated with several carbonates (e.g., siderite, dolomite) and sulfides (e.g., sphalerite, galena, and pyrite) identified (Table 6). Geochemically, this sample was classified as uncertain due to the high NAG pH (i.e., above the pH 4.5 cut-off criterion; Parbhakar-Fox et al. 2011) when plotted against the NAPP value of 61 kg $H_2SO_4$/t (Table 6). Instead, the CARD risk grade identified this sample as high risk, based on the dominance of sulfides, and low proportion of acid neutralizing carbonates.

Sample 6 (from a former Ag-Pb operation) is siderite dominated, with lesser silicate, sulfides and other carbonates identified (Table 5). It was geochemically classified as NAF (Table 6). However, the Sobek test (by which ANC was calculated) has likely overestimated neutralizing capacity, due to the reaction of siderite (White et al. 1999). The CARD risk grade recognizes that siderite is both acid forming, and neutralizing so it is not considered in the calculation, resulting in this sample classified as high risk.

Sample 7 (from an active polymetallic Pb-Zn-Ag operation) is silicate dominated and also contains several sulfides and oxides, with a notable absence of carbonates (Table 5). Geochemically, this sample is classified PAF (Table 6). However, by the CARD risk grade, it is classified as extreme risk which is considered accurate when compared to the sulfide and carbonate mineralogy.

## *Abandoned Sn-Operations, Tasmania*

Bulk waste rock samples were taken from abandoned Sn-operations. Samples 8 and 9 are from a Renison style carbonate-replacement Sn deposit located in western Tasmania. Sample 8 was again siderite dominated, but also contained significant pyrrhotite and magnesite (Table 5). In contrast, sample 9 was dominated by dolomite (Table 5). Geochemical testwork classified both samples as PAF (Table 6), with the CARD classification assigning a high risk to sample 8, and a potential risk to sample 9. Considering the contrast in sulfide and carbonate mineralogy between these samples, the risk classification appropriately indicates that material representative of sample 8 is more hazardous in ARD-terms than sample 9 which is dolomite-bearing.

Sample 10 is from a greisen-style deposit located in eastern Tasmania. It is silicate dominated with pyrite and minor arsenate, sulfate and oxides (Table 5). This sample was geochemically classified as PAF (Table 6) due to the presence of pyrite and absence of ANC. The CARD risk grade refined this classification, identifying it instead as extreme risk.

These examples demonstrate that CARD grading yields greater resolution of ARD risks than conventional ABA testing and classification. This is because risk is calculated based on quantified mineralogy and ARD-relevant mineral properties. Geochemical testwork can lead to misclassification particularly for high siderite samples, as was the case for samples 5 and 6. Moreover, CARD risk grading allows for samples to be classified beyond simply PAF, NAF and UC, which is commonly a limitation of current geochemical tests. This testwork confirmed that the risk categories proposed are appropriate in terms of representing carbonate and sulfide mineralogy, and determining the ARD risk posed.

## Applications of CARD Risk Grading

Unlike other ARD prediction tests, CARD risk grading has the ability to be performed retrospectively on samples which were previously analyzed for other purposes. For example, if mineral abundance data were collected on particle mounts for geometallurgical testwork, then it could be re-processed and used in CARD risk grading, therefore presenting a real opportunity to add significant value to existing automated mineralogy datasets. Whilst our focus is on utilizing MLA, data generated by other automated SEM platforms could also be used. For example, the Zeiss Mineralogic Mining 'feature scan' mode (Graham et al. 2015) may generate appropriate data for CARD risk grading, as might TESCAN TIMA modal analysis and QEMSCAN bulk mineral analysis functions. This remains to be practically tested. In a geochemistry-mineralogy-texture-geometallurgy approach framework, the CARD grade would be regarded as a stage-one tool (i.e., pre-screening stage where cost-effective domaining techniques are used). Based on the outcomes of such analyses, samples would be taken forward for geochemical testwork and more detailed mineralogical and textural evaluations (e.g., using other MLA functions such as XBSE and SPL-Lite analyses which provide additional information on parameters such as mineral association and particle shape). The CARD risk grade protocol can also be used as part of flotation testwork i.e., to characterize potential ARD risks associated with tailings, therefore allowing an ARD index for a tailings storage facility to be formulated (rather than retrospectively determined by drilling and characterizing on closure e.g., Jackson et al. 2015). Further development of the CARD protocol should focus on identifying other acid forming (e.g., secondary iron sulfate phases) and longer-term non-carbonate neutralizing minerals (e.g., chlorite, feldspar, serpentines) and incorporating particle area data from these into the final CARD calculation. This will allow for the evaluation of longer-term ARD risk and leachate quality.

## Conclusions

The CARD grade protocol uses classified MLA-XMOD data and fuses this with BSE images to allow for the extraction of particle area data of both sulfide and carbonate phases. These data are then used with mineral reactivity and acid/neutralising potential values to deduce a CARD grade classification and risk ratio, the latter of which is graded from extreme ARD risk to very low ARD risk. The CARD risk grade protocol was trialed on a mineralogically diverse range of samples (n = 10). These evaluations allowed greater resolution of ARD risks of individual samples than when using routine geochemical or mineralogical assessments. By screening waste materials in this manner the opportunity to improve waste block model accuracy arises as a greater number of waste types can be accurately defined based on this mineralogical risk assessment.

Therefore, the CARD risk grade protocol should be utilized during early life of mine stages (e.g., exploration, pre-feasibility) to improve geoenvironmental domaining practices. Furthermore, it can be performed on both solid (i.e., waste rock) and processed (i.e., tailings) materials. CARD risk grading has additional advantages in that it can be performed retrospectively, providing that mineral abundance data has been collected. Further developmental work should focus on including additional acid forming phases (i.e., secondary iron sulfates) and longer-term neutralizing minerals (e.g., silicates such as chlorite and serpentine) into the CARD calculation. In addition, research should be undertaken into how automated data generated by other instruments (e.g., QEMSCAN, Zeiss Mineralogic, TESCAN TIMA) can be used in this ARD prediction context.

## References

American Society for Testing and Materials (ASTM) 766 D4972–01(2013) (2013) Standard test method for pH of soils.767 ASTM International, West Conshohocken, PA. www.astm.org

Aranda CA, Klein B, Beckie RD, Mayer KU (2009) Assessment of waste rock weathering characteristics at the Antamina Mine based on field cell experiments. In: Proceedings from the 8th international conference on acid rock drainage, Skelleftea, pp 1–10

Blowes DW, Jambor JL (1990) The pore-water geochemistry and the mineralogy of the vadose zone of sulphide tailings, Waite Amulet, Quebec, Canada. Appl Geochem 5:327–346

Brough C, Warrender R, Bowell RJ, Barnes A, Parbhakar Fox A (2013) The process mineralogy of mine wastes. Min Eng 52:125–135

Bruckard WJ, Davey KJ, Jorgensen FRA, Wright S, Bew DRM, Haque N, Vance ER (2010) Development and evaluation of an early removal process for the beneficiation of arsenic-bearing copper ores. Min Eng 23:1167–1173

Buckwalter-Davis M, Jaggard H, Jamieson H (2012) Automated mineralogy of mine tailings using mineral liberation analysis. In: Proceedings from the 9th international conference on acid rock drainage, Ontario, pp 942–949

Chapman NA, Shackleton NJ, Maysiak V, O'Connor CT (2011) The effect of using different comminution procedures on the flotation of platinum group minerals. Min Eng 24:731–736

Dold B (2010) Basic concepts in environmental geochemistry of sulphide minewaste management. In: Kumar S (ed) Waste management, INTECH Open Access Publications, pp 173–198. ISBN 978-953-7619-84-8

Downing BW (1999) ARD sampling and sample preparation. http://technology.infomine.com/enviromine/ard/sampling/intro.html

Downing BW, Madeisky HE (1997) Lithogeochemical methods for acid rock drainage studies and prediction. Explor Min Geol 6:367–379

Egiebor NO, Oni B (2007) Acid rock drainage formation and treatment: a review. Asia Pac J Chem Eng 2:47–62

Fandrich R, Gu Y, Burrows D, Moeller K (2007) Modern SEM-based mineral liberation analysis. Int J Miner Process 84:310–320

GARD (Global Acid Rock Drainage) guide (2015) The international network for acid prevention (INAP). http://www.gardguide.com/

Gottleib, P (2008) The revolutionary impact of automated mineralogy on mining and mineral processing. In: 24th international Mineral Processing Congress. Science Press, Beijing, pp 165–174

Graham SD, Brough C, Cropp A (2015) An introduction to ZEISS mineralogic mining and the correlation of light microscopy with automated mineralogy: a case study using BMS and PGM analysis of samples from a PGE-bearing chromite prospect. In: Precious metals 2015, Cornwall, UK, pp 1–12

Grant WH (1969) Abrasion pH, an index of chemical weathering. Clays Clay Miner 17:151–155

Gu Y (2003) Automated scanning electron microscope based mineral liberation analysis—an introduction to JKMRC/FEI mineral liberation analyser. J Miner Mat Character Eng 2:33–41

Gunsinger MR, Ptacek CJ, Blowes DW, Jambor JL, Moncur MC (2006) Mechanisms controlling acid neutralization and metal mobility within a Ni-rich tailings impoundment. Appl Geochem 21:1301–1321

Hartner R (2012) Integration and analysis of optical and MLA-based microscopy for optimisation of geometallurgical modelling and ore deposit characterisation. PhD thesis, University of Queensland, Australia

Hartner R, Walters S.G, Berry R (2011) Integration and analysis of optical and SEM-based microscopy for automated mineralogical characterisation. In: Proceedings from the 10th International Congress for Applied Mineralogy, Trondheim, Noway, pp 319–326

Hunt J, Berry RF, Bradshaw D (2011) Characterising chalcopyrite liberation and flotation potential: Examples from an IOCG deposit. Min Eng 24:1271–1276

Jackson L, Parbhakar-Fox A, Hughes A, Agius J, Ferguson T, Lester D (2015) Microan-alytical evaluations of the Savage River old tailings dam, north-west Tasmania. In: AUSIMM tailings and mine waste management for the 21st century, Sydney, Australia, pp 1–14

Jambor JL, Dutrizac JE, Raudsepp M (2007) Measured and computed neutralization potentials from static tests of diverse rock types. Environ Geol 52:1019–1031

Lawrence RW, Wang Y (1996) Determination of neutralization potential for acid rock drainage prediction. MEND Project Report 1.16.3, MEND, Ottawa, ON

Lawrence RW, Scheske M (1997) A method to calculate the neutralization potential of mining wastes. Environ Geol 32:100–106

Moncur MC, Jambor JL, Ptacek CJ, Blowes DW (2009) Mine drainage from the weathering of sulfide minerals and magnetite. Appl Geochem 24:2362–2373

Moncur MC, Jambor JL, Ptacek CJ, Blowes DW (2015) Long-term mineralogical and geochemical evolution of sulfide mine tailings under a shallow water cover. Appl Geochem 57:178–193

Noble TN, Lottermoser BG, Parbhakar-Fox A (2015) Evaluation of pH testing methods for sulfidic mine waste. Mine Water Environ. doi:10.1007/s10230-015-0356-2

Paktunc AD (1999) Mineralogical constraints on the determination of neutralising potential and prediction of acid mine drainage. Environ Geol 39:103–112

Parbhakar-Fox A, Edraki M, Walters S, Bradshaw D (2011) Development of a textural index for the prediction of acid rock drainage. Min Eng 24:1277–1287

Parbhakar-Fox A, Lottermoser BG (2014) Domaining acid rock drainage risks using geometallurgical data. In: Proceedings from the 8th Australian workshop on acid and metalliferous drainage, pp 483–494

Parbhakar-Fox AK, Edraki M, Hardie K, Kadletz O, Hall T (2014) Identification of acid rock drainage sources through mesotextural classification at abandoned mines of Croydon, Australia: implications for the rehabilitation of waste rock repositories. J Geochem Explor 137:11–28. doi:10.1016/j.gexplo.2013.10.017. ISSN 0375-6742

Plante B, Bussiere B, Benzaazoua M (2012) Static test response on 5 Canadian hard rock mine tailings with low net acid-generating potentials. J Geochem Explor 114:57–69

Plumlee GS (1999) The environmental geology of mineral deposits. In: Plumlee, GS, Logsdon MJ (eds) The environmental geochemistry of mineral deposits part A: processes, techniques and health issues. reviews in economic geology, vol 6A, pp 71–116

Price WA (2009) Prediction manual for drainage chemistry from sulphidic geologic materials. CANMET Mining and Mineral Sciences Laboratories, Canada

Rizmanoski V (2011) The effect of microwave pre-treatment on impact breakage of copper ore. Min Eng 24:1609–1618

Stevens RE, Carron MK (1948) Simple field test for distinguishing minerals by abrasion pH. Am Miner 33:31–50

# Predictive Waste Classification Using Field-Based and Environmental Geometallurgy Indicators, Mount Lyell, Tasmania

**Anita Parbhakar-Fox and Bernd Lottermoser**

**Abstract** Best practice for acid rock drainage (ARD) risk assessment predominately relies on the geochemical properties of sulfidic rocks. Consequently, a plethora of geochemical tests are routinely utilised by the mining industry to predict ARD formation. Due to limitations associated with these tests and their relatively high costs, analysis of recommended best practice sample numbers is rarely achieved, thus reducing the accuracy of waste management plans. This research aimed to address this through identifying potential geometallurgy indicators using drill core samples (n = 70) obtained from the Comstock Chert, a new prospect proximal to Mount Lyell, western Tasmania, Australia. Samples were subjected to a range of mineralogical analyses, routine ARD geochemical tests (i.e., paste pH; acid-base accounting, ABA; net acid generation, NAG), field-based techniques (e.g., portable X-ray fluorescence, pXRF; short-wave infrared spectrometry, SWIR), and geometallurgical analyses (i.e., HyLogger, Equotip). This study demonstrated: (1) HyLogger data allows identification of acid-neutralizing carbonate minerals; (2) Equotip hardness data provide a conservative indication of lag-time to acid formation; (3) CARD risk grading accurately identifies high and low risk ARD domains; and (4) pXRF data provides a sound indication of the abundance of environmentally significant elements. Consequently, the application of geometallurgical techniques to drill core allows the prediction of ARD characteristics that inform waste characterization and management plans.

A. Parbhakar-Fox (✉)
School of Physical Sciences, University of Tasmania, Private Bag 79, Hobart, TAS 7001, Australia
e-mail: Anita.Parbhakar@utas.edu.au

B. Lottermoser
Institute of Mineral Resources Engineering, RWTH Aachen University, Wüllnerstrasse 2, 52062 Aachen, Germany
e-mail: lottermoser@mre.rwth-aachen.de



B. Lottermoser (ed.), *Environmental Indicators in Metal Mining*,
DOI 10.1007/978-3-319-42731-7_9

## Introduction

Determining the propensity of a rock unit to produce ARD is possible through the use of established and emerging geometallurgical tools and techniques. The geochemistry-mineralogy-texture (GMT) approach is one such protocol allowing for improved ARD prediction. Through using the GMT approach, it is possible to pursue best practice sample numbers (cf. Price 2009) for deposit-wide ore and waste characterization, rather than through using other protocols such as the Wheel Approach (Morin and Hutt 1998). Despite the merits of the GMT approach and the use of such simple pre-screening tests for deposit-wide domaining, it can be argued that the undertaking of such specialised ARD focused analyses (e.g., geochemical tests) is financially limiting as these data are fit-for-purpose and cannot be used to characterize other features of the ore body. Instead, to facilitate deposit-wide characterization and to add value to already existing datasets, proxies for ARD data must be identified. Geometallurgical tests and data are the most appropriate proxies. Whilst a vast range of data is collected for geometallurgical modelling, no published examples exist of it being utilised for predictive ARD characterization. Yet, existing sampling strategies of 2 m intervals, utilised as part of geometallurgical campaigns (e.g., Alruiz et al. 2009; Leichliter et al. 2011), represent an appropriate sampling approach for deposit-scale ARD domaining.

This aim of this study was to determine whether geometallurgical data can be utilised effectively to domain acid neutralizing capacity and acid forming potential in drill core materials. Geometallurgical data and its environmental implications examined in detail were: (1) hyperspectral infrared HyLogger data to assess the accuracy of acid neutralizing capacity (ANC) data; and (2) mineral hardness Equotip data to determine the weathering rate of rock units. In addition to geometallurgical data, information derived from field-based instrumentation (i.e., SWIR, pXRF) is also presented and evaluated in terms of application for accurate deposit-wide ARD domaining. For validation, geometallurgical data were compared with data generated from field tools (e.g., staining), and established geochemical (e.g., NAPP and NAG) and mineralogical (e.g., XRD) tests.

## Deposit Geology

The Comstock Valley is located on the northern end of the Mount Lyell mineral field, Queenstown, Tasmania (McLoughlin and Morrison 2013). The deposit is part of the large Cambrian hybrid volcanogenic-magmatic Cu-Au-Ag system at Mount Lyell, which has been exploited for approximately 120 years from 22 separate mine workings. The Mount Lyell mineral field occupies the southern end of a belt of polymetallic base and precious metal deposits within the late Middle Cambrian Mount Read Volcanics (MRV) succession of western Tasmania (Fig. 1).

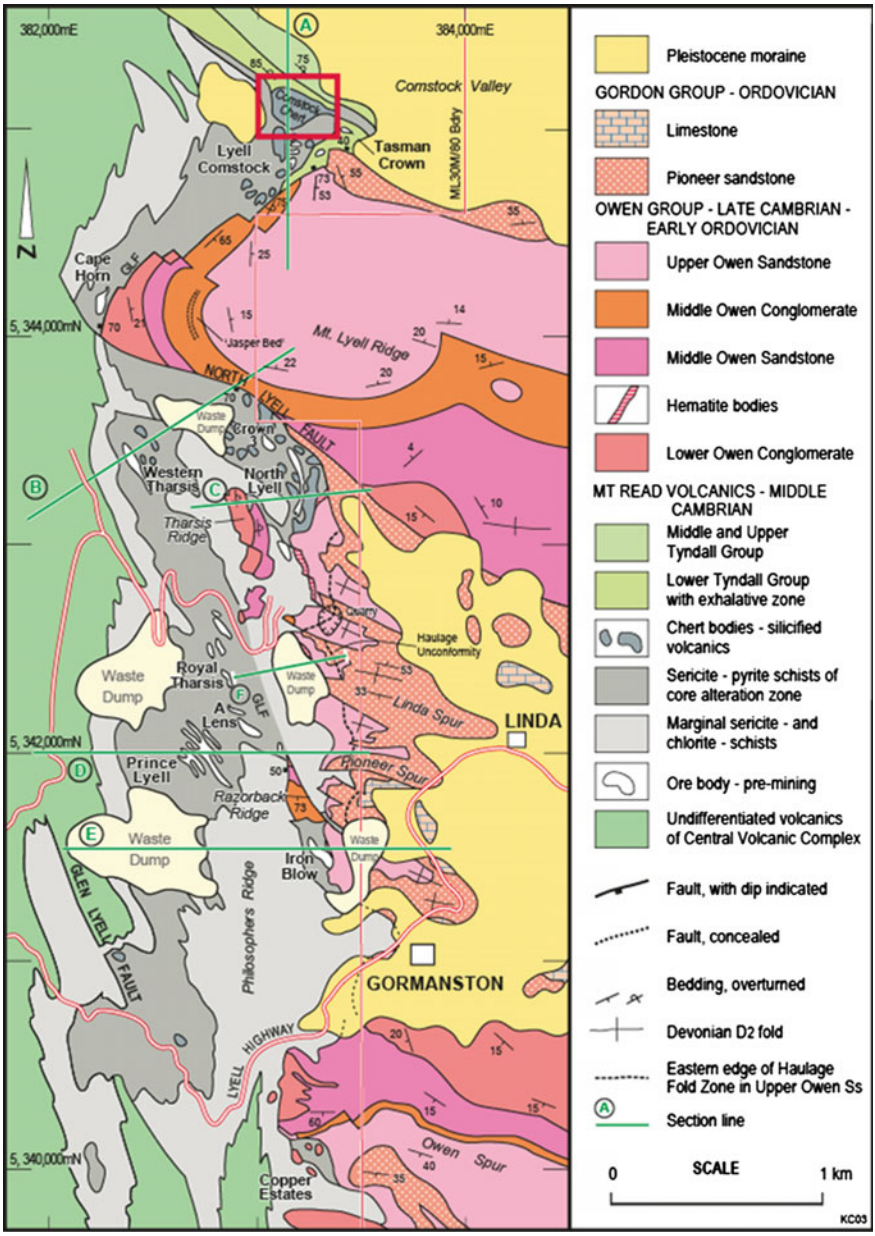


**Fig. 1** Local geology of the Mount Lyell area, with the Comstock Chert shown in the *red box* (Corbett et al. 2014) (reprinted from Corbett et al. 2014, with permission from the Geological Society of Australia) (color figure online)

The Copper Chert deposit is considered to represent a new style of volcanic hosted, copper-rich polymetallic mineralization for the Mount Lyell mineral field (McLoughlin and Morrison 2013). The mineralization is largely Cu-Au-Ag but also contains significant intersections of Pb-Zn-Ag ore. The deposit is hosted in an intense microcrystalline silica alteration package known as the Comstock Chert.

## Acid Rock Drainage at Mount Lyell

ARD is actively produced from mine wastes produced by the former Mount Lyell mine (Fig. 2) and is under the management of the State Government. These mine wastes are the consequence of a century of continuous copper mining and processing at the Mount Lyell mine. Amongst the impacts arising from discharge of metal-enriched ARD, slag and tailings are the pollution of fresh and marine waters and the deposition of tailings and slag in the Queen and King Rivers and Macquarie Harbour. Considering the ARD legacy at Mount Lyell, it is imperative that any new operations such as the Copper Chert adopt and maintain best practice in terms of their ARD testwork and waste management planning.

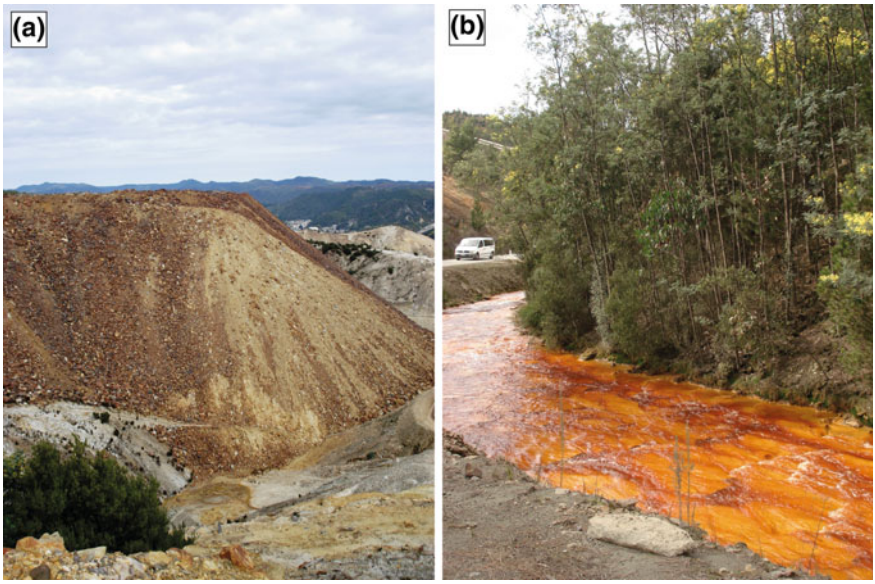


**Fig. 2** **a** Waste rock pile containing pyritic material at the Mount Lyell mine, Tasmania. **b** Haulage Creek, draining the mine site, heavily polluted by acid rock drainage (color figure online)

## Sample Selection and Handling

A 70 m section of drill core (drill hole CCD007), which showed lithological and mineralogical variability, was selected for this study. The upper portion of this drill core section (304–345 m) is representative of the Tyndall Group Lynchford Member, which comprises of sedimentary sandstones, limestones and conglomerates and demonstrated a variety of textures (e.g., fragmental, clastic, veined). The lower portion (345–375 m) sampled the Lyell Schist, which demonstrated increasing degrees of mineralization with depth (i.e., contained greater proportions of chalcopyrite and pyrite towards the base of the drill hole). For the majority of the Tyndall Group Lynchford Member, half core samples were taken. Due to the increased degree of mineralization in the Lyell Schist, only quarter core samples were provided. The materials were shipped directly to Mineral Resources Tasmania (MRT). On receipt of samples, drill core was unpacked and laid out in sequence in metal drill core trays in preparation for HyLogger analysis. However, it was noted that quarter core samples had not transported well and were highly fragmented, causing difficulty when reassembling the drill core material. In some instances, recovery of the whole 1 m interval was not possible. Despite this, the drill core material was arranged so that the best possible fit was achieved, samples were then cleaned thoroughly with water and left to air-dry.

## Geometallurgical Analyses

### *Hyperspectral Mineralogy*

Hyperspectral mineralogy data was collected using a HyLogger instrument housed at MRT. HyLogging$^{TM}$ systems are automated platforms used to rapidly and systematically collect infrared spectroscopic reflectance data at dense sample spacing from drill core, chips or powders (Huntington et al. 2006). 40 m of material (304–345 m; representative of the Tyndall Group Lynchford Member) were analysed both pre- and post-carbonate chemical staining. Approximately >5000 hyperspectral reflectance measurements were collected, with the data acquisition rate ca. 5 min for a three section core tray. Measurements were captured from a 10 × 10 mm field-of-view along the middle of the core, and continuous imagery across the full width of the core was synchronously acquired. Hyperspectral data analysis and mineral interpretation were carried out in version 8.1 of The Spectral Geologist (HotCore). Hylogging derived mineralogy was intended for comparison with: (1) carbonate staining results; (2) SWIR data; (3) XRD data; and (4) domaining of neutralizing capacity using carbonate relative intensity values and total sulfur data.

### *Equotip Analysis*

Circa 3000 measurements were collected from the whole 70 m length of the sampled drill hole using an Equotip 3 instrument (manufactured by Proceq). An average value was calculated for each 1 m interval based on measurements taken at 2.5 cm intervals as recommended by Keeney (2008). Equotip values were compared against total-sulfur values graphically and sample intervals were then classified in terms of lag-time to ARD generation. These classifications were compared against those determined using a NAG pH versus paste pH geochemical plot. This allowed for a critical assessment of the application for ARD risk domaining using Equotip versus total sulfur data.

### *CARD Risk Grading*

Mineralogical and textural data were collected using a mineral liberation analyser (MLA) instrument at the Central Science Laboratory, University of Tasmania (FEI Quanta 600 SEM equipped with 2 EDAX ultra-thin window Si (Li) energy dispersive X-ray detectors). The CARD grade used the XMOD technique, a simpler and lower-cost MLA method than those more routinely used (e.g., XBSE, SPL-Lite). XMOD is based on a point counting method, whereby mineral identification is determined by one X-ray analysis at each counting point. The input parameters used here were: frames, 300; particles, 20,000; time, 60 min; with the BSE standard set to nickel. On average, data acquisition took approximately 30 min or less per sample. Data processing and CARD calculations were performed following the methodology presented in Chap. "Prediction of Acid Rock Drainage from Automated Mineralogy".

## Field Based Tests

### *Chemical Staining*

Only the Tyndall Group Lynchford Member material (304–345 m) was subjected to staining given its high carbonate contents as indicated by the geological logging of these samples. Prior to staining, drill core was etched using dilute HCl for 2–3 min and subsequently washed with water. Samples were then left to dry for approximately 30 min. Next, samples were stained directly with a paintbrush using a dual stain comprising the organic dye Alizarin Red-S (ARS) and Potassium Ferricyanide (PF) dissolved in HCl. After staining, samples were re-run on the HyLogger to collect high-resolution photographic images for comparison against unstained core images.

## Geochemical and Mineralogical Testwork

### *Sulfur Analysis*

Rapid and accurate measurement of sulfur (wt%) for comparison against Equotip and HyLogger values and calculation of maximum potential acidity (MPA) was performed on all samples using an Eltra C-S 2000 instrument at UTAS. Analysis requires the use of two accelerants (tungsten and iron) which were carefully weighed into a crucible, with a measure (c. 200 mg) of powdered (<63 μm) sample added. Individual crucibles were placed onto the instrument stage, loaded into the machine, and heated to >800 °C. The evolved gases were measured and values for carbon and sulfur calculated, in under 1 min. The instrument was regularly calibrated (i.e., once after every 10 samples analysed), using two calibration materials provided by the instrument supplier (calcium carbonate and barium sulfate). As a further measure, two ore standards (purchased from Choice Analytical) were also run in addition to sample blanks (i.e., before instrument calibration).

### *Paste and NAG pH*

The ASTM D4972-01 (2007) paste pH method was used in this study. These data were used in this study for comparison against NAG pH to geochemically classify ARD risk. This pH test measures pH in a 0.01 M $CaCl_2$ solution at a 1:1 solid to solution ratio. The pH value of each sample (n = 55) was measured in triplicate, with the standard deviation calculated as <0.5. To compliment NAPP testing and for comparison against paste pH values, multi-addition net acid generation (mNAG) pH tests were performed following the method of Smart et al. (2002). Essentially, the mNAG test procedure involves the stepped addition of $H_2O_2$ in three increments (100 ml, 100 ml and 50 ml). This allows more time for sulfide oxidation. Powders (<63 μm) from all samples (n = 51) were tested with appropriate sample duplicates used during the analysis.

### *Acid Neutralizing Capacity (ANC)*

All samples from the Tyndall Group Lynchford Member material (304–345 m; CCD007) were sent to ALS Brisbane for the calculation of acid neutralizing capacity (ANC) by the Sobek method (ALS code: EA013). This data was collected to determine NAPP values for the carbonate-rich Tyndall Group Lynchford Member materials. This data was also used to assist in determining whether carbonate staining and hyperspectral mineralogy data had identified calcite in the correct intervals.

### *X-ray Diffractometry (XRD)*

To determine the mineralogy of supplied drill core (for evaluation of field-based and geometallurgical data), milled material from each 1 m interval was subjected to powder XRD analysis. A benchtop Bruker D2 Phaser X-ray diffractometer with a Co X-ray source was used to perform these analyses. Prior to each daily sample run, a corundum standard was analysed to check the X-ray beam alignment and ensure the correct collection of peaks. Each sample was ground in an agate pestle and mortar and loaded into the sample holder and placed into the machine chamber. Samples were analysed for 1 h (fixed divergence slit: 1 mm; range 4–900 2-theta; 0.020 step size, Fe-filter), with the resulting spectra processed in Eva 2.1 software, where minerals were identified using the ICDD PDF 2012 database. In addition, nine samples were chosen for further processing using Topas 2.0 software, to verify the accuracy of carbonate staining. A fundamental parameters approach was applied, and preferred crystal orientation corrected for.

## Results

### *Domaining Acid Neutralizing Capacity*

#### Static Geochemical Data

Acid neutralizing capacity (ANC) measurements collected for the Tyndall Group Lynchford Member (304–345 m) are shown in Fig. 3a. ANC values ranged from 40 to 954 kg $H_2SO_4$/t. On consultation of geological logs for this drill hole, zones of very high ANC correlated to the presence of sandy limestone (e.g. 339–343 m). However, consistent zones of ANC were not observed due to abundance of limestone clasts in the Tyndall Group Lynchford Member.

Paste pH values for select samples of the Tyndall Group Lynchford Member (n = 21) indicated that currently, all tested samples are non-acid forming (Fig. 5b; range: pH 7.6–8.2), when using a cut-off value of pH 5.5 to classify acid forming from non-acid forming materials (Parbhakar-Fox et al. 2011). All values plotted to the left of the pure calcite paste pH line (shown at pH = 8.33), suggesting that minerals such as dolomite and magnesite, which have higher paste pH values (8.87 and 9.32 respectively; Noble et al. 2015), are not present in these samples.

Downhole total-sulfur values (Fig. 3c) identified four distinct zones of relatively high sulfur with potential for acid formation when using a cut-off value of 0.3 wt% sulfur (Parbhakar-Fox et al. 2011). This indicated that either sulfur is present in sulfide species which are slow to react in water (e.g., chalcopyrite) or lesser acid forming sulfides dominate in these samples (e.g., galena and sphalerite). Net acid producing potential (NAPP) values classified 15 % of samples as potentially acid forming (PAF > 20 kg $H_2SO_4$/t), with a distinct zone identified from 330 to 335 m.

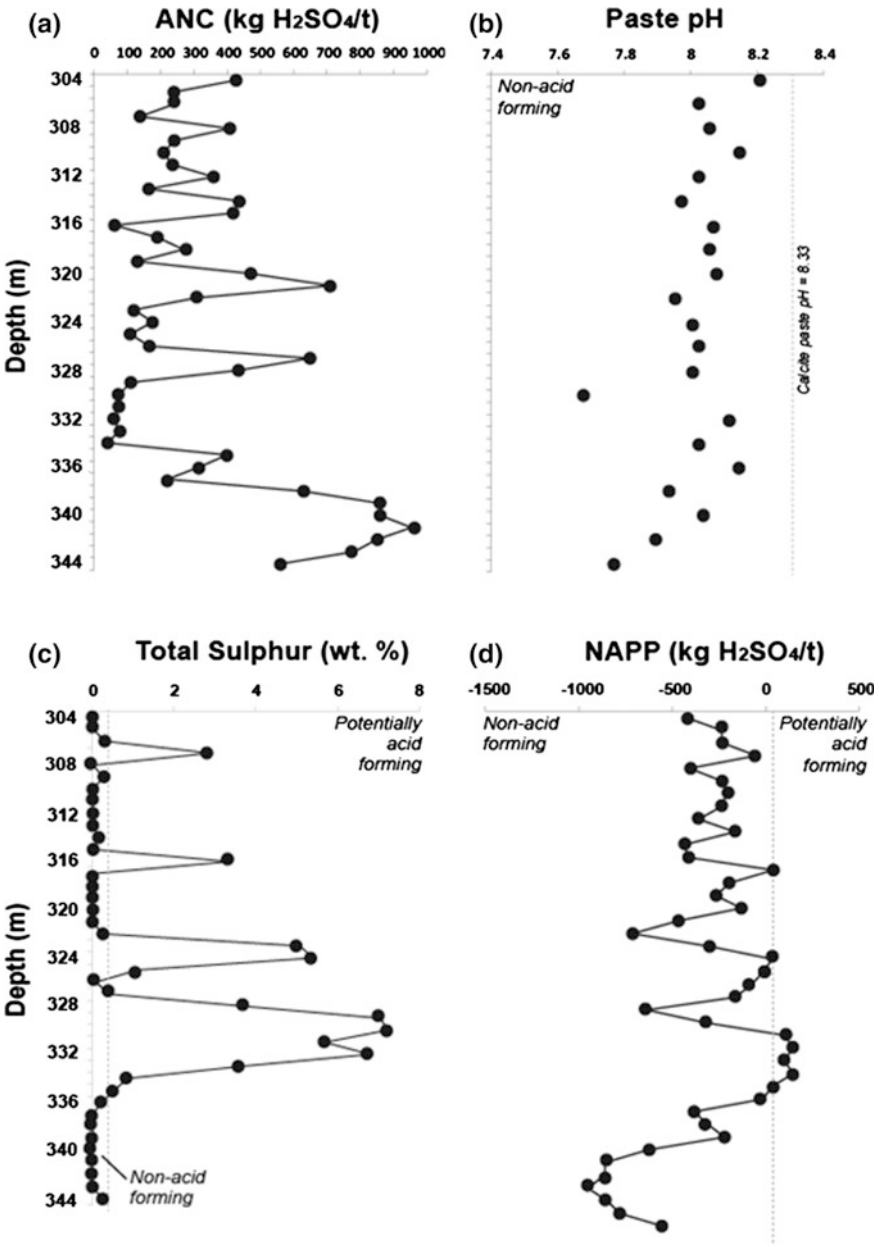


**Fig. 3** Downhole static geochemical results for Tyndall Group Lynchford Member samples (n = 40): **a** acid neutralizing capacity (ANC) values (kg $H_2SO_4$/t); **b** paste pH values (n = 21) with the pure calcite paste pH line shown for comparison, and the paste pH cut-off criterion of pH 5.5 used to classify acid forming from non-acid forming materials; **c** total sulfur values (wt%) with 0.3 wt% used as the classification cut-off criterion (Parbhakar-Fox et al. 2011); **d** net acid producing potential (NAPP) values (kg $H_2SO_4$/t) with a cut-off value of 20 kg $H_2SO_4$/t (Parbhakar-Fox et al. 2011) used to classify non-acid forming from potentially acid forming samples (reprinted from Parbhakar-Fox and Lottermoser (2014), with permission from ACMER)

This was logged as green, chloritic, polymict conglomerate, with fragments of chert, volcanics, limestone and sulfides.

As both carbonate and sulfide minerals are present in the Tyndall Group Lynchford Member, a geochemical plot of ANC versus MPA (calculated conservatively from total-sulfur values) is shown in Fig. 4. The same 15 % of samples were classified as having an increased risk for acid formation, indicating that there is not sufficient ANC in these samples to neutralize any acid formed.

## Carbonate Staining

The dominant carbonate textures observed in this material comprised of clasts (in limestone conglomerates) and veins. The ARS-PF stain appropriately reacted with calcitic material in both textural forms, with a pink stain indicating the presence of calcite (cf. Hitzman 1999) (Fig. 5). Towards the base of the stained portion of CCD007, a blue-purple colour was observed suggesting the presence of either ferroan calcite or ferroan dolomite (Fig. 6). As dolomite was not logged, it is considered that these bluish portions represent ferroan-calcite. However, to confirm the staining colours, specific verification samples were carefully chosen, prepared and analysed by XRD, with an example presented in Fig. 7. Interpretation of XRD patterns indicated the presence of ferroan dolomite rather than ferroan calcite. Considering the overall slight discoloration of the drill core in the Tyndall Group Lynchford Member after staining, and the measured range of ANC values (Fig. 3a), it is most likely that the matrix of this lithology contains calcite, hence why it has consistently been identified downhole by XRD. However, in terms of domaining

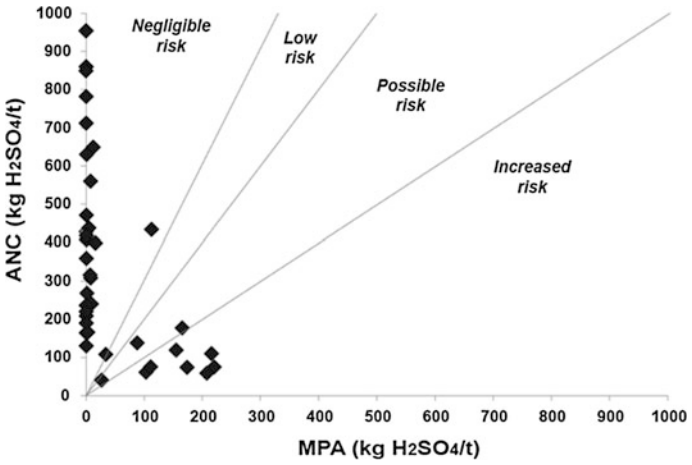


**Fig. 4** Acid neutralizing capacity (ANC) versus maximum potential acidity (MPA) for Tyndall Group Lynchford Member samples (CCD007: 304–344 m; n = 40), with potential acid forming risk fields shown (from Parbhakar-Fox 2012)

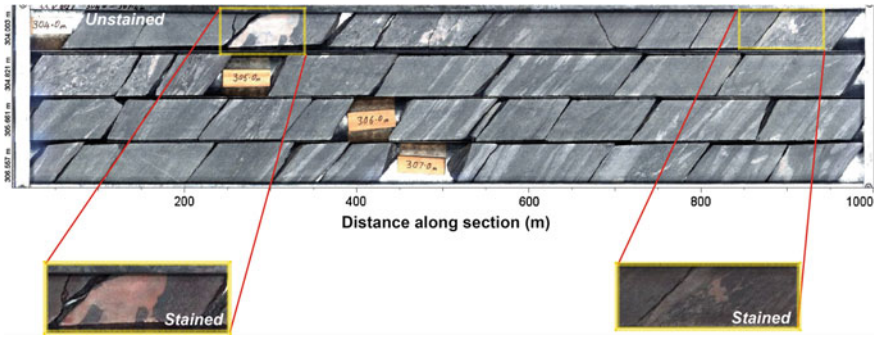


**Fig. 5** Photographic images of drill core CCD007 304–307 m (unstained) with two carbonate stained portions shown, with the *pink colour* indicating the presence of calcite, thus confirming domains of high acid neutralizing capacity within the Tyndall Group Lynchford Member. (Reprinted from Parbhakar-Fox et al. (2015), with permission from Gecamin) (color figure online)

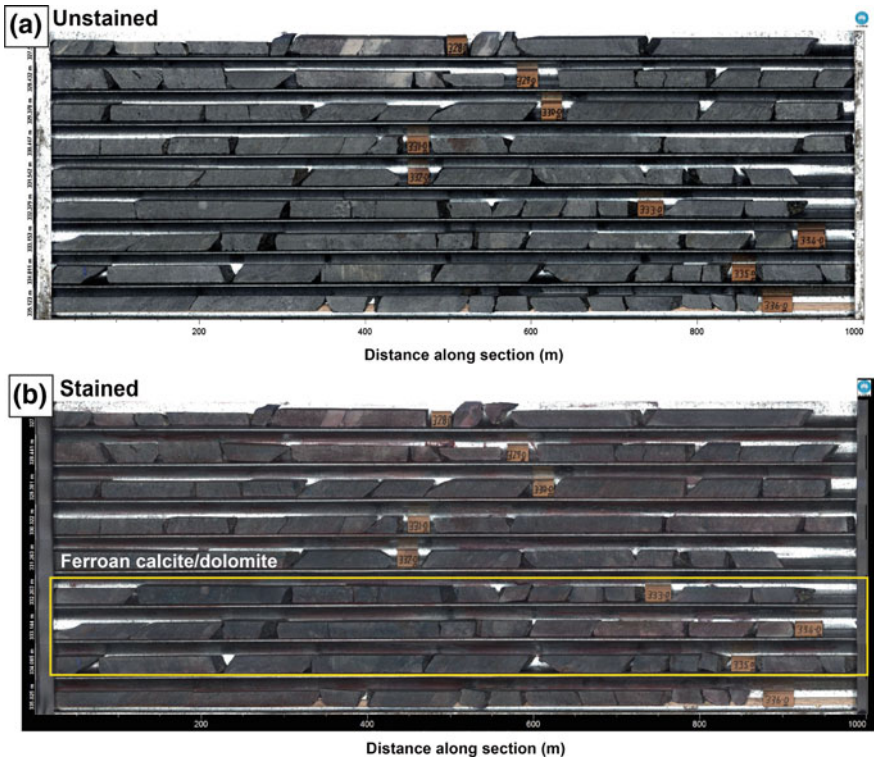


**Fig. 6** Photographic images of drill core CCD007 327–336 m: **a** unstained and **b** carbonate stained, with the *blue-purple colour* (shown in the *yellow box* in **b**) indicating the presence of either ferroan calcite or ferroan dolomite in the Tyndall Group Lynchford Member (color figure online)

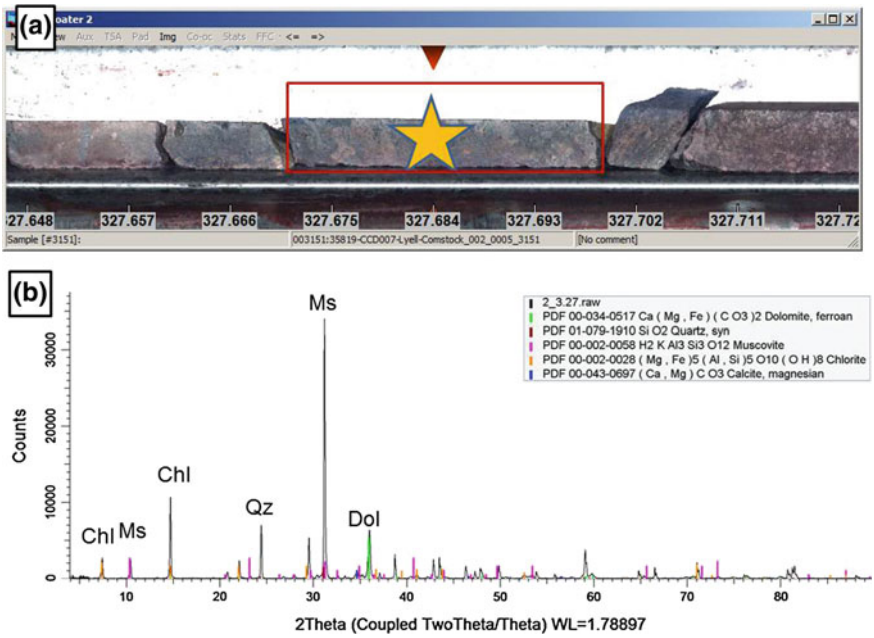


**Fig. 7** **a** Carbonate stained drill core sample from drill core CCD007 327 m, *blue colour* indicating the presence of ferroan calcite or dolomite; **b** X-ray diffraction pattern of area starred in (**a**) confirming the dominance of ferroan dolomite, however traces of calcite were also identified. *Abbreviations Cal* calcite, *Dol* dolomite, *Ms* muscovite, *Qz* quartz (color figure online)

effective ANC, precisely resolving the presence of calcite against dolomite is of lesser significance when considering their similar ANC values (1000 and 1086 kg $H_2SO_4$/t respectively; Jambor et al. 2007). Thus, carbonate staining using the ARS-PF stain can be considered a very useful domaining tool for recognising effective neutralizing minerals in drill core materials.

## Hyperspectral Logging

Thermal infrared (TIR) data collected by HyLogger from the Tyndall Group Lynchford Member samples identified the dominant mineralogy as quartz, chlorite, muscovite and carbonate. Two distinct zones of high carbonate were identified and correlated directly with two zones of high acid neutralizing capacity (Fig. 8).

Comparison of qualitative (i.e., relative proportions) carbonate mineralogy measured by HyLogger against normalised carbonate XRD data is shown in Fig. 9. In general, HyLogger identified more carbonate phases than XRD analyses with the presence of minor siderite identified and distinct ankerite dominated zones,

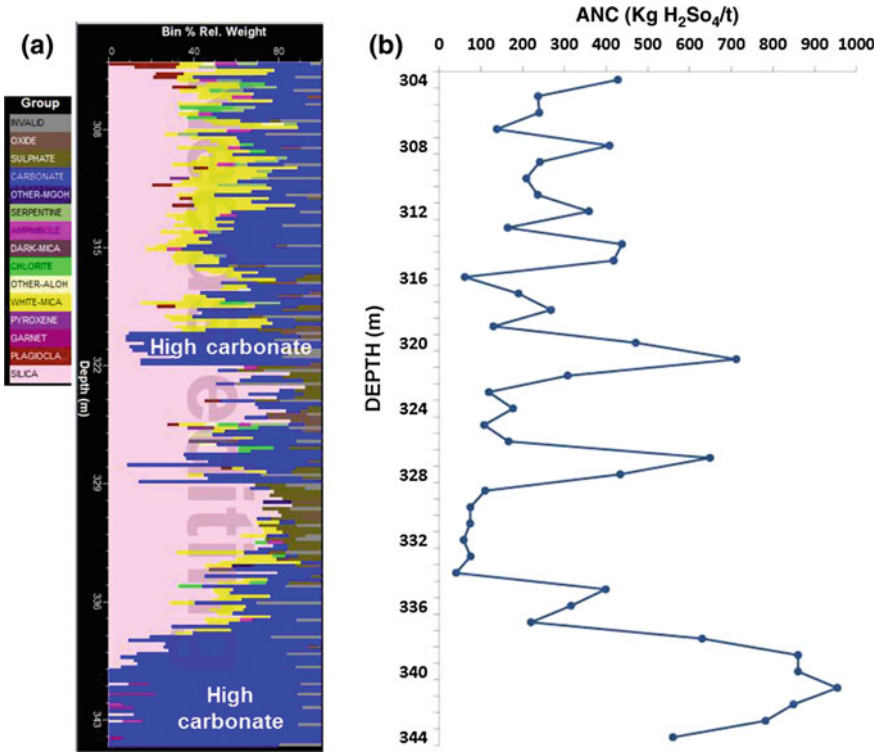


**Fig. 8** **a** Mineralogical identification performed by HyLogger (Thermal infrared; TIR) of drill core material from CCD007 (304–345 m; Tyndall Group Lynchford Member); **b** measured downhole acid neutralizing capacity (ANC) values, with zones of high ANC correlating to high carbonate zones identified by HyLogger (reprinted from Parbhakar-Fox and Lottermoser 2014, with permission from ACMER) (color figure online)

particularly towards the base of the Tyndall Group Lynchford Member. However, during XRD data interpretation, common carbonates minerals were searched for and siderite phases were not recognised, suggesting that carbonate mineral identification by HyLogger is not wholly accurate. For ANC domaining, distinguishing between calcite, dolomite and ankerite is of lesser importance when considering their neutralizing potential values (1000, 1086, and 970 kg $H_2SO_4$/t respectively; Jambor et al. 2007). However, it is necessary to correctly recognise the presence of siderite, as its neutralizing potential is often disregarded due to its potential to form acid (cf. Plumlee 1999). Based on these data, HyLogger should primarily be used to indicate the relative presence of carbonates, and not be relied upon exclusively to resolve carbonate mineralogy. Such data can be used to guide additional mineralogical testwork (i.e., XRD, electron probe microanalysis), which will allow the identification of individual carbonate minerals.

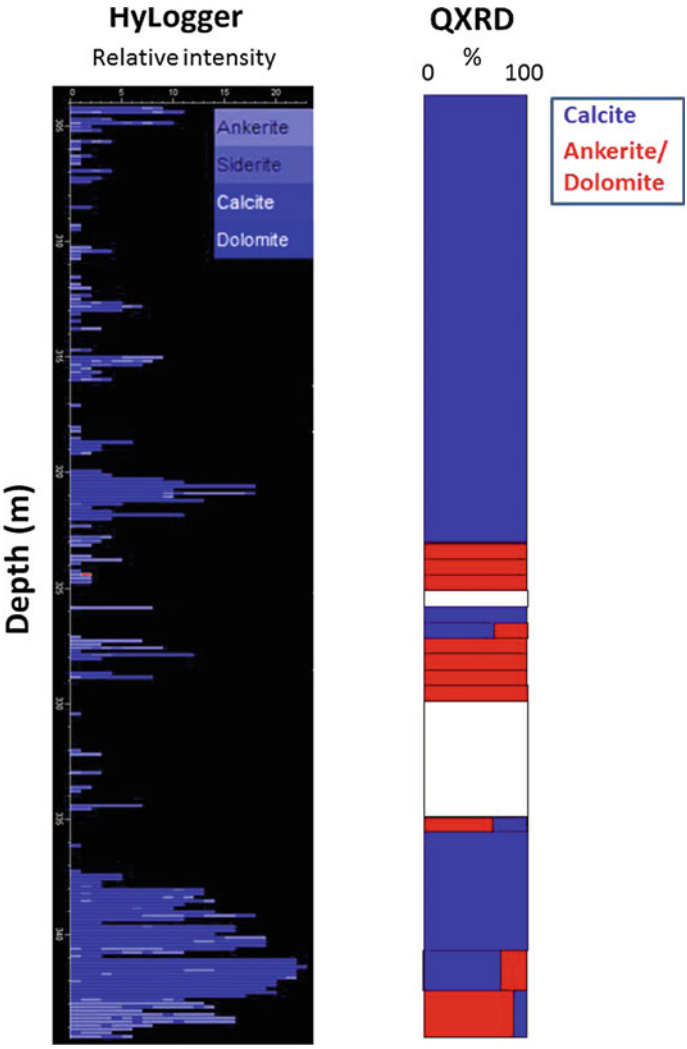


**Fig. 9** Carbonate mineralogy measured by HyLogger (relative intensities shown) and XRD (normalised to 100 % for comparison). NB. white areas in the XRD *bar chart* indicate the absence of carbonate minerals (color figure online)

Parbhakar-Fox et al. (2013) demonstrated the application of HyLogger and total-sulfur values for ARD domaining, thus this dataset was considered as such (Fig. 10). Carbonate relative intensity (Fig. 10a) and total sulfur (Fig. 10b) were used to produce classifications shown in Fig. 10c. When compared against ANC (Fig. 3a) and NAPP classifications (Fig. 3d), HyLogger/total sulfur domaining appears reasonably accurate, with ANC and PAF zones clearly identified. Thus, these results confirm the application of HyLogger for ANC domaining when used

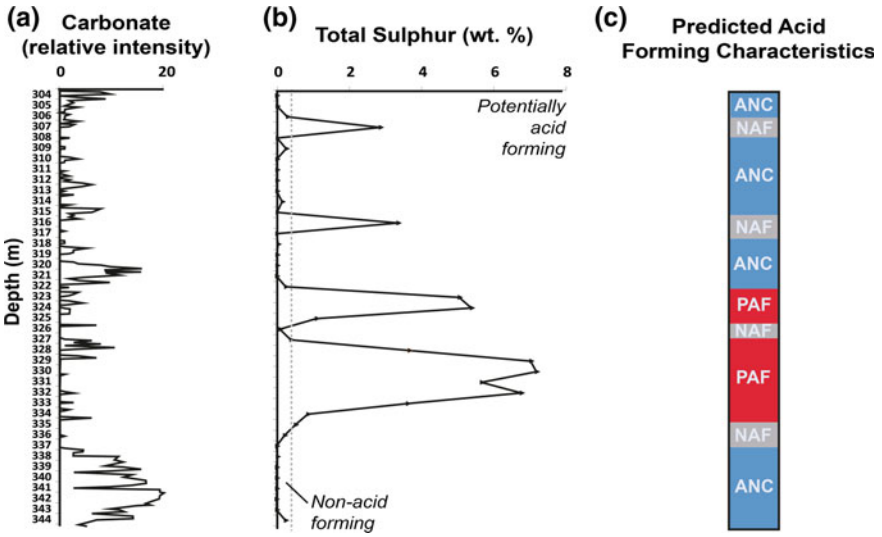


**Fig. 10** Downhole static geochemical results from the Tyndall Group Lynchford Member samples: **a** carbonate relative intensity measured by HyLogger; **b** Total sulfur values (wt%; n = 40) with 0.3 wt% used as the classification cut-off criterion (Parbhakar-Fox et al. 2011); **c** Predicted acid forming characteristics based on HyLogger relative carbonate intensity data and total-sulfur values. Abbreviations: *ANC* acid neutralizing capacity, *NAF* non-acid forming, *PAF* potentially acid forming (reprinted from Parbhakar-Fox and Lottermoser 2014, with permission from ACMER) (color figure online)

alongside total-sulfur values (using the criteria: relative intensity, >5; total-sulfur, <0.3 wt%). In addition, this information can be used to guide sampling campaigns (e.g., for geochemical testwork) through identifying zones with distinct ARD characteristics.

## *Classification of ARD Risk*

### NAG pH Versus Paste pH

The use of NAG pH versus paste pH values was proposed by Weber et al. (2006). However, its application has not been widely demonstrated, despite the fact that it offers an assessment of lag-time to ARD and thus classifies risk. The use of this classification was performed on Lyell Schist drill core material (345–375 m; n = 30) as shown in Fig. 11. All samples but one were identified as either acid-forming or potentially acid forming, and classified as medium-low risk, with the rate of ARD formation determined as rapid to having a short-lag time (in the case of potentially acid forming samples). This assessment confirms: (1) the necessity of undertaking systematic sampling down drill holes due to the geological

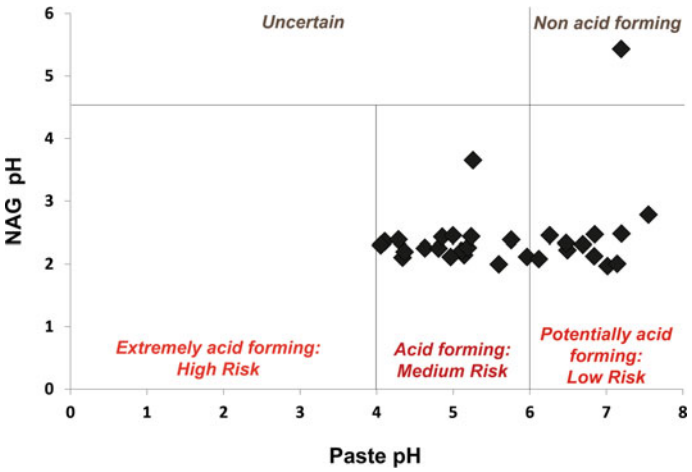


**Fig. 11** ARD risk assessment screening plot of NAG pH versus paste pH for Lyell Schist drill core materials (CCD007, 345–375 m). Modified from Weber et al. (2006) (reprinted from Parbhakar-Fox and Lottermoser 2014, with permission from ACMER)

and mineralogical heterogeneity and variability indicated by these static geochemical data; and (2) the suitability of the Lyell Schist drill core material for evaluating the application of Equotip for classifying ARD risk.

## Mineral Hardness

Mineral hardness (using Equotip) data was collected from all drill core materials. Comparisons against total sulfur and paste pH values are shown in Fig. 12. When considering the Tyndall Group Lynchford Member, if a mineral hardness value (measured in leeb—Ls) was measured as <648 Ls, it was classified as soft in accordance with Keeney (2008). If samples were identified as non-acid forming by both paste pH and total-sulfur classifications and also classified as soft (e.g., 309–315 m; Fig. 12d), then these materials were considered to represent the most effective short-term neutralizers. The Lyell Schist was classified in a similar manner, with samples identified as potentially acid forming by paste pH and total sulfur methods and with soft mineral hardnesses (i.e., greater likelihood of acid formation) here classified as acid forming at a relatively rapid rate. These findings are in agreement with data shown in Fig. 11, thus indicating the potential application of Equotip when performing ARD domaining. Moreover, in the absence of paste pH

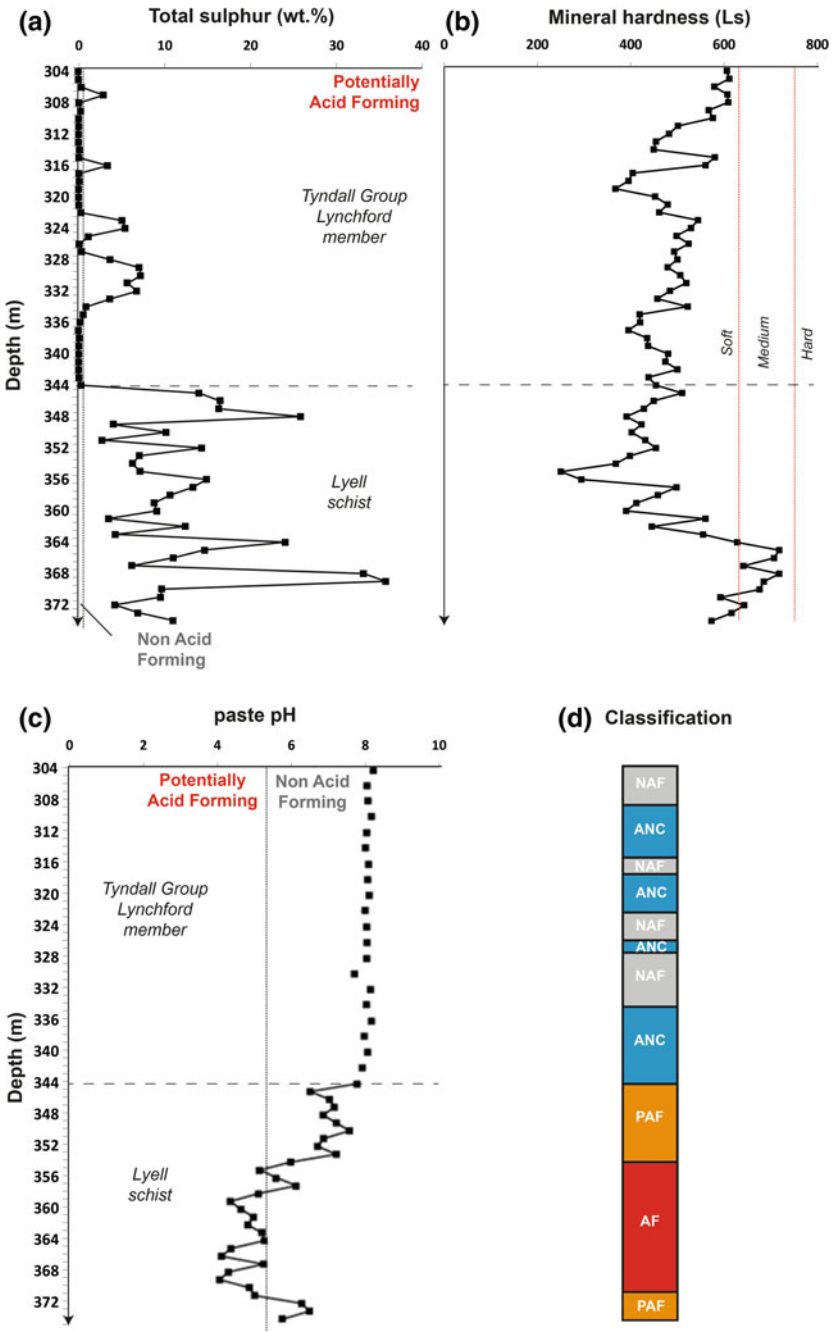
(a)
Total sulphur (wt.%)
0
10
20
30
40
Depth (m)
304
308
312
316
320
324
328
332
336
340
344
348
352
356
360
364
368
372
Potentially Acid Forming
Tyndall Group Lynchford member
Lyell schist
Non Acid Forming
(b)
Mineral hardness (Ls)
0
200
400
600
800
Soft
Medium
Hard
(c)
paste pH
0
2
4
6
8
10
Potentially Acid Forming
Non Acid Forming
Tyndall Group Lynchford member
Lyell schist
(d) Classification
NAF
ANC
NAF
ANC
NAF
ANC
NAF
ANC
PAF
AF
PAF

◀ **Fig. 12** Geochemical and geometallurgical data from drill hole CCD007 (304–375 m): **a** total sulfur values (wt%; n = 70) with 0.3 wt% used as the classification cut-off criterion (Parbhakar-Fox et al. 2011); **b** mineral hardness values as measured by Equotip and reported in Ls, with criteria for defining hard, medium and soft samples shown (Keeney 2008); **c** Paste pH values (n = 55) with pH 5.5 used as the classification cut-off criterion (Parbhakar-Fox et al. 2011); **d** ARD classifications based on total sulfur, mineral hardness and paste pH values. Abbreviations: *AF* acid forming, high risk with rapid ARD formation (after Weber et al. 2006); *ANC* acid neutralizing capacity, *NAF* non-acid forming, *PAF* potentially acid forming, medium risk with lag-time to ARD formation (after Weber et al. 2006) (reprinted from Parbhakar-Fox and Lottermoser 2014, with permission from ACMER) (color figure online)

data, mineral hardness and total sulfur data would have been sufficient to conservatively classify the behaviour of these materials.

## CARD Risk Grading

CARD risk grading performed downhole (Fig. 13) confirmed classifications assigned by routine geochemical methods for both lithologies. In general, the Tyndall Group Lynchford Member was classified as very low risk, with the exception of a low-potential risk zone (i.e., CARD risk ratio = 1–9.9) at approximately 330–335 m depth, which correlates with the PAF zone identified by

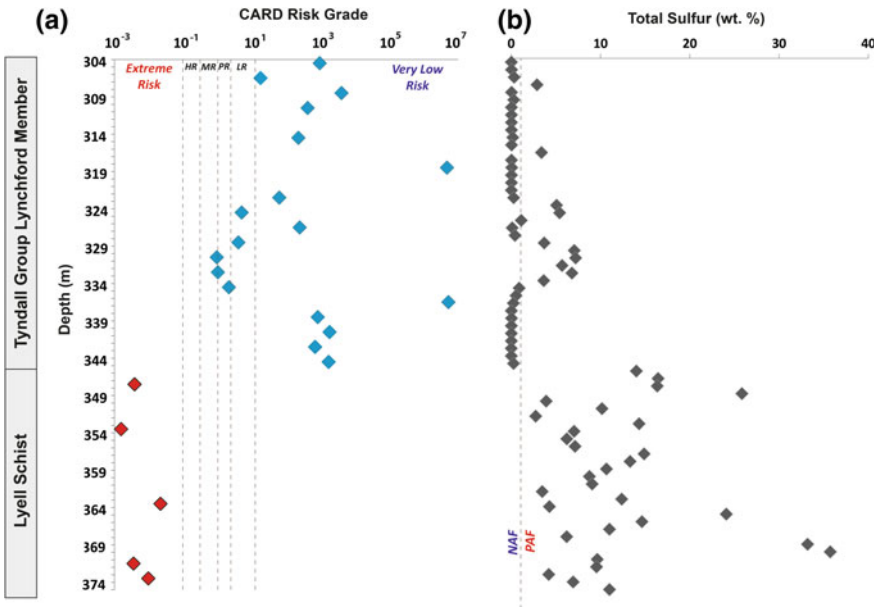


**Fig. 13** **a** CARD risk classification and **b** total sulfur (wt%) values for Tyndall Group Lynchford Member and Lyell Schist drill core materials (CCD007, 304–375 m)

geochemical methods (Fig. 3d). All Lyell schist samples were classified as extreme risk by CARD risk grading, but were identified as intermediate-low risk by NAG pH versus paste pH. However, these samples contained 2.7–35.7 wt% total sulfur which can be taken to represent sulfide sulfur (i.e., chalcopyrite and pyrite) as only trace (<1 wt%) sulfate phases were identified in XRD analyses of these materials. Therefore, geochemical classifications underestimated the ARD risk of these samples. Based on these results; the Tyndall Group Lynchford Member represents a significant ANC source, and the Lyell Schist is extremely acid forming. Such accurate information is critical for designing an appropriate waste management strategy.

## Conclusions

The objective of this study was to determine whether geometallurgical data can be utilised effectively to domain acid neutralizing capacity and acid forming potential in selected drill core from the Comstock Chert prospect, Tasmania. We evaluated the application of two geometallurgical techniques (HyLogger and Equotip) and chemical staining for domaining acid rock drainage (ARD) characteristics. The major outcomes and implications from this study for site-specific ARD recognition and waste classification were as follows:

- Paste pH testing successfully identified materials with significant neutralizing capacity and inferred that calcite was the dominant carbonate mineral in drill core materials of the Tyndall Group Lynchford Member.
- Carbonate staining was confirmed as a simple and accurate technique appropriate for drill core from the Copper Chert deposit (inspite of the textural diversity of carbonates present i.e., breccia clasts, veins). Staining allows for rapid identification of calcite and ferroan dolomite, information which will enable deposit-wide ANC domaining at early stages of operations and guide the selection of samples for in-depth geochemical static testing.
- Thermal infrared data from HyLogger testing accurately reported carbonate intensity. However, it was less accurate when speciating carbonate minerals compared to quantitative XRD data. If used in conjunction with total-sulfur values, accurate ANC domaining when compared against laboratory measured ANC values was achieved.
- The Equotip hardness versus total sulfur geometallurgical classification is best used to provide a conservative indication only of lag-time to acid formation. It allows for the classification of ARD risk for potentially acid forming materials like the Lyell Schist.
- Utilisation of Equotip hardness and total sulfur data alongside paste pH data also allows for further domaining of effective acid neutralizing capacity.
- CARD risk grading better classified ARD risk, with the Tyndall Group Lynchford Member classified as very low risk (with the exception of one

moderate risk zone correlating to the presence of chalcopyrite and pyrite). The Lyell Schist was classified as extreme risk.

- Adoption of such an environmental geometallurgy approach for further exploration in an area, where there is a legacy of ARD, is recommended. This will allow cost-effective domaining of ARD risks.

## References

Alruiz OM, Morrell S, Suazo CJ, Naranjo A (2009) A novel approach to the geometallurgical modelling of the Collahuasi grinding circuit. Min Eng 22:1060–1067

Corbett KD, Quilty PG, Calver CR (2014) Geological evolution of Tasmania. Geological Society of Australia (Tasmanian Division), Hobart

Hitzman MW (1999) Routine staining of drill core to determine carbonate mineralogy and distinguish carbonate alteration textures. Mineralium Deposita 34: 794–798

Huntington JF, Quigley M, Yang K, Roache T, Young C, Roberts I, Whitbourn LB, Mason P (2006) A geological overview of HyLogging 18,000 m of core from the Eastern Goldfields of Western Australia. In: Proceedings from the 6th international mining geology conference, AusIMM publication series no. 6, Darwin, Australia, pp 45–50

Jambor JL, Dutrizac JE, Raudsepp M (2007) Measured and computed neutralization potentials from static tests of diverse rock types. Environ Geol 52:1019–1031

Keeney L (2008) EQUOtip hardness testing: Aqqaluk (including a guide on how to use EQUOtip). Technical report 2, P843 GeM, Australian Mineral Industries Research Association (AMIRA), Melbourne

Leichliter S, Hunt J, Berry R, Keeney L, Montoya PA, Chamberlain V, Jahoda R, Drews U (2011) Development of a predictive geometallurgical recovery model for the La Colosa, Porphyry Gold Deposit, Colombia. In: Proceedings from the 1st AusIMM international geometallurgy conference. THE Australasian Institute of Mining and Metallurgy, Melbourne, pp 85–92

McLoughlin J, Morrison K (2013) The copper chert discovery, Mount Lyell mineral field Tasmania. In: AUSIMMM mines and wines conference, Orange, NSW, Australia, pp 1–5

Morin KA, Hutt NM (1998) Kinetic test and risk assessment for ARD. In: Proceedings of the 5th annual BC metal leaching and ARD workshop, Vancouver, Canada

Noble TN, Lottermoser BG, Parbhakar-Fox A (2015) Evaluation of pH testing methods for sulfidic mine waste. Mine Water Environ. doi:10.1007/s10230-015-0356-2

Parbhakar-Fox A (2012) Establishing the value of an integrated geochemistry-mineralogy-texture approach for acid rock drainage prediction. PhD thesis, University of Tasmania, Australia

Parbhakar-Fox A, Lottermoser BG (2014) Domaining acid rock drainage risks using geometallurgical data. In: Proceedings from the 8th Australian workshop on acid and metalliferous drainage, ACMER, Brisbane, pp 483–494

Parbhakar-Fox A, Edraki M, Walters S, Bradshaw D (2011) Development of a textural index for the prediction of acid rock drainage. Min Eng 24:1277–1287

Parbhakar-Fox A, Lottermoser BG, Bradshaw D (2013) Evaluating waste rock mineralogy and microtexture during kinetic testing for improved acid rock drainage prediction. Min Eng 52:111–124

Parbhakar-Fox AK, Aalders J, Lottermoser BG (2015) Effective field-based testing tools for rapid ARD prediction. In: 10th international conference on acid rock drainage and IMWA annual conference, Santiago, Chile, pp 890–905

Plumlee GS (1999) The environmental geology of mineral deposits. In: Plumlee GS, Logsdon MJ (eds) The environmental geochemistry of mineral deposits part a: processes, techniques and health issues. Reviews in economic geology, vol 6A, pp 71–116

Price WA (2009) Prediction manual for drainage chemistry from sulphidic geologic materials. CANMET Mining and Mineral Sciences Laboratories, Canada

Smart R, Skinner WM, Levay G, Gerson AR, Thomas JE, Sobieraj H, Schumann R, Weisener CG, Weber PA, Miller SD, Stewart WA (2002) ARD test handbook: project P387A, prediction and kinetic control of acid mine drainage. AMIRA International Ltd, Melbourne

Weber PA, Hughes JB, Conner LB, Lindsay P, Smart RC (2006) Short-term acid rock drainage characteristics determined by paste pH and kinetic NAG testing: cypress prospect, New Zealand. In: Proceedings from the 7th international conference on acid rock drainage, Missouri, pp 2289–2310

# Predictive Waste Classification Using the Geochemistry-Mineralogy-Texture-Geometallurgy (GMTG) Approach at a Polymetallic Mine

**Anita Parbhakar-Fox and Bernd Lottermoser**

**Abstract** Management of mine wastes, particularly waste rock, requires careful planning to reduce the likelihood of sulfide oxidation, and generation of ARD. Such a waste management strategy must be based on a thorough understanding of the environmental characteristics of the future waste rock materials. In this study, a waste management strategy for characterizing underground waste rock was developed at a polymetallic mine to determine which materials were appropriate for surficial placement. The criteria for surficial placement set by the regulator were that materials had to be non-acid forming and non-metalliferous. A range of cost-effective field based tools and state-of-the-art laboratory techniques were used on a suite of representative samples collected from the site to determine an appropriate waste management strategy. Ultimately, a modified geochemistry-mineralogy-texture-geometallurgy (GMTG) approach was designed, whereby ARD focused logging and simple pre-screening tools such as paste pH and sulfur analyses were used at stage-one; routine acid base accounting and leachate tests at stage-two, and validation tools including X-ray diffractometry and laser ablation ICPMS at stage-three. Such an approach should be considered for other mine sites at all life-of-mine stages with similar deposit characteristics to ensure correct screening and placement of potentially hazardous waste materials.

A. Parbhakar-Fox (✉)
School of Physical Sciences, University of Tasmania, Private Bag 79, Hobart, TAS 7001, Australia
e-mail: Anita.Parbhakar@utas.edu.au

B. Lottermoser
Institute of Mineral Resources Engineering, RWTH Aachen University, Wüllnerstrasse 2, 52062 Aachen, Germany
e-mail: lottermoser@mre.rwth-aachen.de



B. Lottermoser (ed.), *Environmental Indicators in Metal Mining*,
DOI 10.1007/978-3-319-42731-7_10

## Introduction

Volcanic-associated massive sulfide deposits are ranked as one of the most acid rock drainage (ARD) prone deposit types by Kwong (1993), as demonstrated by Rio Tinto, Spain (Hudson-Edwards and Edwards 2005; Aguilera et al. 2006; Romero et al. 2006) and Iron Mountain, California (Jamieson et al. 2005; Nordstrom et al. 2000). Typically, they contain zones or lenses of massive sulfide minerals, with sulfide mineral contents exceeding 90 vol% (Taylor et al. 1995; Seal II and Piatak 2012). Most deposits also contain extensive zones of semi-massive sulfide rock (25–50 vol%) that contain economically exploitable ore (Taylor et al. 1995; Seal II and Piatak 2012). Stringer zone ore zones typically contain 5–20 % sulfide minerals hosted in quartz veins and disseminated in chloritic wall rocks (Taylor et al. 1995; Seal II and Piatak 2012). Disseminated sulfide rock is extensively developed in footwall alteration zones, with sulfide mineral abundances decreasing with depth below the massive sulfide zone horizon (Taylor et al. 1995; Seal II and Piatak 2012). Lateral development of disseminated pyrite can be continuous for large distances at and immediately below the stratigraphic horizon of the massive sulfide lens (Fig. 1; Taylor et al. 1995; Seal II and Piatak 2012). Iron and base metal sulfide minerals are typically hosted by rocks with low buffering capacity (e.g., basalt-rhyolite; Taylor et al. 1995). Consequently, the propensity to produce ARD is significant, with high concentrations of As, Bi, Cd,

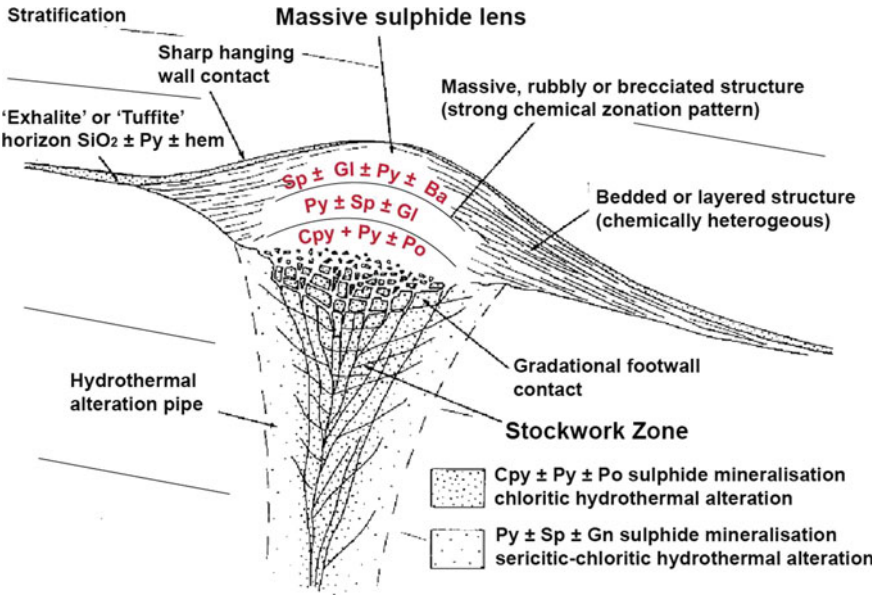


**Fig. 1** Essential characteristics of an idealised volcanogenic massive sulfide deposit (redrawn after Taylor et al. 1995). *Ba* barite, *Cpy* chalcopyrite, *Gn* galena, *Hem* hematite, *Po* pyrrhotite, *Py* pyrite, *Sp* sphalerite

Hg and Sb reported, (Taylor et al. 1995; Seal II and Piatak 2012). Indeed, analyses of waters draining such deposits plot in the extreme metal-extreme acidity field on a Ficklin plot (Taylor et al. 1995). Secondary minerals formed from intermediate stages of alteration can result in the formation of a wide-range of iron and base metal sulfate and sulfate hydrate minerals (Taylor et al. 1995; Seal II and Piatak 2012). Typically, these include goethite, crystalline and amorphous silica, jarosite, a variety of metal-bearing hydroxy-sulfate minerals (e.g., beudantite and plumbojarosite), scorodite, native gold, native silver, native bismuth, barite, anglesite, litharge, covellite, chalcocite, digenite, enargite, luzonite and acanthite (Taylor et al. 1995; Seal II and Piatak 2012).

The study site is an operational polymetallic volcanic-hosted massive sulfide (VHMS) mine (Pb-Zn-Cu-Ag-Au). The mineralization comprises a series of massive sulfide lenses hosted within quartz- and feldspar-phyric, rhyolitic volcaniclastic sandstones and siltstones. The volcanic package, which hosts this, is a 200 km long and 20 km wide belt of Middle to Late Cambrian age. Compositionally and texturally diverse lavas, syn-volcanic intrusions and syneruptive volcaniclastic units are the predominant volcanic facies associations of the volcanics. Virtually all facies were emplaced in a sub-aqueous environment below wave base. The lavas and intrusions are submarine, calc-alkaline primarily felsic bodies. Thick and extensive pumice-rich and crystal-rich units and in situ and re-sedimented hyaloclastites are typical of the volcaniclastic facies associations. The sedimentary facies are interbedded with the volcanic facies and include black mudstone and graded, bedded sandstone derived from volcanic and metasedimentary basement sources.

At this site, mining is through underground operations, with waste currently dumped at surface. However, the current waste repository is approaching maximum capacity therefore a new dump is required. A former open pit was recognised as a potential candidate for a repository, however, the regulator imposed the criteria that only non-acid forming (NAF) and non-metalliferous (NM) wastes can be dumped at surface. All other waste must remain underground. Therefore, a strategy which allows the rapid assessment of these wastes was required. In this study, a waste management strategy based on the geochemistry-mineralogy-texture-geometallurgy (GMTG) approach was developed for this site.

## Sampling and Sample Preparation

Drill core samples (n = 51) were selected from five drill holes to provide a range of materials from non-mineralized or marginal lithologies i.e., those likely to be designated waste. Table 1 provides a list of lithologies sampled along with a brief geological description. Full drill-core samples were selected and transported back to UTAS. Each sample was sawn in two to allow for photography and logging of a fresh surface. One portion was subjected to crushing and milling to <63 µm for geochemical and mineralogical testwork. The other portion was kept intact for non-destructive mineralogical, geochemical and textural analyses.

**Table 1** Lithologies sampled by this study

| Lithological unit code | Geological description | Number of samples |
|---|---|---|
| A | Black, moderately carbonate altered, fine grained, 'black slates', displaying a pervasive dissolution (carbonate) cleavage | 3 |
| B | Massive carbonate clast materials selected from unit H | 2 |
| C | Transitional zone between units D and F. Disseminated sulfides (5–70 %) present | 3 |
| D | Green to cream grey, chlorite-silica altered, coarse grained, poorly sorted, rhyolitic pumice breccia, disseminated sulfides (5–70 %) present | 14 |
| E | As for D, but with a lower (<5 %) content of sulfides | 8 |
| F | Green, sericite altered, medium grained, quartz-phyric sandstone hosting disseminated vein controlled red sphalerite. Disseminated sulfides (5–70 %) present | 11 |
| G | Dull pink, massive carbonate as rhodochrosite with minor patchy chlorite alteration. Trace sulfides (<5 %) present | 6 |
| H | Green to grey, chlorite-silica altered, coarse grained, polymictic, poorly sorted, lithic bearing volcaniclastic sandstone. Lithics include amygdaloidal dacite to rhyolitic clasts hosted within a medium grained, pumiceous crystal rich matrix. Disseminated sulfides (5–70 %) present | 3 |
| I | As for H, but with a lower (<5 %) content of sulfides | 1 |

## Mineralogical Characterization

### Environmental drill core logging

The acid rock drainage index (ARDI) was performed on these samples following the protocol by Parbhakar-Fox et al. (2011). At this site, a modified ARDI was developed to allow for the performance of simpler, more time-efficient assessments. An assessment was performed on all samples, over an 8.5 × 5.5 cm size area, with the area most dominated by sulfide chosen for assessment, as the most conservative ARDI value was sought.

### X-ray diffractometry (XRD)

To determine the bulk mineralogy of supplied drill core, milled material from each sample was subjected to XRD analysis. A benchtop Bruker D2 PHASER X-ray diffractometer instrument with a Co X-ray source was used to perform these analyses. Each sample was ground with an agate pestle and mortar and loaded into the sample holder and placed into the machine chamber. Samples were analysed for 1 h (fixed divergence slit: 1 mm; range 4–900 2theta; 0.020 step size, Fe-filter), with the resulting spectra processed in Eva 2.1 software, where minerals were identified using the ICDD PDF 2012 database.

## *Geochemical Testwork*

**Total sulfur analyses**
Rapid and accurate measurement of total sulfur concentrations (wt%) for the calculation of maximum potential acidity (MPA) was performed on all samples (n = 51) using an Eltra C-S 2000 instrument at UTAS. Analysis requires the use of two accelerants (tungsten and iron) which were carefully weighed into a crucible, with a measure (ca. 200 mg) of powdered (<63 µm) sample added. Individual crucibles were placed onto the instrument stage, loaded into the machine, and heated to >800 °C. The instrument was regularly calibrated (i.e., once after every 10 samples analysed) using two calibration materials provided by instrument supplier (calcium carbonate and barium sulfate). As a further measure, two ore standards (purchased from Choice Analytical) were also run in addition to sample blanks (i.e., before instrument calibration).

**Paste pH testing**
Following a detailed validation study, Noble et al. (2015a) identified the best paste pH method for use in ARD characterization testwork on fresh drill core as the ASTM D4972-01 (2007) method. These measurements were performed, with the data used against total-sulfur and NAG pH values to classify ARD risk. The pH value of each sample (n = 51) was measured in triplicate, with the standard deviation for each sample calculated as <0.5.

**Field portable XRF (pXRF)**
Field portable XRF analyses were conducted on homogenized sample powders that had been filled into sample containers (n = 51). A hand-held Olympus-InnovX instrument was used with reference standards NIST 2781, GXR3-538 and GXR4-2843 analysed throughout.

**Static testing**
Routine ARD geochemical analyses include net acid producing potential (NAPP) testing, and therefore such tests were performed to validate results obtained in previous steps. As total-sulfur values were collected at UTAS, only acid neutralizing capacity (ANC) analysis was performed at Australian Laboratory Services (ALS). Appropriate sample blanks, standards and duplicates were used during the analyses.

Net acid generation (NAG) pH tests were performed at UTAS. Parbhakar-Fox et al. (2011) reported that the standard single addition NAG test is inappropriate for use when samples contain <0.3 wt% sulfur. Therefore, multi addition tests (mNAG) were performed following the method of Smart et al. (2002). Essentially, the mNAG test procedure involves the stepped addition of $H_2O_2$ in three increments (100, 100 and 50 ml). This allows more time for sulfide oxidation. Powders (<63 µm) from all samples (n = 51) were tested. Appropriate sample duplicates were used during the analysis, with standard deviation calculated as <0.5.

**MATE pH and leachate testing**

Kinetic trials provide the most reliable information for predicting the long term water chemistry of mine waste. However, this information is only generated on the time scale of years, and therefore is not often included in mine planning decisions. Therefore, a proxy test for kinetic testing called the Microwave Assisted Thermal Energy (MATE) pH was trialed. This test, developed by Noble et al. (2015b), provides the industry with a predictive static test, which allows a more accurate and rapid assessment of the leachate chemistry of sulfidic wastes. The MATE pH test was performed on all sample powders (n = 51) at UTAS, with the derived leachates filtered (<0.45 μm), acidified and sent to ALS for element analysis by ICP-MS/AES methods with appropriate QA/QC protocols followed.

**USGS field leach testing**

The USGS field leach test is regarded as one of the most rapid (ca. 5 min) and cost-effective leach tests available as it attempts to simulate the reactions that occur when materials are leached by water. Thus, it is used to predict, assess and characterize the geochemical interactions between water and mine wastes (Hageman 2007). Based on this, it was selected here to provide a comparison against leachate data derived from the MATE pH test. The methodology was adapted (considering the limited amount of powdered sample available) with 5 g of material suspended in 100 mL deionised water and shaken for 5 min, and left to stand for a further 10 min. The pH of the solution was recorded, and the leachates were subsequently filtered (<0.45 μm), acidified in $HNO_3$, and sent to ALS for elemental analysis by ICP-MS/AES methods again with appropriate QA/QC protocols followed.

**Laser ablation ICPMS (LA-ICPMS)**

One inch polished laser mounts (n = 9) were prepared from nine samples, with six chosen to determine the trace element chemistry of pyrite and chalcopyrite. The remaining samples were analysed to determine the trace element chemistry of the dominate carbonate minerals (i.e., rhodochrosite and calcite) to determine which elements may be leached following acid neutralization (i.e., carbonate dissolution) if this material is placed into the waste rock dump. Spot analyses were performed on these samples using LA-ICPMS instruments at UTAS (Agilent HP4500 Quadripole ICPMS for sulfides, and the EXCIMER for carbonates). Calibration was performed using in-house standards (STDGL2b-2; MACS-3 and NIST612) comprising powdered sulfides doped with certified element solutions and fused to a lithium borate glass disk (Danyushevsky et al. 2011). Finally, data was processed using in-house software.

## Results

### *Mineralogical Characterization*

The dominant mineralogy in all samples was quartz, muscovite and chlorite, with pyrite, albite, orthoclase, sphalerite, rhodochrosite and calcite occasionally detected. Within each group, the concentration range of individual mineral phases was broad, indicating that based on their mineralogy, the grouping could be further refined (i.e., waste units may be defined based on waste properties and not lithologies). Considering this, measured total carbonate (calcite + rhodochrosite + ankerite + dolomite) values were plotted against sulfide (pyrite) contents (Fig. 2). The results strongly confirm the unsuitability of disseminated sulfide groups (e.g., Units D, F and H) for surface placement. However, several samples from Units A, B and C appear to offer acid neutralizing capacity, and therefore may be appropriate for surface placement.

### *Waste Classification Based on Geochemical Data*

Paste pH values plotted against total sulfur ($S_{Total}$) values (wt%) are shown in Fig. 3. This classification allows for samples to be identified as potentially acid forming (PAF), non-acid forming (NAF) or acid forming (AF). Whilst paste pH values were generally greater than pH 6 (indicating that currently, these samples are

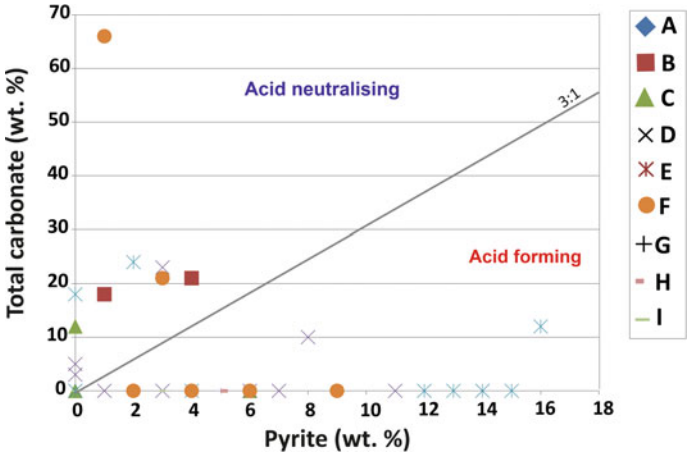


**Fig. 2** Mineralogical classification of acid forming potential based on pyrite versus total carbonate (calcite + rhodochrosite + ankerite + dolomite), measured and quantified by XRD. For lithological descriptions, see Table 1

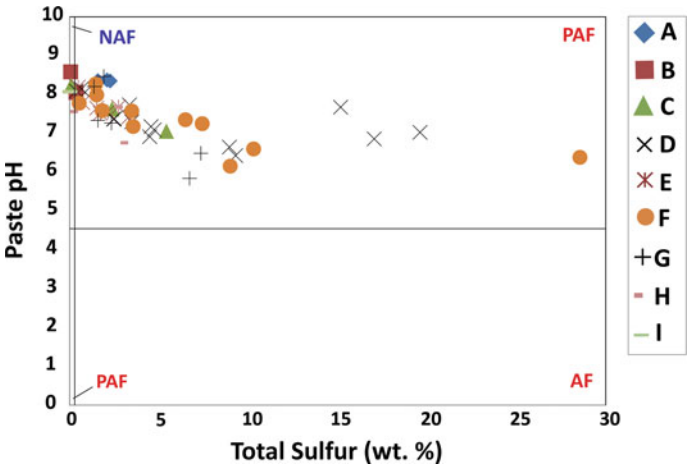


**Fig. 3** Paste pH versus total sulfur (wt%) for all drill core samples (n = 51) with classification fields after Parbhakar-Fox et al. (2011). *NAF* non-acid forming, *PAF* potentially acid forming, *AF* acid forming. For lithological descriptions, see Table 1

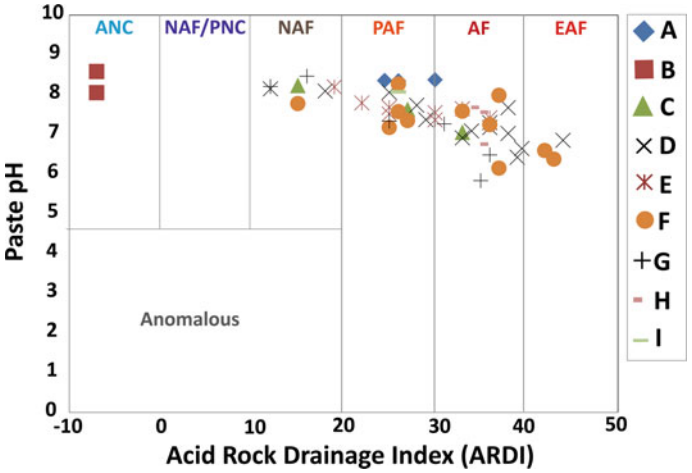


**Fig. 4** Paste pH versus acid rock drainage index values for all drill core samples (n = 51) with classification fields after Parbhakar-Fox et al. (2011). *AF* acid forming, *A/PNC* acid/potential neutralizing capacity, *EAF* extremely acid forming, *NAF* non-acid forming, *PAF* potentially acid forming. For lithological descriptions, see Table 1

not acid forming), a large range of sulfur values were retuned (0.06–28.5 wt%) for these samples, with the majority of samples therefore classified as PAF.

Acid rock drainage index (ARDI) values were plotted against paste pH values (Fig. 4). This type of geochemical plot can be regarded as depicting a 'worst case' scenario. Both carbonate lithology samples were identified as having an acid

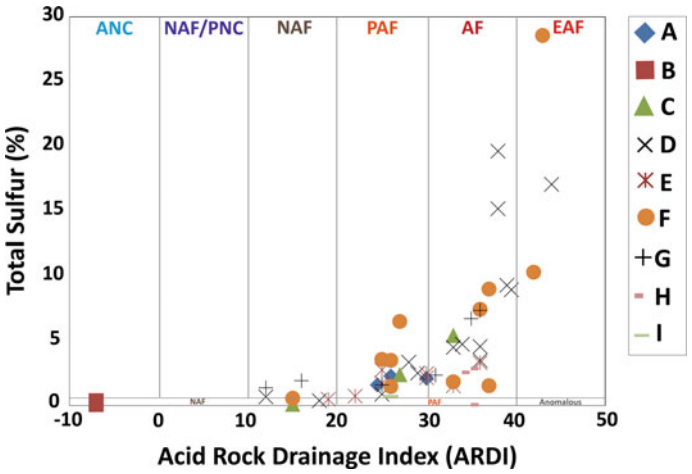


**Fig. 5** Total sulfur (wt%) versus acid rock drainage index values for all drill core samples (n = 51) with classification fields after Parbhakar-Fox et al. (2011). *AF* acid forming, *A/PNC* acid/potential neutralizing capacity, *EAF* extremely acid forming, *NAF* non-acid forming, *PAF* potentially acid forming. For lithological descriptions, see Table 1

neutralizing capacity and seven samples (from a range of lithologies) as NAF. However, the majority of samples were PAF and AF, with three disseminated sulfide samples classified as EAF.

Total sulfur values were compared against ARDI values as shown in Fig. 5, and largely confirmed the classifications given in the previous figures. A range of classifications (from NAF to EAF) were returned for both the Units D and F, suggesting that no clear decision regarding placement can be made based on a visual classification/assumed behaviour of a lithology group alone. Instead, these three tests (ARDI, paste pH and $S_{Total}$) must all be performed in order to fully understand the acid forming characteristics as was recommended by Parbhakar-Fox et al. (2011). These classifications suggest that disseminated sulfide samples (e.g., Units D, F and H) are inappropriate for surface placement, however, Units A, B and C may contain materials which can be brought to surface.

Consideration of NAG pH against paste pH allows for an assessment of both ARD risk, and the lag time to its formation, as shown in Fig. 6. Twelve samples (from eight of the units) were NAF and one sample (Unit G) was acid forming/intermediate risk with rapid ARD formation likely. The remaining samples were PAF/low risk, with a lag-time to ARD formation. Following this classification, Unit G materials are strongly recommended for underground storage, and Units B and C materials are potential candidates for surface storage. The spread of results for other classes demonstrates the difficulty in determining ARD characteristics for each lithology when using geochemical data alone. Therefore, visual logging (as per the ARDI) is critical for correct classification. However, the definition of groups used here (based on lithological classes) also needs to be re-evaluated, and

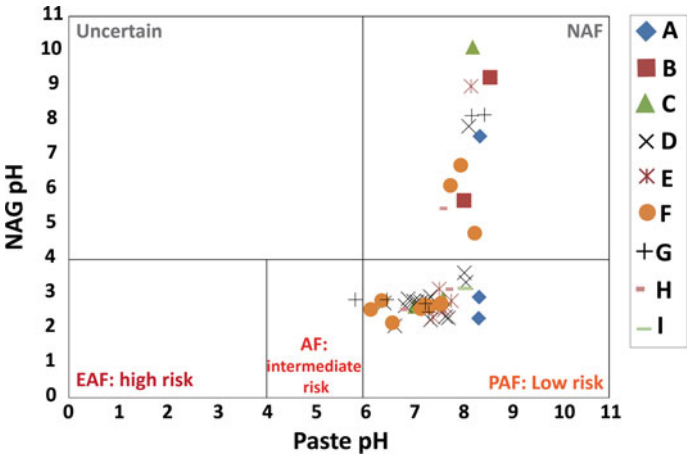


**Fig. 6** NAG pH versus paste pH for all drill core samples (n = 51) with classification fields after Weber et al. (2006). *NAF* non-acid forming, *PAF* potentially acid forming, *AF* acid forming. For lithological descriptions, see Table 1

following a grouping scheme independent of lithology or alteration style may facilitate more effective grouping. In general, more trace sulfide as opposed to disseminated sulfide groups feature in the NAF field as would be expected, therefore, based on this classification, trace sulfide units (e.g., E, G and I) are the most likely to be nominated for surface placement.

The NAPP (kg $H_2SO_4$/t) versus NAG pH classification method is routinely used by industry, and therefore was used here (Fig. 7). The majority of samples were classified as PAF, with twelve samples again identified as NAF. Materials from Unit B were consistently NAF, confirming its suitability for surface storage. Some samples from Units A and C were also NAF. With further testing of samples from these groups, it will be possible to deduce whether they should be brought to surface, or remain underground. Based on the current data, it is not possible to confidentially decide this. Whilst Units D and F showed a large range in NAPP values (−63 to 868; and −131 to 535 kg $H_2SO_4$/t, respectively), materials from both groups are recommended for underground storage. Overall, they are the most acid forming groups of the lithologies sampled by this study as indicated in the previous geochemical plots.

Samples were classified using modified Ficklin plots with paste pH and NAG pH data used (Figs. 8 and 9, respectively) as recommended by Parbhakar-Fox et al. (2011). No samples are currently high risk, with the majority classified as intermediate risk when paste pH data are considered against total metal abundance (measured by pXRF) as shown in Fig. 8.

The criteria set by the regulator for non-metalliferous wastes to be placed on surface is unlikely to be satisfied by Units D and F materials, with >1000 ppm metals measured for the majority of samples from these groups. Unit A consistently

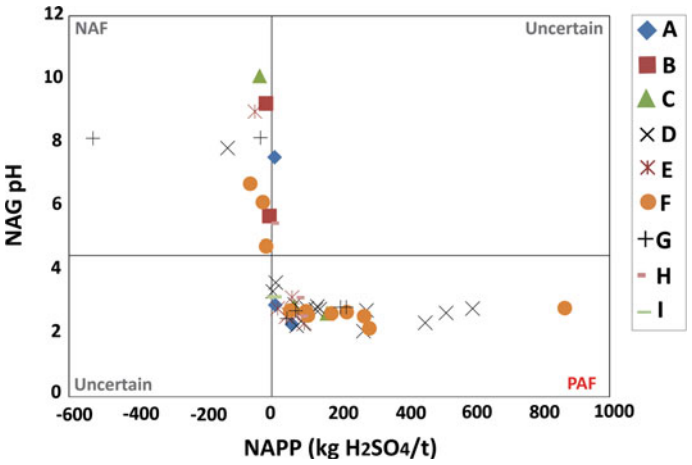


**Fig. 7** NAPP (kg $H_2SO_4$/t) versus NAG pH for all drill core samples (n = 51) with classification fields after Smart et al. (2002). *NAF* non-acid forming, *PAF* potentially acid forming. For lithological descriptions, see Table 1

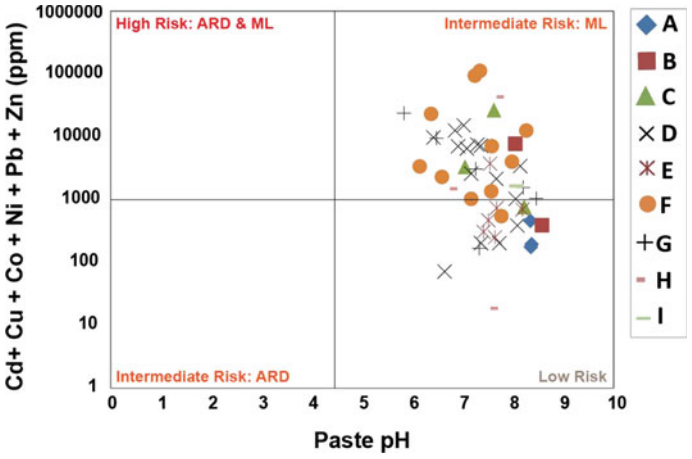


**Fig. 8** Paste pH versus total metals (ppm; as measured by pXRF on sample powders) for all drill core samples (n = 51) with classification fields after Parbhakar-Fox et al. (2011). *NAF* non-acid forming, *ML* metal leaching, *PAF* potentially acid forming. For lithological descriptions, see Table 1

contained the least quantity of metals, however, one Unit B sample was classified as intermediate risk due to a combined metal content of >10,000 ppm measured. This confirmed the necessity for LA-ICPMS analyses on Unit B samples to establish the presence or absence of metals, as it is possible that the metals are sourced from disseminated sulfide phases in the host rock. When considering total metals against

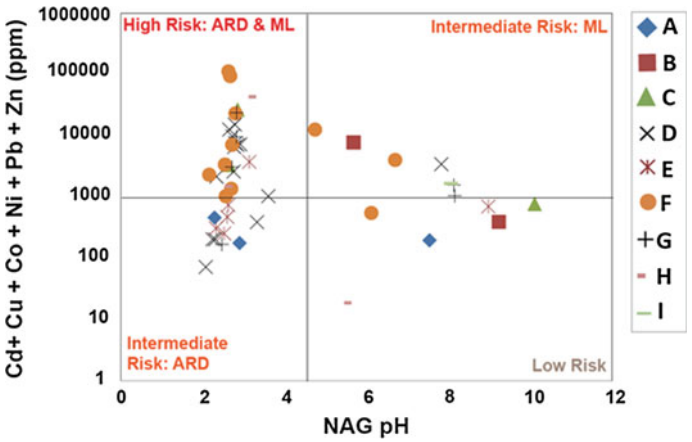


**Fig. 9** NAG pH versus total metals (ppm; as measured by pXRF on sample powders) for all drill core samples (n = 51) with classification fields after Parbhakar-Fox et al. (2011). *NAF* non-acid forming, *ML* metal leaching, *PAF* potentially acid forming. For lithological descriptions, see Table 1

NAG pH values, the 'worst-case' scenario is predicted. All data shifts to the left (i.e., lower pH values) with the majority of samples now plotting in the high-risk (with ARD formation and metal leaching anticipated) and intermediate (with ARD formation likely) fields. Only one sample from units A, B and C remain as low-risk. These results confirm that potentially, these three lithologies could be nominated for surface placement, but more samples from these lithologies are required to confirm their ARD characteristics, and the potential for metal leaching. All other groups would be recommended for underground storage.

## *Leachate Characteristics*

A comparison of the three pH tests performed (paste, NAG and MATE pH) is shown in Fig. 10. Paste pH values return the highest results as anticipated given that the solute used in this test is deionised water, with the current acid forming characteristics measured. The NAG pH is regarded as measuring the 'worst-case' scenario, and MATE pH represents the most realistic case describing future water quality. NAG and MATE pH values are near identical ($R^2 = 0.93$), with classifications (i.e., pH > 4.5 = NAF; pH < 4.5 = PAF) unchanged between both tests, except for two Unit H samples. MATE pH values are generally slightly higher than NAG pH values, as it is anticipated that secondary neutralizing minerals (i.e., chlorite) may be reacting.

To examine the extent of future leachable metals, MATE pH values were plotted against their corresponding leached metals on a modified Ficklin plot (after

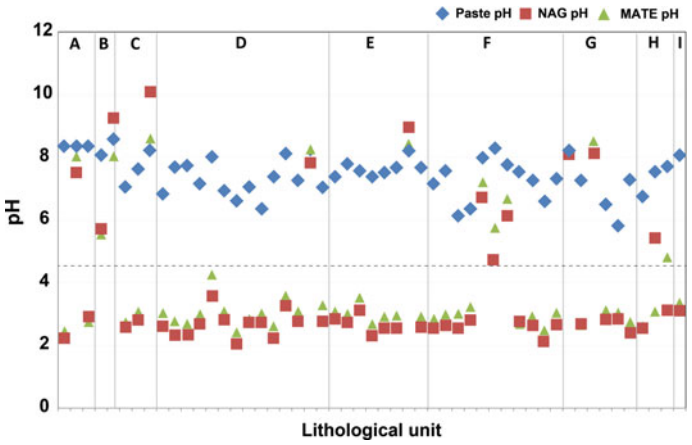


**Fig. 10** Paste pH, NAG pH and MATE pH values for all drill core samples (n = 51) with vertical lines grouping samples by lithological unit (descriptions provided in Table 1). The *horizontal dashed line* indicates the cut-off criterion for NAF (pH > 4.5) and PAF (pH < 4.5)

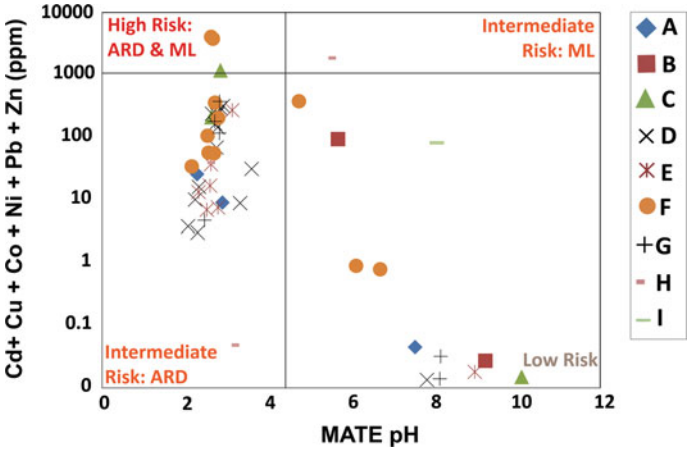


**Fig. 11** MATE pH versus leached metals (ppm) (as measured from MATE pH leachates by ICP-MS methods) for all drill core samples (n = 51) with classification fields after Parbhakar-Fox et al. (2011). *ARD* acid rock drainage, *ML* metal leaching. For lithological descriptions, see Table 1

Parbhakar-Fox et al. 2011; Fig. 11). The majority of samples are classified as intermediate risk with only one sample identified as high risk (Unit F), and twelve samples as low risk. When USGS field leach test data are plotted against NAG pH values (Fig. 12), all samples are classified as intermediate risk (ARD formation) or low risk. This indicates that despite the high total metals content (Figs. 8 and 9), only a very low portion are leachable under near-natural conditions (as mimicked by the USGS field leach test) and sulfide oxidised 'worst-case' conditions (as

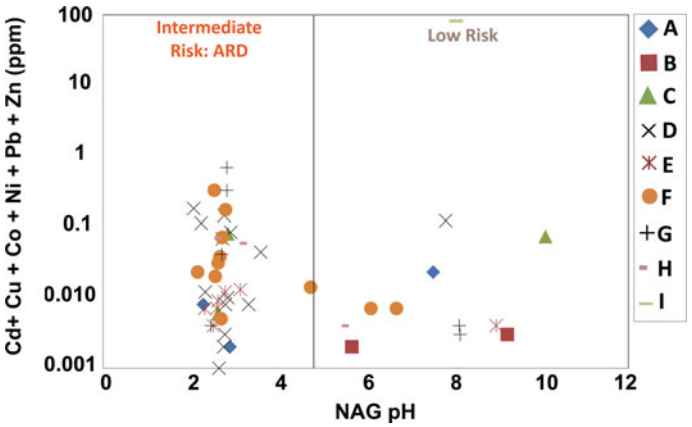


**Fig. 12** NAG pH versus leached metals (ppm) (as measured from USGS FLT leachates by ICP-MS methods) for all drill core samples (n = 51) with classification fields after Parbhakar-Fox et al. (2011). *ARD* acid rock drainage, *ML* metal leaching. For lithological descriptions, see Table 1

mimicked by MATE pH testing). Based on these analyses, only Unit B appears appropriate for surface storage in terms of both ARD and metal leaching.

## *Trace Element Chemistry*

Considering that only materials from Unit B have been identified as appropriate for the surface waste rock dump, only LA-ICPMS data for these materials is shown here. These analyses were performed to determine whether there could be any metal-leaching posed by the dissolution of carbonate minerals. Very little carbonate material was deemed appropriate for LA-ICPMS analysis as the carbonates were weathered and finely intergrown with other phases e.g., quartz (i.e., making quantification using an appropriate internal standard difficult). Therefore, results presented are only indicative of the trace element contents. A total of 46 spots were analysed in two samples, with the dominant carbonate analysed identified as calcium-rich rhodochrosite. A statistical summary of the elements observed above detection is shown in Table 2, with crustal abundance values for each element also shown for comparison. In general, a high concentration of As was measured. Whilst there appear to be Sn- and Zn-rich inclusions within the rhodochrosite, generally, average values were low. Only minor Pb, Sb and several rare earth elements were detected as inclusions. The MATE pH leachate data reported low dissolved metals (<90 ppm) and As from these samples. Additionally, very low concentrations (<1 ppm) of both were measured in USGS test leachates. These carbonates can be regarded as 'clean' with respect to metals, but may contain high As and REEs.

**Table 2** Element contents of calcium-rich rhodochrosite present in Unit B measured by LA-ICPMS in ppm (n = 46)

| | As | Pb | Sb | Sn | U | W | Yb | Y | Zn |
|---|---|---|---|---|---|---|---|---|---|
| Maximum | 340 | 872 | 10 | 730 | 27 | 41 | 24 | 148 | 505 |
| Minimum | 2 | 0 | 0 | 0 | 0 | 1 | 0 | 4 | 13 |
| Average | 106 | 52 | 3 | 70 | 3 | 13 | 7 | 47 | 71 |
| Median | 83 | 16 | 2 | 17 | 2 | 4 | 5 | 40 | 60 |
| Crustal abundance[a] | 2.1 | 10 | 0.2 | 2.2 | 1.8 | 1.1 | 2.8 | 29 | 79 |

[a]Values from www.webelements.com

Therefore, they may not satisfy the 'non-metalliferous' criteria set. Only further testing will resolve this.

## Waste Management Strategy

Following this investigation, a waste management strategy was developed for the site. This strategy essentially follows a modified GMTG style approach to achieve appropriate waste classification. Each stage is outlined in the following section.

### *Stage One: Pre-screening Tool*

Stage-one focusses on the application of simple-to-use (and low-cost) pre-screening methods which can be performed on-site (i.e., core shed and field-laboratory). The data collected from the tests used at this stage allows for an accurate first-pass assessment of the ARD generating characteristics on best practice sample numbers in accordance with Australian Government (2007) guidelines (Price 2009). These tests are to be performed systematically on drill core materials. When considering the relative ease of performing these geochemical tests (paste pH testing and carbon-sulfur analysis), it is recommended that a field-laboratory is established and utilised by environmental staff to increase the throughput of samples analysed (access to a carbon-sulfur analyser is required if assay data is not available). Based on these data, the most appropriate cut-off value to determine NAF from PAF materials is 0.3 wt%, which aligns with best practice guidelines published by Price (2009). Whilst the value of a visual field-based geoenvironmental logging scheme can be considered subjective, logging following a modified ARDI approach will improve accuracy. This final score is compared with geochemical paste pH and $S_{Total}$ data, with resulting classifications comparable to established NAPP versus NAG classifications as demonstrated in Parbhakar-Fox et al. (2011).

## *Stage Two: Screening Tool*

Following stage-one, only samples identified as NAF and PAF are recommended for stage-two where screening analyses are to be performed on at least 50 % of samples using established geochemical screening tests. Materials identified at stage-one as extremely acid forming (EAF) or acid forming (AF) do not require further testing as they must remain below ground by the criteria set by the regulator. Care must be taken to ensure that a multi-addition (as opposed to single-addition) NAG test is performed to allow for more efficient sulfide oxidation to take place. Additionally, the leachate must be kept and scheduled for ICP-MS analyses (with appropriate standards and blanks used as part of a rigorous QA/QC protocol). Performance of the USGS field leach test (FLT) is recommended to measure leachable metals. After this stage, a decision as to the fate of the waste materials can be made, with PAF-high risk samples identified and therefore nominated for underground storage. PAF-low risk and NAF materials can be bought to surface. Elemental analyses as performed by the USGS FLT and NAG testing will allow for the determination of NAF materials, and therefore provide an indication if materials should be placed on the inner or outer segment of the surface dump.

## *Stage Three: Validation Tool*

This stage focuses on using state-of-the art analytical tools to validate the waste classifications made at stage-two (i.e., carefully selected NAF and PAF samples are tested). XRD is to be performed to allow for the mineralogical calculation of ARD forming potential. Laser ablation ICPMS analysis is recommended on both sulfide and carbonate materials nominated for surface placement in order to confirm the element loads, thus helping to identify whether they are to be placed on the outer or inner section of the surface waste rock dump.

## *QA/QC During Waste Placement*

Validation sampling should be performed following the waste management strategy (focusing on the use of stage-one tests) during waste rock placement. This ensures that are placed in the appropriate destination. The initial validation frequency should be at least one sample per 1,000 tonnes for waste headings. To ensure full QA/QC, this number should not be dropped down as the sulfide mineralogy and texture observed in these drill core materials is highly heterogeneous even in waste zones. If any major classification discrepancies are identified, then measures should be taken to resolve the classification error.

## Conclusions

Polymetallic massive sulfide ore deposits represent potential sources of ARD due to their exceptionally high content of sulfide minerals (i.e., >50 %) including pyrite, pyrrhotite, sphalerite and galena. Considering this, a volcanic hosted polymetallic massive sulfide mine was presented with a management challenge to minimise environmental impacts. Only non-acid forming and non-metalliferous waste from underground mining activities were permitted to be brought to surface, and placed into a new waste repository. The study site required an innovative waste management scheme by which to classify the materials. Therefore, a set of samples representative of waste and marginal ore were collected from nine lithological Units (A to I). These were subjected to various simple, established and state-of-the art geochemical and mineralogical tests to develop a waste classification scheme.

A modified GMT approach was used to classify wastes. At stage-one, logging and field-portable methods are used, but these techniques are not be sufficient to decide upon the final location of samples. Instead, these must be supplemented with simple geochemical methods that will have to be used including paste pH and measurement of total sulfur. At stage two, established geochemical tests are performed to characterize NAF and PAF materials only, with leachate tests including the MATE pH and USGS FLT used to predict the future water chemistry. At stage-three, a representative subset of samples are taken for detailed characterization whereby the mineralogy of the samples is determined. Through the combined use of these methods, materials can be identified for surface placement, particularly from Unit B which contains carbonate breccia materials. Ultimately, this study has demonstrated that a solid relationship between mining operators, regulators and researchers must be established in order to develop a well-informed and efficient best practice waste management strategy.

## References

Aguilera A, Manrubia SC, Gómez F, Rodríguez N, Amils R (2006) Eukaryotic community distribution and its relationship to water physicochemical parameters in an extremely acidic environment, Río Tinto (Southwestern Spain). Appl Environ Microbiol 72:5325–5330

Australian Government Department of Industry, Tourism and Resources (2007) Managing acid and metalliferous drainage. Leading Practice Sustainable Development Program for the Mining Industry, Canberra

Danyushevsky L, Robinson P, Gilbert S, Norman M, Large R, McGoldrick P, Shelley M (2011) Routine quantitative multi-element analysis of sulphide minerals by laser ablation ICP-MS: standard development and consideration of matrix effects. Geochem Explor Environ Anal 11:51–60

Hageman PL (2007) U.S. Geological Survey field leach test for assessing water reactivity and leaching potential of mine wastes, soils, and other geologic and environmental materials. U.S. Geological Survey Techniques and Methods, Book 5, D3, United States

Hudson-Edwards KA, Edwards SJ (2005) Mineralogical controls on storage of As, Cu, Pb and Zn at the abandoned Mathiatis massive sulphide mine, Cyprus. Mineral Mag 69:695–706

Jamieson HE, Robinson C, Alpers CN, Nordstrom DK, Poustovetov Al, Lowers HA (2005) The composition of coexisting jarosite-group minerals and water from the Richmond mine, Iron Mountain, California. USGS Published Research 475. http://digitalcommons.unl.edu/usgsstaffpub/475

Kwong YTJ (1993) Prediction and prevention of acid rock drainage from a geological and mineralogical perspective. MEND Report 1.32.1, Ottawa, Ontario

Noble TN, Lottermoser BG, Parbhakar-Fox A (2015a) Evaluation of pH testing methods for sulfidic mine waste. Mine Water Environ. doi:10.1007/s10230-015-0356-2

Noble TN, Aalders JA, Lottermoser BG (2015b) Development of the Microwave Assisted Thermal Energy (MATE) pH test. CRC ORE Technical Report 94, CRC for Optimising Resource Extraction, Brisbane

Nordstrom DK, Alpers CN, Ptacek CJ, Blowes DW (2000) Negative pH and extremely acidic mine waters from Iron Mountain, California. Environ Sci Technol 34:254–258

Parbhakar-Fox AK, Edraki M, Walters S, Bradshaw D (2011) Development of a textural index for the prediction of acid rock drainage. Min Eng 24:1277–1287

Price WA (2009) Prediction manual for drainage chemistry from sulphidic geologic materials. CANMET Mining and Mineral Sciences Laboratories, Canada

Romero A, Gonzalez I, Galan E (2006) Estimation of potential pollution of waste mining dumps at Peña del Hierro (Pyrite Belt, SW Spain) as a base for future mitigation actions. Appl Geochem 21:1093–1108

Seal II RR, Piatak N (2012) Geoenvironmental features in volcanogenic massive sulfide occurrence model. US Geological Survey Scientific Investigations Report 20, United States

Smart R, Skinner WM, Levay G, Gerson AR, Thomas JE, Sobieraj H, Schumann R, Weisener CG, Weber PA, Miller SD, Stewart WA (2002) ARD test handbook: Project P387A, Prediction and kinetic control of acid mine drainage. AMIRA International Ltd, Melbourne

Taylor CD, Zierenberg RA, Goldfarb RJ, Kilburn JE, Seal II RR, Kleinkopf MD (1995) Volcanic-associated massive sulfide deposits. In: Preliminary Compilation of descriptive geoenvironmental mineral deposit models. U.S Geological Survey Open-File Report 90-831, pp 137–144

Weber PA, Hughes JB, Conner LB, Lindsay P, Smart RStC (2006) Short-term acid rock drainage characteristics determined by paste pH and kinetic NAG testing: cypress prospect. Paper presented at the 7th International Conference on Acid Rock Drainage (ICARD), New Zealand

# Part III
# Water Quality

# pH Testing Methods for Sulfidic Mine Wastes

**Taryn L. Noble, Bernd Lottermoser and Anita Parbhakar-Fox**

**Abstract** pH tests are useful screening tools for assessing the characteristics of first flush waters draining sulfidic rocks and waste materials at mine sites. Rinse and paste pH tests are part of a suite of static tests used in acid-base accounting assessments. This study presents a comparison of eleven different pH tests (e.g., rinse and paste pH tests as well as soil tests of the International Organization for Standardization ISO 10390:2005, American Society for Testing and Materials ASTM D4972-01(2007) and Standards Australia AS4969.2-2008) using three different sulfidic rock samples and the acid-base accounting standard KZK-1. We show that different rinse and paste pH methodologies using different grain sizes and extraction solutions can result in different risk classification for ARD assessments. We suggest pH testing should be standardized in their grain size and solid to solution ratio. pH tests conducted using unweathered materials (e.g., drill core) should be carried out using a 0.01 M $CaCl_2$ solution.

## Introduction

Exposure and subsequent weathering of sulfidic rocks brought to the surface during mining operations can result in acid rock drainage (ARD). Accurate deposit-wide environmental characterization of geological units is therefore essential for understanding the acid-generating capacity of sulfidic rocks. Many different static tests

T.L. Noble (✉) · A. Parbhakar-Fox
School of Physical Sciences, University of Tasmania, Private Bag 79, Hobart, TAS 7001, Australia
e-mail: Taryn.Noble@utas.edu.au

A. Parbhakar-Fox
e-mail: Anita.Parbhakar@utas.edu.au

B. Lottermoser
Institute of Mineral Resources Engineering, RWTH Aachen University, Wüllnerstrasse 2, 52062 Aachen, Germany
e-mail: lottermoser@mre.rwth-aachen.de



B. Lottermoser (ed.), *Environmental Indicators in Metal Mining*,
DOI 10.1007/978-3-319-42731-7_11

exist, which aim to provide information on the acid generating and acid neutralizing characteristics of mine waste (e.g. Price 2009; Smart et al. 2002). Rinse and paste pH tests measure the pH of slurries of crushed rock and water to provide an estimate of the current net acidity and first flush characteristics, while Net Acid Generation pH tests use hydrogen peroxide to estimate the future acidity by oxidizing the sulfide minerals.

pH analyses of waters, soils and wastes yield fundamental and useful data because: (1) measurements can be easily made using inexpensive equipment; (2) values are readily interpreted and widely understood; and (3) pH controls the behaviour of elements through changes in speciation, sorption and mobility of metals (Lottermoser 2010). This study evaluates different pH test methods that are used in ARD risk assessments and provide recommendations for the most suitable pH testing method.

Rinse and paste pH tests commonly used include those by Sobek et al. (1978), Morin and Hutt (1997), Smart et al. (2002) and Price (2009). There is no accepted standards method that allows interlaboratoy comparison between different pH methods applied to weathered and unweathered sulfidic wastes. The analytical protocols all rely on deionized (DI) water as the extraction solution. However, they all vary in their prescribed methodologies, e.g., the sample particle size for testing purposes is recommended as <0.075 mm (Smart et al. 2002), <0.25 mm (Sobek et al. 1978), and <2 mm (Morin and Hutt 1997; Price 2009). Furthermore, the analytical protocols used to prepare the supernatant or paste rely on different solid:solution proportions, ranging from 1:1 (Morin and Hutt 1997; Price 2009), to 1:2 (Smart et al. 2002) and 2:1 (Sobek et al. 1978). Moreover, the equilibration time between the sample and extracting solution also varies, from instant pH measurement (Sobek et al. 1978) to a period of equilibration ranging from 10 min (Price 2009) to 12–16 h (Smart et al. 2002). These factors can significantly influence pH readings.

The soil science community also has numerous methods to measure soil pH, which include the use of different solid to solution ratios and electrolytes as extraction solutions. Also in this area, numerous standard methods exist through national (e.g., Standards Australia) and international [e.g., International Organisation for Standardisation (ISO)] bodies. Previous research in soil science has shown that the use of 0.01 M $CaCl_2$ relative to DI water helps to: (1) reduce the junction potentials through coagulation of soil particles in suspension; (2) stabilize the ionic conductivity which can vary due to seasonal fluxes in soluble salts; (3) eliminate variability observed in pH measurements of moist and dry soils; and (4) reduce fluctuations in pH observed with different shaking times (Conyers and Davey 1988; Davey and Conyers 1988; Sumner 1994).

The purpose of this study was to demonstrate the need for a standardized method for the assessment of pH in weathered and unweathered sulfidic rocks for the purposes of ARD risk assessment. We assessed: (a) whether the use of different pH test protocols influences pH measurements on unweathered and weathered sulfidic rock samples; (b) which major variable of the analytical protocols (i.e. grain size; solid:solution ratio; equilibration time) leads to the most pronounced variation in

measured pH values; and (c) which existing or modified pH test provides the best indication of the propensity of a sample to produce ARD. Furthermore, we present data on the NAG pH of corresponding samples used in the pH assessment.

## Materials and Methods

### *pH Tests*

The accuracy of the various pH testing methods was evaluated using three different sulfidic waste rock samples. The pH tests included in this study were the rinse and paste pH tests of Sobek et al. (1978) and Smart et al. (2002), and the United States Geological Survey (USGS) Field Leach Test method (Hageman 2007). Standard soil tests used in this work were from the International Organisation for Standardisation (ISO) 1090:2005, American Society for Testing and Materials (ASTM) D4972-01(2007) and Standards Australia (AS) 4969.2-2008. The samples were further tested by the commercial laboratory Intertek (Perth) using the 1:5 soil pH test of Rayment and Lyons (2010), which is similar in experimental design to ISO 1090:2005. Each test required particular solid:solution ratios (1:1, 2:1, 1:2, 1:5, 1:20, 1:40), extracting solutions (DI water, $CaCl_2$, KCl), sample masses (5–25 g), solution volumes (5–50 ml), grain size fractions (<0.075, <0.25, <2 mm), equilibration times (0, 1, <3, <16 h), and procedural steps (Table 1).

A Mettler Toledo S47 SevenMulti™ dual pH/conductivity meter was used to measure the pH and electrical conductivity (EC) of the samples' supernatant or paste. The pH was measured by an InLab®Expert Pro electrode and the EC by an InLab®731 probe. The pH electrode was calibrated using a four-point calibration with buffer solutions (pH 2, 4, 7.0, 9.21) at 25 °C. The EC probe was calibrated using three conductivity solutions (500, 1413 and 12.88 μS $cm^{-1}$) at 25 °C.

The pH and EC of distilled water, prepared in a conventional glass distillery, was an average of 5.44 ± 0.25 (n = 26) and 7 μS $cm^{-1}$ ± 40 (n = 26), respectively. The pH is within error of the theoretical pH of 5.65 (Langmuir 1997), but the large standard deviation reflects that precise pH measurements are difficult to achieve in low ionic strength solutions. The electrolyte 0.01 M $CaCl_2$ had an average pH and EC of 6.40 ± 0.04 (n = 10) and 1594 ± 16 μS $cm^{-1}$ (n = 10), respectively. The average pH and EC of 1 M KCl was 6.56 ± 0.04 (n = 10) and 114,000 ± 769 (n = 10) μS $cm^{-1}$, respectively.

### *Samples*

The accuracy of the various pH testing methods was evaluated using the acid-base accounting reference material KZK-1, which is a sericite schist made from a mixture of drill cores from the Kudz Ze Kayah copper-lead-zinc project, Canada

**Table 1** Summary of the protocols required for each of the pH methods evaluated

| pH test | Solid to solution | Solution | Mass | Grain size (mm) | Equilibration time (h) |
|---|---|---|---|---|---|
| Rinse pH (Sobek et al. 1978) | 1 to 1 | DI water | 10 g:10 ml | <2 | 0 |
| Paste pH (Sobek et al. 1978) | 2 to 1 | DI water | 10 g:5 ml | <0.25 | 0 |
| Paste pH (Smart et al. 2002) | 1 to 2 | DI water | 25 g:50 ml | <0.075 | 12–16 |
| USGS Field Leach Test | 1 to 20 | DI water | 50 g:100 ml | <2 | <1 |
| ASTM D4972-01 (2007) | 1 to 1 | DI water | 10 g:10 ml | <2 | >1 |
| ASTM D4972-01 (2007)(E) | 1 to 1 | 0.01 M $CaCl_2$ | 10 g:10 ml | <2 | >1 |
| ISO 10390:2005 | 1 to 5 | DI water | 5 ml:25 ml | <2 | >2 |
| ISO 10390:2005(E) | 1 to 5 | 0.01 M $CaCl_2$ | 5 ml:25 ml | <2 | >2 |
| ISO 10390:2005(E) | 1 to 5 | 1 M KCl | 5 ml:25 ml | <2 | >2 |
| AS 4969, Method 2-2008 | 1 to 40 | 1 M KCl | 2 g:80 ml | <0.075 | >12 |

American Society for Testing and Materials (*ASTM*); International Organization for Standardization (*ISO*); Standards Australia (*AS*), electrolyte (*E*)

(CANMET Certificate of Analysis KZK-1 2007). The tested material was operationaly defined as −74 μm and contains quartz, albite, muscovite, biotite, rutile, ilmenite, ankerite, calcite, monazite, zircon, pyrite, and pyrrhotite. Trace amounts of clinochlore, kaolinite and sphalerite are also present.

Two bulk sulfidic rock samples were collected from the Mt Lyell Cu-Au mine (41°04′S, 145°34′E), Australia, from the run-of-mine ore stockpile (CMT-ROM1) and waste rock dump (CMT-WRD1). Mt Lyell ore and waste rocks consist of chalcopyrite and pyrite within a quartz-sericite-chlorite gangue (cf. Hills 1990; Raymond 1996). The Mt Lyell ore sample (CMT-ROM1) derived from underground workings and represents a freshly extracted, unweathered sulfidic ore. By contrast, the Mt Lyell waste rock sample (CMT-WRD1) has been subjected to limited weathering (possibly months) since the waste was extracted from underground workings and placed into the above-ground waste repository.

The third bulk waste rock sample (RG-WRD1) was acquired from an abandoned waste rock pile of the historical Royal George Sn mine site, Australia (41°49′S, 147°53′E). Royal George ore and waste rocks contain cassiterite, pyrite and chalcopyrite, and the gangue minerals feldspar, quartz, biotite and tourmaline (cf. McIntosh Reid and Henderson 1929; Green 1990). The Royal George sample (RG-WRD1) represents oxidized material, which has been exposed to atmospheric conditions since abandonment of the site in the 1920s (Hills 1990).

The fourth sample suite comprises several waste rock samples (n = 35) from piles at the historical Croydon Au mine site, Australia (18°12′S, 142°14′E). The waste rocks contain major quartz, potassium feldspar, muscovite and plagioclase, minor illite, kaolinite, pyrite, arsenopyrite, sphalerite and galena, and traces of pyrrhotite and chalcopyrite (Van Eck and Child 1990; Parbhakar-Fox 2012).

The acid-base accounting characteristics of CMT-ROM, CMT-WRD and RG-WRD were assessed using the following static tests: NAG pH measurements (Smart et al. 2002) provided a preliminary evaluation of the material's net acidity. The total sulfur ($S_{Total}$) content of samples was assumed to represent the maximum potential acidity (MPA) calculated in kg $H_2SO_4$/t. The acid neutralizing capacity (ANC) of rocks was determined by standard acid reaction and titration. The difference between MPA and ANC yielded the net acid producing potential (NAPP).

Particle surface area analyses were carried out on each grain size fraction of the three bulk samples (CMT-ROM1, CMT-WRD1, RG-WRD1), following the single point BET method (Brunauer et al. 1938) and using a Micrometrics Flowsorb II 2300 at Intertek, Melbourne.

The mineralogy of samples was determined using Siemens D500 and D501 X-ray diffractometers at Federation University, Ballarat. Mineral phases were identified using computer-aided search/match of the 2010 ICDD PDF4/minerals subfile. SiroQuant™ (version 3.0) was applied to obtain semi-quantitative mineral abundances (wt%).

## Results and Discussion

The pH tests methods were evaluated using the acid-base accounting reference material KZK-1, which has a certified paste pHvalue of 8.8 (±0.21 between laboratories; CANMET Certificate of Analysis KZK-1 2007). Analysis of the KZK-1 standard demonstrated that there is significant variation in the measured pH when applying different test protocols. Overall, pH tests using DI water showed variable pH values deviating by up to +0.68 relative to the certified reference value. In contrast, pH tests using electrolyte solution such as 0.01 M $CaCl_2$ and 1 M KCl resulted in pH values deviating by −0.61 pH units and +0.6–0.9 pH units, respectively (Fig. 1). The most accurate pH test methods were the paste pH protocol by Smart et al. (2002) and ASTM D4972-01(2007) (DI water), while the pH methods using 0.01 M $CaCl_2$ were the most precise.

The evaluation of pH methods using sulfidic rock samples showed greater variability in pH compared to the standard reference material (Fig. 2). However, the same trend was observed with more precise results obtained from pH methods using 0.01 M $CaCl_2$, and the largest variability was observed in the pH tests using DI water (Fig. 2).

For each sulfidic sample analyzed, we observed a 100-fold difference in the $H^+$ ion concentration between different pH test protocols (Fig. 3). The pH assessment of the unweathered CMT-ROM1 showed circum-neutral pH values with a

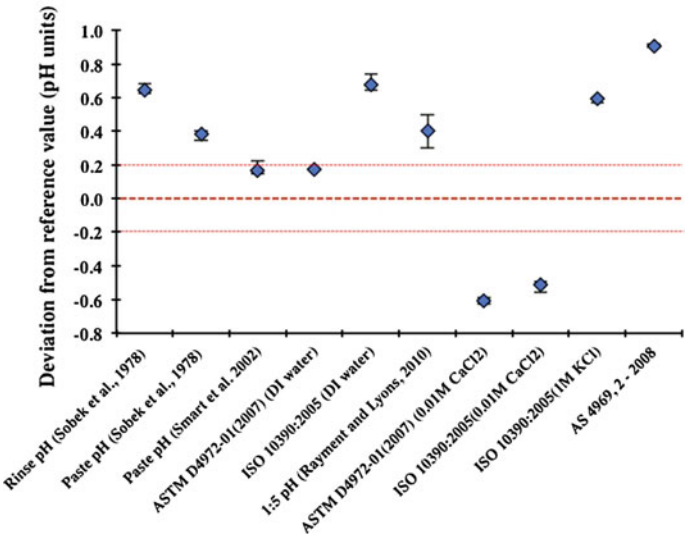


**Fig. 1** The difference between the median pH value (n = 3) measured using nine pH methods and the certified reference pH value for the acid-base accounting standard KZK-1. The 1:5 pH test (Rayment and Lyons 2010) was measured by Intertek, Perth. The *error bars* show the 25th percentile (*lower*) and 75 % percentile (*upper*) of data

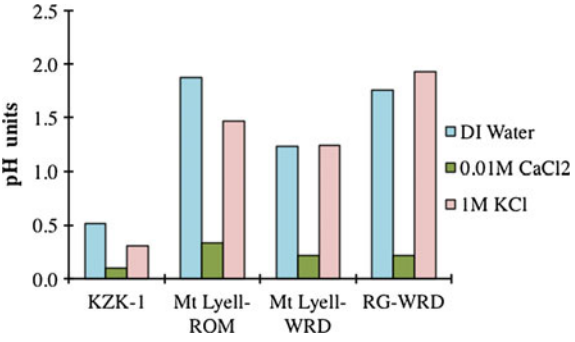


**Fig. 2** The difference between the maximum and minimum pH values for pH test protocols using DI water, 0.01 M $CaCl_2$ and 1 M KCl for the reference standard KZK-1, CMT-ROM1, CMT-WRD1 and RG-WRD1 (color figure online)

minimum of pH 6.22 (USGS FLT) and a maximum of pH 8.18 (paste pH; Smart et al. 2002). The high pH value observed for CMT-ROM1, using the method by Smart et al. (2002), can be explained by the presence of calcite and dolomite and the greater surface area. The smaller size fraction (0.075 mm) has a surface area of 2.06 $m^2/g$ compared to 0.32 $m^2/g$ in the <2 mm size fraction, which therefore provides greater exposure of mineral surfaces.

The weathered waste rock samples also showed a wide range of pH values according to pH methodology. CMT-WRD1 has acidic pH values varying from 3.37 (rinse pH; Sobek et al. 1978) to 5.23 (AS 4969, 2-2008). RG-WRD1 showed a similar range of acidic pH values from 3.11 (paste pH; Sobek et al. 1978) to 5.49

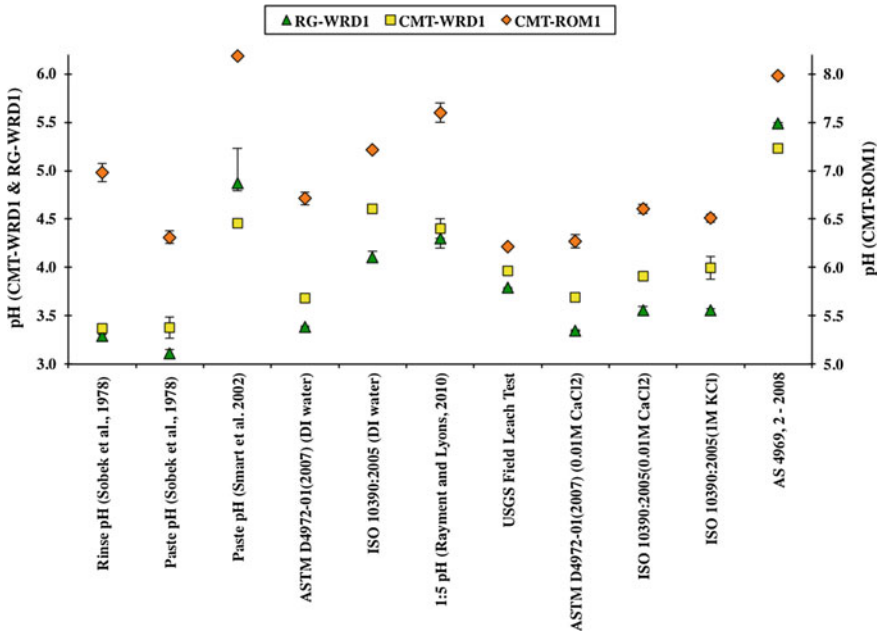


**Fig. 3** Mean pH values (n = 5 per analysis) sulfidic rock samples (CMT-ROM1, CMT-WRD1, RG-WRD1), using 11 different pH test methods. The upper and lower percentiles are plotted for the five replicates. The analyses for the 1:5 pH test (Rayment and Lyons 2010) were carried out by Intertek (Perth) on the <2 mm size fraction

(AS 4969-2, 2008). The lower pH values of the weathered samples measured in the rinse and paste method of Sobek et al. (1978) can be explained by the high solid:solution ratio of the tests, which results in less dilution of $H^+$ ions. In contrast, the highest pH value was consistently measured using AS 4969-2 (2008), which has the lowest solid:solution ratio of 1:40.

The electrical conductivity values measured varied from 200 to 118,000 μS $cm^{-1}$ across the tests, with the lowest values observed in the unweathered sample CMT-ROM1. For all samples using DI water as the extraction solution, the EC of the tests was dependent on the solid to solution ratio specified for each test (Fig. 4), and the proportion of soluble phases present in each sample. The EC of the extraction solutions increased as the solid:solution ratio increased, which corresponded to a decrease in the pH for both the circum-neutral and acidic samples (Fig. 4). Overall, the solid to solution ratio was a major control on the pH values observed between different methods. For example, similar pH values were observed for the rinse pH (Sobek et al. 1978) and ASTM D4972-012007) (DI water) method for CMT-ROM1 (EC) and RG-WRD1 (pH), where the solid:solution ratio was 1 for both tests. The negative relationship between solid to solution ratio and pH is consistent with previous studies (e.g. Afzal and Yasin 2002; Miller and Kissel 2010), and relates simply to the dilution of $H^+$ ions released into solution.

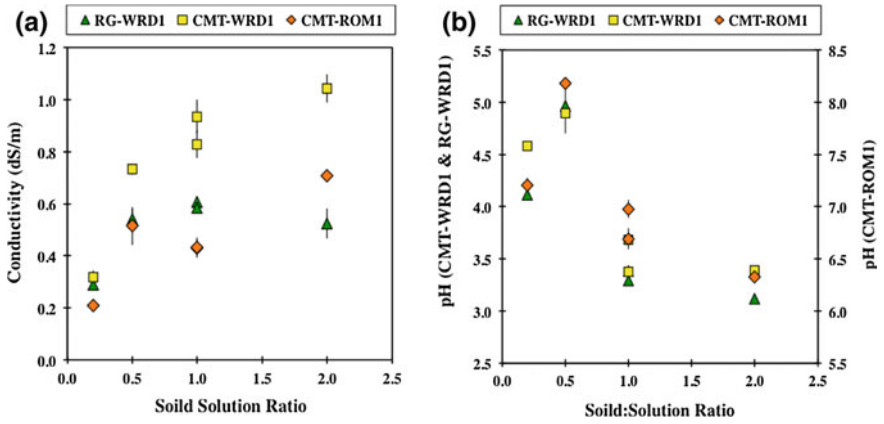


**Fig. 4** **a** EC and **b** pH data for rinse and paste tests that used DI water as the extracting solution

Grain size was the dominant control on the pH observed between different pH methods. Grain size controls chemical reactions through changes in particle surface area, which can increase rates of sulfide oxidation and weathering (Liu et al. 2008), and therefore the release rate of elements into waters (cf. Förstner and Salomons 1980).

The effect of grain size on rinse and paste pH values was determined by carrying out two pH tests [ISO 10390:2005(E) and ASTM D4972-01(2007) (E)], using two grain size fractions of the Croydon waste rock samples (<0.075 and <2 mm). The extraction solution used was 0.01 M $CaCl_2$. The pH values increased as the particle size decreased. For a given sample, we observed more alkaline pH values in the 0.075 mm size fraction for 80 % of the sample suite. This relationship may be explained by an increase in the release of alkalinity and exposure of acid consuming minerals (e.g. muscovite, k-feldspar) as the surface area available for reactions increased with decreasing particle size (cf. Shaw et al. 2000; Lapakko et al. 2006).

For a given grain size, we observed similar pH results for both tests, despite the differences in pH protocol relating to the solid to solution ratio and sample mass and the equilibration time. Using <2 mm grain size, 57 % of the pH values, resulting from the ISO 10390:2005(E) and ASTM D4972-01(2007) (E)) protocols, were within 2σ error. In comparison, 46 % of the pH values produced from both pH tests were consistent within 2σ error for the 0.075 mm grain size fraction. Overall, the pH data for the <2 and <0.075 mm size from both pH test protocols plot along a straight line, with a slope of 0.982 ($R^2$ = 0.98) for the 0.075 mm data and 1.012 ($R^2$ = 0.95) for the <2 mm data (Fig. 5).

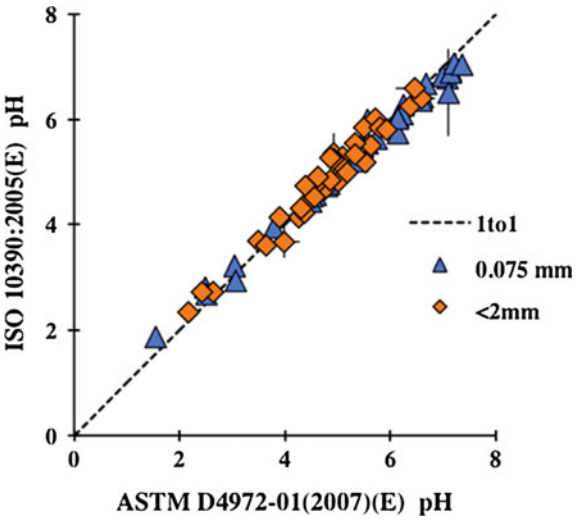


**Fig. 5** pH data relating to grain size from waste rock samples from the historical Croydon Au mine site. The pH tests ISO 10390:2005(E) and ASTM D4972-01(2007) (E) use 0.01 M $CaCl_2$ as the extraction solution. Each test was carried out using both 0.075 and <2 mm grain size fractions

## The Application of pH Tests to ARD Risk Assessment

The evaluation of pH methods using KZK-1 suggests that methods with a high solid:solution ratio (e.g. Sobek et al. 1978) and/or long equilibration time (e.g. Smart et al. 2002) produced the most accurate pH values. The dilution of $H^+$ has shown to be an important bias in the pH method evaluation. The degree of sulfide oxidation and therefore release of soluble salts into solution can therefore influence rinse and paste pH measurements.

This study has shown that pH measurements made in DI water are less precise, in contrast to higher ionic strength solutions which lead to more stable pH readings (cf. Sumner 1994). Considering that ARD risk assessment relies predominantly on testing of unweathered sulfidic rocks (e.g. drill core), the dilution of $H^+$ ions released from the rock may result in a wide range of pH values as shown here. For example, we observed pH values within 2 sigma variation using Sobek's et al. (1978) rinse and paste pH tests for the weathered sulfidic samples (CMT-WRD1 and RG-WRD1). In contrast for the unweathered sulfidic sample (CMT-ROM1), a difference of 0.6 was observed between these two pH tests. The use of DI water with high solid to solution ratios results in the most accurate pH assessment (Fig. 1). However, the pH methods using 0.01 M $CaCl_2$ [e.g., ISO 10390:2005(E) and ASTM D4972-01(2007) (E)] lead to more precise pH measurements. This is demonstrated by the smaller pH difference (0.2 pH units) between the pH values measured at CMT-ROM1 using ISO 10390:2005(E) and ASTM D4972-01(2007) (E), despite large differences in the solid:solution ratio between these tests protocols.

NAG pH measurements of the unweathered CMT-ROM1 sample revealed a median NAG pH value of 2.9, while the 11 different pH test protocols produced a

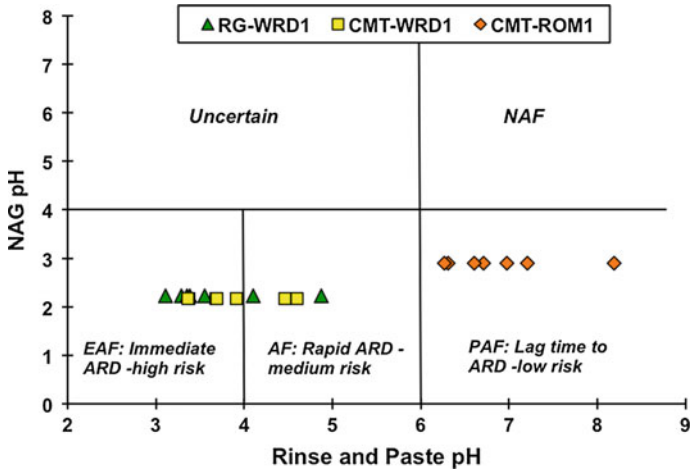


**Fig. 6** Classification of bulk sulfidic samples according to rinse and paste pH using DI water as the extraction solution and NAG pH. Data for rinse and paste pH are plotted by sample type, and include pH measurements from the rinse and paste pH method by Sobek et al. (1978), Smart et al. (2002) and the standard soil tests ISO 10390:2005(E) and ASTM D4972-01(2007)(E)

much higher median pH value of 6.71 (± 0.70 interquartile range between tests). Clearly, the latter pH value does not reflect the sample's ability to produce acid in the long term but rather its first flush characteristics. NAG pH measurements of the weathered sulfidic waste rocks revealed a value of 2.2 for both samples (CMT-WRD1, RG-WRD1). Similarly acidic pH values were also found by the 11 different pH test protocols, with median pH values of 3.91 (±0.77) and 3.55 (±0.76), respectively.

Combining rinse and paste pH data obtained on unweathered sulfidic rocks with parameters such as total S (wt%), metal or NAG pH (e.g. Weber et al. 2006) can provide a more reliable ARD risk assessment using low cost environmental tests. This study highlights that wide variability in rinse and paste pH can affect ARD risk classification based on the NAG pH-paste pH classification scheme (Fig. 6). In particular, the ARD classification falls between medium and high ARD risk according to the rinse and paste pH method used (Fig. 6).

## Conclusions

Rinse and paste pH tests are used as screening tests to assess the environmental risks associated with mining and mineral processing of sulfidic rock materials. This study compares the use of eleven different rinse, paste and soil pH test protocols on three sulfidic rock materials and the international reference material KZK-1. The measured pH values showed significant variability according to the methodology.

The most important factors that influenced the measured pH values are: (1) type of extracting solution (DI water, $CaCl_2$, KCl); (2) ionic conductivity; and (3) grain size. The use of DI water as the sole extracting solution results in pH values that are strongly dependent on methodology. The most accurate pH methods included the paste pH tests as documented by Sobek et al. (1978) and (Smart et al. 2002). However, the most precise pH methods used 0.01 M $CaCl_2$ as the extraction solution [e.g., ISO 10390:2005(E) and ASTM D4972-01(2007) (E)]. The use of 0.01 M $CaCl_2$ helps to stabilise the pH measurement due to the modest EC of the extraction solution (1200 μS $cm^{-1}$). This is particularly significant when testing unweathered sulfidic materials such as drill core, which will have a low EC due to the low proportion of soluble salts present.

## References

Afzal M, Yasin M (2002) Effect of soil to water ratios on chemical properties of saline-sodic and normal soils. Pak J Agri Res 17:379–386

American Society for Testing and Materials ASTM D4972-01(2007) (2007) Standard test method for pH of soils. ASTM International, West Conshohocken

Brunauer S, Emmett PH, Teller E (1938) Adsorption of gases in multimolecular layers. J Am Chem Soc 60:309–319

CANMET Certificate of Analysis KZK-1 (2007) CANMET mining and mineral sciences laboratories, 555 Booth Street, Ottawa, Ontario, Canada, K1A 0G1. http://www.nrcan.gc.ca/sites/www.nrcan.gc.ca/files/mineralsmetals/pdf/mms-smm/tect-tech/ccrmp/cer-cer/kzk-1-eng.pdf

Conyers MK, Davey BG (1988) Observations of some routine methods for soil pH determination. Soil Sci 145:29–36

Davey BG, Conyers MK (1988) Determining the pH of acid soils. Soil Sci 146:141–150

Förstner U, Salomons W (1980) Trace metal analysis on polluted sediments. Part I: assessment of sources and intensities. Environ Technol Lett 1:494–505

Green GR (1990) Palaeozoic geology and mineral deposits of Tasmania. In: Hughes FE (ed) Geology of the mineral deposits of Australia and Papua New Guinea. Australasian Institute of Mining and Metallurgy, Melbourne, pp 1207–1223

Hageman PL (2007) U.S. Geological Survey field leach test for assessing water reactivity and leaching potential of mine wastes, soils and other geologic and environmental materials: U.S. Geological Survey Techniques and Methods, book 5, chap. D3

Hills PB (1990) Mount Lyell copper-gold-silver deposits. In: Hughes FE (ed) Geology of the mineral deposits of Australia and Papua New Guinea. Australasian Institute of Mining and Metallurgy, Melbourne, pp 1257–1266

International Organization for Standardization ISO 10390:2005(E) (2005) Soil quality—determination of pH. International Organization for Standardization, Geneva

Lapakko KA, Engstrom JN, Antonson DA (2006) Effects of particle size on drainage quality from three lithologies. In: Proceedings of the 7th international conference on acid rock drainage (ICARD), pp 1026–1050

Liu R, Wolfe AL, Dzombak DA, Stewart BW, Capo RC (2008) Comparison of dissolution under oxic acid drainage conditions for eight sedimentary and hydrothermal pyrite samples. Environ Geol 56:171–182

Lottermoser BG (2010) Mine wastes: characterization, treatment and environmental impacts, 3rd edn. Springer, Berlin

McIntosh Reid A, Henderson QJ (1929) Avoca mineral district, Geological Survey Bulletin no. 40, Department of Mines, Hobart, Tasmania

Miller RO, Kissel DE (2010) Comparison of soil pH methods on soils of North America. Soil Sci Soc Am J 74:310–316

Morin KA, Hutt NM (1997) Environmental Geochemistry of minesite drainage: practical theory and case studies. MDAG Publishing, Vancouver

Parbhakar-Fox A (2012) Establishing the value of an integrated geochemistry-mineralogy-texture approach for acid rock drainage prediction. PhD Thesis. University of Tasmania, Australia

Price WA (2009) Prediction manual for drainage chemistry from sulphidic geological materials MEND report 1.20.1. CANET Mining and Mineral Sciences Laboratories, Smithers British Columbia. CA

Rayment GE, Lyons DJ (2010) Soil chemical methods: Australasia. CSIRO Publishing, Melbourne

Raymond OL (1996) Pyrite composition and ore genesis in the Prince Lyell copper deposit, Mt Lyell mineral field, western Tasmania, Australia. Ore Geol Rev 10:231–250

Shaw SC, Robertson AM, Maehl WC (2000) Material characterization and prioritization of remediation measures at the Zortman/Landusky mine sites. In: Proceedings of the billings land reclamation symposium, BLRS'00, Billings, Montana, USA, pp 346–358

Smart R, Skinner WM, Levay G, Gerson AR, Thomas JE, Sobieraj H, Schumann R, Weisener CG, Weber PA, Miller SD, Stewart WA (2002) ARD test handbook: project P387A, Prediction and kinetic control of acid mine drainage. AMIRA International Ltd, Melbourne

Sobek AA, Schuller WA, Freeman JR, Smith RM (1978) Field and laboratory methods applicable to overburdens and mine soils. EPA-600/2-78-054, US EPA, Cincinnati

Standards Australia AS4969.2-2008 (2008) Analysis of acid sulfate soil—dried samples—methods of test—determination of $pH_{KCl}$ and titratable actual acidity (TAA). Standards Australia, Sydney

Sumner ME (1994) Measurement of soil pH: problems and solutions. Commun Soil Sci Plant Anal 25:859–879

Van Eck M, Child R (1990) Croydon gold deposits. In: Hughes FE (ed) Geology and mineral deposits of Australia and Papua New Guinea, vol 14. The Australian Institute of Mining and Metallurgy, Monograph, pp 979–982

Weber PA, Hughes JB, Conner LB, Lindsay P, Smart R St C (2006) Short-term acid rock drainage characteristics determined by paste pH and kinetic NAG testing: Cypress prospect, New Zealand. In: Proceedings of the 7th international conference on acid rock drainage (ICARD), pp 2289–2310

# Modified Abrasion pH and NAGpH Testing of Minerals

**Taryn L. Noble and Bernd Lottermoser**

**Abstract** The original abrasion pH test of Stevens and Carron (1948) is based on grinding and wetting of minerals and subsequent pH measurements of the minerals' paste and suspensions. Such pH values allow insights into the behaviour of individual minerals upon fluid:mineral reactions in surface environments including mine sites and waste repositories. This study proposes a modified abrasion pH method which includes the use of 0.01 M $CaCl_2$, an operationally defined grain size (<0.075 mm), and high precision pH measurements. Several mineral specimens (n = 20) were obtained from commercial suppliers for the modified abrasion pH testwork, with the acquired specimens having a range of purities and resultant pH values. The modified abrasion pH testwork demonstrates that small admixtures to monomineralic samples caused significant pH changes. Only pure monomineralic samples provide a true indication of the modified abrasion pH of that mineral type. The NAGpH method aims to oxidize sulfide minerals but the reliability of this method in waste classification can be compromised depending on the sample mineralogy. This study demonstrates that NAGpH measurements of some carbonate minerals led to very alkaline pH values that are possibly due to the formation of Ca and Mg hydroxides. Such reactions do not occur in waste environments and therefore, NAGpH measurements of carbonate-rich wastes may overestimate their acid buffering capacity.

## Introduction

Characterization of the mineralogical composition and acid generating properties of mine waste is an essential component of environmental prediction and acid base accounting. The environmental impact caused by the release of acidity as a result of

T.L. Noble (✉)
School of Physical Sciences, University of Tasmania, Hobart, TAS 7001, Australia
e-mail: Taryn.Noble@utas.edu.au

B. Lottermoser
Institute of Mineral Resources Engineering, RWTH Aachen University, Wüllnerstrasse 2, 52062 Aachen, Germany
e-mail: lottermoser@mre.rwth-aachen.de



B. Lottermoser (ed.), *Environmental Indicators in Metal Mining*,
DOI 10.1007/978-3-319-42731-7_12

metal sulfide oxidation by oxygen or $Fe^{3+}$ and the precipitation of metal hydroxides is well documented (Lottermoser 2010). In addition, metal sulfates, which are extremely soluble can store significant amounts of acidity and deleterious metals. pH tests such as rinse and paste pH and NAGpH are fundamental indicators of the current acid-base characteristics used in the assessment of acid rock drainage (ARD). It is therefore important to have a good understanding of which minerals contribute acidity or alkalinity when interpreting data that provide information about the current net acidity (e.g., paste and rinse pH).

The pH of mineral solutions dissolved in water varies depending on the release of $H^+$ and $OH^-$ during dissolution. In addition, the presence of trivalent ions (e.g., $Al^{3+}$ and $Fe^{3+}$) that undergo hydrolysis and the presence of soluble mineral salts (e.g., copiapite $Fe^{2+}Fe_4^{3+}(SO_4)_6(OH)_2 20H_2O$; Jerz and Rimstidt 2003), can contribute significantly towards the net acidity.

The abrasion pH was established as a simple field test to identify minerals based on measurement of their particle suspensions. This method was first presented by Stevens and Carron (1948) and primarily focused, but not limited to the identification of secondary mineral salts. The procedure for determining the abrasion pH of mineral suspensions involved: (i) using a streak plate, whereby soft non-absorbent minerals were scratched and a drop of water applied; and (ii) using a pestle and mortar, whereby hard minerals were ground with a few drops of water and the suspension measured using indicator papers. The use of pH as a means to distinguish between minerals is based simply upon the theory that the hydrolysis of a mineral results in the production of acid (Eq. 1) or alkali (Eq. 2) accordingly:

$$Fe_2(SO_4)_3 9H_2O + H_2O \leftrightarrow 6H^+ + 3SO_4^{2-} + 2Fe(OH)_3 + 4H_2O \quad (1)$$

$$CaCO_3 + H_2O \leftrightarrow Ca^{2+} + HCO_3^- + OH^- \quad (2)$$

Minerals that release cations such as Ca during hydrolysis reactions result in alkaline pH solutions (e.g. Eq. 2). Grant (1969) used the abrasion pH as a weathering index, related to the release of alkalinity from granites. The study showed how the abrasion pH increased with increasing grinding time, which was associated with an increase in the concentration of cations such as K, Na, Ca and Mg (Grant 1969).

The initial work by Stevens and Carron (1948) demonstrated that minerals, which undergo isomorphous cation substitution have variable abrasion pH values (e.g., Mg and Fe substitution in biotite varied the abrasion pH between 8 and 9 for the Fe rich end member to pH 10 and 11 for the Mg end member). Minerals with fixed compositions had the same abrasion pH (e.g., abrasion pH of 6 for pyrophyllite). The abrasion pH was shown to be a useful test to distinguish between carbonate minerals, with pH 8 for calcite, pH 9–10 for dolomite and pH 10–11 for magnesium containing carbonates. In contrast, different end-member minerals of the plagioclase feldspar series did not have large enough pH differences to be distinguished.

Rinse, paste and NAGpH tests are commonly conducted on sulfidic wastes and ores and are part of static testing procedures to understand the propensity of samples to generate ARD (e.g. Price 2009). Rinse and paste pH measurements provide information on the current state of net acidity by measuring the pH in suspensions of crushed or pulverised rock and water (e.g. Sobek et al. 1978). NAGpH analyses provide a preliminary evaluation of the materials' future acid generation potential by oxidizing sulfides present in the powdered sample using hydrogen peroxide (Smart et al. 2002). The NAGpH method was developed primarily for the oxidation of sulfide minerals, but there is evidence for the dissolution of carbonate minerals due to the slightly acidic pH of $H_2O_2$ (Faimona et al. 2003).

In this chapter, we present a series of modified abrasion pH measurements to establish the propensity of different minerals to influence pH measurements during rinse and paste pH testing. Such data allow insights into weathering reactions of tailings and waste rocks and more informed interpretations of rinse and paste pH measurements during waste characterization. In addition, the corresponding NAGpH is presented for the minerals used in the modified abrasion pH testwork and plagioclase-rich Au ore samples. We note that the NAGpH of minerals containing carbonates result in unnaturally high pH values, which can underestimate the assesment of ARD risk.

## Methods

### *Samples*

Several mineral specimens (n = 22) were obtained from commercial suppliers for abrasion pH testwork, with the aim of selecting high purity monomineralic specimens where possible. Mineral specimens included carbonates (calcite, dolomite, malachite, azurite, siderite, magnesite), silicates (plagioclase, K-feldspar, olivine), sulfides (pyrite, pyrrhotite, chalcopyrite, sphalerite, arsenopyrite, galena), sulfates (celestine, gypsum, jarosite), and native sulfur.

Three run-of-mine samples from the Newcrest Mining Cadia Valley operation (33.28°S; 149.10°E) were also analysed. The ore is associated with a complex of quartz monzonite intrusive complexes, hosted by central stockworks and sheeted quartz-sulfide-carbonate vein systems. The Cadia East sample (CE-ROM) represents run-of-mine material, taken at the Cadia East underground mining operation. The Cadia Hill (CHOP-ROM1) and Ridgeway (RDW-ROM1) samples are run-of-mine waste materials taken at the Cadia Hill open pit and Ridgeway deposit.

The mineral specimens and bulk samples were characterized by QXRD using a Siemens D500 and D501 X-ray diffractometers at Federation University, Ballarat. Mineral phases were identified using computer-aided search/match of the 2010 ICDD PDF4/minerals subfile. SiroQuant™ (version 3.0) was applied to obtain semi-quantitative mineral abundances (wt%).

### *Modified Abrasion pH Method*

The modified abrasion pH method included: (1) the use of 0.01 M $CaCl_2$ solution; (2) an operationally defined grain size (<0.075 mm); and (3) high precision pH measurements using a Mettler Toledo S47 SevenMulti™ dual pH/conductivity meter. The pH and electrical conductivity (EC) of each mineral was measured by mixing 10 g of <0.075 mm fraction with 10 ml of 0.01 M $CaCl_2$ solution. The paste was stirred for 10 s and the pH recorded after 10 min. For background on the use of 0.01 M $CaCl_2$ in pH testwork for ARD evaluation, see Chap.11. We also present data for the NAGpH for each mineral specimen using the method of Smart et al. (2002).

The pH electrode was calibrated using a four-point calibration with buffer solutions (pH 2, 4, 7.0, 9.21), and the EC probe was calibrated using three conductivity solutions (500, 1413 and 12.88 μs $cm^{-1}$) at 25 °C. The pH and EC of 0.01 M $CaCl_2$ measured was 6.40 ± 0.04 and 1594 ± 16 μs $cm^{-1}$ (n = 10), respectively. Each mineral was measured in triplicate, and each replicate was measured three times giving a total of nine measurements per sample.

## Results and Discussion

### *Mineral Specimens*

We present modified abrasion pH values with the corresponding mineralogical composition according to XRD analyses. Only calcite, malachite, pyrite, chalcopyrite and sulfur were monomineralic specimens, while Iceland spar, galena and gypsum had a purity of >99 wt% (Table 1). The sulfide minerals investigated showed modified abrasion pH values that ranged from 3.86 (1σ ± 0.08) for pyrite to 8.04 (1σ ± 0.01) for sphalerite. Pyrrhotite and galena had pH values of 7.38 and 6.70, respectively, containing trace amounts of calcite ($\leq$ 1 wt%), while sphalerite contained 3.9 wt% calcite. Alkaline pH values were not limited to sulfides specimens containing carbonate minerals. Chalcopyrite (II) contained 2.7 wt% sphalerite and measured a higher modified abrasion pH of 6.56 compared to 4.22 for the pure chalcopyrite specimen. The arsenopyrite specimen contained 98 wt% arsenopyrite and minor amounts of quartz and traces of chalcopyrite, and a modified abrasion pH of 5.34 was measured. Overall, we expected the modified abrasion pH to decrease with increasing Fe content, since Fe in particular $Fe^{3+}$ is a strong oxidizing agent. This hypothesis could only be tested with the monomineralic specimens pyrite and chalcopyrite, where we observed a positive relationship between iron content and $H^+$ concentration (Table 2) (i.e. higher Fe content lower pH). The modified abrasion pH for sulfide minerals is largely controlled by the degree of oxidation at the time of measurement.

The calcite specimen tested had a modified abrasion pH of 8.33 (1σ ± 0.08), which was within error of the modified abrasion pH measured for Iceland spar. The offset between the modified abrasion pH and the theoretical value could be due to

**Table 1** Mineralogical composition of mineral specimens analyzed by QXRD

| Mineral | Mineralogical composition (wt%) |
|---|---|
| Calcite | 100 calcite |
| Iceland spar | 99.8 calcite, trace dolomite |
| Dolomite | 97.1 dolomite, 1.8 calcite, trace: apatite, quartz |
| Malachite | 100 malachite |
| Azurite | 97.3 azurite, 2.1 malachite, trace: quartz |
| Siderite | 85.6 siderite, 5.8 goethite, 4.4 hematite, 4.3 quartz |
| Magnesite | 87.3 magnesite, 12 dolomite, trace: quartz |
| Olivine | 78.9 forsterite, 18 enstatite, 3.1 clinopyroxene |
| Plagioclase | 82.6 albite, 16.1 muscovite, 1.3 chlorite |
| K-Feldspar | 84.9 microcline, 14.8 albite, trace: quartz, ankerite |
| Pyrite | 100 pyrite |
| Pyrrhotite | 95.7 pyrrhotite, 1.9 pyrite, 1.1 chalcopyrite, trace: calcite, quartz |
| Chalcopyrite | 100 chalcopyrite |
| Chalcopyrite II | 96.3 chalcopyrite, 2.7 sphalerite, trace: quartz, pyrite |
| Spalerite | 89.5 sphalerite, 4.4 magnetite, 3.9 calcite, trace: pyrite, quartz |
| Arsenopyrite | 98.7 arsenopyrite, 1.1 quartz, trace: chalcopyrite |
| Galena | 99.2 galena, trace: fluorite, sphalerite, calcite |
| Celestine | 97.1 celestite, 2 gypsum, trace: quartz, clay |
| Gypsum | 99.6 gypsum, trace: unidentified |
| Jarosite | 84.4 jarosite, 15.6 quartz |
| Native sulfur | 100 sulfur |

Trace components are $\leq 1$ %. The detection limit was 0.2 %

the consistently lower pH values measured using 0.01 M $CaCl_2$ as the extraction solution Noble et al. (2016). Dolomite could be distinguished from calcite by the higher modified abrasion pH of 8.87 ($1\sigma \pm 0.03$). The copper minerals azurite and malachite showed alkaline modified abrasion pH values of 6.93 ($1\sigma \pm 0.07$) and 7.71 ($1\sigma \pm 0.09$) respectively. The modified abrasion pH of siderite was 7.71 ($1\sigma \pm 0.02$), which is within error of the value for malachite. Stevens and Carron (1948) reported pH values for siderite as pH 5, 6 and 7, which likely reflects differences in trace mineral compositions.

The acid forming mineral jarosite yielded a modified abrasion pH value of $6.28 \pm 0.01$ (Table 2). The jarosite specimen was difficult to dissolve and behaved hydrophically in suspension with 0.01 M $CaCl_2$. The corresponding NAGpH of jarosite was acidic with a NAGpH of $3.1 \pm 0.01$ (Table 3), which is lower than the value of 4.12 observed when treated with $H_2O_2$ by Jennings et al. (2000) and higher than the paste pH value of <2.5 reported for jarosite-rich tailings by Hammarstrom et al. (2005).

NAGpH measurements were performed on minerals to provide baseline data for individual mineral pH values resulting from the interaction with hydrogen peroxide and heat treatment. In this study, the pH of the NAG solution was measured after the initial reaction with hydrogen peroxide (NAGpH (i)), prior to heat treatment, and finally after heating on the hot plate (85 °C) for 2 h (NAGpH (f)) (Table 3).

**Table 2** The median modified abrasion pH and EC (μs $cm^{-1}$) values for mineral specimens

| 0.01 M $CaCl_2$ | Median pH | IQR | Median EC (μs $cm^{-1}$) | IQR |
|---|---|---|---|---|
| *Sulfides* | | | | |
| Arsenopyrite | 5.34 | 0.06 | 1450 | 38 |
| Chalcopyrite | 4.22 | 0.08 | 1607 | 23 |
| Chalcopyrite II | 6.56 | 0.20 | 2100 | 40 |
| Galena | 6.70 | 0.03 | 1362 | 127 |
| Pyrite | 3.86 | 0.12 | 3390 | 60 |
| Pyrrhotite | 7.38 | 0.13 | 1773 | 80 |
| Spalerite | 8.04 | 0.01 | 1324 | 43 |
| *Carbonates* | | | | |
| Azurite | 6.93 | 0.07 | 1071 | 25 |
| Calcite | 8.33 | 0.08 | 940 | 22 |
| Dolomite | 8.87 | 0.03 | 1392 | 31 |
| Iceland spar | 8.43 | 0.07 | 947 | 21 |
| Magnesite | 9.32 | 0.01 | 1018 | 26 |
| Malachite | 7.71 | 0.09 | 1053 | 16 |
| Siderite | 7.80 | 0.02 | 1810 | 219 |
| *Sulfates* | | | | |
| Celestine | 7.92 | 0.03 | 2010 | 58 |
| Gypsum | 6.94 | 0.04 | 1674 | 29 |
| Jarosite | 6.28 | 0.02 | 4815 | 315 |
| *Silicates* | | | | |
| K-Feldspar | 9.26 | 0.04 | 971 | 10 |
| Plagioclase | 8.29 | 0.06 | 1170 | 22 |
| Olivine | 9.78 | 0.06 | 1077 | 60 |
| *Other* | | | | |
| Native sulfur | 7.29 | 0.08 | 519 | 117 |

*IQR* interquartile range on three replicates each measured three times

After heating on the hotplate for 2 h, the pH of calcite increased from NAGpH (i) 7.4 to NAGpH (f) 9.6. The increase in alkalinity above that observed for the abrasion pH of calcite (8.3) may be due to the formation of minor amounts of calcium oxide (pH 12.8). Carbonate disequilibrium caused by heating has also been suggested to result in highly alkaline NAGpH values observed during ABA (Charles et al. 2015). Therefore, NAGpH measurements of carbonate-rich samples may lead to artificially high pH values that do not reflect actual field conditions. Moreover, classification of carbonate-rich waste rocks and tailings using their NAGpH could lead to underestimation of their ARD risks and buffering capacity.

The very alkaline NAGpH results observed for calcite were not observed in other carbonate minerals in this study. In contrast, the intermediate and final NAGpH values were lower for Iceland Spar, malachite and magnesite compared to their respective modified abrasion pH values.

**Table 3** The average NAGpH of mineral specimens (n = 3)

| Mineral | NAGpH (i) | IQR | NAGpH (f) | IQR |
|---|---|---|---|---|
| Calcite | 7.4 | 0.01 | 9.6 | 0.01 |
| Iceland Spar | 7.3 | 0.00 | 7.5 | 0.00 |
| Malachite | 7.5 | 0.00 | 6.8 | 0.00 |
| Siderite | 8.1 | 0.09 | 7.8 | 0.03 |
| Magnesite | 7.4 | 0.00 | 8.0 | 0.27 |
| Pyrite | 1.7 | 0.03 | 1.6 | 0.05 |
| Chalcopyrite | 2.6 | 0.00 | 3.1 | 0.00 |
| Arsenopyrite | 1.9 | 0.02 | 1.8 | 0.01 |
| Galena | 4.0 | 0.06 | 4.5 | 0.97 |
| K-Feldspar | 5.8 | 0.00 | 5.9 | 0.00 |
| Plagioclase | 6.3 | 0.01 | 6.4 | 0.03 |
| Gypsum | 5.5 | 0.14 | 5.5 | 0.07 |
| Jarosite | 3.9 | 0.01 | 3.1 | 0.10 |

The intermediate NAGpH (NAGpH i) reflects the pH of the samples after reaching with 15 % hydrogen peroxide for 24 h, while the NAGpH final (NAGpH f) is the pH after heating the samples on a hotplate (85 °C) for 2 h, or until the reaction ceased
*IQR* interquartile range

## *Bulk Samples*

Mineralogical assessment of samples CE-ROM1, CHOP-ROM1 and RDW-ROM1 revealed a plagioclase-dominated matrix. Two distinct plagioclase varieties were identified in CE-ROM1. The gangue minerals included a sodic variety of plagioclase with a low albite structure and a more calcic plagioclase (labrodorite) and diverse minor and trace phases including pyrite and chalcopyrite (Table 4). CHOP-ROM1 consisted of major Na-plagioclase, orthoclase, quartz and calcite as well as minor pyrite and other minerals (Table 4). RDW-ROM1 consisted of quartz, Na-plagioclase, orthoclase, hornblende and calcite with trace amounts of pyrite and chalcopyrite (Table 4).

Alkaline modified abrasion pH values were measured for the plagioclase-rich ore samples CE-ROM1, CHOP-ROM1 and RDW-ROM1 (Table 5). Their modified

**Table 4** QXRD results for the <75 μm fraction of ore samples

| Mineral | Mineralogical composition (wt%) |
|---|---|
| CE-ROM1 | 21 labradorite, 20 albite, 14 quartz, 14 chlorite, 9 orthoclase, 7 actinolite, 7 calcite, 3 dolomite, 2 muscovite, 2 pyrite, trace: chalcopyrite, clinozoisite |
| CHOP-ROM1 | 39 Na-plagioclase, 28.6 orthoclase, 20 quartz, 5 calcite, 2 muscovite, 2 pyrite, 1 chlorite, 1 magnetite, trace: kaolinite, dolomite |
| RDW-ROM1 | 29 Na-plagioclase, 23 quartz, 19 orthoclase, 8 hornblende, 6 calcite, 4 muscovite, 2 chlorite, 2 dolomite, 2 epidote, 1 chalcopyrite, trace: pyrite, chalcopyrite |

**Table 5** The median modified abrasion pH and NAGpH of plagioclase-rich bulk samples (n = 3)

| Sample | Modified abrasion pH | IQR | NAGpH | IQR |
|---|---|---|---|---|
| CE-ROM1 | 8.2 | 0.00 | 10.9 | 0.0 |
| CHOP-ROM1 | 8.3 | 0.01 | 8.9 | 0.8 |
| RDW-ROM1 | 8.3 | 0.00 | 8.7 | 0.2 |

Each replicate was measured in triplicate (*IQR* inter quartile range)

abrasion pH values are most similar the modified abrasion pH of calcite and plagioclase (pH 8.3, respectively) (Table 2). Higher NAGpH values were measured for CHOP-ROM1 and RDW-ROM1, but most significantly for CE-ROM1 where a NAGpH of 10.9 was observed (Table 5). Note that CE-ROM1 has the highest proportion of carbonate of all three samples. These pH results provide a preliminarily assessment of the basic nature of CE-ROM1, CHOP-ROM1 and RDW-ROM1 when exposed to weathering. The inconsistency in NAGpH values between the samples has been observed in other samples, where replicates diverged significantly or in the case of the NAGpH results of Iceland spar and calcite. Differential heating on the hotplate is suspected, where some samples are heated more than others, or the differences in the crystallization history or trace metal content of the minerals present. The heating step in the NAGpH method (Smart et al. 2002) is also sample depended, and stipulates that heating should continue until effervescence stops. So samples with an abundance of carbonates, which react strongly with hydrogen peroxide, are often heated for longer.

## Conclusions

The abrasion pH was originally presented as a field based test by Stevens and Carron (1948) to assess the acidic or basic nature of minerals. The abrasion pH was foremost used to test for secondary minerals released during weathering, particularly sulfate salts. The original methodology has been adapted in this work. The protocol for the modified abrasion pH is as follows:

- Pulverised materials are sieved to <75 μm
- A 10 g subsample of the <75 μm material is weighed out into a small (e.g. 50 ml) glass beaker
- 10 ml of 0.01 M $CaCl_2$ solution is added to the 10 g subsample and mixed into a paste
- The pH of the paste is measured after 10 min

The modified abrasion pH is controlled by the mineralogy of the sample and the degree of weathering (i.e. presence of soluble salts). Mineralogical characterization by QXRD and modified abrasion pH data has been presented for twenty different mineral specimens, including carbonates, silicates, sulfides and sulfates. In this

sample suite, only calcite, malachite, chalcopyrite and sulfur where monomineralic. The modified abrasion pH of the: (i) carbonates ranged from 6.9 for azurite to 9.2 for magnesite; (ii) silicates ranged from 8.3 for plagioclase to 9.8 for olivine; and (iii) silicates ranged from 3.7 for pyrite to 8.0 for sphalerite (containing trace calcite).

Three ore samples from the Cadia Valley deposit were also tested. These bulk samples showed a modified abrasion pH of 8.2 to 8.3 and have gangue mineralogy dominated by plagioclase. Given that the abrasion pH of plagioclase and calcite mineral specimens were the same, some knowledge of the mineralogy plus abrasion pH data can provide a first pass assessment of the chemical characteristics of bulk samples.

The NAGpH of monomineralic and polymineralic specimens was also measured. In addition, the intermediate pH was measured after reacting with hydrogen peroxide and prior to heating on the hotplate. Significant differences were observed for calcite where the intermediate pH measured was 7.4 compared to the final NAGpH of 9.6. A similar observation was made for CE-ROM1, where a NAGpH value of 10.9 was measured. The inconsistencies in NAGpH values observed in this study highlight the need for caution when interpreting NAGpH values. Classification schemes to domain samples using NAGpH values for carbonate-rich waste rocks could lead to underestimation of their ARD risks and buffering capacity. Consequently, results of this study highlight the need for caution when interpreting NAGpH values of bulk samples containing carbonate minerals.

## References

Charles J, Barnes A, Declercq J, Warrender R, Brough C, Bowell R (2015) Difficulties of interpretation of NAG test results on net neutralizing mine: initial observations of elevated pH conditions and theory of $CO_2$ disequilibrium. In: Proceedings of the 10th international conference on acid rock drainage and IMWA annual conference, 21–24 April 2015, Santiago, Chile, pp 1–10

Faimona J, Stelcl J, Kubesova S, Zimak J (2003) Environmentally acceptable effect of hydrogen peroxide on cave "lamp-flora", calcite speleothems and limestones. Environ Poll 122:417–422

Grant WG (1969) Abrasion pH, an index of chemical weathering. Clays Clay Miner 17:151–155

Hammarstrom JM, Seal RR II, Meier AL, Kornfeld JM (2005) Secondary sulphate minerals associated with acid drainage in the eastern US: recycling of metals and acidity in surficial environments. Chem Geol 215:407–431

Jennings SR, Dollhop JD, Inskeep WP (2000) Acid production from sulfide minerals using hydrogen peroxide weathering. Appl Geochem 15:235–243

Jerz JK, Rimstidt JD (2003) Efflorescent iron sulfate minerals: Paragenesis, relative stability, and environmental impact. Am Mineral 88:1919–1932

Lottermoser BG (2010) Mine wastes: characterization, treatment and environmental impacts, 3rd edn. Springer, Berlin

Noble TL, Parbhakar-Fox A, Lottermoser BG (2016) pH Testing Methods for Sulfidic Mine Wastes. In: Lottermoser B (ed) Environmental Indicators in Metal Mining, Springer, Switzerland. doi:10.1007/978-3-319-42731-7_11

Price WA (2009) Prediction manual for drainage chemistry from sulphidic geologic materials. CANMET Mining and Mineral Sciences Laboratories, Canada

Smart R, Skinner B, Levay G, Gerson A, Thomas J, Sobieraj H, Schumann R, Weisener C, Weber P, Miller S, Stewart W (2002) ARD test handbook. AMIRA P387A, prediction and kinetic control of acid mine drainage. AMIRA International Ltd, Melbourne

Stevens RE, Carron MK (1948) Simple field test for distinguishing minerals by abrasion pH. Am Mineral 33:31–50

# Prediction of Leachate Quality for a Gossan Dump, Angostura, Spain

**Anita Parbhakar-Fox, Julie Hunt, Bernd Lottermoser, Eleanor M. van Veen and Nathan Fox**

**Abstract** The Iberian Pyrite Belt (IPB) is one of the largest of the world's massive sulfide provinces. Since the Chalcolithic era, gossans formed from massive sulfide mineralization have been worked for copper, silver and gold. Consequently many historical mine sites have abandoned dumps of gossanous material. One such example is located at Angostura, a historical copper mine which operated from 1906 to 1931. The aims of this study are to determine the mineralogical hosts of environmentally significant elements (As, Ba, Bi, Co, Cu, Hg, Mo, Sb, Se, Ni, Pb, Zn) in gossanous waste rocks dumped adjacent to the Angostura open cut, using geochemical, optical, SEM-MLA and laser ablation techniques. Our findings demonstrate that the gossan materials are enriched in environmentally significant elements with several hosted by iron oxides and iron-oxyhydroxides. Leaching of these gossan materials was performed using three extractants to represent different conditions which may be experienced in a surficial environment (i.e., deionized water, hydrogen peroxide and sulfuric acid). Results from these experiments indicated that under ambient surface conditions all analyzed elements will not be

A. Parbhakar-Fox (✉) · N. Fox
School of Physical Sciences, University of Tasmania, Private Bag 79, Hobart, TAS 7001, Australia
e-mail: Anita.Parbhakar@utas.edu.au

N. Fox
e-mail: Nathan.Fox@utas.edu.au

J. Hunt
GeMMe, University of Liege, Sart Tilman B52, 4000 Liege, Belgium
e-mail: jahunt@ulg.ac.be

B. Lottermoser
Institute of Mineral Resources Engineering, RWTH Aachen University, Wüllnerstrasse 2, 52062 Aachen, Germany
e-mail: lottermoser@mre.rwth-aachen.de

E.M. van Veen
Camborne School of Mines, Environment and Sustainability Institute, University of Exeter, Penryn Campus, Penryn, Cornwall TR10 9FE, UK
e-mail: E.M.Van-Veen@exeter.ac.uk



B. Lottermoser (ed.), *Environmental Indicators in Metal Mining*,
DOI 10.1007/978-3-319-42731-7_13

released from their goethite and hematite hosts. However, under ARD conditions, elements such Co, Cu, Pb and Zn will be mobilized.

## Introduction

The Iberian Pyrite Belt (IPB) is one of the world's largest massive sulfide provinces with a total estimated tonnage of 1600 Mt of massive sulfides, and approximately 250 Mt in the underlying sub-economic stockwork (Tornos 2006). It has been continuously explored and mined since prehistoric times resulting in more than 80 mines across Spain and Portugal, including the large Rio Tinto and Neves Corvo deposits (e.g. Leistel et al. 1998; Sáez et al. 2003; Nocete et al. 2005; Pérez-López et al. 2011). Associated with these deposits are gossans (typically up to 70 m thick; Núñez et al. 1987), which formed as a result of supergene oxidation of such massive sulfide deposits (Velaso et al. 2013; Fig. 1). In the IPB, gossanous rocks are characterized by a high content of hematite, amorphous and poorly crystalline Fe oxyhydroxides, goethite and quartz (Romero et al. 2006; Velaso et al. 2013). In addition, metals such as Co, Cu, Ni, Pb and Zn were released into solution at high concentrations during supergene oxidation (Thornber and Wildman 1984). Gossan minerals such as goethite and hematite are typically insoluble, a useful property when undertaking exploration studies (Andrew 2000; Wilhelm and Kosakevitch 1979 *in* Velaso et al. 2013). However, they may contain elevated concentrations of several environmentally significant elements typically associated with massive sulfide deposits (e.g., As, Ag, Pb, Bi, Cd, Sn, Zn) (cf. Thornber and Wildman 1984; Taylor et al. 1995; Atapour and Aftabi 2007; Fakih et al. 2009). Therefore, when gossan materials are dumped at the surface, they represent potential point sources of these elements, with García Palomero et al. (1986) and Craddock et al. (1987) reporting elevated As, Sb, Cu, Ag, Pb, Bi, Au, Sn and Hg (±Mo, Co) in such materials.


**Fig. 1** Examples of gossans observed in the Iberian Pyrite Belt (IPB), Spain with iron-oxide (*red-brown colour*) rich gossans observed in the upper benches; **a** Rio Tinto mine; **b** Tharsis mine (Color figure online)

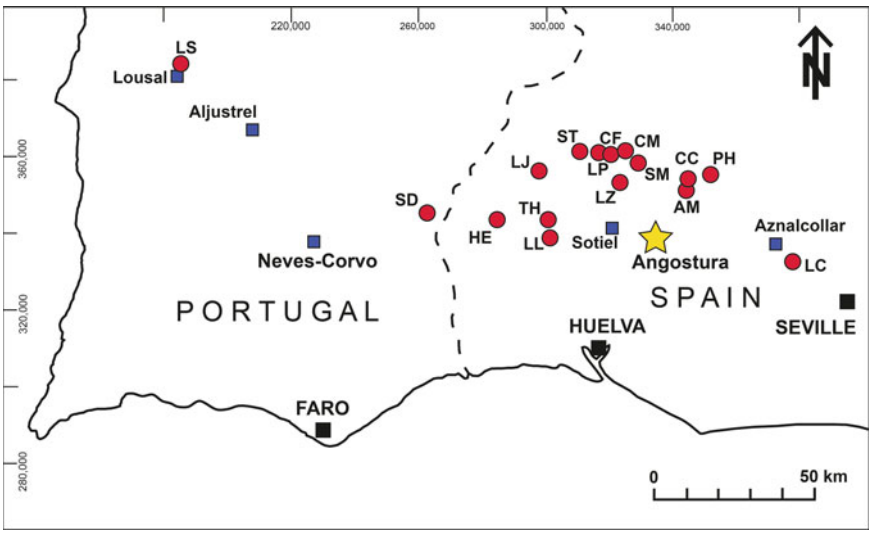


**Fig. 2** Location map of the main massive sulfide occurrences and deposits in the Iberian Pyrite Belt (*blue squares*), with Angostura shown. The main gossans outcrops/deposits are shown as red circles as follows: *AM* Alto de la Mesa (Rio Tinto); *CM* Cueva de la Mora; *CC* Cerro Colorado (Rio Tinto); *CF* Confesionarios; *HE* Herrerías; *LC* Las Cruces; *LS* Lagoa-Salgada; *LJ* La Joya; *LL* La Lapilla; *LP* Lomero-Poyatos; *LZ* La Zarza; *PH* Peñadel Hierro; *TH* Tharsis (Filón Norte); *SD* Sao Domingos; *SM* San Miguel; *ST* San Telmo (modified after Velaso et al. 2013) (Color figure online)

Considering the number of gossan outcrops and dumps in the IPB (Fig. 2), an understanding of the leach characteristics of these materials is required to determine whether they are potentially hazardous materials posing environmental risks to downstream ecosystems. To study this, materials from the Angostura gossan dump were collected and subjected to a series of geochemical leach tests designed to replicate surficial conditions which may be experienced by such materials. The aim of this study was to determine whether these gossan materials release environmentally significant trace elements (i.e. As, Ba, Bi, Co, Cu, Hg, Mo, Sb, Se, Ni, Pb, Zn) into pore and surface waters.

## Geological Setting and Site Description

The massive sulfides of the Iberian Pyrite belt occur in the Volcano-Sedimentary Complex (VSC) with ages of 350 Ma (i.e., close to the Devonian-Carboniferous transition; *in* Velaso et al. 2013). The VSC is up to 1300 m in thickness and comprises volcanic and volcaniclastic rocks ranging from basalt to rhyolite composition, interbedded with epiclastic and chemical sedimentary rocks, and abundant shales (Tornos 2006). The massive sulfides occur within the VSC as

stratiform bodies hosted by shale interbedded with felsic volcanic rocks (Tornos et al. 2002). The orebodies occur as large lenses with an extensive underlying stockwork mainly composed of pyrite with lesser amounts of sphalerite, chalcopyrite, and galena (Tornos 2006; Velaso et al. 2013). The Angostura mine (37° 46′02.50″N; 6°42′50.90″W) is situated approximately 80 km north east of Seville (Fig. 2).

Angostura experiences a Mediterranean climate with an annual temperature range of 6–33 °C, and rainfall range of 0.8–108 mm (World Weather Online 2016). It was operated by Esperanza Copper and Sulfur Ltd from 1906 to 1931. It was mined as both an open pit and underground operation which in conjunction with the historical Esperanza Mine (located 3 km to the east), produced a total of 1.84 Mt at 1.55 % Cu (Cadillac Ventures 2016). Cadillac Ventures (2016) estimate grades of 1.6 g/t Au and 5 g/t Ag in these gossan materials. The site comprises the open cut, with the gossan dump located to the west (Fig. 3a, b). The gossan dump dimensions are approximately 30 × 80 × 20 m. The gossan dump surface has no apparent lithological zonation. The dump surface comprises of deep-red iron-oxide fragments (ranging from sub-cm to dm-scale; Fig. 3c, d), with some patchy vegetation. Run-off from the dump collected to the west (Fig. 3e), where some evidence of acid rock drainage (ARD) is observed (e.g., jarosite staining), but is likely sourced from the overflowing open pit and other waste rock materials present at the site.

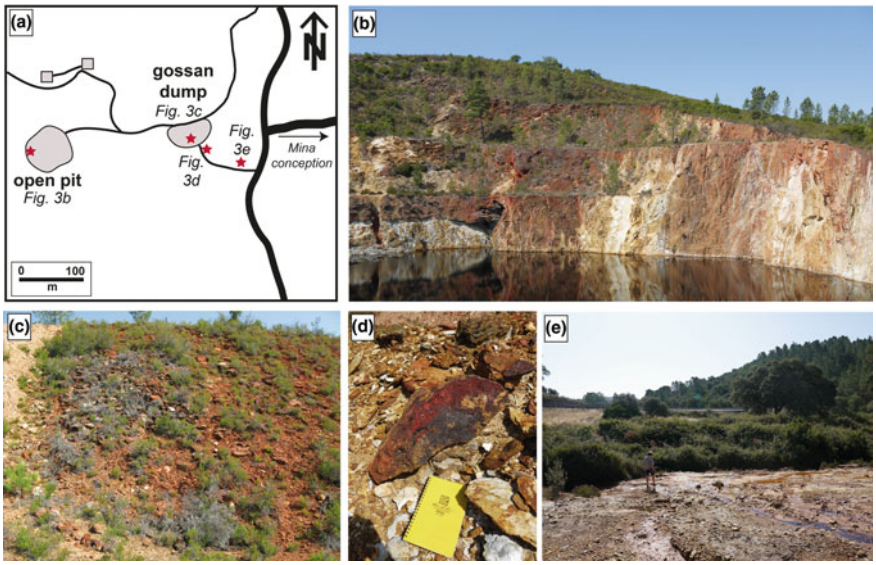


**Fig. 3** The Angostura mine site: **a** sketch map of site features; **b** view of the open pit; **c** the surface of the sampled gossan dump (*red-brown*) partially vegetated; **d** deep red oxidised gossan boulder at the foot of the dump; **e** run-off from the dump, with pH < 4 measured, and minerals indicative of ARD (jarosite and copper sulfates) also observed (Color figure online)

## Materials and Methods

### *Sampling and Sample Preparation*

Fieldwork was conducted in June 2014, with the collection of gossan samples for mineralogical and geochemical characterization. Samples of waste rock materials were representative rock chip composites (n = 12) taken from waste repositories faces, and constituted several kilograms. Composite materials collected at the base of the gossan dump were termed sample AG01, with sample numbers incrementally increasing with height (i.e., sample AG12 is the uppermost composite sample). In addition, a selection of corresponding grab samples (prefix AGS; n = 13) were collected for mineralogical analysis. Samples were dried at room temperature, and composite samples were crushed with a jaw crusher and ground with a chrome-steel ring mill.

### *Mineralogical Characterization*

Sawn pieces from grab samples and particulate material from the chip samples were mounted in resin for mineralogical analyses. Analyses included X-ray diffraction (XRD), reflected light microscopy, scanning electron microscope-mineral liberation analysis (SEM-MLA) and laser-ablation-inductively coupled plasma mass spectrometry (LA-ICPMS).

#### X-Ray Diffractometry (XRD)

XRD analyses of chip samples were performed at Federation University, Australia, on micronized sample splits, with a Panalytical XPert Powder Diffractometer, using CoKα radiation and a graphite monochromator. Operating conditions were 40 kV/30 mA, step scan 0.02θ at 1o/2 θ/min, 1o divergence and receiving slits and a 0.15° scatter slit. Scan range was 5° to 76° 2Θ. Phases were identified by computer aided search/match of the ICDD PDF4 2014 Minerals Database. Quantitative results were determined using SiroQuant© (a whole pattern Rietveld technique) version 3.1, with refinement of the most suitable structures for each phase present conducted.

#### Reflected Light Microscopy

Reflected light images for whole grain mounts (n = 17) representative of both composite and grab samples were collected using a Leica DM6000 automated microscope at the University of Tasmania (UTAS). The microscope has a high

precision stage (position reproducibility better than 1 μm) which allows direct tiling of frames. The samples were photographed with a 5 × objective lens, as this provided the best balance between resolution and field of view. The automated microscope was driven by Leica Q-WIN © software under constant lighting and temperature conditions to achieve the best image results. All images were adjusted for colour balance and shading corrections. Once collection of each frame was complete, images were stitched together using the LeicaQ gallery function.

### Scanning Electron Microscopy

Scanning electron microscopy (SEM) was performed using an FEI Quanta 600 environmental scanning electron microscope (ESEM) at the Central Science Laboratory, UTAS. These analyses were performed to allow for observations of gossan minerals and their textures. In addition, these samples were analyzed using a Hitachi SU-70 field emission SEM, with data collected and processed data using Oxford software. This instrument allows for high resolution imaging, allow for the observation of μm-scale inclusions. Additionally, this instrument permits element X-ray mapping. The objective of using this instrument was to determine the location of As and Sb in iron-oxide phases prior to LA-ICPMS analyses.

### Laser Ablation ICPMS

LA-ICPMS analysis was performed on polished mounts (n = 13) using a Resonetics Resolution 193 nm Excimer Laser Ablation system coupled with an Agilent 7700 s ICP-MS at UTAS. Both spots and lines were measured. A beam diameter of 22 μm was used for ablation of lines, with an ablation depth of ~1–2 μm. Lines were ablated with a repetition rate of 10 Hz, moving horizontally at 10 μm/s for 50 s giving a line length of ~500 μm. Laser energy was 50 mJ; fluence of 3.5 J/cm$^2$ for lines and 35 mJ; fluence of 3.0 J/cm$^2$ for spots. Beam diameter for spots was 33 μm, with a frequency of 5 Hz and dwell time on all masses of 10 ms. Laser energy was 50 mJ; fluence of 3.5 J/cm$^2$. Ablation was performed in an ultra-high purity He atmosphere, and the resulting aerosol was mixed with an Ar carrier gas before introduction to the ICP-MS. Data was collected over 50 s intervals with a 20 s pre-ablation acquisition (background) interval and 30 s ablation of the samples. The calibration standards GSD-1G and STDGL2b-2 were used (Danyushevsky et al. 2011). GSD-1G is a synthetic basaltic glass with nominal trace element contents of approximately 30 ppm and is available for purchase from the USGS. STDGL2b-2 is a lithium-borate fused disc of ore concentrate powder doped with certified element solutions. It was used to calculate contents and correct for instrument drift. Analyses were corrected for linear drift and data reduction was undertaken following the methodology developed by Longerich et al. (1996).

## *Geochemical Testwork*

### Bulk Geochemistry

To determine the bulk geochemistry of these materials, homogenized powders from the composite samples (n = 12) were analysed for 48 elements. A four-acid-digest was used followed by inductively coupled plasma atomic emission spectrometry (ICP-AES) and inductively coupled plasma mass spectrometry (ICP-MS; procedure ME-MS61) at Australian Laboratory Services (ALS), Loughrea, Ireland. Replicate analyses of a sample and the Certified Reference Material (CRM) NIST 2710a (Montana soil I) were included. Replicate determinations, including those for Au, agreed to within 5 % (10 % for Ba) for the samples. Replicate determinations agreed to within 5 % (10 % for Ni) for the CRM. Elemental recoveries for the CRM were in the range 95–105 % (90–110 % for Cd, Co and V and 85–115 % for Ni). In addition, these samples were also analysed for total Hg and 1 M HCl extractable Hg at ALS, Brisbane, Australia (procedures EG035T and EG035-SDH).

### Total Sulfur

Rapid and accurate measurement of sulfur (wt%) for calculation of maximum potential acidity (MPA) was performed on all composite samples using an Eltra C-S 2000 instrument at UTAS. Analysis requires the use of two accelerants (tungsten and iron) which were carefully weighed into a crucible, with a measure (ca. 200 mg) of powdered (<63 μm) sample added. Individual crucibles were placed onto the instrument stage, loaded into the machine, and heated to >800 ºC. The instrument was regularly calibrated (i.e., once after every 10 samples analysed) using two calibration materials provided by the instrument supplier (calcium carbonate and barium sulfate). As a further measure, two ore standards (purchased from Choice Analytical) were also run in addition to sample blanks (i.e., before instrument calibration).

### Paste pH Leach

The ASTM D4972-01(2007) paste pH method was used in this study. This test measures pH in a 0.01 M $CaCl_2$ solution at a 1:1 solid to solution ratio. 10 g of homogenised powdered from each of the composite samples (n = 12) was tested. The pH value of each sample (n = 12) was measured in triplicate, with the standard deviation calculated as <0.3. Following the pH measurement, the supernatants were filtered through a 0.45 μm Millipore filter, acidified with 1 % $HNO_3$ and submitted to ALS for ICP-MS analyses (procedure EG005c) to determine the concentrations of metals in the water soluble fraction.

### Hydrogen Peroxide ($H_2O_2$) Leach

Oxidation of organic matter and sulfides occurs on the addition of $H_2O_2$ (Tessier et al. 1979). Considering this, multi-addition net acid generation (mNAG) tests were performed to determine which elements will leach on oxidation of any remnant sulfides in these gossan materials following the procedure of Smart et al. (2002). Essentially, the mNAG test procedure involves the stepped addition of 15 % $H_2O_2$ in three increments (100 ml, 100 ml and 50 ml) to allow for more time for sulfide oxidation. The pH was measured as 4.5. Powders (<63 μm) from all composite gossan samples (n = 12) were tested. Appropriate sample duplicates were used during the analysis, with standard deviation calculated as <0.3. After the pH was measured, the samples were filtered through a 0.45 μm Millipore filter and sent to ALS for ICP-MS analyses (procedure EG005c).

### Sulfuric Acid ($H_2SO_4$) Leach

In order to determine which metals may leach under ARD conditions, a sulfuric acid leach test was conducted. In this procedure, pH 2.5 was maintained to replicate such an ARD environment. The synthetic leach precipitation procedure (SPLP) was adapted and performed at ALS. In this experiment, 400 ml of $H_2SO_4$ was added to 20 g of homogenized powdered samples (n = 12), and tumbled for 18 h. This solution was then left to settle for 2 h, filtered through a 0.6 μm glass filter and analyzed by ICP-MS (procedure EG005c).

## Results and Discussion

### *Bulk Mineralogy*

The gossanous waste dump material is largely composed of goethite (avg. 46 %) and quartz (avg. 44 %) with lesser hematite, barite and mica, and minor gypsum, feldspar and pyrite (Table 1). Jarosite is rare in contrast to other gossans in the IPB (cf. Velaso et al. 2013; Yesares et al. 2014). Furthermore, there does not appear to be any vertical stratification of the mineralogy, however, in general, chlorite and muscovite content decreased with elevation. In terms of the three gossan zones identified by Velaso et al. (2013), these gossan materials appear to be characteristic of the upper zone, which is characterized by hematite and quartz, with an absence of jarosite. Minor pyrite was detected, indicating that these gossan materials are extremely mature (i.e., well weathered).

**Table 1** Summary of bulk mineralogy (%) for composite gossan samples as measured by XRD

| | Goethite | Quartz | Hematite | Barite | Chlorite | Muscovite | Albite | Gypsum | Pyrite | Jarosite |
|---|---|---|---|---|---|---|---|---|---|---|
| 1 | 33.4 | 35.2 | 7.9 | 7 | 5.8 | 10.1 | 0 | 0.4 | 0 | 0 |
| 2 | 37.1 | 58.6 | 1.6 | 1.3 | 0.6 | 0 | 0.2 | 0.5 | 0 | 0 |
| 3 | 48.7 | 46.5 | 3 | 0.3 | 0.3 | 0.6 | 0 | 0.6 | 0 | 0 |
| 4 | 56.4 | 31.5 | 7.4 | 3.3 | 0.2 | 0.5 | 0 | 0.6 | 0.1 | 0 |
| 5 | 44.5 | 44 | 2.3 | 3.8 | 1.6 | 3 | 0 | 0.8 | 0 | 0 |
| 6 | 45.4 | 47 | 3.3 | 1.7 | 1 | 1 | 0 | 0.5 | 0.1 | 0 |
| 7 | 60.3 | 27.7 | 9.3 | 1.5 | 0.1 | 0.5 | 0 | 0.4 | 0.2 | 0 |
| 8 | 29.6 | 66.5 | 2.3 | 0.1 | 0.2 | 0.2 | 0.3 | 0.8 | 0 | 0 |
| 9 | 33.1 | 58.6 | 4.4 | 2.4 | 0.5 | 0.3 | 0 | 0.7 | 0 | 0 |
| 10 | 49.6 | 44.4 | 4.1 | 0.5 | 0.2 | 0.6 | 0 | 0.6 | 0 | 0 |
| 11 | 52.3 | 37.9 | 3.7 | 4.9 | 0.5 | 0.4 | 0 | 0.3 | 0 | 0 |
| 12 | 56.7 | 35.8 | 5 | 0.5 | 0.3 | 1.1 | 0 | 0.4 | 0 | 0.1 |
| Avg | 45.6 | 44.5 | 4.5 | 2.3 | 0.9 | 1.5 | 0 | 0.6 | 0 | 0 |

## *Gossan Textures*

Petrographic observations of the gossan grab samples confirm the predominance of goethite, with a range of textures observed (Figs. 4 and 5) including massive, boxwork, banded, bladed, frothy and dull forms, which are locally intergrown with hematite. Varying thicknesses of goethite are observed, with coarse to fine aggregates seen (Fig. 5), indicating different stages of redissolution, transformation and loss of volume during alteration (Velaso et al. 2013). Colloform goethite textures were observed that fell into two sub-textural types. For example, in Fig. 5b, c, goethite appears to overgrow quartz, leaving it with a serrated texture, with minor barite inclusions seen. However, in Fig. 5i, r goethite is interlayered with hematite, which also forms in the interstitia between each nodule (Fig. 4o). Typically, these spherical, botryoidal textures precipitate from highly supersaturated fluids (Velaso et al. 2013). Occasionally, anhedral patchy goethite was rimmed by bernalite ($FeOH_3$) (Fig. 4f).

Hematite was prevalent in two samples (AGS 04, Fig. 4j–l; AGS 11, Fig. 5j–l), where it appeared to be undergoing dissolution, with a porous, spongy texture demonstrated. Barite was identified in all samples, and showed a range of textural forms including vein, anhedral and patchy textures (Figs. 4, 5). Muscovite was observed in voids adjacent to goethite (Fig. 4r). Quartz is present either as microcrystalline (Fig. 4h) or larger primary grains (Fig. 5c).

## *Primary Sulfide Mineralogy*

One grab sample (AGS10) is dominated by pyrite (Fig. 6). The texture can be described as massive, with large pyrite grains appearing heavily fractured with iron oxides precipitated in fractures and rims. The grain size was non-uniform; however, the general morphology exhibited by all grains is subhedral-anhedral. These grains are associated with quartz, with no other primary minerals identified. Such primary sulfide mineralogy is typical of IPB deposits (Tornos 2006; Velaso et al. 2013; Yesares et al. 2014).

The trace element chemistry of pyrite grains in this sample was measured (n = 17, Fig. 7) to provide an indication of the leach fluids potentially encountered by these gossan materials since dump establishment. The content of environmentally significant elements is generally low, with Co and As dominating (averages: 90 and 10 ppm, respectively). The distribution of these elements appears lattice-bound; however, the concentrations with depth are non-uniform, indicating a spatially zoned distribution (i.e., reflecting compositional fluctuations in the ore forming fluids). Locally, high concentrations of both Pb and Zn were measured (480 and 165 ppm respectively; Fig. 7). Both appear present as inclusions within pyrite (Fig. 8), therefore, these elements may represent as minor inclusions of sphalerite and galena within pyrite, which is not uncommon for such deposits.

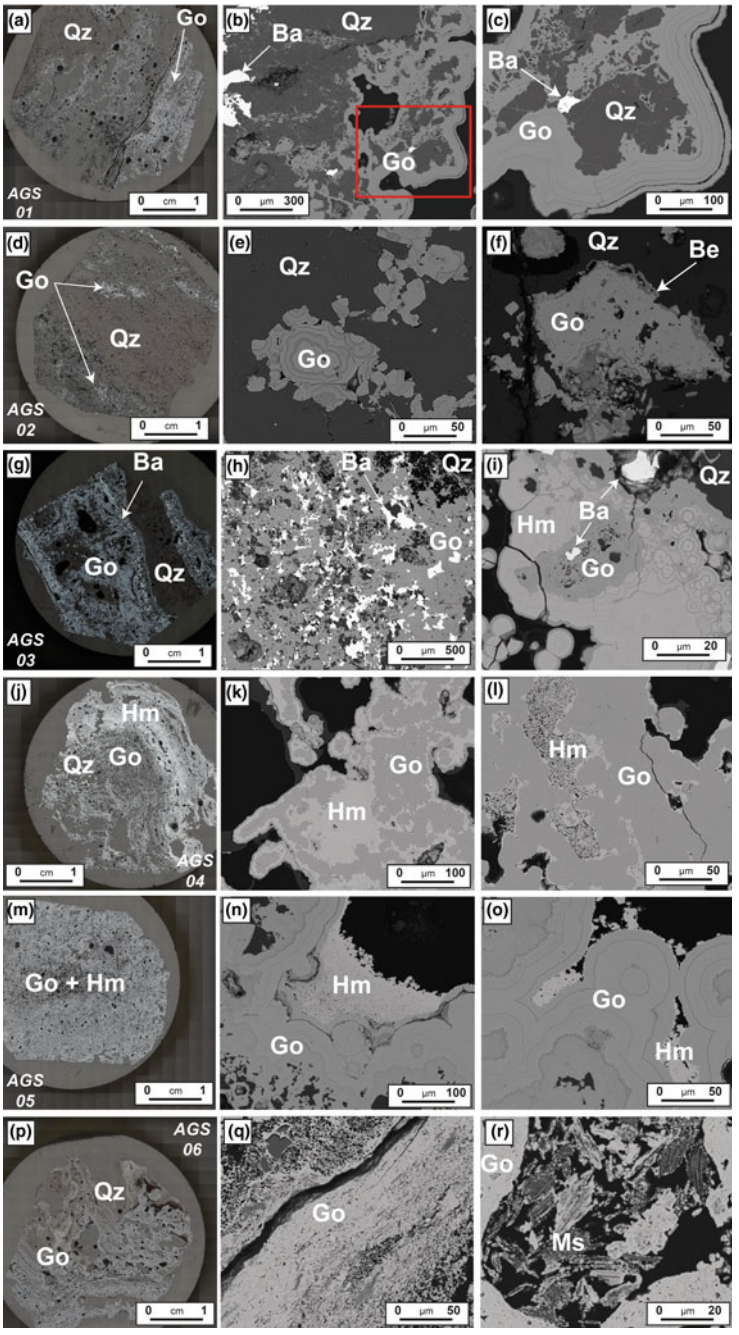


**Fig. 4** Reflected light (*left*) and back scattered electron (BSE) images (*centre* and *right*) of gossan grab samples AGS 01 to AGS 06. *Ba* barite; *Be* bernalite; *Hm* hematite; *Go* goethite, *Ms* muscovite, *Qz* quartz

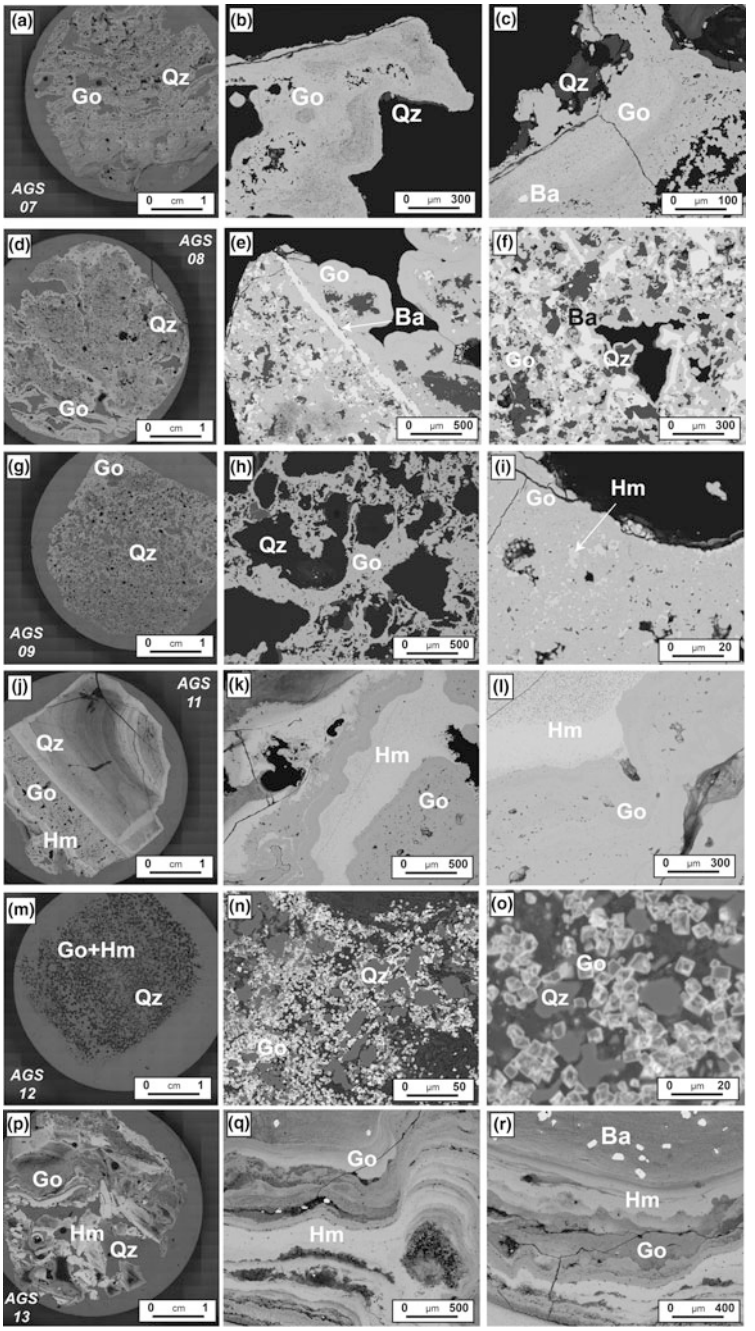


**Fig. 5** Reflected light (*left*) and back scattered electron (BSE) images (*centre* and *right*) of gossan grab samples AGS 07 to AGS 09, 11 to 13. *Ba* barite; *Be* bernalite; *Hm* hematite; *Go* goethite, *Ms* muscovite, *Qz* quartz

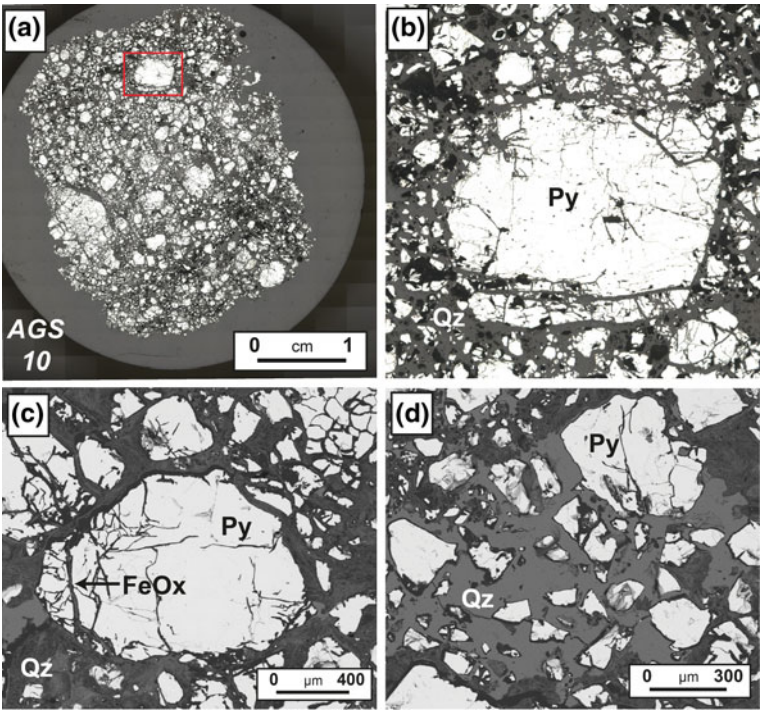


**Fig. 6** Example of primary sulfide mineralogy at Angostura (AGS 10): **a**, **b** reflected light; **c**, **d** back scattered electron images. *FeOx* iron oxide, *Py* pyrite, *Qz* quartz

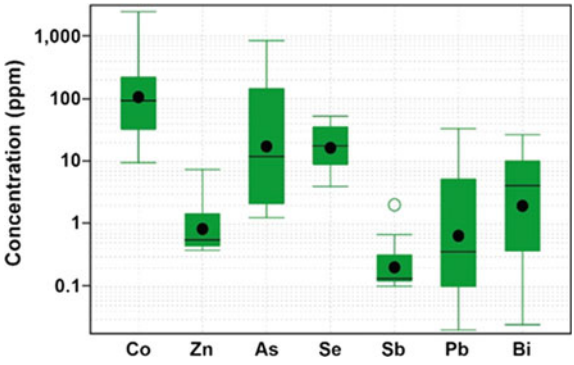


**Fig. 7** Tukey box plot showing pyrite chemistry (measured in AGS 10) with select environmentally significant elements shown (n = 17). NB. The *box* covers the interquartile range, the *line* is the median and the circle the mean. The *whiskers* are drawn at the threshold to identify near and far outliers based on the Tukey statistic

Selenium and Bi were measured (maximum: 40 and 30 ppm, respectively), potentially indicating the presence of precious metals (e.g., Ag and Au) as in gossans selenides and bismuthides have been reported as their hosts (Andreu et al. 2015).

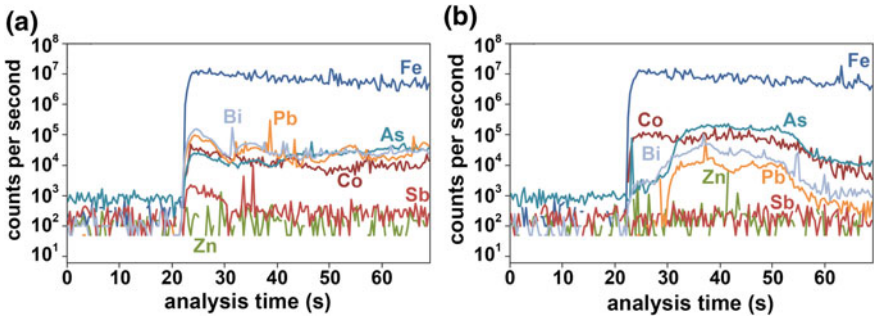


**Fig. 8** LA-ICPMS traces from pyrite in Angostura gossan material, showing clean intervals (*left hand side*) and inclusion-rich or bulk intervals (*right hand side*) (color figure online)

## *Leaching Characteristics*

Total sulfur is low across the gossan face, indicating that very little primary sulfide remains in the pile, therefore, acidic conditions (arising as a consequence of sulfide oxidation) are unlikely to be experienced at the gossan pile. Results from the various leaching experiments compared to the whole rock geochemical data are shown in Fig. 9 and summarised in Table 2. Arsenic is significantly elevated in these materials, with an average content of approximately 1320 ppm, and showed a consistent content across the gossan face (Fig. 9). Such an elevated As signature is typical of gossan materials formed in association with IPB massive sulfide deposits (e.g., Pérez-López et al. 2011). Arsenic was not extracted under the three leach conditions, with concentrations below the WHO (2008) drinking water guideline (DWG) value.

Under these pH conditions, As present in goethite (Fig. 10) is strongly adsorbed to goethite (Fig. 11). Similarly, high Sb was consistently measured between the samples in the total digestion (average 130 ppm), but was not extracted in the leach experiments. Typically, Sb is strongly sorbed and co-precipitates with goethite (Watkins et al. 2006; Ritchie et al. 2013) as observed in these samples (Fig. 10). Like As, Sb is pervasively distributed in goethite (Fig. 11). Both will leach under alkaline pH values (Mamindy-Pajany et al. 2009; Ritchie et al. 2013). Therefore, under current site conditions, both are likely to remain contained within these gossan materials.

Cobalt, Cd and Ni are typically low in these materials (Fig. 9; Table 2) in contrast with other gossans (cf. Atapour and Aftabi 2007). Cobalt appears to be hosted in goethite (Figs. 10, 11 and 12), however, element distribution maps show a low content of Cd and Ni in goethite, potentially suggesting their hosting in other iron oxide phases (e.g., hematite). The distribution of cobalt among iron phases is controlled by pH and temperature (Pivovarov 2001; Beukes et al. 2000). Consequently, concentrations in all leach experiments for Co, Cd and Ni were below WHO (2008) DWGs. Whilst Cu values may appear relatively high (average

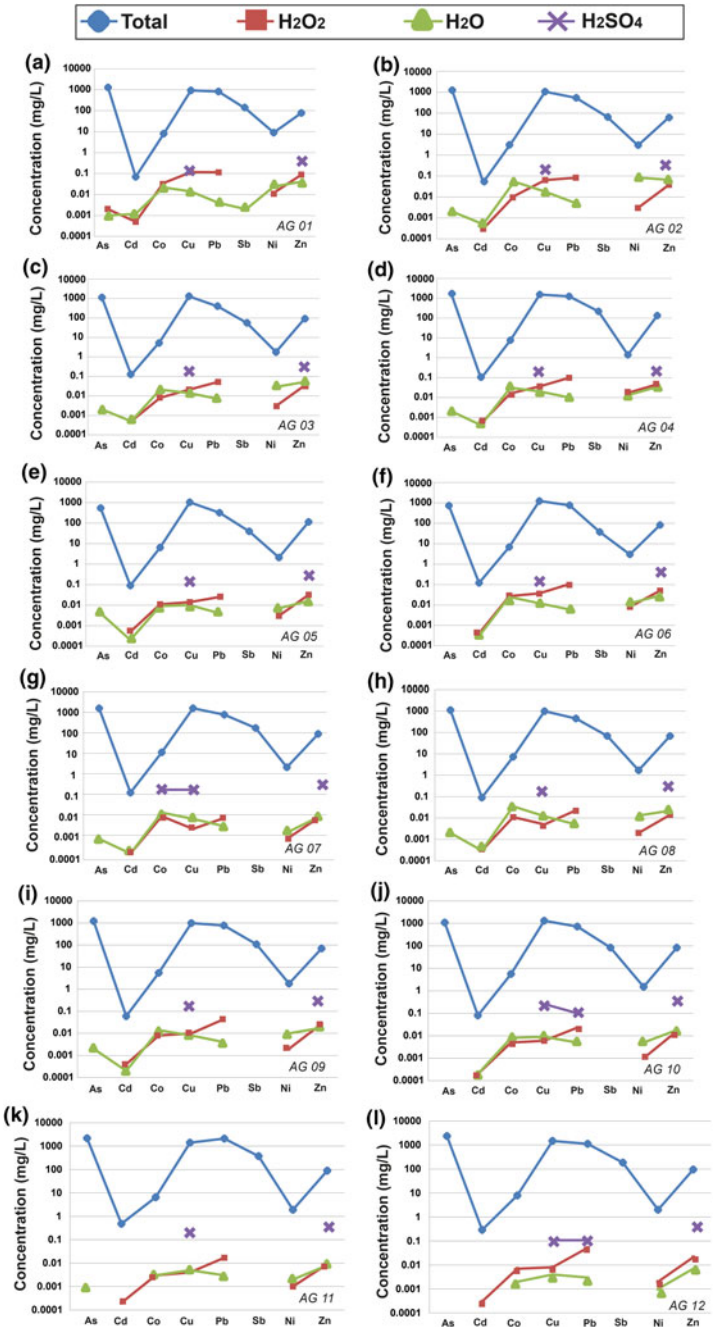


**Fig. 9** Total content and leachate chemistry ($H_2O$, $H_2O_2$, $H_2SO_4$ extracts) for Angostura gossan composite samples (AG1 to 12) (color figure online)

**Table 2** Summary of geochemical data (ppm for total, mg/L for leach results) for composite gossan samples (n = 12) as measured by ICPMS

| | | As | Cd | Co | Cu | Hg | Ni | Pb | S | Sb | Zn |
|---|---|---|---|---|---|---|---|---|---|---|---|
| Total | Max | 2350 | 0.48 | 13.4 | 1700 | 53 | 9 | 2100 | 1.7 | 371 | 132 |
| | Min | 540 | 0.05 | 5.5 | 928 | 1 | 1.4 | 320 | 0.4 | 37.8 | 63 |
| | Avg | 1328 | 0 | 7 | 1243 | 13 | 3 | 838 | 0.8 | 129 | 89 |
| WHO (2008) | | 0.01 | 0.003 | ND | 2 | | 0.07 | 0.01 | | 0.02 | ND |
| $H_2O$ leach | Max | 0.004 | 0.001 | 0.05 | 0.020 | | 0.084 | 0.01 | | 0.002 | 0.066 |
| | Min | 0.001 | BDL | 0.001 | 0.001 | | 0.001 | 0.001 | | 0.001 | 0.005 |
| | Avg | 0.002 | BDL | 0.019 | BDL | | 0.016 | 0.005 | | 0.002 | 0.025 |
| $H_2O_2$ leach | Max | 0.002 | 0.0005 | 0.035 | 0.117 | | 0.017 | 0.116 | | 0.001 | 0.088 |
| | Min | 0.002 | 0.0002 | 0.003 | 0.003 | | 0.001 | 0.01 | | 0 | 0.009 |
| | Avg | 0.002 | 0.0003 | 0.01 | 0.025 | | 0.004 | 0.05 | | 0.001 | 0.03 |
| $H_2SO_4$ leach | Max | BDL | BDL | 0.2 | 0.3 | | BDL | 0.1 | | BDL | 0.5 |
| | Min | BDL | BDL | BDL | 0.1 | | BDL | BDL | | BDL | 0.3 |
| | Avg | BDL | BDL | BDL | 0.19 | | BDL | BDL | | BDL | 0.4 |
| 1 M HCl leach | Max | | | | | 1.09 | | | | | |
| | Min | | | | | 0.1 | | | | | |
| | Avg | | | | | 0.36 | | | | | |

WHO (2008) drinking water guidelines are also shown
*BDL* below detection limit, *ND* no data

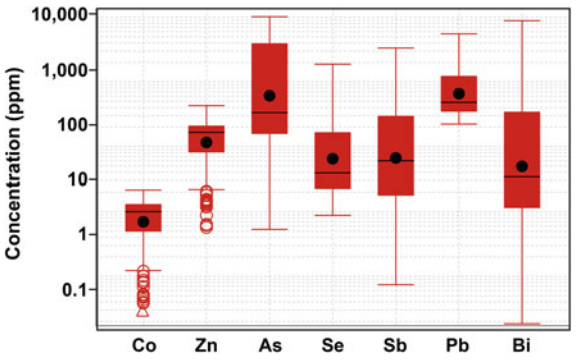


**Fig. 10** Tukey box plot summarizing goethite chemistry (n = 211) with selected elements shown. NB. The *box* covers the interquartile range, the *line* is the median and the circle the mean. The *whiskers* are drawn at the threshold to identify near and far outliers based on the Tukey statistic

1240 ppm), these values are below those reported by others (e.g., Tornos 2006; Velaso et al. 2013). Low Cu concentrations were leached in the $H_2O$ and $H_2O_2$ experiments; with comparatively higher values extracted in the $H_2SO_4$ experiment, though values are still below the WHO (2008) DWG. This confirms that under ARD conditions, Cu is likely to leach significantly from these materials.

Lead was considerably high in these materials (average 840 ppm, Table 2), with a consistent total concentration measured across the vertical transect (Fig. 9). Other gossans in the IPB have reported high Pb concentrations (e.g., Cerro Colarado,

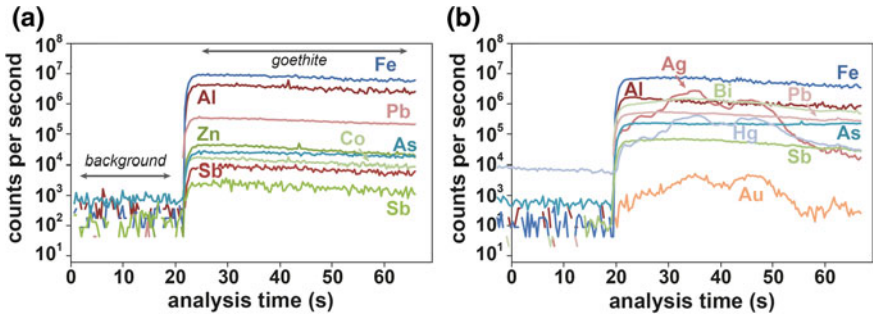


**Fig. 11** LA-ICPMS traces from goethite in Angostura gossan material showing clean intervals (*left hand side*) and inclusion-rich or bulk intervals (*right hand side*) (color figure online)

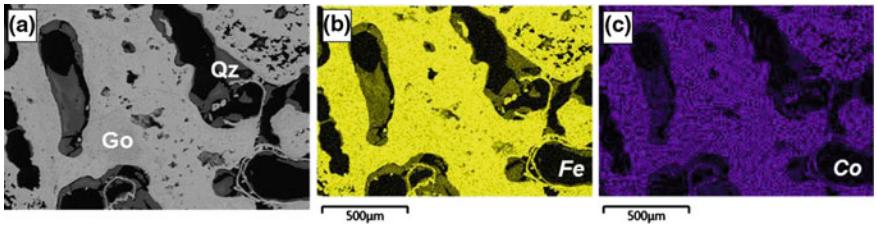


**Fig. 12** Images of sample AG01: **a** Back scattered electron image of goethite with quartz. **b** X-ray element map showing the distribution of Fe. **c** X-ray element map showing the distribution of Co. *Go* goethite; *qz* quartz (color figure online)

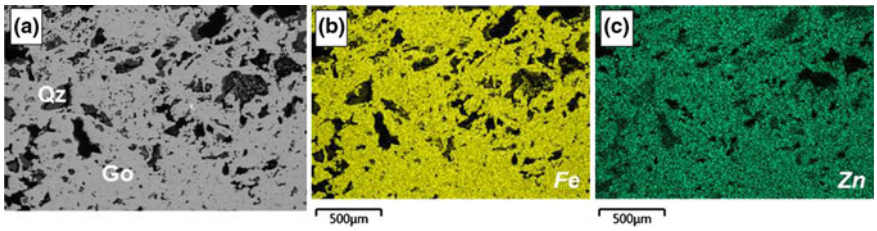


**Fig. 13** Images of sample AG09: **a** Back scattered electron image of goethite with quartz. **b** X-ray element map showing the distribution of Fe. **c** X-ray element map showing the distribution of Zn. *Go* goethite; *qz* quartz (color figure online)

Tornos 2006). Only under $H_2SO_4$ leach conditions, Pb concentrations were greater than WHO (2008) DWG (maximum 0.1 mg/L). Lead is hosted by goethite, and in these materials, appears to be lattice bound (Figs. 10 and 11). Zinc is primarily hosted by goethite (Fig. 13) with characteristically low concentrations measured (average 90 ppm, Table 2; Tornos 2006). The highest leachable Zn was measured from the $H_2SO_4$ experiments; however, there are no WHO (2008) guideline values for comparison.

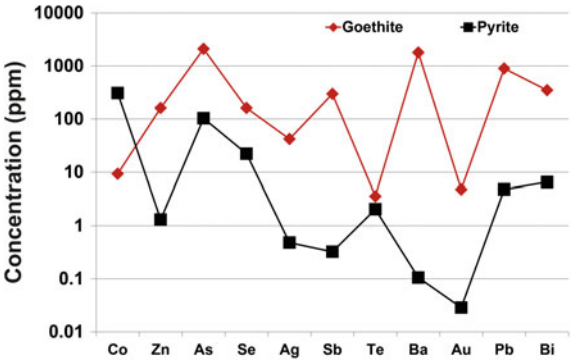


**Fig. 14** Geochemical comparison of goethite (n = 211) and pyrite (n = 17) chemistry (averages shown) as measured by LA-ICPMS, with data for select environmentally significant and precious metals shown

Mercury is typically detected in IPB gossans (e.g., Velaso et al. 2013; Las Cruces, Yesares et al. 2014) and was detected across the Angostura gossan face (Table 2). Mercury is present as Ag-Hg halide inclusions in goethite as indicted by LA-ICPMS data (Fig. 11b). Finally, elevated Hg relative to WHO (2008) guidelines were measured in the 1 M HCl leach (Table 2).

## *Precious Metals*

A comparison of pyrite and goethite chemistry (Fig. 14) indicated that goethite hosts a greater content of both environmentally significant elements and precious metals. This confirms that significant leaching of the primary sulfides has occurred under surface conditions, leaving them comparatively barren.

Silver and Au occur within the iron oxide as inclusions of gold and electrum and as inclusions and bands/intergrowth of Ag-Hg halides (Hunt et al. 2016). Within the iron oxide the inclusions may be hosted directly by goethite ± hematite, or be in or next to quartz or barite encapsulated by goethite (Hunt et al. 2016). Inclusions of electrum range in size from <2 to ~15 μm (equivalent circle diameter) with an average of 4 μm (Hunt et al. 2016). Ag-Hg halide occurs as bands and inclusions, and it is more difficult to determine a representative size. Equivalent circle diameter ranges from <2 to ~60 μm with an average of 9 μm (Hunt et al. 2016). Analysis of the boundaries of precious metal inclusions, using SEM-MLA techniques, indicates that electrum is largely encapsulated in iron oxide (mainly goethite), more rarely it is within quartz or barite; approximately 18 % has a free surface (Hunt et al. 2016). Ag-Hg halide inclusions occur dominantly within quartz and barite; about 28 % has a free surface.

Similar oxide material (i.e. goethite-hematite rich gossan) containing Au and Ag halides are processed at the Cerro de Maimón deposit using cyanide leaching and Merrill-Crowe Au-Ag precipitation (Andreu et al. 2015). The average gold grade of our samples (1.07 g/t) and the size of gold grains (<2–15 μm) are similar to those

of the oxide ore processed at Cerro de Maimón (1.04 g/t Au; Au grains 1-10 µm in size). However, Au grains at Cerro de Maimón are reported as largely occurring in fractures/voids, i.e. are free, thus providing access for cyanide solutions. Ag occurs in Ag halides in both locations, but the composition of the Ag halides is different. In these materials, Ag occurs dominantly as Ag-Hg-Cl phases, whereas oxide ore at Cerro de Maimón is reported to contain dominantly AgI (Andreu et al. 2015). Both compositions of Ag halide are potentially leachable by cyanide solutions.

## Conclusions

Percolation of meteoritic water within massive sulfides at the Iberian Pyrite Belt (IPB) and associated stockworks induced the formation of gossans. At the Angostura gossan dump, both goethite and hematite were identified along with quartz and barite. In general, goethite dominates and is the host of several environmentally significant metals (e.g., As, Sb, Co, Zn), which are surface or lattice bound. Higher contents of these elements were measured in the secondary iron oxides relative to primary sulfides (i.e., pyrite). Goethite also contained inclusions of Ag-Hg-halides which is not uncommon for such gossan material.

Leach experiments confirm goethite's stable nature under ambient surficial conditions, with no environmentally significant elements (i.e., As, Sb, Co, Cd, Cu, Ni, Pb, Zn) leached from these materials when using deionized water as the extractant. Similarly, under mildly acidic and oxidizing conditions (e.g., pH 4.5, $H_2O_2$), these elements remain attenuated by their iron oxide hosts with the exception of Pb, with slightly elevated concentrations measured relative to WHO (2008) drinking water guideline values. In addition, Co, Cu and Zn were extracted in the leach experiment replicating an environment dominated by ARD fluids (i.e., $H_2SO_4$ extractant), however, these values were below WHO (2008) DWGs. As very little primary sulfide minerals were observed in the pile, these metals are unlikely to elute. However, further experiments using organic acids should be pursued to determine their mobility, whether natural regrowth of vegetation on the dump and associated production of humic and fulvic acids in root zones could lead to element mobility. Under current pH conditions, As and Sb are expected to remain bound to goethite. As this dump is not a point source of ARD, no high pH additives (e.g., carbonate, quick lime) are likely to be emplaced, thus these metalloids are likely to remain bound to Fe phases. The dump has been identified as an economic resource, with processing of these materials likely to occur in future for Ag and Au extraction.

## References

Andrew RL (2000) Short course in evaluation of gossans in mineral exploration. ADIMB, Brasilia, pp 57

Andreu E, Torró L, Proenza JA, Domenech C, García-Casco A, Villanova de Benavent C, Chavez C, Espaillat J, Lewis JF (2015) Weathering profile of the Cerro de Maimón VMS deposit (Dominican Republic): textures, mineralogy, gossan evolution and mobility of gold and silver. Ore Geol Rev 65:165–179

Atapour H, Aftabi A (2007) The geochemistry of gossans associated with Sarcheshmeh porphyry copper deposit, Rafsanjan, Kerman, Iran: Implications for exploration and the environment. J Geochem Explor 93:47–65

Beukes JP, Giesekke EW, Elliot W (2000) Nickel retention by goethite and hematite. Min Eng 13:1573–1579

Cadillac Ventures (2016) http://www.cadillacventures.com/s/Home.asp

Craddock PT, Freestone IC, Hunt Ortiz M (1987) Recovery of silver from Speiss at Rio Tinto (SW Spain). IAMS 10–11:8–11

Danyushevsky L, Robinson P, Gilbert S, Norman M, Large R, McGoldrick P, Shelley M (2011) Routine quantitative multi-element analysis of sulphide minerals by laser ablation ICP-MS: standard development and consideration of matrix effects. Geochem Explor Environ Anal 11:51–60

Fakih M, Davranche M, Dia A, Nowack B, Morin G, Petitjean P, Châtellier X, Gruau G (2009) Environmental impact of As(V)–Fe oxyhydroxide reductive dissolution: an experimental insight. Chem Geol 259:290–303

García Palomero F, Bedia Fernández JL, García Magarinño M, Sides EJ (1986) Nuevas investigaciones y trabajos de evaluacioón de reservas de gossan en minas de Río Tinto. Bol Geol Miner 97:622–642

Hunt J, Lottermoser BG, Parbhakar-Fox A, van Veen E, Goemann K (2016) Precious metals in gossanous waste rocks from the Iberian Pyrite Belt. Min Eng 87:45–53

Leistel JM, Marcoux E, Thiéblemont D, Quesada C, Sánchez A, Almodóvar GR, Pascual E, Sáez R (1998) The volcanic-hosted massive sulfide deposits of the Iberian Pyrite Belt. Review and preface to the thematic issue. Miner Deposita 33:2–30

Longerich HP, Jackson SE, Günther D (1996) Laser ablation inductively coupled plasma-mass spectrometric transient signal data acquisition and analyte concentration calculation. J Anal At Spectrom 11:899–904

Mamindy-Pajany Y, Hurel C, Marmier N, Roméo M (2009) Arsenic adsorption onto hematite and goethite. C R Chim 12:876–881

Nocete F, Álex E, Nieto JM, Sáez R, Bayona MR (2005) An archaeological approach to regional environmental pollution in the South-Western Iberian Peninsula related to Third Millennium BC mining and metallurgy. J Archaeol Sci 32:1566–1576

Núñez C, Roca A, Espiell F (1987) Improved gold and silver recovery from Spanish gossan ores by sulphidization prior to cyanidation. Trans Inst Min Metal 96:171

Pérez-López R, Asta MP, Roman-Ross G, Nieto JM, Ayora C, Tucoulou R (2011) Synchrotron-based X-ray study of iron oxide transformations in terraces from the Tinto-Odiel river system: influence on arsenic mobility. Chem Geol 280:336–343

Pivovarov S (2001) Adsorption of cadmium onto hematite: temperature dependence. J Colloid Interface Sci 234:1–8

Ritchie VJ, Ilgen AG, Mueller SH, Trainor TP, Goldfarb RJ (2013) Mobility and chemical fate of antimony and arsenic in historic mining environments of the Kantishna Hills district, Denali National Park and Preserve, Alaska. Chem Geol 335:172–188

Romero A, Gonzalez I, Galan E (2006) Estimation of potential pollution of waste mining dumps at Pena del Hierro (Pyrite Belt, SW Spain) as a base for future mitigation actions. Appl Geochem 21:1093–1108

Sáez R, Nocete F, Nieto JM, Capitán MA, Rovira S (2003) The extractive metallurgy of copper from Cabezo Juré, Huelva, Spain: chemical and mineralogical study of slags dated to the Third Millenium B.C. Can Mineral 41:627–638

Smart R, Skinner WM, Levay G, Gerson AR, Thomas JE, Sobieraj H, Schumann R, Weisener CG, Weber PA, Miller SD, Stewart WA (2002) ARD test handbook: project P387, a prediction and kinetic control of acid mine drainage. AMIRA, International Ltd., Melbourne, Australia, pp 42

Taylor CD, Zierenberg RA, Goldfarb RJ, Kilburn JE, Seal II RR, Kleinkopf MD (1995) Volcanic-associated massive sulfide deposits. In: Preliminary Compilation of Descriptive Geoenvironmental Mineral Deposit Models. U.S Geological Survey Open-File Report 90–831, pp 137–144

Tessier A, Campbell PGC, Bisson M (1979) Sequential extraction procedure for the speciation of particulate trace metals. Anal Chem 51:844–851

Thornber MR, Wildman JE (1984) Supergene alteration of sulphides VI: the binding of Cu, Ni, Zn, Co and Pb with gossan (iron-bearing) minerals. Chem Geol 44:399–434

Tornos F, Casquet C, Relvas J, Barriga F, Saez R (2002) The relationship between ore deposits and oblique tectonics: the SW Iberian Variscan Belt. In: Blundell D, Neubauer F, von Quadt A (eds) The timing and location of major ore deposits in an evolving orogen. Geol Soc London Spec Publ, 204, pp 179–198

Tornos F (2006) Environment of formation and styles of volcanogenic massive sulfides: the Iberian Pyrite Belt. Ore Geol Rev 28:259–307

Velaso F, Herrero JM, Suarez S, Yusta I, Alvaro A, Tornos F (2013) Supergene features and evolution of gossans capping massive sulphide deposits in the Iberian Pyrite Belt. Ore Geol Rev 53:181–203

Watkins R, Weiss D, Dubbin W, Peel K, Coles B, Arnold T (2006) Investigations into the kinetics and thermodynamics of Sb(III) adsorption on goethite (α-FeOOH). J Colloid Interface Sci 303:639–646

Wilhelm EK, Kosakevitch A (1979) Utilisation des chapeaux de fer comme guide de prospection. Bull BRGM Sect 2: Geol Gites Miner 2/3, 109–140

World Health Organisation (2008) Drinking water guideline values. http://www.who.int/water_sanitation_health/dwq/fulltext.pdf

World Weather Online (2016) http://www.worldweatheronline.com/Seville-weather-averages/Andalucia/ES.aspx

Yesares L, Sáez R, Nieto JM, Ruiz de Almodóvar G, Cooper S (2014) Supergene enrichment of precious metals by natural amalgamation in the Las Cruces weathering profile (Iberian Pyrite Belt, SW Spain) Ore Geol Rev 58:14–26

# Prediction of Metal Mobility from Sulfidic Waste Rocks Using Micro-analytical Tools, Baal Gammon, Northern Australia

**Nathan Fox, Anita Parbhakar-Fox and Bernd Lottermoser**

**Abstract** Predictions on the behavior of environmentally significant elements at mine sites requires the use of advanced laboratory techniques. The aim of this contribution is to demonstrate the use of electron microprobe analysis (EMPA) and laser ablation inductively coupled plasma mass spectrometry (LA-ICPMS) to gain an understanding of likely element behaviour. Sulfidic boulders sampled from an acid rock drainage (ARD) impacted ephemeral stream adjacent to the historical Baal Gammon workings are dominated by chalcopyrite, arsenopyrite, pyrrhotite and lesser pyrite. Micro-analytical investigations using EMPA and LA-ICPMS reveal that chalcopyrite contains significant quantities of Ag, Cd, Sn, In and Zn either substituted directly into the crystal lattice or occurring as discrete sphalerite and stannite inclusions. Arsenopyrite, comprising more than 50 % of some boulders, is most notably rich in Co, Ni, Sb and Se, but it also contains inclusions of sphalerite, chalcopyrite and stannite. By contrast, pyrrhotite contains relatively few trace elements, but it may be a significant contributor to ARD development. The trace element composition of Fe-oxides in the oxidized rinds of these boulders is likely directly influenced by the mineralogy of the sulfidic boulders on which they precipitate. Although significant quantities of As, Bi, Cu, In, Pb and Zn occur in Fe-oxides at Baal Gammon, these elements may be liberated during acid flushing of the ephemeral stream. Consequently, EMPA and LA-ICPMS represent valuable tools for evaluating the source and potential mobility of environmentally significant elements at mine sites.

N. Fox (✉) · A. Parbhakar-Fox
School of Physical Sciences, University of Tasmania, Hobart, TAS 7001, Australia
e-mail: Nathan.Fox@utas.edu.au

A. Parbhakar-Fox
e-mail: Anita.Parbhakar@utas.edu.au

B. Lottermoser
Institute of Mineral Resources Engineering, RWTH Aachen University, Wüllnerstrasse 2, 52062 Aachen, Germany
e-mail: lottermoser@mre.rwth-aachen.de



B. Lottermoser (ed.), *Environmental Indicators in Metal Mining*,
DOI 10.1007/978-3-319-42731-7_14

## Introduction

The Herberton tin-tungsten province in north Queensland, Australia (Fig. 1) has been a significant contributor to Australia's total tin production since the 1880s (Blake 1972). At least 2000 historical lode and alluvial mines and workings occur in the province, yielding over 150 kt of tin and 4 kt of tungsten (Solomon and Groves 1994). Tin mineralization largely occurs in greisen, skarn and breccias associated with Late Carboniferous granites forming polymetallic deposits that contain cassiterite, wolframite, chalcopyrite, sphalerite and galena with gangue arsenopyrite, pyrrhotite and pyrite. The rising global demand for tin and critical metals, particularly indium and tantalum (Skirrow et al. 2013), has driven a resurgence in mining and exploration in and around historical tin-tungsten provinces including the Herberton province, Queensland.

Baal Gammon, located 7 km west of Herberton (Fig. 1), is a polymetallic deposit that was mined historically for Sn, Cu, Ag and Bi. Intermittently active during the last decade, Baal Gammon operated as a Cu-Ag mine with no documented recovery of Sn. Indium is associated with Sn-W ores and related Cu-Zn-Pb mineralization.

The Herberton area has a tropical climate characterized by seasonal rainfall and ephemeral run-off, which in turn leads to episodic leaching of waste repositories from historical and active mines, leading to potential downstream environmental

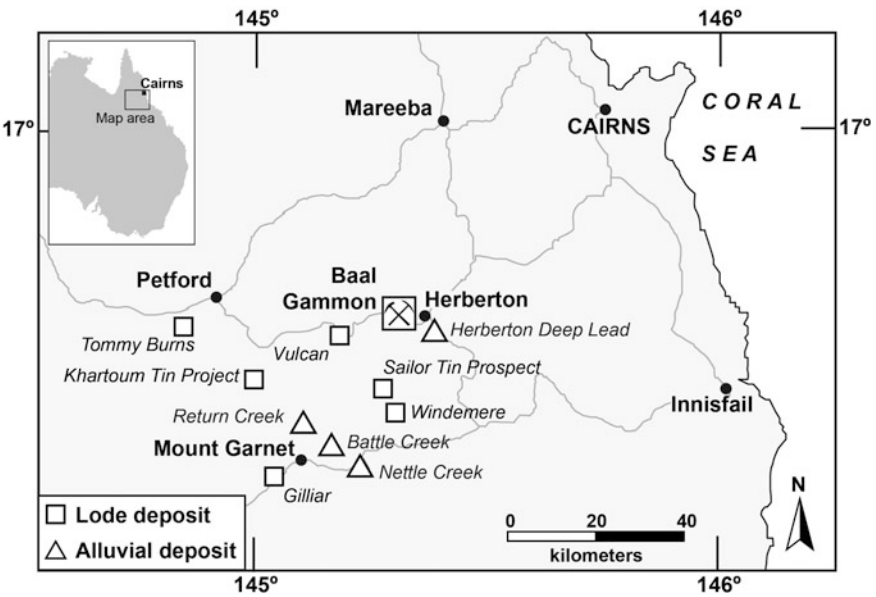


**Fig. 1** Location of lode and alluvial tin deposits in the Herberton area, north Queensland, Australia (modified from Lam 2009)

hazards. This study provides a detailed examination of the mineralogy and trace element content of sulfidic waste rock boulders present in an ephemeral creek adjacent to the Baal Gammon mine. Evaluation of the mineralogical siting of metals and metalloids allows prediction of anticipated element mobility from mine wastes.

## Site Description and Mining History

Baal Gammon is located approximately 100 km southwest of Cairns in north Queensland (Fig. 1), an area characterized by a tropical savannah-type climate with an annual rainfall typically exceeding 800 mm/year. Access to site is by the Herberton-Petford sealed road from Herberton (Fig. 1). The Herberton area is

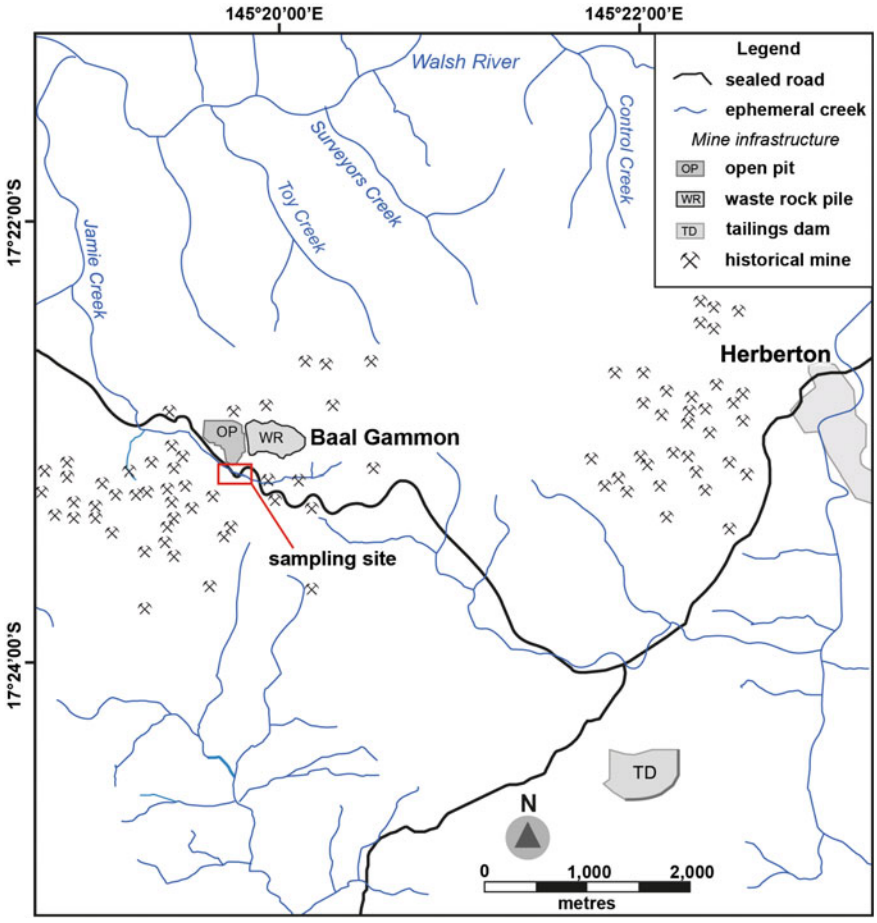


**Fig. 2** Location of the Baal Gammon deposit, infrastructure, historical and active mine workings and local drainage. Modified from Natural Systems Research (1980) and Monto Minerals (2014)

subject to heavy seasonal rainfall and tropical cyclones. The Baal Gammon site was flooded during the 2011 and 2012 wet seasons discharging metal-rich leachate containing As, Cd, Cu, Pb and Zn into the nearby Jamie Creek and Walsh River (Fig. 2; Dally-Watkins 2014).

Small scale historical tin and copper mining started at Baal Gammon in the 1930s, when the site was operated by the United Northern Australian (UNA) battery (Lam 2009). Intermittent copper, silver and tin mining also occurred at Baal Gammon between 1967 and 1979. Baal Gammon (then also known as UNA) was the subject of numerous exploration joint ventures between 1979 and 1985, managed by Newmont Holdings Pty until their withdrawal from the area in 1985 (Lam 2009). Several exploration and drilling campaigns between 2006 and 2008 defined significant ore reserves of tin, indium, silver and copper (Lam 2009). In 2011, Kagara Pty Ltd commenced open pit mining at Baal Gammon extracting 38 kt of ore at an average grade of 1.9 % Cu, 41 g/t Ag which was processed at the nearby Mount Garnet copper processing facility (Champion and McKay 2013). Operations at Baal Gammon ceased in 2012 as Kagara Pty Ltd entered into voluntary administration. Currently, the site is owned by Monto Minerals Limited and mining operations at Baal Gammon have been carried out by Snow Peak International since 2013. Indicated and inferred resources of 2.8 Mt of ore at 1.0 % copper, 0.2 % tin, 40 g/t silver and 38 g/t indium make Baal Gammon one of the world's highest grade indium resources (Geological Survey of Queensland 2014; Monto Minerals 2014).

## Geological Setting and Mine Geology

The regional geology of the area around Baal Gammon comprises Devonian mudstone, siltstone, limestone and conglomerate of the Hodgkinson Formation which is unconformably overlain by late Carboniferous rhyolite and welded tuffs of the Featherbed Volcanics (Blake 1972). The region is extensively intruded by Late Carboniferous granites, including the highly greisenized Elizabeth Creek Granite (318 Ma; Champion and Heinemann 1994; Champion et al. 2009) and younger granites, including the Early Permian Watsonville Granite (289–281 Ma; Garrad and Bultitude 1999). Mineralization in the Herberton-Wastonville region is interpreted to be associated with the Elizabeth Creek Granite, rather the younger intrusions (Watsonville Granite) which characteristically lack greisens and associated mineralization (Blake 1972).

Mineralization at Baal Gammon is hosted by thinly bedded mudstones of the Hodgkinson Formation which is intruded by a porphyry sill, named the UNA Sill, interpreted to represent a highly-fractionated, late-stage product of the regionally extensive Elizabeth Creek Granite (Fraser 1972; Monto Minerals 2014). The UNA Sill is extensively greinsenized and altered to an assemblage of quartz, muscovite and fluorite, topaz (Fraser 1972; Monto Minerals 2014). Mineralization at Baal

Gammon is zoned from massive chalcopyrite, arsenopyrite and pyrrhotite which grades laterally into semi-massive pyrrhotite and pyrite (Fraser 1972). Tin and minor tungsten mineralization occurs as mostly as cassiterite, stannite and trace scheelite.

## Waste Rock Sample Descriptions

A series of large boulders were sampled from Jamie Creek adjacent to historical mine workings at Baal Gammon (Fig. 3). The boulders comprise massive sulfide minerals (arsenopyrite, pyrrhotite, chalcopyrite) with lesser oxide ore minerals (e.g., cassiterite, wolframite) and silicate gangue minerals (quartz, feldspar). Under the acidic and oxidizing ephemeral stream environment, the sulfidic boulders have developed thick (10–20 mm thick) exterior rinds dominated by secondary Fe-oxide minerals (Fig. 3). Fe-oxides also occur locally in the interior of the boulders infilling fractures. The sulfide and oxide mineralogy of the boulders was determined using a combination of reflected light microscopy, backscatter electron (BSE) imaging and electron microprobe analysis (EMPA).

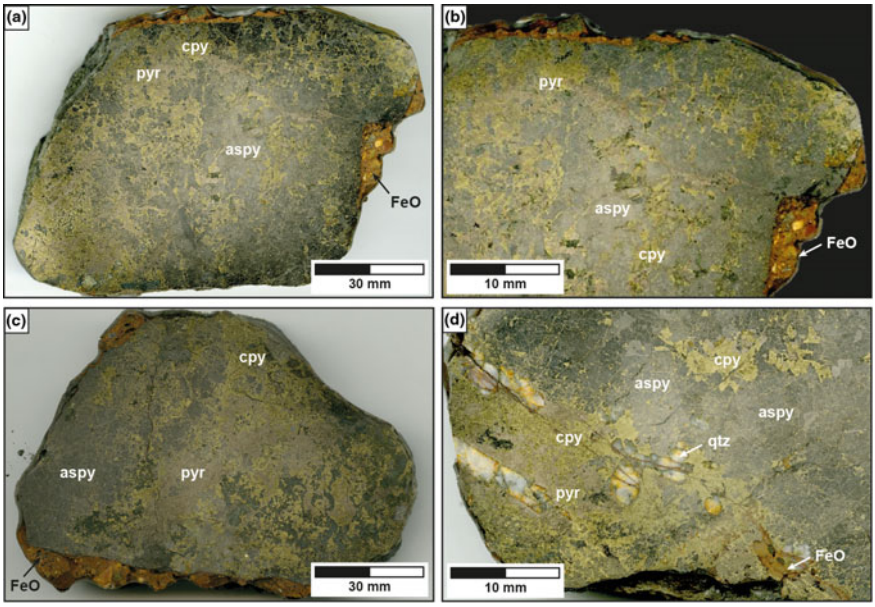


**Fig. 3** Hand specimen photos of waste rock samples collected from Jamie Creek adjacent to Baal Gammon historical workings. **a** Massive arsenopyrite, pyrrhotite, and chalcopyrite with Fe-oxide dominated rind (*BG14A*); **b** Fe-oxide rind (BG14A). **c** Massive arsenopyrite, pyrrhotite and chalcopyrite with oxidized rind (BG14B). **d** Arsenopyrite, chalcopyrite and pyrrhotite with quartz gangue and localized Fe-oxide developed along a fracture (BG14E). *aspy* arsenopyrite; *cpy* chalcopyrite; *FeO* iron oxide; *pyr* pyrrhotite; *qtz* quartz (color figure online)

## Analytical Methodology

### *Field-Emission Scanning Electron Microscopy (FE-SEM)*

Polished blocks were analyzed at the Central Science Laboratory, University of Tasmania (UTAS), using a Hitachi SU-70 field-emission scanning electron microscope (FE-SEM) fitted with a 5-segment solid state BSE detector and an Oxford Instruments Aztec EDS system equipped with an X-max 80 SDD EDS detector. Samples were carbon coated prior to analysis using a 17 kV operating voltage for imaging and in situ semi-quantitative chemical analysis using energy dispersive X-ray spectroscopy spectrometry (EDS) and X-ray chemical mapping.

### *Electron Microprobe Analysis (EMPA)*

Fully quantitative chemical analyses of individual minerals was carried out using a Cameca SX100 electron microprobe, also housed at the Central Science Laboratory, UTAS. Carbon coated samples were analyzed at 20 kV for sulfide minerals and 15 kV for iron oxide minerals using an effective spot size of 1 to 2 μm. Quantitative measurements were carried out using wavelength dispersive (WDS) X-ray spectrometry on 5 WDS analyzing crystals. Measurements were calibrated using secondary standard reference materials, including cassiterite, hessite, chalcopyrite, sphalerite, greenockite, zinc selenide, lead telluride, pentlandite, stibnite, cobalt metal and pyrite. Data was corrected for X-ray interferences (e.g., Sn on Sb peaks) using Probe for EMPA software developed by Probe Software Inc. Due to X-ray interferences and overlapping X-ray peaks between Sn and In, In concentrations were not determined by electron microprobe analysis.

### *Laser Ablation Inductively Coupled Plasma Mass Spectrometry (LA-ICPMS)*

The trace element concentration of individual minerals was determined by LA-ICPMS analysis carried out at the Discipline of Earth Sciences, UTAS. Analyses were performed on a Resonetics RESOlution system equipped with a 193 nm wavelength Coherent COMPex Pro ArF excimer laser with a custom built Laurin Technic constant geometry ablation cell. Sulfide and oxide minerals were analyzed using a 30–50 μm diameter laser spot size, 5 Hz frequency and 45 mJ energy. The laser is coupled to an Agilent 7700 quadrupole mass spectrometer for quantification of each laser ablation spot analysis. Data for each spot analysis was collected over a total of 60 s on the mass spectrometer comprising 30 s of background followed by 30 s of mineral ablation. A doped lithium borate fused disc

developed in house (STDGL2B-2) and GSD-1G, developed by the USGS were used as primary standards for quantification and to account for instrumental drift on the mass spectrometer. Data reduction and quantification was carried out using in house Excel-based software that corrects for linear drift. Mass-bias interferences occur on mass-spectrometers when elements with the same isotopes (e.g., $Cd^{112}$, $Sn^{112}$; $Cd^{113}$, $In^{113}$; $Cd^{114}$, $Sn^{114}$; $In^{115}$, $Sn^{115}$ and $Cd^{116}$, $Sn^{116}$) are analyzed together in the same mineral. Indium has two isotopes ($In^{113}$ and $In^{115}$) but because neither isotope is unique to In alone, mass-bias corrections were performed to account for simultaneous measurement of $Cd^{113}$ and $Sn^{115}$ during LA-ICPMS analysis. Mass-based interferences were corrected using a dedicated analytical element suite for accurate quantification of Cd, In and Sn.

## Results

### *Primary Mineralogy*

The primary mineralogy of the boulders reflects the polymetallic mineralization at Baal Gammon and is dominated by sulfide minerals (Fig. 4). The sulfide ore mineralogy comprises chalcopyrite, stannite and minor sphalerite and galena. Cassiterite occurs as inclusions in chalcopyrite, commonly rimmed by stannite (Fig. 5). Wolframite is less common, occurring sporadically as individual grains, mostly within chalcopyrite. The dominant gangue sulfide minerals include arsenopyrite, pyrrhotite and lesser pyrite. One sample (BG14C) was dominated by pyrite and contained comparatively minor chalcopyrite, arsenopyrite and pyrrhotite (Fig. 4d). Other gangue phases likely related to primary mineralization include quartz, muscovite, fluorite, garnet (almandine), alkali feldspar and rutile. Stannite, cassiterite, sphalerite and wolframite occur as discrete phases and as micro-inclusions within the major sulfides. Backscattered electron imagery was most effective at distinguishing individual grains of these minerals, whereas LA-ICPMS analysis revealed the composition of micro-inclusions.

### *Secondary Mineralogy*

Oxidized rinds, up to 20 mm thick (Fig. 3a) are developed on the exterior of the massive sulfide boulders. They are characteristically red to ochre yellow in colour (Fig. 3) and are dominated by Fe-oxides (Fig. 6) that typically form an apparent cement supporting angular clasts of brecciated primary quartz, alkali feldspar, chalcopyrite, arsenopyrite and pyrrhotite (Figs. 3b and 6a, b). Fe-oxides have locally filled open spaces within samples dominated by pyrite (Figs. 3b and 6c, d) and also form concentrically zoned precipitates on the surface of Fe-oxide cemented breccias (Fig. 6b).

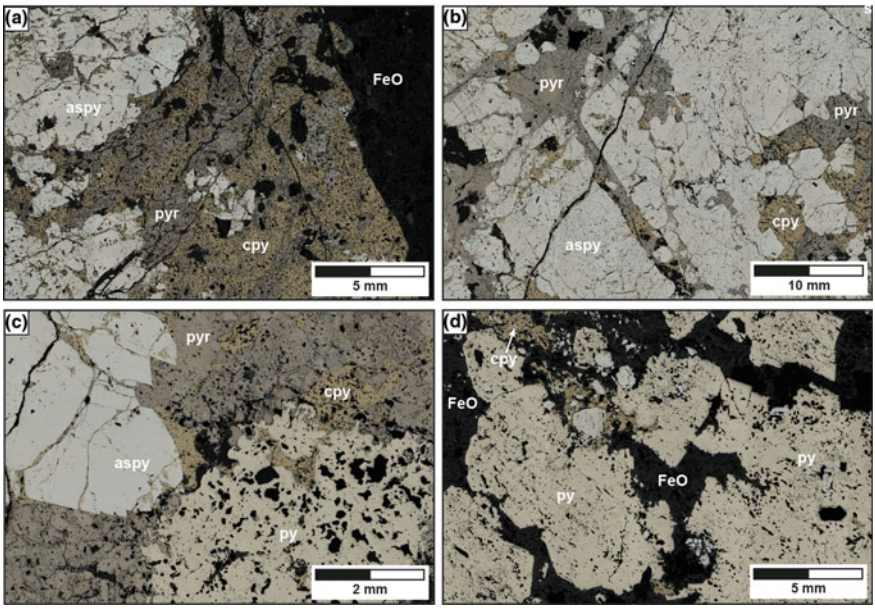


**Fig. 4** Reflected light photomicrographs of Baal Gammon waste rock samples: **a** arsenopyrite, inclusion-rich pyrrhotite intergrown with inclusion-rich chalcopyrite (BG14A), **b** massive arsenopyrite intergrown with chalcopyrite and pyrrhotite, locally altered to marcasite (BG14A); **c** arsenopyrite, pyrrhotite and chalcopyrite with pyrite (BG14E). **d** Inclusion-rich pyrite with minor chalcopyrite and arsenopyrite. Fe-oxide occurs as a main constituent between pyrite on the interior of the boulder (BG14C). *aspy* arsenopyrite; *cpy* chalcopyrite; *FeO* iron oxide; *py* pyrite; *pyr* pyrrhotite (color figure online)

## *Electron Microprobe Analyses*

Representative analyses from the major sulfide minerals (chalcopyrite, pyrrhotite, arsenopyrite, pyrite, stannite and sphalerite) as determined by electron microprobe are listed in Table 1. Chalcopyrite ($CuFeS_2$) from Baal Gammon typically contains measureable Sn, Ag and Zn but As, Se, Pb, Cd, Co and Ni are typically below the limit of detection (Table 1). Only trace quantities of As occur in pyrrhotite with nearly all other elements analyzed being below the limit of detection. Arsenopyrite contains Sb together with minor amounts of Co and Ni (Table 1) whereas only Sn tends to occur above the limit of detection in pyrite. Variation in the Fe content of stannite between 12.8 and 17.0 wt% is compensated by variable Sn contents (21.5–27.0 wt%). Zn occurs in stannite ranging from 0.45 to 2.87 wt% (Table 1). Sphalerite displays a narrow range in Fe (9.0 and 11.4 wt% Fe), but also contains Cu, Cd and Mn (Table 1). Average limits of detection for elements measured on the microprobe ranges from 0.02 wt% (200 ppm) for Co, Ni and Mn, 0.03 wt%

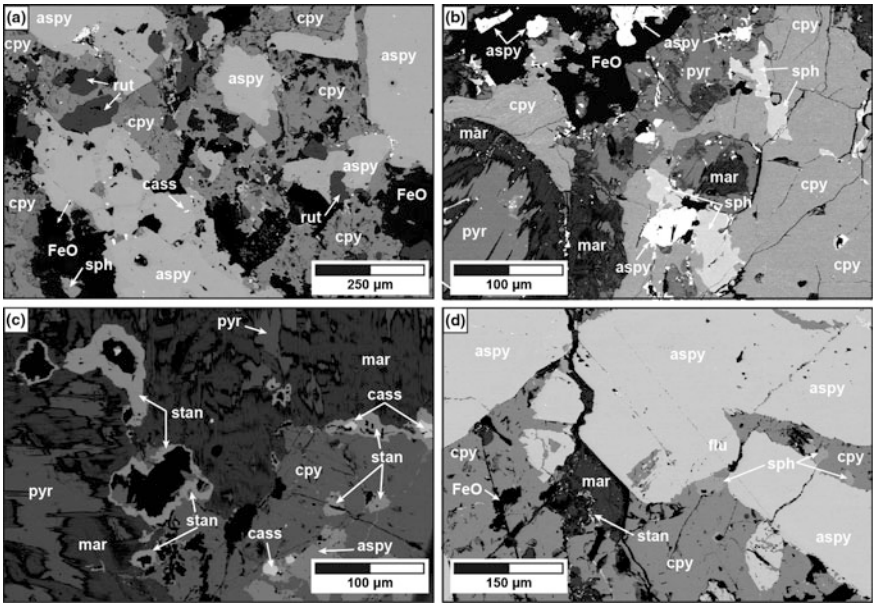


**Fig. 5** Backscattered electron (BSE) images of ore mineralogy and textures from Baal Gammon. **a** Arsenopyrite, chalcopyrite and trace sphalerite intergrown with rutile and secondary iron oxides (BG14A), **b** massive chalcopyrite, pyrrhotite and marcasite with lesser arsenopyrite and sphalerite (BG14A); **c** cassiterite rimmed by stannite intergrown with chalcopyrite and occurring within marcasite, which has altered primary pyrrhotite (BG14B). **d** Massive arsenopyrite and chalcopyrite with lesser sphalerite and trace stannite (BG14A). *aspy* arsenopyrite; *cass* cassiterite; *cpy* chalcopyrite; *FeO* iron oxide; *mar* marcasite; *pyr* pyrrhotite; *rut* rutile; *sph* sphalerite; *stan* stannite

(300 ppm) for Ag, As, Cu, Sb and Sn, and 0.04 wt% (400 ppm) for Cd, Pb, Se and Zn. With a highly focused electron beam (1–2 µm) EMPA analyses likely represent inclusion- or impurity-free analyses of the major sulfide minerals at Baal Gammon. Together with the relative high limits of detection, the microprobe data therefore, represents a conservative measurement of the total abundance of trace elements that could be leached from sulfide minerals during oxidation at Baal Gammon.

Electron microprobe analyses of Fe-oxides from two contrasting samples—BG14A, a poly-sulfide sample and BG14C dominated by pyrite (Table 2), reveal subtle differences between Fe-oxides developed in mineralogically different host rocks. Fe-oxides in BG14A contain higher Zn and Al than those from BG14C, which in contrast contain higher Si, Mn and Ca than BG14A. Considering the higher limits of detection using the electron microprobe, the trace element composition of Fe-oxides at Baal Gammon was investigated by LA-ICPMS.

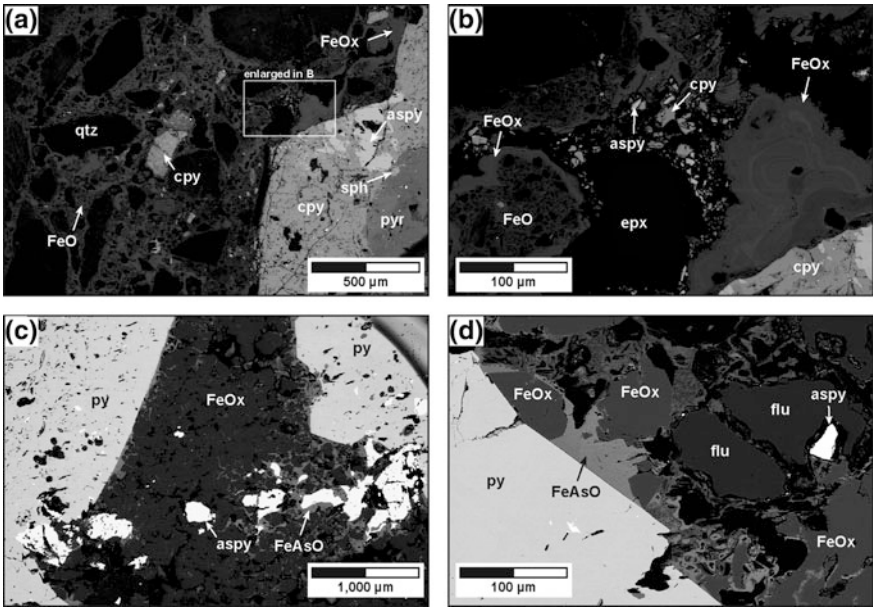


**Fig. 6** Backscattered electron (BSE) images of secondary iron oxide minerals and textures. **a** Secondary Fe-oxide rind developed on primary sulfides (BG14A); **b** enlargement from **a** showing concentric texture in Fe-oxides and a spongey Fe-oxide (BG14A); **c** interior of sulfidic sample dominated by pyrite. Fe-oxide infills spaces between pyrite grains (BG14C); **d** Fe-oxide and fluorite with trace arsenopyrite in spaces between pyrite, and an unnamed arsenic-rich Fe-oxide occurs as a rimming phase on the Fe-oxide (BG14C). *aspy* arsenopyrite; *AsFeO* unnamed As-rich Fe-oxide; *cpy* chalcopyrite; *epox* epoxy resin; *FeO* iron oxide; *flu* fluorite; *py* pyrite; *pyr* pyrrhotite; *sph* sphalerite; *stan* stannite

## Laser Ablation ICPMS Analyses

Laser ablation ICPMS analyses allow measurement of trace element concentrations to significantly lower limits of detection (typically <0.2 ppm or less) compared to electron microprobe techniques. Lower limits of detection can also be attained by using larger laser spot sizes (e.g. 32 µm) for ablation. Similar to EMPA, LA-ICPMS analysis can measure clean, inclusion-free parts of individual crystals, therefore giving an indication of trace element substitutions into a pure-mineral phase (e.g., substitution of Ni, Co, and Cu for Fe in pyrite). An example of the output from the LA-ICPMS for such clean analyses in chalcopyrite, pyrrhotite, arsenopyrite and pyrite is shown in Fig. 7. Commonly, LA-ICPMS analyses will sample micro-inclusions of other mineral phases either exsolved from, or trapped within, a growing crystal. These inclusions are commonly recognized as irregular spikes in elements specific to the mineralogy of particular inclusions (e.g., Cu-Sn-S spikes indicate stannite inclusions). Examples of LA-ICPMS traces for each sulfide mineral, with and without mineral inclusions, are shown in Fig. 7.

**Table 1** Representative electron microprobe analyses (in wt%) of sulfide minerals at Baal Gammon, north Queensland

| Sample | Chalcopyrite | | | | Pyrrhotite | |
|---|---|---|---|---|---|---|
| | 14B | 14D | 14E | 14D | 14E | 14D |
| Analysis | 1 | 2 | 3 | 1 | 2 | 3 |
| S | 34.2 | 34.8 | 33.9 | 39.1 | 37.3 | 38.9 |
| Ag | <0.03 | 0.08 | 0.06 | <0.02 | <0.02 | <0.03 |
| Cu | 33.9 | 34.1 | 33.9 | <0.03 | <0.03 | 0.04 |
| Zn | 0.20 | 0.05 | <0.03 | <0.03 | <0.03 | <0.03 |
| Sb | <0.02 | <0.03 | <0.03 | <0.03 | <0.02 | <0.02 |
| As | <0.03 | <0.03 | 0.04 | 0.07 | 0.04 | <0.03 |
| Fe | 30.0 | 30.1 | 30.0 | 59.9 | 59.7 | 59.4 |
| Se | <0.03 | <0.03 | <0.03 | <0.02 | <0.02 | 0.05 |
| Pb | <0.05 | <0.05 | <0.04 | <0.04 | <0.05 | <0.04 |
| Cd | <0.03 | <0.03 | <0.03 | <0.03 | <0.03 | <0.03 |
| Mn | <0.01 | <0.01 | <0.01 | <0.01 | <0.01 | <0.01 |
| Ni | <0.02 | <0.02 | <0.02 | <0.02 | <0.02 | <0.02 |
| Co | 0.02 | <0.01 | <0.01 | <0.01 | <0.01 | <0.01 |
| Sn | 0.07 | 0.07 | 0.12 | <0.02 | <0.02 | 0.03 |
| Total | 98.4 | 99.2 | 98.0 | 99.2 | 97.1 | 98.4 |
| Sample | Arsenopyrite | | | Pyrite | | |
| | 14C | 14E | 14D | 14C | 14C | 14E |
| Analysis | 1 | 2 | 3 | 1 | 2 | 3 |
| S | 20.7 | 20.1 | 20.8 | 53.0 | 52.5 | 51.6 |
| Ag | <0.03 | 0.04 | <0.03 | <0.02 | <0.02 | <0.02 |
| Cu | <0.03 | 0.04 | <0.03 | <0.03 | <0.03 | <0.03 |
| Zn | <0.03 | <0.03 | <0.03 | <0.03 | <0.03 | <0.03 |
| Sb | 0.06 | 0.22 | <0.03 | <0.03 | <0.02 | <0.03 |
| As | 42.9 | 43.4 | 43.0 | <0.03 | <0.02 | 0.07 |
| Fe | 34.7 | 35.3 | 35.1 | 46.5 | 46.7 | 46.8 |
| Se | <0.05 | <0.05 | 0.09 | <0.02 | <0.02 | <0.02 |
| Pb | <0.05 | <0.05 | <0.05 | <0.05 | <0.05 | <0.05 |
| Cd | <0.03 | <0.03 | <0.03 | <0.03 | <0.03 | <0.03 |
| Mn | <0.01 | <0.01 | <0.01 | <0.01 | <0.01 | <0.01 |
| Ni | 0.11 | <0.02 | 0.03 | <0.02 | <0.02 | <0.02 |
| Co | 0.07 | <0.01 | 0.17 | <0.01 | <0.01 | <0.01 |
| Sn | <0.02 | <0.02 | <0.02 | 0.05 | 0.03 | <0.02 |
| Total | 98.5 | 99.1 | 99.2 | 99.4 | 99.3 | 98.5 |
| Sample | Stannite | | | Sphalerite | | |
| | 14B | 14B | 14E | 14D | 14A | 14B |
| Analysis | 1 | 2 | 3 | 1 | 2 | 3 |
| S | 29.8 | 30.6 | 28.9 | 33.3 | 33.5 | 33.2 |

(continued)

**Table 1** (continued)

| Sample | Stannite | | | Sphalerite | | |
|---|---|---|---|---|---|---|
| | 14B | 14B | 14E | 14D | 14A | 14B |
| Analysis | 1 | 2 | 3 | 1 | 2 | 3 |
| Ag | <0.03 | 0.04 | <0.03 | <0.03 | <0.03 | 0.04 |
| Cu | 28.2 | 29.9 | 28.6 | 0.62 | 0.73 | 1.54 |
| Zn | 2.87 | 0.65 | 0.46 | 55.3 | 53.8 | 55.0 |
| Sb | <0.04 | <0.03 | <0.04 | <0.03 | <0.03 | <0.03 |
| As | <0.03 | <0.03 | <0.03 | <0.03 | <0.03 | <0.04 |
| Fe | 12.8 | 17.0 | 14.0 | 9.5 | 11.4 | 9.0 |
| Se | <0.04 | <0.03 | <0.03 | <0.04 | <0.03 | <0.03 |
| Pb | <0.05 | <0.05 | <0.05 | <0.05 | <0.05 | <0.05 |
| Cd | <0.03 | <0.03 | <0.03 | 0.31 | 0.31 | 0.27 |
| Mn | <0.01 | <0.01 | <0.01 | 0.04 | <0.01 | 0.04 |
| Ni | <0.02 | <0.02 | <0.02 | <0.02 | 0.02 | <0.02 |
| Co | <0.02 | <0.01 | <0.01 | <0.01 | <0.01 | <0.01 |
| Sn | 25.74 | 21.46 | 27.00 | <0.02 | <0.02 | <0.02 |
| Total | 99.2 | 99.7 | 98.9 | 99.0 | 99.7 | 99.0 |

**Table 2** Results of EMPA analyses (in wt%) of Fe-oxides from two samples at Baal Gammon

| Sample | BG14A | BG14A | BG14A | BG14C | BG14C | BG14C |
|---|---|---|---|---|---|---|
| Analysis | 1 | 2 | 3 | 1 | 2 | 3 |
| Mg | <0.02 | <0.02 | <0.02 | <0.02 | <0.02 | <0.02 |
| Al | 0.40 | 0.45 | 0.35 | 0.17 | 0.22 | 0.31 |
| Si | 0.05 | 0.06 | 0.07 | 0.30 | 0.35 | 0.41 |
| Zn | 0.19 | 0.17 | 0.12 | <0.02 | <0.02 | <0.02 |
| Ni | <0.02 | <0.02 | <0.01 | <0.02 | <0.01 | <0.01 |
| Fe | 57.6 | 57.4 | 57.0 | 57.3 | 57.4 | 57.2 |
| Mn | <0.02 | <0.02 | <0.02 | 0.06 | 0.06 | 0.07 |
| Cr | <0.02 | <0.02 | <0.02 | <0.01 | <0.01 | <0.01 |
| V | <0.01 | <0.01 | <0.01 | <0.01 | <0.01 | <0.01 |
| Ca | <0.00 | <0.00 | <0.00 | 0.02 | 0.02 | 0.03 |
| Ti | <0.00 | <0.01 | <0.01 | <0.00 | <0.01 | <0.00 |
| O | 39.9 | 38.8 | 39.6 | 37.9 | 36.7 | 37.1 |
| S | 0.98 | 0.88 | 1.09 | 1.23 | 1.43 | 0.97 |
| Total | 99.1 | 97.8 | 98.2 | 97.0 | 96.2 | 96.1 |

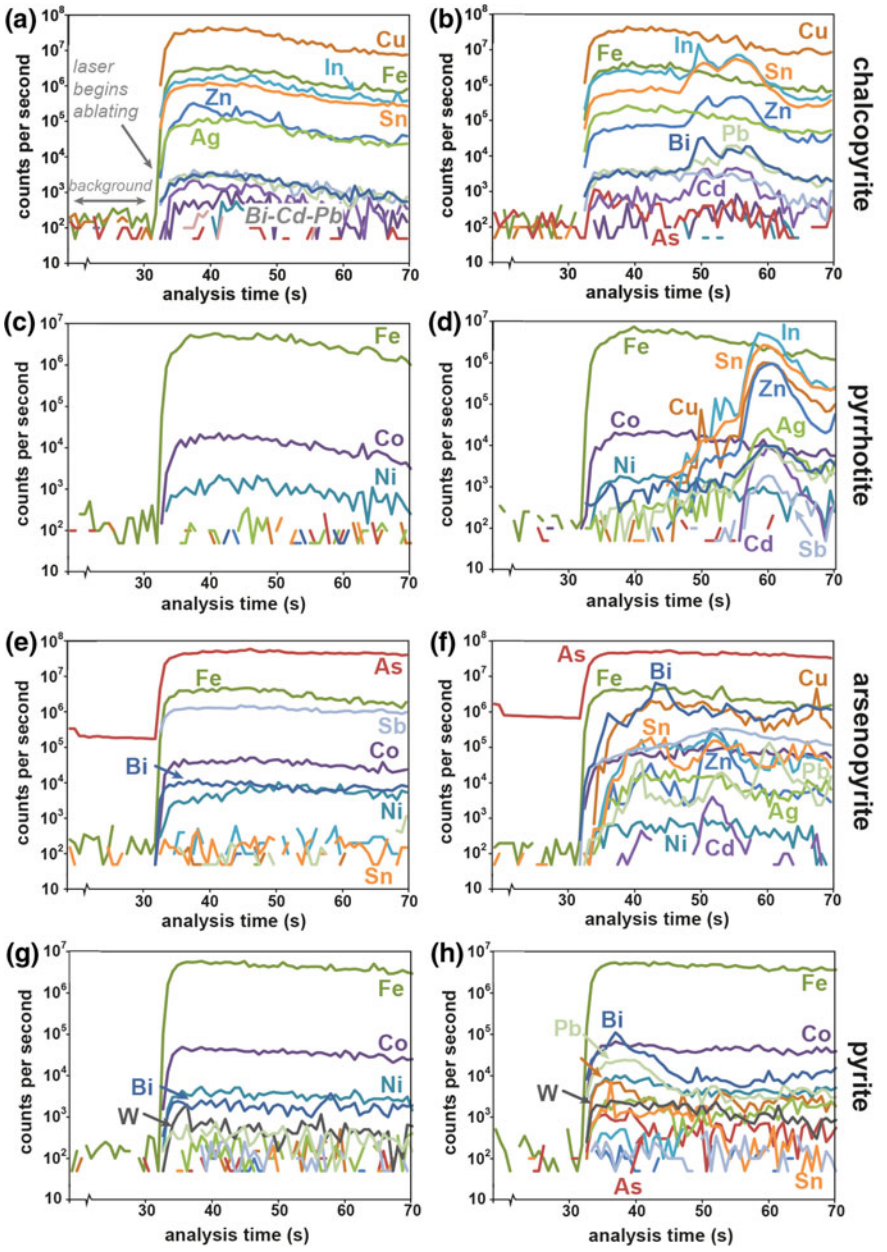


**Fig. 7** LA-ICPMS traces from major sulfide minerals showing clean intervals (*left hand side*) and inclusion-rich intervals (*right hand side*) (color figure online)

Consequently, the trace element content of a clean analytical interval within a mineral that excludes inclusions, represents only a conservative estimate of the total content of trace elements that may be liberated from that mineral during oxidation and leaching. To account for the total amount of trace elements that may be liberated from each mineral phase, intervals that include micro-inclusions of other mineral phases are reported as "bulk intervals" together with data for "inclusion-free" intervals (Table 3). Mass-bias corrected values for Cd, In and Sn are reported in Table 3 together with a suite of elements from the LA-ICPMS analysis.

## *Sulfide Minerals*

Chalcopyrite from Baal Gammon is highly enriched in trace metals including Ag, Zn, Sn, In and Cd (Figs. 7a, b and 8; Table 3). Flat LA-ICPMS traces for Ag, Cd, In, Sn and Zn shown in Fig. 7a are consistent with substitution of these elements into the crystal structure, as opposed to discrete sphalerite inclusions (Cd-In-Sn-Zn) shown in Fig. 7b. Consequently, even the cleanest LA-ICPMS analytical intervals in chalcopyrite are enriched in additional trace metals. Relative to other mineral phases, inclusion-free chalcopyrite has moderately low As (<5 ppm; Table 3), low Co and low Ni (Fig. 8d). Micro-inclusions of arsenopyrite account for locally elevated As in bulk intervals ($\sim$550 ppm; Table 3; Fig. 8f). Concentrations of Bi and Pb also increase from clean to bulk intervals (Table 3) suggesting greater liberation of these elements during oxidation and leaching of chalcopyrite.

In contrast to chalcopyrite, pyrrhotite has considerably lower concentrations of Ag, As, Bi, Cd, In, Pb, Sn and Zn than chalcopyrite. Clean pyrrhotite LA-ICPMS analyses typically only contain elevated Co and Ni (Figs. 7c, 8d). Inclusions of sphalerite and/or chalcopyrite (Fig. 7d) account for the increase in trace element concentrations in the bulk intervals (Table 3).

Inclusion-free and inclusion-rich arsenopyrite at Baal Gammon typically has the lowest concentrations of Ag, Cd, In, Sn and Zn but it is more enriched in Bi, Co, Se, Sb and Ni than all other sulfides analyzed (Figs. 7e, f and 8; Table 3). The cleanest arsenopyrite intervals show Bi, Co, Ni and Sb likely incorporated into the crystal structure (Fig. 7e), whereas chalcopyrite, stannite or sphalerite inclusions increase the concentrations of Cd, Cu, In and Zn (Fig. 7f; Table 3).

Clean pyrite intervals analyzed in BG14C also indicate elevated Co and Ni likely substituted for Fe in pyrite but also reveal elevated W in the cleanest analyses (Fig. 7g; Table 3). Inclusions containing Cu, Bi, Pb and Sn occur in pyrite also correlating with locally elevated As (Fig. 7h). However, relative to all other sulfides analyzed, pyrite only appears to have elevated concentrations of Bi, Co and Ni with slightly elevated As (Fig. 8).

**Table 3** Representative LA-ICPMS analyses from sulfide minerals at Baal Gammon

| | Isotopic mass | Chalcopyrite | | Pyrrhotite | |
|---|---|---|---|---|---|
| | | 14A | 14A | 14E | 14E |
| | | Clean interval (ppm) | Bulk interval (ppm) | Clean interval (ppm) | Bulk interval (ppm) |
| Sc | 45 | 0.18 | 0.24 | 0.17 | 0.3 |
| Ti | 49 | 2.62 | 7.26 | 2.85 | 6.2 |
| V | 51 | 0.09 | 0.31 | 0.06 | 0.5 |
| Cr | 52 | 0.76 | 1.13 | 0.82 | 0.8 |
| Mn | 55 | 4.19 | 42.73 | 1.12 | 76.6 |
| Co | 59 | 1.76 | 3.52 | 51.05 | 54.3 |
| Ni | 60 | 1.79 | 1.50 | 9.39 | 10.3 |
| Cu | 65 | 339,275 | 336,272 | 0.40 | 1654 |
| Zn | 66 | 2263 | 4280 | 0.49 | 270 |
| As | 75 | 4.35 | 543 | 0.67 | 12.9 |
| Se | 77 | 64.8 | 68.5 | 53.93 | 60.1 |
| Mo | 95 | 0.04 | 0.04 | 0.46 | 0.5 |
| Ag | 107 | 575 | 528 | 1.15 | 13.3 |
| Cd | 111 | 18.3 | 33.1 | 0.02 | 3.5 |
| In | 113 | 20.7 | 49.0 | 0.1 | 20.9 |
| Sn | 117 | 1224 | 1271 | 0.2 | 104 |
| Sb | 121 | 5.52 | 8.12 | 0.08 | 1.2 |
| Te | 125 | 0.40 | 0.41 | 0.16 | 0.2 |
| W | 182 | 1.26 | 2.68 | 0.02 | 2.3 |
| Pt | 195 | 0.03 | 0.05 | 0.03 | 0.0 |
| Au | 197 | 0.02 | 0.12 | 0.02 | 0.0 |
| Tl | 205 | 0.05 | 0.22 | 0.01 | 0.0 |
| Pb | 206 | 6.42 | 13.5 | 0.86 | 5.32 |
| Bi | 209 | 2.30 | 8.44 | 0.34 | 3.1 |
| Th | 232 | 0.04 | 0.03 | 0.01 | 0.5 |
| U | 238 | 0.07 | 0.08 | 0.01 | 0.4 |
| | Isotopic mass | Arsenopyrite | | Pyrite | |
| | | 14E | 14E | 14C | 14C |
| | | Clean interval (ppm) | Bulk interval (ppm) | Clean interval (ppm) | Bulk interval (ppm) |
| Sc | 45 | 0.13 | 0.13 | 0.12 | 0.14 |
| Ti | 49 | 1.11 | 1.29 | 2.09 | 2.88 |
| V | 51 | 0.04 | 0.04 | 0.07 | 0.20 |
| Cr | 52 | 0.95 | 0.97 | 0.57 | 0.55 |
| Mn | 55 | 0.55 | 1.16 | 0.78 | 3.38 |
| Co | 59 | 737 | 1187 | 148 | 123 |
| Ni | 60 | 71.4 | 56.2 | 80.2 | 63.2 |

(continued)

**Table 3** (continued)

| | Isotopic mass | Arsenopyrite | | Pyrite | |
|---|---|---|---|---|---|
| | | 14E | 14E | 14C | 14C |
| | | Clean interval (ppm) | Bulk interval (ppm) | Clean interval (ppm) | Bulk interval (ppm) |
| Cu | 65 | 0.99 | 303 | 0.56 | 25.4 |
| Zn | 66 | 0.73 | 4.26 | 0.58 | 1.21 |
| As | 75 | ≫ | ≫ | 2.82 | 316 |
| Se | 77 | 201 | 244 | 60.8 | 48.5 |
| Mo | 95 | 3.53 | 2.42 | 0.39 | 0.39 |
| Ag | 107 | 0.06 | 20.5 | 0.62 | 3.19 |
| Cd | 111 | 0.04 | 0.13 | 0.07 | 0.04 |
| In | 113 | 0.0 | 59.0 | 0.02 | 0.14 |
| Sn | 117 | 0.2 | 101 | 0.23 | 0.79 |
| Sb | 121 | 2200 | 2049 | 0.31 | 0.48 |
| Te | 125 | 0.38 | 0.88 | 0.11 | 0.20 |
| W | 182 | 0.25 | 0.17 | 3.37 | 3.51 |
| Pt | 195 | 0.01 | 0.01 | 0.02 | 0.02 |
| Au | 197 | 0.04 | 0.06 | 0.01 | 0.02 |
| Tl | 205 | 0.00 | 0.03 | 0.10 | 0.13 |
| Pb | 206 | 0.34 | 1954 | 5.82 | 8.51 |
| Bi | 209 | 6.14 | 3045 | 2.04 | 42.4 |
| Th | 232 | 0.00 | 0.03 | 0.01 | 0.01 |
| U | 238 | 0.00 | 0.17 | 0.01 | 0.01 |

Results for clean intervals are compared to inclusion-rich (bulk) intervals

## *Fe-Oxide Minerals*

The grain size of most Fe-oxides were not large enough to be routinely analyzed by LA-ICPMS. Coarse Fe-oxide, developed on the exterior rind of sample BG14A which comprises massive arsenopyrite, pyrrhotite and chalcopyrite, contains elevated Cd, Co, Cr, Cu, In, Pb, Sn, Th, U, V and Zn relative to Fe-oxide in sample BG14C (Figs. 8 and 9). Fe-oxide in sample BG14C is elevated in Bi, Mn and W relative to Fe-oxide in BG14A, elements that are shown to be enriched in pyrite at Baal Gammon (Table 4). The Fe-oxides contain comparable As concentrations in both BG14A and BG14C (1329 ppm and 1811 ppm, respectively; Table 4), despite sample BG14C containing only trace quantities of arsenopyrite.

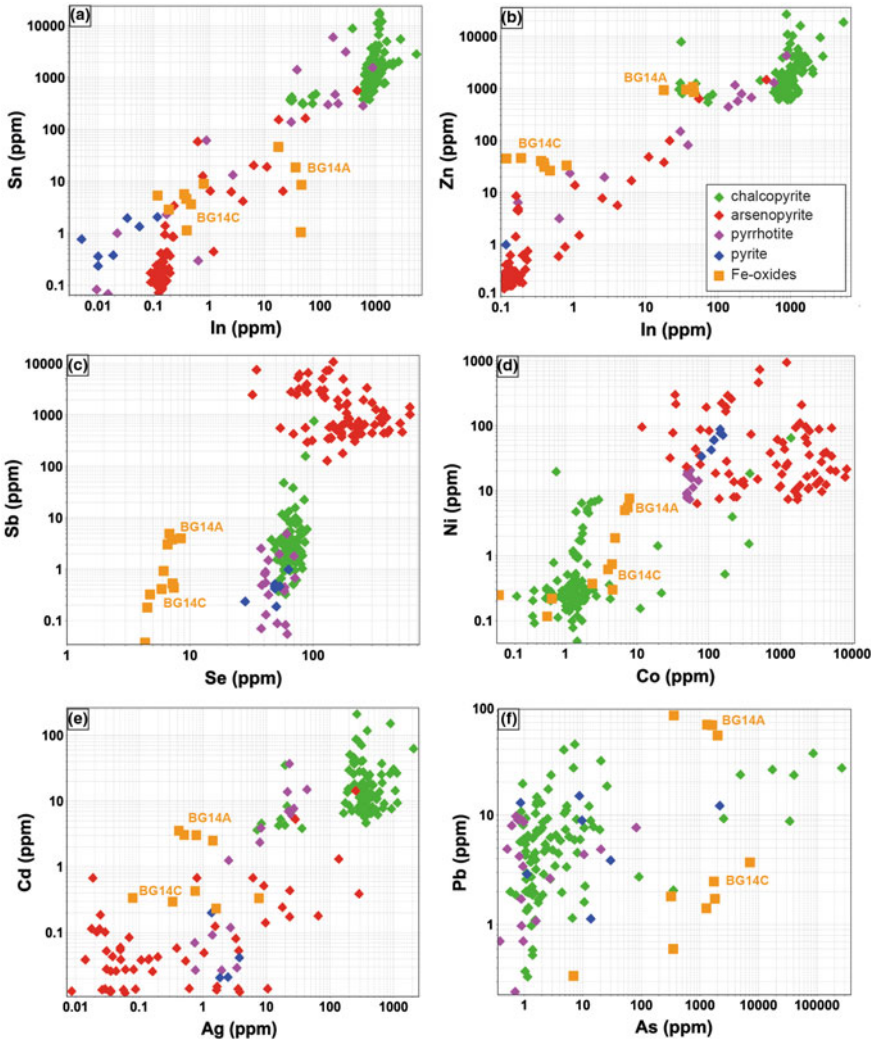


**Fig. 8** Binary plots showing element correlations in individual LA-ICPMS spot analyses of sulfide minerals and Fe-oxide. The data shown represents integration of the full LA-ICPMS output, including inclusions (see Fig. 7) (color figure online)

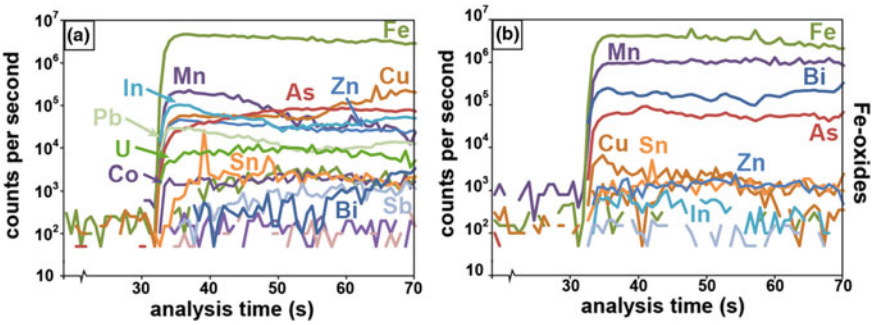


**Fig. 9** LA-ICPMS traces from Fe-oxide. **a** Fe-oxide developed in polysulfidic sample; **b** Fe-oxide developed in pyrite-rich sample (color figure online)

**Table 4** LA-ICPMS analyses of Fe-oxide from two samples with contrasting mineralogies

| | Isotopic mass | Fe-oxide within poly-sulfidic rock | Fe-oxide within pyrite dominated rock |
|---|---|---|---|
| | | BG14A | BG14C |
| | | Clean interval (ppm) | Clean interval (ppm) |
| Sc | 45 | 4.0 | 0.6 |
| Ti | 49 | 241 | 2.5 |
| V | 51 | 10.2 | 0.6 |
| Cr | 52 | 6.4 | 1.0 |
| Mn | 55 | 354 | 4171 |
| Co | 59 | 6.8 | 2.4 |
| Ni | 60 | 5.0 | 0.4 |
| Cu | 65 | 1604 | 162 |
| Zn | 66 | 952 | 37 |
| As | 75 | 1329 | 1811 |
| Se | 77 | 6.6 | 6.1 |
| Mo | 95 | 0.1 | 0.1 |
| Ag | 107 | 0.8 | 1.6 |
| Cd | 111 | 3.0 | 0.2 |
| In | 113 | 36.3 | 0.39 |
| Sn | 117 | 18.6 | 4.61 |
| Sb | 121 | 3.0 | 0.9 |
| Te | 125 | 0.4 | 0.2 |
| W | 182 | 1.8 | 4.7 |
| Pt | 195 | 0.0 | 0.1 |
| Au | 197 | 0.0 | 0.0 |
| Tl | 205 | 0.5 | 0.1 |
| Pb | 206 | 63.4 | 1.69 |
| Bi | 209 | 2.3 | 202 |
| Th | 232 | 9.1 | 0.2 |
| U | 238 | 6.5 | 0.4 |

## Implications for Element Mobility

Trace elements, either substituted into the crystal lattice or as discrete inclusions within sulfide minerals, will be liberated during oxidation in the near surface environment. Chalcopyrite at Baal Gammon contains the highest concentrations of Ag, In, Sn and Zn within both its crystal lattice and as discrete inclusions of sphalerite and stannite. Arsenopyrite is the most As-rich phase at Baal Gammon. It contains the highest concentrations of Co, Ni, Sb and Se.

The trace element composition of Fe-oxides likely developed in the low pH conditions of the ARD affected streams and is determined by the mineralogy of the sulfidic boulders on which it forms, either as rinds or as space fill. Significant quantities of As, Bi, Cu, In, Pb and Zn occur in Fe-oxides at Baal Gammon, although their mode of occurrence has not been determined (i.e., adsorpted onto mineral surfaces or incorporated into crystal lattices).

Leachate derived from sulfidic boulders will be enriched in these elements most mobile in oxidized, low pH fluids. ARD impacted water has previously discharged from the Baal Gammon site into Jamie Creek, which feeds the larger Walsh River, during seasonal flooding (Fig. 2). The ARD leachate was elevated in As, Cd, Cu, Pb and Zn, exceeding safe drinking water guidelines (Dally-Watkins 2014). The poly-sulfidic nature of mineralization at Baal Gammon and the quantities of trace metals in each mineral phase detected by this study indicate that sulfidic waste rock boulders within Jamie Creek will continue to be a source of environmentally deleterious metals without ongoing management or remediation.

## Conclusions

Sulfidic boulders collected from an ephemeral stream adjacent to the Baal Gammon mine site contain a large amount of arsenopyrite, pyrrhotite and chalcopyrite. Micro-analysis of the sulfide phases has revealed appreciable quantities of trace elements including Ag, As, Bi, Cd, Co, Cu, In, Ni, Sb, Sn and Zn. Thick Fe-oxide rinds have developed on the surfaces of the boulders, indicative of oxidation. Micro-analysis of these Fe-oxides reveals that As, Bi, Cu, In, Pb and Zn are included into their crystal structure or are adsorbed onto mineral surfaces. These elements are derived from the oxidation of sulfide minerals and leaching of trace elements. Although deleterious metals and metalloids (i.e. Ag, As, Bi, Cd, Co, Cu, In, Ni, Sb, Sn, Zn) are leached from the sulfides during oxidation, at least some of these are incorporated and therefore incorporated into Fe-oxide minerals.

The waste material at Baal Gammon and adjacent abandoned mines is extremely vulnerable to oxidation under the tropical conditions of north Queensland. Acid run-off waters may mobilize metals and metalloids either from trace element rich sulfides or Fe-oxides into surface waters. Hence, the use of micro-analytical tools

such as EMPA and LA-ICPMS allows for the prediction of element mobility upon oxidation, by determining the deportment and concentration of trace elements within sulfide minerals prone to oxidation.

## References

Blake D (1972) Regional and economic geology of the Herberton/Mount Garnet Area—Herberton Tinfield, North Queensland. Department of National Development Bureau of Mineral Resources. Geol Geophys Bull 124:293

Champion DC, Kositcin N, Huston DL, Mathews E, Brown C (2009) Geodynamic synthesis of the phanerozoic of eastern Australia and implications for metallogeny. Geoscience Australia Record No. 2009/18, 254 pp

Champion D, McKay A (2013) Australian Atlas of minerals resources, mines & processing centres. Geoscience Australia. http://www.australianminesatlas.gov.au/aimr/commodity/tin.html

Champion DC, Heinemann MA (1994) Igneous rocks of northern Queensland 1:500 000 map and GIS explanatory notes. Australian Geological Survey Organisation. Record 1994/11, 98 pp

Dally-Watkins R (2014) Company fined for Queensland waterway pollution. Austr Mining Rev I71:4

Fraser N (1972) Geology and mineralisation, United North Australian mine, Watsonville, north Queensland. BSc Hons thesis, James Cook University, Townsville

Garrad PD, Bultitude RJ (1999) Geology, mining history and mineralisation of the Hodgkinson and Kennedy Provinces, Cairns Region, North Queensland. Queensland Minerals and Energy Review Series, Queensland Geological Survey, 306 pp

Geological Survey of Queensland (2014) Indium opportunities in Queensland. https://www.dnrm.qld.gov.au/__data/assets/pdf_file/0019/238105/indium.pdf

Lam J (2009) Tin deposits in the Hodgkinson Province, current company exploration status. Queensland Gov Mining J 31–39

Monto Minerals (2014) http://montominerals.com/sites/montominerals.com/files/140314%20MOO%20Investor%20Pres%20Fnl_Optimised.pdf

Natural Systems Research Pty Ltd (1980) Environmental baseline investigation Baal Gammon project, north Queensland: vegetation, fauna, water quality and archaeology, 16 pp

Skirrow RG, Huston DL, Mernagh TP, Thome JP, Dulfer H, Senior AB (2013) Critical commodities for a high-tech world: Australia's potential to supply global demand. Australian Government Geoscience Australia, 118 pp

Solomon M, Groves DI (1994) The geology and origin of Australia's mineral deposits. Oxford monographs on geology and geophysics series 24. Clarendon Press, Oxford, 951 pp

# Prediction of Metal Mobility from Sulfidic Waste Rocks Using Micro-Analytical Tools, Spray, Tasmania

**Nathan Fox, Anita Parbhakar-Fox and Bernd Lottermoser**

**Abstract** The Zeehan Pb-Zn field in western Tasmania (Australia) contains over one hundred abandoned and historical mine sites. Combined with a temperate rainforest climate and abundant waste rock material, many sites are affected by acid rock drainage (ARD). The Spray mine, located southwest of the town of Zeehan, was one of the field's largest historical producers of Pb and Ag. Abandoned in the early 1900s, the site contains numerous adits and waste rock piles which contribute to ARD in the region. The aim of this study was to predict the likely ARD surface water quality, using the major and trace element chemistry of sulfide minerals present within waste materials on site. Major ore sulfides are galena and sphalerite with associated Sb-rich sulfosalt minerals including boulangerite and geocrocite. These minerals contain minor concentrations of Ag, Bi, Cd, In and Sn. Minor arsenopyrite and abundant pyrite (average 7500 ppm As) represent the main repository for As. Siderite is a major gangue mineral, containing slightly elevated In, Pb, Sb and Zn (250–50 ppm). Metals and metalloids (Ag, As, Bi, Cd, Cu, In, Pb, Zn) contained within sulfides and siderite may be mobilized upon mineral dissolution into ARD waters. Consequently, micro-analytical analyses of sulfides and associated gangue minerals can assist in the prediction of aqueous metal and metalloid mobility from sulfidic waste rock piles.

N. Fox (✉) · A. Parbhakar-Fox
School of Physical Sciences, University of Tasmania, Hobart, TAS 7001, Australia
e-mail: Nathan.Fox@utas.edu.au

A. Parbhakar-Fox
e-mail: Anita.Parbhakar@utas.edu.au

B. Lottermoser
Institute of Mineral Resources Engineering, RWTH Aachen University, Wüllnerstrasse 2, 52062 Aachen, Germany
e-mail: lottermoser@mre.rwth-aachen.de



B. Lottermoser (ed.), *Environmental Indicators in Metal Mining*,
DOI 10.1007/978-3-319-42731-7_15

## Introduction

The discovery of Sn mineralization on Tasmania's west coast in 1876 was followed in 1882 with discoveries of significant Pb and Ag mineralizations, which defined the Zeehan Field, east of Heemskirk (Fig. 1). Peak production in the Zeehan Field was reached in 1896 before rapidly declining Ag-Pb grades with increased depth forced most mines to close by 1913 (Both and Williams 1968). The Montana and Oceana mines (Fig. 1) were the last mines to close in the 1950s and 1960s respectively (Besley 1971). Total production from the Zeehan Field was approximately 200,000 t Pb, 27 Moz Ag and 2700 t Zn (Both and Williams 1968). Table 1 summarises the production from the Zeehan Field's largest producers, which includes the Spray Mine (also known as Silver Spray), one of the most productive

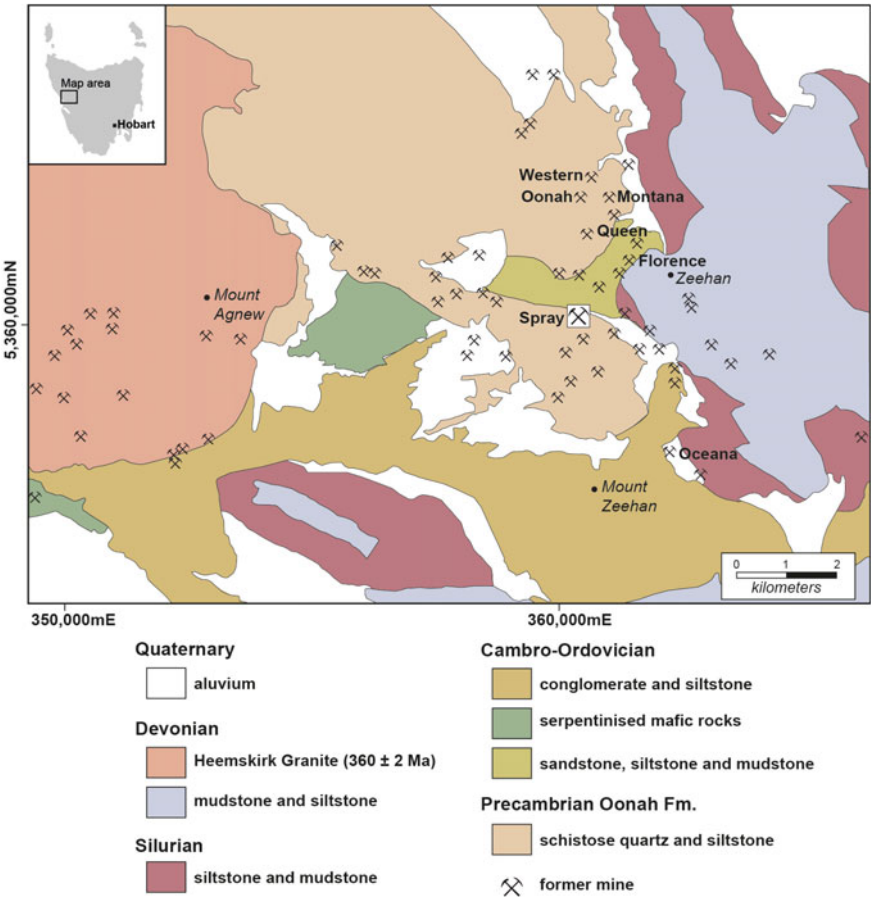


**Fig. 1** The geology of the Zeehan Field in western Tasmania showing the location of the Spray mine and other abandoned mines around the town of Zeehan. Modified from Seymour et al. (2007) (color figure online)

**Table 1** Historical production from selected polymetallic mines in the Zeehan field (after Both and Williams 1968)

| Mine | Pb (tonnes) | Ag (oz) | Additional commodities |
|---|---|---|---|
| Spray | 41,700 | 6,456,674 | |
| Montana | 49,580 | 7,058,122 | |
| Queen | 16,532 | 1,973,746 | |
| Western | 26,300 | 4,800,000 | |
| Oonah | 11,724 | 2,050,135 | 941 tonnes Cu |
| Oceana | 14,902 | 614,981 | 12.8 tonnes Zn |
| Florence | 10,200 | 140,000 | |

See Fig. 1 for locations

mines in the Zeehan Field, located approximately 2 km southwest of the town of Zeehan in western Tasmania (Fig. 1).

The Spray Mine was operational from 1889 until closure in 1910, following peak production in 1906 (Besley 1971). Reconnaissance exploration drilling and sampling of underground adits between the 1970s and 1990s (Besley 1971; Crossing 1992) failed to identify any economic Pb, Zn and Ag mineralization at depth in the Zeehan Field. Consequently, there are now more than 50 sub-economic, abandoned polymetallic mines around Zeehan (Fig. 1), many of which have flooded adits and sulfidic waste rock piles posing potential ARD hazards.

This study documents the mineralogical and geochemical characterization of polymetallic sulfidic mine waste from the Spray property, which includes the Spray, Colonial North, Foam, Wave and Nubeena historical mines (Fig. 2). Characterization of major and trace element chemistry of major sulfide minerals allows predictions to be made regarding the ARD water quality emanating from waste rock piles.

## Geological Setting and Mineralization

Mineralization at Zeehan is hosted by the Precambrian Oonah Formation, which comprises mostly schistose quartzite and siltstone, locally intercalated with basaltic lava and tuff (Both and Williams 1968; Seymour et al. 2007). Cambro-Ordovician sandstone, mudstone and siltstone overly the Oonah Formation and locally hosts mineralization (Fig. 1). The Heemskirk Granite is a composite monzo-granite to alkali feldspar granite that intruded the Zeehan stratigraphy in the Late Devonian ($360 \pm 1.9$ Ma; Black et al. 2005). Tin mineralization associated with the Heemskirk Granite extends from the central to southeastern margin of the granite (Fig. 1). Polymetallic Ag-Pb-Zn mineralization at Zeehan forms the outermost hydrothermal zone that surrounds the Heemskirk Granite (Both and Williams 1968). The most distal expression of these granite-related fluids generated Zn- and Pb-rich fissure infill veins characterized by galena and sphalerite but a general absence of Ag-bearing minerals such as argenitite (Both and Williams 1968;

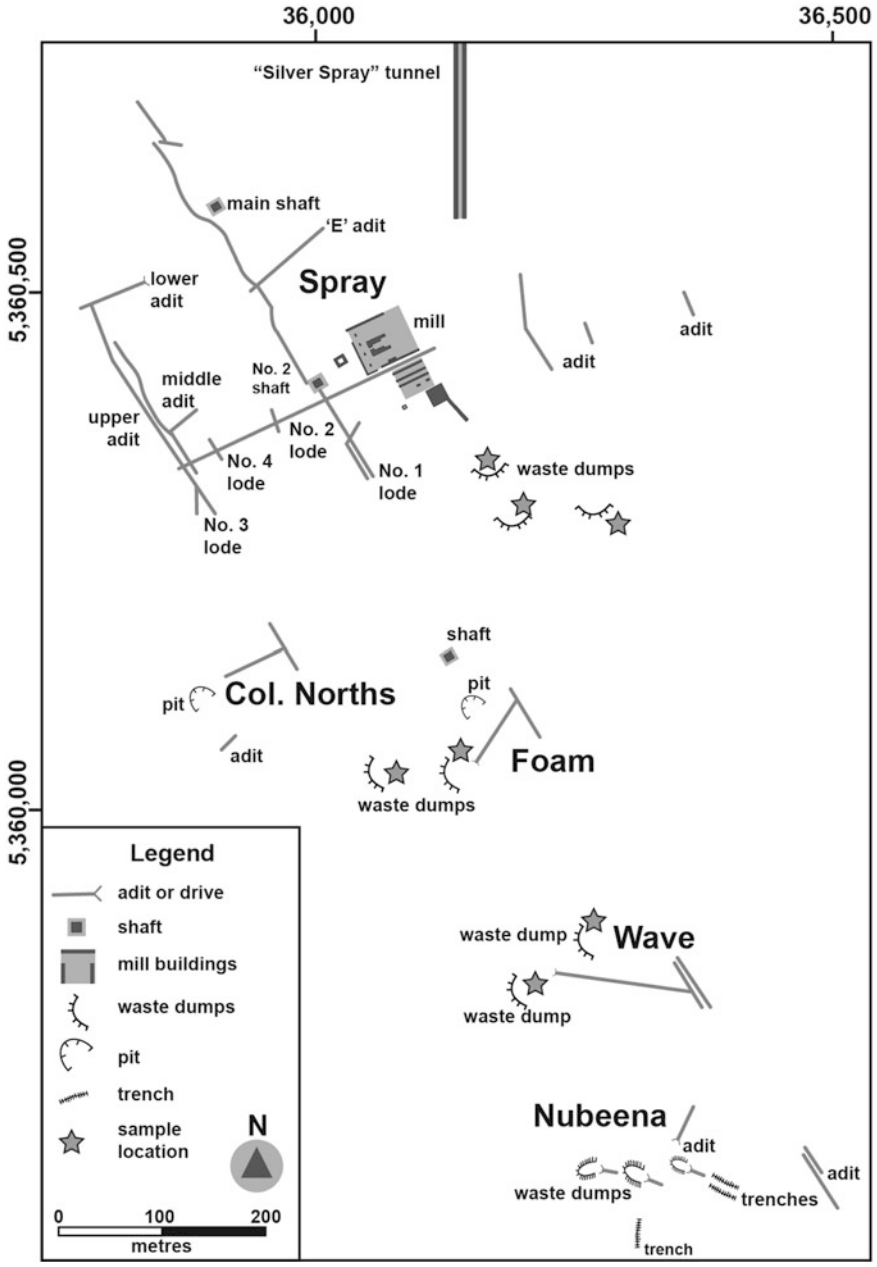


**Fig. 2** Plan of the Spray property including relict infrastructure and adits at the main Spray mine and waste dumps and pits associated with smaller workings to the south. Redrawn and modified from Besley (1971)

Green 1973). The mineralogical zonation surrounding the Heemskirk Granite proposed by Both and Williams (1968) places the Zeehan Field in the outermost siderite-pyrite subzone with abundant base metal and sulfosalt mineralization. The gangue mineralogy at Spray is consistent with this model, dominated by quartz, siderite, pyrite and arsenopyrite. Significantly, the Zeehan Field contains abundant Sb-rich sulfosalt minerals including boulangerite, tetrahedrite and bournonite (Both and Williams 1968; Green 1973). Metallurgical problems associated with the increasing abundance of Sb-rich sulfosalts (Green 1973), combined with declining Ag and Pb grades, contributed to eventual closure of the Spray Mine in 1910.

### *Site Description and Access*

Spray property is located approximately 1.5 km SW of the township of Zeehan, in western Tasmania (Fig. 1). The climate is temperate with an excess of 2400 mm of annual rainfall. The site is accessed from Zeehan via unsealed roads that pass through the town's golf course. Surface features at the Spray mine include derelict foundations of a processing mill and boiler shed, together with several vertical shafts and horizontal adits which access the now flooded underground workings at Spray, Colonial Norths, Foam, Wave and Nubeena lodes (Fig. 2). Ore was extracted at Spray from underground adits and stopes on at least nine individual mine levels, which were operated to a maximum depth of about 200 m (Besley 1971). The smaller mines located on the Spray property were also mined from underground adits and locally from small pits (Fig. 2). The site is highly vegetated with steep gradients on the surrounding hills. Numerous waste dumps and spoil heaps occur on site (Fig. 1) and are locally partially vegetated (Fig. 3). Streams draining the site appear characteristically brick-red in colour due to the effects of ARD (Fig. 3).

## Materials and Methods

Twenty-five sulfidic waste rock samples were selected from spoil heaps and waste rock piles in and adjacent to the Spray Mine (Fig. 2). The samples displayed abundant Fe-oxide staining on the outer surfaces, and when broken contained visible sulfide minerals including bright yellow pyrite and silver grey galena. The samples were cut using a diamond saw to expose fresh surfaces, and 2.5 cm diameter round polished blocks were prepared for petrological examination prior to microanalysis.

**Fig. 3** ARD affected stream and historical waste rock piles at the Spray mine, Zeehan Field, western Tasmania (color figure online)

## *Mineralogical Characterization*

All polished blocks were examined and photographed in reflected light using an automated Lecia DM6000 automated microscope at the University of Tasmania. The microscope has a high precision stage (position reproducibility better than 1 μm) which allows direct tiling of frames. The samples were photographed with a 5x objective lens under constant lighting and temperature conditions to achieve the best image results. All images were optimized for colour balance and shading correction. The images were stitched together using the LeicaQ gallery function to produce a tiled composite image of each polished mount. Scanning electron microscopy (SEM) was performed using an FEI Quanta 600 environmental scanning electron microscope (ESEM) at the Central Science Laboratory, UTAS.

### *Electron Microprobe Analysis (EMPA)*

The major element composition of sulfide minerals was determined using a Cameca SX100 electron microprobe at the Central Science Laboratory, University of Tasmania (UTAS). Samples were carbon coated (20 nm thickness) and analyzed using at 20 kV with an effective spot size of 1–2 µm. Wavelength dispersive X-ray spectrometry (WDS) provided fully quantitative chemical measurements of individual sulfide minerals. All measurements were calibrated using secondary standard reference materials including cassiterite, hessite, chalcopyrite, sphalerite, greenockite, zinc selenide, lead telluride, pentlandite, stibnite, cobalt metal and pyrite. The data was corrected for X-ray interferences (e.g., Sn on Sb peaks).

### *Laser Ablation Inductively Coupled Plasma Mass Spectroscopy (LA-ICPMS)*

The trace element concentration of individual sulfide minerals was determined by laser ablation inductively coupled plasma mass spectroscopy (LA-ICPMS) at the Discipline of Earth Sciences, UTAS. A Resonetics RESOlution system equipped with a 193 nm wavelength Coherent COMPex Pro ArF excimer laser was used to generate mineral particulates in situ from a 30 to 50 µm diameter spot. The laser was operated at 5 Hz frequency and 45 mJ energy. The material from each analytical spot was quantitatively analysed using an Agilent 7700 quadrupole mass spectrometer. Each spot analysis was analysed for a total of 60 s on the mass spectrometer comprising 30 s of background followed by 30 s of mineral ablation. Primary standards for quantification included a doped lithium borate fused disc (STDGL2B-2) and the USGS GSD-1G. Data reduction and quantification was carried out using in house Excel-based software that includes corrections for instrumental drift on the mass spectrometer. To minimize mass-bias interferences on isotopes of elements that share the same mass numbers (e.g., Cd112, Sn112; Cd113, In113; Cd114, Sn114; In115, Sn115 and Cd116, Sn116) mass-bias corrections were performed to account for simultaneous measurement isotopes of In, Cd and Sn during LA-ICPMS analysis.

## Results

### *Waste Rock Mineralogy*

The mineralogy of the waste rock samples used in this study is consistent with petrological studies at the Spray mine by Both and Williams (1968), Williams and Both (1971) and Green (1973). In hand specimen, the samples contain patches of

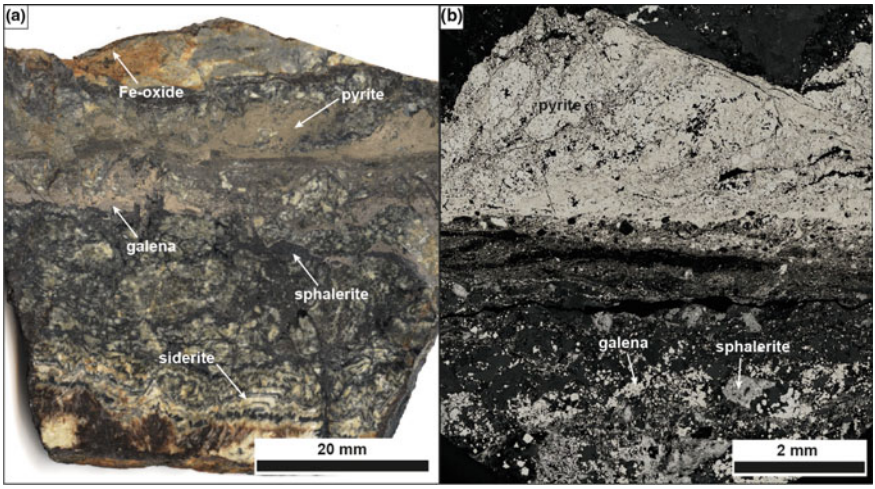


**Fig. 4** **a** Representative sample of Spray waste rock, showing the dominant mineralogy and textures. **b** Reflected light photomicrograph of representative mineral assemblages in Spray waste rock (color figure online)

euhedral pyrite, commonly intergrown with fine-grained arsenopyrite and is associated with pale white to grey quartz (Fig. 4). Colloform banded white siderite is rhythmically interlayered with dark-grey siderite and is intergrown with irregular bands of silver-grey galena and darker-grey sulfosalt minerals including boulangerite (Fig. 4). In reflected light, the pyrite contains abundant inclusions and micro-fractures infilled by galena.

## *Major Element Composition of Sulfide Minerals*

Electron microprobe analyses of sulfide minerals indicate that pyrite from the Spray Mine contains variable concentrations of As ranging from <0.02 (limit of detection) to 1.61 wt%. A negative correlation between As and Fe (Fig. 5a) and positive correlation between Fe and S (Fig. 5b) suggests stoichiometric substitution of Fe by As and S occurs within the pyrite structure. Whilst most trace elements in pyrite are largely below the limit of detection (LOD) of the electron microprobe (typically 0.02–0.05 wt%) maximum concentrations of Pb (0.15 wt%), Sb (0.04 wt%), Co (0.03 wt%) and Se (0.05 wt%) were reported. In galena only Ag (0.07–0.25 wt%) and Sb (0.07–0.17 wt%) occur in concentrations systematically above the LOD (Fig. 5a; Table 2). Arsenopyrite contains traces of Sb (0.8–1.4 wt%), Se (0.18–0.20 wt%) and Mn (0.04–0.22 wt%), whereas all other elements analysed are typically below the LOD. Sphalerite is moderately Fe-rich (2.65–5.27 wt%) and contains elevated Cu (0.16–0.77 wt%), Cd (0.20–0.39 wt%) and Sn (0.14–0.40 wt%). Boulangerite, a sulfosalt mineral with the formula $Pb_5Sb_4S_{11}$, is the dominant

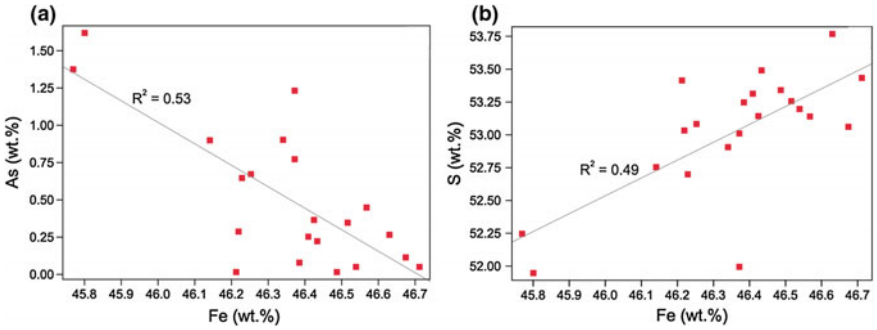


**Fig. 5** Substitution of Fe in pyrite for: **a** arsenic and **b** sulfur

antimony bearing phase at Spray. Although locally containing Zn (0.06–1.00 wt%) and Cd (0.08–0.15 wt%), boulangerite contains few other trace elements in concentrations above the limit of detection of the electron microprobe (Table 2). Geocrocite ($Pb_{14}(Sb, As)_6S_{23}$) is an antimony- and lead-rich sulfosalt mineral that has not previously been documented at Spray.

Geocrocite is found in close association with galena and boulangerite and is dominated by Pb (66.8 wt%) and Sb (14.9 wt%), with elevated Sn (0.62 wt%) and Mn (0.21 wt%) and low concentrations of As (0.03 wt%). Concentrations of Zn, Cu and Cd in geocrocite were all typically below the limit of detection of the electron microprobe (Table 2).

## *Trace Element Concentration of Sulfide Minerals*

The electron microprobe analysis indicated that waste rock samples at Spray contain abundant Pb-, Sb-, Zn-, and As-sulfide minerals including galena, sphalerite, boulangerite and arsenopyrite. Although pyrite is abundant in the waste rock samples, the microprobe analysis is less sensitive to trace element concentrations of these elements compared to LA-ICPMS analysis, which has significantly lower limits of detection (Danyushevsky et al. 2011). Furthermore, LA-ICPMS analysis can give a good indication of the mode of occurrence of these trace elements either as substitutions within the pyrite lattice or as micro-inclusions of other sulfide minerals.

### Pyrite

SEM analysis of pyrite indicates the presence of abundant micro-inclusions of galena, ranging from 1 to 20 μm in diameter (Fig. 6). The LA-ICPMS output traces for analyses with galena inclusions are identified by the occurrence of distinctive spikes or peaks in Pb with associated elevated Sn, Bi and Ag (Fig. 7). Pyrites that

**Table 2** Representative electron microprobe analyses (wt%) of sulfide minerals in waste rock from the Spray Mine, Zeehan Field, Tasmania

| Sample | SP02 | SP01 | SP02 |
|---|---|---|---|
| | Pyrite | Arsenopyrite | Sphalerite |
| S | 53.03 | 22.74 | 33.19 |
| Ag | <0.02 | <0.03 | 0.04 |
| Cu | 0.03 | 0.04 | 0.55 |
| Zn | <0.03 | <0.03 | 62.53 |
| Sb | <0.02 | 1.37 | <0.03 |
| As | 0.29 | 39.60 | <0.03 |
| Fe | 46.22 | 35.60 | 2.65 |
| Se | <0.02 | 0.20 | <0.03 |
| Pb | 0.07 | <0.05 | <0.05 |
| Cd | <0.03 | <0.03 | 0.20 |
| Mn | <0.01 | 0.05 | <0.01 |
| Ni | <0.02 | <0.02 | 0.02 |
| Co | <0.01 | 0.03 | <0.01 |
| Sn | <0.02 | <0.02 | 0.40 |
| Total | 99.64 | 99.62 | 99.58 |
| Sample | SP06 | SP05 | SP05 |
| | Galena | Boulangerite | Geocrocite |
| S | 13.32 | 17.84 | 15.06 |
| Ag | 0.22 | <0.04 | <0.04 |
| Cu | <0.04 | <0.04 | <0.04 |
| Zn | <0.04 | <0.04 | <0.04 |
| Sb | 0.12 | 27.08 | 14.97 |
| As | <0.03 | <0.03 | 0.04 |
| Fe | <0.02 | 0.10 | 1.58 |
| Se | <0.03 | <0.03 | <0.03 |
| Pb | 86.34 | 54.86 | 66.83 |
| Cd | <0.06 | <0.05 | <0.05 |
| Mn | <0.01 | <0.01 | 0.21 |
| Ni | <0.02 | <0.02 | <0.02 |
| Co | <0.02 | <0.02 | <0.02 |
| Sn | <0.04 | <0.03 | 0.62 |
| Total | 99.99 | 99.88 | 99.31 |

are free of galena inclusions have distinctly flat traces for As, Cu, Fe, Sb and Zn as well as notably flatter traces for Ag, Bi, Pb and Sn (Fig. 7).

Pyrite from Spray contains elevated As (mean 7490 ppm) relative to galena and sphalerite (Table 3; Fig. 8) and is also notably lead-rich from galena inclusions and Pb-substitutions. Mean concentrations of Sb, Ni, Co, Cu and Zn are also generally low compared to other sulfide minerals analysed (Table 3; Fig. 8a).

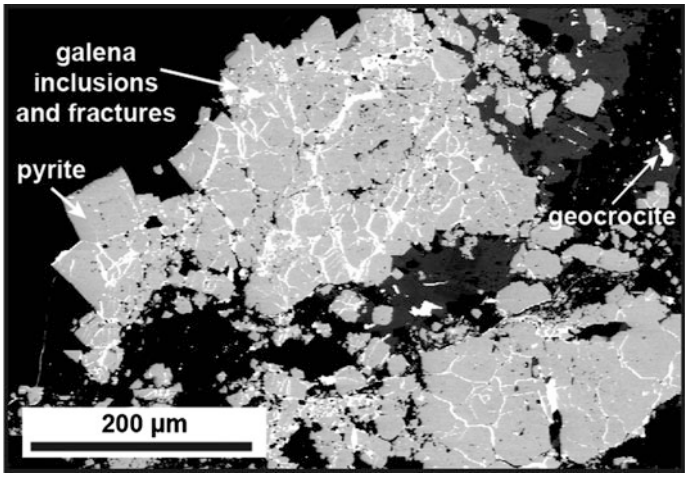


**Fig. 6** Backscattered scanning electron (BSE) image of pyrite (*mid-grey*) with abundant macro- and micro-inclusions of galena, boulangerite and geocrocite (*bright white*)

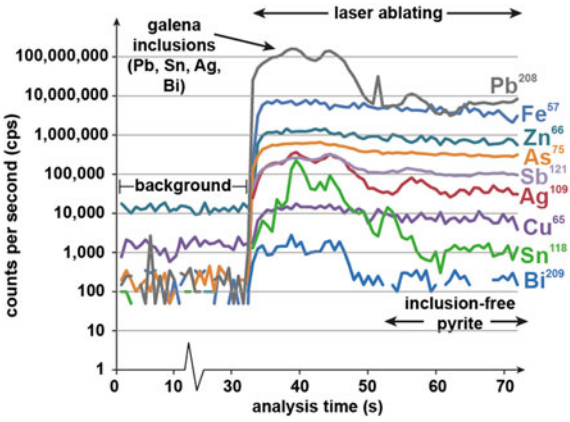


**Fig. 7** Output element traces from a single LA-ICPMS analysis of pyrite from the Spray mine. Flat traces for As, Cu, Fe, Sb and Zn are from pyrite, whereas irregular or erratic spikes in Pb, Ag, Bi and Sn indicate ablation of galena micro-inclusions (color figure online)

## Sphalerite

Sphalerite has the highest concentration of Pb, Cu, Cd, Sn, and In relative to other sulfides analysed at Spray (Table 3; Fig. 8b). The elevated concentration of these elements appears to be due to substitutions into the structure of sphalerite as opposed to the presence of micro-inclusions (e.g., chalcopyrite disease). The concentration of As in sphalerite has a wide range (Fig. 8), but a low mean concentration relative to pyrite (Table 3).

**Table 3** Mean concentration of selected trace elements in sulfide minerals from waste rock at the Spray Mine, as determined by LA-ICPMS

| | As (ppm) | Sb (ppm) | Pb (ppm) | Zn (ppm) | In (ppm) | Sn (ppm) | Ag (ppm) | Cu (ppm) |
|---|---|---|---|---|---|---|---|---|
| Pyrite | 7490 (*4735*) | 388 (*199*) | N/A | 32.6 (*4.1*) | 1.9 (*0.9*) | 13.6 (*3.4*) | 81 (*35*) | 61(*45*) |
| Sphalerite | 123 (11.9) | 546 (351) | 9550 (2664) | N/A | 1475 (1112) | 3161 (2442) | 767 (552) | 7552 (6100) |
| Galena | 2.5 (*0.9*) | 1713 (*1678*) | N/A | 0.88 (*0.78*) | 2.1 (*2.0*) | 129 (*78*) | 1502 (*1486*) | N/A |
| Siderite | 3.4 (*3.3*) | 43 (*9.9*) | 89 (*35.6*) | 88 (*71*) | 127(*110*) | 6.8(*5.4*) | 0.2(*0.1*) | 7.1 (*1.9*) |

Values italicized in brackets represent the mean of the natural logarithm ($\log_{(x)}$) of the analysed values as displayed in Fig. 8

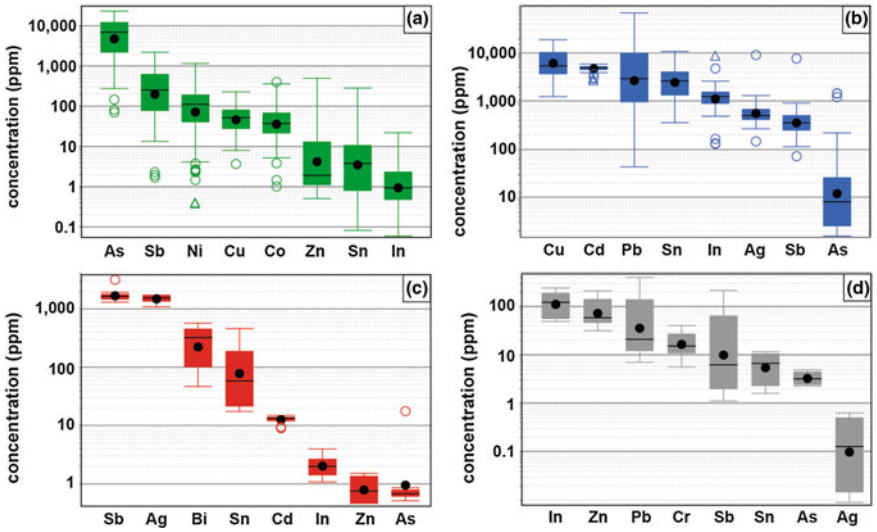


**Fig. 8** Tukey plots showing trace element concentrations (log scale) of: **a** pyrite; **b** sphalerite; **c** galena; and **d** siderite from the Spray mine waste rock. Data representation is based on logged values. *Black circles* indicate the mean, *black line* the median, *whiskers* are the maximum and minimum values omitting outliers (*open circles*) and far outliers (*open triangles*) (Color figure online)

## Galena

Galena contains the highest concentration of Ag, Bi and Sb relative to all other sulfides analysed (note that boulangerite and geocrocite were not analysed by LA-ICPMS; Table 3; Fig. 8). Overall, the concentration of Sn in galena is only slightly elevated (mean 129 ppm) relative to pyrite, but it contains lower concentrations of As and Zn (Table 3; Fig. 8).

## Siderite

Siderite from Spray was analysed by LA-ICPMS to determine the trace element concentration of this major gangue phase. Overall, the siderite contains low concentrations of trace elements (overall range 250–0.01 ppm) relative to the sulfide minerals analysed (Fig. 8). However, the concentrations of In and Zn in siderite is higher than that in pyrite (Fig. 8).

### *Implications for Predicting Leachate Quality*

The mineralogy of the waste rock at Spray reflects the overall metal budget of the ore forming environment on the distal fringes of the Heemskirk Granite, one of the world's major Sn-W provinces (Both and Williams 1968; Solomon and Groves 1992). As a major Pb-Zn producing region, galena and sphalerite from Spray represent the dominant sources of Pb and Zn into surface waters draining the mine site.

In addition, the occurrence of Sb-rich phases including boulangerite and the newly identified geocrocite in close association with galena indicate that Sb may be a significant contaminant in the local area. The trace element concentration of sphalerite indicated that this phase also contains abundant Ag, Cd, Cu, In and Sb but comparatively low concentrations of As. Sphalerite therefore represents a major potential source of these deleterious elements during sulfide oxidation. In contrast, galena with low concentration of As, Cd, In and Zn represents a significant source of Ag, Bi and Sb during oxidation.

Pyrite is a significant gangue sulfide mineral at Spray, occurring ubiquitously in all waste rocks sampled. Pyrite is extremely enriched in Pb, most likely as inclusions of galena, but it also represents a significant source of As with a mean concentration of 7500 ppm (Table 3). Relative to other sulfide phases analysed, pyrite has variable, but comparatively low, concentrations of most other trace elements including Sn, In and Zn. During oxidative dissolution of pyrite, the leachate would likely be enriched in As and may facilitate further oxidation of other sulfide minerals in waste rock at Spray.

Siderite, as the main non-sulfide gangue mineral, may represent a potential acid-neutralizing phase, partially mitigating the effects of ARD generation. However, with trace element concentrations of In, Pb, Sb and Zn between 10 and 200 ppm (Table 3) siderite may represent an additional source of these contaminants.

## Conclusions

Waste rock samples from the historical mine workings at the Spray mine are highly sulfidic and contain a large amount of galena and sphalerite with associated Sb-rich sulfosalt minerals including boulangerite and geocrocite. Micro-analysis of the sulfide phases has revealed variable quantities of trace metals and metalloids. Furthermore, the gangue mineral siderite contains detectable In, Pb, Sb and Zn concentrations. Considering the fact that sulfide and gangue minerals presently oxidize within the exposed waste rock piles, it is likely that the contained metals (Ag, Bi, Cd, Cu, In, Pb, Zn) and metalloids (As, Sb) are mobilized into ARD drainage waters.

## References

Besley RE (1971) Final report Spray mine evaluation, E.L. 44/70, Tasmania. Tenneco Australia Inc. 39 pp

Black LP, McClenaghan MP, Korsch RJ, Everard JL, Foudoulis C (2005) Significance of Devonian-Carboniferous igneous activity in Tasmania as derived from U-Pb SHRIMP dating of zircon. Aust J Earth Sci 52:807–829

Both RA, Williams KL (1968) Mineralogical zoning in the lead-zinc ores of the Zeehan field, Tasmania, Part II: Paragenetic and zonal relationships. J Geol Soc Aust 15:217–244

Crossing DJF (1992) Zeehan area annual report for the period Oct. 1991 to Sept. 1992. RGC Exploration Pty. Ltd. Report T/92-17, 351 pp

Danyushevsky LV, Robinson P, Gilbert S, Norman M, Large R, McGoldrick P, Shelley M (2011) Routine quantitative multi-element analysis of sulphide minerals by laser ablation ICP-MS: standard development and consideration of matrix effects. Geochem Explor Environ Anal 11:51–60

Green G (1973) Mineragraphy of the Spray Mine, Zeehan. Tas Mines Dept Tech Dept 16:16–18

Seymour DB, Green GR, Calver CR (2007) The geology and mineral deposits of Tasmania: a summary. Tas Geol Surv Bull 72:1–32

Solomon M, Groves DI (1992) The geology and origin of Australia's mineral deposits. Oxford monographs on geology and geophysics series 24, Clarendon Press, Oxford, 951 pp

Williams KL, Both RA (1971) Mineralogy of the mines and prospects of the Zeehan Field. Rec Geol Surv Tasm 11:1–46

# Part IV
# Air Quality

# Mineral Dust Emissions at Metalliferous Mine Sites

**Taryn L. Noble, Anita Parbhakar-Fox, Ron F. Berry and Bernd Lottermoser**

**Abstract** Mineral dusts produced from mining activities pose a risk to human health and the surrounding environment. The particle size distribution of dust is important for determining environmental, occupational health and physiological impacts. Dust is generally thought of as particulates with a diameter of between 1 and 60 μm, but it can be further divided into nuisance dust or total suspended particulates, fugitive dust, inhalable dust, thoracic dust, and respirable dust. This review considers aspects of mineral dust related to the mining of metalliferous ores including: (a) sources of mineral dust at mine sites (i.e. land clearing, drilling and blasting, transport operations, crushing, milling, screening, stockpiles); (b) control measures to reduce dust generation; (c) monitoring techniques; (d) mineral dust characterization to quantify particle concentration, size and morphology and chemical composition; and (e) prediction of mineral dust properties. Predicting the physical and mineralogical characteristics of dust is important for effective dust management and control strategies. At present, there are no appropriate testing procedures available to predict the chemical and mineralogical properties of mineral dust from mining operations. Further work is required to understand mineral fractionation according to grain size and to provide a rapid test methodology that would predict dust composition.

T.L. Noble (✉) · A. Parbhakar-Fox · R.F. Berry
School of Physical Sciences, University of Tasmania, Private Bag 79, Hobart, TAS 7001, Australia
e-mail: Taryn.Noble@utas.edu.au

A. Parbhakar-Fox
e-mail: Anita.Parbhakar@utas.edu.au

R.F. Berry
e-mail: Ron.Berry@utas.edu.au

B. Lottermoser
Institute of Mineral Resources Engineering, RWTH Aachen University, Wüllnerstrasse 2, 52062 Aachen, Germany
e-mail: lottermoser@mre.rwth-aachen.de



B. Lottermoser (ed.), *Environmental Indicators in Metal Mining*,
DOI 10.1007/978-3-319-42731-7_16

## Introduction

Atmospheric transport of dust is an important mechanism for the distribution of contaminants over large spatial scales and prolonged time periods. Mining processes provide multiple pathways for the production and dispersal of mineral dust into the surrounding environment. Dust source activities include removing overburden, blasting, crushing, hauling on unsealed roads, and dispersion from waste dumps or ore stockpiles. Dust dispersal represents a significant risk to human health and the local environment. The health risks associated with inhalation of dust depends on the physical properties of dust, such as the particle size and shape, composition, solubility, and reactivity in respiratory fluids (Plumlee and Ziegler 2003). Mineral dusts sourced from mining activities that are of particular concern include those rich in crystalline silica (e.g. quartz, tridymite, cristobalite), coal, and dusts containing metals and metalloids such as As, Pb, Cd and U (NIOSH 2002). Mining remains one of the most dangerous occupations in the world, but it is through exposure to hazardous mineral dusts that long term health implications are realized (Stephens and Ahern 2001).

This review aims to provide an overview of the existing literature on dust from metalliferous mining operations. The literature presented relates to: (i) dust sources and control measures; (ii) monitoring techniques; (iii) mineral dust characterization; and (iv) predicting dust composition. This review does not include computational methods relating to modeling of mine dust emissions and dispersal and excludes discussion of aerosols produced from industrial activities, carbon (black soot) from vehicular transport and fossil fuel burning and emissions from underground mine workings.

### *Definitions*

- A range of terms exists to describe the different classes of dust for the purpose of sampling and monitoring (*Australian Department of Environment's Best Practice Dust Control Handbook* 1998; WHO 1999) and occupational health impacts (ISO 1995): *Mineral dust* is a primary particle emitted directly into the atmosphere, as individual grains or aggregates. It is usually <60 μm in diameter but can be up to 100 μm. The composition of the mineral dust varies widely according to the source.
- *Nuisance dust* describes dust that results in adverse aesthetic effects, such as settling on surfaces and causing discoloration and soiling. It ranges in size from 0.001 to 50 μm, and is generally termed *total suspended particulates* (TSP). The larger particles are inhalable and can cause irritation of the mucosal membranes (i.e. nose, throat, eyes).

- *Fugitive dust* refers to dust derived from a mixture of sources which may not be easily defined. For example, mine dust is frequently derived from multiple sources, including during transport of material (vehicular or conveyor) and processing (crushing and grinding).
- The proportion of *particulate matter* (PM) that can be inhaled into the body can be defined through sampling conventions. These conventions describe the fraction of particles penetrating the respiratory regions according to specified conditions (e.g. wind speed and direction of air movement near the body) and the relationship with aerodynamic diameter (British Standard Institute 1993).
- *Inhalable dust* is the proportion of dust that can be inhaled through the nose and mouth and deposited there. It includes a range of particle sizes generally between 5 and 10 μm and larger (<100 μm) (ISO 1995). Human health effects tend to be associated with particles with an aerodynamic diameter of less than 10 μm ($\leq$ PM10).
- *Thoracic fraction* is the mass fraction of inhalable dust that penetrates beyond the larynx (ISO 1995). The PM10-2.5 fraction makes up >50 % of the inhalable particles which can be deposited into the upper airways and lungs.
- *Respirable dust* is the particulate fraction that can be inhaled beyond the terminal bronchioles into the alveoli or gas exchange region of the lungs and pose a greater health risk through absorption of trace elements into the blood stream. The respirable fraction makes up >50 % of the inhalable particles less than 4 μm in diameter. This dust fraction is termed the $PM_{2.5}$ fraction.

Dust can also be divided into sub-classes of environmental, occupational health and physiological effects, as presented by Petavratzi et al. (2005) (Table 1).

## Implications of Dust Dispersal

The dispersal of dust and aerosols from mining activities to the surrounding environment via wind deposition provides a pathway for the accumulation of heavy metals and contaminants in the environment. Exposure to heavy metals by ingestion or inhalation of contaminated soils and directly emitted particulates can result in absorption of soluble substances or physiological responses in the body

**Table 1** Classification of dust types (Petavratzi et al. 2005)

| Environmental effect classes | Occupational health effect classes | Physiological effect classes |
|---|---|---|
| Generated dust<br>Total suspended dust<br>Nuisance dust<br>Fugitive dust | Inhalable dust<br>Thoracic dust<br>Respirable dust | Toxic dust<br>Carcinogenic dust<br>Fibrogenic dust<br>Explosive dust<br>Nusiance dust |

**Table 2** Hazardous mineral dust generated during metalliferous mining

| Mineral types | Description | Analysis | Health impacts |
|---|---|---|---|
| Asbestos | Highly fibrous silicate minerals. Two groups: serpentine (chrysotile) and amphiboles (actinolite, tremolite, anthophyllite, amosite and crocidolite). Long, thin, strong fibres | TEM | Carcinogen (US EPA 1986) |
| Crystalline silica | Microcrystalline quartz and polymorphs: cristobalite and tridymite are hazardous | XRD and IR | Silicosis. Lung cancer (IARC 1997) |
| Sheet silicates | Talc, pyrophyllite, kaolinite, vermiculite and zeolite (erionite) | XRD | Talcosis, bronchitis and emphysema (Ross et al. 1993) |
| Mineral dusts | Dusts containing U, Pb, Hg, As | FESEM | Child development (e.g. Boreland and Lyle 2006) |

*TEM* transmission electron microscopy, *XRD* X-ray diffraction, *IR* infrared spectrophotometry

(e.g. production of fluid in the respiratory tract) to remove foreign particles (Plumlee and Zeiger 2003). The World Health Organization air quality guidelines for reducing the effects on health from air pollution (WHO 2000) should be referred to for the latest summary on the risks associated with inhalation of particulate matter. As described in the Air Quality Guidelines Global Update 2005 (WHO 2006), current scientific research suggests that guidelines cannot be proposed that will completely protect against adverse health impacts of particulate matter. The guidelines presented by the WHO should be applied with caution as health effects have been reported for relatively low ambient PM concentrations and with a range of different individual responses to PM exposure. While particle size is the main focus of regulatory standards, the health risk of particles is also influenced by their chemistry and shape. In the case of mine dusts, understanding the mineralogy and geochemistry is imperative to managing the hazards posed by different dusts (Table 2) (Best Practice Handbook: Airborne Contaminants, Noise and Vibrations 2009). The US National Research Council's Committee on Research Priorities for Airborne Particulate Matter (National Research Council 2004) summarized the characteristics of PM that may be important to health responses in relation to toxicity and bioaccessibility. These factors include size mode, mass concentration, acidity, particle surface chemistry and area, particle chemistry (metals, carbon) and solubility. Plumlee and Zieger (2003) provided a summary of heavy metals and metalloids sources, pathways and known or postulated health effects associated with deficiencies of constituents (e.g., essential minerals Ca, Fe), as well as health effects associated with excessive exposure to non-essential elements that are toxic (e.g., Pb, Cd, Hg).

## Dust Generation and Control in Mining

The quantity and nature of dust generated at mine sites is controlled by many different factors. The mineralogy of the rock will influence rock-breakage characteristics, while the climatic conditions (e.g., precipitation, wind gustiness) will control the degree of dust dispersal. Dust sources can either be point sources (e.g., rock breakage circuits), which are more easily managed relative to fugitive sources (e.g., unsealed roads). Over the past 30 years the US Bureau of Mines (USBM) and now the National Institute for Occupational Safety and Health (NIOSH) have conducted extensive research to lower silica concentrations in dust from metal/non-metal operations. Various control technologies are recommended, as described in Cecala et al. (2012).

Accurate quantification of dust emissions at mine sites facilitates the development of appropriate dust control strategies. The US Environmental Protection Agency's (US EPA) *AP-42 Compilation of Air Pollutant Emission Factors,* now in it in its fifth edition, provides emission factors for more than 200 categories of air pollution sources. The emission factors are a representative estimate of the quantity of a pollutant emitted to the atmosphere in relation to a specific activity involved in the release of that pollutant. These factors are usually expressed as the weight of pollutant divided by a unit weight, volume, distance or duration of the activity emitting the pollutant (e.g. kilograms of particulate emitted per megagram of coal burned). The emission factors are calculated based on averages of data that aim to reduce biases from site specific or short-term variability.

Exposure to respirable dust at surface mines primarily results from (i) overburden drilling and (ii) haul road dust. In minerals processing, sources of dust include belt conveyors, transfer chutes, crushing, milling, storage bins/hoppers and stockpiles. Unpaved roads generated most of the dust emissions in open pit mines but these emissions can be reduced by up to 72 % by spraying with water (Huertas et al. 2012a). Ghose and Majee (1998) showed that dust production in Indian opencast mines was predominately from coal processing (72 % from crushing, conveyor belts, unloading), wind erosion (17 %), overburden removal (7 %), coal extraction (3 %), and topsoil removal (1 %). The following section highlights the main dust sources at mine sites and the control measures used to mitigate dust dispersal.

### *Land Clearing*

Surface mining operations require topsoil and overburden to be removed and relocated. The dust generated from land clearing is nuisance dust since it originates from diffuse sources (Best Practice Dust Control Handbook 1998). The larger size fraction of mineral dust generated from land clearing limits the spatial distribution of dust generated by this activity.

**Table 3** Total dust generated per meter coal, limestone and iron ore drilled according to drill hole diameter (DDH) (Pandey 2012)

| DHH (mm) | Coal (kg $m^{-1}$) | Limestone (kg $m^{-1}$) | Iron ore (kg $m^{-1}$) |
|---|---|---|---|
| 60 | 3.7 | 7.8 | 12.7 |
| 100 | 10.2 | 21.5 | 35.5 |
| 150 | 23 | 48.6 | 79.5 |
| 200 | 40.9 | 86.4 | 144.5 |
| 250 | 63.8 | 134.9 | 220.7 |
| 300 | 92 | 194.5 | 318.2 |

Control options to reduce dust emission rate for dozing activities are limited to changing the material moisture content by wet spray systems, which can suppress dust emission. Meteorological conditions can also be considered to avoid clearing during gusty conditions. Cecala et al. (2012) outline the theory behind wet spray systems and operational and maintenance issues for these dust control mechanisms.

## *Drilling and Blasting*

The process of drilling for blasting operations at mines is a notorious source of respirable dust, which can lead to high exposure levels for the workforce involved (Cecala et al. 2012). The rate of dust generation during blast hole drilling has been shown to increase with the diameter of the drill, as well as rock hardness (Table 3). A study quantifying the rate of dust generation from sources in gold and platinum mines in South Africa concluded that blasting generated extensive amounts of dust, and that higher levels of mechanization led to higher generation rates (Biffi and Belle 2003).

Blasting is the first step in the comminution sequence to liberate valuable minerals from waste by initial fragmentation of the rock. At open pit and strip mines blasting is a controlled operation, which occurs intermittently to fragment the rock being mined. Blasting can be optimised to reduce the cost of crushing and grinding and to suit the processing requirements of each individual mine. Blasting results in the initial formation of a concentrated dust cloud that can affect the local region. The particle size distribution generated during blasting is highly variable but can produce a high proportion of fines (PM10).) Updated estimates of emission factors for TPS (<30 μm) and PM10 can be found in the *Emission Estimation Technique Manual for Mining Version 3.1* (EA 2000, 2012). The surface mining dust control strategies for drilling and blasting were reviewed by Cecala et al. (2012).

## *Transport*

Transport of ore, waste rock and tailings and ore concentrate can generate significant quantities of fugitive dust. The transport of waste rock and ore at a mine site by haul trucks on unsealed roads can be one of the largest sources of particulate emission, requiring the most expensive dust control mechanisms (e.g. Amphonsah-Dacosta 1997). Dust emissions at sites of loading, unloading and stockpiling of processed materials (e.g. coal, iron ore, phosphorites) can have significant impacts on the surrounding environment. The grain size fraction of the final products is often fine (50–100 μm) and therefore easily dispersed. There are numerous published examples of dust emission studies at ports during handling of iron ore (e.g. Port Headland, BHP Billiton), coke (e.g. Valencia Harbour; Moreno et al. 2009), and phosphorites (Silva et al. 2012).

Control technologies to reduce dust emissions from unpaved roads are limited by the availability of water, particularly during dry seasons. Different methods available include a range of additives that are mixed with water to reduce the evaporation and agglomeration of particulates over unpaved roads. Huertas et al. (2012a) summarized the advantages and disadvantages of each of these methods (Table 4).

**Table 4** Comparison of control technologies for unpaved roads (Huertas et al. 2012a)

| Substance | Mechanism | Advantage | Disadvantage |
|---|---|---|---|
| Water | Wets the particles, increasing their mass and agglomeration | Low cost<br>Minimum environmental impact | Requires regular application<br>Overwatering can lead to problems |
| Salts | Hydroscopic substances that attract and retain soil moisture | Reduce evaporation to a third<br>Compact material | Corrosive<br>Removed by rain<br>Environmental impacts |
| Surfactants | Reduce surface tension of water | Easy to apply | Low residual effects |
| Resin emulsions | Act as adhesives to agglomerate the fines | Low solubility<br>Non-corrosive<br>Seals the surface | Disappear with road maintenance<br>Require heavy use |
| Lignin derivatives | Act as adhesives to agglomerate the fines | No water requirement<br>Not removed with road maintenance | Disappear with rain<br>Slippery when wet<br>Environmental impacts |
| Bitumen | Paves the road | Insoluble to water<br>Seals against water<br>Long lasting | Expensive |
| Polymers | Act as adhesives to agglomerate the fines | More effective agglomeration than resins<br>Suitable for long-term applications<br>Low environmental impact | Require regular application<br>Expensive |

## *Crushing, Milling and Screening*

Crushing, milling and screening operations can be major sources of dust due to major reductions in grain size during comminution and segregation processes. Estimates of dust emissions from common mineral processes demonstrate that dust emissions increase as the size of the material processed decreases (US EPA 2004). For example, in the case of coal, a mean particle size as fine as 5 μm may be necessary (Mankosa et al. 1989). In contrast, in Australia a number of fine grinding stirred mills are being used for beneficiation of fine grained base metal ores (e.g. Century Zinc, McArthur River, George Fisher) (Jankovic et al. 2000).

Crushing is performed in a series of size reduction steps, which vary from hard ores (Cu, Au, Fe ores), which may require three stages of crushing to soft ores (uranium, bauxite) that require little or no crushing. Crushing can be achieved by different equipment through either slow compression of particles against rigid surfaces or by impact. The next stage of size reduction for mineral processing generally involves wet grinding in tumbling mills where breakage occurs by compression, chipping and abrasion using an assortment of grinding media. The product of primary grinding can result in particles between 40 and 300 μm for tumbling mills but varies according to the type of mill (Table 5). In the case of stirred mills, particle sizes of a few microns (<15 μm) can be achieved but with high energy costs (Herbst et al. 2003; Cecala et al. 2012). Grinding is most often performed with a slurry, which reduces dust emissions to negligible levels, but where dry grinding is used dust emissions can be considerable. Since grinding operations can produce particles that are within the respirable size range, this source of dust dispersal poses a significant health threat to workers.

Cecala et al. (2012) discuss in detail the dust control mechanisms for crushing, grinding and screening. Briefly, dust suppression during crushing can be achieved through the application of water, by enclosure of the dust source with or without exhaust ventilation or a combination of wet and dry methods. Milling or grinding operations that utilize dry milling should use enclosed milling circuits and transfer points to contain dust dispersal. Dust control systems during the screening process should also be fully enclosed to minimize dust dispersal.

## *Stockpiles*

Storage piles of ore (short-term), waste rock and tailings (long-term) and other aggregate materials are integral to any mining operation. Storage piles are usually

**Table 5** Summary of grain size reduction parameters for milling (Herbst et al. 2003)

| Comminution equipment | Feed size (cm) | Product size (μm) | Conditions |
|---|---|---|---|
| Ball mill | 1 | >20 | Wet or dry |
| Autogenous mill | <25.4 | >200 | Wet or dry |
| Stirred ball mill | <150 | >0.2 | Wet |

left uncovered due to the access requirements for frequent material transfer. Dust emissions can occur throughout the storage cycle, during loading and unloading of material and erosion by strong winds. Dust emission from stockpiles will depend on the grain size of the aggregate material, age of the pile and moisture content. The US EPA AP-42 (US EPA 2006), provides emission factors for particulate emissions from stockpiles which depend on the particle size of the storage material, wind speed and material moisture content.

Fine-grained tailings in tailings dams or other storage facilities are susceptible to wind erosion and therefore, dispersion of dust. The particle size distribution of tailings is heterogeneous with sizes ranging from fine silt to sand. There are numerous studies documenting the contamination of the surrounding environment by metal and metalloid bearing dusts sourced from abandoned tailings. For example, Abdelouas (2006) described the geochemistry and mineralogy of radioactive dust dispersed from tailings produced during uranium mining, which is known to cause lung cancers; high As concentrations were observed in the >8 μm fraction of dusts generated at an abandoned mine tailings site in Nova Scotia, Canada (Corriveau et al. 2011). A study in southeast Spain showed that the PM10 fraction of dust sourced from oxidised ferruginous tailings was preferentially enriched in metalloids such as As and Sb (Moreno et al. 2007).

There are several control mechanisms for reduction of dust generated from various stockpiles (Cecala et al. 2012). Factors that can reduce wind erosion include: (i) material that is compacted, roughened or kept moist; (ii) material that contains stable clods that are large and dense enough to resist wind erosion; and (iii) vegetated surfaces or surfaces that are covered in vegetative materials (e.g. straw). Reduction of wind velocity near the ground surface using vegetation or barriers reduces erosion. Various chemical suppressants are available to the mining and minerals industry which include wetting agents, binders, crushing agents, foaming agents and foam binders. However, the most effective coating as a dust control method is the formation of a crust on the surface of the material, preferably a non-toxic crust. These can be produced by mixing bentonite clay with soil or the application of Guar Gum polymer to the surface of a tailings pond. The orientation and configuration of storage piles can be optimized according to wind conditions and pile height to reduce fugitive dust emissions (Badr and Harion 2007).

## Mineral Dust Measurement and Monitoring

Since the 1950s the minerals industry has had in place preventative measures to limit its workers exposure to dust through the implementation of Occupational Exposure Limit values (OELs) at the work place in European Union member states and other countries including Australia (e.g. Guidance on the interpretation of workplace exposure standards for airborne contaminants; Safe Work Australia 2012). Accurate measurement and monitoring of dust concentrations are essential for the management of dust-related lung diseases. Dust monitoring is particularly

**Table 6** Permissible exposure limits (PEL) for different mineral dusts (SME Mining Engineering Handbook 2011)

| Dust type | PEL |
|---|---|
| Crystalline silica | 0.01 mg/m$^3$ |
| *Silicates* | |
| Asbestos | 5 fibres/cc |
| Mica | 706/million m$^3$ |
| Cement | 1056/million m$^3$ |
| Talc | 706/million m$^3$ |
| Coal dust | 2 mg/m$^3$ or 10 % crystalline silica |
| *Metallic dusts* | |
| Mercury | 0.05 mg/m$^3$ |
| Lead | 0.15 mg/m$^3$ |
| Antimony, arsenic | 0.5 mg/m$^3$ |
| Manganese | 5 mg/m$^3$ |
| Iron, zinc, molybdenum | 5 mg/m$^3$ |
| Uranium (insoluble) | 0.2 mg/m$^3$ |
| Vanadium ($V_2O_3$) | 0.5 mg/m$^3$ |

concerned with the particle size of dust, since particle size determines the exposure route and consequently the health impacts. At mine sites, the monitoring of dust emissions is an integral part of the dust control strategies. Dust management plans for the minerals industry aim to reduce and control dust emissions around mine sites. Dust management plans include: (i) identifying potential dust sources; (ii) implementing measures to avoid and or minimize dust generation; (iii) complying with legislation and other obligations; (iv) reducing negative environmental and human health impacts of dust; and (v) rigorous monitoring and reporting, and systematically investigating dust related incidents (e.g. Lingard and Gibson 2011).

Meteorological monitoring (wind speed and direction, precipitation) may also be required to enable accurate interpretation of dust monitoring data. According to the agency overseeing the mine approval process, baseline air quality conditions prior to mining need to be assessed as part of a monitoring program. The air quality monitoring programs are implemented according to the specifics of each operation, in order to meet air quality guidelines regulated by state and federal bodies (Airborne Contaminants, Noise and Vibration 2009). For example, in Australia, the National Environment Protection Measure for Ambient Air Quality recommends a maximum concentration of 50 μg/m$^3$ over a day. The more hazardous finer particulates PM2.5 are limited to an annual average of 8 and a 25 μg/m$^3$ maximum over a 24-h period (DSEWPC 2013). The permissible exposure limits (PEL) for the exposure to various respirable dusts is shown in Table 6. The PELs are taken from SME Mining Engineering Handbook (2011) showing PELs for various respirable dusts, adapted from the general guidelines provided by the American Conference of Governmental Industrial Hygienists (ACGIH 1972).

The 50 μg/m$^3$ PM10 criterion has proved problematic in its interpretation and compliance for the mining industry as explained in the Best Practice Handbook for Airborne Contaminants, Noise and Vibrations (2009). An example is given from the Hunter Valley, where the combined emissions of multiple mines can affect the air quality in nearby communities. Invariably, background sources of emissions can be significant. Therefore, the 50 μg/m$^3$ criterion is often applied as an incremental goal, that is, the concentration above background emissions from other sources. Also, consideration must be given to the fact that this standard can be breached when there are bushfires, deliberate burning-off or dust storms.

## *Monitoring Methods*

Dust monitoring methods vary in sophistication and are fit for purpose according to the compliance monitoring required. The specific locations of dust monitoring instruments should reflect the nature of the dust sources and include control sites, which provide an indication of background levels during the mining operations. The frequency of sampling will vary according to the objectives of the monitoring programme and sampling equipment.

In general, there are two approaches to dust monitoring, passive techniques that generally monitor TSP and do not require a power source, so are relatively inexpensive (e.g. dust deposition gauges; personal exposure samples); and active systems that require a power source to measure nuisance dust and different particle sizes (e.g. high volume samplers; continuous particle monitors).

## *Dust Deposition Gauges*

Dust deposition gauges are ideal for longer term and remote monitoring of dust deposition at low cost. Settable particulate matter can be sampled using a high-density polyethylene. (HDPE) funnel connected to a HDPE bottle similar to a rain gauge style of passive fallout collectors. The dust gauges are left in position for set periods of time (months) before the gauge is removed. The contents can then be filtered in the laboratory and the total dust deposition measured. This monitoring method provides information about the rate of atmospheric deposition but cannot provide data on short timescales or high-resolution particle size information.

## *High Volume Air Samplers*

High volume air sampling (HVAS) devices (Fig. 1) are recommended for monitoring of TSP and PM10. Precise volumes of air are continuously drawn through a

**Fig. 1** Two high volume air samplers monitoring TSP and PM10 at an offsite location near a mine (*left*). Close up of the filter paper shown under the lid of the TSP sampler (*centre*). The PM10 high volume sampler situated adjacent to the TSP sampler (*right*) (color figure online)

filter paper beneath a protective hood, which prevents particulates from falling onto the paper. The sampling is carried out for a set time period (24 h cycle/week) onto a filter of known weight, which can be reweighed to determine the mass of particulates collected. The concentration can then be calculated together with the total volume of air drawn in during the 24-h period according to the standard method for TSP and PM10. For PM10, a size selective inlet attached to the sampler ensures that only particles with a diameter less than 10 μm are collected. Deleterious elements such as Pb, Cd and Zn can be measured on the TSP and PM10 fraction collected on the filters, by chemically digesting the filter paper and analysing the metal concentrations using atomic absorption spectrometry (AAS) or inductively coupled plasma mass spectrometry (ICPMS).

## *Dichotomous Samplers*

The dichotomous sampler (dicot) is another particulate sampler that can be used to meet requirements of the regulator (e.g., US EPA 1999; AS 3580.97:1990). The instrument separates particulate matter into coarse (2.5–10 μm) and fine (<2.5 μm) fractions by removing the larger particles through impact, while the finer inhalable particles are separated by a virtual impactor technique. The filter papers are weighed in the laboratory prior to dust sampling under controlled climatic conditions, and the mass of particulates collected during a 24-h period is determined gravimetrically. Teflon can be used as a filter media, which can then be analyzed for the chemical composition of the particulate matter.

## *Real Time Air Quality Monitoring*

A wide range of dust monitors are available, which can provide information about dust concentration in real time. The most common type of sampler used to measure dust in mine air is the gravimetric sampler. This is described in detail in Colinet (2010).

A tapered element oscillating microbalance (TEOM), is a sampling device designed to monitor size specific particulates on a continuous near real-time basis, without the delay required for laboratory-based gravimetric determination of PM concentration or data averaged over a 24-h period. For details on how the TEOM system works see Patashnick and Rupprecht (1991).

Light scattering devices, can also be used in real-time dust monitoring. These incorporate a near-infrared light emitting diode source, a silicon detector, and collimating optics. Particulates passing though the sensing chamber scatter light, which is proportional to their concentration. For example, the DustTrak™ DRX Aerosol Monitor 8533 can simultaneously measure size-segregated mass fraction concentrations corresponding to PM1, PM2.5, PM10 and total PM size fractions. Real time monitoring can be implemented to prevent the measurement of concentrations exceeding trigger levels or compliance levels.

## *Personal Dust Exposure Monitoring*

Personal dust samplers are an extremely important part of work place health and safety in industries such as coal and metalliferous mining. The personal dust samplers were originally developed to measure respirable coal mine dust mass to provide accurate exposure data at the end of a work shift in an effort to reduce the incidence of coal workers pneumoconiosis (Volkwein et al. 2004). The National Institute developed an advanced type of personal dust sampler for Occupational Safety and Health (NIOSH) in partnership with industry. This instrument, known as the personal dust monitor (PDM), provides continuous information about the amount of respirable coal mine dust in the breathing zone of an individual. This device incorporates a miniaturized tapered-element oscillating microbalance mass sensor that can provide time resolved measurements on a screen display. The PDM then gives the wearer information on the cumulative dust concentration, and the permissible exposure limit that has been reached. The PDM performance in underground coal mines shows that this device provides data that is equal to or better than manual dust collection and analysis methods available (Volkwein et al. 2006).

The personal DataRam (pDR) is another common personal dust sampler that provides real time information (Colinet 2010). This operates by dust-laden air passing through a sensing chamber in the sampler. A light beam passes through the dust. A sensor in the sampler measures the amount of light scatter caused by the dust and relates this scatter to a relative dust concentration. This concentration is correlated to the time when the sample was measured and stores this information in

the internal data logger. The logged data can be analyzed for specific time intervals (e.g., loading a cut), with average dust concentrations calculated for these intervals.

### *Biomonitoring*

Lichens have been used in biomonitoring studies for more than 50 years to monitor the levels of pollution resulting from human activities (Nimis et al. 2000). Lichens are ubiquitous throughout the natural environment as well as in urban areas. They are perennial organisms and therefore provide year round monitoring of pollutants predominantly from aerial sources. There are numerous examples of the use of lichen in environmental biomonitoring programs to monitor trace elements (e.g. Al, As, Ba, Cd, Cu, Fe, Mg, Ni, Pb, Zn) in the atmosphere on large spatial scales (e.g. Sloof and Wolterbeek 1991; Conti and Cecchetti 2001). Different methods can be applied to lichens in biomonitoring studies which include: (i) index of atmospheric purity, where compositional changes in the lichen community are correlated with changes in the levels of atmospheric pollution; and (ii) direct analysis of contaminants in the thallus (tissue of lichen) in high pollution zones, which are transplanted from low pollution areas and fixed to suitable surfaces in the monitoring areas (Conti and Cecchetti 2001).

Fugitive dust in zones associated with mining can be sampled using lichens on yearly timescales, providing valuable information to distinguish the background signal from the deleterious metals associated with industrial activities. Samples of lichen are processed by microwave acid digestion to dissolve the heavy metals, which can be measured by ICP-AES, ICP-MS or electrothermal atomic absorption spectrometry (ETAAS) (Dolgopova et al. 2006). Furthermore, systematic scanning electron microscopy (SEM) investigation of particulates on the surfaces of the thalli can be carried out using back-scatter mode and scanning electron microscopy energy-dispersive X-ray spectrometry (SEM-EDS) to quantify the mineralogy and qualitative estimates of elemental abundance (Williamson et al. 2004). However, lichen cannot be used to assess the ambient air quality relating to human health studies. Williamson et al. (2008) demonstrated that lichen were able to trap larger blast-furnace particulates (mean equivalent spherical diameter of 2.2 μm) derived from a Cu smelter in Karabash, Russia, but the smaller particles were not captured by the lichens. Furthermore, due to the size selective bias, the composition (and therefore source) of the TSP sampled by sampling pumps was different to that of the lichen.

## Mineral Dust Characterization

Understanding the mineralogy and morphology of dust has important implications for the heath risks associated with dust inhalation. The toxicity of individual mineral dusts has been investigated, with examples for silica (Richards and

Wusteman 1974; Fubini et al. 1999), kaolinite (Lapenas et al. 1984), talc (El Ghawabi et al. 1970), and mica (Shanker et al. 1975). The following sections describe techniques used to determine the mineral composition of dust. A summary of research techniques relating to dust characterization is shown in Table 7.

## *IR and XRD Techniques*

Infrared (IR) spectrophotometric and X-ray diffraction (XRD) methods are two techniques applied to dust samples, specifically to monitor quartz which is a lung carcinogen (Ferg et al. 2008). X-ray diffraction can distinguish between complex mixtures of minerals, whereas IR techniques have been used in particular to measure polymorphs of silica. There are three main crystalline forms of silica; quartz, tridymite and cristobalite of which there are two variations of each (high and low). Measurement of crystalline silica from filters is typically performed as per the NIOSH IR analytical Method 7602 and XRD analytical Method 7500.

Madsen et al. (1995) reviewed IR, XRD and colorimetry methods for quartz analysis. IR analysis is based on the bonding energy of minerals. It measures the vibrational energy of the covalent bonds between silicon and oxygen. However, interferences are possible due to overlapping spectral peaks at 798 $cm^{-1}$ from other phases of silica and silicates with similar tetrahedral $SiO_4$ structures (Madsen et al. 1995). An understanding of the sample matrix is therefore important when considering IR analysis, as chemical and heat treatments can be applied to remove some interferences. This method is not suitable for all sample matrix but is less expensive than powdered XRD.

XRD is more costly that IR, however it is less prone to interferences. Gualtieri et al. (2009) used XRD to monitor asbestos dust in Italian communities. This study explains how samples must be prepared to prevent interference of the filter on the analysis of the dust composition. Dust samples were analysed for different polymorphs of minerals by scanning different diffraction lines characteristic of each polymorph. Treatment in a muffle furnace at 500 °C for 1 h was necessary to separate the overlap of the main basal diffraction peaks of kaolinite and chrysotile. At 500 °C, the crystal lattice of chrysotile remains unmodified, while kaolinite decomposes (Criado et al. 1984; Cattaneo et al. 2003).

## *Particle Size Distribution*

The particle size distribution of mineral dusts generated during mining is an important factor controlling the depth of dust deposition in the respiratory system. The particle size distribution of dust collected on filters can be measured using a Coulter Counter Multisizer. This instrument is a multi-channel analyzer based upon the electrical sensing zone (ESZ) or Coulter principle. The number and size of the

**Table 7** Summary of techniques used to establish the mineralogical composition of mineral dust

| Study | Location | Sampling | Particle concentration | Size and morphology | Chemical composition |
|---|---|---|---|---|---|
| Jones et al. (2002) | Openpit coal mine, Margam, South Wales | HVAS with PM10 selective inlet or TSP head on polycarbonate filter | Gravitational method | FESEM | SEM-EDX<br>TEM-EPXMA |
| Moreno et al. (2005) | Almadén, Spain | polycarbonate filter | | FESEM | SEM-EDX<br>XRD<br>ICP-MS |
| Panigrahi et al. (2006) | Chromite mine, Sukinda valley, India | Respirable particulate matter samplers; HVAS | Laser particle size analyser Cascade Impactor | | Cr(VI) extracted from dust using colorimetric method |
| Meza-Figueroa et al. (2009) | Nacozari de García, tailings impoundment, Mexico | Mine tailings; efflorescences; soils; residential soils and road dust | | | XRD |
| Gualtieri et al. (2009) | Bologna, Modena, Reggio Emilia, Italy | HVAS on a Whatman cellulose nitrate membrane (PM10); fallout particulates; soil samples | Gravitational method | Optical microscopy SEM | SEM<br>TEM |
| Magiera et al. (2011) | Various industry dusts | Fly ashes; dust from lignite combustion; cement dusts; dusts from coke production | | SEM | XRD, Mossbauer spectroscopy |
| Pachauri et al. (2013) | Agra, North Central India | TSP collected by HVAS onto quartz fiber filter paper | Gravitational method | SEM | SEM-EDX |

particles is measured by suspending the sample in a conductive liquid and monitoring the electrical current that passes between two electrodes, on either side of a small aperture. As the particles pass through the aperture, it changes the impedance of the current between the two electrodes, producing a pulse with a magnitude proportional to the particle volume. The small quantity of sample required make the Coulter Multisizer ideal for quantifying the grain size distribution of dust (McTanish et al. 1997). The Coulter Counter Multisizer has been used to determine the particle size distribution of TSP collected on filters using low volume samplers mostly in relation to agricultural sources of dust (e.g. Sweenten et al. 1998) and in studies comparing the PM10 fraction measured using different sampling devices (Capareda et al. 2005).

Other studies have analyzed the particle size distribution of the samples using particle laser diffraction in a Malvern Mastersizer by dispersion in a surfactant (Ferg et al. 2008) or a Scanning Mobility Particle Sizer, which consists of a Condensation Particle Counter (CPC) combined with an electrostatic classifier (Beccaceci et al. 2010). The Malvern Mastersizer provides a range of different particle sizing products for the analysis of sub-nano meter to millimeter. These specific laser diffraction or light scattering devices for measuring the particle size distribution have been shown to be more accurate than SEM techniques, which are limited by the sample preparation and the statistics of small sample sizes (Ghosal et al. 1995). However, little to no mineralogical information is available with these methods.

## *Scanning Electron Microscopy*

Since the 1970s, scanning electron microscopy (SEM) fitted with X-ray Energy Dispersive Spectrometers (EDS) has been applied to characterize the physical and chemical characteristics of mine dust (DeNee 1972; White and DeNee 1972). Dust particles can be analyzed by mounting them on a stud or plate distributed evenly over a sticky carbon tape; or attaching segments of inert filters on to the studs. SEM-EDS has been used in numerous studies to characterize airborne particulate matter because it can simultaneously provide information about the size, morphology and chemical composition of particles (Jones et al. 2002; Reynolds et al. 2003, Vassilev and Vassileva 2004; Casuccio et al. 2004).

The limitations of SEM-EDS analysis include: (i) it only provides an approximate particle composition in terms of elemental composition; (ii) low efficiency in the detection of elements with low atomic masses (Jones et al. 2002); and (iii) when using filters (e.g. composed of quartz; polycarbonate) from HVAS, the experience of the SEM operator is required to accurately identify the spectra which can be affected by the composition of the filters. To obtain quantitative particle composition the filter should be composed of Teflon, which does not cause spectral interferences. An alternative method, X-ray photoelectron spectroscopy (XPS or electron spectroscopy for chemical analysis or ESCA) could be used (Huertas et al. 2012b).

## *Transmission Electron Microscopy*

Transmission electron microscopy (TEM) is a powerful method for the semi-quantitative to quantitative characterization of individual dust particles. This technique is recommended as ISO standard for determining the concentration of asbestos fibres in ambient air and includes the measurement of the length, width and aspect ratios of asbestos structures (ISO 10312:1995). Transmission electron microscopes fitted with EDS can: (i) detect elements with masses larger than carbon ($Z \geq 6$); (ii) observe particles as small as 0.001 μm (in comparison a FESEM can image 0.1 μm); and (iii) determine the crystalline structure of the particle by the electron diffraction pattern. The phase identification of particles by analysis of electron diffraction patterns is time consuming, therefore this method is applied to selective particles, in addition to analysis of chemical composition by SEM (e.g. Kandler et al. 2007). For identification of an asbestos fibre using typical TEM analysis the definition specifying a minimum aspect ratio of 3:1 for particles longer than 5 μm is not valid. Many non-asbestos particles would fit this definition, therefore, Harris et al. (2007) developed a protocol that supplements FESEM with the TEM analysis method. This method allows the overall particle shape, surface topography and the side and termination (particle end) geometries to be characterized and reduces the number of non-asbestiform particles identified. This combined FESEM-TEM analysis was applied to the characterization of mineral dust from a former vermiculite mine in Montana, USA, where amphibole particles were classified into six primary groups: fibre, acicular, prismatic, bladed, columnar and bundle. Unique morphological features can be observed with FESEM that cannot be observed in a standard TEM image, which allows asbestos and non-asbestos particles to be differentiated (Harris et al. 2007).

## *Raman Spectroscopy*

Raman spectroscopy is a powerful technique for identifying structural details of minerals (i.e. to differentiate between polymorphs), and information on elemental speciation and crystallinity (Das and Hendry 2011). Raman spectroscopy has been widely applied to characterize the chemical composition of atmospheric aerosols and dust, for example: (i) respirable diesel and coal particulates in coal mines (Suhartono et al. 1996) and carbonaceous aerosols in urban environments (Sze et al. 2001); (ii) the chemical interactions between mineral dust and organic acids (Laskina et al. 2013); and (iii) chemical species and mineral dust in polar ice cores in Antarctica (Sakurai et al. 2010).

Raman mapping is a valuable tool that can be used to determine how various chemical components are spatially distributed within a single particle and has been used to determine the spatial distribution of chemical species within dust particles (Laskina et al. 2013). Instrument that map both physical and chemical characteristics

of submicron particles are now available (e.g. Malvern MorphologiG3-ID). A study by Rinaudo et al. (2003) applied FT-Raman spectroscopy to distinguish between the three principle minerals of the serpentine group (chrysotile, antigorite and lizardite), which have a very similar chemical composition but a significantly different structure.

## *Geochemical Assessment*

Dust management plans for mine sites are to comply with set limits for the concentration of deleterious elements in the TSP and PM10 fraction collected using HVAS. Also, a thorough assessment of the geochemical composition of dust, particularly from metalliferous mines is important for understanding metal and metalloid loading and transfer of environmentally significant elements. The concentrations of metals and metalloids in dust can be established using appropriate sampling protocols and analytical tools such as AAS, ICP-AES or ICP-MS. For example, elevated trace metal contents (Cu, Zn, As, Pb) of size segregated soil samples analyzed by ICP-AES and ICP-MS has been used to identify anthropogenic sources from smelter facilities (Parra et al. 2014).

Guidelines for metal and metalloid concentrations in air pollutants know to have health effects are reported by WHO (2000). Arsenic is a human carcinogen and no guideline for a safe level of inhalation exposure has been recommended considering a linear-dose response (WHO 2000). Heavy metals such as Pb, Co, Cd, Cu, and Cr are toxic at certain levels and are considered hazardous contaminants that can accumulate in the human body. For example, Cd has a half-life of 10 years in the human body. Experiments on animals demonstrate that Cd can produce acute toxic effects on organs such as the kidney, liver, pancreas and lung (Godt et al. 2006). Chromium (VI) compounds can cause chrome ulcers, corrosive reactions on nasal septum and eczematous dermatitis. The toxicity of Pb has been explained by its interference with different enzyme systems or displacement of essential metal ions (WHO 2000). The toxicity of metals and metalloids is also dependent on their ion speciation and redox state. For example, chemical species with net neutral charges are most easily transferred across cell membranes; while elements such as Cr and As are more toxic in their hexavalent and trivalent states, respectively (Plumlee and Ziegler 2003).

## *Methods for Predicting Particle Size and Mineralogy of Dust*

Traditional dust emission estimation factors used in the mining industry do not take into account geological variability or rock type. The dust emission factors for blasting, comminution and road haulage are the same for both coal and metalliferous mine operations (NPI 2012). Methods for predicting dust characteristics could

be developed following a similar approach to those used to predict rock fragmentation during blasting and comminution. Over the past few decades there has been a push to optimise rock breakage for metal extraction. This has led to research predicting rock fragmentation and blast size distribution of rocks (McKee et al. 1995). A new dust prediction tool has been developed by Michaux (2009), who adapted a small scale comminution crush test to characterize rock, in terms of its texture and propensity to generate dust. The GeM Comminution Index (GeM Ci), developed in the AMIRA P843 project, takes discrete pieces of drill core and measures the size distribution after applying energy (Kojovic et al. 2010). The resulting particle size distribution represents the rock breakage signature, which can be used to calculate the GeM Ci Dust Index (GeM Ci DI) for each rock type (Eq. 1) (Michaux 2009).

$$GeM\ Ci\ DI = \frac{\beta}{\tau} \tag{1}$$

where:

β (%) of whole sample passing 106 μm after GeM Ci crushing

τ (%) of whole sample passing 1.18 mm after GeM Ci crushing

The shape of the size distribution of the cumulative (%) passing fragmentation was shown to be similar for crushing and blasting of the same rock type (Moser et al. 2003; Michaux 2009). The GeM Comminution Index can therefore be used to estimate the size distribution of particles <100 μm, released during blasting and crushing processes, as well as during transport of material. The <100 μm fraction produced can: (i) provide information on the ratio of TSP, PM10 and PM2.5 fractions produced for each rock type; (ii) be analysed for morphology and mineralogy of each size fraction; and (iii) simulate the proportion of particles that may become airborne.

A second method, applied to understanding mineral fractionation during crushing to predict mineral liberation and flotation behaviour, could also be adapted to understand the morphological and mineralogical characteristics of dust. There is very little data available in the literature on the mineralogy of different size fractions produced during comminution. Only one such study by Berry et al. (2013) is presented. In this research, 32 samples from two IOGC deposits were crushed to −3.3 mm and the resulting size fractions analysed using QXRD. The bulk mineralogy was calculated by weighted least squares to calculate the preferred weight percent minerals, by combining the chemical assay with the QXRD results (Berry et al. 2011). This provided a robust estimate of the high abundance minerals based on QXRD with the higher precision of chemical assay used to define less common minerals.

The fractionation of minerals into different size fractions varies according to mineral hardness, which controls how minerals crack and fracture. Therefore, weaker minerals are expected to experience greater size reduction than harder minerals for the same crushing energy. Berry et al. (2013) observed that coarse size fractions were enriched in harder minerals such as quartz, while softer minerals like

barite were concentrated in the finer fractions. Mineral fractionation into size fractions was not always predictable; in some samples K feldspar was enriched in both the coarser fractions (+475 μm) and the finer fraction (−53 μm). Furthermore, pyrite and magnetite fractionation was determined by the grain size of the mineral, in contrast to chalcopyrite, which fractionated according to the rock hardness (Berry et al. 2013). Data collected on rock hardness (e.g. Equotip; Keeney 2008) and mineral fractionation by size (Berry et al. 2013), may be used to understand the mineralogical fractionation in dusts. This could add significant value to the analyses undertaken as part of geometallurgy data collection, since understanding mineral grain size fractionation is an important factor in mineral processing.

## Conclusions

This review presents details on mineral dust generated during metalliferous mining and processing activities. Dust generated during mining activities provides a pathway for the accumulation of heavy metals and contaminants in the surrounding environment. The amount of mineral dust generated, its dispersal, and types of health and environmental risks depend on many factors. These include geology, local climate, topography, working methods and mine operations, dust control measures, mineralogy and metallurgical characteristics of some ores, and the land use of the area around the mine.

At mine sites, fugitive dust generation can result from land clearing, drilling and blasting, transport on unsealed roads, and the release of fine particles from waste repositories and ore stockpiles. Finer grain size fractions are produced from crushing milling and screening operations, which act as point sources for dust dispersal. Similarly, dust emissions from transport and stockpiling of ore concentrate and tailings repositories are well known sources of mineral dust. Dust suppression and control mechanisms can reduce dust produced by wind erosion. These include wetting and chemical agents to bind the material together, and enclosure of crushing circuits and transfer points.

Dust monitoring methods are generally determined by the specifications for work place health and safety to meet the air quality guidelines regulated by federal organizations. Low-cost technologies include dust deposition gauges for long term monitoring dust deposition. High volume air samplers provide size specific (e.g., PM2.5 and PM10) determinations of dust flux while a range of options exit for real time dust monitoring. Biomonitoring methods are also used to monitor the trace metal flux to the surrounding environment.

Geochemical and mineralogical characterization of dust is required to understand potential risks to human health and local environment. Particle shape is another important factor in determining the hazardous nature of dust particles. Geochemical characterization is carried out through ICP-MS and ICP-AES methods, while SEM a powerful tool for characterizing mineralogical attributes of mineral dust.

Grain size is the major control on the risk of exposure to mineral dust through digestion and inhalation. Predictive tools are required to evaluate the risks of dust generated by mining operations and facilitate the selection of appropriate dust management strategies. Existing predictive tool focus on dust dispersion modelling however, there has been little research on predicting the dust properties (e.g., mineralogy of grain size fractions). Future work should consider appropriate methodologies for predicting mineral fractionation across the size spectrum, which would allow more advanced dust management schemes.

## References

Abdelouas A (2006) Uranium mill tailings: geochemistry, mineralogy and environmental impact. Elements 2:335–341

Amphonsah-Dacosta FA (1997) Cost-effective strategies for dust control in an opencast coal mine. MSc. Thesis, University of the Witwatersrand

Australian Standard AS 3580.97:1990 (1990) Methods for sampling and analysis of ambient air. Method 9.7: Determination of suspended particulate matter—PM10 dichotomous sampler—Gravimetric method. Standards Australia, Sydney

Badr T, Harion JL (2007) Effect of aggregate storage piles configuration on dust emissions. Atmos Environ 41:360–368

Beccaceci S et al (2010) CPEA 28: Airborne particulate concentrations and numbers in the United Kingdon (Phase 2). Annual Report 2010. NPL Report AS 65. Teddington. Middlesex. ISSN 1754-29-2928

Berry RF, Hunt JH, McKnight SW (2011) Estimating mineralogy in bulk samples. In: Proceedings 1st AusIMM international geometallurgy conference, Brisbane, pp 153–156

Berry RF, Hunt J and McKnight SW (2013) Mineral fractionation during crushing and grinding. AMIRA P843A technical report, vol 11, pp 112–131

Best Practice Handbook on Air Borne Contaminants, Noise and Vibration (2009) Australian Government, Department of Resources, Energy and Tourism. http://www.ret.gov.au/resources/Documents/LPSDP/AirborneContaminantsNoiseVibrationHandbookweb.pdf

Biffi M, Belle BK (2003) Quantification of dust generating sources in gold and platinum mines. Safety in Mines Research Advisory Committee, GAP 802:28

Boreland F, Lyle DM (2006) Lead in Broken Hill homes: effect of remediation on indoor lead levels. Environ Res 100:276–283

British Standards Institute (1993) Workplace atmospheres—size fraction definitions for measurement of airborne particles. BS EN 481:1993. Section 3.5. European Committee for Standardization

Capareda S, Parnell C, Shaw B, Wanjura J (2005) Particle size distribution analysis of cotton gin dust and its impact of PM10 concentration measurement. In: Proceedings 2005 Beltwide cotton conferences. National Cotton Council, Memphis, TN

Casuccio G, Schlaegle S, Lersch T, Huffman G, Chen Y, Shah N (2004) Measurement of fine particulate matter using electron microscopy techniques. Fuel Process Technol 85:763–779

Cattaneo A, Gualtieri AF, Artiolo G (2003) Kinetic study of the dehydroxylation of chrysotile asbestos with temperature by in situ XRPD. Phys Chem Miner 20:177–183

Cecala AB, O'Brien AD, Schall J, Colinet JF, Fox WR, Franta RJ, Joy J, Reed WR, Reeser PW, Rounds JR, Schultz MJ (2012) Dust control handbook for industrial minerals mining and processing. Report of investigations 9689, National Institute for Occupational Safety and Health

Colinet J (2010) Sampling to quantify respirable dust generation. Best practices for dust control in metal/ non-metal mining, IC9521, NIOSH, pp 15–21
Conti ME, Cecchetti G (2001) Biological monitoring: lichens as bioindicators of air pollution assessment—a review. Environ Pollut 114:471–492
Corriveau MC, Jamieson HE, Parsons MB, Campbell JL, Lanzirotti A (2011) Direct characterization of airborne particles associated with arsenic-rich mine tailings: particle size, mineralogy and texture. Appl Geochem 26:1639–1648
Criado JM, Ortega A, Real A, De Torres E (1984) Re-examination of the kinetics of the thermal dehydroxylation of kaolinite. Clay Miner 19:653–661
Das S, Hendry MJ (2011) Application of Raman Spectroscopy to identify iron minerals commonly found in mine wastes. Chem Geol 290:101–108
DeNee PB (1972) Mine dust characterisation using the scanning electron microscope. Am Ind Hyg Assoc J 33:654–660
Dolgopova A, Weiss DJ, Seltmann R, Kober B, Mason TFD, Coles B, Stanley CJ (2006) Use of isotope ratios to assess sources of Pb and Zn dispersed in the environment during mining and ore processing within the Orlovka-Spokoinoe mining site (Russia). Appl Geochem 21:563–579
DSEWPC (2013) Air quality standards. http://www.environment.gov.au/atmosphere/airquality/standards.html
El Ghawabi SH, El Samra GH, Mehasseb H (1970) Talc pneumoconiosis. J Egypt Med Assoc 53:330–339
Ferg EE, Loyson P, Gromer G (2008) The influence of particle size and composition on the quantification of airborne quartz analysis on filter paper. Ind Health 46:144–151
Fubini B, Zanetti G, Altilia S, Tiozzo R, Lison D, Safflotti U (1999) Relationship between surface properties and cellular responses to silica: studies with heat-treated cristobalite. Chem Res Toxicol 12:737–745
Ghosal S, Ebert JLK, Self SA (1995) Chemical composition and size distribution for fly ashes. Fuel Proc Technol 44:81–94
Ghose MK, Marjee SR (1998) Assessment of dust generation due to opencast coal mining—an Indian case study. Environ Monit Assess 61:255–263
Godt J, Scheidig F, Grosse-Siestrup C, Esche V, Brandenburg P, Reich A, Groneberg DA (2006) The toxicity of cadmium and resulting hazards for human health. J Occup Med Tox 1:22
Gualtieri AF, Mangano D, Lassinantti Gualtieri M, Ricchi A, Foresti E, Lesci G, Roveri N, Mariotti M, Pecchini G (2009) Ambient monitoring of asbestos in selected Italian living areas. J Environ Manage 90:3540–3552
Harris KE, Bunker KL, Strohmeier BR Hoch R, Lee RJ (2007) Discovering the true morphology of amphibole minerals: complementary TEM and FESEM characterization of particles in mixed mineral dust. In: Méndez-Villas A, Díaz J (eds) Modern Research and Educational Topics in Microscopy, FORMATEX, pp 643–650
Herbst JA, Yi CL, Flintoff B (2003) Size reduction and liberation. In: Fuerstenau MC, Han KN (eds) Principals of mineral processing. SME, Colorado, pp 69–95
Huertas JI, Camacho DA, Huertas ME (2012a) Standardized emissions inventory methodology for open pit mining. Environ Sci Pollut Res Int 19:2784–2794
Huertas J, Huertas ME, Solís DS (2012b) Characterization of airborne particles in an open pit mining region. Sci Total Environ 423:39–46
IARC (1997) International Agency for Research on Cancer. Silica. IARC Monograph 68 on the Evaluation of the carcinogenic risk of chemicals to humans
International Organisation for Standardization ISO 7708:1995(E) (1995) Air quality—particle size fraction definitions for health-related sampling, Geneva
Jankovic A, Valery W, La Rosa D (2000) Fine grinding in Australian mineral industry. J Min Metall A 36:51–61
Jones T, Blackmore P, Leach M, Berube K, Sexton K, Richards R (2002) Characterisation of airborne particles collected within and proximal to an open cast coalmine: South Wales, U.K. Environ Monit Assess 75:293–312

Kandler K, Benker N, Bundke U, Cuevas E, Ebert M, Knippertz P, Rodriguez S, Schutz L, Weinbruch S (2007) Atmos Environ 41:8058–8074

Keeney L (2008) EQUOtip hardness testing: Aqqaluk (including a guide on how to use EQUOtip). AMIRA P843 2, pp 17.1–17.20

Kojovic T, Michaux S, Walters S (2010) Development of new comminution testing methodologies for geometallurgical mapping of ore hardness and throughput. In: XXV international mineral processing congress IMPC conference, Brisbane

Lapenas D, Gale P, Kennedy T, Rawlings W Jr, Dietrich P (1984) Kaolin Pnumoconiosis: radiologic, pathologic and minerlogic findings. Am Rev Respir Dis 130:282–288

Laskina O, Young MA, Kleiber PD, Grassian VH (2013) Infrared extinction spectroscopy and micro-Raman spectroscopy of selected components of mineral dust with organic compounds. J Geophys Res Atmos 118:6593–6606

Lingard J, Gibson N (2011) Management, mitigation and monitoring of nuisance dust and PM10 emissions arising from the extractive industries: an overview. The Mineral Industry Research Organisation Didcot, Oxfordshire

Madsen FA, Rose MC, Cee R (1995) Review of quartz analytical methodologies: present and future needs. Appl Occup Environ Hyg 10:991–1002

Magiera T, Jablonska M, Strzyszcz Z, Rachwal M (2011) Morphological and mineralogical forms of technogenic magnetic particles in industrial dusts. Atmos Environ 45:4281–4290

Mankosa MJ, Adel GT, Yoon RH (1989) Effect of operating parameters in stirred ball mill grinding of coal. Powder Technol 59:255–260

McKee DJ, Chitombo GP, Morrell S (1995) The relationship between fragmentation in mining and comminution circuit throughput. Min Eng 8:1265–1274

McTanish GH, Lynch AW, Hales R (1997) Particle-size analysis of Aeolian dust, soils and sediments in very small quantities using a Coulter Multisizer. Earth Surf Process Land 22:1207–1216

Meza-Figueroa D, Maier RM, de la O-Villanueva M, Gómez-Alvarez A, Moreno-Zazueta A, Rivera J, Campillo A, Grandlic C, Anaya R, Palafox-Reyes J (2009) The impact of unconfined mine tailings in residential areas from a mining town in a semi-arid environment: Nacozari, Sonora, Mexico. Chemosphere 77:140–147

Michaux SP (2009) Sub-populations and patterns in blast induced fine fragmentation. Miner Eng 22(7–8):576–586

Moreno T, Higuerasb P, Jonesc T, McDonald I, Gibbons W (2005) Size fractionation in mercury-bearing airborne particles (HgPM10) at Almaden, Spain: implications for inhalation hazards around old mines. Atmos Environ 39:6409–6419

Moreno T, Oldroyd A, McDonald I, Gibbons W (2007) Preferential fractionation of trace metals–metalloids into PM10 resuspended from contaminated gold mine tailings at Rodalquilar, Spain. Water Air Soil Pollut 179:93–105

Moreno N, Viana M, Pandolfi M, Alastuey A, Querol X, Chinchon S, Pinot JF (2009) Determination of direct and fugitive PM emissions in a Mediterranean harbor by means of classic and novel tracer methods. J Environ Manage 91:133–141

Moser P, Olsson M, Ouchterlony F, Grasedieck A (2003) Comparison of the blast fragmentation from lab-scale and full-scale tests at Bararp. Proceedings of EFEE 2nd world conference on explosives and blasting technique. Czech Republic, Prague, pp 449–458

Nimis PL, Lazzarin A, Lazzarin G, Skert N (2000) Biomonitoring of trace elements with lichens in Veneto (NE Italy). Sci Total Environ 255:97–111

NIOSH (National Institute for Occupational Safety and Health) (2002) NIOSH hazard review: health effects of occupational exposure to respirable crystalline silica. US Department of Health and Human Services, Centers for Disease Control and Prevention, DHHS (NIOSH) Publication No. 2002-129

National Research Council (2004) Research Priorities for Airborne Particulate Matter. The National Academies Press, Washington

National Pollutant Inventory (2012) Emission estimation technique manual for explosives detonation and firing ranges. January 2012. Department of Sustainability, Environment, Water, Population and Communities. ISBN 978-0-642-55384-3

Pachauri T, Singla V, Satsangi A, Lakhani A, Kumari KM (2013) Characterization of major pollution events (dust, haze, and two festival events) at Agra, India. Environ Sci Pollut Res Int 20:5737–5752

Pandey JK (2012) Dust control practices in the Indian mining industry. In: 12th coal operators' conference University of Wollongong & the Australasian Institute of Mining and Metallurgy, pp 185–192

Panigrahi DC, Pandey JK, Udaybhanu G (2006) Pattern of hexa-valent chromium in air borne respirable dust generated at various workplaces in open cast chromite mines. Environ Monit Assess 114:211–223

Parra S, Bravo MA, Quiroz W, Moreno T, Karanasiou A, Font O, Vidal V, Cereceda F (2014) Distribution of trace elements in particle size fractions for contaminated soils by a copper smelting from different zones of the Puchuncaví Valley (Chile). Chemosphere 111:513–521

Patashnick H, Rupprecht EG (1991) Continuous PM-10 measurement using the tapered element oscillating microbalance. J Air Waste Manag Assoc 41:1079–1083

Petavratzi E, Kingman S, Lowndes I (2005) Particulates from mining operations: A review of sources, effects and regulations. Mineral Eng 18:1183–1199

Plumlee GS, Ziegler TL (2003) The medical geochemistry of dusts, soils, and other earth materials: Treatise Geochem 9(7):263–310

Reynolds L, Jones T, Berube K, Wise H, Richards R (2003) Toxicity of airborne dust generated by opencast coal mining. Mineral Mag 67:141–152

Richards RJ, Wusteman FS (1974) The effects of silica dust and alveolar macrophages on lung fibroblasts grown in vitro. Life Sci 14:355–364

Rinaudo C, Gastaldi D, Belluso E (2003) Characterization of chrysotile, antigorite and lizardite by FT-Raman spectroscopy. Can Mineral 41:883–890

Ross M, Nolam RP, Langer AM, Cooper WC (1993) Health effects of mineral dusts other than asbestos. In: Guthrie GD, Mossman BT (eds) Health Effects of Mineral Dusts. Rev Mineral 28:361–409. Mineralogical Society of America, Washington

Safe Work Australia (2012) Guidance on the interpretation of workplace exposure standards for airborne contaminants. ISBN 978-0-642-33396-4

Sakurai T, Ohno H, Horikawa S, Iizuka Y, Uchida T, Hondoh T (2010) A technique for measuring microparticles in polar ice using micro-Raman spectroscopy. Int J Spectrosc. doi:10.1155/2010/384956

Silva AV, Almeida AM, Freitas MC, Marques AM, Silva AI, Ramos CA, Pinheiro T (2012) INAA and PIXE characterisation of heavy metals and rare earth element emissions from phosphorate handling in harbours. J Radioanal Nucl Chem 294:277–281

Sloof JE, Wolterbeek HT (1991) National trace-element air pollution monitoring survey using epiphytic lichens. Lichenologist 23:139–165

Shanker R, Sahu AP, Dogra RKS, Zaidi SH (1975) Effects of intertracheal injection of mica dust on the lymph nodes of guinea pigs. Toxicol 5:193–199

Stephens C, Ahern M (2001) Worker and community health impacts related to mining operations internationally: a rapid review of the literature. Mining, mineral and sustainable development working paper no 25

Suhartono L, Cornilsen BC, Johnson JH, Carlson DH (1996) Quantitative measurement of diesel particulate matter in an underground coal mine using laser raman spectroscopy. Appl Occup Environ Hyg 11:790–798

Sweenten JM, Parnell CB, Shaw BW, Auvermann BW (1998) Particle size distribution of cattle feedlot dust emission. Trans ASAE 41:1477–1481

Sze S-K, Siddique N, Sloan JJ, Escribano R (2001) Raman spectroscopic characterization of carbonaceous aerosols. Atmos Environ 35:561–568

US EPA (1986) Airborne asbestos health assessment update. EPA/6000-8-84/003F

US EPA (1999) Compendium method for the determination of inorganic compounds in ambient air. EPA/625/R-96/010a. United States EPA, Office of Research and Development, Washington, DC

US EPA (2004) Section 11.19.2, crushed stone processing and pulverized mineral processing. AP 42, fifth edition, volume 1, chapter 11. Mineral Products Industry, http://www.epa.gov/ttn/chief/ap42/ch11/

US EPA (2006) Section 13.2.4, aggregate handling and storage piles (fugitive dust sources). AP 42, fifth edition, volume 1, chapter 13: miscellaneous sources. http://www.epa.gov/ttn/chief/ap42/index.html

Vassilev S, Vassileva C (2004) Methods for characterization of composition of fly ash from coal-fired power station: a critical overview. Energy Fuel 19:1084–1098

Volkwein JC, Vinson RP, McWilliams LJ, Tuchman DP, Mishchler SE (2004) Performance of a new personal respirable dust monitor for mine use. Report investigations 9663, NIOSH publication no. 2004-151

Volkwein JC, Vinson RP, Page SJ, McWilliams LJ, Joy GJ, Mischler SE, Tuchman DP (2006) Laboratory and field performance of a continuously measuring personal respirable dust monitor. Report of investigations 9669. NIOSH publication no. 2006-145

White EW, DeNee PB (1972) Characterisation of coal mine dust by computer processing of scanning electron microscope information. Annals of the New York Academy of Sciences 200, Coal Workers' Pneumoconiosis, pp 666–675

WHO (1999) Hazard prevention and control in the work environment: airborne dust. Protection of the human environment occupational health and environmental health series, Geneva, 1999. World Health Organization WHO/SDE/OEH/99.14

WHO (2000) Air quality guidelines for Europe, 2nd edn. World Health Organization, Copenhagen

WHO (2006) Air quality guidelines global update 2005. World Health Organization, Copenhagen

Williamson BJ, Udachin V, Purvis OW, Spiro B, Cressey G, Jones GC (2004) Characterisation of airborne particulate pollution in the Cu smelter and former mining town of Karabash, south Ural mountains of Russia. Environ Monit Assess 98:235–259

Williamson BJ, Purvis OW, Mikhailova IN, Spiro B, Udachin V (2008) The lichen transplant methodology in the source apportionment of metal deposition around a copper smelter in the former mining town of Karabash, Russia. Environ Monit Assess 141:227–236

# Mineral Dust Properties at the Mt Lyell Cu-Au Mine Site, Australia

**Taryn L. Noble, Ron F. Berry and Bernd Lottermoser**

**Abstract** Mine sites operating dust monitoring programs use a variety of techniques to comply with legislative constraints and maintain high standards of environmental and human health protection. One low cost option is the use of dust deposition gauges, which provide information on the total, soluble and insoluble dust fluxes. The aim of this study was to identify methods that could provide information on likely dust sources of samples, which were collected using dust deposition gauges at the Mt Lyell Cu-Au mine, Australia. Elemental analyses of archived dust samples combined with known dust deposition rates allowed quantification of annual metal fluxes. The highest annual metal fluxes were measured for Cu (1–33 g $m^{-2}$ $year^{-1}$) followed by Pb (8–343 mg $m^{-2}$ $year^{-1}$), Cr (3–59 mg $m^{-2}$ $year^{-1}$) and As (1–79 mg $m^{-2}$ $year^{-1}$). X-ray diffractometry and scanning electron microscopy permitted characterization of the mineralogical and morphological properties of dust samples. These analyses revealed that the analysed samples derived from at least four different dust sources. Consequently, geochemical and mineralogical characterization of mineral dust samples combined with a detailed site knowledge allows identification of dust sources at mine sites.

## Introduction

Dust emissions from mine sites pose potential contamination issues for the surrounding environment and local communities through human health consequences. The chemical composition of mineral dust can impact on human and ecosystem

T.L. Noble (✉) · R.F. Berry
School of Physical Sciences, University of Tasmania, Private Bag 79, Hobart, TAS 7001, Australia
e-mail: Taryn.Noble@utas.edu.au

B. Lottermoser
Institute of Mineral Resources Engineering, RWTH Aachen University, Wüllnerstrasse 2, 52062 Aachen, Germany
e-mail: lottermoser@mre.rwth-aachen.de



B. Lottermoser (ed.), *Environmental Indicators in Metal Mining*,
DOI 10.1007/978-3-319-42731-7_17

health. Human health effects from exposure to dust depends on the diameter (particularly particles $\leq 10$ μm), shape, solubility, and reactivity of particulate matter (Plumlee and Ziegler 2003). A thorough assessment of the physical and chemical composition of mineral dust requires the use of advanced laboratory tools. Empowered with information on mineral dust properties at mine sites, it is possible to evaluate dust sources on mine leases and to respond to possible site risks with appropriate dust control measures.

Since the 1950s the minerals industry has had in place preventative measures to limit its workers exposure to dust through the implementation of Occupational Exposure Limit values (OELs) (e.g., Safe Work Australia 2012). Dust management plans for the minerals industry aim to reduce and control dust emissions around mine sites. Dust management plans include: (i) identifying potential dust sources; (ii) implementing measures to avoid and or minimise dust generation; and (iii) complying with legislation and other obligations to reduce negative environmental and human health impacts of dust. The specific locations of dust monitoring instruments should reflect the nature of the dust sources and include control sites, which provide an indication of background levels during the mining operations (AS 2007). The frequency of sampling will vary according to the objectives of the monitoring programme and sampling equipment. In general, there are two approaches to dust monitoring around mine sites: (i) passive techniques that generally monitor total suspended solids (TSP) and do not require a power source, so are relatively inexpensive (e.g. dust deposition gauges; personal exposure samples); and (ii) active systems that require a power source to measure nuisance dust and different particle sizes (e.g., high volume air samplers; continuous particle monitors).

The objective of this study was to identify dust sources using mineralogical and geochemical characteristics of mineral dust collected at the Mt Lyell Cu-Au mine, Australia. Dust samples collected using deposition gauges, positioned across the Mount Lyell dust-sampling network, were analyzed using mineralogical and geochemical techniques. The study demonstrates that additional laboratory analyses on mineral dust samples at mine sites provide valuable information for operators and regulators.

## *Mount Lyell Mine Operation*

The Mount Lyell Cu-Au mine is situated in northwest Tasmania, Australia (41°04′ S, 145°34′E). The mine has been in operation since the early 1890s after the discovery of gold in 1883. It has produced over 1.3 Mt Cu, 750 t Ag, and 45 t Au (McQuade et al. 1995). Prior to 1995, no environmental controls were enforced resulting in an extensive environmental legacy. The environmental impacts ranged from denudation of the landscape as a result of deforestation and acid rain from pyritic smelting, to widespread degradation of the natural river systems through the disposal of acid rock drainage (ARD) , slag and pyritic tailings into the King and Queen River systems. It is estimated that 1.5 Mt of tailings were flushed into the King River since 1916, and 95 Mt of tailings, 10 Mt of topsoil and 1.4 Mt of

smelter slag were discharged into the Queen River (McQuade et al. 1995; Locher 1997). After efforts to remediate the effected region during a period of mine closure, the Mount Lyell lease and mine were re-opened in 1995 by Copper Mines of Tasmania (CMT), operated by Vedanta.

The mined ore body consists of disseminated pyrite and is hosted in the Cambrian quartz-sericite felsic volcanics of the Mount Read Volcanic complex (Corbett and Solomon 1989). This geological unit predominantly consists of felsic lavas and pyroclastic deposits that have been subjected to low grade metamorphism and a high level of regional deformation and hydrothermal alteration. At the time of sampling, ore is extracted in an underground mining process, involving a sub-level caving method to mine the ore about 1000 metres below the surface. Primary crushing of the ore is carried out below the surface after which, the ore is hoisted up to the surface and transported over 1.2 km to the treatment plant for further processing. At the surface, the plant uses secondary, tertiary and quaternary crushing to produce a final product (P80).

A significant source of dust at Mount Lyell is likely generated during the production of the sulfide concentrate. Dust dispersal may also be caused during transport on unpaved roads. The degree of dust dispersal from either of these sources will be controlled by the regional precipitation rate. Dust control measures in operation at the mine site included enclosure of the crushing and concentrator plant and management of a dust-monitoring program.

## *Climate*

Meteorological data collected at Mount Lyell indicate that dominant winds are westerly, to north-westerly with gusts averaging around 45 km/h (Copper Mines Tasmania). Rainfall in this region is highest during winter (Fig. 1). The average

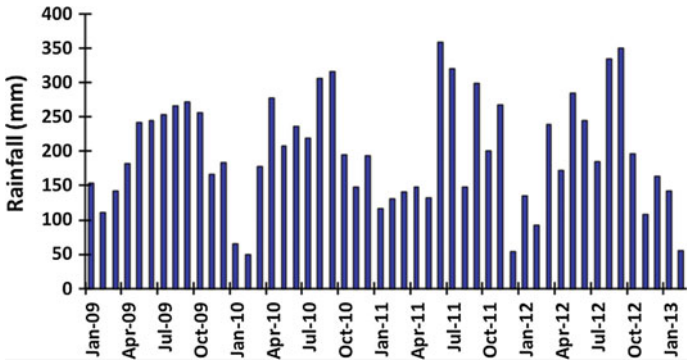


**Fig. 1** Monthly average rainfall at Mt Lyell between 2009 and 2013, which corresponds to the period of the dust monitoring program investigated by this study (*data source* Copper Mines of Tasmania)

monthly rainfall from 1997 to 2013 for the month of August was 294 mm with a maximum of 554 mm (BOM 2013). Dust dispersion to the surrounding environment from Mount Lyell is likely to be strongly damped by the high rainfall regime.

### *Dust Monitoring Program*

The environmental program at Mt Lyell operates an extensive network of dust deposition gauges, which monitor monthly dust fluxes around the mine site (Fig. 2). Dust deposition gauges are ideal for long term and remote monitoring of dust deposition at low cost. The mine site was required by the regulator to monitor the total dust deposition rate (g $m^{-2}$ $month^{-1}$) and the fraction of insoluble and soluble components. This investigation aimed to provide additional information using the samples collected in the years 2009–2013. Parameters of interest included particle morphology and size distribution as well as the composition of individual dust grains.

## Methods

### *Settle Dust*

Dust deposition gauges were composed of high-density polyethylene (HDPE) funnels connected to a HDPE bottle (Fig. 3). The rate of dust deposition was measured in g $m^{-2}$ $month^{-1}$ and the insoluble and soluble masses determined according to the standard procedure AS (2003). This method documents how the contents of the dust deposition gauge are sieved to <1 mm and evaporated on a hotplate. The mass of the solids is recorded as total, while re-dissolving the evaporated sample in deionized water and filtering it under vacuum through a filter paper, allowing the insoluble and soluble fractions to be determined (Fig. 4).

Once the dust deposition rate was measured and the soluble and insoluble mass determined, the filter papers from each site were added to the sample container each month. As a result, this study used bulk samples of dust collected from each site spanning the length of the sampling regime (2009–2013) (Table 1). Distinct colour variations were observed between different filter papers for all the settled dust samples (Fig. 5), suggesting monthly variations in the source of dust at a given sampling site.


**Fig. 2** Location of dust deposition gauges at the Mount Lyell mine site. The samples used in this study are highlighted in *grey boxes*. *Source* Copper Mines of Tasmania (Color figure online)

**Fig. 3** Dust deposition gauge with stand (DG18)

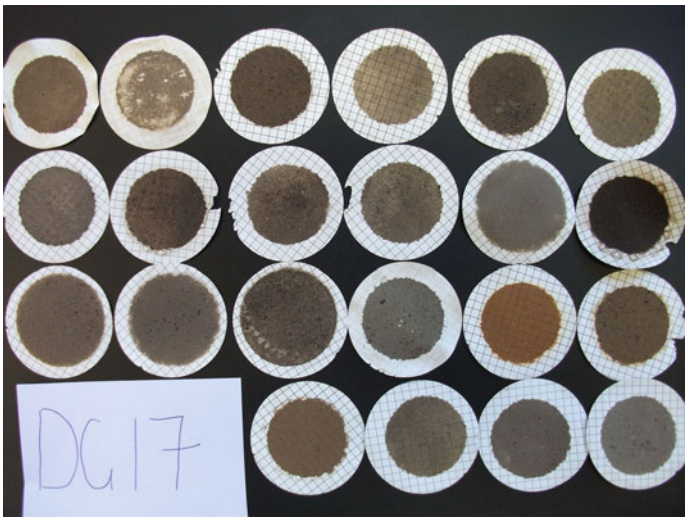


**Fig. 4** Filter papers with dust collected in dust deposition gauges from site DG17 near the core store.*Each square* on the filter paper is 3 × 3 mm (color figure online)

**Table 1** Sample sites selected for this study, and their distance relative to the crushers

| Site | Description of location | Relative to crusher plant |
|---|---|---|
| DG03 | Core lay-down area near environment store, under power lines, 184 m | Proximal |
| DG06 | Corner at the 100 ft thicker, 117 m | Proximal |
| DG09 | Hill top looking over Mt Lyell operation, 198 m | Proximal |
| DG10 | Filter Plant shed near the river, 163 m | Distal |
| DG13 | Corner laydown and surge bin area, 182 m | Proximal |
| DG14 | Adjacent stores laydown area 190 m | Proximal |
| DG15 | Near the red tank 192 m | Proximal |
| DG17 | Core shed fence 164 m | Distal |
| DG19 | Slag dump 191 m | Distal |

Proximal sites are near to the crushers, while distal ones are on the boundary of the lease

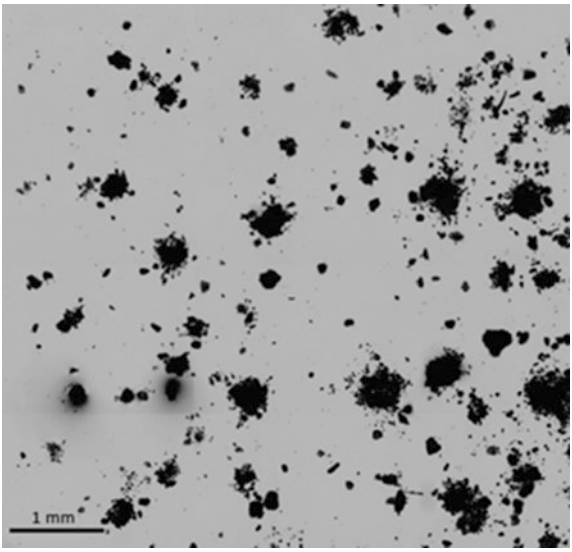


**Fig. 5** Transmitted light image of a mineral dust sample (DG03), using a Leica DM6000 automated optical microscope

## *Geochemistry*

The elemental concentrations (As, Be, Cd, Co, Cr, Cu, Mn, Ni, Pb, Se, Zn) for each sample were determined by solution chemistry using an *ELEMENT* (Finnigan MAT) High-Resolution Inductively Coupled Plasma Mass Spectrometer (HR-ICP-MS) at the University of Tasmania (UTAS). The samples were dissolved on a hotplate (180 °C) in 7 ml Savillex vials, using a three-acid (HF; $HNO_3$; aqua regia) digestion method to ensure that both the silicate and sulfide fractions were completely dissolved. The samples were spiked with indium as the internal standard

at a concentration of 100 ppb prior to ICP-MS analysis. QA/QC was assured by analysing RTS-3 and RTS-4, certified reference materials for sulfide ores. Analytical accuracy was estimated by comparing the certified reference values to the measured values of each element, with some excellent recoveries noted (98–111 %) (Table 2). External precision was estimated by triplicate analysis of DG15, which reflects heterogeneity between aliquots tested from the bulk dust sample (Table 3).

## *Mineralogy and Morphology*

The approach taken to assess the mineralogical composition of dust samples involved using optical microscopy, Scanning Electron Microscopy (SEM) , Laser Raman spectrometry and X-ray Diffraction (XRD). Sample preparation for mineralogy and morphological assessment is critical in analysing dust due to the small

**Table 2** The recovery of each element, calculated as the ratio of the measured relative to the 'true' standard reference value

| Element | RTS-3 (% recovery) |
|---|---|
| Cr | 146 |
| Mn | 111 |
| Co | 98 |
| Ni | 100 |
| Cu | 108 |
| Zn | 109 |
| As | 75 |
| Se | 85 |
| Se | 94 |
| Cd | 96 |
| Pb | 111 |

**Table 3** The average concentration of elements in sample DG15 measured in triplicate and the associated standard deviation

| Element | Average (ppm) | 1σ error (%) |
|---|---|---|
| Be | 0.9 | 23 |
| Cr | 28 | 18 |
| Mn | 1379 | 20 |
| Co | 134 | 19 |
| Ni | 26 | 24 |
| Cu | 15,190 | 22 |
| Zn | 34 | 22 |
| As | 34 | 38 |
| Se | 8.0 | 32 |
| Se | 7.1 | 13 |
| Cd | 2.8 | 25 |
| Pb | 172 | 16 |

particle size. Development of methods to re-suspend the dust particles collected from the filters is required to suit the limitations of each mineralogical technique.

After scraping the dust particles off the filters, the dust tended to clump together as a result of static forces. Several trials to separate the dust onto glass slides to allow individual particles to be assessed for shape, size distribution, and composition, were unsuccessful in dispersing the particles evenly (Fig. 5). A second method involved mounting the dust in a one-inch mould with a fine coating of dust covering the bottom surface of double-sided tape, filled with epoxy resin.

Mineralogical identification was carried out using XRD analyses of dust samples. This method could be applied because materials were taken from large bulk dust samples, which were made up using all the filters collected during 2009–2013. XRD analyses were performed at UTAS using a benchtop Bruker D2 Phase Analyser X-ray Diffractometer with a Co X-ray source (30 kV, 10 mA) and Lynxeye detector. The analyses provided identification of minerals with abundances of >1 %. A corundum standard was used to calibrate the X-ray beam alignment and the detected peaks. Each sample was placed into sample holder for 1-hour analytical runs, which produced spectra that were processed by using Eva 2.1 mineral identification software using the ICDD PDF 2012 database.

Further mineralogical characterization was carried out using a Hitachi SU-70 field emission scanning electron microscope (FESEM) at UTAS. A 15 kV electron beam was applied to produce a backscattered electron (BSE) grey-scale image, which reflects mean atomic number variations within the sample. Semi-quantitative elemental analyses were made using an Oxford Instrument's energy dispersive X-ray spectrometer (EDS) fitted to the FESEM. The epoxy resin sample mounts were coated with a 20 nm carbon film to prevent surface charging. Representative spectra were collected for each sample, which were interpreted offline using MinIdent to identify minerals based on the % of each element.

Laser Raman spectroscopy was also trialled as a method for mineralogical characterization, using the Renishaw® laser Raman system at UTAS. Laser Raman spectrometry has traditionally been used in mineral identification and is a type of vibrational spectroscopy. A laser excites a target, resulting in inelastic scattering of photons (Raman scattering). The scattered photons have a characteristic frequency defined by the chemical bonds of the material represented by peaks in the Raman spectra. The Renishaw® laser Raman system at the University of Tasmania is optimized for fast mapping and initial tests indicate high quality spectral data can be recorded at 50 ms/pixel (0.7 micron pixels for 100 × objective, 3 micron pixel at 20×) (Berry et al. 2012). However, the dust samples proved difficult to analyze for the following reasons: (1) small particle size and/or small particle adhered to each other, resulting in a mixed spectra that was difficult to interpret; and (2) intense fluorescence resulted in a board spectrum which overprinted the spectra produced by Raman scattering. Several different laser wavelengths were trialled to avoid fluorescence, which included 532 nm (green), 633 (red), 785 (NIR) and 830 nm (NIR). Infra-red light could potentially be used to avoid the problem of fluorescence, however, a statistical library of mineral spectra for each study site would be required to interpret the mineral spectra for accurate mineral identification.

## Results and Discussion

### *Dust Deposition Fluxes*

Nine dust collection sites operating between August 2009 and May 2013 were investigated. The median dust deposition fluxes per month are reported for the four-year collection period, since the geochemical and mineralogical characterization of the samples was carried out on the bulk material collected over the same period. The highest monthly deposition fluxes for total dust was observed at DG15, located near the crusher plant, which recorded dust fluxes that are an order of magnitude higher than the surrounding stations (Fig. 6). The lowest monthly dust deposition flux over the same period was observed at DG09, a site located at the highest point (198 m) to the northwest of the crusher plant (Fig. 6). DG19 is a recent addition to the sampling station and showed similarly low median monthly dust flux of 6.3 g $m^{-3}$ $month^{-1}$ over the collection period August 2012 to May 2013.

The proportion of insoluble versus soluble fluxes was operationally defined according the method AS/NZS 3580.10.1:2003. The proportion of insoluble and soluble fluxes at each site varied with proximity to the crusher and concentrator

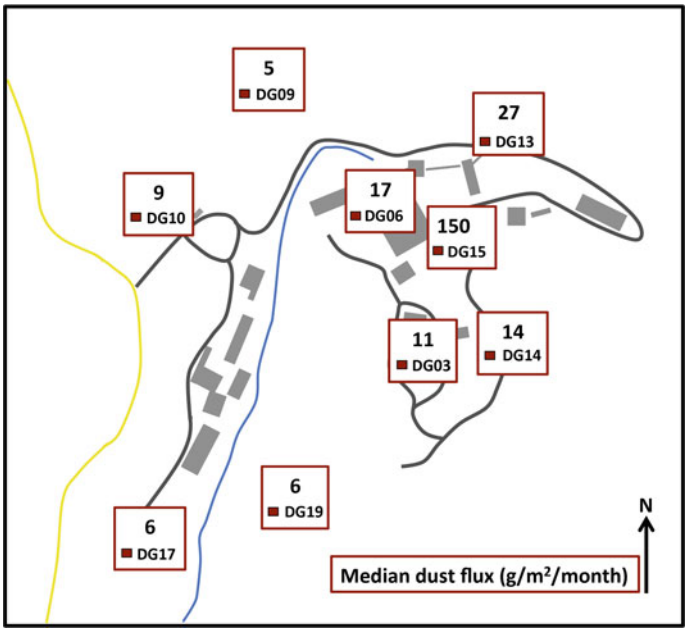


**Fig. 6** Median total dust deposition flux ($g/m^2$/month) for each station over a period from August 2009 to May 2013. Except for station DG19, which represents the median value between August 2012 to May 2013 (color figure online)

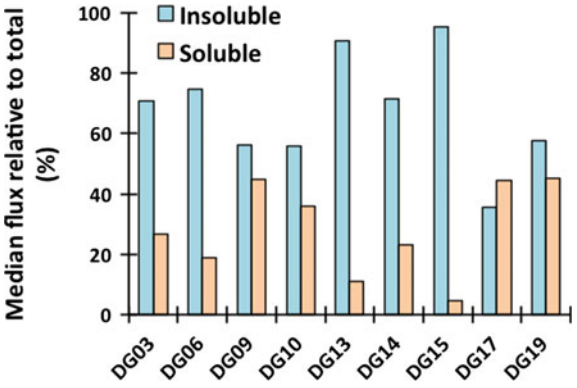


**Fig. 7** The percentage insoluble and soluble dust fraction relative to the total dust deposition flux at each site. The estimates are based on the median values for the periods August 2009 to May 2013 and August 2012 to May 2013 for DG09 (color figure online)

plant. The median insoluble fluxes were larger than the soluble fluxes at all the sites investigated except DG17 (Fig. 7). The monitoring sites furthest from the crushing plant (DG09, DG17 and DG19), exhibit the highest soluble fraction relative to the insoluble fraction. In comparison, the sites nearest to the crushing plant have the largest insoluble dust deposition fluxes.

## *Metal Fluxes*

Eleven element concentrations presented in mg/kg, were measured for each dust sample (Table 2). In general the dust samples showed minor (>1000 mg/kg) Cu, Zn and Mn, subminor (>100 mg/kg) Pb and Co, and trace amounts of Be, Cd, Cr, Ni, As and Se. Overall DG10 (in the west of the sampling network) showed the highest cumulative metal content, primarily driven by the high Cu concentration (21,632 mg/kg); while DG19 located to the south showed the lowest metal enrichment compared to the other eight samples, including the lowest Cu concentration (3,485 mg/kg) (Fig. 8). The DG10 is located near the filter plant, therefore an abundance of fines with high Cu concentrations are expected. In contrast, DG19 is located to the west of the waste rock dump near the banks of the Queen River, therefore high metal dust fluxes are not expected. The distribution of Pb measured in the dust samples showed a similar spatial distribution compared to the Cu concentration, with the highest Pb concentration at DG10 (205 mg/kg) and the lowest at DG19 (108 mg/kg) (Fig. 9).

Zinc concentrations in the settle dust ranged from 1080 to 2919 mg/kg across the dust-sampling network (Fig. 10). The highest Zn concentration was observed at DG17 (in the south of the dust-sampling network), whereas the lowest Zn concentration was measured to the NNE at DG13. DG09 situated in the NW also had a notably high Zn concentration (1831 mg/kg) and intermediate Cu and Pb values. Elevated Zn at the distal sites (DG17, DG19) may be due to dust from legacy slag, which will have higher Zn concentrations (Table 4).

**Table 4** Elemental concentrations of Mt Lyell dust samples measured by ICP-MS

| mg/kg | DG03 | DG06 | DG09 | DG10 | DG13 | DG14 | DG15 | DG17 | DG19 |
|---|---|---|---|---|---|---|---|---|---|
| Be | 0.8 | 0.9 | 0.6 | 0.6 | 0.8 | 0.8 | 1.0 | 0.5 | 0.5 |
| Cd | 2.3 | 2.7 | 2.5 | 3.2 | 2.7 | 2.1 | 3.3 | 2.1 | 0.7 |
| Pb | 176 | 180 | 165 | 205 | 163 | 147 | 191 | 176 | 108 |
| Cr | 54.5 | 57.6 | 42.0 | 76.1 | 39.3 | 37.5 | 32.9 | 93.3 | 34.3 |
| Mn | 1202 | 1499 | 1142 | 476 | 1416 | 1102 | 1635 | 768 | 385 |
| Co | 108 | 135 | 81 | 52 | 111 | 87 | 157 | 54 | 37 |
| Ni | 36.7 | 33.9 | 49.0 | 24.6 | 25.7 | 24.0 | 32.7 | 56.2 | 17.0 |
| Cu | 13,713 | 14,581 | 12,825 | 21,362 | 13,927 | 12,105 | 18,374 | 6416 | 3485 |
| Zn | 1516 | 1204 | 1831 | 1318 | 1080 | 1308 | 1102 | 2919 | 1663 |
| As | 34.1 | 38.1 | 22.5 | 22.8 | 25.4 | 22.0 | 43.9 | 18.7 | 6.1 |
| Se | 6.1 | 6.5 | 6.0 | 5.8 | 5.5 | 5.0 | 6.1 | 4.0 | 1.2 |

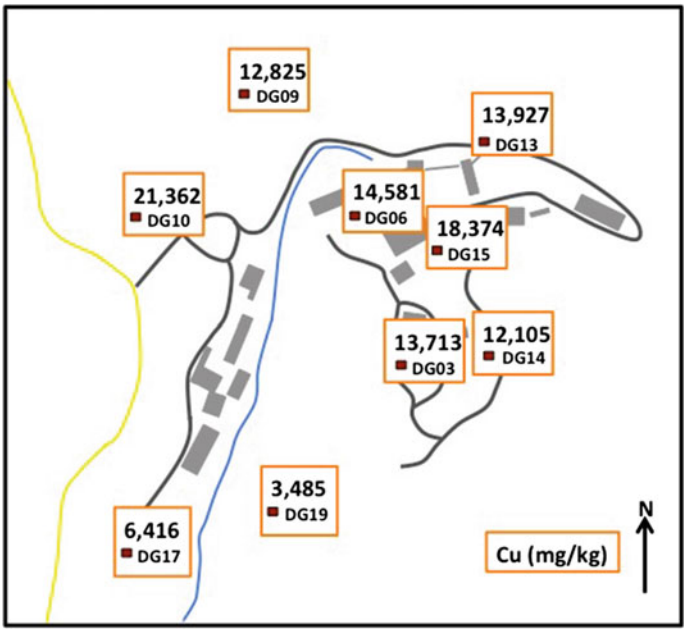


**Fig. 8** Distribution of Cu concentration, measured in mineral dusts across the settled dust-sampling network at the Mt Lyell mine site. The Queen River is shown in *blue* and the Lyell Highway in *yellow* (Color figure online)

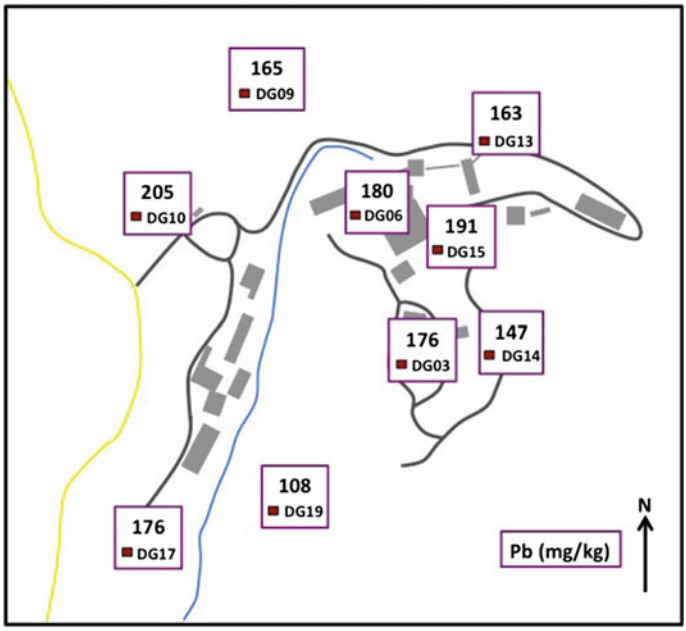


**Fig. 9** Distribution of Pb concentration, measured in mineral dusts across the settled dust-sampling network at the Mt Lyell mine site. The Queen River is shown in *blue* and the Lyell Highway in *yellow* (Color figure online)

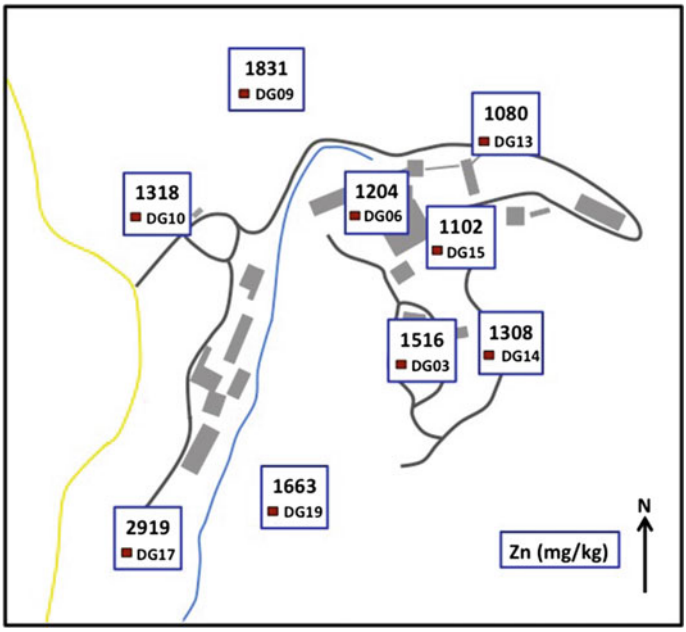


**Fig. 10** Distribution of Zn concentration, measured in mineral dusts across the settled dust-sampling network at the Mt Lyell mine site. The Queen River is shown in *blue* and the Lyell Highway in *yellow* (color figure online)

Arsenic concentrations measured in the dust-sampling sites showed a median value 26 mg/kg and a range of 6 mg/kg at DG19 to 44 mg/kg at DG15. Higher As (>34 mg/kg) concentrations were focused towards the centre of the sampling network at DG15, DG06 and DG03, which are proximal to the crushers and concentrator. In contrast, the lowest values were observed at DG19, located to the south of the dust generating activities (Fig. 11).

Annual metal deposition fluxes were estimated for As, Cr, Cu, Ni, Pb and Zn based on the total median settled dust fluxes and the elemental concentrations measured by ICP-MS. The total fluxes were used rather than insoluble or soluble metal fluxes since the partitioning of metals between these two phases is unknown. However, we present the total, soluble and insoluble metal fluxes for comparison (Table 5). The flux of soluble metal constituents would be of particular concern since this proportion is likely to pose a greater risk to the surrounding environment. The total metal fluxes likely overestimate the true metal fluxes at sites DG09, DSG17 and DG19, where the insoluble fraction ranges from 36 to 56 % of the total. The soluble fraction is likely to be sourced predominately from marine aerosols of the Southern Ocean (e.g., NaCl, KCl; Andreae 1989).

Cu fluxes were the highest ranging from 1 to 33 g $m^{-2}$ $year^{-1}$ across the dust sites. Overall the highest metal deposition fluxes were observed at DG15, despite the fact that the highest metal concentrations were generally observed at DG10.

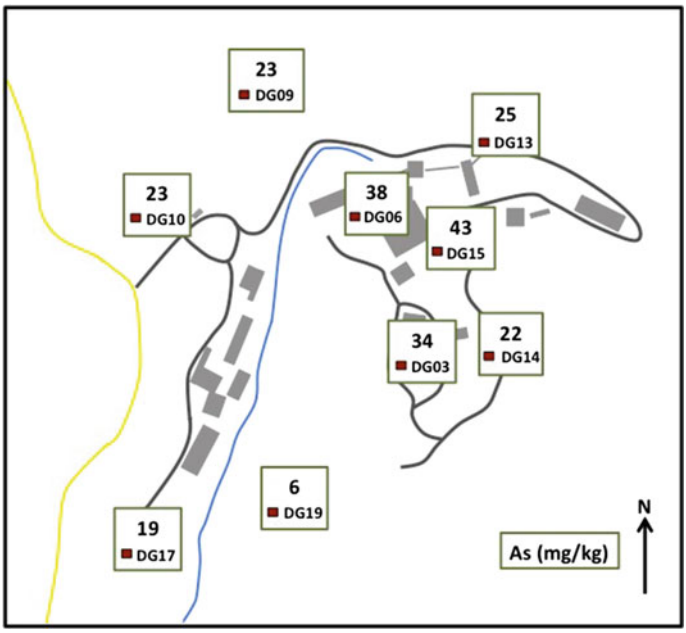


**Fig. 11** Distribution of As concentration, measured in mineral dusts across the settled dust-sampling network at the Mt Lyell mine site. The Queen River is shown in *blue* and the Lyell Highway in *yellow* (Color figure online)

Thus additional dust suppression mechanisms are required to reduce the dust fluxes at the crushing and concentrating circuits. The lowest metal fluxes were observed at DG19 (Table 5) suggesting that metal enriched dust dispersal from the mining activities does not pose a problem for the Queenstown settlement.

The geochemical data provides some constraints on the composition of dust sources. The data indicate that four different end members of dust can be distinguished using Cu, Pb, Zn, Mn, Ni and Se concentrations (Fig. 12). The four geochemical domains were: (i) a dust source with a low Cu:Pb ratio and relatively low Zn, Mn and Ni concentrations which dominates at site DG19 (slag-component); (ii) a dust source with a low Cu:Pb ratio and relatively high Zn, Mn and Ni concentrations, which dominates site DG17 (depleted ore signature/waste); (iii) a dust source with a high Cu:Pb ratio as well as low Zn and Ni but high Mn concentrations (enriched ore signature I); and (iv) a dust source with a high Cu:Pb ratio but low Mn concentrations (enriched ore signature II).

**Table 5** Total, insoluble and soluble dust deposition metal fluxes (mg $m^{-2}$ $year^{-1}$) at the Mt Leyll mine site, based on median total deposition dust fluxes and elemental concentrations

| Metal flux ($mg/m^2$/year) | DG03 | DG06 | DG09 | DG10 | DG13 | DG14 | DG15 | DG17 | DG19 |
|---|---|---|---|---|---|---|---|---|---|
| Total Pb | 24 | 36 | 10 | 23 | 52 | 24 | 343 | 13 | 8 |
| Insoluble | 17 | 27 | 6 | 13 | 47 | 17 | 327 | 5 | 5 |
| Soluble | 6 | 7 | 5 | 8 | 6 | 6 | 16 | 6 | 4 |
| Total Cr | 7.4 | 11.6 | 2.6 | 8.5 | 12.6 | 6.2 | 59 | 6.9 | 2.6 |
| Insoluble | 5.3 | 8.7 | 1.5 | 4.8 | 11.4 | 4.4 | 56 | 2.5 | 1.5 |
| Soluble | 2.0 | 2.2 | 1.2 | 3.1 | 1.4 | 1.4 | 3 | 3.1 | 1.2 |
| Total Cu | 1871 | 2937 | 792 | 2384 | 4458 | 1985 | 33,032 | 474 | 264 |
| Insoluble | 1328 | 2198 | 446 | 1334 | 4051 | 1418 | 31,511 | 169 | 152 |
| Soluble | 497 | 553 | 356 | 858 | 500 | 456 | 1539 | 211 | 119 |
| Total Ni | 5.0 | 6.8 | 3.0 | 2.7 | 8.2 | 3.9 | 58.8 | 4.2 | 1.3 |
| Insoluble | 3.5 | 5.1 | 1.7 | 1.5 | 7.5 | 2.8 | 56.0 | 1.5 | 0.7 |
| Soluble | 1.3 | 1.3 | 1.4 | 1.0 | 0.9 | 0.9 | 2.7 | 1.8 | 0.6 |
| Total Zn | 1.9 | 2.5 | 0.9 | 1.1 | 3.4 | 2.1 | 24 | 1.4 | 0.7 |
| Insoluble | 1.5 | 1.9 | 0.8 | 0.8 | 2.9 | 1.7 | 19 | 1.0 | 0.4 |
| Soluble | 2.3 | 2.9 | 1.1 | 1.6 | 4.5 | 2.3 | 28 | 1.6 | 0.9 |
| Total As | 4.7 | 7.7 | 1.4 | 2.5 | 8.1 | 3.6 | 79 | 1.4 | 0.5 |
| Insoluble | 3.3 | 5.7 | 0.8 | 1.4 | 7.4 | 2.6 | 75 | 0.5 | 0.3 |
| Soluble | 1.2 | 1.4 | 0.6 | 0.9 | 0.9 | 0.8 | 4 | 0.6 | 0.2 |

## *Mineralogy*

Mineral phases in each dust sample were identified by XRD analysis. Overall, the following minerals were identified: calcite, chalcopyrite, chlorite, clinochlore, muscovite, pyrite and quartz. The silicate minerals such as chlorite, muscovite and quartz were observed at all sites. Chalcopyrite and pyrite were observed across all sites except for DG19, located near the slag and waste dumps (Fig. 13).

Mineral phases present in minor (<1 %) or trace amounts were identified using the SEM and included Fe oxides phases, illite and rutile. However, the mineral phases identified using the SEM are biased towards larger particles due to loss of the finest fraction during polishing of the mount to create a smooth surface for imaging. The larger particles embedded in the epoxy resin were often coated with finer particles, and many of the smaller grains were coagulated making image analysis, using software packages (e.g., eCognition) more difficult (Fig. 14). Thus, development of a method to automate the mineral and morphological properties of the dust using the epoxy mounts was not pursued further.

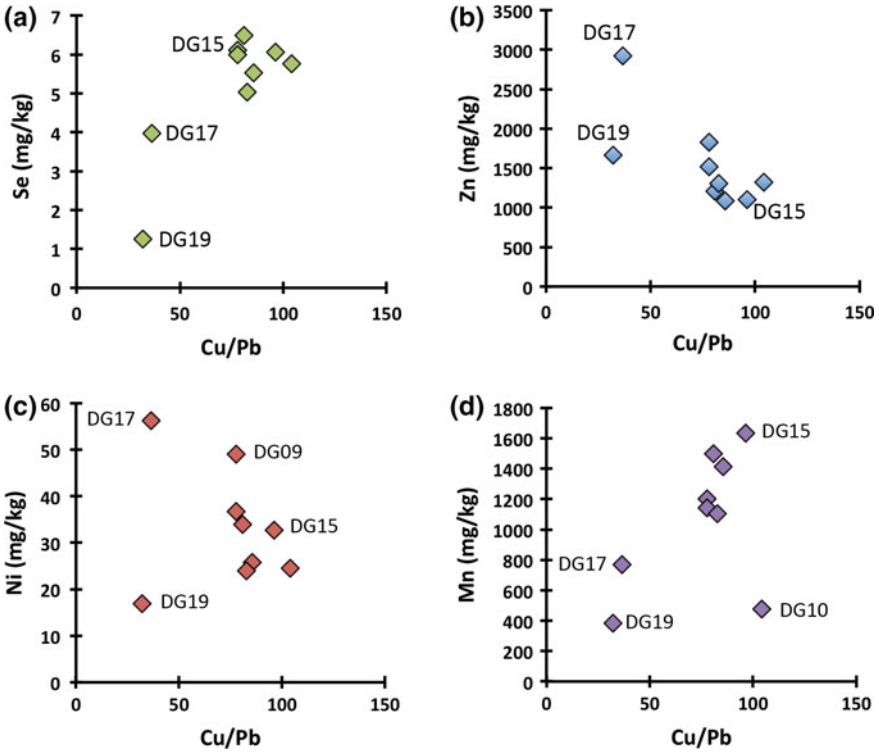


**Fig. 12** Chemical composition of settled dust from the Mt Lyell mine site, showing their Cu:Pb ratio plotted versus concentrations of **a** Se **b** Zn **c** Ni and **d** Mn (mg/kg) (color figure online)

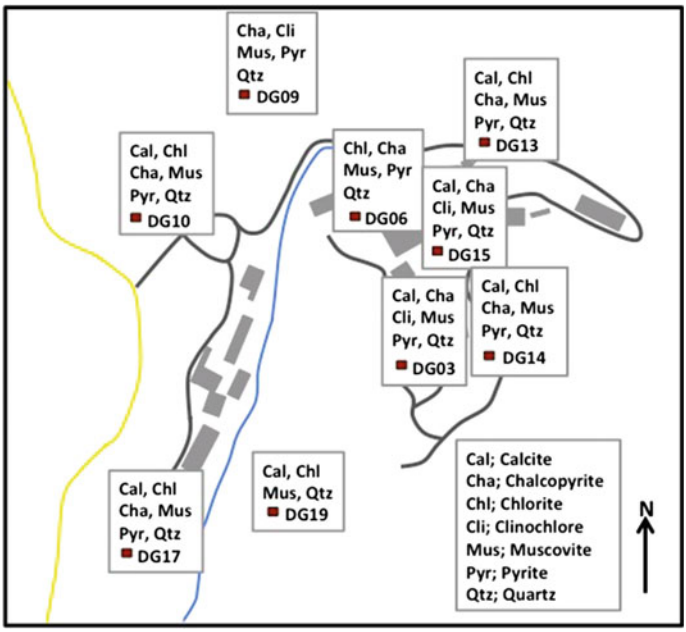


**Fig. 13** Minerals detected in dust samples collected from the dust sampling network at the Mt Lyell mine site (color figure online)

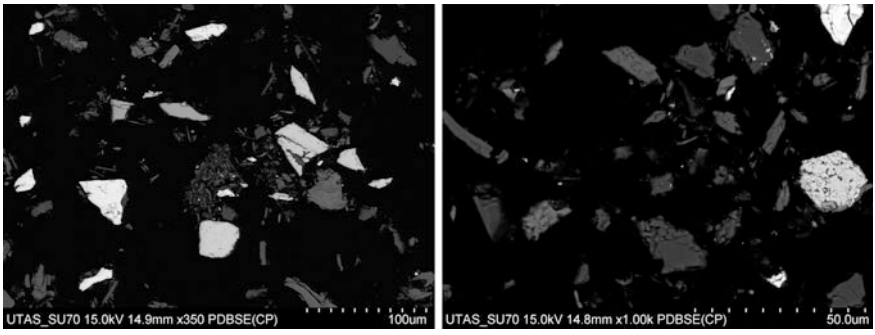


**Fig. 14** BSE images of mineral dust (DG03, *left*; DG07, *right*). The *grey-scale* reflects mineral composition with heavy elements making up the brightest minerals

## Conclusions

The aim of this study was to identify methods that could provide information on likely dust sources of samples, which were collected using dust deposition gauges at the Mt Lyell Cu-Au mine, Australia. Dust filters from the monitoring period 2009–2013 were bulked to create bulk dust samples.

Four geochemical domains were identified using elemental concentrations at each site, which implied that there are at least four different dust sources: (i) enriched ore signature I; (ii) enriched ore signature II; (iii) depleted ore signature/waste; and (iv) slag-component. Annual metal flux estimates, evaluated using the median dust flux recorded at each site, demonstrated the Cu flux to be the largest (1–33 g $m^{-2}$ $year^{-1}$) followed by Pb (8–343 mg $m^{-2}$ $year^{-1}$), Cr (3–59 mg $m^{-2}$ $year^{-1}$) and As (1–79 mg $m^{-2}$ $year^{-1}$). X-ray diffractometry (XRD) proved to be a useful methods of mineralogical characterization of bulk dust composition, which was possible due to the large amount of sample material available. Calcite, chalcopyrite, chlorite, muscovite, pyrite and quartz were the dominant mineral phases identified, in addition to variable contents of other minerals (e.g., Fe-oxide, illite, rutile) associated with individual sampling sites. This case study demonstrates that the use of advanced analytical tools allows fingerprinting of individual dust sources at metalliferous mine sites.

## References

Andreae MO (1989) Marine aerosol chemistry at Cape Grim, Tasmania, and Townsville, Queensland. J Geophys Res 87:8875–8885

AS (Australian Standard) (2003) AS 3580.93:2003, Methods for sampling and analysis of ambient air. Method 9.3: determination of suspended particulate matter—total suspended particulate matter (TSP)—high volume sampler gravimetric method. Standards Australia, Sydney

AS (Australian Standard) (2007) AS 3580.1.1:2007, methods for sampling and analysis of ambient air—determination of suspended particulate matter—Dichotomous sampler (PM10, coarse PM and PM2.5)—gravimetric method. Standards Australia, Sydney

Berry R, Bonnici N, Danyushevsky L, Goemann K, Hutchison D, Meffre S, Parbhakar-Fox A, Rodemann T (2012) Review of micro-analytical technologies for mineral mapping and trace element deportment. CRC ORE Technical Report, CRC for Optimising Resource Extraction, Brisbane

BOM (Bureau of Meterology) (2013) Monthly rainfall Queenstown. http://www.bom.gov.au/jsp/ncc/cdio/weatherData/av?p_nccObsCode=139&p_display_type=dataFile&p_startYear=&p_c=&p_stn_num=097091

Corbett M, Solomon M (1989) Cambrian Mt Read volcanics and associated mineral deposits. In: Burrett CF, Martin EL (eds) Geology and mineral resources of Tasmania, Geological Society of Australia Special Publication, vol 15, pp 84–153

Locher H (1997) Sediment transport in the King River, Tasmania. Mount Lyell remediation research and demonstration program. Office of the Supervising Scientist, Canberra, Report 120

McQuade CV, Johnston JF, Innes SM (1995) Review of historical literature and data on the sources and quality of effluent from the Mount Lyell lease site. Mount Lyell remediation research and demonstration program. Office of the Supervising Scientist, Canberra, Report 104

Plumlee GS, Ziegler TL (2003) The medical geochemistry of dusts, soils and other Earth materials. In: Sherwood Lollar B (eds) Treaties on Geochemistry, vol 9, pp 263–310

Safe Work Australia (2012) Guidance on the interpretation of workplace exposure standards for airborne contaminants. Canberra

# Assessing Mineral Dust Properties Using Passive Dust Samplers and Scanning Electron Microscopy

**Taryn L. Noble, Ron F. Berry, Karsten Goemann and Bernd Lottermoser**

**Abstract** This study presents a novel method to characterize dust particles using a passive dust sampler (PDS). Six different PDS were deployed around six different metal mine sites (Tasmania, Australia) and left in the field for 1 month. Dust particles were analyzed directly on the PDS using a Field Emission Scanning Electron Microscope. Backscattered electron (BSE) images were collected with a resolution of 0.5 μm per pixel and used to characterize the size and composition of dust particles. Those particles >2 μm in diameter were classified according to the range of BSE brightness values, which correspond to mineralogical compositions. Particles were grouped according to BSE brightness and categorized as organic particles, silicates, Fe silicates and oxides, and sulfides. Dust sources with unique particle size:composition relationships were identified at particular mine site domains (e.g. rock crusher, concentrator plant, tailings dam). The documented method can be used to monitor the dispersal of mineral dust and provide information on the mineralogical composition of particle size fractions relevant to occupational health risks at metalliferous mine sites.

T.L. Noble (✉) · R.F. Berry
School of Physical Sciences, University of Tasmania, Private Bag 79, Hobart, TAS 7001, Australia
e-mail: Taryn.Noble@utas.edu.au

R.F. Berry
e-mail: Ron.Berry@utas.edu.au

K. Goemann
Central Science Laboratory, University of Tasmania, Private Bag 74, Hobart, TAS 7001, Australia
e-mail: Karsten.Goemann@utas.edu.au

B. Lottermoser
Institute of Mineral Resources Engineering, RWTH Aachen University, Wüllnerstrasse 2, 52062 Aachen, Germany
e-mail: lottermoser@mre.rwth-aachen.de



B. Lottermoser (ed.), *Environmental Indicators in Metal Mining*,
DOI 10.1007/978-3-319-42731-7_18

## Introduction

Atmospheric particulate matter can result from a diverse range of natural and anthropogenic sources, resulting in a complex mixture of mineral (e.g. silicates, sulfides, sulfates) and biological (e.g. organics, pollen, microbial contaminants) particulates. Mineral dust originating from mine sites is commonly rich in silicate minerals. Depending on the size and nature of dust particles, they can have significant human health impacts (Plumlee and Ziegler 2003). The most hazardous dust particles are those that are <2.5 μm in diameter. These are referred to as "respirable" particles as they can be inhaled deep into the lungs and get trapped in the alveoli, where gaseous exchange occurs. Particles that are between 2.5 and 10 μm in diameter can penetrate beyond the larynx and be deposited in the upper airwards and lungs. This is conventionally referred to as the "thoracic" fraction of inhalable dust (BSI 1993). However, it is not just the size of dust particle which is important, but other physical properties such as shape, solubility and reactivity. In addition to the potential occupational health effects, dust dispersion can also lead to contamination of the surrounding environment. For example, dispersion of metalliferous dust from a mine site and deposition of such dust on agricultural land can lead to contamination of food products (e.g. Zhuang et al. 2009). Dust monitoring therefore forms an integral part of a mine's environmental monitoring activities.

Dust monitoring at mine sites traditionally involves a combination of dust deposition gauges and high volume air samplers in accordance with national standards. Dust deposition gauges are ideal for the long term monitoring of dust deposition rates. High volume air samplers allow the rate of dust deposition for a particular fraction of the dust to be quantified (e.g. <10 μm fraction). The concentration of deleterious metals (e.g. Pb, Zn, Cd) in dust particles collected on the filter papers can also be measured by chemical digestion and inductively coupled plasma mass spectrometry (ICP-MS).

Considering the capital costs of dust deposition gauges and high volume air samplers and the regulatory requirements to monitor dust dispersion, other low-cost dust sampling techniques are required. This study demonstrates a new method to collect dust particles using passive dust samplers (PDS) that can be easily deployed in the field and rapidly analyzed for their mineralogical composition.

## Methods

### *Passive Dust Samplers*

Passive dust samplers (PDS) were designed and made at the University of Tasmania. The design centred on using a scanning electron microscopy (SEM) mount to directly collect the airborne fraction of particulates. This design prevented methodological issues relating to sample preparation for SEM imaging as

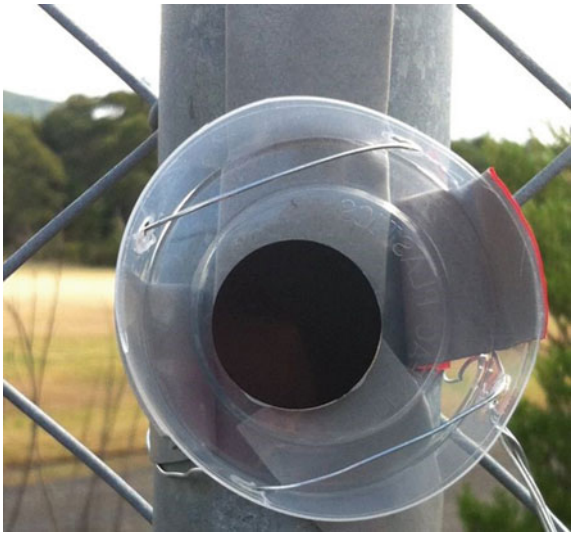

**Fig. 1** Passive dust samplers were attached to posts, trees and fences using either metal wire or double-sided tape (color figure online)

well as potential contamination. Since the particulates adhere to the adhesive surface of the mount, they can be imaged directly without sample transfer to another SEM mount.

The PDS were attached at a height of approximately 1.7 m and at different locations around six selected mine sites (Fig. 1). All samples were left in the field for one month during the summer period. At some locations, PDS were also placed at ground-level. The selected domains of the different mine sites include: (i) a rock crusher of a base metal mine; (ii) a concentrator plant; (iii) two tailings sites; (iv) a waste rock dump; and (v) a background site situated at significant distance from mining activities.

## *Imaging and Analysis*

Backscattered electron (BSE) images were collected from each PDS at the Central Science Laboratory (UTAS) using the Hitachi SU-70 field emission scanning electron microscope (FESEM) fitted with an Oxford Aztec XMax80 silicon drift detector energy dispersive spectroscopy system. Prior to analysis the mounts were carbon coated to 20 nm. Each BSE image was exported as 8-bit image (256 grey values), such that the BSE brightness value for the background stub was 2, and Mn metal was 253. For this setup, polished quartz has a BSE brightness value of 72. For each sample, two images corresponding to two different areas on the stub were collected. Each area had a mosaic image composed of $2 \times 2$ frames mapped at $60 \times$ magnification with a frame resolution of $4096 \times 2816$ pixels. The frames have $\sim 10$ % frame overlap so that the final stitched size depends on the stitching

adjustment, however, each image is approximately 7800 × 5400 pixels. At this magnification and SEM set up, the nominal pixel size was 0.515 × 0.515 μm squared, giving the area for one 2 × 2 map of around 4 × 2.8 mm. After initial test work to finalize the image analysis method, the total time taken to analyze each sample was around 30 min. The BSE images were exported in a TIF format from the Oxford Aztec software and cropped to remove white edges using Corel PhotoPaint.

The software package eCognition Developer v8 was used to analyze the two BSE images taken of each PDS. Particles were recognized using the "contrast split" function in the range of BSE brightness (2–253). The particles recognized were then segmented again, and classified into objects as "very bright" (>190), "bright" (>100), "medium" (>45), and "other". The statistical data on size, shape and average brightness was exported for these objects (typically 2000–10,000 for each image) and the data from the two images were combined.

The effective diameter of each object was calculated according to Berry and Hunt (2013), which provides the best estimate of the average diameter for near spherical objects. BSE brightness is a function of mean atomic weight of elements in a material (Howell et al. 1998). However for very small particles, the apparent brightness is also a function of the grain size. To account for this grain size affect, a provisional function was used based on empirical observations of quartz dust. Particles smaller than 2 μm diameter did not fit the relationship and so are excluded from the study.

While BSE brightness is a strong function of mean atomic weight, it is also sensitive to topographic effects. BSE brightness is sensitive to detector distance, shadowing and preferential BSE emission at edges. Sample preparation for these experiments does not include polishing the sample. Thus, there is an additional error in classifying particles into compositional groups using the BSE brightness alone. Classification of individual particles has a high error. To reduce this effect, we only report the range (histogram) of BSE brightness across the particle population.

## Results and Discussion

### *Dust Sampling*

At all site locations, the PDS recorded atmospheric particulates with a range of different BSE brightness values. The BSE brightness values presented are the effective BSE brightness values, which take into account the effect of variable particle size on the apparent brightness. The proportion of the total area of the sampler covered by particulates varied from 1 % at the background site to 35 % at an active tailings dam (Table 1). The proportion of the area of the PDS covered in particulate matter is likely to be a function of the dust flux at each site, and the

**Table 1** The proportion of the image covered in particles is represented as the total dust coverage at each sampling site

| PDS site | Total dust coverage (%) |
|---|---|
| Background 1 | 1 |
| Crusher plant | 5.9 |
| Concentrator plant | 2.6 |
| Remediated tailings dam | 1.5 |
| Tailings dam | 35.1 |
| Waste rock dump | 2.8 |

efficiency of the PDS. The total particulate coverage provides some indication of low to high dust flux sites although no quantitative relationship was established in this study.

The particle size range observed using the analyses protocol ranged from 0.61 to 102 μm in diameter. Given that reliable BSE brightness values can only be reported for particles with diameters >2 μm using the current method, the 2–5, 5–10 and 10–20 μm (and in one case the 20–50 μm) particle size fractions are reported in conjunction with the BSE brightness values for each PDS. The dominant size fraction varied from site to site.

## *Dust Composition*

The range of adjusted BSE brightness values observed were interpreted using the method recommended in Howell et al. (1998). The particles were grouped by composition according to the range of values for adjusted BSE brightness. Particles with a low brightness <50 were interpreted to represent biogenic particles (e.g. plant matter such as pollen) that are composed of light elements (C, N, O, H) and marine aerosols (e.g. Na, Mg, Cl, S). Particles with adjusted BSE brightness from 60 to 100 were interpreted as silicates. This brightness class should include albite, quartz, tourmaline, muscovite, K-feldspar, as well as carbonate minerals (Table 2). Particles within this composition class could be derived from a wide range of sources, both local and distant ones, as indicated by particle size. Brighter particles with adjusted BSE brightness values from 110 to 190 were interpreted to represent iron silicates and iron oxides (Fig. 2). The brightest particles with BSE brightness values >200 where classed as sulfides (Table 2). In this study, the particle brightness could be interpreted as a proxy for anthropogenic dust sources derived from current or past mine operations that have exposed heavy minerals. This method is most suitable for characterizing the dust composition, size fraction and dispersal of sulfidic mine sites or tailings deposits where silicate and heavy minerals that may contain deleterious trace metals.

The "organics" class (BSE brightness value <50) is perhaps the least well constrained in terms of the exact composition of particles. In addition to biogenic

**Table 2** BSE coefficient calculated according to Howell et al. (1998)

| Phase | BSE coefficient | BSE brightness |
|---|---|---|
| resin | 0.082 | 2 |
| sulfate | 0.104 | 28 |
| $NH_4$-sulfate | 0.125 | 52 |
| Mg-chlorite | 0.139 | 69 |
| dolomite | 0.143 | 74 |
| albite | 0.146 | 78 |
| quartz | 0.147 | 79 |
| tourmaline | 0.149 | 81 |
| muscovite | 0.153 | 86 |
| K-feldspar | 0.159 | 93 |
| calcite | 0.161 | 96 |
| clinozoisite | 0.161 | 96 |
| FeMg-chlorite | 0.171 | 107 |
| epidote | 0.175 | 112 |
| Ca-sulfate | 0.174 | 111 |
| titanite | 0.187 | 127 |
| Fe-chlorite | 0.195 | 136 |
| NaCl | 0.194 | 134 |
| rutile | 0.203 | 146 |
| greenalite | 0.204 | 147 |
| F-apatite | 0.212 | 156 |
| magnetite | 0.243 | 193 |
| hematite | 0.239 | 188 |
| pyrite/marcasite | 0.249 | 200 |
| chalcopyrite | 0.272 | 228 |
| bornite | 0.285 | 243 |
| sphalerite | 0.284 | 242 |
| barite | 0.315 | 279 |
| galena | 0.463 | 455 |
| Mn metal | 0.294 | 254 |

Brightness values are based on a linear map from BSE coefficients, using the high (Mn metal) and low (resin) from the BSE map setup as the calibration

particles, the airborne particulate fraction can comprise of marine aerosols with a BSE brightness around <50 (Heintzenberg et al. 2000). Background aerosol can be made up of a significant amount of organic matter, sulfur (natural and/or anthropogenic) and ammonium sulfate (Andreae 1989). In many PDS analysed by this study, the finest fraction (2–5 μm) was dominated by a peak in frequency of particles with BSE brightness 25–35. This could indicate the presence of sulfate, which has a brightness value of 28, compared to ammonium sulfate, which is

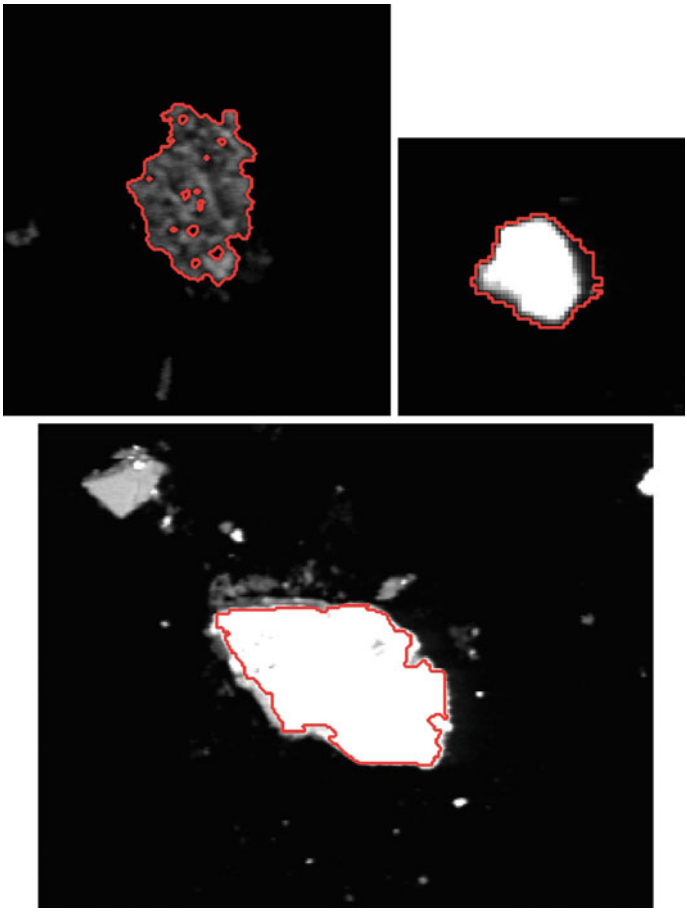

**Fig. 2** *Top left* organic particle from the background 1 PDS with a brightness of 20 and diameter of 50 µm. *Top right* silicate particle from the crusher plant PDS with a brightness of 118 and diameter of 20 µm. *Bottom* Fe silicate/Fe oxide particle from the concentrator plant PDS with a brightness of 200 and diameter of 70 µm (color figure online)

expected to have a value of around 52 (Table 2). The EDS spectra of a leaf imaged using BSE showed the presence of Mg, P, S, K and Ca (Talbot and White 2013), which could also contribute to the brightness range <50. Aerosols typically make up the submicron fraction, however, the contribution of elements (e.g. Na, Mg and S) from both organic- and marine-derived sources, to the >2 µm fraction observed in this study is possible.

## *Characterizing Dust Composition by Size Fraction*

### Crusher Plant

A PDS was attached to a post nearby the crushing circuit of a base metal mine. The total particulate coverage on the PDS was 5.9 %. The proportion of particles with a diameter between 10 and 20 μm was 42 %, compared to 31 % in the 5–10 μm size fraction, while only 13 % were in the 2–5 μm size fraction (Fig. 3). The BSE brightness histogram for each size fraction is based on the analyses of 13,000 particles for the 2–5 μm size fraction, 3000 particles in 5–10 μm size fraction, and 1000 particles in the 10–20 μm size fraction. No fractionation in BSE brightness and particle size was observed for particles >5 μm, however, the finest size fraction is skewed slightly to the left (Fig. 4). The average BSE brightness range for this population of particles was 74 % for 60–100, followed by 15 % in the 110–190 range, 6 % < 50 and 5 % > 200.

The PDS monitoring dust generated at the crusher plant reflects the mineralogical characteristics of the ore. The dust particles contain five times more silicate minerals than Fe silicates and oxides (Fig. 4). There was no fractionation of minerals between different grain sizes, indicating that the crushing circuit is the major dust source at this sampling point, with no input from other sources.

### Concentrator Plant

The PDS was attached to an electricity pole outside the concentrator plant. The total area of the PDS covered in particulates was 2.6 %. Analysis of the particle size distribution showed that 42 % of the particles had a diameter between 10 and

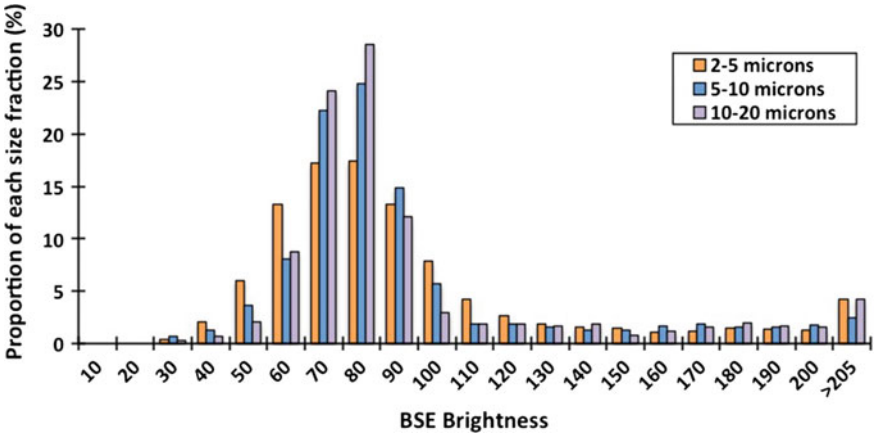


**Fig. 3** The range of BSE brightness values for the PDS overlooking the crusher plant (CP). The distribution of BSE brightness observed was very similar for all size fractions (color figure online)

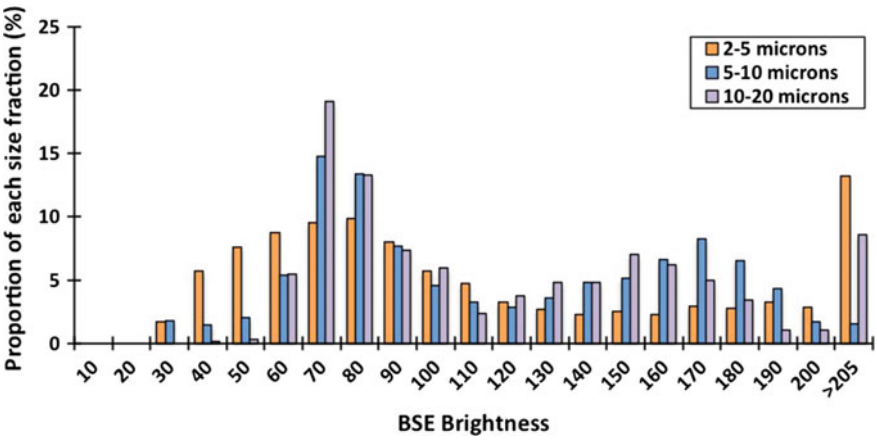


**Fig. 4** The range of BSE brightness values for the concentrator plant PDS. The highest proportion of particles with BSE brightness values >200 was observed in the 2–5 μm size fraction (color figure online)

20 μm and 30 % between 5 and 10 μm (Fig. 4). Only 13 % of the particles had a diameter between 2 and 5 μm. The BSE brightness histogram for each size fraction is based on the analyses of ~4000 particles in the 2–5 μm size fraction, 1400 particles in 5–10 μm, and ~600 particles in the 10–20 μm. A similar BSE brightness distribution was observed for the 5–10 and 10–20 μm size fractions in the 60–190 BSE brightness range. However, the smallest size fraction showed a higher frequency of particles with BSE brightness <50 (Fig. 4). This site had the highest proportion (16 %) of particles with a BSE brightness >200 in the 2–5 μm size fraction compared to the other PDS analysed.

Dust collected by the concentrator plant PDS showed the highest proportion of sulfides recorded across the sample suite (Fig. 5). Upgrading of the ore to concentrate is preserved in the dust signature, with a reduction in silicate minerals and an increase in sulfides. The bimodal distribution in mineralogy (BSE brightness) (Fig. 4) may reflect two different dust sources: (i) very fine concentrate possibly from slimes; and (ii) bulk concentrate (<50 μm). The dust signature at the concentrator plant can be recognized by the ~1:1 ratio of silicates to Fe silicates and oxides.

## Remediated Tailings Dam

At the remediated tailings dam (RT) site, tailings have been flooded and tailings are no longer exposed to atmospheric conditions. The total particulate coverage at this site was 2.4 %. The proportion of particles in the 2–5 μm size fraction was the largest (30 %). As the particle size increases, the proportion of particles with a BSE brightness of <50 decreases from 96 % in the 2–5 μm fraction to 54 % in the 20–50 μm fraction. By contrast, the proportion of particles with BSE brightness values

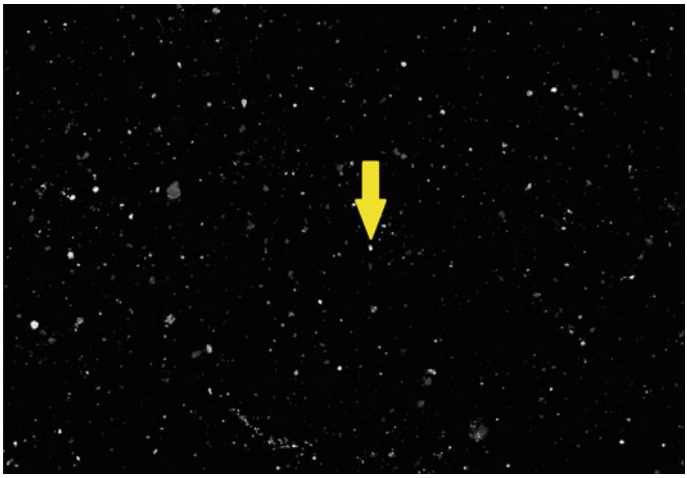

**Fig. 5** BSE mosaic image of PDS sample collected from the concentrator plant. The mosaic image is composed of 2 × 2 frames mapped at 60× magnification used in the image analysis. The *yellow arrow* points to a particle that is 23 μm in diameter (x-axis) (color figure online)

between 60 and 100 increases as particle size increases, from 4 % in the 2–5 μm fraction to 43 % in the 20–50 μm fraction (Fig. 6).

The ground-level sampler placed at the site of the RT PDS had very low total particle coverage (0.2 %). The number of particles analysed for BSE brightness is therefore much lower than at any other site (e.g., ~600 particles in the 2–5 μm size fraction, ~80 in the 5–10 μm fraction and ~20 in the 10–20 μm fraction). The distribution of BSE brightness values in the ground-level sampler differed

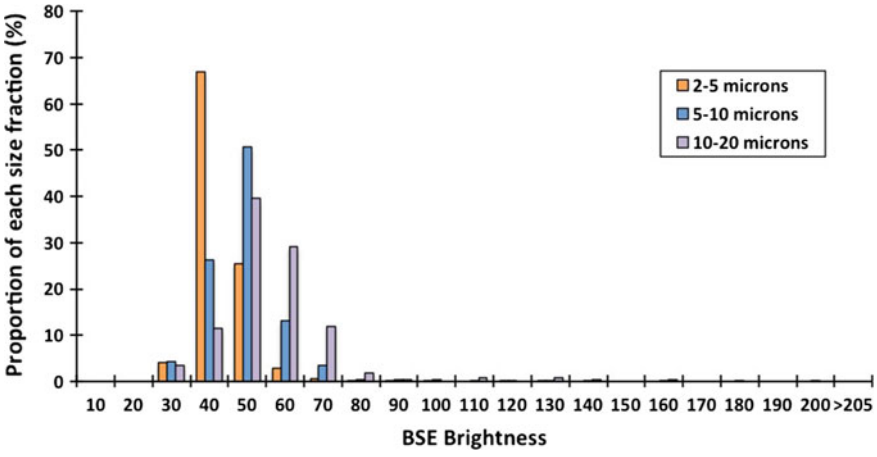


**Fig. 6** The range of BSE brightness values for the remediated tailings dam (RT) PDS (color figure online)

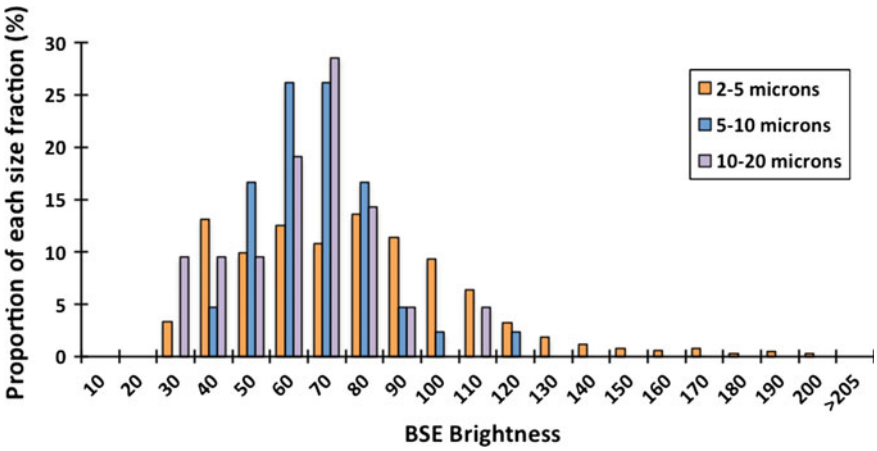


**Fig. 7** BSE brightness for the ground-level sampler at the remediated tailings (RT) dam (color figure online)

significantly from the PDS at 1.7 m. The brightest particles observed were the smallest particles, as 16 % of the 2–5 μm particle population had a BSE brightness of 110–190, compared to only 2 and 5 % in the 5–10 μm and 10–20 μm fractions respectively (Fig. 7). These differences suggest that the PDS does indeed sample the airborne fraction, which is dominated by organics in the finest size fraction rather than mineral particles as observed at ground-level.

The composition of dust at the remediated tailings dam was characterized by high organics ($\geq$70 %) and low silicate ($\leq$30 %) minerals in the <10 μm fraction. The dust fingerprint at the remediated tailings dam site suggests a background source, without influence of mining derived materials. The ground-level sampler showed a higher proportion of silicates and iron silicates. The greater proportion of silicates, Fe silicates and Fe oxides at ground-level reflects the signature of the exposed overburden at this site, which was likely sourced from mine wastes previously disposed at this particular site.

## *Tailings Dam*

A high total particulate coverage was observed at this site (35 %) due to the high proportion of unconsolidated material present at the tailings site. The smallest size fractions (i.e., 2–5 and 5–10 μm fractions) contained μμa high proportion of organic particles with a BSE brightness <50 (94 and 90 %, respectively). The BSE brightness range for larger dust particles between 20 and 50 μm was considered because this size fraction contributes significantly to the overall BSE brightness distribution for this population of particles. It is the only site where a significant proportion (43 %) of particles collected were present in the 20–50 μm size range (Fig. 8). The BSE

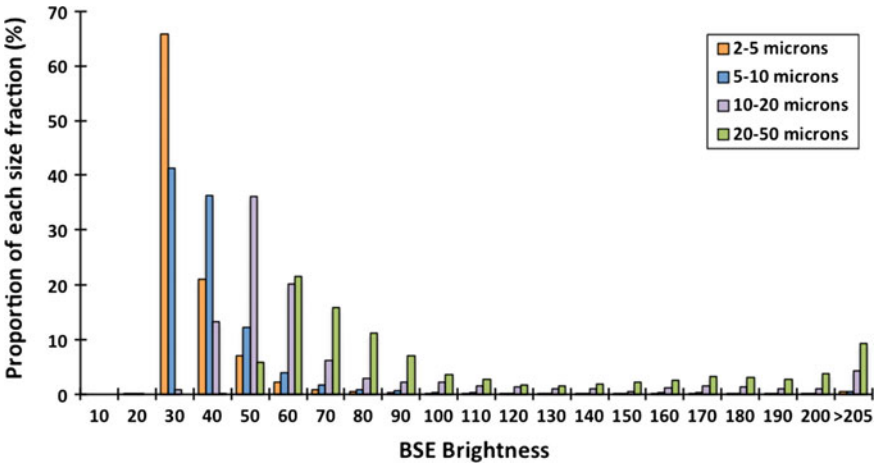


**Fig. 8** BSE brightness values shown according to particle size fraction for the tailings dam PDS (color figure online)

brightness values are bi-modally distributed for this size fraction, showing a peak in frequency for BSE brightness values between 55 and 65 and >200.

Ground-level particulates were sampled at the tailings dam site (Fig. 9). The BSE image of the ground level sampler showed a non-uniform distribution of particles across the surface of the sampler and much larger particulates (Fig. 10). The total area covered in particles was 13 % at the ground level. The BSE brightness range for the ground-level sampler was similar to the PDS above, but the frequency of particles with BSE brightness >50 was higher in the upper PDS.

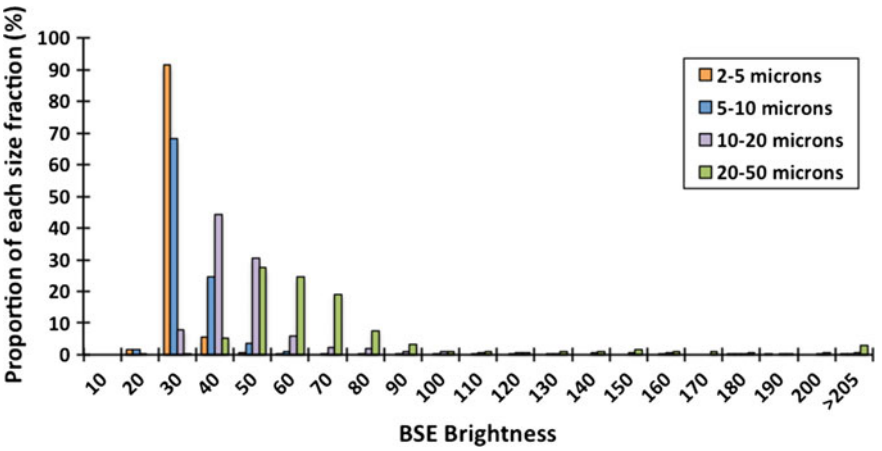


**Fig. 9** BSE Brightness range for the ground-level sampler placed below the tailings dam PDS (color figure online)

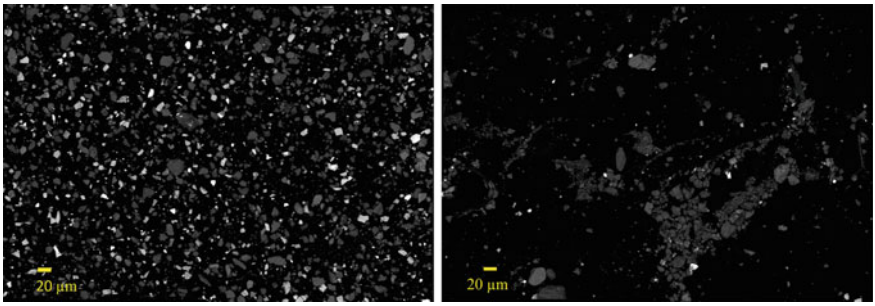


**Fig. 10** *Left* BSE image of the tailings dam PDS which was placed at a height of 1.7 m. *Right* BSE image of dust sample taken using a ground-level sampler placed below the PDS

The tailings dam PDS recorded two different dust sources. The first is composed mostly of organic particles and a low proportion of silicates (<10 %). This composition likely reflects the "natural" dust signature of this region, which is densely covered in vegetation. The second dust source is prevalent in the larger size particles as shown by the composition of the 20–50 µm fraction, which made up a significant proportion of the particle population at this site. This dust source is depleted in organic material and enriched in silicates and heavy minerals. This high silicate-high sulfide source is derived from wind erosion and suspension of tailings dust and is only observed in the larger size fraction (20–50 µm). However, the 10–20 µm fraction is enriched in Fe silicates/Fe oxides and sulfides relative to the finest particles. The ground-level sampler at this site reflects a similar compositional distribution compared to the PDS at 1.7 m. However the number of particles was much larger in the PDS compared to that placed at ground-level, and the distribution of particles across the surface of the PDS was much more uniform in the upper PDS (Fig. 10). The distribution of particles on the ground-level PDS may have resulted from backsplash of particles onto the sampler during rain events and/or transport of particles by saltation.

## Waste Rock Dump

The waste rock dump site is located on a hillside, overlooking an operational waste pile from a base metal mine. The total particulate coverage measured was 2.8 %. The majority of the particles observed had a diameter of 5–60 µm. The BSE brightness histogram is based on the analysis of 2700 particles for 2–5 µm fraction, 2000 particles for the 5–10 µm fraction and 300 particles for the 10–20 µm fraction. Low BSE brightness values for the 2–5 µm and 5–10 µm particle size fraction were observed, with 100 and 99 % of the BSE brightness values <50, respectively

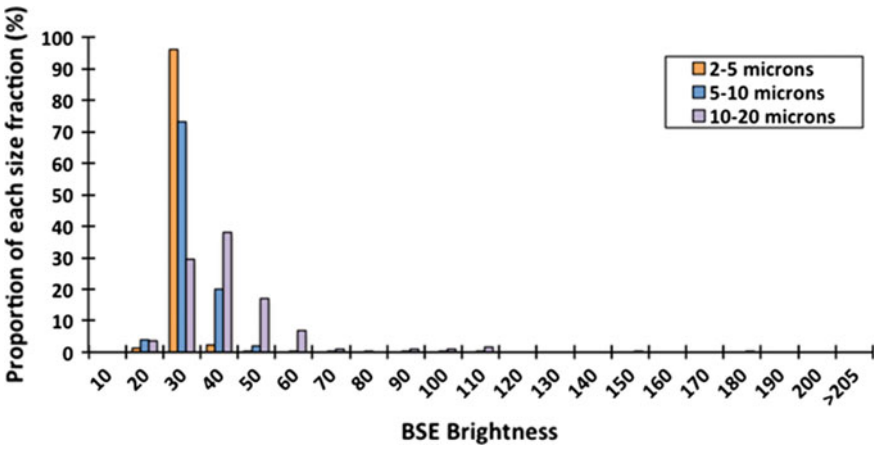


**Fig. 11** The range of BSE brightness values for the PDS located above the current waste rock dump (AW) for the 5–10 and 10–20 μm fraction of particles (color figure online)

(Fig. 11). BSE brightness values for the particles in the 10–20 μm size fraction were also dominated by BSE brightness values <50, but with 10 % of particles in the 60–100 range and 2 % in the 110–190 range (Fig. 11).

The results indicate that the dust source at this site is dominated by organic particles, with only a minor contribution from mineral dust in the larger grain size fraction (10–20 μm).

## Background Site 1

Background 1 site is located sufficiently far away from mining activities to represent the background dust flux. The total particulate coverage at this site was low (1 %). At this site, particles with a diameter <5 μm dominated (>40 %) the population of particles, with 30 % in the 2–5 μm fraction. The proportion of particles with a diameter between 5 and 10 μm and 10–20 μm was about 20 % in each fraction (Fig. 12). The 10–20 μm fraction was distinguished by a higher frequency of particles with a brightness range between 110 and 190 (11 %).

The presence of dust composed of Fe silicate and oxide minerals in the 10–20 μm fraction at the Background 1 site was most likely mobilized by nearby road traffic. Historical haulage of ore by road in mining districts is a potential source of the Fe silicate and oxide dust fraction observed at this site.

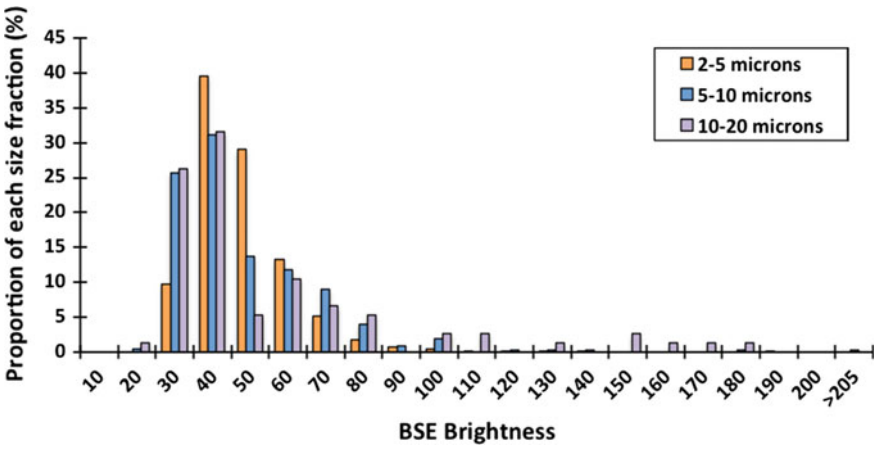


**Fig. 12** BSE brightness range for the PDS sample collected from the background 1 site. The 2–5 and 5–10 μm fractions show similar distributions of brightness values, while the 10–20 μm fraction is distinguished by brightness values >100 and <190 (color figure online)

## Conclusions

Dust was collected using a novel passive dust sampler across six different mine site domains. BSE images of the PDS were imaged using FESEM and analysed using eCognition Developer v8 software. Particles were recognized according to their brightness (2–253) and split into categories representing mineralogical groups. The size and brightness of dust particles were presented for each site. The mineralogical composition of dust at each site was characterized by the range of BSE brightness values: organic particles (BSE brightness <50), silicate particles (60–100), Fe silicate and Fe oxide particles (110–190), and sulfide particles (>200).

Differences in dust compositions were identified at the investigated sites. The crusher plant showed dust generated with a uniform composition across the 2–20 μm size fractions, with materials composed of >70 % silicates, <20 % Fe silicates/Fe oxides and <10 % sulfides. Mineral dust collected at the concentrator plant had a lower proportion of silicate particles (>40 %) but a higher proportion of Fe silicates/oxides (>30 %) and sulfides (>10 %) in the 2–5 and 10–20 μm size range. Mineral dust generated at an active tailings dam was dominated by larger particles (20–50 μm), composed mostly of silicate minerals.

The documented method can provide information on particle size distribution and composition and has the potential to classify particle shape, in particular for phases with fibrous habits. The PDS method can be used in dust monitoring programs to provide important information relating to the hazardous nature of dust generated during but not limited to mining activities.

## References

Andreae MO (1989) Marine aerosol chemistry at Cape Grim, Tasmania, and Townsville, Queensland. J Geophys Res 87:8875–8885

Berry RF, Hunt J (2013) Grain size in geometallurgy: revised version. AMIRA P843A Technical Report 11, pp 83–111

British Standards Institute (1993) Workplace atmospheres—size fraction definitions for measurement of airborne particles. BS EN 481:1993. Section 3.5. European Committee for Standardisation

Heintzenberg J, Covert DC, van Dingenen R (2000) Size distribution and chemical composition of marine aerosols: a compilation and review. Tellus 52B:1104–1122

Howell PGT, Davy KMW, Boyde A (1998) Mean atomic number and backscattered electron coefficient calculations for some materials with low mean atomic number. Scanning 20:35–40

Plumlee GS, Ziegler TL (2003) The medical geochemistry of dusts, soils and other Earth materials. In: Sherwood Lollar B (ed) Treaties on geochemistry, vol 9, pp 263–310

Talbot MJ, White RG (2013) Cell surface and cell outline imaging in plant tissue using the backscattered electron detector in variable pressure scanning electron microscope. Plant Methods 9:40

Zhuang P, ZouB Li NY, Li ZA (2009) Heavy metal contamination in soils and food crops around Dabaoshan mine in Guangdong, China: implication for human health. Environ Geochem Health 31:707–715

# Prediction of Mineral Dust Properties at Mine Sites

**Taryn L. Noble, Ron F. Berry, Karsten Goemann and Bernd Lottermoser**

**Abstract** Predicting the properties of dust generated at mine sites is important for understanding the impact of dust dispersal to the surrounding environment. This chapter presents a new approach to predicting the mineralogical properties of the PM2.5 and PM10 dust fractions. A purpose-built dust resuspension machine was fitted with a size selective sampler to collect dust fractions. Dust particles were collected onto a polycarbonate filter, which was analyzed using a scanning electron microscope (SEM). Backscattered electron (BSE) maps of the polycarbonate surface were imaged and processed to determine dust properties. For a given population of particles, the BSE brightness distribution of the 2–5 and 5–10 μm size fractions were quantified. The mineralogical composition of the dust size fractions were inferred by the BSE brightness as biogenic particles and sulfates (30–50), silicates (60–100), iron silicates and oxides (110–190), and sulfides (>200). The method was validated by comparing laboratory-generated dust fractions with those collected from dust monitoring stations at a tailings repository site. Similar dust composition and size fractions were observed for both laboratory and field samples. Consequently, the purpose-built dust resuspension device and associated laboratory procedures allow the prediction of mineralogical properties of dust at mine sites.

T.L. Noble · R.F. Berry (✉)
School of Physical Sciences, University of Tasmania, Private Bag 79, Hobart, TAS 7001, Australia
e-mail: Ron.Berry@utas.edu.au

T.L. Noble
e-mail: Taryn.Noble@utas.edu.au

K. Goemann
Central Science Laboratory, University of Tasmania, Bag 74, Hobart, TAS 7001, Australia
e-mail: Karsten.Goemann@utas.edu.au

B. Lottermoser
Institute of Mineral Resources Engineering, RWTH Aachen University, Wüllnerstrasse 2, 52062 Aachen, Germany
e-mail: lottermoser@mre.rwth-aachen.de



B. Lottermoser (ed.), *Environmental Indicators in Metal Mining*,
DOI 10.1007/978-3-319-42731-7_19

## Introduction

Mineral dusts are derived from multiple sources at mine sites, leading to heterogeneous compositions in terms of particle size distribution, morphology, mineralogy and geochemistry. It is the physical and mineralogical composition of dust, which determines its risk to human health and the surrounding environment (Gelencser et al. 2011). Therefore, predicting these physical and mineralogical characteristics is important for effective dust management and control strategies. At present, there are no appropriate testing procedures available to predict the morphological and mineralogical properties of mineral dust from mining operations. Models exist to predict the dispersal of dust plumes under certain climatic and meteorological conditions, as part of a mine site dust mitigation strategies. Computer modelling of dust dispersion from mine sources can allow health and safety hazards to be identified and result in improved dust control techniques (Reed 2005). However, properties such as morphology and mineralogical composition are generally not considered in current modelling methods for dust prediction.

The dispersion of dust containing deleterious elements (e.g. As and Hg) is often associated with abandoned mine sites or tailings facilities (e.g. Corriveau et al. 2011; Kribek et al. 2014). The high concentration of trace metals prevents stabilization of the unconsolidated waste surface resulting in wind and water erosion. The aim of this study was to develop a new method that combines a dust re-suspension chamber adapted from Moreno et al. (2005), with a size selective aerosol sampler (SKC IMPACT®) and analysis by scanning electron microscopy (SEM). The purpose of the method is to provide compositional information on the inhalable dust fraction (<10 μm) fraction of ore and waste materials. In turn, such information allows forecasting of environmental risks to air quality at mine sites.

## Methodology

### *Experimental Design*

A dust resuspension machine was designed and built at RIMS Engineering, Australia. The design was adapted from information described in Moreno et al. (2005), to study Hg-bearing airborne particles around abandoned mines in Spain. To sample a potential dust fraction, crushed or powdered material is placed inside a rotating metal cylinder under unidirectional airflow driven by a vacuum pump (Fig. 1). A HEPA filter is attached to the air-intake end of the cylinder to remove contamination from any ambient dust that may be in the laboratory. The rotation speed of the cylinder can be set from a minimum of 3 revolutions per minute (rpm) to 36 rpm. The inside of the cylinder has two 2 cm high fins that help to disturb the sample which slides and cascades during each rotation. The fine airborne

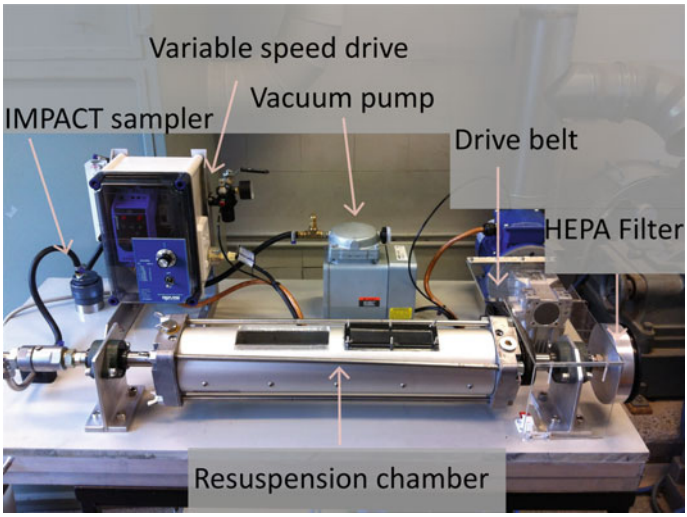


**Fig. 1** Purpose-built dust resuspension machine (color figure online)

fraction of the material is resuspended into the airspace of the drum and sucked into the dust-sampling unit.

An IMPACT Sampler was used as the dust-sampling unit. It is designed and patented by SKC Inc. and has been engineered to function within the design of the dust machine. The IMPACT Sampler, is based on an inertial impactor, which removes particles larger than 10 μm by capturing them on a disposable 37 mm oiled impaction disc (Figs. 2 and 3). Particles smaller than 10 μm are collected on a 37 mm filter. A polycarbonate filter (SKC Inc.) was chosen for this work since the lighter elements making up the filter are distinct from the dust particles of interest, when imaged using SEM. The IMPACT Sampler is designed to operate with a flow rate of 10 L/min. Flow rates above this specification were trialled and showed that particles larger than 10 μm were collected on the polycarbonate filter. The major components of the dust machine in contact with the sample material have been designed to be easily cleaned to prevent cross contamination between samples.

Operational variables of the dust machine were tested to optimize the sampling of resuspended dust. These parameters included: (i) sample mass (g); (ii) duration of the experiment (minutes); (iii) rotational speed of the chamber (rpm); and (iv) flow rate (L/min). The operationally defined limit for using the IMPACT sampler to collect the <10 μm particulate fraction was 10 L/min (Table 1). The optimum method required at least 5000 particles for statistically significant analyses. In this study, the method was optimised for tailings material.

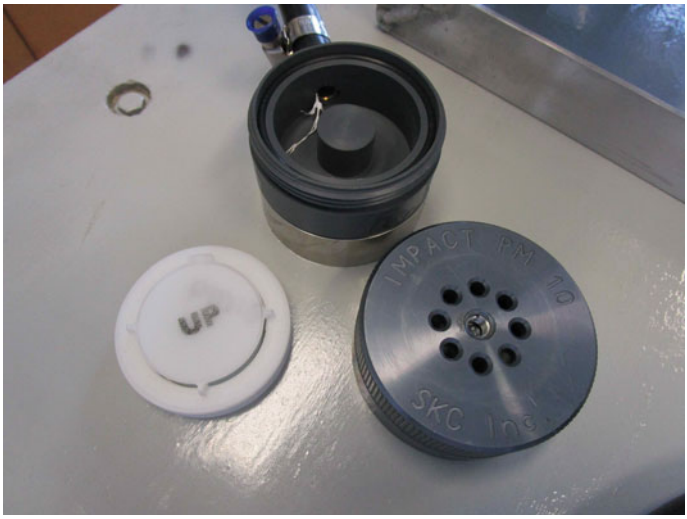


**Fig. 2** The IMPACT sampler engineered to function between the sampling cylinder and vacuum pump of the dust machine (*centre*)

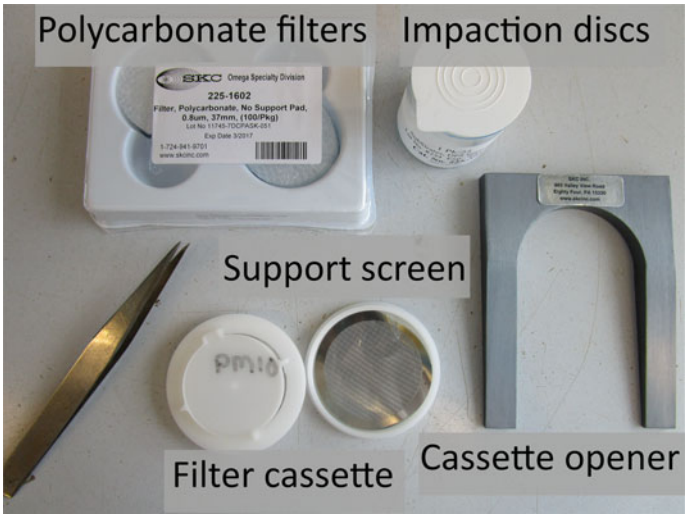


**Fig. 3** Collection filter for the IMPACT sampler with stainless steel mesh and tweezers to handle the polycarbonate filters and impaction discs. The filter cassette opener is used to exchange the filters and impaction disc

**Table 1** Operational limits defined for the dust machine and IMPACT sampler

| Operation | Control mechanism | Limit |
|---|---|---|
| Flow rate | Vacuum flow control | 10 L/min for IMPACT sampler |
| Chamber rotation | Speed controller | 36 rotations per minute |

## Samples for Method Development

Samples for method development were collected from the Mathinna tailings dump, Fingal region, NE Tasmania. The Mathinna tailings occur at the historical Golden Gate Au mine in a NW-SE trending valley 41°29′4.97″S and 147°53′38.70″E (Fig. 4). The site is approximately 100 × 650 m in area and is estimated to hold 321,000 t of sands and slimes and 112,000 t of residues from treatment plants, with the materials containing high (∼1 wt%) As concentrations (King 1964). The site has not been rehabilitated. Patches of vegetation growing at the edges and in depressions, where the moisture and organic contents are likely to be higher, were observed (Fig. 4).

Four different tailings samples were collected along the length of the Mathinna tailings dump: MT1, MT2, MT3 and MT4. Each of these samples was processed using the dust resuspension machine, applying the following experimental protocol:

- 5 g of tailings sample
- flow rate of 7.5 L/min
- 23 rotations of the cylinder per minute
- 3 min sampling duration

The polycarbonate filter was attached to 25 mm diameter aluminium pin mount (ProSciTech) with an adhesive carbon tab (Fig. 5). The mount is designed for used SEM analysis and fits easily into a standard sample holder.

**Fig. 4** The Mathinna tailings site, looking southeast (*left*) and northwest (*right*) (color figure online)

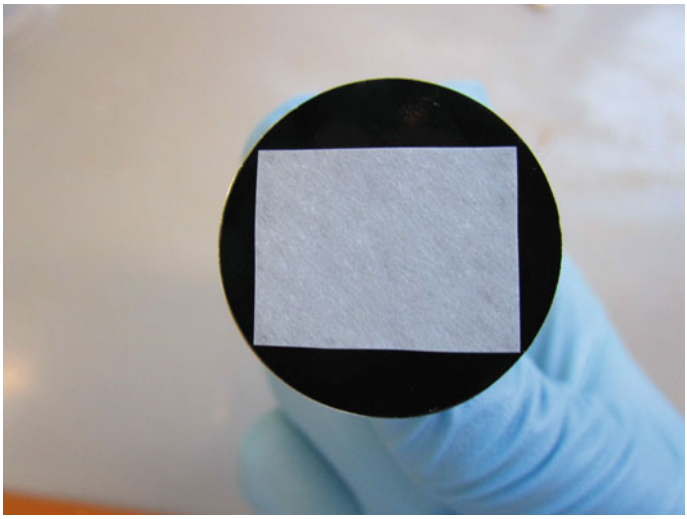

**Fig. 5** The polycarbonate filter was cut to size and placed onto a 25 mm aluminum SEM mount

## *Imaging of the Dust Particles*

Scanning electron microscopy was used to analyse the dust collected on polycarbonate filters from the dust machine. Back-scattered electron (BSE) imaging produce a grey scale image. The brightness of the objects detected using BSE varies as a function of the mean atomic number of compounds. Very bright objects correspond to high contents of elements with a high atomic number and vice versa. The general mineralogical character of the object can therefore be inferred. A variety of different methods have been used to calculate the mean BSE coefficient of a compound and the corresponding BSE brightness (Howell et al. 1998). However, polished surfaces rather than individual particles sitting on top of filter are generally used. This study presents corrected BSE brightness values (referred to as effective BSE brightness), which have been empirically corrected for the effects of particle size. Therefore, only particles >2 μm are included in this study.

Backscattered electron (BSE) images were collected at the Central Science Laboratory (UTAS) using the Hitachi SU-70 field emission scanning electron microscope (FESEM) fitted with an Oxford Aztec XMax80 silicon drift detector energy dispersive spectroscopy system. Prior to analysis the mounts were carbon coated to 20 nm. The sample holder allowed each batch to consist of four samples and one standard mount containing Mn metal. Samples were imaged using a voltage of 15 kV and a standard working distance of 14.8 mm. Mn metal and the background resin of the standard mount were used to calibrate the brightness and contrast. This calibration was checked periodically throughout the period of analysis. The background resin had a BSE brightness value of 2 and Mn metal 253.

The software program eCognition Developer v8 was used to analyze the BSE images of resuspended dust. Particles were recognized using the "contrast split" function in the range of BSE brightness. The background of the polycarbonate filters was much brighter than the carbon tab, therefore the lower range of BSE brightness values was set to 30 to exclude the fibers making up the filter. The objects were classified into "very bright" (>190), "bright" (>100), "medium" (>45) and "other" objects. The statistical data on size, shape and average brightness was exported for these super-objects (typically 2000–10,000 on each image).

The particles were grouped by composition according to the range of values for adjusted BSE brightness. Particles with a low brightness 30–50 were interpreted to represent biogenic particles (e.g. plant matter such as pollen) that are composed of light elements (C, N, O, H) and marine aerosols (e.g. Na, Mg, Cl, S). Particles with adjusted BSE brightness from 60 to 100 were interpreted as silicates. This brightness class should include albite, quartz, tourmaline, muscovite, K-feldspar as well as carbonate minerals (Howell et al. 1998). BSE brightness values between 110 and 190 were interpreted to represent iron silicates and iron oxides and the brightest particles with BSE brightness values >200 where classified as sulfides.

## Validation Study

To validate the method, dust fractions generated from Mathinna tailings material using the dust machine method were compared to actual mineral dust collected in the field. Such dust samples were collected at the Mathinna tailings dump using Passive Dust Samplers (PDS). The PDS are designed to collect airborne particles that stick onto adhesive carbon tab. A 25 mm aluminium SEM mount with an adhesive carbon tab (ProSciTech) was placed in the field at a height of $\sim$1.7 m (Fig. 6). The dust collected on the adhesive carbon tape can be easily analyzed by SEM techniques. Two PDS were deployed at the north and south end of the tailings dump facing inwards towards the centre of the tailings dump (PDS-1 and PDS-2). Dust from this site is known to be a problem during dry, high wind conditions, with large dust plumes observed from the Fingal fire station (26 km to the south).

The effective BSE brightness distribution is presented for the 2–5 and 5–10 μm size fractions collected in the field and using the dust machine. The results are reported for the population of particles in each image. Dust particles >10 μm are negligible in the dust machine filters since the IMPACT sampler selects only PM10 size range. By contrast, the PDS sampled a wider range of particle sizes.

The dust sampler PDS 1 was located on the northern boundary facing inwards toward the tailings dump. The dust collected at this site showed a BSE rightness range between 50 and 130 (Fig. 7). The 2–5 μm size fraction had the highest number of particles with a BSE brightness of 80. The 5–10 μm size fraction has the highest number of particles with a BSE brightness of 70. The second dust sampler, PDS 2 was placed at the southern boundary of the tailings dump, facing inwards to

**Fig. 6** Site PDS-1 with dust sampling devices deployed in the field for one month, Mathinna tailings dump. Dust sampling devices are ~1.7 m above ground (color figure online)

the north. PDS 2 showed the same BSE brightness range as for PDS 1 (50 and 130) (Fig. 7). Lower maximum BSE brightness values of 70 for the 2–5 μm size fraction and 60 the 5–10 μm size fraction were observed.

For tailings sample MT1, analysis of resuspended dust on the polycarbonate filter from the dust machine showed a larger range of BSE brightness values from 50 to 190 compared to the field dust sample. The peak value in the BSE brightness distribution was 90 for the 2–5 μm fraction and 70 for the 5–10 μm fraction (Fig. 8). Tailings sample MT2 showed a BSE brightness range from 60 to 200. The maximum frequency in the BSE brightness distribution for all four images was 100 for the 2–5 μm fraction and 80 for the 5–10 μm fraction. The effective BSE brightness distribution for MT3 did not show a normal distribution (Fig. 8). The 2–5 μm size fraction showed two peaks in BSE brightness, at values of 100 and 200. In contrast, the peak in BSE brightness for the 5–10 μm size fraction was between 80 and 90. MT4 had a different constituency compared to tailings samples MT1–MT3. For sample MT4, two distinct dust types were observed. The 2–5 μm size fraction showed a BSE brightness peak at 90 and 80 for the 5–10 μm size fraction (Fig. 9).

Dust collected from the tailings samples using the dust machine showed a broader range in BSE brightness distribution, compared to field dust samples. Overall, the BSE brightness distribution in samples generated by the small-scale

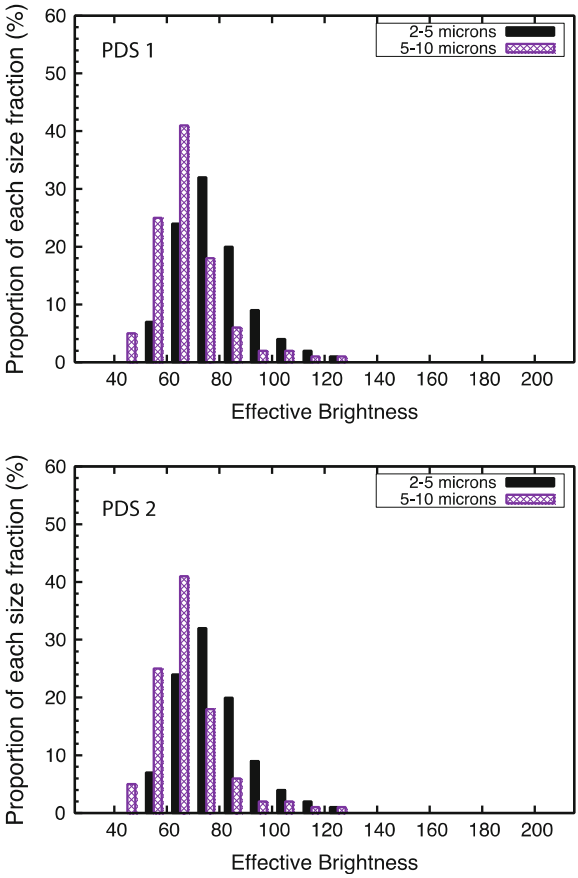


**Fig. 7** Particle properties collected from the PDS-1 and PDS-2 site, Mathinna tailings dump, Tasmania (color figure online)

dust test exceeds the proportion of bright objects between 130 and 200, compared to the field dust samples. This may be related to the aerodynamics of different mineral types. The heaviest minerals (and brightest) are unlikely to be airborne across a significant distance or height, relative to lighter minerals (e.g. quartz). The dust machine collects fractions of tailings material, with such fractions having similar compositions to ground level dust. In all cases, the coarser 5–10 μm dust fraction collected in the field is composed of a greater proportion of particles with a lower BSE brightness, while the 2–5 μm fraction contains dust with a higher BSE brightness.

Regardless, samples obtained with the resuspension dust chamber and samples collected in the field have similar particle size and BSE brightness properties. The resuspension method allows production of mineral dust samples similar to those actually present in the field. Consequently, the purpose-built device provides material for a rapid determination of mineralogical dust properties according to grain size.

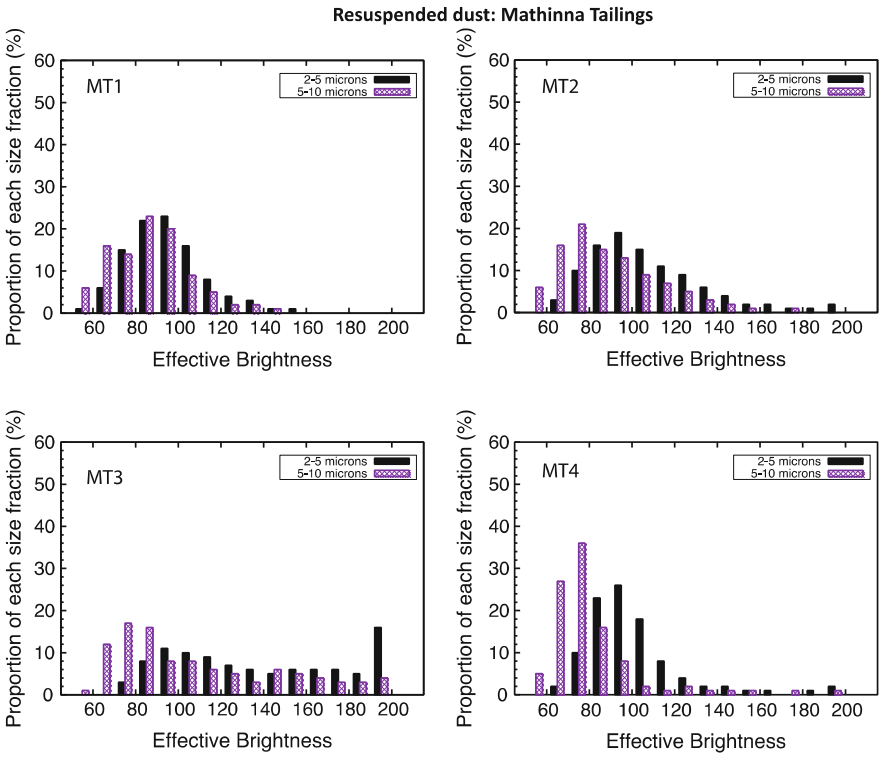


**Fig. 8** Particle properties of samples MT1–MT4, Mathinna tailings dump, Tasmania (color figure online)

The empirical relationship determined to correct for biases in BSE brightness according to size assigns values of 60 to quartz and 160 to pyrite. The dust fraction sampled by the dust resuspension device generated particles with a BSE brightness above 160 to a maximum BSE brightness value of 190. The particles observed to have a BSE brightness greater than 160 are likely to be a combination of mixed sulfides (i.e. atomically heavier than $FeS_2$) and oxide phases. This assumption was tested by the analysis of individual particle composition using Energy Dispersive Spectroscopy (EDS) on the SEM. We observed minerals such a Fe-As and Zn oxides (Fig. 9). Quartz and clay minerals such as muscovite are the dominant silicates observed, in addition to a range of metal sulfates containing hosting trace elements such as Pb, As, Zn and Fe.

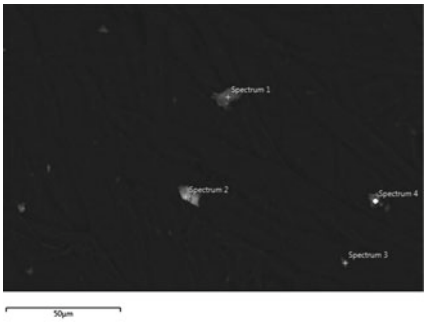


| | |
|---|---|
| Spectrum 1 | Muscovite |
| Spectrum 2, 4 | As-Fe oxide |
| Spectrum 3 | Quartz |
| Spectrum 4 | As-Fe oxide |

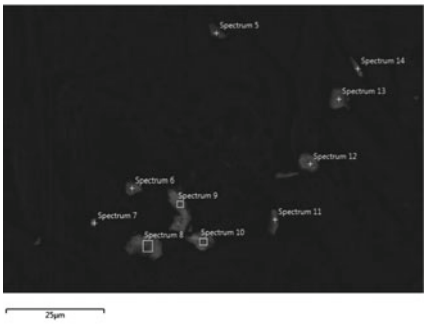


| | |
|---|---|
| Spectrum 5 | Fe oxide |
| Spectrum 6, 11, 13 | Quartz |
| Spectrum 7 | Zn oxide |
| Spectrum 8, 9, 11 | Muscovite |

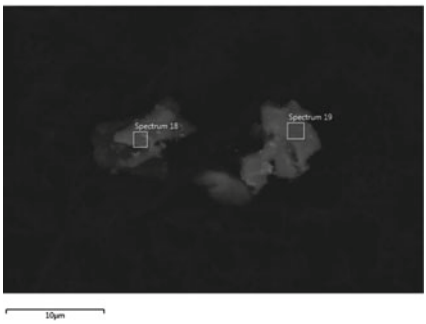


| | |
|---|---|
| Spectrum 18,19 | Muscovite |

**Fig. 9** BSE images of particles collected using the dust resuspension device from the Mathinna tailings sample MT2

## Conclusions

This report details a new method to generate mineral dust samples in the laboratory and to predict the mineralogical composition of airborne mineral dust. A purpose-built dust resuspension device was fitted with an IMPACT sampler to allow selective trapping of particular dust size fractions.

The documented method provides a good estimation of the mineralogical composition of a population of dust particles as inferred from the BSE brightness values and the BSE brightness distribution of the 2–5 and 5–10 µm fractions. The

relationship between BSE brightness and particle size was quantified for quartz and pyrite, since BSE brightness is also sensitive to topographic effects, detector distance, shadowing, and preferential BSE emission at edges.

The method was validated on mineral dust samples collected using PDS at the Mathinna tailings repository, Tasmania. The results demonstrate that the purpose-built device and associated sampling and analytical protocols overestimate the proportion of heavy minerals that are less likely to be dispersed widely. However, the laboratory method provides a preliminary indication of the likely silicate fraction of mineral dust observed in real dust samples.

## References

Corriveau MC, Jamieson HE, Parsons MB, Campbell JL, Lanzirotti A (2011) Direct characterization of airborne particles associated with arsenic-rich mine tailings: particle size, mineralogy and texture. Appl Geochem 26:1639–1648

Gelencser A, Kovats N, Turocz B, Rostasi A, Hoffer A, Imre K, Nyiro-Kosa I, Csaberenyi-Malasics D, Toth A, Czitrovsky A, Nagy A, Nagy S, Acs A, Kovacs A, Ferincz A, Hartyani Z, Posfai M (2011) The red mud accident in Ajka (Hungary): characterization and potential health effects of fugitive dust. Environ Sci Technol 45:1608–1615

Howell PGT, Davy KMW, Boyde A (1998) Mean atomic number and backscattered electron coefficient calculations for some materials with low mean atomic number. Scanning 20:35–40

King RWL (1964) Survey of mineral resources tasmanian tailing dumps. Bureau of Mineral Resources Geology and Geophysics

Kribek B, Majer V, Pasava J, Kamona F, Mapani B, Keder J, Ettler V (2014) Contamination of soils with dust fallout from the tailings dam at the Rosh Pinah area, Namibia: Regional assessment, dust dispersion modeling and environmental consequences. J Geochem Explor 144:391–408

Moreno T, Higueras P, Jones T, McDonald I, Gibbons W (2005) Size fractionation in mercury-bearing airborne particles ($HgPM_{10}$) at Almaden, Spain: implications for inhalation hazards around old mines. Atmos Environ 39:6409–64419

Reed WR (2005) Significant dust dispersion models. Information circular 9478, NIOSH, 29 pp

# Part V
# Land Quality

# Bioaccessibility Testing for Metals at Mine Sites

**Eleanor M. van Veen and Bernd Lottermoser**

**Abstract** Knowledge of bioaccessible metals in soils is relevant to the rehabilitation of mine sites and remediation of mined land. Soils of metal mine sites are commonly enriched in metals and metalloids due to mine waste dumping, atmospheric fallout from smelter emissions as well as dust deposition and erosion of particles originating from ore stockpiles, tailings storage facilities, waste rock dumps and exposed mine workings. Upon mine closure, the establishment of an effective and sustainable vegetation community represents an integral part of mine site rehabilitation. Only a vegetated and uncontaminated landscape will lead to site stability, effectiveness of dry covers, minimization of deleterious offsite effects and return of the mined land to a condition that allows a particular post-mining land use. Moreover, plants may represent pathways of metals and metalloids from contaminated substrates into local foodchains. Consequently, a solid understanding of the current and future bioaccessibility of metals and metalloids is of key relevance for assessing mined land for rehabilitation purposes. This paper presents a review of the literature concerning tests that are used to assess and predict the bioaccessibility of metals in contaminated and mining environments.

## Introduction

Plants acquire the bulk of their metal content from the substrate on which they grow, but the plants only take up a portion of that metal content. This portion is referred to as the bioavailable fraction. The portion that is present in soil solution

E.M. van Veen (✉)
Environment and Sustainability Institute/Camborne School of Mines, University of Exeter, Penryn Campus, Penryn, Cornwall TR10 9FE, UK
e-mail: E.M.Van-Veen@exeter.ac.uk

B. Lottermoser
Institute of Mineral Resources Engineering, RWTH Aachen University, Wüllnerstrasse 2, 52062 Aachen, Germany
e-mail: lottermoser@mre.rwth-aachen.de



B. Lottermoser (ed.), *Environmental Indicators in Metal Mining*,
DOI 10.1007/978-3-319-42731-7_20

and freely available and/or temporarily physically or chemically constrained is referred to as the bioaccessible fraction. Some plants have evolved strategies to take up or exclude metals from their biomass, which allows them to survive in environments with high metal and metalloid concentrations. Uptake also depends on the local environmental geochemical and physical conditions which influence the forms in which the elements exist. The first section in this chapter discusses the different strategies that plants have evolved to survive in environments with elevated concentrations of potentially toxic trace elements such as mine sites, and highlights the applications for which such plants are therefore suited. The second section reviews methods that have been used to determine the operationally defined bioaccessible fraction, i.e. that fraction of metals that is accessible for uptake by the roots of plants in the environment.

## Bioaccessibility of Metals to Plants

Plants that colonize high metal environments have evolved mechanisms to tolerate metal toxicity which generally involve internal detoxification rather than the suppression of metal uptake (Baker 1981). Plants can be described as accumulators, indicators or excluders depending on the way in which the aerial portions of these plants respond to increasing soil metal levels (Fig. 1). Accumulators tend to concentrate metals in the aerial parts of the plant from either high or low soil levels; the root uptake and transport of metals to the shoots are more or less in balance in this type of plant. Indicators regulate the uptake and transport of metals, and the concentration in the above-ground plant parts reflects external levels. Excluders maintain a constant, low metal concentration in the shoot over a wide range of soil concentrations by restricting transport from root to shoot. However, above a certain concentration the exclusion mechanism can break down with resultant unrestricted transport. Plants employing all three types of response can be found at mine sites.

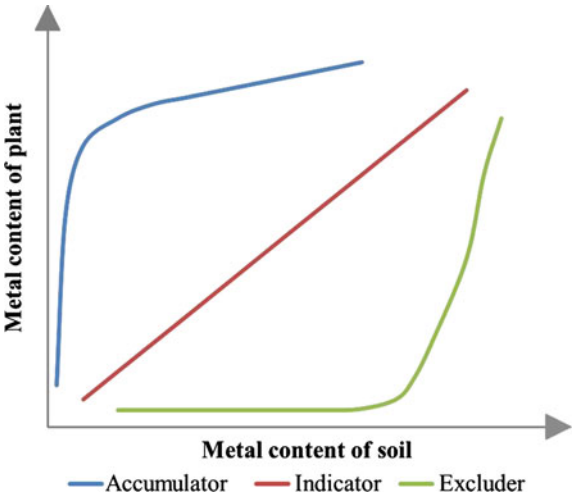


**Fig. 1** Three different plant responses to increasing soil metal content (after Baker 1981) (color figure online)

## *Hyperaccumulators*

Some plants that grow on metalliferous soils have developed the ability to accumulate high levels of metals and metalloids in their tissues without symptoms of toxicity. Plants which are able to take up high concentrations of heavy metals are known as accumulators and those who are capable of acquiring extreme metal concentrations as hyperaccumulators. A hyperaccumulator plant must be able to accumulate Cd to >100 mg $kg^{-1}$, and/or As, Cu, Ni and Pb to >1000 mg $kg^{-1}$, and/or Zn to >10,000 mg $kg^{-1}$ as dry shoot matter (Garcia-Salgado et al. 2012). In a few plant taxa, the concentration of metals and metalloids accumulated in above ground biomass is more than one and up to four orders of magnitude higher than in other adjacent plants. This accumulation of potentially toxic trace elements like Ni, Zn, Cd, Se, As, Mn, Co, Cu, Pb, Sb and Tl can approach or even exceed the concentrations of the macronutrient cations K and Ca. A review of metal hyperaccumulation in plants by Krämer (2010) states that hyperaccumulation of trace metals has been reported in approximately 500 plant taxa (ca. 0.2 % of all angiosperms). The author indicates that the selective advantage of metal hyperaccumulation, in excess of physiological needs, remains elusive but most likely it acts as an elemental defence against herbivore and/or pathogen attack. Metal hyperaccumulation is inevitably associated with metal hypertolerance, and metal hypertolerance is an example of an extreme abiotic stress resistance trait (Krämer 2010).

Heavy metal uptake and accumulation studies in ten native Spanish plant species spontaneously growing in soils polluted by mining activities found high element concentrations in the above ground parts of *Corrigola telephiifolia* (As and Pb), *Jasione Montana* (Cd and Zn) and *Digitalis thapsi* (As, Cd, Cu, Pb and Zn) (Garcia-Salgado et al. 2012). *Noccaea caerulescens* (formerly *Thlaspi caerulencens*) is known to hyperaccumulate Zn (Shen et al. 1997) and has been recommended for in situ decontamination of soils (Kabata-Pendias 2011).

Some native plants from locations associated with serpentinite or other Ni-rich soils accumulate Ni leaf concentrations of over 6000 mg $kg^{-1}$. High Ni concentrations recorded include 5500 mg $kg^{-1}$ in the shoots of *Berkheya coddi*, an endemic plant that grows on Ni-enriched ultramafic soils in South Africa (Robinson et al. 1997). Other plant species known for their great tolerance and hyperaccumulation of Ni include the *Brassicaceae, Boraginaceae, Cruciferae, Cunoniaceae, Flacortiaceae, Myrtaceae, Leguminosae, Caryophyllaceae and Violaceae* families (Kabata-Pendias 2011; Sheoran et al. 2009).

*Pterris vittata* is the first identified As hyperaccumulator which has received much attention since its discovery in 2001 (Ma et al. 2001). Since then, many As hyperaccumulators have been found, these naturally evolved As accumulators all belong to the fern family and the majority of them are members of the *Pteris* genus. Xie et al. (2009) provide a full list of these plants. Arsenic is transported from the root systems of *P. vittata* through the xylem to the above-ground part of the plants, with the highest levels of As in the fronds. Arsenic accumulated in the fronds can be up to 93 % of the total As content in the plants and 25 times more than that in the

roots. Old fronds can accumulate 13,800 mg As $kg^{-1}$ dry biomass, which is approximately 142 times higher than the As in the soil in which the plants were grown.

Gonzaga et al. (2012) assert that As hyperaccumulators can access As in soils which is not bioavailable to typical crop plants. They consider that this is probably due to root exudates and highlight that increases in dissolved organic content (DOC) have been reported in pot studies in the rhizosphere of As hyperaccumulators (Gonzaga et al. 2006). Furthermore, more phytic acid and oxalic acid is produced by the hyperaccumulator *P. vittata* than by the non As hyperaccumulator *N. exaltata* and this difference increases under As stress (Tu et al. 2004). Organic acids based on root exudates may therefore be effective in measuring plant As availability. Gonzaga et al. (2012) suggest that these organic acids may act by forming complexes with Fe or Al, releasing As into the soil, increasing As availability by blocking As absorption sites on soil particles, or forming complexes with cations on soil mineral surfaces. Details of specific plants which hyperaccumulate Cd, Co, Cu, Au, Pb, Mn, Ni, Ag, Th, U and Zn are tabulated in Sheoran et al. (2009).

## *Excluders*

Metal excluders follow an alternative strategy of hypertolerance in their response to metalliferous soils. In these plants differential uptake and transport between roots and shoots leads to low shoot levels over a wide range of soil metal concentrations (Baker 1981). Such tolerance was first reported by Prat in 1934 who showed that that seeds from a normal population of *Silene vulgaris* (bladder campion) failed on copper contaminated soil, whilst seeds from a mine site population thrived (Terry and Banuelos 2010).

*Calluna vulgaris* (heather) and *Ulex europaeus* (gorse, Fig. 2) are opportunistic plant species that have colonized many abandoned mine and metalliferous tailings sites in Cornwall, UK. Lottermoser et al. (2011a) report that both species demonstrate a subdued biogeochemical signature, reflecting the exclusion of metals and As from their above-ground biomass. Other hypertolerant plants include the grasses; *Festuca avina, Agrostis tenuis, Trachypogon spicatus* and *Stereochlaena cameronii, Stachys sylvatica* (Antosiewicz et al. 2008; Baker 1981; Krämer 2010).

Some plants can exhibit more than one tolerance mechanisms. For example, mean concentration factors calculated for *Armeria maritima* (thrift, Fig. 3) growing on a Cu-rich bog in Wales show that the roots and living leaves generally exclude Cu, whilst the decaying leaves accumulate the metal (Brewin et al. 2003). Neumann et al. (1995) proposed four possibilities by which *A. maritima* may avoid enrichment in the cytoplasm: (1) excretion by salt glands; (2) Cu chelation with phenolic compounds; (3) Cu chelation by particular cell wall proteins; and (4) Cu binding by particular cytoplasmic or organellar proteins. In a study of *A. maritima* seedlings

**Fig. 2** Metal-excluding *Ulex europaeus* (gorse) growing in a contaminated mining landscape in Cornwall, UK (color figure online)

**Fig. 3** *Armeria maritima* (sea thrift) growing at a contaminated historic mineral processing plant, Poldice valley, Cornwall, UK (color figure online)

from a Zn-Pb calamine heap in Boleslaw, Poland, Olko et al. (2008) found that malate and citrate play a role in the transport of heavy metals to the aerial portions of the plant as these compounds significantly decreased in the roots and increased in the leaves after treatment with heavy metals.

## *Indicators*

Plant indicator species, or phytoindicators, may serve as a measure of the chemical status of a given site or area. Geobotanical prospecting using plant chemical status is a very old practice for the exploration of metal ores. The biogeochemistry of indicator plants reflects the physiologically controlled uptake of metals from a substrate that is enriched with metals to varying degrees. A good phytoindicator accumulates the elements of interest whilst being tolerant to those elements. The plant should be common with a wide distribution in the area to be investigated. A good correlation between substrate concentration and accumulation is required without seasonal differences in availability and applicability (Kabata-Pendias and Mukherjee 2007).

The potential use of metallophytes growing on and in the vicinity of Pb-Zn gossans in northwest Queensland, Australia as indicators in geobotanical and biogeochemical prospecting was investigated by Lottermoser et al. (2008). Of 16 plants investigated, they found that *Triodia molesta* (porcupine grass) and *Eriachne mucronata forma* were the plant species best suited for biogeochemical prospecting for base metals in the region. In China, *Elsholtzia haichowensis* and *Commelina communis* L. are widely distributed in areas that are rich in Cu. Work by Tang et al. (2001) suggests that *E. haichowensis* may be a better biogeochemical indicator for ore exploration than *C. communis*, but that both may be used for phytostablization of toxic mine soils.

## *Phytostabilization*

Plant based in situ stabilization or so called “phytostabilization” is a management strategy for stabilizing or deactivating contaminants which are potentially toxic. It decreases the contaminants bioavailability using plants and also sometimes soil amendments that strongly reduce the availability of pollutants to plant uptake, limiting the toxicity to the plants and allowing re-vegetation of contaminated sites. Plants suitable for phytostabilization are excluders, i.e. those which do not translocate metals to shoot tissues (Fig. 4). The ratio of shoot to root (or soil) should be less than one and concentrations in the above ground portion of the plant should not pose a risk to foraging animals (Mendez and Maier 2008).

The establishment of a vegetative cover on tailings repositories also decreases leaching and prevents dispersal of contaminated dusts through wind and water erosion. This leads to attenuation of the impact both on site and to adjacent ecosystems; preventing further spread and transfer into food chains. Such in situ deactivation can be simple, non-invasive and cost-effective and has the potential to be a valuable strategy for a wide range of contaminated sites. Successful plant establishment should stabilize metals, create an abundant and diverse heterotrophic microbial community and serve as the basis for a successional development that

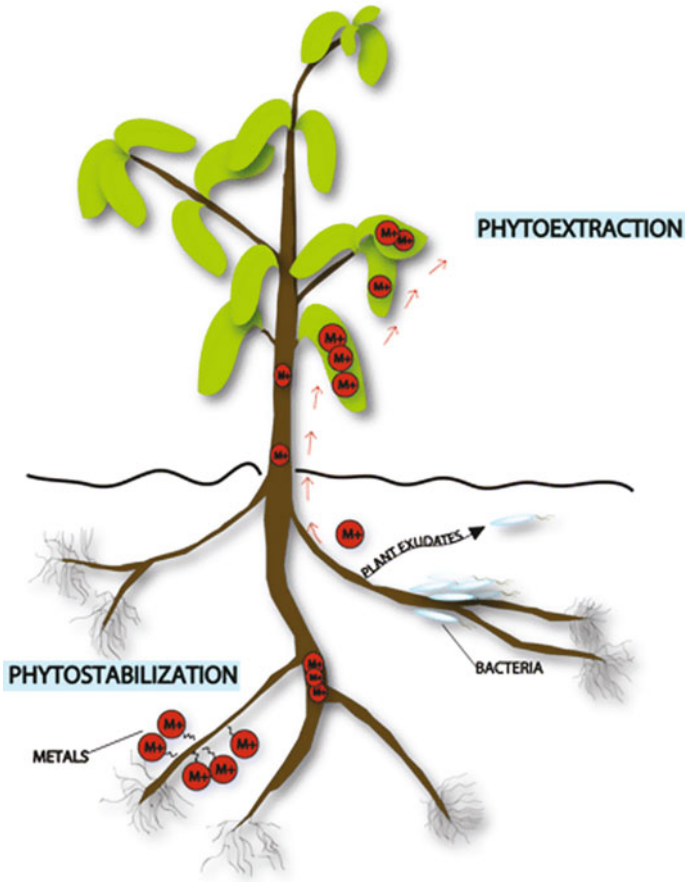


**Fig. 4** Phytoremediation of metals includes both phytoextraction and phytostabilization (Mendez and Maier 2008); reprinted from Mendez and Maier (2008), with permission from Springer and Springer Science and Business Media BV (color figure online)

ultimately leaves the site with a self-sustaining vegetative cap that minimizes erosion and leaching from the site.

Typical soil amendments for stabilizing trace elements include liming agents, phosphates, Fe–Mn oxy-hydroxides, organic materials, zeolites, ash and steel shot (Vangronsveld et al. 2009). Plants may also help to stabilize contaminants by accumulating and precipitating trace elements in the roots or root zone or by adsorption onto root surfaces. They may change the soil physical-chemical environment (e.g. pH, redox potential) around plant roots, thereby assisting in altering the chemical form of the contaminants. Microorganisms (bacteria and mycorrhiza) living in the rhizosphere of these plants may play an important role in changing the chemical speciation in the soil and assisting the plant in overcoming phytotoxicity

(Vangronsveld et al. 2009). Element mobility can be reduced by accumulation in plant roots and absorption onto root surfaces, as well as precipitation within the root zone resulting from plant-induced changes in pH or oxidation of the root environment (Antosiewicz et al. 2008).

The most suitable plant species for a site selected for phytoremediation will depend on the local climate. In temperate environments, grasses such as *Festuca* spp and *Agrostis* spp are often used because of their extensive rooting systems and rapid growth. In arid and semi-arid climates, drought- and salt-tolerant plants are required such as the halophyte *Atriplex* (Chenopodiaceae family) are more suitable. An inventory of field experiments on phytostabilization and metal inactivation in Europe is given in Vangronsveld et al. (2009), whilst Mendez and Maier (2008) list plant families of potential phytostabilization candidates. They also note that future challenges in this field include the identification of suitable regional- and climatic-specific native plants for phytostabilization and the definition of minimum inputs of soil improvers necessary to establish a sustainable plant community.

## *Phytoextraction*

Phytoextraction involves translocation of metals from the root to the plant shoot biomass (Fig. 4). The plant is harvested once plant maturity or suitable metal concentrations have been reached. Phytoextraction can be used in the phytoremediation of contaminated land and for phytomining. In the former, the plants are used to remove or reduce metals at contaminated locations, the plants are then harvested and disposed of as hazardous waste or incinerated for metal recovery (Mendez and Maier 2008). In the latter, the plant material can act as a sulfide-free "bio-ore" from which the target metal can be smelted and recovered if it is of sufficient economic value (Sheoran et al. 2009). For either application, metal tolerance, fast growth, ease of harvest and the ability to translocate metals to the above ground biomass which can then be cropped are key characteristics in a candidate plant.

Vangronsveld et al. (2009) note the development of three basic strategies of trace element phytoextraction: (1) natural phytoextraction using hyperaccumulators; (2) natural extraction using fast growing accumulators with deep root systems such as *Salix* (willow); and (3) chemically assisted phytoextraction using soil amendments such as chelators (e.g. EDTA; ethylene diamine tetraacetic acid) to increase trace element mobility in the soil. They report a promising prognosis for a decontamination time of a few years using *Nicotiana tabacum* (tobacco) at a Zn contaminated site in Switzerland. Total Zn concentrations ranged from 500 to 55,000 mg $kg^{-1}$ with soluble Zn concentrations (0.1 M $NaNO_3$) ranging from 0.2 to 35 mg $kg^{-1}$. A reduction in the soluble Zn concentration of 40–50 % after one year's cultivation was observed and the phytoextraction also lead to a higher pH and decreased mobility of metals in the soil.

The most common Ni accumulators are *Alyssum sps.* (Kabata-Pendias 2011). In situ phytoextraction of Ni by a native population of *Alyssum murale* has been reported on an ultramafic site in Albania (Bani et al. 2007). Nickel was present in the soil in two Ni-bearing phases: high Mg smectite (1.3 % Ni) and serpentine (0.7 % Ni). The smectite was identified as the sources of available Ni to the plants. Phytoextracted Ni in the experiment reached 25 kg $ha^{-1}$ on fertilized plots but only 3 kg $ha^{-1}$ on unfertilized plot, the difference was due to a reduction in yield rather than in the Ni content of the shoots.

## Plant Bioaccessibility Test Methods

The different approaches applied to the determination of metals and metalloids in soils can be seen in Fig. 5, which illustrates the effect of different extractions on various fractions of metals in soils. Column leaching techniques describe only the currently mobile phase, they do not describe the plant bioaccessible metal content and hence such techniques are not reviewed further. Pseudo-total and total digestions of the sample are both aggressive techniques and determine a greater proportion of the total metal concentration of a sample than is available to plant roots for uptake. They are also not discussed further. Thus, the following section is concerned with single and sequential extraction techniques. Whilst it is clear from the section above that the actual bioavailability of a metal to a plant will depend on a range of factors such as substrate, climate and plant specific parameters, sequential and single extractions offer the best prospect with which to operationally determine the fraction of an element which is, or may become, bioaccessible to a plant.

### *Sequential Extraction*

In sequential extraction, a sample is reacted with a series of extraction reagents in order to partition the trace elements and determine the availability of those elements within different geochemical fractions. There are many different procedures, and many slight variations on accepted procedures but a common feature is that extractants are applied successively, and each extractant is chemically more active than the previous one. In a typical sequence, the first species to be isolated are those in soil solution and those loosely attached at cation-exchange sites. Following this, there is usually a successive attack on the carbonates, Fe and Mn oxy-hydroxides, as well as organic matter and sulfides. The more refractory components, sometimes including the primary silicates, are dissolved last or on occasion not at all. The main advantage of sequential extraction over single extraction is the improved phase specificity and hence a more comprehensive understanding of the element fractionation within a sample.

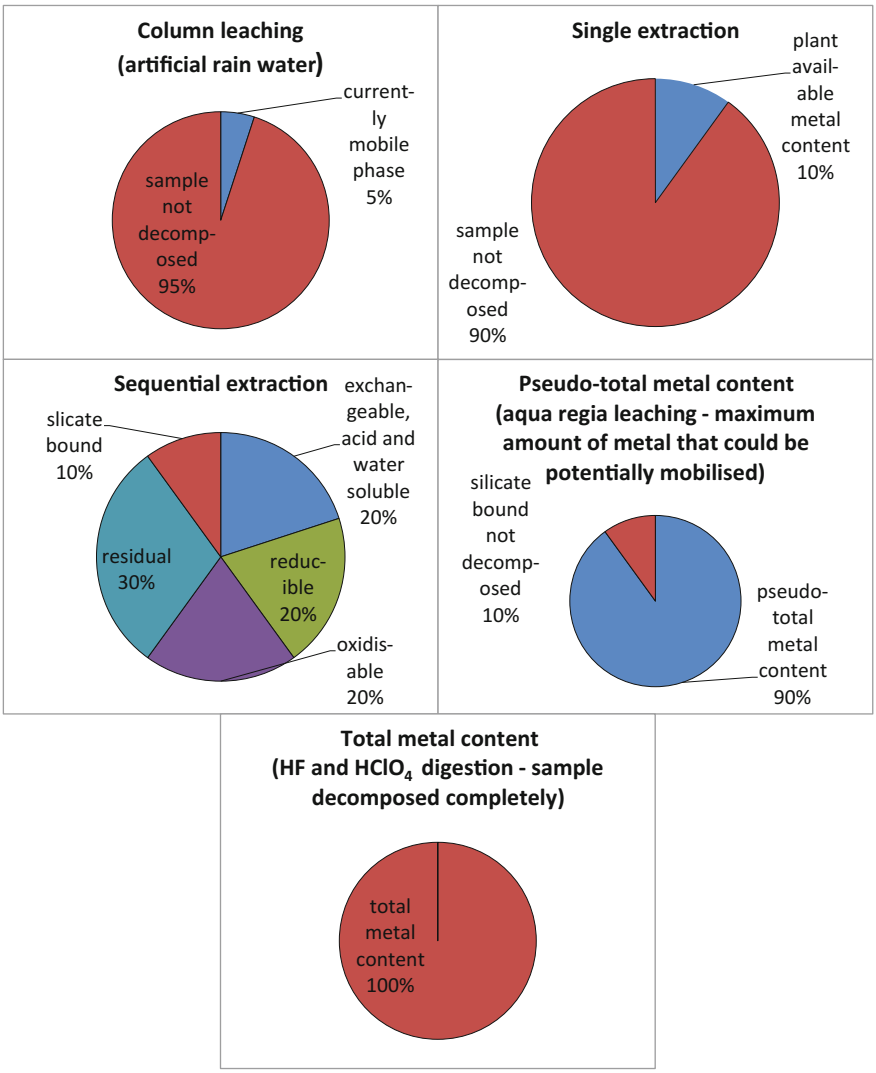


**Fig. 5** Different approaches applied in general to the determination of heavy metals in soil (% values shown above are only tentative as they are metal and matrix dependent) (after Rao et al. 2008); reprinted from Rao et al. (2008), with permission from Springer and Springer Science and Business Media BV (color figure online)

The Tessier scheme (Tessier et al. 1979) and the BCR® sequential extractions (Community Bureau of Reference, now known as the Standards, Measurement and Testing Program) (Rauret et al. 1999) outlined below are the most commonly adopted. These have been reviewed and summarized by Rao et al. (2008). The Tessier scheme in particular forms the basis of many adapted methods, for example,

the revised sequential extraction method used for geochemical studies of Cu sulfide mine waste by Dold (2003) and in the characterization of Fe and Al preciptates from an acid mine water passive remediation systems (Caraballo et al. 2009; Zhao et al. 2012). The CISMeD extraction procedure is also discussed; it uses only one extractant, nitric acid, at increasing concentrations. A major limitation to the widespread adoption of the sequential extraction procedures is the lengthy sample processing time. Some accelerated methods have been proposed with varying success. Lu et al. (2003) applied microwave extraction procedures for rare earth elements using a single extraction and achieving a shorter operational time and improved precision.

## Tessier Sequential Extraction Procedure

Tessier et al. (1979) developed a technique for the partitioning of the trace elements Cd, Co, Cu, Ni, Pb, Zn, Fe and Mn in fluvial sediments. The operating conditions are outlined in Table 1; they involve a four stage procedure with increasingly aggressive reagents, the overall sample processing time is 18 h. Adapted versions of this technique have been used to fractionate trace metals in phosphate rocks from mines in Jordan (Al-Hwaiti et al. 2014), mineral processing waste from an abandoned Cu mine facility in Nevada, USA (Al-Abed et al. 2006) and in weathered tailings from Sudbury, Ontario, Canada and Montevecchio, Sardinia (Fanfani et al. 1997; Ribeta et al. 1995). Heavy metal dispersion in a Fe-Cu sulfide deposit associated with ophiolitic rocks in the mining area of Vigonzano (northern Italy) has also been investigated using an adapted version of the Tessier technique (Dinelli and Tateo 2001).

**Table 1** Operating conditions required in the Tessier sequential extraction procedure for 1 g of sample (Rao et al. 2008)

| Stage | Fraction | Reagent | Experimental conditions |
|---|---|---|---|
| 1 | Exchangeable | 8 ml of 1 mol $L^{-1}$ $MgCl_2$ (pH 7) | 1 h at 25 °C |
| 2 | Associated with carbonates | 8 ml of 1 mol $L^{-1}$ NaOAc (pH 5 with acetic acid) | 5 h at 25 °C |
| 3 | Associated with Fe-Mn oxides | 20 ml of 0.4 mol $L^{-1}$ $NH_2OH{\cdot}HCl$ in 25 % w/v HOAc (pH ca. 2) | 6 h at 96 °C |
| 4 | Associated with organic matter | 3 ml of 0.02 mol $L^{-1}$ $HNO_3$/5 ml of 30 % m/w $H_2O_2$ | 2 h at 85 °C |
| | | +3 ml of 30 % m/v $H_2O_2$ | 3 h at 85 °C |
| | | +5 ml of 3.2 mol $L^{-1}$ $NH_4OAc$ | 30 min t 25 °C |

Reprinted from Rao et al. (2008), with permission from Springer and Springer Science and Business Media BV

## The BCR® Sequential Extraction Procedure

The BCR® optimized sequential extraction procedure was originally developed for heavy metals in sediments (Bacon and Davidson 2008; Rauret et al. 1999). The standardized technique is outlined in Table 2. A certified reference material, BCR®-701, is available for the technique that has certified extractable contents of Cd, Cr, Cu, Ni, Pb and Zn for all three steps and indicative values for the *aqua regia* extractible content of the six elements in the sediment and the residue obtained after the sequential extraction (Pueyo et al. 2001). Step 3 is of particular interest when attempting to predict the future bioaccessibility of metals in sulfidic mine wastes because it targets metals contained in sulfide minerals.

The BCR® technique has been successfully applied to a variety of mine-site related matrices including: (1) 10 and 20 year old mine tailings from northeastern Namibia (Sracek et al. 2014a, b); (2) 30 year old sulfidic mine tailings from the Monte Romero abandoned mining district and the Sao Domingos mine in the

**Table 2** The BCR® [Community Bureau of reference, now the Standards, Measurement and Testing Program (SM&T)] optimized sequential extraction procedure for 1 g sample (Rao et al. 2008)

| Step | Extractant | Fraction | Nominal target phase(s) | Experimental conditions |
|---|---|---|---|---|
| 1 | 40 ml of 0.11 mol $L^{-1}$ acetic acid solution | Exchangeable, acid- and water-soluble | Soil solution, exchangeable cations, carbonates | Room temperature, 16 h, constant shaking |
| 2 | 40 ml of 0.5 mol $L^{-1}$ hydroxyl amine hydrochloride solution at pH 1.5 (with nitric acid) | Reducible | Iron and manganese oxy-hydroxides | Room temperature, 16 h constant shaking |
| 3 | 10 ml of 30 % w/v $H_2O_2$ | Oxidizable | Organic matter and sulfides | Room temp, 1 h, occasional agitation +85 °C, 1 h |
| | 10 ml of 30 % w/v $H_2O_2$ | | | 85 °C, 1 h, Reduce volume to a few ml |
| | 50 ml of 1 mol $L^{-1}$ ammonium acetate at pH 2 | | | Room temperature, 16 h, constant shaking |
| 4 | Aqua regia[a] | Residual | Non-silicate minerals | ISO 11466 (ISO 1995) method adopted |

Reprinted from Rao et al. (2008), with permission from Springer and Springer Science and Business Media BV

[a]Recommended, to allow comparison for quality control purposes of sequential extraction (Σ = Step 1 + Step 2 + Step 3 + residual) with results obtained by a separate aqua regia digestion of original material

Iberian pyrite belt (IPB) (Pérez-López et al. 2008; Quispe et al. 2013); and (3) environmental samples following the Anzalcollar mine tailings dam spill in 1998 (Lacal et al. 2003). A modified version of the technique was used to extract trace metals from waste rock taken at a zinc mine in northern Finland (Kaakinen et al. 2012).

The first two BCR® extraction steps were used to assess metal mobility and availability in mine tailings taken from an old Pb-Zn treatment factory in Spain (Marguí et al. 2007). The effectiveness of DTPA extraction was also investigated in the same study. The extracted metals were compared with accumulated metals found in the silver birch tree (*Betula pendula*) grown in the mining spoils. These plants demonstrated a high degree of metal accumulation, particularly of Pb and Zn, with concentrations in some cases over 20x the background value for this species. Bioaccessibility studies based on a DTPA extraction procedure seemed useful in samples with pH values higher than 5, however, the extractable metals fractions determined by using steps 1 and 2 of the BCR® method were found to be a poor indication of bioavailability, possibly indicating a reservoir of Pb and Zn sited in the sulfidic material that was not extracted by the first two BCR® steps.

## CISMeD Extraction Procedure

The CISMeD extraction procedure developed by Cave et al. (2004) assumes that the physical-chemical components of a soil dissolve at different rates in increasing concentrations of nitric acid. Fourteen sequential extracts are performed on the sample by passing increasing concentrations of $HNO_3$, from highly diluted to 5 mol $L^{-1}$ nitric acid, through the soil using centrifugation. Each extract is analyzed for major and trace element contents. The method assumes that more easily extractable phases such as carbonates are dissolved in the dilute acid extracts and less soluble phases, such as Fe oxides, are dissolved in the more concentrated acid extracts. The aluminosilicate components of the soil are mostly resistant to nitric acid attack. A data processing algorithm identifies the number of physico-chemical components extracted, their composition and contribution to each extract. Nine chemically distinct soil compartments have been identified using this technique: pore-water residual solutes; organic; easily exchangeable; a Cu–Zn dominated phase; a Pb-dominated phase; amorphous Fe oxide/oxy-hydroxide; crystalline Fe oxide; Fe–Ti oxide; and Mn oxide. The technique allows an estimate of which identified physico-chemical component within the soil hosts which trace element (Cave et al. 2003, 2004).

### *Single Step Extraction*

For almost half a century, the use of chemical extractants for the assessment or prediction of agricultural crop plant contents, plant growth or health and the estimation of the likelihood of plant or animal deficiency or toxicity has been studied in agricultural laboratories (Rao et al. 2008). Many different reagents are used, and there exists a large body of information on how plant contents are correlated with soil extractable contents for different crops and soil types. The reason for the wide variety of extractants used to evaluate the quality of agricultural soils is primarily historic and not necessarily due to intrinsic differences in the physical-chemical properties of the nutrients (Houba et al. 1996). However, the validity of the link between plant and extractable soil metal contents is less well established in industrial polluted soils that contain metal concentrations well in excess of agricultural soil contents.

Each additional metal specific extraction method represents a significant increase in cost; the ideal scenario is therefore to find one extractant which provides an acceptable estimate of plant bioaccessibility of all metals of interest in the sample. The major benefits of using a single universal extractant include the simultaneous measurement of many elements, automation of laboratory labour, and minimization of the number of chemicals used, reducing the environmental impact of the technique itself.

An extensive review of Cd, Zn, Ni, Cu and Pb phytoavailability across a range of soils and concentrations (Menzies et al. 2007) recommend that neutral salt extracts such as 0.01 mol $L^{-1}$ $CaCl_2$, 0.1 mol $L^{-1}$ $NaNO_3$ and 1.0 mol $L^{-1}$ $NH_4OAc$ provide the most useful indication of metal phytoavailability. Menzies et al. (2007) also found that there was no correlation between total metal concentration and phytoavailable concentration and similarly, trace metal concentrations using DTPA (diethylene triamine pentaacetic acid) and EDTA complexing agents or 0.1 mol $L^{-1}$ HCl acid extractants were poorly correlated with plant uptake. Further research was recommended to investigate the effectiveness of the neutral salt extractants.

The different single extractants proposed in the literature fall into three broad categories: neutral salts, weak acids, and chelating agents. Examples of all three types are discussed below, along with brief examples of agricultural tests and more unusual extraction reagents such as cola soft drinks.

## Salt Solutions

Salt solutions are used to extract the exchangeable or electrostatically weakly bound fraction. Several studies have shown that such weak neutral salt solutions are suitable as metal extractants in soils because they are good models for simulating rainfall and flooding events (Garcia-Salgado et al. 2012). pH is one of the more

important factors that influence the relationship between metal concentration and metal activity. Although buffers can be used to maintain a relatively constant pH value during extraction, solutions of inorganic salts which are not pH buffered are often used, so that the pH of the reaction is determined mainly by the sample being extracted (Sahuquillo et al. 2003). Houba et al. (1996) state that "usually the results achieved with salt solutions such as 0.1 or 0.01 mol $L^{-1}$ $CaCl_2$, 0.1 mol $L^{-1}$ $NaNO_3$ and 1 mol $L^{-1}$ $NH_4NO_3$ are superior—meaning more strongly correlated with appearance of toxicity symptoms—to results achieved by extractions with (diluted) acid solutions or solutions containing complexing agents. This is also the case for correlations with the content of heavy metals in crops".

Interest in the use of mild extractants such as $CaCl_2$ and $NaNO_3$ has increased with improvements in detection limits when using analytical techniques such as inductively coupled plasma mass spectrometry (ICP-MS) to determine the low metal concentrations usually found in the extractant. Previously these methods were limited, because the concentrations extracted were too low for the usual analytical techniques of flame atomic absorption spectrometry (FAAS) and inductively coupled plasma optical emission spectrometry (ICP-OES).

National preferences exist for the extractant with which to estimate soil contamination and trace metal availability to plants using neutral salt solutions. The Netherlands uses 0.01 mol $L^{-1}$ $CaCl_2$, Switzerland uses 0.1 mol $L^{-1}$ $NaNO_3$, and Germany uses 1 mol $L^{-1}$ $NH_4NO_3$ (Prüeß 1997; Rao et al. 2008). The procedures have been found to be precise (typically ±10 % for all metals) and whilst trace metal extraction efficiency obtained with each procedure was slightly different, the three methods provided the same prediction of relative trace metal mobility (Cd > Zn > Cu > Pb) (Menzies et al. 2007; Pueyo et al. 2004).

**Calcium chloride ($CaCl_2$)** has been used as early as the 1970s to find correlations between concentrations of Al and Mn in acidic soils and toxicity to plants. It was later used to study Zn, Cd and Ni in soils and has been shown to provide an index for Cd-uptake by crops. Strong correlations exist between 0.1 mol $L^{-1}$ $CaCl_2$ extractable Zn and Cd in soil and plant concentrations in maize, and it is useful in predicting the phytoavailability of lead to spinach (Houba et al. 1996). Good correlations were found between rare earth element concentrations in wheat *(Troticum aestivum L.)* and single extractions using $CaCl_2$, and also $CH_3COOH$ (Lu et al. 2003).

Pueyo et al. (2004) recommend that the 0.01 mol $L^{-1}$ $CaCl_2$ extraction procedure as described by Houba et al. (1996) is the most suitable method for the determination of Cu, Cd, Pb and Zn mobility in soils, because it combines an appropriate extraction capacity with the lowest salt concentration in the extract, and therefore a simple matrix for analysis. Considerations highlighted by Houba et al. (1996) when choosing $CaCl_2$ as the universal extractant are: (1) the similar salt concentration of 0.01 mol $L^{-1}$ $CaCl_2$ and soil solutions; (2) coagulation caused by $Ca^{2+}$ in suspension; (3) the presence of $Ca^{2+}$ as the primary cation on adsorption sites in soils; and (4) the fact that various metals and nutrients can be determined in the extract.

The recommended procedure is to air dry soil with a particle size of <2 mm particle size. 10 g of sample is shaken with 100 ml of 0.1 mol $L^{-1}$ $CaCl_2$ for 2 h at 20 °C ± 2 °C, the pH is measured in the settling suspension which is subsequently centrifuged (3000×*g*) for 10 min. Various elements and nutrients can then be determined in the centrifugate (Houba et al. 1996). This extraction of metals with 0.01 mol $L^{-1}$ $CaCl_2$ cannot simply be regarded as a determination of the exchangeably adsorbed fraction (as is the case for the cations of K, Mg, Na and $NH_4$). The metal concentration achieved after the soil is suspended with $CaCl_2$ is controlled by desorption or solubilization of mineral phases. The electrolyte concentration stays almost constant and the metal concentration is affected by differences in binding strength and solubility of minerals in the different soils.

Sodium nitrate ($NaNO_3$) is used as a neutral soil extractant at a concentration of 0.1 mol $L^{-1}$ $NaNO_3$ and provides similar but less useful information to $CaCl_2$. An early agricultural application was the extraction of chlorides from soil samples in an attempt to identify the cause of leaf scorch in *Glycine* max (L.) Merr. (soybean) in America (Gaines et al. 1984). It has also been used as a "weak extractant" in an interlaboratory study on sewage sludge amended soils (Quevauviller 1998) and was favored by Switzerland as a standard protocol to assess the bioavailability of metals in different polluted soils (Häni and Gupta 1986; Rao et al. 2008; Sahuquillo et al. 2003).

Calcium nitrate ($Ca(NO_3)_2$) is used in a method initially developed to investigate the desorption of Cd in New Zealand soils (Gray et al. 1999). The technique involves shaking 5 g of soil with 30 ml of 0.01 mol $L^{-1}$ $Ca(NO_3)_2$ for 2 h at 20 °C. An analysis of soil metal bioavailability data from experiments spanning 6 months to 13 years was undertaken for wheat and ryegrass on agricultural soils and soils treated with biosolids and metal salts (Black et al. 2011). The neutral salt solution $Ca(NO_3)_2$ gave the best correlations between soil metal bioavailability and shoot concentration for Ni ($r^2 = 0.72$) and Zn ($r^2 = 0.64$) compared with measurements of total metal, EDTA, soil solution, DGT (diffusive gradients in thin films) and free ion activity. DGT gave the best estimation of Cd bioavailability.

Ammonium acetate ($NH_4OAc$) is the ammonium salt of a weak acid and tends, in contrast to ammonium nitrate, to raise the pH with the potential precipitation of metal hydroxides. However, metal complexation by acetate counters this effect (Ure 1996). In an assessment of trace metal bioavailability to vegetables in garden soils (Cu, Zn, Pb and Cd), transfer factors showed a trend of Cd > Zn > Cu > Pb (Xu et al. 2013). The extraction method for ammonium acetate is to add 4.0 g of soil to 20 ml of 1.0 mol $L^{-1}$ $NH_4OAc$ (pH 7) and shake for 2 h (Ure 1996). A study by Ure (1996) tested different extractants (DTPA, EDTA, HCl, $NO_4NO_3$, $NH_4OAc$) and found that overall $NH_4OAc$ provided the best estimate of Cd and Zn bioavailability to vegetables in multi-element contaminated soils.

Ammonium nitrate ($NH_4NO_3$) became the extractant used in a German national standard to determine mobile amounts of trace elements in soils in 1995 (Prüeß 1997). The chemical species extracted using 1 mol $L^{-1}$ ammonium nitrate are exchangeable and thus easily available for supplying soil solutions during plant growth (Baize et al. 2009). The procedure involves shaking 20 g of soil with 50 g

of 1 mol $L^{-1}$ $NH_4NO_3$ for 2 h. Ammonium salts of strong acids (e.g. ammonium nitrate or chloride) can lower the pH and promote the hydrolysis of clays (Ure 1996). Baize et al. (2009) found Cd in wheat grain to be positively correlated with $NH_4NO_3$ extracted Cd.

Potassium phosphate buffer is often recommended for the evaluation of plant bioavailable, easily extractable As (Antosiewicz et al. 2008). The phosphate anions complete for exchange sites and can replace the oxyanion As in the soil, releasing As into the soil solution (Gleyzes et al. 2001). In the method used by Antosiewicz et al. (2008), approximately 2 g of soil sample is weighed into a centrifuge tube and 20 ml of a 0.1 mol $L^{-1}$ $KH_2PO_4$/0.1 mol $L^{-1}$ $K_2HPO_4$ solution at pH 7.2 is added. The mixture is shaken at room temperature for 2 h at 30 rpm, and then the extract is separated from the solid residue by centrifugation at 14,000×*g* for 10 min. The final extracts are diluted with deionized water up to 25 ml. Antosiewicz et al. (2008) found that *S. sylvatica* had a smaller pool of potassium phosphate accessible As (5 % of total As) in its rhizosphere than other species which had around three times more, this plant was also distinguished by a low concentration of As in its shoots.

## Complexing Agents

In early investigations of single extractants complexing agents were widely used because they were successful in releasing measureable concentrations of metals into extraction solutions and were thought to extract all the metals in the non-silicate bound soil phases, thus reflecting metal availability in the long and short term (Ure 1996). However, levels of metals released from soils by complexing extractants have not been convincingly correlated with plant bioavailability in either pot or field trials and with advances in analytical technologies allowing lower limits of detection it is likely future research will focus on the full evaluation of neutral salt extractants.

**Diethylene triamine pentaacetic acid (DTPA)** is used at a concentration of 0.005 mol $L^{-1}$ in a procedure developed by Lindsay and Norvell (1978); 0.1 mol $L^{-1}$ TEA (triethanolamine), 0.01 mol $L^{-1}$ $CaCl_2$ are also present in the mixed solution which is adjusted to pH 7.3. DTPA has less extraction capacity than EDTA but is stronger than salt solution extractions and is best adapted for neutral and alkaline pH soils. In a study investigating the relationship between concentrations of trace metals in wheat grains and soil, Baize et al. (2009) found that Cd extracted from the soil using DTPA is positively correlated with grain Cd. They also found that Zn extracted from the soil by this method was negatively correlated with Cd in the wheat, possibly due to the antagonism between Zn and Cd.

**Ethylene diamine tetraacetic acid (EDTA)** is a very strong chelating compound that is often used for the extraction of both cations and anions. It gives the highest estimation of potential metal leaching when compared with phosphate buffer and acetic acid extractants. It has been used to estimate the potential As

leaching by natural organic ligands and the mobile fraction of As in the root zone. Arsenic in soils can occur as compounds of Al, Fe and Ca and complexation of these elements with EDTA can release As into solution (Gleyzes et al. 2001).

Antosiewicz et al. (2008) has used a concentration of 0.05 mol $L^{-1}$ EDTA at pH 7 to evaluate the mobile As fraction in samples taken close to a former As and Au mine and smelter in the Góry Zlote Mountains, Poland. 1 g of soil was mixed with 50 ml of reagent and subjected to shaking at 180 rpm at room temperature for 2 h, filtered, acidified and used for elemental analysis. Quevauviller et al. (1997) proposed a standardized method for the evaluation of Cd, Cr, Cu, Ni, Pb and Zn mobility where 5 g of soil is added to 25 ml of 0.05 mol $L^{-1}$ Na-EDTA at pH 7 and shaken for 1 h at 20 °C. The method was used by González-Corrochano et al. (2014) on soils and sediments from the vicinity of La Union, an abandoned Pb-Zn sulfide mine in central Spain.

Sahuquillo et al. (1999) compared the effectiveness of DTPA and EDTA. In soils with low carbonate content, metals bound with the carbonate and organically soil fractions were assumed to be extracted by EDTA. However, in calcareous soils DTPA buffered with triethanolamine was considered more suitable. In all cases, the EDTA extracted higher percentages of metals than DTPA.

## Weak Acids

Weak acids are commonly used to determine trace element mobility. Inorganic acids simulate the effect of an acid input onto soils, for example through acid rain, accidental spill or acid rock drainage. Organic acids have been used as a proxy for the root exudates to predict the bioaccessibility of As to hyperaccumulators.

**Acetic acid ($CH_3COOH$)**, also known as ethanoic acid, is thought to release As bound to carbonates. Antosiewicz et al. (2008) used a concentration of 0.11 mol $L^{-1}$ to investigate As bound to carbonate complexes from samples collected near an As and Au mine in Poland and found that only 2–5 % of total As was released into solution. This low percentage was expected because carbonates are not the most important As-binding phase in the studied area. Extractions on contaminated soils using both 0.11 mol $L^{-1}$ and 0.43 mol $L^{-1}$, found that for the most mobile elements, Cd and Zn, the increase in acidity did not have a significant effect on extractability. For elements with intermediate mobility, Cu and Ni, and for "fixed" elements, Pb and Cr, an increase in acidity caused a considerable increase in extractability due to increased carbonate dissolution (Sahuquillo et al. 1999). Ure (1996) notes that the effect of progressive acidification of a soil would be better predicted with the higher concentration of acetic acid. They report correlations between the acetic acid (0.4 mol $L^{-1}$) extractible Cd, Co, Cr, Ni, Pb and Zn contents and plant metal content in arable crops and herbage. This extraction solution dissolves the exchangeable species, releases the more tightly bound exchangeable forms and may also partly attack silicate and carbonate phases and dissolve Cu from some sites on oxide minerals.

**Hydrochloric acid (HCl)** is used in dilute form to isolate the non-residual phase in a variety of environmental media. The acid is assumed to extract metals on exchange sites, by dissolving calcareous materials, and also via the strong ligand action of the chloride ion. 0.1 mol $L^{-1}$ and 0.5 mol $L^{-1}$ HCl have been used to extract available metals and a concentration of 1 mol $L^{-1}$ HCl has been recommended as a standard method for assessing metal concentrations (Snape et al. 2004). Studies on the use of HCl as a single extractant are not encouraging (Leleyter et al. 2012).

**Organic acids** have been used in a method to predict As availability to hyperaccumulators in contaminated soils with the aim of improving estimates of the time frame for site clean-up during phytoremediation (Gonzaga et al. 2012). The method using root-exudate based organic acids was developed following observations that As hyperaccumulators are able to access some As in soils that is unavailable to non-hyperaccumulators, and that this was probably achieved by root exudates, the major constituents of which are low molecular weight organic acids. The organic acid extractable arsenic was determined in this method using a 1:20 soil to solution ratio (1.4 mmol $L^{-1}$ phytic acid + 0.2 mmol $L^{-1}$ oxalic acid), shaking for 24 h and centrifuging at 3500 rmp for 15 min. These concentrations of organic acid were similar to those reported in the root exudates of *P. vittata* (Gonzaga et al. 2012).

## Agricultural Tests

Several agricultural tests were developed to predict nutrient uptake by agricultural crops. These tests were based on fertilizer need and little information is available regarding extraction in contaminated soils and related metal bioavailability to hyperaccumulators (Gonzaga et al. 2012). Mehlich 3 is a dilute acid solution at pH 2.5 consisting of a mixture of 0.2 mol $L^{-1}$ $CH_3COOH$, 0.25 mol $L^{-1}$ $NH_4NO_3$, 15 mmol $L^{-1}$ $NH_4F$, 13 mmol $L^{-1}$ $HNO_3$ and 1 mmol $L^{-1}$ EDTA that has been widely used to predict nutrient availability from crops. The Mehlich 3 extractant removes As bound to Fe–Al minerals along with dissolved and adsorbed As. The organically-bound As fraction is targeted by the EDTA in the extraction solution (Dinelli and Tateo 2001; Mehlich 1984). The Mehlich 3 was developed as a universal extractant for soils of differing pH (Mallarino 1995).

The Bray P1 and Olsen methods are the most widely used soil-test methods to estimate available phosphorus in the North-Central region of the US (Mallarino 1995). The Bray P1 test has been shown to be reliable for the estimation of available P in neutral or acid soils but it underestimates available P on calcareous soils. The Olsen test is more reliable in calcareous soils. Ammonium lactate/acetic acid extract is used for the determination of P, K and some minor elements (Houba et al. 1996).

## Cola Soft Drinks

Many of the conventional single and sequential extraction techniques discussed above require distilled or deionized water and high quality chemical reagents. These requirements can become problematic when working in developing nations where such facilities are not available, yet there is a need for soil testing procedures that are scientifically sound and quantitative as well as simple, rapid, cheap and readily available and with the potential to be applied in the field to avoid costly transportation of test material. Lottermoser et al. (2011b) compared the trace element bioaccessibility achieved using DTPA and $CaCl_2$ with their bioaccessibility as determined using soft drinks (Coca-Cola Classic®, Diet Coke® and Coke Zero®). The data from the single extraction tests demonstrate that soft drink extractable As, Cu, La, Mn, Ni, Y and Zn correlate with DTPA- and $CaCl_2$ extractable metals. These unconventional reagents are superior in terms of availability, cost, preparation and disposal when compared to traditional chemicals (Lottermoser et al. 2011b). However, regional variations in ingredients mean the reproducibility of data obtained using cola drinks may be questionable.

## Conclusions

The bioavailability of metals and metalloids to plants growing at mine sites will depend on the strategies that those plants possess to tolerate high concentrations of these elements. Some plants will hyperaccumulate an elevated potentially toxic trace element, such as *Pterris vittata* (Chinese brake fern), others will exclude it by limiting transport from root to shoot, such as *Silene vulgaris* (bladder campion). A third category of plants are indicators. These take up the element in a proportion related to its concentration in the substrate, such as *Triodia molesta* (porcupine grass). The strategies used by these plants will in turn determine their usefulness for application in phytoextraction, phytostabilization and biogeochemical prospecting.

Tests to determine the actual uptake of a particularly element by a particular plant are expensive and lengthy to perform (e.g. using pot or lysimeter trials). An alternative is the use of tests to evaluate the bioaccessibility of an element to plants. These tests determine the operationally defined fraction of an element in a substrate that is available, or may become available, to a plant growing on that substrate. The most useful tests to determine the bioaccessibility of elements in sulfidic rocks and wastes are those which include an element of sample oxidation. It is the oxidation of sulfides in the substrate that will release potentially toxic trace elements into a more mobile form which will be more likely to be bioavailable to plants growing at mine sites.

## References

Al-Abed SR, Hageman PL, Jegadeesan G, Madhavan N, Allen D (2006) Comparative evaluation of short-term leach tests for heavy metal release from mineral processing waste. Sci Total Environ 364:14–23

Al-Hwaiti M, Tardio J, Reynolds H, Bhargava S (2014) Selectivity assessments of a sequential extraction procedure for potential trace metals' mobility and bioavailability in phosphate rocks from Jordan phosphate mines. Soil Sed Contam 23:417–436

Antosiewicz D, Escudě-Duran C, Wierzbowska E, Skłodowska A (2008) Indigenous plant species with the potential for the phytoremediation of arsenic and metals contaminated soil. Water Air Soil Pollut 193:197–210

Bacon JR, Davidson CM (2008) Is there a future for sequential chemical extraction? Analyst 133:25–46

Baize D, Bellanger L, Tomassone R (2009) Relationships between concentrations of trace metals in wheat grains and soil. Agron Sustain Dev 29:297–312

Baker AJM (1981) Accumulators and excluders—strategies in the response of plants to heavy-metals. J Plant Nutr 3:643–654

Bani A, Echevarria G, Sulçe S, Morel JL, Mullai A (2007) In-situ phytoextraction of Ni by a native population of *Alyssum murale* on an ultramafic site (Albania). Plant Soil 293:79–89

Black A, McLaren RG, Reichman SM, Speir TW, Condron LM (2011) Evaluation of soil metal bioavailability estimates using two plant species (*L. perenne and T. aestivum*) grown in a range of agricultural soils treated with biosolids and metal salts. Environ Pollut 159:1523–1535

Brewin LE, Mehra A, Lynch PT, Farago ME (2003) Mechanisms of copper tolerance by Armeria maritima in Dolfrwynog Bog, North Wales—initial studies. Environ Geochem Health 25:147–156

Caraballo MA, Rotting TS, Nieto JM, Ayora C (2009) Sequential extraction and DXRD applicability to poorly crystalline Fe- and Al-phase characterization from an acid mine water passive remediation system. Am Mineral 94:1029–1038

Cave M, Wragg J, Palumbo B, Klinck BA (2003) Measurement of the bioaccessibility of arsenic in UK soils. Environment Agency Technical report P5-062/TR02. Almondsbury, Bristol, UK

Cave MR, Milodowski AE, Friel EN (2004) Evaluation of a method for identification of host physico-chemical phases for trace metals and measurement of their solid-phase partitioning in soil samples by nitric acid extraction and chemometric mixture resolution. Geochem Explor Environ Anal 4:71–86

Dinelli E, Tateo F (2001) Factors controlling heavy-metal dispersion in mining areas: the case of Vigonzano (northern Italy), a Fe-Cu sulfide deposit associated with ophiolitic rocks. Environ Geol 40:1138–1150

Dold B (2003) Speciation of the most soluble phases in a sequential extraction procedure adapted for geochemical studies of copper sulfide mine waste. J Geochem Explor 80:55–68

Fanfani L, Zuddas P, Chessa A (1997) Heavy metals speciation analysis as a tool for studying mine tailings weathering. J Geochem Explor 58:241–248

Gaines T, Parker M, Gascho G (1984) Automated determination of chlorides in soil and plant tissue by sodium nitrate extraction. Agron J 76:371–374

Garcia-Salgado S, Garcia-Casillas D, Quijano-Nieto MA, Bonilla-Simon MM (2012) Arsenic and heavy metal uptake and accumulation in native plant species from soils polluted by mining activities. Water Air Soil Pollut 223:559–572

Gleyzes C, Tellier S, Sabrier R, Astruc M (2001) Arsenic characterisation in industrial soils by chemical extractions. Environ Technol 22:27–38

Gonzaga MIS, Ma LQ, Pacheco EP, dos Santos WM (2012) Predicting arsenic bioavailability to hyperaccumulator *Pteris Vittata* in arsenic-contaminated soils. Int J Phytorem 14:939–949

Gonzaga MIS, Santos JAG, Ma LQ (2006) Arsenic chemistry in the rhizosphere of *Pteris vittata L.* and *Nephrolepis exaltata L.* Environ Pollut 143:254–260

González-Corrochano B, Esbrí JM, Alonso-Azcárate J, Martínez-Coronado A, Jurado V, Higueras P et al (2014) Environmental geochemistry of a highly polluted area: the La Union Pb–Zn mine (Castilla-La Mancha region, Spain). J Geochem Explor 144:345–354

Gray C, McLaren R, Roberts A, Condron L (1999) Solubility, sorption and desorption of native and added cadmium in relation to properties of soils in New Zealand. Eur J Soil Sci 50:127–137

Häni H, Gupta S (1986) Chemical methods for the biological characterization of metal in sludge and soil. In: L'Hermite P (ed) Processing and use of organic sludge and liquid agricultural wastes. Springer, Netherlands, pp 157–167

Houba VJG, Lexmond TM, Novozamsky I, van der Lee JJ (1996) State of the art and future developments in soil analysis for bioavailability assessment. Sci Total Environ 178:21–28

ISO (1995) Soil quality. Extraction of trace elements soluble in Aqua Regia, ISO 11466

Kaakinen J, Kuokkanen T, Kujala K, Välimäki I, Jokinen H (2012) The use of a five-stage sequential leaching procedure for risk assessment of heavy metals in waste rock utilized in railway ballast. Soil Sed Contam 21:322–334

Kabata-Pendias A (2011) Trace elements in soils and plants. CRC Press, Boca Raton

Kabata-Pendias A, Mukherjee AB (2007) Trace elements from soil to human. Springer, Heidelberg

Krämer U (2010) Metal hyperaccumulation in plants. Annu Rev Plant Biol 61:517–534

Lacal J, da Silva MP, García R, Sevilla MT, Procopio JR, Hernandez L (2003) Study of fractionation and potential mobility of metal in sludge from pyrite mining and affected river sediments: changes in mobility over time and use of artificial ageing as a tool in environmental impact assessment. Environ Pollut 124: 291–305

Leleyter L, Rousseau C, Biree L, Baraud F (2012) Comparison of EDTA, HCl and sequential extraction procedures for selected metals (Cu, Mn, Pb, Zn) in soils, riverine and marine sediments. J Geochem Explor 116–117:51–59

Lindsay W, Norvell WA (1978) Development of a DTPA soil test for zinc, iron, manganese, and copper. Soil Sci Soc Am J 42:421–428

Lottermoser BG, Ashley PM, Munksgaard NC (2008) Biogeochemistry of Pb-Zn gossans, northwest Queensland, Australia: implications for mineral exploration and mine site rehabilitation. Appl Geochem 23:723–742

Lottermoser BG, Glass HJ, Page CN (2011a) Sustainable natural remediation of abandoned tailings by metal-excluding heather (*Calluna vulgaris*) and gorse (*Ulex europaeus*), Carnon Valley, Cornwall, UK. Ecol Eng 37:1249–1253

Lottermoser BG, Schnug E, Haneklaus S (2011b) Cola soft drinks for evaluating the bioaccessibility of uranium in contaminated mine soils. Sci Total Environ 409:3512–3519

Lu A, Zhang S, Shan X-Q, Wang S, Wang Z (2003) Application of microwave extraction for the evaluation of bioavailability of rare earth elements in soils. Chemosphere 53:1067–1075

Ma LQ, Komar KM, Tu C, Zhang W, Cai Y, Kennelley ED (2001) A fern that hyperaccumulates arsenic. Nature 409:579

Mallarino AP (1995) Comparison of Mehlich-3, Olsen, and Bray-P1 procedures for phosphorus in calcareous soils. In: Proceedings of the 25th North Central extension-industry soil fertility conference, St. Louis, Missouri, pp 96–101

Marguí E, Queralt I, Carvalho M, Hidalgo M (2007) Assessment of metal availability to vegetation (*Betula pendula*) in Pb-Zn ore concentrate residues with different features. Environ Pollut 145:179–184

Mehlich A (1984) Mehlich 3 soil test extractant: a modification of Mehlich 2 extractant. Comm Soil Sci Plant Anal 15:1409–1416

Mendez MO, Maier RM (2008) Phytoremediation of mine tailings in temperate and arid environments. Rev Environ Sci Bio/Technol 7:47–59

Menzies NW, Donn MJ, Kopittke PM (2007) Evaluation of extractants for estimation of the phytoavailable trace metals in soils. Environ Pollut 145:121–130

Neumann D, Zurnieden U, Lichtenberger O, Leopold I (1995) How does *Armeria maritima* tolerate high heavy metal concentrations. J Plant Physiol 146:704–717

Olko A, Abratowska A, Zylkowska J, Wierzbicka M, Tukiendorf A (2008) *Armeria maritima* from a calamine heap–initial studies on physiologic-metabolic adaptations to metal-enriched soil. Ecotoxicol Environ Saf 69:209–218

Pérez-López R, Álvarez-Valero AM, Nieto JM, Sáez R, Matos JX (2008) Use of sequential extraction procedure for assessing the environmental impact at regional scale of the São Domingos Mine (Iberian Pyrite Belt). Appl Geochem 23:3452–3463

Prüeß A (1997) Action values for mobile ($NH_4NO_3$-extractable) trace elements in soils based on the German national standard DIN 19730. Les Colloques de l'INRA 415–423

Pueyo M, López-Sánchez JF, Rauret G (2004) Assessment of $CaCl_2$, $NaNO_3$ and $NH_4NO_3$ extraction procedures for the study of Cd, Cu, Pb and Zn extractability in contaminated soils. Anal Chimica Acta 504:217–226

Pueyo M, Rauret G, Lück D, Yli-Halla M, Muntau H, Quevauviller P, Lopez-Sanchez JF (2001) Certification of the extractable contents of Cd, Cr, Cu, Ni, Pb and Zn in a freshwater sediment following a collaboratively tested and optimised three-step sequential extraction procedure. J Environ Monit 3:243–250

Quevauviller P (1998) Operationally defined extraction procedures for soil and sediment analysis I. Standardization. Trends Anal Chem 17:289–298

Quevauviller P, Rauret G, Rubio R, López-Sánchez JF, Ure A, Bacon J, Muntau H (1997) Certified reference materials for the quality control of EDTA-and acetic acid-extractable contents of trace elements in sewage sludge amended soils (CRMs 483 and 484). Fresenius' J Anal Chem 357:611–618

Quispe D, Pérez-López R, Acero P, Ayora C, Nieto JM, Tucoulou R (2013) Formation of a hardpan in the co-disposal of fly ash and sulfide mine tailings and its influence on the generation of acid mine drainage. Chem Geol 355:45–55

Rao C, Sahuquillo A, Sanchez JL (2008) A review of the different methods applied in environmental geochemistry for single and sequential extraction of trace elements in soils and related materials. Water Air Soil Pollut 189:291–333

Rauret G, Lopez-Sanchez JF, Sahuquillo A, Rubio R, Davidson C, Ure A, Quevauviller P (1999) Improvement of the BCR® three step sequential extraction procedure prior to the certification of new sediment and soil reference materials. J Environ Monit 1:57–61

Ribeta I, Ptacek CJ, Blowes DW, Jambor JL (1995) The potential for metal release by reductive dissolution of weathered mine tailings. J Contam Hydrol 17:239–273

Robinson BH, Brooks RR, Howes AW, Kirkman JH, Gregg PEH (1997) The potential of the high-biomass nickel hyperaccumulator Berkheya coddii for phytoremediation and phytomining. J Geochem Explor 60:115–126

Sahuquillo A, Lopez-Sanchez JF, Rubio R, Rauret G, Thomas RP, Davidson CM, Ure AM (1999) Use of a certified reference material for extractable trace metals to assess sources of uncertainty in the BCR® three-stage sequential extraction procedure. Anal Chim Acta 382:317–327

Sahuquillo A, Rigol A, Rauret G (2003) Overview of the use of leaching/extraction tests for risk assessment of trace metals in contaminated soils and sediments. Trends Anal Chem 22:152–159

Shen ZG, Zhao FJ, McGrath SP (1997) Uptake and transport of zinc in the hyperaccumulator Thlaspi caerulescens and the non-hyperaccumulator Thlaspi ochroleucum. Plant Cell Environ 20:898–906

Sheoran V, Sheoran AS, Poonia P (2009) Phytomining: a review. Miner Eng 22:1007–1019

Snape I, Scouller RC, Stark SC, Stark J, Riddle MJ, Gore DB (2004) Characterisation of the dilute HCl extraction method for the identification of metal contamination in Antarctic marine sediments. Chemosphere 57:491–504

Sracek O, Mihaljevič M, Kříbek B, Majer V, Filip J, Vaněk A, Mapani B (2014a) Geochemistry and mineralogy of vanadium in mine tailings at Berg Aukas, northeastern Namibia. J Afr Earth Sci 96:180–189

Sracek O, Mihaljevič M, Kříbek B, Majer V, Filip J, Vaněk A, Mapani B (2014b) Geochemistry of mine tailings and behavior of arsenic at Kombat, northeastern Namibia. Environ Monit Assess 186:4891–4903

Tang SR, Wilke BM, Brooks RR (2001) Heavy-metal uptake by metal-tolerant *Elsholtzia haichowensis* and *Commelina communis* from China. Commun Soil Sci Plant Anal 32:895–905

Terry N, Banuelos G (2010) Phytoremediation of contaminated soil and water. CRC Press, Boca Raton

Tessier A, Campbell PGC, Bisson M (1979) Sequential extraction procedure for the speciation of particulate trace-metals. Anal Chem 51:844–851

Tu S, Ma L, Luongo T (2004) Root exudates and arsenic accumulation in arsenic hyperaccumulating *Pteris vittata* and non-hyperaccumulating *Nephrolepis exaltata*. Plant Soil 258:9–19

Ure A (1996) Single extraction schemes for soil analysis and related applications. Sci Total Environ 178:3–10

Vangronsveld J, Herzig R, Weyens N, Boulet J, Adriaensen K, Ruttens A, Thewys T, Vassilev A, Meers E, Nehnevajova E, van der Lelie D, Mench M (2009) Phytoremediation of contaminated soils and groundwater: lessons from the field. Environ Sci Pollut Res 16:765–794

Xie Q-E, Yan X-L, Liao X-Y, Li X (2009) The arsenic hyperaccumulator fern *Pteris vittata L.* Environ Sci Technol 43:8488–8495

Xu DC, Zhou P, Zhan J, Gao Y, Dou C, Sun Q (2013) Assessment of trace metal bioavailability in garden soils and health risks via consumption of vegetables in the vicinity of Tongling mining area, China. Ecotoxicol Environ Saf 90:103–111

Zhao H, Xia B, Qin J, Zhang J (2012) Hydrogeochemical and mineralogical characteristics related to heavy metal attenuation in a stream polluted by acid mine drainage: a case study in Dabaoshan Mine, China. J Environ Sci China 24:979–989

# Prediction of Plant Metal Bioaccessibility in Mineralized and Sulfidic Rocks

**Eleanor M. van Veen, Bernd Lottermoser and Taryn L. Noble**

**Abstract** Successful rehabilitation of mine sites requires a solid knowledge of waste and mine soil properties. In particular, there is a need for a predictive test that allows forecasting of risks to plant growth on contaminated mine soils and waste repositories. In this contribution, a new plant bioaccessibility test is described that meets this need. The methodology for the new test oxidizes the sample with hydrogen peroxide and then extracts the solubilized metals and metalloids from the sample using 1 M ammonium acetate solution. The test is based on aspects of two established tests: (1) the sequential NAG test, which is suitable for sulfidic samples but does not determine metals and metalloids; and (2) the BCR® extraction, which gives information on the geochemical fractionation of these elements but is not suitable for highly sulfidic samples. Learnings from the method development, a stepwise test protocol and a simplified flow diagram for the test are presented. The proposed new plant bioaccessibility test represents a predictive tool that allows forecasting of metal fractions that may become available to plants upon colonization of sulfidic soils and wastes at mine sites.

E.M. van Veen (✉)
Environment and Sustainability Institute/Camborne School of Mines, University of Exeter, Penryn Campus, Penryn, Cornwall TR10 9FE, UK
e-mail: E.M.Van-Veen@exeter.ac.uk

B. Lottermoser
Institute of Mineral Resources Engineering, RWTH Aachen University, Wüllnerstrasse 2, 52062 Aachen, Germany
e-mail: lottermoser@mre.rwth-aachen.de

T.L. Noble
School of Physical Sciences, University of Tasmania, Private Bag 79, Hobart, TAS 7001, Australia
e-mail: Taryn.Noble@utas.edu.au



B. Lottermoser (ed.), *Environmental Indicators in Metal Mining*,
DOI 10.1007/978-3-319-42731-7_21

## Introduction

Metal and metalloid contamination in the environment has many causes and the source of the contamination will influence the form in which these potentially toxic trace elements are present and hence their availability to plants. Metals and metalloids are found in many crystalline minerals and amorphous materials and their siting in these materials is one factor that will influence the extent to which they are taken up into the biomass of plants growing on contaminated substrates. In sulfidic mine waste, metals and metalloids associated with sulfide minerals may become more mobile and hence available to plants as their host minerals oxidize in the surficial environment.

The terms bioavailability and bioaccessibility have been used interchangeably in the literature and many slightly different definitions have been proposed for both terms (Bryan and Langston 1992; Cave et al. 2003; Ruby et al. 1996; Semple et al. 2004; Templeton et al. 2000). Confusion can arise when comparisons are made between human/animal bioaccessibility and plant (phyto) bioaccessibility. However, comparison and harmonization of these meanings are beneficial to clarity and understanding in the field. In human bioaccessibility, a case has been made for referring to the bioaccessible fraction of a substance as "the fraction that is soluble in the gastrointestinal environment and is available for absorption" (Cave et al. 2003). In plant bioaccessibility, a comparable definition of the bioaccessible fraction as "that which is available to cross an organism's cellular membrane from the environment" seems appropriate (Semple et al. 2004). The principal difference between these two definitions is therefore that in the human/animal field the bioaccessibility is internal to the organism, and therefore influenced by the conditions inside the gut or lumen of the species of interest (such as mineralogy, temperature, pH, enzymes). By contrast in the plant field, the factors influencing bioaccessibility are external to the plant (such as mineralogy, pH, temperature, redox potential, root exudates).

Having defined the bioaccessible fraction, definition of the bioavailable fraction is straight forward. The bioavailable fraction of a substance is the fraction that can enter the organism and hence potentially cause toxic effects. In humans and animals, this refers to the fraction of the substance that can enter the systemic circulation (bloodstream). It is further defined according to the route of entry such as the mouth "oral bioavailability", skin "dermal bioavailability", or lungs "pulmonary bioavailability". The plant bioavailable fraction of a compound is the fraction that can enter the organism by crossing its cellular membrane (Semple et al. 2004). Metal and metalloid uptake in plants primarily occurs through the roots, this route of entry is therefore implicit in the term and a more specific distinction is not usually applied.

The processes that determine the exposure to contaminants in a substrate of organisms that interact with that substrate are summarized by Semple et al. (2004). They encompass: (a) sorption and release of a soil bound contaminants; (b) transport of released contaminants; (c) transport of bound contaminants; (d) uptake across a physiological membrane; and (e) incorporation of the absorbed contaminant into a living system. In the definitions proposed by Semple et al. (2004) and

adopted here plant bioavailability encompasses process (d), whereas plant bioaccessibility encompasses processes (a) to (d). The boundary between a bioaccessible and a non-bioaccessible substance is not sharp and the potential for a substance to become bioaccessible will depend on mineralogical siting, temporal factors and the local environmental conditions to which the substrate is exposed.

Information on the bioavailability of a substance to plants can be obtained by analyzing vegetation growing naturally on the substrate (e.g. Lottermoser et al. 2011). Greenhouse pot or lysimeter trials (e.g. Gonzaga et al. 2012) can enable quantification of the plant uptake of the substance in question. However, these methods are slow and results will depend on the strategies that the plant has evolved to adapt to the contaminated environment. Information on the bioaccessibility of a substance can be plant, site and substrate specific; a bioaccessible substrate may be freely available, but it may also be temporarily physically or chemically constrained and tests must be suited to the aspect characteristics of the material that is under consideration.

For example, Pb present in carbonates such as cerrussite, $PbCO_3$, (e.g. Schaider et al. 2007; Sracek et al. 2014) would become mobile in an acidic environment caused by acid rain or mine drainage and a test to evaluate the bioaccessibility in this scenario could involve extraction with acid reagents. Elements associated with sulfidic minerals such as pyrrhotite, arsenoprite, chalcopyrite and galena can be released due to oxidation processes and tests should be designed accordingly (Amos et al. 2015; Parbhakar-Fox and Lottermoser 2015).

This chapter describes the method development and details the protocol for a new bioaccessibility test for mineralized and sulfidic mine soils, rocks and wastes. First, two existing procedures that can be used for assessing these materials are discussed along with their limitations. The method development for the new test is then detailed with learnings from both useful and inappropriate modifications. The recommended protocol for the new plant bioaccessibility test is described with a simplified flow diagram of the procedure. The new test is designed to predict the bioaccessibility of potentially toxic trace elements in sulfidic wastes. It is suitable for use as part of a suite of predictive tests and methodologies that should be used at the beginning of the life-of-mine cycle to achieve more cost effective end environmentally benign mine closure outcomes in the long term.

## Current Tests for Mineralized and Sulfidic Wastes

Numerous single and sequential tests have been described which endeavor to assess the mobility and bioaccessibility of metals and metalloids in various contaminated substrates. However, widely accepted standardized tests devised specifically for mineralized and sulfidic wastes are somewhat limited. One such test is the sequential NAG (net acid generating) test. This is an adapted form of the single NAG test and recommenced for samples with >1.5 % sulfides or samples with high Cu concentrations, both of which can catalyze the decomposition of hydrogen peroxide. The sequential NAG test is a multi-stage process with repeated cycles of

15 % hydrogen peroxide ($H_2O_2$) addition followed by heating and filtration until either there is no further catalytic decomposition of the $H_2O_2$, or the NAGpH is greater than pH 4.5 (Smart et al. 2002).

The standard BCR® test described by Rauret et al. (1999) has been applied to sulfidic wastes and rocks. The technique has been used by: (1) Quispe et al. (2013) on pyritic (30–80 %) flotation tailings from the Monte Romero abandoned mining district in the IPB; (2) by Lacal et al. (2003) on pyritic (80–85 %) sludges collected after the Aznalcollar tailings dam break in 1998; and (3) by Pérez-López et al. (2008) on pyritic slags (10–15 %), fine grained smelting ashes (1–5 % pyrite) and pyrite rich (15–40 %) waste dumps sampled from the São Domingos Mine area (IPB). Due to the high pyrite content in some of the samples extracted in these studies, very slow addition of hydrogen peroxide during the third step to extract the oxidizable fraction would have been key to avoiding sample loss in these studies. A certified sediment reference material (BCR® 701) is available that can be used to evaluate the accuracy of the analysis achieved using the extraction procedure. This was used by Lacal et al. (2003) to evaluate analytical performance.

The BCR® procedure has the advantage of providing detailed information on the geochemical fractionation of potentially toxic trace elements. However, it is too lengthy to be useful in its entirety as a rapid, cheap and targeted test to evaluate the plant bioaccessibility of metals in sulfidic wastes at mine sites. Step 3 of the procedure targets the metals associated with sulfides and organic matter by using hydrogen peroxide to oxidize the sample. Since the aim of the proposed test is to evaluate the "first flush" of sulfide oxidation of sulfidic wastes and waste rocks, the BCR® step 3 offers a useful foundation on which to build the plant bioaccessibility test. Determination of metals bound to sulfides is necessary when attempting to predict the environmental impact of mineralized and sulfidic rock samples at a mine site. These elements have the potential to be released via oxidation reactions when the minerals are exposed to weathering processes. This provides a transfer route for metals and metalloids out of the solid material and into the more mobile and phytoavailable aqueous phase.

## Test Method Development

### *Samples*

Waste rock samples were taken from several mine sites in Australia and include unoxidized run-of-mine (ROM) material and partly oxidized waste rocks. Samples were homogenized, passed through a steel jaw crusher and dry sieved to obtain two different size fractions (<75 μm and <2 mm). A representative portion was pulverized in a chrome steel ring mill to produce a powdered sample of each particle size fraction. These were sent to external laboratories for full characterization using standard tests in order to gain a full understanding of the samples' mineralogical and geochemical properties. The samples used were:

- CMT-WRD1. This is a bulk sulfidic waste rock sample collected from the Mt Lyell Cu-Au mine, Tasmania. It had been subject to limited weathering (possibly months), since the waste was extracted from underground workings. It contains 21.1 % pyrite, 0.5 % chalcopyrite, 690 mg/kg Cu in the <75 μm fraction and 16.2 % pyrite, 0.5 % chalcopyrite and 360 mg/kg Cu in the <2 mm size fraction.
- CMT-ROM1. This is a bulk ROM sample collected from the Mt Lyell Cu-Au mine, Tasmania. The sample contains 5.9 % pyrite, 3.9 % chalcopyrite, 9660 mg/kg Cu in the <75 μm size fraction and 6.8 % pyrite, 3.3 % chalcopyrite and 9740 mg/kg Cu in the <2 mm size fraction.
- MB4K. This is a bulk sulfidic waste rock sample collected from the Mount Bischoff Sn mine, Tasmania. The sample contains 3.9 % pyrite, 15.8 % pyrrhotite, 39.3 % siderite and 410 mg/kg Cu (magnesite is not detected) in the <75 μm size fraction and 15.7 % pyrite, 35.1 % pyrrhotite, 14.9 % siderite, 11.8 % magnesite and 420 mg/kg Cu in the <2 mm size fraction.
- MB5K. This is a bulk sulfidic waste rock sample collected from the Mount Bischoff Sn mine, Tasmania. It contains 7 % pyrite, 15.1 % pyrrhotite, 23.4 % dolomite, 21.2 % siderite and 360 mg/kg Cu in the <75 μm size fraction and 9.8 % pyrite, 19.6 % pyrrhotite, 18.4 % dolomite, 29.9 % siderite and 470 mg/kg Cu in the <2 mm size fraction.
- OS4K. This is a bulk sulfidic waste rock sample collected from the historic Spray Pb-Zn mine, Tasmania. It has been subject to weathering (>90 years), since the waste was extracted from underground workings. The sample contains 1 % pyrite, 6.6 % sphalerite, 4.2 % galena, 2.7 % dolomite, 5.2 % Pb and 3.5 % Zn in the <75 μm size fraction and 1.7 % pyrite, 5.7 % sphalerite, 5.1 % galena, 3.2 % dolomite, >1 % Pb and >2 % Zn in the <2 mm size fraction.
- RG-WRD1. This is a bulk sulfidic waste rock sample collected from the historic Royal George Sn mine, Tasmania. It has been subject to weathering (>90 years) since the waste was extracted from underground workings. It contains 1.5 % pyrite, 0.3 % jarosite and 4270 mg/kg As in the <75 μm size fraction and 1.7 % pyrite, 0.2 % scorodite and 2980 mg/kg As in the <2 mm size fraction.
- CE-ROM. This is a bulk ROM sample collected from the Cadia East Cu-Au mine, New South Wales. It contains 1.8 % pyrite, 0.2 % chalcopyrite, 10.8 % calcite, 9100 mg/kg Cu in the <75 μm fraction and 0.7 % pyrite, 0.6 % chalcopyrite, 6.8 % calcite and 2410 mg/kg Cu in the <2 mm size fraction.
- CHOP-ROM. This is a bulk ROM sample collected from the Cadia Hill Cu-Au mine, New South Wales. It contains 1 % pyrite, 6.1 % calcite and 2740 ppm Cu in the <75 μm size fraction and 1 % pyrite, 4.6 % calcite and 1730 ppm Cu in the <2 mm size fraction.
- RDW-ROM. This is a bulk ROM sample collected from the Ridgeway Cu-Au mine, New South Wales. It contains 0.8 % pyrite, 1.8 % chalcopyrite, 9.9 % calcite, 0.4 % scorodite and 9130 mg/kg Cu in the <75 μm size fraction and 0.2 % pyrite, 0.9 % chalcopyrite, 7.8 % calcite, 0.6 % scorodite and 6240 mg/kg Cu in the <2 mm size fraction.

## *Pilot Testing of BCR® Method*

The first phase of method development was to perform the standardized three step BCR® extraction technique on the entire sample set to observe the response of the samples. After one addition of 30 % $H_2O_2$, it was immediately clear that the unmodified step 3 was not workable as a rapid test for sulfidic samples. The high sulfide content in some samples caused a vigorous and exothermic reaction, leading to extensive sample loss from the vials. The option of adding the $H_2O_2$ in small aliquots as suggested by the BCR® protocol was investigated, but the time period necessary to avoid sample loss for even small (<0.5 ml) would make the test too labor intensive and onerous. Hence, the concentration of $H_2O_2$ was reduced so that larger aliquot additions can be made.

## *Selecting an Appropriate $H_2O_2$ Concentration*

Concentrations of 15 and 5 % $H_2O_2$ were tested on samples which had previously produced a vigorous reaction with 30 % $H_2O_2$. Whilst 15 % $H_2O_2$ produced a vigorous reaction that had to be quenched, 5 % $H_2O_2$ was found to be suitable for rapid addition as two 5 ml aliquots. Although the addition of 10 ml of 5 % $H_2O_2$ to 1 g of MB4K, MB5K and CMT-WRD1 initiated an exothermic effervescent reaction, the sample mixture remained within the vial and the reaction did not cause sample loss. The recommendation is to follow step 3 of the BCR® extraction technique but modify the hydrogen peroxide concentration to 5 % $H_2O_2$.

## *Modification of BCR® Step 3 to Achieve Total Sulfide Oxidation*

The hypothesis was that successive aliquot additions of 10 ml 5 % $H_2O_2$ will induce oxidation of sulfide minerals within the sample, releasing metals into the liquid phase. The daily additions, followed by a heating and evaporation cycle as per Step 3 of the BCR® technique, were anticipated to cease when adding hydrogen peroxide to the sample no longer caused effervescence indicating the destruction of the sulfide minerals.

Step 1 and 2 of the BCR® sequential extraction proceeded as stipulated in the method (Rauret et al. 1999) with minor changes to allow for use of equipment available in the laboratory. In the modified step 3, 5 % $H_2O_2$ was added to the sample in 2 × 5 ml aliquots. The response of each sample was recorded and photographed. The reaction proceeded for 1 h at ambient laboratory temperature (20 °C) and 1 h at 85 °C in a covered water bath, the temperature was then raised to

maximum (99 °C), the water bath was uncovered and the samples were heated until the volume of the liquid in the vials was reduced to <3 ml.

After 18 cycles this phase of test development was halted, without achieving the anticipated end-point of cessation of effervescence on addition of hydrogen peroxide. Samples were indeed oxidizing, with an orange precipitate likely to be iron hydroxides and oxyhydroxides developing in several samples. The precipitate was particularly evident in samples MB4K and MB5K, which have elevated pyrite (3.9 and 15.7 % respectively), pyrrhotite (15.8 and 35.1 %) and siderite (39.3 and 14.9 %) but also in sample CMT-WRD1 which is very high in pyrite (21.1 %). Observations indicated that samples CMT-WRD1 and CMT-ROM1 were still reacting after 18 cycles. The destruction of sulfides in the sample by roasting at high temperature to reduce the vigour of the subsequent reaction with $H_2O_2$ was then attempted.

## *Roasting to Achieve Sulfide Oxidation*

Samples were roasted in an attempt to achieve sulfide oxidation. Thermal decomposition temperatures of sulfides vary from 400 to 800 °C and samples have been reported to oxidize within minutes depending on sulfide mineralogy and roasting temperature. Two trial samples were selected for their high (CMT-WRD1) and low (CH-OP ROM) sulfide content. BCR® steps 1 and 2 were performed on 5 replicates of each sample. Following the rinse and decant stage for BCR® step 2, a composite was made of the five replicates for each samples. After drying until no further weight loss the samples were lightly dis-aggregated using a spatula and roasted in a ceramic crucible at 600 °C for 20 min.

1 g of each roasted sample was accurately (3 dp) weighed into 50 ml PP (polypropylene) vials ready for extraction using step 3 of the un-modified BCR® procedure. As the addition of very small aliquots is prohibitively time consuming, the intention was to add 2 × 5 ml of 30 % $H_2O_2$ to the vials. Three minutes after addition of 5 ml 30 % $H_2O_2$, the vial containing CMT-WRD1 began to effervesce and fume furiously and had to be brought under control by the addition of 2 × 5 ml of DIW. Hence, the recommendation is to use conical beakers as the reaction vessels in place of the smaller vials; these allow more head space and liquor surface area during the reaction period.

## *Modification Inspired by the Sequential NAG Test*

The sequential NAG test method uses 500 ml conical beakers as the vessel in which 2.5 g of sample is reacted with 250 ml of 15 % $H_2O_2$ (Smart et al. 2002). This approach was adapted for use in the bioaccessibility test by using 250 ml conical beakers. However, the sample mass of 1 g, $H_2O_2$ concentration of 30 %, solid to liquid ratios of 1:10 (wt/vol) and temperatures used in the BCR® step 3 were retained.

Although still reacting vigorously, the CMT-WRD1 sample mixture remained within the conical beaker and sample loss did not occur. An additional benefit to using conical beakers is that for sulfidic samples, which react rapidly and vigorously with the $H_2O_2$, the objective of heating the samples in the water bath becomes the reduction of the liquor volume to <3 ml, rather than a step to increase the rate of reaction between the $H_2O_2$ and the sample. This happens far more efficiently (approximately 5 times more quickly) in the 250 ml conical beakers than in the 50 ml vials both due to the increased surface area and the fact that the temperature of the water bath can be set to maximum more quickly.

## *Learnings from the Bioaccessibility Test Method Development*

The learnings from observations and experience gained during method development work for the bioaccessibility test are summarized in Table 1. They emphasize the importance of both successful and not-successful results in the development of a new technique. The final recommended design for the bioaccessibility test, detailed

**Table 1** Summary of learnings from method development of the plant bioaccessibility test

| Objective | Solution trialed | Learnings |
|---|---|---|
| Identify a technique that can extract plant bioaccessible metals from a sulfidic or mineralized sample in a rapid, inexpensive and reproducible manner | BCR® three step extraction scheme | The tiny additions required to avoid the violent reaction of the sample with 30 % $H_2O_2$ in step 3 made the unmodified method too laborious and onerous |
| Reduce the concentration of $H_2O_2$ to a level at which the addition of larger aliquots is possible without violent reaction | Concentrations of 15 % and 5 % $H_2O_2$ in a single 10 ml addition | On samples MB4K, MB5K and CMT-WRD1 an exothermic effervescent reaction was observed with 5 % $H_2O_2$ but there was no sample loss |
| Achieve total oxidation of the susceptible sulfide minerals using repeated additions of 5 % $H_2O_2$ | Daily additions of 5 % $H_2O_2$ were made to the samples followed by a heating and evaporation cycle | After 18 cycles the samples were still reacting with the $H_2O_2$. An alternative way to achieve total oxidation of the susceptible sulfide minerals was required |
| Achieve sulfide oxidation by roasting | A high and low sulfide sample were roasted at 600 °C for 20 min. They were then subject ed to step 3 of the BCR® extraction | The reaction with 30 % $H_2O_2$ was still to vigorous and there was sample loss from the vials |
| Use a reaction vessel with a larger volume | 250 ml conical beakers were used as the reaction vessels in order to allow more head space and liquor surface area | Reaction with 30 % $H_2O_2$ added in one 10 ml aliquot was possible without sample loss. Quicker evaporation was an additional benefit of using this apparatus |

in the next section, incorporates reagent concentrations, solid to liquid ratios and heating and evaporation cycles specified in step 3 of the Standards, Measurements and Testing Programe (formally BCR) three step sequential extraction procedure (Rauret et al. 1999) whilst the apparatus is inspired by the protocol for the sequential NAG test (Smart et al. 2002).

## Test Method Design

### *Aspects of the BCR® Sequential Extraction Procedure*

The sample mass (1 g) and solution volume (10 ml) recommended in the bioaccessibility test are the same as those specified in Step 3 of the BCR® procedure (Rauret et al. 1999). Both are smaller than the 2.5 g and 250 ml used in the sequential NAG test. This will reduce costs, environmental impact and the time necessary for evaporation.

The concentration of the $H_2O_2$ solution is 30 %; the same as is recommended in the BCR® procedure. The BCR® method specifies that the $H_2O_2$ solution should be used as supplied, i.e. 30 % and acid stabilized. The $H_2O_2$ used in the test development was Perdrogen® (30 % $H_2O_2$) that is acid stabilized with 40 mg $l^{-1}$ dipicolin acid. This is in contrast to the single and sequential NAG method which specifies that the pH of the $H_2O_2$ must be re-adjusted to pH 4.5–6 with NaOH and that the concentration must be reduced to 15 %. The rationale for using the solution as supplied by the manufacturer is that the bioaccessibility test aims to measure the concentration of metals that have been liberated from solid phases and the low pH of the acid stabilized $H_2O_2$ solution will ensure the metals stay in solution. The rationale for using the higher concentration is to maximize oxidation of sulfides in the sample.

The recommended temperature of the $H_2O_2$ for use in the bioaccessibility test is approximately 5 °C, i.e. straight from the refrigerator. This is in contrast to the recommendation in the sequential NAG that the $H_2O_2$ solution should be at room temperature. No specific instruction is given as to the temperature of the hydrogen peroxide solution in the BCR® methodology. The rationale behind using a temperature of 5 °C is: (a) minimal decomposition of $H_2O_2$ due to time spent out of the refrigerator; (b) reaction kinetics are not being monitored in the bioaccessibility test; (c) the temperature of the liquor will rise upon exothermic oxidation of any sulfides in the sample; (d) standardization of the test is facilitated if less steps (e.g. allowing the $H_2O_2$ to come to room temperature) are required.

In the BCR® procedure, ammonium acetate solution is shaken with the sample residue for 16 h to prevent re-adsorption or precipitation of the released metals following oxidation with $H_2O_2$. This approach is also recommended in the bioaccessibility test to target metals released into solution (Rao et al. 2008). The BCR® method specifies that the extract should be separated from the solid residue by

centrifuging at 3000*g* for 20 min and decanting the supernatant. The bioaccessibility test recommends that centrifuging is done at 2700*g* due to equipment availability. If a centrifuge is not available filtration of the sample to <0.45 μm may be appropriate.

## *Aspects of the Single and Sequential Net Acid Generation (NAG) Tests*

The single and sequential NAG tests use a 500 ml conical beaker as the reaction vessel with a watchglass placed on top of the vessel. The recommendation for the new bioaccessibility test is to use a 250 ml conical beaker as a reaction vessel with a watch glass placed on top if necessary. The reason for the smaller flask volume is the fact that the recommended solution volume in the bioaccessibility test is much smaller (10 ml) than in the NAG tests (250 ml) and smaller flasks allow higher sample throughput.

## *Operational Experience*

The sequential NAG test recommends samples are reacted with 15 % $H_2O_2$ for approximately 2 h at room temperature, or until "boiling" or effervescence ceases, the beaker is then heated on a hot plate at a temperature of 150–200 °C for 1.5 h and the sample volume is maintained by the addition of de-ionized water (Smart et al. 2002). The BCR® procedure recommends that samples are reacted for 1 h at room temperature with 30 % $H_2O_2$ followed by 1 h at 85 °C in a water bath, the volume is then reduced to <3 ml by heating the uncovered tube (Rauret et al. 1999). Operational experience using mine site samples indicates that high sulfide samples, (e.g. CMT-WRD1, 21.1 % pyrite) react violently and quickly (<5 min, vigorous reaction) with 30 % $H_2O_2$ at room temperature and that on heating there is no further reaction.

Samples that are rich in organic matter may react more slowly with 30 % $H_2O_2$ at room temperature with further effervescence upon heating in a water bath. However, this is not relevant for sulfidic and mineralized rocks and wastes, which are unlikely to be high in organic matter. If fast reacting sulfides are present in the sample, the $H_2O_2$ will be consumed within an hour. In the new bioaccessibility test it is therefore recommended that samples are reacted with 10 ml of $H_2O_2$ for up to 1 hour at room temperature, or until effervescence ceases if this is sooner.

The single NAG test is recommended for samples with low total sulfide sulfur contents (<ca. 1.5 % S) and with low concentrations of metals such as copper which can catalyze the decomposition of $H_2O_2$. For NAG testing of samples with higher sulfide contents, this limitation is overcome by applying a sequential NAG; a

multi stage process with repeated cycles of $H_2O_2$ addition followed by heating and filtration until either there is no further catalytic decomposition of $H_2O_2$ or the NAGpH is greater than pH 4.5. Operational experience with repeated additions to high sulfide samples (e.g. 21.1 % pyrite) showed that the endpoint of no further catalytic decomposition of $H_2O_2$ was not achieved after the cyclic addition and evaporation of 18 × 10 ml of 5 % $H_2O_2$. Although, observational evidence for sulfide oxidation was clear from the colour change of the sample. Likewise, the same sample continued to react after 12 cyclic addition and evaporations of 10 ml of 30 % $H_2O_2$. Determining the pH of the sample was not considered a suitable endpoint for the new bioaccessibility test, because it could introduce between-sample contamination with the elements of interest.

An operationally defined limit of three cycles of addition and evaporation of $H_2O_2$ is recommended for the new bioaccessibility test. This will allow a comparison of the relative bioaccessibility of metals released into pore-water upon incipient sulfide oxidation.

The single NAG test is not recommended for use on high Cu samples due to the potential for catalytic decomposition of $H_2O_2$ by this metal. The solution suggested by Smart et al. (2002) is to use the sequential NAG test, aspects of which are already incorporated into the new bioaccessibility test. However, it is interesting to note that any catalyzed decomposition of $H_2O_2$ during the method development for the bioaccessibility test was not attributable to the high Cu content of the sample. Two samples with similar elevated Cu concentrations responded in a very different way to the additions. The response of CE-ROM (1.8 % pyrite, 9100 ppm Cu) decreased with repeated additions until the main response was observed only on heating. However, sample CMT-ROM1 (5.9 % pyrite, 9660 ppm Cu) continued to react vigorously at room temperature after 18 additions of 10 ml 5 % $H_2O_2$.

The fast reacting sulfides induce a vigorous reaction with 30 % $H_2O_2$ within 10 min at room temperature. The purpose of heating the sample is therefore to decompose any $H_2O_2$ remaining in the sample and to evaporate to a volume of <3 ml (or <1 ml on the final cycle) rather than to induce any further oxidation of the samples. The recommendation for the new bioaccessibility test is that the samples should be heated in an uncovered water bath set at its maximum temperature to reduce sample volume by evaporation at a temperature of ca. 90–99 °C. The lower temperature recommended in the BCR® technique of 85 °C leads to long evaporation times and the higher temperature recommended in the sequential NAG of heating on a hotplate at a temperature of 150–200 °C may lead to a greater loss of volatile elements of interest such as As, Hg, Sb and Tl. The loss of volatile elements such as these remains a potential limitation of the recommended technique. However, the use of the water bath for evaporation of the samples is more standardized and will therefore produce more reproducible results than heating on a hot plate. Evaporation of volatile elements may also occur during the vigorous "boiling" that occurs during the reaction between the sample and $H_2O_2$ at room temperature, this is a potential limitation of the technique.

### *Sample Preparation*

In common with NAG tests (Smart et al. 2002) the bioaccessibility test can be performed on drill core, blast rock samples and blast hole cuttings. Large samples of rock are crushed to a nominal size of 4 mm and a representative sub-sample taken. The sub-sample is then sieved to a grain size of <2 mm. Unlike the NAG test, the new bioaccessibility test should be performed on sieved samples because grinding will greatly affect, and potentially exaggerate, metal extractability.

### *Reagents*

The hydrogen peroxide solution ($H_2O_2$) should be Analar Analytical Reagent grade $H_2O_2$ 30 % w/v and used as supplied (i.e. acid stabilized). A suitable product is Perdrogen® 30 % $H_2O_2$ puriss, p.a., reag. Ph.. The ammonium acetate solution ($NH_4C_2H_3O_2$) is 1.0 mol $L^{-1}$ and should be acid stabilized to pH 2 using concentrated nitric acid. 18 MΩ de-ionized water should be used to prepare the reagents.

## Protocol for a New Plant Bioaccessibility Test for Mineralized and Sulfidic Rocks

(a) Homogenize the <2 mm particulate sample for 5 min, then accurately (3 dp) weigh a 1 g aliquot into a 250 ml conical beaker.
(b) Add 10 ml of 30 % $H_2O_2$ to the conical beaker in a fume hood. The hydrogen peroxide should be used straight from the refrigerator.
(c) Leave the beaker in the fume hood and if necessary place a watch glass over the top of the beaker. Exercise caution as the mixture may react vigorously and exothermically.
(d) Allow the sample to react at room temperature for approximately 1 h or until "boiling" or effervescence ceases, if this is sooner.
(e) Place beaker in a water bath at maximum temperature in a fume cupboard and heat until the volume is reduced to <3 ml.
(f) Cool the sample to room temperature. Stage 1 of the test has been completed.
(g) Repeat steps "b" to "f" in the same vessel using the residue from Stage 1. This is called Stage 2
(h) Repeat steps "b" to "e" in the same vessel using the residue from Stage 2, but continue to reduce the volume to <1 ml before cooling. This is called Stage 3.
(i) Add 50 ml of ammonium acetate solution to the cool, moist residue in the conical beaker. Cover conical beaker with e.g. parafilm.
(j) Shake immediately for 16 h (overnight) on an orbital shaker.

(k) Separate by centrifugation (2700*g* for 20 min) and retain the resulting bioaccessibility liquor for metal and metalloid analysis using ICP-MS/ICP-O(A)ES techniques.

A flow chart for this procedure for the new test designed to determine the bioaccessibility of metals and metalloids in sulfidic and mineralized rock samples is outlined in Fig. 1.

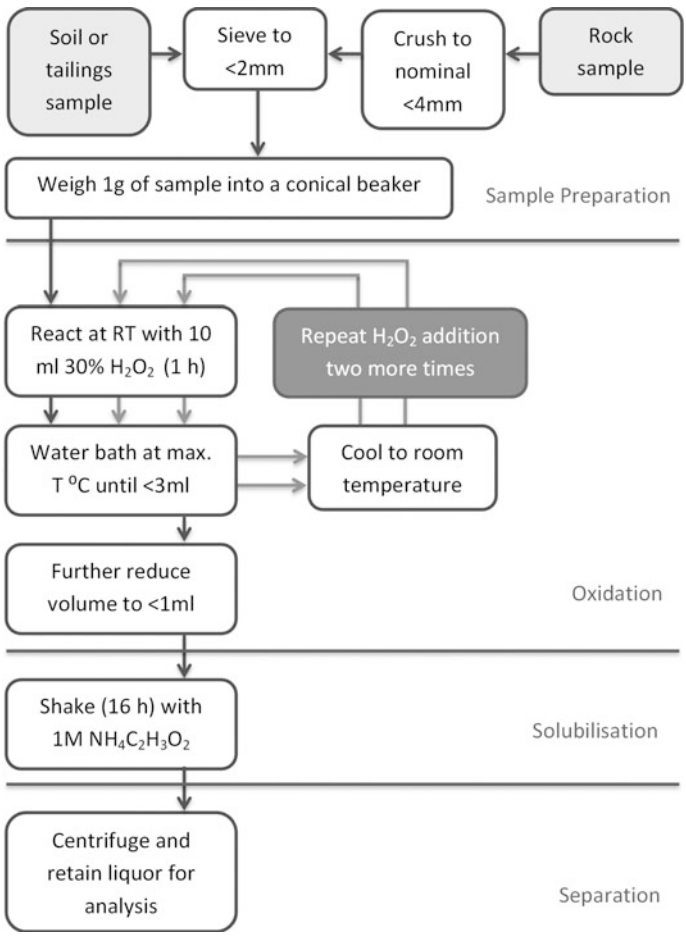


**Fig. 1** Flowchart for the plant bioaccessibility test. *RT* room temperature

## Conclusions

Information on contaminant bioaccessibility to plants is important to predict the environmental impact of wastes at mine sites and allow appropriate risk assessments to be designed. Current methods used in environmental and agricultural science to predict plant bioaccessibility include: (a) sequential extractions (e.g. Rauret et al. 1999; Tessier et al. 1979), which can be lengthy to perform; and (b) weak single solution extractions (e.g. Houba et al. 1996; Pueyo et al. 2004), which do not access metals and metalloids bound in the sulfide fraction. A new rapid, reliable and inexpensive test for the bioaccessibility of metals and metalloids in sulfidic mine wastes is required to predict the release of these contaminants upon oxidation. This will enable better risk assessment and waste management at an early stage of mine life development.

The new bioaccessibility test method proposed here includes: (1) aspects of the BCR® extraction scheme; (2) aspects of the sequential NAG test; and (3) aspects from operational experience extracting sulfidic rocks and wastes. The new test is performed on 1 g of <2 mm air dried particulate sample in a 250 ml conical beaker. To oxidize the samples, 3 × 10 ml additions of 30 % $H_2O_2$ are made. Each addition is followed by an evaporation and cooling cycle. To solubilize the metals and metalloids released following oxidation, 50 ml of acidified 1 mol $L^{-1}$ ammonium acetate solution is added to the cool, moist residue. The sample is shaken for 16 h and then centrifuged to separate the solid and liquid fractions. The resulting bioaccessibility liquor is then analyzed for metals and metalloids using ICP-MS/ICP-O(A)ES techniques.

Use of the new bioaccessibility test should be restricted to sulfidic wastes, rocks and mine soils. The test provides one tool that should be used as part of a suite of tests to enable an improved risk assessment of these mine site materials. A consideration of plant bioaccessibility of potentially toxic trace elements at mine sites should also include a consideration of the native and/or introduced plant species present at the site. Their tolerance to potentially toxic trace elements and their tendency to exclude or accumulate these elements will impact upon the transport of these elements into the biosphere. The new test is not suitable for samples that are high in organic matter or for samples where the mineral assemblage or preliminary testing indicates that the elements of concern are primarily associated with the reducible fraction. Whilst the test is operationally defined and cannot predict what fraction of the elements of interest will be taken up by plant material, it can be used to classify wastes in terms of the plant bioaccessibility of any potentially toxic elements they contain.

## References

Amos RT, Blowes DW, Bailey BL, Sego DC, Smith L, Ritchie AIM (2015) Waste-rock hydrogeology and geochemistry. Appl Geochem 57:140–156

Bryan GW, Langston W (1992) Bioavailability, accumulation and effects of heavy metals in sediments with special reference to United Kingdon estuaries: a review. Environ Pollut 76:89–131

Cave MR, Wragg J, Palumbo B, Klinck BA (2003) Measurement of the bioaccessibility of arsenic in UK soils, Environment Agency and the British Geological Survey

Gonzaga MIS, Ma LQ, Pacheco EP, dos Santos WM (2012) Predicting arsenic bioavailability to hyperaccumulator *Pteris Vittata* in arsenic-contaminated soils. Int J Phytorem 14:939–949

Houba VJG, Lexmond TM, Novozamsky I, van der Lee JJ (1996) State of the art and future developments in soil analysis for bioavailability assessment. Sci Total Environ 178:21–28

Lacal J, da Silva MP, García R, Sevilla MT, Procopio JR, Hernandez L (2003) Study of fractionation and potential mobility of metal in sludge from pyrite mining and affected river sediments: changes in mobility over time and use of artificial ageing as a tool in environmental impact assessment. Environ Pollut 124: 291–305

Lottermoser BG, Glass HJ, Page CN (2011) Sustainable natural remediation of abandoned tailings by metal-excluding heather (*Calluna vulgaris*) and gorse (*Ulex europaeus*), Carnon Valley, Cornwall, UK. Ecol Eng 37:1249–1253

Parbhakar-Fox A, Lottermoser BG (2015) A critical review of acid rock drainage processes and practices. Miner Eng 82:107–124

Pérez-López R, Álvarez-Valero AM, Nieto JM, Sáez R, Matos JX (2008) Use of sequential extraction procedure for assessing the environmental impact at regional scale of the São Domingos Mine (Iberian Pyrite Belt). Appl Geochem 23:3452–3463

Pueyo M, López-Sánchez JF, Rauret G (2004) Assessment of $CaCl_2$, $NaNO_3$ and $NH_4NO_3$ extraction procedures for the study of Cd, Cu, Pb and Zn extractability in contaminated soils. Anal Chimica Acta 504:217–226

Quispe D, Pérez-López R, Acero P, Ayora C, Nieto JM, Tucoulou R (2013) Formation of a hardpan in the co-disposal of fly ash and sulfide mine tailings and its influence on the gen-eration of acid mine drainage. Chem Geol 355:45–55

Rao C, Sahuquillo A, Sanchez JL (2008) A review of the different methods applied in environmental geochemistry for single and sequential extraction of trace elements in soils and related materials. Water Air Soil Pollut 189:291–333

Rauret G, Lopez-Sanchez JF, Sahuquillo A, Rubio R, Davidson C, Ure A, Quevauviller P (1999) Improvement of the BCR® three step sequential extraction procedure prior to the certification of new sediment and soil reference materials. J Environ Monit 1:57–61

Ruby MV, Davis A, Schoof R, Eberle S, Sellstone CM (1996) Estimation of lead and arsenic bioavailability using a physiologically based extraction test. Environ Sci Technol 30:422–430

Schaider LA, Senn DB, Brabander DJ, McCarthy KD, Shine JP (2007) Characterization of zinc, lead, and cadmium in mine waste: implications for transport, exposure, and bioavailability. Environ Sci Technol 41:4164–4171

Semple KT, Doick KJ, Jones KC, Burauel P, Craven A, Harms H (2004) Defining bioavailability and bioaccessibility of contaminated soil and sediment is complicated. Environ Sci Technol 38:228A–231A

Smart R, Skinner WM, Levay G, Gerson AR, Thomas JE, Sobieraj H, Schumann R, Weisener C, Weber P, Miller S, Stewart WA (2002) ARD test handbook: Project P387, a prediction and kinetic control of acid mine drainage. AMIRA, International Ltd, Ian Wark Research Institute, Melbourne, Australia

Sracek O, Mihaljevič M, Kříbek B, Majer V, Filip J, Vaněk A, Mapani B (2014) Geochemistry of mine tailings and behavior of arsenic at Kombat, northeastern Namibia. Environ Monit Assess 186:4891–4903

Templeton DM, Ariese F, Cornelis R, Danielsson LG, Muntau H, van Leeuwen HP, Lobinski R (2000) Guidelines for terms related to chemical speciation and fractionation of elements. Definitions, structural aspects, and methodological approaches (IUPAC Recommendations 2000). Pure Appl Chem 72:1453–1470

Tessier A, Campbell PGC, Bisson M (1979) Sequential extraction procedure for the speciation of particulate trace-metals. Anal Chem 51:844–851

# Predicting Plant Metal Bioaccessibility at the Historic Wheal Maid Tailings Lagoons, Cornwall, UK

**Eleanor M. van Veen, Bernd Lottermoser, Anita Parbhakar-Fox and Julie Hunt**

**Abstract** Abandoned mine sites with their metal-rich substrates pose significant challenges to naturally colonizing plants. In this study, the abandoned Sn-Cu tailings lagoons at Wheal Maid (Cornwall, UK) have been investigated to establish the bioaccessibility of metals and metalloids (As, Cd, Cu, Pb, Sb, Zn) in exposed tailings and wastes using a new plant bioaccessibility test. Four main substrate types were sampled: (1) mine waste used to construct the lagoons, a relatively uncontaminated material with variable particle size; (2) granular capping material used in the upper lagoon to cover the tailings and relatively uncontaminated; (3) grey tailings a fine to medium grained material with visible sulfides and white secondary salts, extremely high in near-total Zn concentrations; and (4) marbled tailings a fine grained brown/red/yellow material with extremely high near-total As concentrations. The analytical quality of results produced by a new plant bioaccessibility test was monitored using blanks, spiked solutions and repeat analyses. The grey tailings had the highest bioaccessible metal and metalloid content. As this material oxidizes, it will release As, Cd, Cu, Sb, Zn and to a lesser extent Pb in a form which will be more available to plants. This will inevitably delay re-vegetation at the site. The new bioaccessibility test is recommended for sulfidic rocks and waste samples and

E.M. van Veen (✉)
Environment and Sustainability Institute/Camborne School of Mines, University of Exeter, Penryn Campus, Penryn, Cornwall TR10 9FE, UK
e-mail: E.M.Van-Veen@exeter.ac.uk

B. Lottermoser
Institute of Mineral Resources Engineering, RWTH Aachen University, Wüllnerstrasse 2, 52062 Aachen, Germany
e-mail: lottermoser@mre.rwth-aachen.de

A. Parbhakar-Fox
School of Physical Sciences, University of Tasmania, Private Bag 79, Hobart, TAS 7001, Australia
e-mail: Anita.Parbhakar@utas.edu.au

J. Hunt
GeMMe, University of Liege, Sart Tilman B52, 4000 Liège, Belgium
e-mail: jahunt@ulg.ac.be



B. Lottermoser (ed.), *Environmental Indicators in Metal Mining*,
DOI 10.1007/978-3-319-42731-7_22

should be employed at an early mine-life stage to allow appropriate waste classification and improve mine closure outcomes.

## Introduction

Abandoned mine sites undergo natural colonization by plants (Lottermoser, 2011; Jiménez 2011). Establishment of a sustainable post-mining vegetation is essential for successful mine site rehabilitation and should be planned for at an early mine-life stage. To predict re-vegetation processes and challenges a thorough knowledge of the substrate is required. Characterization of the bioaccessibility of potentially toxic trace elements in mine site substrates provides useful data to help forecast re-colonization. This can be achieved using sequential extraction tests to define the geochemical fractionation of these elements (e.g. Al-Abed et al. 2006; Dold 2003; Khorasanipour et al. 2011). However these tests are lengthy and therefore expensive to preform, prohibiting their routine application. This study presents the results of a case study using a new test to determine the plant bioaccessibility of trace elements in sulfidic wastes and rocks. The test is rapid, repeatable and inexpensive. It can be used to obtain operational plant bioaccessibility data for mine site samples on a routine basis. This will improve environmental risk assessments and hence waste management plans and mine closure outcomes at these sites.

## The Wheal Maid Site

### *Location and Physiography*

The Wheal Maid site is located in the Gwennap Mining district and forms part of the Cornwall and West Devon Mining Landscape, which has been on the UNESCO world heritage list since 2006. The Gwennap Mining district is one of the most intensively mined in the Cornwall and Devon Sn and Cu mining province. During the 18th and 19th century this was the richest mining district in Cornwall and was referred to by contemporary writers as “the richest square mile to be found anywhere on the earth” (Cornish Mining 2015).

Approximately 10 km northwest of Falmouth, the site has its center at 50°14′14.61″N and 5°9′37.85″W. The site comprises two lagoons which are bordered by a path which runs around the perimeter of the site. The western lagoon is referred to as the upper lagoon and has some vegetation cover and some standing water (Fig. 1). The eastern lagoon is referred to as the lower lagoon, this has no vegetation and the standing water is a striking orange colour (Fig. 2) due to the Fe oxides present in the water.

**Fig. 1** Granular capping at the upper Wheal Maid tailings lagoon, with evidence of some re-vegetation (foreground) and mine waste used to construct the lagoons (beyond the standing water, middle distance) (color figure online)

**Fig. 2** Marbled tailings (foreground) and standing water at the lower Wheal Maid tailings lagoon (color figure online)

## Geology

Mineralization in this area is largely hosted by a series of upper Devonian metamorphosed sediments (dominantly shales) known locally as "killas". Deformation of the sediments occurred prior to and during the period of granite intrusion with later minor deformation. The major period of deformation took place during the Variscan orogeny (mountain building) and in the later part of this orogeny the granites were intruded with associated tin and copper mineralization, forming the Cornubain Orefield which covers the whole of the county of Cornwall and part of the county of Devon (Camm and Hedley 2005).

Most of the tailings in the lagoons were deposited as waste from the nearby Mount Wellington mine during the late 1970s (Freeborn 2006). The mineralogy of the lodes exploited by this mine is therefore relevant when evaluating the environmental impact of those wastes decades later. The Mount Wellington mine lies approximately 2 km south east of the Wheal Maid site, approximately 3 and 4 km from the nearest outcrops of the Carnmarth and Carmenellis granites. Kettaneh and Badham (1978) detailed the mineralization and paragenesis at the Mount Wellington Mine at a time when the mine was still operational. They highlight six lodes in the mine; numbers 1, 2 and 3 and the Wheal Andrew, the Trenares and the Hot lodes. The main lodes were numbers 1, 2 and 3 which produced Sn, Cu and Zn concentrates and contained Fe, Zn, Sn, As, Cu, Ti and lesser Pb, Ag, Au, W, Bi and Sb. The mineralization in these three lodes was very similar and the bulk of mineralization is accounted for by two main phases. Initially following emplacement and cooling of the intrusion, extensive fracturing permitted the introduction of mineralizing fluids in phase A; these fluids precipitated considerable amounts of quartz, tourmaline and cassiterite with minor amounts of wolframite. Renewed movements in the fractures permitted the introduction of phase B where quartz, chlorite and sulfides are abundant. No cassiterite was introduced and there is therefore a dilution of the tin grade in this phase. During phase B, chlorite, quartz, pyrrhotite, arsenopyrite and chalcopyrite were the first minerals precipitate. These were followed by more quartz with sphalerite (containing exsolved chalcopyrite), rutile, minor galena and probably small grains of gold. The phase ended with the precipitation of large amounts of pyrite which overgrew earlier minerals and cemented the rock. It is unclear when the secondary marcasite and covellite observed in this association formed.

## Climate and Vegetation

The local climate is influenced by its position on the southwest peninsular which forms the most southerly part of the British Isles. There is strong maritime control of temperatures and annual averages are close to the surrounding sea temperatures at 11–12 °C. Frost frequency is highly variable and the region has a reputation for

mildness. Rainfall totals are approximately 900–1000 mm and the area is prone to rare but heavy rainfall events lasting from 5 to 15 h (Met Office 2015).

Plant cover around the site is patchy and the extent of re-vegetation of the upper and lower lagoons is very different. Very little re-vegetation has occurred over the lower lagoon, there is no vegetation present on the exposed grey or marble tailings although some *Calluna vulgaris* (heather) has begun to colonize the periphery. This is in contrast to the granular capping of the upper lagoon which was seeded in the 1980s. The area of the upper lagoon which is slightly elevated and distant from the standing water appears to have benefited from the remedial measures and shows a variety of vegetation. Colonizers at the site occur mainly at the margins of the mine waste constructed paths around the lagoons and include predominantly *Calluna vulgaris* (heather) and *Ulex europaeus* (gorse) which have the ability to exclude metals and arsenic from their above ground biomass (Lottermoser et al. 2011) and are often found at abandoned mine sites because of this. Outside the perimeter path of the lagoons grow *Pinus radiata* (Monterey Pine) trees, a native of rocky headlands and islands on the Pacific coast of California. This salt tolerant tree is often planted as an amenity or shelter plant and has the ability to tolerate harsh conditions. There are records of them being planted at the nearby United Mines, St. Day in the early 1980s (CC 2015) and it is likely that these larger specimens date from that period. In addition to trees that have likely been planted, there are some younger plants that may well have self-seeded.

## *Site History*

The tailings lagoons were built in two separate construction phases between 1976 and 1981 and contain approximately 220,000 $m^3$ of fine grained mineral processing waste. The downstream and intermediate embankments were constructed during the first stage between 1976 and 1978 whilst the land was under the ownership of Cornwall Tin and Mining Ltd. This mining company used the site to dispose of mill tailings from the nearby Mount Wellington mine by pumping them along the valley in slurry form. Part of phase one also involved diverting the Wheal Maid stream into a 1200 mm concrete pipe which ran beneath the depository for approximately 440 m. After Billiton Minerals purchased the surface plant at Mount Wellington mine and the Wheal Maid tailings dams in 1979, an upstream embankment and a further 396 m of culvert were constructed. Material from the downstream dam, along with other material from the Carnon Valley, were reprocessed, and the reworked deposits were pumped into the upstream dam. Mount Wellington mine closed in 1981. In 1982 Carnon Consolidated Tin Mines Ltd. purchased Billiton's interest including the Wheal Maid site and no further waste was deposited in the dams. An attempt was made at the time to prevent wind-blown dust by trial seeding of the upper dam, which was partially successful with the growth of a variety of vegetation across the dam surface (Freeborn 2006; Gwennap 2015).

Gwennap Council now owns the site (CDC 2008), having purchased the site in 2002 for £1 from Carnon Enterprises. There is no right of access onto the site, although it is freely accessible via a footpath on the western boundary and a section of the mineral tramway footpath runs along the southern boundary. The site is regularly used by walkers, mountain bikers and horse riders, also on occasion by motorcyclists and four wheel drive vehicles, although this is not permitted. In 2013 a section of the perimeter formed part of the course for the British Cycling National Cross Country MTB competition.

## *Previous Investigations*

A record of determination of the Wheal Maid tailings lagoons as contaminated land was made by Carrick District Council in 2008 (CDC 2008) due to the risk of significant harm to young children using the site and the risk of pollution of controlled water through leaching of potentially toxic trace metals and metalloids (As, Cd, Cu, Cr, Fe, Pb, Ni and Zn). The evidence on which the determination was based is detailed in the record of determination (CDC 2008) and includes: (a) monitoring data from the Environment Agency suggesting the site could be causing a failure of Environmental Quality Standards (EQSs) in the St. Day Stream; (b) a desk study to establish a conceptual model for the site; and (c) an intrusive investigation carried out in 2007 which undertook soil, groundwater and surface water sampling and analysis. The four main soil samples identified during the intrusive investigation were:

1. Mine Waste (MW). This material was used in the construction of the dams and is located around the perimeter of the lagoons. It is a granular material with a variable particle size (Fig. 1).
2. Granular Capping (GC). This material was used in the upper lagoon to cover the tailings; some of it was subsequently seeded in an attempt to remediate the land (Fig. 2).
3. Marbled Tailings (MT). This material was located around the lower lagoon. It is a fine grained brown/red/yellow material (Fig. 2).
4. Grey Tailings (GT). This material was located at one end of the lower lagoon. It is a fine to medium grained material (Fig. 3). Grains of sulfide material can be seen by eye and there are white effervescent salts evident on the surface of the material in some places.

Variable high metal and metalloid concentrations were reported for all four materials (CDC 2008). A water leachate test showed that the proportion of metals and metalloids in the four materials upon a heavy rainfall event was very different. Leach testing of the grey tailings showed that there was a high leaching potential for As, Cd, Cu, Pb, Ni and Zn, and a likelihood that the exposure, erosion and weathering of the pyritic grey tailings in the lower lagoon contribute to the very poor, acidic water

**Fig. 3** Grey tailings at the lower Wheal Maid tailings lagoon (color figure online)

quality within the lower lagoon and the St. Day Stream, to which seepage occurs at the lower end of the retaining dam. The leachable metals in the mine waste and granular capping material were generally Cu and Zn with some Cr. In the marbled tailings, As concentrations were high, however As did not appear to be readily leached. Cu and Zn did leach from the marbled tailings but to a lesser extent than from the other materials on the site. Of the four materials, the grey tailings were considered to pose the most significant contamination risk (CDC 2008).

## Mineralogy and Geochemistry

Forty one bulk surface samples (ca. 500 g) were collected from the Wheal Maid site. These were grouped by the four different sample types: mine waste (MW), grey tailings (GT), marbled tailings (MT), and granular capping (GC). Samples were dried and sieved to <2 mm. At ALS laboratories, the samples were subsequently pulverized to 85 % <75 µm, aliquots of the sample were then digested with perchloric, nitric, hydrofluoric and hydrochloric acid and analyzed using ICP-AES. Analysis included replicate analyses of the NIST 2710a Montana soil I standard reference material, for which the relative standard deviations of analysis were <5 % and recoveries were in the range 90–110 %. The mean geochemistry (± standard

deviation) for the major and environmentally relevant trace elements was calculated for each of the four main soil types and is given in Table 1 below.

Concentrations of As are particularly high in the marbled tailing samples. Positive correlation coefficients of the log normalized Fe and S concentrations suggest that arsenopyrite (FeAsS) is the source of these elevated concentrations. Copper is elevated in both the granular capping and grey tailings. Cu correlates well with S and Zn in the granular capping. This possibly indicates an association between sphalerite and chalcopyrite as was suggested by Kettaneh and Badham (1978). There is no obvious single mineral responsible for Cu in the grey tailings; when all the samples are considered the only correlation observed is between Cu and In. However, when only the five high copper grey tailing samples are considered, correlations with Zn and Cd but also to a lesser extend Pb and S become more important. This also possibly supports the sphalerite/chalcopyrite association suggested by Kettaneh and Badham (1978). The Zn in the grey tailings correlates only with Cd when all samples are considered, however, if only the five samples with the highest Zn concentrations are considered the correlation with Fe and S increase, indicating that sphalerite is the likely source of Zn in the high zinc grey tailings samples.

The multi-addition NAG technique (mNAG) (Smart et al. 2002) involves three cycles of addition of 15 % $H_2O_2$, effervescence and heating. The results (Table 1) give an indication of the acid generating capacity of the sample when sulfides within the sample become oxidized over time. The mNAG pH is lowest in the grey tailings, as this is a substrate type with visible pyrite in many of the collected samples. However, the mean $CaCl_2$ paste pH is lower in the marbled tailings indicating that the sulfides have undergone some oxidation, releasing immediate acidity rather than requiring oxidation of the sulfides to effect the acidity. Both the grey and marbled tailings have a lower pH than the mine waste and granular capping materials.

## Bioaccessibility Testing

The test for metal and metalloid bioaccessibility as described previously was applied to each of the 41 samples (<2 mm) collected from the Wheal Maid site. In a similar method to the mNAG, the samples were reacted with hydrogen peroxide, heated, evaporated and the cycle was repeated three times. The resultant soluble metals and metalloids in the moist sample were then extracted using ammonium acetate solution and submitted for analysis at ALS, Ireland. Analytical quality of the test was monitored by the inclusion of blank extracts (determinations all $<2 \times$ LOD), spiked solutions (recoveries 85–115 % except for Sb (78 %)) and replicate analyses of a single sample (relative standard deviations all <10 %). The results are presented in Table 2.

Some of the detected metals and metalloids are contained in sulfide minerals. However, following oxidation of the material these elements will become available

**Table 1** Mean and standard deviations for selected elemental concentrations and pH values determined for the four sample types

| Mean value (standard deviation) by material type | | | | |
|---|---|---|---|---|
| | MW (n = 10) | GC (n = 10) | GT (n = 10) | MT (n = 11) |
| Major elements (wt%) | | | | |
| Al | 8.31 (0.94) | 7.11 (0.87) | 3.58 (1.43) | 4.98 (1.24) |
| Ca | 0.12 (0.14) | 0.11 (0.05) | 0.04 (0.01) | 0.04 (0.02) |
| Fe | 5.9 (0.7) | 5.8 (1) | 15.4 (8.2) | 20.3 (4.5) |
| S | 0.31 (0.25) | 0.12 (0.09) | 6.4 (1.13) | 2.44 (0.56) |
| Minor elements (ppm) | | | | |
| As | 1081 (653) | 2470 (1010) | 2332 (1260) | 13,325 (5350) |
| Cd | 0.43 (0.32) | 1.6 (1.27) | 18.8 (22.5) | 0.88 (0.57) |
| Cu | 378 (202) | 893 (577) | 694 (755) | 141 (57) |
| Pb | 130 (53) | 416 (136) | 395 (258) | 304 (109) |
| Sb | 8.8 (5.7) | 13.9 (5.2) | 12.6 (5.9) | 13.4 (3.2) |
| Zn | 271 (81) | 399 (287) | 11,590 (16,790) | 364 (319) |
| pH measurements | | | | |
| mNAG | 4.08 (0.98) | 6.55 (0.45) | 1.93 (0.12) | 2.63 (0.11) |
| Paste $CaCl_2$ | 4.11 (0.99) | 4.46 (0.25) | 2.58 (0.36) | 2.42 (0.11) |

mine waste (*MW*), granular capping (*GC*), grey tailings (*GT*) and marbled tailings (*MT*)

**Table 2** Bioaccessibility of metals and metalloids in MW, GC, GT and MT samples expressed as a percentage of the total element concentrations

| Mean value (standard deviation) by material type | | | | |
|---|---|---|---|---|
| Element (%) | MW (n = 10) | GC (n = 10) | GT (n = 10) | MT (n = 11) |
| As | 2.4 (1.6) | 2.8 (2.5) | 60.2 (12.1) | 1.4 (0.4) |
| Cd | nr | nr | 65.7 (9.8) | nr |
| Cu | 33.9 (14.9) | 42.3 (15.8) | 55.6 (12.6) | 38.7 (13.5) |
| Pb | 3.9 (2.4) | 6.7 (6.6) | 18.1 (22.9) | 0.6 (0.2) |
| Sb | nr | nr | 35.1 (13.0) | nr |
| Zn | 16.9 (13.9) | 13.2 (15.3) | 57.5 (20.3) | 48.7 (19.5) |

*nr* not reported because a high number of results for the bioaccessible fraction were below the limit of detection

to plants either planted on, or colonizing the substrate. The hydrogen peroxide in the bioaccessibility test accelerates the oxidation process and the ammonium acetate solubilizes the elements liberated by this accelerated oxidation.

All results for As are above the LOD for the bioaccessibility liquior and it is clear that As is particularly bioaccessible (62 %) in the grey tailings. Arsenic in the marbled tailings is far less bioaccessible (1.4 %) since there is a much larger reservoir of total As in these samples.

Many of the results for the determination of Cd in the bioaccessibility leachate were less than or near the limit of detection. However, the bioaccessibility of Cd in

the grey tailings seemed to be consistently high, particularly in two samples of the white precipitate present on the surface of the grey tailings which had a Cd bioaccessibility of 74 and 84 %. The grey tailings is the sample set with the highest total concentration of Cd, and the log normalized concentrations correlate highly with those of Zn.

Cu bioaccessibility is consistently high in all four sample types, although slightly higher in the grey tailings. Lead in the grey tailings was found to be the most bioaccessible (18 %). However, the standard deviation for this figure was relatively large (23 %), indicating high variability in the bioaccessibility of Pb in these samples. Lead concentration in the white precipitate associated with the samples is very low, and when these samples are excluded, the Pb bioaccessibilities range from 2.6 to 70 %.

The bioaccessibility analysis for Sb suffered from the same limitation as Cd in that many of the results for the bioaccessibility liquor were below or close to the limit of detection. However, it is interesting that for Sb whilst the grey tailings were the only samples with a measureable bioaccessibility of 35 %; these were not the samples with the highest total Sb concentrations.

Zinc is particularly bioaccessible in the grey and marbled tailings and is also bioaccessible in the granular capping and mine waste materials. Within the grey tailings, Zn bioaccessibility in the white precipitate is particularly high at 82 and 94 %. These samples also have high total Zn concentrations and will provide a large input of this element into the mobile phase upon oxidation. Apart from these two samples, the grey tailings generally have both high bioaccessibility and total concentrations for Zn. It is likely that the oxidation of sphalerite in these high zinc samples is the source of the bioaccessible Zn.

## Conclusions

The current use of bioaccessibility testing for contaminated land assessment is dominated by the assessment of oral bioaccessibility of potentially harmful elements to humans (e.g. Denys et al. 2012; Ruby et al. 1996; Van De Wiele et al. 2007). Revegetation of historic mine sites is important for successful rehabilitation and can be delayed if environmentally significant elements are elevated and bioaccessible. Sequential extraction techniques (e.g. Dold 2003) determine the association of potentially toxic trace elements with different geochemical fractions and as such can help predict plant bioaccessibility. However, these tests are time-consuming and expensive and are consequently not used by the mining industry on a routine basis (Parbhakar-Fox and Lottermoser 2015). Moreover, they provide detailed but unnecessary information on inert geochemical fractions. In sulfidic wastes and rocks, it is the potentially toxic elements associated within sulfide minerals that are bioaccessible as they may become mobile and available to plants upon oxidation (Amos et al. 2015; Kossoff et al. 2014). A rapid, inexpensive and reliable technique to determine this fraction is therefore required before plant

bioaccessibility measurements will become fully integrated into mine site risk assessments. A protocol for such a test has been presented previously in this monograph and the results of its application in a case study site are presented here.

The Wheal Maid historic mine site is part of the Cornish mining heritage landscape. It lies on the southwest UK peninsular in an area that was heavily mined during the 18th and 19th century. Disposal of sulfidic tailings in two adjacent lagoons in the 1970s and 80s caused the site to become a major source of potentially toxic trace elements and acid water contamination. The walls and walkways of the lagoons were constructed with mine waste. Colonization by pioneer and intentionally seeded plants has begun to occur on the upper lagoon which has been capped with a granular material. The lower lagoon shows no sign of re-vegetation and there are exposed pyritic (grey) tailings and weathered (marbled) tailings. Standing water in the upper lagoon is not visibly contaminated but in the lower lagoon it is a striking orange colour due to the presence of Fe oxides in the water.

Geochemical analysis shows that the marbled tailings have extremely elevated near-total levels of As whilst the grey tailings are extremely elevated in near-total Zn. Near total concentrations for other elements and materials are of approximately the same order of magnitude, apart from S which is elevated in both the grey and marbled tailings and Cd which is elevated in the grey tailings. Results for the new bioaccessibility test reveal that As bioaccessibility in the marbled tailings is relatively low. It is the grey tailings that contain the most bioaccessible As, Cd, Cu, Sb, Zn and to a lesser extent Pb.

Weathering and oxidation of the grey tailings at the Wheal Maid case study site will continue to release the bioaccessible elements present in this material into a potentially available form for plant uptake. If no remedial action is taken, mine site rehabilitation reliant on a sustainable vegetation cover will inevitably be delayed. The application of the new bioaccessibility test on Wheal Maid samples demonstrate its potential application for other site assessments. In particular, the new test is useful for site scenarios where sulfide oxidation and acid rock drainage are likely.

## References

Al-Abed SR, Hageman PL, Jegadeesan G, Madhaven N, Allen D (2006) Comparative evaluation of short term leach tests for heavy metal release from mineral processing waste. Sci Total Environ 364:14–23

Amos RT, Blowes DW, Bailey BL, Sego DC, Smith L, Ritchie AIM (2015) Waste-rock hydrogeology and geochemistry. Appl Geochem 57:140–156

Camm S, Hedley P (2005) CSM virtual museum. http://projects.exeter.ac.uk/geomin-centre

CC (2015) Monterey Pines, Cornwall Council web page. http://www.cornwall.gov.uk/environment-and-planning/trees-hedges-and-woodland/monterey-pines

CDC (2008) Carrick District Council. Record of determination of Wheal Maid tailings lagoon, Gwennap, Cornwall as contaminated land

Cornish Mining (2015) The Gwennap-Chacewater Mining District, Cornish Mining World Heratage. https://www.cornish-mining.org.uk/fr/delving-deeper/industrial-settlements

Denys S, Caboche J, Tack K, Rychen G, Wragg J, Cave M, Jondreville C, Feidt C (2012) In vivo validation of the unified BARGE method to assess the bioaccessibility of arsenic, antimony, cadmium, and lead in soils. Environ Sci Technol 46:6252–6260

Dold B (2003) Speciation of the most soluble phases in a sequential extraction procedure adapted for geochemical studies of copper sulfide mine waste. J Geochem Explor 80:55–68

Freeborn (2006) History of Mount Wellington mine up until 2006. http://www.mountwellington.co.uk

Gwennap (2015) The history of the Wheal Maid Tailings Lagoon, Information board at the Wheal Maid site owned by Gwennap Parish Council

Jiménez MN, Bacchetta G, Casti M, Navarro FB, Lallena AM, Fernández-Ondoño E (2011) Potential use in phytoremediation of three plant species growing on contaminated mine-tailing soils in Sardinia. Ecol Eng 37:392–398

Kettaneh Y, Badham J (1978) Mineralization and paragenesis at the Mount Wellington Mine, Cornwall. Econ Geol 73:486–495

Khorasanipour M, Tangestani MH, Naseh R, Hajmohammadi H (2011) Hydrochemistry, mineralogy and chemical fractionation of mine and processing wastes associated with porphyry copper mines: a case study from the Sarcheshmeh mine, SE Iran. Appl Geochem 26:714–730

Kossoff D, Dubbin WE, Alfredsson M, Edwards SJ, Macklin MG, Hudson-Edwards KA (2014) Mine tailings dams: characteristics, failure, environmental impacts, and remediation. Appl Geochem 51:229–245

Lottermoser BG, Glass HJ, Page CN (2011) Sustainable natural remediation of abandoned tailings by metal-excluding heather (*Calluna vulgaris*) and gorse (*Ulex europaeus*), Carnon Valley, Cornwall, UK. Ecol Eng 37:1249–1253

Met Office (2015) South West England: climate. http://www.metoffice.gov.uk/climate/uk/regional-climates/sw

Parbhakar-Fox A, Lottermoser BG (2015) A critical review of acid rock drainage processes and practices. Miner Eng 82:107–124

Ruby MV, Davis A, Schoof R, Eberle S, Sellstone CM (1996) Estimation of lead and arsenic bioavailability using a physiologically based extraction test. Environ Sci Technol 30:422–430

Smart R, Skinner WM, Levay G, Gerson AR, Thomas JE, Sobieraj H, Schumann R, Weisener C, Weber P, Miller S, Stewart WA (2002) ARD test handbook: Project P387, a prediction and kinetic control of acid mine drainage. AMIRA, International Ltd, Ian Wark Research Institute, Melbourne, Australia

Van de Wiele TR, Oomen AG, Wragg J, Cave M, Minekus M, Hack A, Cornelis C, Rompelberg CJM, De Zwart LL, Klinck B, Van Wijnen J, Verstraete W, Sips AJ (2007) Comparison of five in vitro digestion models to in vivo experimental results: lead bioaccessibility in the human gastrointestinal tract. J Environ Sci Health A 42:1203–1211

# Index





B. Lottermoser (ed.), *Environmental Indicators in Metal Mining*,
DOI 10.1007/978-3-319-42731-7